ANNUAL REPORTS ON NMR SPECTROSCOPY

Volume 17

ANNUAL REPORTS ON

NMR SPECTROSCOPY

This Page Intentionally Left Blank

ANNUAL REPORTS ON

NMR SPECTROSCOPY

Edited by

G. A. WEBB

Department of Chemistry, University of Surrey, Guildford, Surrey, England

VOLUME 17

1986

ACADEMIC PRESS

LIST OF CONTRIBUTORS

T. Drakenberg, *Department of Physical Chemistry 2, University of Lund, Sweden.*

F. Heatley, *Department of Chemistry, University of Manchester, Manchester M13 9PL, UK.*

C. J. Jameson, *Department of Chemistry, University of Illinois at Chicago, Chicago, Illinois 60680, USA.*

H. Jörg Osten, *Academy of Sciences of the GDR, Central Institute of Physical Chemistry, 1199 Berlin, Rudower Chaussee 6, German Democratic Republic.*

P. S. Pregosin, *Laboratorium für Anorg. Chemie, ETH-Zentrum Universitatstr. 6, CH-8092 Zürich, Switzerland.*

J. D. Satterlee, *Department of Chemistry, University of New Mexico, Albuquerque, New Mexico 87231, USA.*

This Page Intentionally Left Blank

PREFACE

Volume 17 of Annual Reports consists of state of the art accounts of five rather distinct areas of NMR spectroscopy.

The review on Theoretical Aspects of Isotope Effects on Nuclear Shielding by Prof. C. J. Jameson and Dr. J. Osten, is a welcome complement to the account by Dr. P. E. Hansen in Volume 15 of this series. It is a pleasure to include the account on Relaxation Processes in Synthetic Polymers by Dr. F. Heatley which is the first time that this particular area of NMR has been visited in the present series.

The other three reports cover fields of NMR which have been treated *inter alia* in earlier volumes. The continuing burgeoning of the literature in these areas has resulted in complete chapters being required to provide adequate current coverage. Prof. J. D. Satterlee deals with the NMR of Paramagnetic Haem Proteins, Dr. T. Drakenberg covers the NMR of Less Common Quadrupolar Nuclei which was last treated in Volume 9 and Prof. P. Pregosin reviews Platinum NMR.

I am very grateful to all of the contributors for their diligence and kind cooperation in the production of this volume.

University of Surrey   G. A. WEBB
Guildford, Surrey,   November 1985
England

This Page Intentionally Left Blank

CONTENTS

Theoretical Aspects of Isotope Effects on Nuclear Shielding

CYNTHIA J. JAMESON AND H. JÖRG OSTEN

NMR Spectroscopy of Paramagnetic Haem Proteins

JAMES D. SATTERLEE

Nuclear Magnetic Relaxation and Models for Backbone Motions of Macromolecules in Solution

F. HEATLEY

Nuclear Magnetic Resonance of Less Common Quadrupolar Nuclei

TORBJÖRN DRAKENBERG

Platinum NMR Spectroscopy

P. S. PREGOSIN

This Page Intentionally Left Blank

Theoretical Aspects of Isotope Effects on Nuclear Shielding

CYNTHIA J. JAMESON

Department of Chemistry, University of Illinois at Chicago, Chicago, Illinois, USA

H. JÖRG OSTEN

Academy of Sciences of the GDR, Central Institute of Physical Chemistry, Berlin, German Democratic Republic

I. INTRODUCTION

Isotope shifts have long been observed in high resolution NMR in the gas phase, in liquids and in solutions. There are large shifts associated with the mass dependence of rate constants for chemical reactions or changes in

conformational structure. We do not consider these equilibrium or kinetic isotope effects, only intrinsic isotope effects. The review by Batiz-Hernandez and Bernheim[1] and the more recent one by Hansen[2a] in this series include most of the published data up to 1982. There is also a recent discussion of ^{13}C isotope shifts by Forsyth.[2b] Here we review the theory underlying the interpretation of isotope shifts in NMR. The interpretation of isotope shifts involves a consideration of the vibrational and rotational averaging of nuclear shielding. For this reason the isotope shift is intimately related to the observed temperature dependence of nuclear shielding in the gas phase in the zero-pressure limit. These two measurable properties share the same electronic factors – the change in shielding with bond extension or bond angle deformation.

We follow the notation introduced by Gombler[3] for the isotope shift observed for nucleus A upon substitution of the neighbouring ^mX isotope in the molecule with the heavier $^{m'}X$ isotope:

$$^n\Delta A(^{m'/m}X) = \frac{\nu_A(A\,^{m'}X\cdots) - \nu_A(A\,^mX\cdots)}{\nu_A(A\,^mX\cdots)} \qquad (m' > m) \qquad (1a)$$

where $\nu_A(A\,^{m'}X\cdots)$ is the resonance frequency of the A nucleus in the molecule having the heavier $^{m'}X$ isotope which is n bonds away from the observed nucleus. The molecules $(A\,^{m'}X\cdots)$ and $(A\,^mX\cdots)$ are isotopomers. The isotope shift can also be written in terms of the nuclear shielding difference:

$$^n\Delta A(^{m'/m}X) = \sigma^A(A\,^mX\cdots) - \sigma^A(A\,^{m'}X\cdots) \qquad (1b)$$

$$= \sigma - \sigma^*$$

where the asterisk applies to the heavy isotopomer. Just as for spin–spin couplings, this notation becomes ambiguous when A and X are atoms in cyclic compounds in which there are at least two paths connecting the observed nucleus and substituted atom. In this case the observed quantity is an isotope shift corresponding to two or more bond paths.

There are several general observations which have been made about magnitudes and signs of isotope shifts:[1]

(i) Upon substitution with a heavier isotope the NMR signal of the nearby nucleus usually shifts towards lower frequencies (higher shielding). Thus, as defined in equation (1), isotope shifts are generally negative in sign.

(ii) The magnitude of the isotope shift is dependent on how remote the isotopic substitution is from the observed nucleus. Although there are exceptions, one-bond isotope shifts are larger than two-bond or three-bond isotope shifts.

(iii) The magnitude of the shift is a function of the observed nucleus and reflects its chemical shift range.

(iv) The magnitude of the shift is related to the fractional change in mass upon isotopic substitution.

(v) The magnitude of the shift is approximately proportional to the number of equivalent atoms which have been substituted by isotopes. In other words, isotope shifts exhibit additivity.
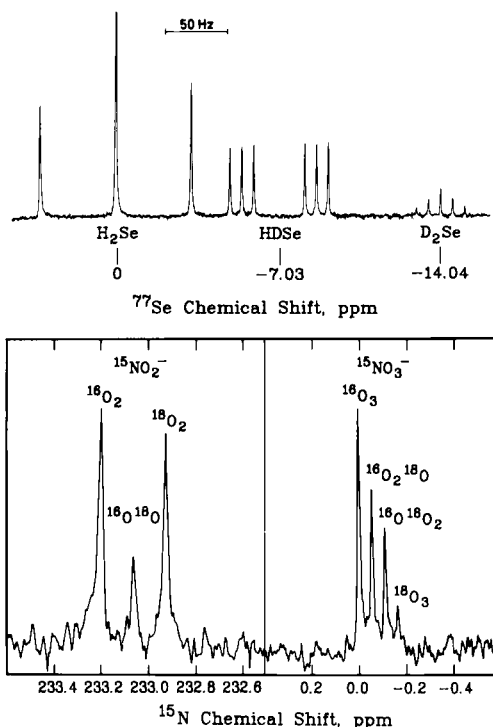
FIG. 1. ^{77}Se FT NMR spectrum of a mixture of H_2Se, HDSe and D_2Se, and ^{15}N spectra of $^{18/16}O$ derivatives of NO_2^- and NO_3^-. From references 4 and 5, respectively, with permission.

Examples of isotope shifts in Fig. 1 illustrate these trends. The ^{77}Se shifts on D substitution in H_2Se are proportionately large (-7.02 ppm per D) compared to ^{17}O shifts on D substitution in H_2O (-1.54 ppm per D), reflecting the large chemical shift range of ^{77}Se compared to ^{17}O. ^{15}N shifts in NH_3 on D substitution (-0.65 ppm per D) are large compared to that for ^{15}N on ^{18}O substitution in NO_2^- (-0.138 ppm) showing the more favourable fractional mass changes in D substitution compared to O substitution. Figure 1 also clearly shows the additivity of isotope shifts; the isotope shift is proportional to the number of substituted atoms, giving rise to

spectra exhibiting equal spacing of characteristic peaks for each isotopomer. We shall discuss the theory underlying these general observations.

There are some less general trends which have been observed, correlating isotope shift with molecular structure.

(a) One-bond isotope shifts tend to increase with increasing bond order[6-8] and decreasing bond length[3] between the observed nucleus and the substituted atom.

(b) The magnitudes of isotope shifts in similar bonds increase with the magnitude of the spin–spin coupling between the observed nucleus and the substituted atom.[9-11]

(c) The magnitudes of one-bond isotope shifts correlate with the chemical shift of the observed nucleus, i.e. the less shielded nuclei have larger isotope shifts.[11-13]
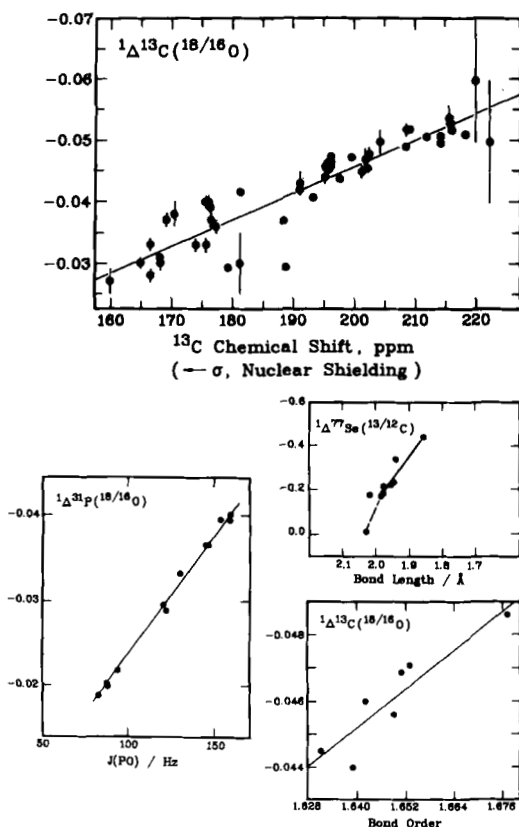
FIG. 2. Correlations between one-bond isotope shifts and various indices of the chemical bond: bond order, bond length, spin–spin coupling, nuclear shielding. From references 12, 10, 3 and 6, with permission.

(d) There is a lone pair effect on the isotope shifts. A nucleus with a σ lone pair tends to have a larger isotope shift in comparison with a related bond in which there is no lone pair on the observed nucleus; for example, the isotope shift for ^{15}N in NH_3 (-0.65 ppm per D) with one lone pair may be compared to that in NH_4^+ (-0.307 ppm per D) with zero lone pairs, or ^{15}N in NO_2^- can be compared with ^{15}N in NO_3^- (see Fig. 1).[14]

(e) The isotope shift tends to be larger when electronegative substituents are introduced at the nuclear site.[8]

Trends (a)-(c) are demonstrated in Fig. 2. These trends are interesting and require interpretation with a suitable theory. It is important to know which aspects of isotope shifts are due to dynamical factors (to rovibrational averaging) and which aspects can be attributed to electronic factors (changes in nuclear shielding with bond extension or bond angle deformation). If the theory can sort out the former, isotope shifts can be used to extract the latter, thus providing chemically interesting information which would make the isotope shift an easily measurable index of the chemical bond.

II. ROVIBRATIONAL EFFECTS ON NUCLEAR SHIELDING

The effects of intramolecular dynamics (vibration and rotation) on nuclear shielding were theoretically predicted by Ramsey[15] and have been observed in two ways. First, there is an observable temperature dependence of the resonance frequency even for the "isolated" molecule (apart from the temperature dependence due to intermolecular interactions).[16] Second, there is an observable shift upon isotopic substitution of neighbouring nuclei. Both are effects of differences in averaging over nuclear configuration as the molecule undergoes vibration and rotation. The temperature dependence of nuclear shielding is observed in the dilute gas phase, where the average shielding can be written as a virial expansion in the gas density ρ,

$$\sigma(T, \rho) = \sigma_0(T) + \sigma_1(T)\rho + \sigma_2(T)\rho^2 + \cdots \tag{2}$$

The intermolecular effects are contained in the density dependent terms.

The nuclear shielding in an "isolated" molecule, $\sigma_0(T)$, is actually observed as the nuclear shielding in the limit of pressure approaching zero. Yet, the pressure must be high enough so that collisional interactions cause a given molecule to pass through a representative number of thermally accessible vibrational and rotational states in a time that is short compared to the reciprocal of the NMR frequency difference between nuclei in different rovibrational states. Thus, mathematically speaking, one does not extrapolate the results to a true zero pressure, but to a pressure so low that collisional deformation of the molecule no longer contributes to σ, while there are still

enough collisions to provide the required rate of transition between vibrational and rotational states.

The observed isotropic nuclear shielding of a nucleus in an isolated molecule, $\sigma_0(T)$, is a statistical average of the nuclear magnetic shielding tensor over all possible orientations of the molecule in the magnetic field. It is also an average over all possible rovibrational states of the molecule weighted according to the fraction of molecules occupying that state at that temperature. Thus, the value of the shielding of a nucleus in a gas sample extrapolated to zero density at a given temperature is a weighted average of the values characteristic of each occupied state.

The average shielding for a given rovibrational state is different for each of several isotopically related species because the masses enter into the solution of the vibrational-rotational hamiltonian. Thus, the thermal average shielding $\sigma_0(T)$ is different for the isotopomers. These differences are measured as isotope shifts. It has been found that mass effects on intermolecular interactions (except in hydrogen-bonding or complex-formation) are not significant, i.e. the mass dependence of $\sigma_1(T)$ in equation (2) is small.[17] Therefore, even isotope shifts measured in condensed phase can sometimes be interpreted as the differences between $\sigma_0(T)$ values of the isotopically related species.

A. Basic principles

The Born–Oppenheimer approximation allows us to consider the nuclear motion in rotation and vibration separately from the electronic motion. Within the Born–Oppenheimer approximation, we can consider a shielding surface which gives the values of nuclear shielding at rigidly fixed nuclear configurations. The interpretation of the experimentally observed nuclear magnetic shielding then involves the two surfaces, the potential energy surface and the nuclear shielding surface, with simultaneous averaging on both surfaces. Figure 3 shows the proton shielding surface[18] and the potential energy surface of the H_2^+ molecule.[19] The shielding surface gives the ^1H nuclear shielding calculated with the relativistic theory for fixed nuclear configurations. For a given rovibrational state, there will be a characteristic average shielding which can be evaluated from the vibrational and rotational wavefunctions and the nuclear shielding function such as the one shown in the figure. The vibrational levels of the HD^+ and D_2^+ isotopomers (which have lower vibrational frequencies than H_2^+) sit lower in the potential well and thus will give different average values of proton shielding. In this case the shielding surface is known for a wide range of nuclear configurations. For most systems, however, there is very limited information, the shielding surface being calculated for just a few points in the vicinity of r_e. For semirigid molecules that we often observe in NMR (excluding molecules
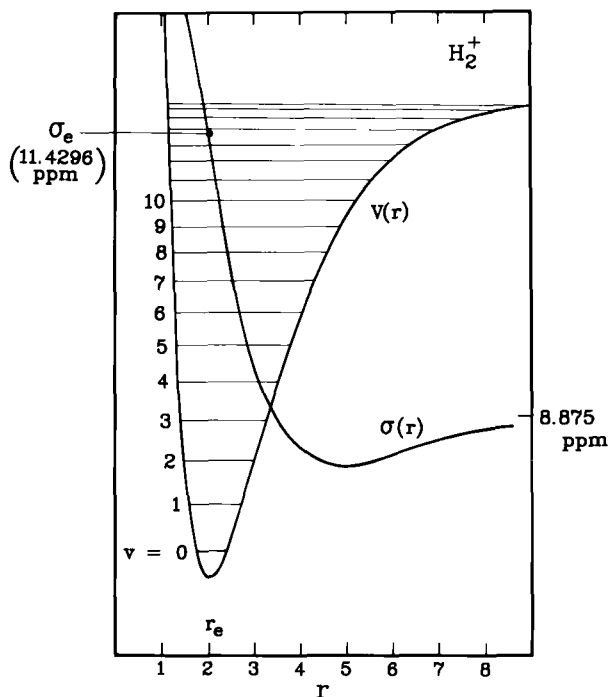
FIG. 3. The ^{1}H shielding surface and the potential energy surface for ^{1}H$_2$$^+$. From references 18 and 19, with permission.

which are fluxional or which undergo low frequency torsion), the motions involved in the averaging take place in a small pocket of the potential energy surface close to the equilibrium configuration. Therefore this corresponds to averaging over small displacements on the shielding surface. Then it makes physical sense to expand the nuclear shielding in terms of the normal coordinates Q_s (a concept of significance only for small displacements):

$$\sigma = \sigma_e + \sum_s \left(\frac{\partial \sigma}{\partial Q_s}\right)_e Q_s + \frac{1}{2} \sum_{s,r} \left(\frac{\partial^2 \sigma}{\partial Q_r \partial Q_s}\right)_e Q_r Q_s + \cdots \tag{3}$$

where the shielding derivatives are taken at the equilibrium configuration. The application of this equation to a general molecular electronic property (not just nuclear shielding) for a general molecular type (an asymmetric rotor) as well as for specific types (spherical tops and symmetric tops) has been formulated.[20-22] Normal coordinates are a logical choice for this expansion since methods of evaluating the average values $\langle Q_s \rangle$, $\langle Q_r Q_s \rangle$ are well known in vibrational spectroscopy. However, the derivatives of the nuclear shielding with respect to the normal coordinates are not invariant under isotopic substitution. For the purpose of discussing the isotope shift

it is more convenient to expand the shielding in terms of internal displacement coordinates:

$$\sigma = \sigma_e + \sum_i \left(\frac{\partial \sigma}{\partial \mathcal{R}_i}\right)_e \mathcal{R}_i + \frac{1}{2} \sum_{i,j} \left(\frac{\partial^2 \sigma}{\partial \mathcal{R}_i \, \partial \mathcal{R}_j}\right)_e \mathcal{R}_i \, \mathcal{R}_j + \cdots \tag{4}$$

where $\mathcal{R}_i$ stands for the bond displacements (Δr_i) and the bond angle deformations $(\Delta \alpha_{ij})$.

The theoretical interpretation of isotope shifts in NMR therefore involves the mass-independent electronic quantities such as

$$(\partial \sigma / \partial \mathcal{R})_e = (\partial \sigma / \partial \Delta r)_e, (\partial \sigma / \partial \Delta \alpha)_e, \ldots$$

which describe the change in nuclear shielding with bond extension or angle deformation, and the mass-dependent thermal averages $\langle \mathcal{R}_i \rangle^T$ which are $\langle \Delta r \rangle^T, \langle \Delta \alpha \rangle^T, \ldots$ and $\langle \mathcal{R}_i \, \mathcal{R}_j \rangle^T$ which are $\langle (\Delta r)^2 \rangle^T, \langle (\Delta \alpha)^2 \rangle^T, \langle \Delta r \, \Delta \alpha \rangle^T, \ldots$ The isotope shift is given by

$$\sigma - \sigma^* = \sum_i \left(\frac{\partial \sigma}{\partial \mathcal{R}_i}\right)_e [\langle \mathcal{R}_i \rangle^T - \langle \mathcal{R}_i \rangle^{T*}]$$

$$+ \frac{1}{2} \sum_{i,j} \left(\frac{\partial^2 \sigma}{\partial \mathcal{R}_i \, \partial \mathcal{R}_j}\right)_e [\langle \mathcal{R}_i \, \mathcal{R}_j \rangle^T - \langle \mathcal{R}_i \, \mathcal{R}_j \rangle^{T*}] + \cdots \tag{5}$$

B. Effect of vibration and rotation on the internuclear distance

1. The vibrational average bond extension

In order to be able to evaluate $\langle \mathcal{R}_i \rangle^T, \langle \mathcal{R}_i \, \mathcal{R}_j \rangle^T, \ldots$ etc. we need a potential surface in which the vibrational motion of the molecule takes place. The known derivatives of this surface are the quadratic, cubic, etc. force constants. Normal coordinate analysis with the quadratic force constants gives the solutions to the harmonic problem whch are the harmonic frequencies (ω), the normal coordinates (Q), and the L matrix.[23] The internal displacement coordinates $\mathcal{R}_i = \Delta r_i, \Delta \alpha_{ij}$, etc. can be expressed in terms of these normal coordinates as follows:

$$\mathcal{R} = \mathbf{L} \mathbf{Q} \tag{6}$$

where $\mathbf{L}$ is a tensor which contains the transformation coefficients between the curvilinear internal coordinates and various powers of Q. The vibrational part of Δr_i is then

$$\Delta r_i = \sum_r L_i^r Q_r + \frac{1}{2} \sum_{r,s} L_i^{rs} Q_r Q_s + \frac{1}{6} \sum_{r,s,t} L_i^{rst} Q_r Q_s Q_t + \cdots \tag{7}$$

Thus the vibrational average $\langle \Delta r \rangle_{vib}$ can be expressed in terms of $\langle Q_r \rangle$,

$\langle Q_r Q_s \rangle$, etc. The analytical expressions for elements of the L tensor are given by Hoy et al.,[24] in which the linear terms L_i^r are identical to the elements L_{ir} of the L matrix. Equation (7) is exact, but in practice of course the series must be truncated; in general it converges well, each term being smaller than the preceding by a factor of about 10 for typical vibrational amplitudes.[25]

If the calculation is confined to the terms of the second order in equation (7), it is necessary to use the wavefunctions of the first order for obtaining the expectation values of Q_r, whereas it is sufficient to use zero-order wavefunctions for those of $Q_r Q_s$.[26] The quantum mechanical hamiltonian for a vibrating rotor has been derived by Wilson and Howard[27] and developed by Nielsen and others.[28,29] There are several equivalent approaches in calculating the desired expectation values from the hamiltonian. Perturbation theory methods and the contact transformation method lead to identical results. The expectation values of only totally symmetric coordinates Q_s are required:

$$\langle Q_s \rangle = -\left(\frac{h}{4\pi^2 c}\right)^{\frac{1}{2}} \omega_s^{-\frac{3}{2}} \left[3k_{sss}(v_s + \tfrac{1}{2}) + \sum_r' k_{srr}(v_r + g_r/2) \right] \qquad (8)$$

where ω_s are the normal frequencies and k_{srr} are the cubic force constants, both in wavenumbers. g_r denotes the degeneracy of the r-th vibration. $\langle Q_r Q_s \rangle = 0$ if $\omega_r \neq \omega_s$ and

$$\langle Q_s^2 \rangle = \left(\frac{h}{4\pi^2 c\omega_s}\right)(v_s + \tfrac{1}{2}) \qquad (9)$$

These two expressions, equations (8) and (9), represent the expectation values for $\langle Q \rangle$ and $\langle Q^2 \rangle$ for one given vibrational level v_s. In an NMR experiment we observe only the average values over all vibrational states for a given temperature:

$$\langle v_s + g_s/2 \rangle^T = \frac{\sum_{v_s} g_s(v_s + g_s/2) \exp[-E(v_s)/kT]}{\sum_{v_s} g_s \exp[-E(v_s)/kT]} \qquad (10)$$

If we assume harmonic energy levels in evaluating the thermal average in equation (10), the infinite sums are calculable in closed form:[30]

$$\langle v_s + g_s/2 \rangle^T = (g_s/2) \coth(hc\omega_s/2kT) \qquad (11)$$

A second approach is that of Bartell.[31] The quantum mechanical law of motion applied to a wave packet is given, in Cartesian coordinates, by

$$m\frac{d^2\langle x \rangle}{dt^2} = -\left\langle \frac{\partial V}{\partial x} \right\rangle \qquad (12)$$

In our molecular applications the system will be in stationary states or an

equilibrium distribution among stationary states. Since the space average displacement $\langle x \rangle$ is independent of time in such a system, it follows that the space average force is zero, or

$$\langle \partial V / \partial x \rangle = 0 \tag{13}$$

Equation (12) is the molecular quantum mechanical analogue to the Ehrenfest theorem.[32] We use the Cartesian displacement coordinates, rather than internal coordinates, because the latter do not necessarily form a complete set of coordinates. For the same reason it is not always possible to use the set of symmetry coordinates. We adopt local molecular Cartesian frames such that the z_i-axis lies along the direction of the A–X_i bond at its equilibrium position and the x-axis is on the plane X_i–A–X_j and perpendicular to z_i. Now we can express the internal displacement coordinates in terms of the Cartesian displacement coordinates:

$$\Delta r_i = \Delta z_i + [(\Delta x_i)^2 + (\Delta y_i)^2]/2r_i + \cdots \tag{14a}$$

$$\Delta \alpha_{ij} = \frac{\Delta x_i}{r_i} + \frac{\Delta x_j}{r_j} - \frac{\Delta x_i \, \Delta z_i}{r_i^2} - \frac{\Delta x_j \, \Delta z_j}{r_j^2} + \cdots \tag{14b}$$

Using equation (14) we are able to calculate the derivatives of the internal coordinates with respect to Δz_k, for example:

$$(\partial \Delta r_i / \partial \Delta z_k) = \delta_{ik} + \cdots \tag{15a}$$

$$(\partial \Delta \alpha_{ij} / \partial \Delta z_k) = -\frac{\Delta \alpha_{kj}}{2r_k} \delta_{ik} = -\frac{\Delta \alpha_{ik}}{2r_k} \delta_{jk} \tag{15b}$$

where δ_{ij} is the Kronecker delta.

We obtain from a potential function in internal coordinates, by applying equation (13), a set of coupled equations which connect the desired mean bond displacements $\langle \Delta r_i \rangle$ and mean bond angle deformations $\langle \Delta \alpha_{ij} \rangle$ with the mean square amplitudes (MSA) of the internal coordinates in a linear way, whereas the coefficients are functions of the quadratic and cubic force constants and geometry parameters.[31,33-35,14] These MSA's (which include non-vanishing cross products) are related to the mean square normal coordinates $\langle Q^2 \rangle$ in the usual way:[36]

$$\langle \mathfrak{R}_i \, \mathfrak{R}_j \rangle \approx L \langle Q^2 \rangle \tilde{L} \tag{16}$$

Equation (7) can be written as[25,37]

$$\langle \Delta r \rangle = \langle \Delta z \rangle + [\langle (\Delta x)^2 \rangle + \langle (\Delta y)^2 \rangle]/2r_e + \cdots \tag{17}$$

in the same local Cartesian coordinate system as equation (14a). $\langle \Delta z \rangle$ can be identified with $\sum_r L_i^r \langle Q_r \rangle$, which represents the part of the average displacement that is along the equilibrium bond axis. Unlike a diatomic

molecule, nuclear motions perpendicular to this z-axis occur in a polyatomic molecule, so we need to add $[(\Delta x)^2 + (\Delta y)^2]/2r_e$ which can be identified with $\frac{1}{2} \sum_s L_i^{ss} \langle Q_s^2 \rangle$. Thus we see in equation (7) that the first term, the average displacement parallel to the equilibrium bond axis, arises from the average displacement in the totally symmetric coordinate due to cubic anharmonicity; the next term, containing the mean square perpendicular amplitudes, involves only the harmonic potential constants and arises from the non-linear nature of the transformation from interatomic distances to normal coordinates.

Fowler[38] has shown that Bartell's approach is mathematically equivalent to the perturbation approach. However, Bartell's method has the advantage of being useful in a convenient form when the cubic force constants are not available. As originally proposed by Bartell, it has been used with a Urey–Bradley quadratic force field augmented with the cubic terms arising from a Morse anharmonicity for the stretching terms and a suitable model for the non-bonded interactions.

2. Effects due to molecular rotation: centrifugal stretching

As a molecule rotates, the atoms tend to move away from the centre of mass. This centrifugal distortion depends only upon the harmonic potential constants to the second-order approximation:[26]

$$\langle Q_s \rangle_{\text{rot}} = \frac{1}{8\pi^2 c^2 \omega_s^2} \cdot \sum_\alpha \frac{a_s^{(\alpha\alpha)}}{I_{\alpha\alpha}^{(e)2}} \cdot (v_1^* \, v_2^* \cdots R|(P_\alpha - p_\alpha^*)^2|v_1^* \, v_2^* \cdots R)$$

$$(18)$$

where $I_{\alpha\alpha}^{(e)}$ are principal moments of inertia along the α axis in the equilibrium configuration, $a_s^{(\alpha\alpha)}$ are coefficients of the normal coordinate expansion of $I_{\alpha\alpha}$, P_α is the component of the total angular momentum along the α axis, and p_α stands for the vibrational angular momentum. The asterisks denote the angular momentum associated with the degenerate vibrations, and R stands for the overall rotation. The complete expression for $\langle Q_s \rangle$ is then obtained by adding the rotational contribution given by equation (18) to the vibrational contribution given in equation (8). Explicit expressions for $a_s^{(\alpha\alpha)}$ have been derived for specific molecular types,[28] and equation (18) can be written in terms of the rotational quantum numbers for specific molecular types.[26] Averaging over these rotational levels in a similar manner to equation (10) can thus be carried out to give $\langle Q \rangle^T_{\text{rot}}$, taking into account the appropriate nuclear spin statistical weights. Except for the H_2 molecule, in which the rotational levels are widely spaced and nuclear spin statistics play an important role in the averaging, the thermal average centrifugal stretching can be calculated classically. The assumption that the spacing of rotational levels is sufficiently small compared with kT

(which is easily satisfied except for the case of extremely low temperatures) allows us to use the law of equipartition of energy for calculating the average value of the angular momentum. If the rotational energy is written in the form

$$E_{\text{rot}} = \sum_\alpha (P_\alpha - p_\alpha{}^*)^2/2I_{\alpha\alpha}{}^{(\text{e})} \tag{19}$$

we obtain

$$\langle (P_\alpha - p_\alpha{}^*)^2 \rangle^{\text{T}} = kTI_{\alpha\alpha}{}^{(\text{e})} \tag{20}$$

$$\langle Q_s \rangle^{\text{T}}{}_{\text{rot}} = \frac{kT}{8\pi^2 c^2 \omega_s{}^2} \sum \frac{a_s{}^{(\alpha\alpha)}}{I_{\alpha\alpha}{}^{(\text{e})}} \tag{21}$$

Toyama et al.[26] have shown that equation (18) can be written alternatively in terms of the usual matrices which arise in a harmonic vibrational analysis, so that equation (21) can be written also as

$$\langle \Delta r \rangle^{\text{T}}{}_{\text{rot}} = kT\tilde{\mathbf{U}}\mathbf{F}_s{}^{-1}\mathbf{G}_s{}^{-1}\mathbf{U}\mathbf{B}\mathbf{\Omega}\mathbf{X} \tag{22}$$

where $\mathbf{\Omega}$ denotes a diagonal matrix with the elements

$$\Omega_{ii}{}^{(\alpha\alpha)} = \Omega_\alpha = \frac{1}{I_{\beta\beta}{}^{(\text{e})}} + \frac{1}{I_{\gamma\gamma}{}^{(\text{e})}}$$

and $\mathbf{X}$ is a vector which has the Cartesian coordinates of the atoms at the equilibrium configuration as its elements. $\mathbf{F}_s{}^{-1}$ and $\mathbf{G}_s{}^{-1}$ are the inverse of the usual $\mathbf{F}$ and $\mathbf{G}$ matrices in symmetry coordinates. $\mathbf{U}$ is the transformation matrix from internal into symmetry coordinates and $\mathbf{B}$ is the transformation from Cartesian displacements into internal coordinates.[23] Simple formulae of the thermal averaged centrifugal distortion for some molecular types have been derived.[26,28] For linear triatomics, for example, we obtain:[34]

$$\langle \Delta r_1 \rangle^{\text{T}}{}_{\text{rot}} = \frac{kT}{8\pi^2 c^2} \left[\frac{L_{11}}{\omega_1{}^2} \sum \frac{a_1{}^{\alpha\alpha}}{I_{\alpha\alpha}} + \frac{L_{13}}{\omega_3{}^2} \sum \frac{a_3{}^{\alpha\alpha}}{I_{\alpha\alpha}} \right]$$

and   (23)

$$\langle \Delta r_3 \rangle^{\text{T}}{}_{\text{rot}} = \frac{kT}{8\pi^2 c^2} \left[\frac{L_{31}}{\omega_1{}^2} \sum \frac{a_1{}^{\alpha\alpha}}{I_{\alpha\alpha}} + \frac{L_{33}}{\omega_3{}^2} \sum \frac{a_3{}^{\alpha\alpha}}{I_{\alpha\alpha}} \right]$$

where ω_1 and ω_3 are the two stretching vibrational frequencies, L_{ij} are elements of the L matrix, and the coefficients of the normal coordinates in the moment of inertia, $a_s{}^{\alpha\alpha}$, can be expressed entirely in terms of measured spectroscopic constants:[28]

$$a_1{}^{xx} = a_1{}^{yy} = 2(2B_e/\omega_1)^{\frac{1}{2}}\zeta_{23}{}^x, \qquad a_1{}^{zz} = 0$$

$$a_3{}^{xx} = a_3{}^{yy} = 2(2B_e/\omega_3)^{\frac{1}{2}}\zeta_{21}{}^x, \qquad a_3{}^{zz} = 0 \tag{24}$$

where B_e is the rotational constant. The Coriolis constants for the symmetrical case are $\zeta_{23}{}^x = 1$ and $\zeta_{21}{}^x = 0$.

For highly symmetrical molecules the rotational effect on the mean bond length can be expressed in even simpler form, for example:[26,39]

For a CO_2 type molecule

$$\langle \Delta r \rangle^T_{\text{rot}} = \frac{kT}{r_e(F_{11} + F_{12})}$$

For a CH_4 type

$$\langle \Delta r \rangle^T_{\text{rot}} = \frac{3kT}{4r_e F_{11}} \quad (25)$$

For a BF_3 type (planar AX_n)

$$\langle \Delta r \rangle^T_{\text{rot}} = \frac{3kT}{nr_e F_{11}}$$

For a SF_6 type

$$\langle \Delta r \rangle^T_{\text{rot}} = \frac{kT}{2r_e F_{11}}$$

where F_{11} and F_{12} are mass-independent quadratic force constants.

Although the rotational contribution to $\langle \Delta r \rangle^T$ is usually one order of magnitude smaller than the vibrational contribution $\langle \Delta r \rangle_{\text{vib}}^T$, it plays an important role in the temperature dependence of nuclear shielding. At the same time, we will find that the rotational effects play no role (or a negligible one) in the isotope shift. This we can predict already for certain cases by examining equations (25). Since these equations involve only mass-independent terms, there will be no rotational contribution to the isotope shift if isotopic substitution preserves the symmetry of the molecule, as in going from CH_4 to CD_4 (but not in CH_4 to CH_3D).[39]

III. ISOTOPE SHIFTS IN DIATOMIC MOLECULES

The general theoretical approach used in the interpretation of isotope shifts in particular and rovibrational effects on nuclear shielding in general has been given in the previous section. However, since some complications arise only in polyatomic molecules, there is some advantage to be gained in understanding isotope shifts in diatomic molecules first.

A. Calculation of isotope shifts in diatomic molecules

For a diatomic molecule it is convenient to expand the shielding as a power series in the reduced coordinate $\xi = (r - r_e)/r_e$. For a particular

molecular state characterized by vibrational and rotational quantum numbers v and J,

$$\langle \sigma \rangle_{vJ} = \sigma_E + (d\sigma/d\xi)_e \langle \xi \rangle_{vJ} + \tfrac{1}{2}(d^2\sigma/d\xi^2)_e \langle \xi^2 \rangle_{vJ} + \cdots \tag{26}$$

Here $\langle \xi \rangle_{vJ}$, $\langle \xi^2 \rangle_{vJ}$, ... are the averages of the reduced coordinate over the vibrational-rotational wavefunction corresponding to the v,J level. The thermal averages $\langle \xi \rangle^T$, $\langle \xi^2 \rangle^T$, ... may then be obtained by

$$\langle \xi^n \rangle^T = \frac{\sum_{vJ} g_{vJ} \langle \xi^n \rangle_{vJ} \exp(-E_{vJ}/kT)}{\sum_{vJ} g_{vJ} \exp(-E_{vJ}/kT)} \tag{27}$$

so that the thermal average shielding is

$$\langle \sigma \rangle^T = \sigma_e + (d\sigma/d\xi)_e \langle \xi \rangle^T + \tfrac{1}{2}(d^2\sigma/d\xi^2)_e \langle \xi^2 \rangle^T + \cdots \tag{28}$$

The potential energy surface of a diatomic molecule can be written in terms of a Dunham potential or more approximately in terms of a Morse potential. Both have been used in the interpretation of isotope shifts.

The Dunham potential function expresses the potential energy in terms of a Taylor series expansion in ξ:[40]

$$V = a_0 \xi^2 (1 + a_1\xi + a_2\xi^2 + a_3\xi^3 + \cdots) \tag{29}$$

The potential parameters $a_0, a_1, \ldots$ can be obtained from the expression for the energy levels of a diatomic molecule:

$$E_{vJ} = \sum_{i=0}^{\infty} \sum_{l=0}^{\infty} Y_{il} (v + \tfrac{1}{2})^i [J(J+1)]^l \tag{30}$$

in terms of the spectroscopic constants Y_{il}. The average values $\langle \xi^n \rangle_{vJ}$ can then be obtained by perturbation theory in terms of the potential parameters. Herman and Short have derived the expressions for the average values:[41]

$$\langle \xi^n \rangle_{vJ} = \sum_{i=0}^{\infty} \sum_{l=0}^{\infty} Z_{il}^{(n)} (v + \tfrac{1}{2})^i [J(J+1)]^l \tag{31}$$

where the $Z_{il}^{(n)}$ are expressed in terms of the vibrational frequency ω_e, the rotational constant B_e and the coefficients $a_1, a_1, \ldots$. Once these averages are known, the thermal average shielding can be obtained. This method has been applied to the H_2 molecule by Raynes et al.[42] and to H_2, LiH and HF by Ditchfield.[43] Typically, terms up to a_6 in equation (29) are used.

Some typical results are shown in Figs 4 and 5 and in Table 1. These were calculated by Ditchfield using shielding functions obtained from coupled Hartree–Fock calculations at various internuclear separations. The σ values so obtained for a range of ξ values are fitted to a power series in ξ and the derivatives $(d\sigma/d\xi)_e$, $(d^2\sigma/d\xi^2)_e$, ... are obtained. These were used in equation (26) to calculate the values shown in Table 1. The thermal averages calculated in equation (28) are shown in Figs 4 and 5.

FIG. 4. Calculated shielding components for H or D in H_2, HD and D_2. From reference 43, with permission.

We note in Table 1 that for any given v,J level the ^{1}H or ^{2}D shielding in HD is greater than that in H_2; in D_2 it is greater than in HD. The calculated rovibrational effects on the average shielding at 300 K are shown in Table 2. First we note that rovibrational averaging usually leads to deshielding, Li in LiH being the only known exception. Secondly, we note that the third-

FIG. 5. Calculated shielding components in HF. From reference 43, with permission.

TABLE 1

Rovibrationally averaged shielding tensor components (in ppm) of individual molecular states for ^{1}H in H$_2$, HD and D$_2$, and ^{19}F in HF.[43]

		H$_2$		HD		D$_2$		HF	
v	J	$\sigma_\perp^H$	$\sigma_\parallel^H$	$\sigma_\perp^H$	$\sigma_\parallel^H$	$\sigma_\perp^H$	$\sigma_\parallel^H$	$\sigma_\perp^F$	$\sigma_\parallel^F$
at	r_e	26.022	27.706	26.022	27.706	26.022	27.706	395.98	482.12
0	0	25.694	27.330	25.738	27.380	25.790	27.440	379.82	482.10
0	1	25.672	27.306	25.721	27.362	25.779	27.427	379.68	482.10
0	2	25.627	27.257	25.688	27.326	25.756	27.403	379.41	482.10
0	3	25.560	27.185	25.637	27.271	25.723	27.367	379.00	482.10
1	0	25.067	26.608	25.191	26.751	25.339	26.922	344.36	482.07
1	1	25.046	26.585	25.175	26.734	25.328	26.910	344.19	482.07
1	2	25.004	26.539	25.143	26.699	25.307	26.887	343.87	482.07
1	3	24.941	26.470	25.095	26.647	25.275	26.852	343.38	482.07

TABLE 2

The linear, quadratic and higher order rovibrational contributions to the thermal average shielding at 300 K, $\langle \sigma \rangle^{300} - \sigma_e$, in ppm.[43]

Nucl.	Mol.	$(d\sigma/d\xi)_e\langle\xi\rangle$	$\begin{Bmatrix} (d\sigma/d\xi)\langle\xi\rangle + \\ \frac{1}{2}(d^2\sigma/d\xi^2)_e\langle\xi^2\rangle \end{Bmatrix}$	up to 6th order
^{1}H	H$_2$	−0.5554	−0.3694	−0.3814
^{1}H	HD			−0.3364
^{1}H	HF	−0.7021	−0.3721	−0.3911
^{2}D	DF			−0.2951
^{19}F	HF	−7.42	−11.113	−11.23
^{19}F	DF			−8.161
^{1}H	LiH	−0.1228	−0.1238	−0.1228
^{2}D	LiD			−0.0978
^{7}Li	LiH	+0.1386	+0.0726	+0.0786
^{7}Li	LiD			+0.0656

TABLE 3

Calculated isotope shifts, in ppm.[43]

Molecule	Nucleus	Calculation	Experiment	Ref.
HD – H$_2$	^{1}H	−0.045	−0.036 ± 0.002	44
D$_2$ – HD	^{2}D	−0.054	−0.0469 ± 0.0005	45
DF – HF	^{19}F	−3.07	−2.5 ± 0.5	46
DLi – HLi	^{7}Li	+0.013		

and higher-order terms in equation (28) have very little effect on the thermal average shielding; terms up to quadratic are sufficient to include nearly all rovibrational effects. The calculated isotope shifts at 300 K are shown in Table 3. ^{7}Li, which shows an unusual temperature dependence, also shows an unusual sign for the D-induced isotope shift.

In order to observe more easily the largest terms which contribute to the above equations and explicitly express their mass dependence, we write only the leading terms, expressed in the measured spectroscopic constants of the molecule. The leading terms in the potential energy are:

$$V(\xi) = (hc\omega_e^2/4B_e)[\xi^2 + a_1\xi^3 + \cdots] - hcB_eJ(J+1)[2\xi - 3\xi^2 + \cdots] \quad (32)$$

where a_1 can also be expressed as

$$a_1 = -[1 + (\alpha_e\omega_e/6B_e^2)] \quad (33)$$

α_e being the vibrational-rotational interaction constant.

An especially useful form of an approximate potential for the diatomic molecule is the Morse function:[47]

$$V = D_e\{1 - \exp[-a(r - r_e)]\}^2 \quad (34)$$

For the Morse potential the ratio $\frac{1}{3}(d^3V/d\xi^3)_e/(d^2V/d\xi^2)_e = -ar_e$ can be identified with a_1, the same a_1 that we have previously defined above. The leading terms in equation (31) are:

$$\langle\xi\rangle_{vJ} = -3(v + \tfrac{1}{2})a_1(B_e/\omega_e) + 4J(J+1)(B_e/\omega_e)^2 \quad (35)$$

$$\langle\xi^2\rangle_{vJ} = 2(v + \tfrac{1}{2})(B_e/\omega_e) \quad (36)$$

These substituted into equation (26) then give the leading terms in the shielding:

$$\langle\sigma\rangle_{vJ} = \sigma_e + (d\sigma/d\xi)_e[-3a_1(B_e/\omega_e)(v + \tfrac{1}{2}) + 4(B_e/\omega_e)^2J(J+1)]$$
$$+ \tfrac{1}{2}(d^2\sigma/d\xi^2)_e 2(B_e/\omega_e)(v + \tfrac{1}{2}) \quad (37)$$

With a classical thermal average for $\langle J(J+1)\rangle^T$ and a further approximation given in equation (11) for $\langle v + \tfrac{1}{2}\rangle^T$, the thermal average shielding is:[48]

$$\langle\sigma\rangle^T = \sigma_e + (B_e/\omega_e)[(d^2\sigma/d\xi^2)_e - 3a_1(d\sigma/d\xi)_e] \times \tfrac{1}{2}\coth(hc\omega_e/2kT)$$
$$+ (d\sigma/d\xi)_e 4(B_e/hc\omega_e^2)kT \quad (38)$$

Of these quantities, a_1 is mass-independent and the others depend on the reduced mass of the diatomic molecule as follows:

$$\omega_e^* = (\mu/\mu^*)^{\frac{1}{2}}\omega_e$$
$$B_e^* = (\mu/\mu^*)B_e \quad (39)$$
$$\alpha_e^* = (\mu/\mu^*)^{\frac{3}{2}}\alpha_e$$

Furthermore the thermal average $\langle v+\tfrac{1}{2}\rangle^T$ is also mass-dependent since the populations of the vibrational energy levels over which this average is taken depend on the vibrational frequency ω_e. We note that B_e/ω_e^2 is mass-independent, so the rotational contribution to the thermal average shielding in the diatomic molecule is independent of mass.

Therefore the isotope shift is given by

$$\langle\sigma\rangle-\langle\sigma\rangle^* = [(d^2\sigma/d\xi^2)_e - 3a_1(d\sigma/d\xi)_e](B_e/\omega_e)$$
$$\times\{\coth(hc\omega_e/2kT)-(\mu/\mu^*)^{\frac{1}{2}}\coth[hc(\mu/\mu^*)^{\frac{1}{2}}\omega_e/2kT]\} \quad (40)$$

Alternatively, equation (38) and equation (40) can be written in terms of the mean bond displacement $\langle\Delta r\rangle^T$ and the mean square amplitude $\langle(\Delta r)^2\rangle^T$:

$$\langle\sigma\rangle^T = \sigma_e + (d\sigma/d\Delta r)_e\langle\Delta r\rangle^T + \tfrac{1}{2}(d^2\sigma/d\Delta r^2)_e\langle(\Delta r)^2\rangle^T + \cdots \quad (41)$$

$$\langle\sigma\rangle-\langle\sigma\rangle^* = (d\sigma/d\Delta r)_e[\langle\Delta r\rangle-\langle\Delta r\rangle^*]$$
$$+\tfrac{1}{2}(d^2\sigma/d\Delta r^2)_e[\langle(\Delta r)^2\rangle-\langle(\Delta r)^2\rangle^*] + \cdots \quad (42)$$

where

$$\langle\Delta r\rangle^T = \langle\Delta r\rangle^T_{rot} + \langle\Delta r\rangle^T_{vib} \quad (43)$$

$$\langle\Delta r\rangle^T_{rot} = \frac{4B_e r_e}{hc\omega_e^2}kT \quad (44)$$

$$\langle\Delta r\rangle^T_{vib} = -(3/2)a_1(B_e/\omega_e)r_e\coth(hc\omega_e/2kT) \quad (45)$$

$$\langle(\Delta r)^2\rangle^T_{vib} = (B_e/\omega_e)r_e^2\coth(hc\omega_e/2kT) \quad (46)$$

We note that including only terms up to quadratic allows us to write $\langle\Delta r\rangle^T_{vib} = -(3/2)(a_1/r_e)\langle(\Delta r)^2\rangle^T$ or, in terms of the Morse parameter:[49]

$$\langle\Delta r\rangle^T_{vib} = (3/2)a\langle(\Delta r)^2\rangle^T \quad (47)$$

For a harmonic oscillator equation (46) is exact, so we shall refer to the term involving this and the second derivatives of the shielding as the "harmonic vibrational contribution". On the other hand, only for an anharmonic vibration is $a_1 \neq 0$, therefore we shall refer to the term involving this and the first derivative of the shielding as the "anharmonic vibrational contribution". The rotational contribution is due to centrifugal stretching. As the molecule rotates, the atoms tend to move away from the centre of mass, thereby contributing to an increase of the mean bond length with increasing rotational energy, or with increasing temperature.

We have calculated the rovibrational corrections to shielding and the isotope shift using equations (38) and (40) and show the rotational (equation (44)), the anharmonic vibrational (equation (45)) and the harmonic vibrational (equation (46)) contributions separately in Tables 4–6 for some

TABLE 4

Rotational, anharmonic vibrational and harmonic vibrational contributions to shielding, $\langle \sigma \rangle^{300} - \sigma_e$, in ppm.[a]

Nucl.	Mol.	Rotational	Anharm. vib.	Harm. vib.	Total
^{1}H	H_2	−0.4238	−0.5342	+0.0669	−0.5096
^{1}H	HD	−0.4238	−0.4619	+0.0578	−0.4464
^{1}H	^{7}LiH	−0.0136	−0.0651	−0.1278	−0.2066
^{1}H	^{6}LiH	−0.0136	−0.0658	−0.1291	−0.2086
^{7}Li	LiH	+0.0380	+0.1816	−0.1035	+0.1160
^{7}Li	LiD	+0.0380	+0.1377	−0.0785	+0.0972
^{1}H	HF	−0.0380	−0.6264	+0.2902	−0.3742
^{2}D	DF	−0.0380	−0.4545	+0.2106	−0.2819
^{19}F	HF	−0.3840	−6.3280	−2.8728	−9.5847
^{19}F	DF	−0.3840	−4.5916	−2.0845	−7.0599
^{13}C	$^{13}C^{16}O$	−0.1594	−1.6432	−0.2285	−2.0311[b]
^{13}C	$^{13}C^{18}O$	−0.1594	−1.6018	−0.2227	−1.9839[b]
^{17}O	$^{12}C^{17}O$	−0.1846	−1.9213	−0.2760	−2.3819[b]
^{17}O	$^{13}C^{17}O$	−0.1846	−1.8775	−0.2697	−2.3319[b]
^{15}N	$^{15}N^{14}N$	−0.2108	−2.4825	−0.8529	−3.5462
^{15}N	$^{15}N_2$	−0.2108	−2.4393	−0.8381	−3.4881

[a] This work, using equation (38).

[b] This may be compared with results of calculations by Raynes and Stanney[55] which are, respectively, −2.23, −2.17, −2.6 and −2.54 ppm.

diatomic molecules. We have used shielding derivatives from the literature for H_2,[42] LiH,[51] HF,[52] CO[53] and N_2.[54]

There are several points worth noting in Table 4. First, as in Table 2, we find that the rovibrational effects lead to deshielding of the nucleus compared to the rigid equilibrium configuration, except in the case of Li in LiH.

TABLE 5

Temperature dependence of nuclear shielding, $\langle \sigma \rangle^{400} - \langle \sigma \rangle^{200}$, in ppm.[a]

Nucl.	Mol.	Rotational	Anharm. vib.	Harm. vib.	Total
^{1}H	H_2	−0.0282	0	0	−0.0282
^{1}H	^{7}LiH	−0.0091	−0.0008	−0.0016	−0.0115
^{7}Li	^{6}LiH	+0.0253	+0.0023	−0.0013	+0.0263
^{1}H	HF	−0.0253	0	0	−0.0253
^{19}F	HF	−0.2560	0	0	−0.2560
^{13}C	$^{13}C^{16}O$	−0.1062	−0.0016	−0.0002	−0.1081
^{17}O	$^{12}C^{17}O$	−0.1231	−0.0020	−0.0003	−0.1254
^{15}N	$^{15}N_2$	−0.1405	−0.0013	−0.0004	−0.1423

[a] This work, using equation (38).

TABLE 6

Anharmonic and harmonic vibrational contributions to the isotope shift, in ppm.[a]

Nucl.	Mol.	Anharm.	Harm.	Total	Expt.	Ref.
^{1}H	$HD - H_2$	−0.0723	+0.0090	−0.0632[b]	−0.036 ± 0.002	44
^{1}H	$^7LiH - ^6LiH$	−0.0007	−0.0013	−0.0020		
^{7}Li	$LiD - LiH$	+0.0438	−0.0250	+0.0188		
^{1}H	$DF - HF$	−0.1719	+0.0796	−0.0923		
^{19}F	$DF - HF$	−1.7364	−0.7883	−2.5248	−2.5 ± 0.5	46
^{13}C	$^{13}C^{18}O - ^{13}C^{16}O$	−0.0414	−0.0058	−0.0472[c]	−0.0476 ± 0.0016	50
^{17}O	$^{13}C^{17}O - ^{12}C^{17}O$	−0.0438	−0.0063	−0.0501	−0.110 ± 0.001	50
^{15}N	$^{15}N_2 - ^{15}N^{14}N$	−0.0432	−0.0148	−0.0581	−0.0601 ± 0.002	141

[a] This work, using equation (40).

[b] For isotopomers of H_2 the classical treatment of rotation leads to significant error. A proper average taking into consideration the nuclear spin statistics gives better results: −0.047,[56] −0.042,[42] −0.045.[43]

[c] This may be compared with −0.06 ppm obtained from calculations including cubic terms.[55]

Second, the anharmonic vibration contribution is the largest one of the three in every molecule (except for LiH) and the rotational contribution is the smallest (except for H_2). Third, neglect of the harmonic vibrational contribution leads to error. Differences in shielding between pairs of isotopically related molecular species give the isotope shifts in Table 6. There is no rotational contribution to the isotope shift in the diatomic molecule. The relative contributions of the anharmonic and harmonic vibrational effects vary so that neglect of the harmonic contribution in calculating the isotope shift can lead to error. The largest error would occur in the case of ^{19}F in the DF–HF system, in which the harmonic vibrational contribution is 31% of the observed isotope shift.

On the other hand, the temperature dependence of the shielding depends nearly entirely on rotation, with vibrational effects accounting for 0–2%. This is easily understood by consulting equation (38). The linear temperature dependence dominates the change of the average shielding with temperature, especially for these diatomic molecules which have very strong bonds characterized by high vibrational frequencies. The $(hc\omega/2kT)$ term is large, for which the coth function is very nearly constant and equal to 1.0. For weaker bonds such as in F_2 and ClF, the rotational contribution still dominates the temperature dependence of the shielding although the anharmonic vibration contribution to the temperature dependence becomes significant.[57] A significant rotational contribution to the temperature dependence means that the term in the first derivative determines the observed temperature dependence in a gas in the limit of zero pressure. A single parameter fit to such data then yields empirical values of $(d\sigma/d\Delta r)_e$.

Ditchfield has noted that for the diatomic molecules H_2, HF and LiH the contributions to the temperature dependence of shielding from second and higher derivatives of shielding are altogether too small to affect the observed temperature dependence in the zero-pressure limit to a measurable extent.

B. The dynamic factor in isotope shifts

In order to be able to discuss general trends in isotope shifts, we need to be able to see what factors determine the isotope effect on $\langle\Delta r\rangle_{\text{vib}}$ and $\langle\Delta r^2\rangle$.

1. Estimation of $\langle\Delta r\rangle - \langle\Delta r\rangle^*$

From equation (45) we see that by making use of the implicit mass dependence of B_e and ω_e (equation (39)) we can write

$$\langle\Delta r\rangle - \langle\Delta r\rangle^* = -(3/2)a_1 r_e\{(B_e/\omega_e)\coth(hc\omega_e/2kT)$$
$$- (\mu/\mu^*)^{\frac{1}{2}}(B_e/\omega_e)\coth[hc(\mu/\mu^*)^{\frac{1}{2}}\omega_e/2kT]\} \qquad (48)$$

There are several approximations which can be invoked to simplify this expression further:

(i) if $\coth(hc\omega_e/2kT)$ is very close to 1.0 and $\coth[hc(\mu/\mu^*)^{\frac{1}{2}}\omega_e/2kT]$ is also very close to 1.0, i.e. for high vibrational frequencies, then $\langle\Delta r\rangle - \langle\Delta r\rangle^*$ reduces simply to

$$\langle\Delta r\rangle - \langle\Delta r\rangle^* \approx [1 - (\mu/\mu^*)^{\frac{1}{2}}]\langle\Delta r\rangle \qquad (49)$$

Similarly

$$\langle(\Delta r)^2\rangle - \langle(\Delta r)^2\rangle^* \approx [1 - (\mu/\mu^*)^{\frac{1}{2}}]\langle\Delta r^2\rangle \qquad (50)$$

(ii) $[1 - (\mu/\mu^*)^{\frac{1}{2}}]$ can be further approximated by $(\mu^* - \mu)/2\mu^*$ so that

$$\langle\Delta r\rangle - \langle\Delta r\rangle^* \approx \langle\Delta r\rangle\left(\frac{\mu^* - \mu}{2\mu^*}\right) = \langle\Delta r\rangle\frac{1}{2}\left(\frac{m' - m}{m'}\right)\left(\frac{m_A}{m_A + m}\right) \qquad (51)$$

$$\langle(\Delta r)^2\rangle - \langle(\Delta r)^2\rangle^* \approx \langle(\Delta r)^2\rangle\left(\frac{\mu^* - \mu}{2\mu^*}\right) = \langle(\Delta r)^2\rangle\frac{1}{2}\left(\frac{m' - m}{m'}\right)\left(\frac{m_A}{m_A + m}\right) \qquad (52)$$

where m_A is the mass of the observed nucleus A and the isotopes m' and m of the other nucleus X in the diatomic molecule.

2. The concept of the reduced isotope shift

Although equation (52) is only an approximate one, it is still a nice simple formula which allows us to separate out most (not all) of the mass dependence of the isotope shift.

$$^1\Delta A(^{m'/m}X) = \langle\sigma\rangle - \langle\sigma\rangle^* \approx \left\{\begin{array}{l}(d\sigma/d\Delta r)_e\langle\Delta r\rangle + \\ \frac{1}{2}(d^2\sigma/d\Delta r^2)_e\langle(\Delta r)^2\rangle\end{array}\right\} \cdot \frac{1}{2}\left(\frac{m' - m}{m'}\right)\left(\frac{m_A}{m_A + m}\right) \qquad (53)$$

If we define a reduced isotope shift as

$$^1\Delta^R(A, X) \equiv {}^1\Delta A(^{m'/m}X)\left(\frac{m'-m}{m'}\cdot\frac{1}{2}\frac{m_A}{m_A+m}\right)^{-1} \tag{54}$$

then

$$^1\Delta^R(A, X) \approx (d\sigma/d\Delta r)_e\langle\Delta r\rangle + \tfrac{1}{2}(d^2\sigma/d\Delta r^2)_e\langle(\Delta r)^2\rangle \tag{55}$$

This definition has the advantage of allowing us to compare isotope shifts of the same nucleus under different isotopic substitutions, for example the $^{37/35}$Cl-induced ^{19}F isotope shift with the $^{2/1}$H-induced ^{19}F isotope shift in ClF and HF respectively. The mass factors have been explicitly removed, leaving a reduced isotope shift which contains primarily electronic information (not entirely since $\langle\Delta r\rangle$ and $\langle(\Delta r)^2\rangle$ are still mass-dependent).

Furthermore, within this approximation the reduced isotope shift gives the rovibrational corrections to shielding at that temperature,

$$\langle\sigma^A\rangle^{300} - \sigma_e{}^A \approx {}^1\Delta^R(A, X). \tag{56}$$

3. Estimation of $\langle\Delta r\rangle$

If we make the approximation of including only the linear term in equation (55), the reduced isotope shifts can be implemented in the determination of the derivatives $(d\sigma/d\Delta r)_e$ or for the prediction of magnitudes of isotope shifts from known or estimated derivatives. To do this we need to be able to estimate $\langle\Delta r\rangle$. For diatomic molecules this is not a problem since there are usually enough known spectroscopic constants to calculate $\langle\Delta r\rangle$ without using estimates. To apply this reduced isotope shift concept to polyatomic molecules we need to be able to estimate $\langle\Delta r\rangle$ for a bond in a polyatomic molecule. Thus we use the known spectroscopic constants for many diatomic molecules to verify how good this estimation method is.

We have already seen in equation (47) that, for diatomic molecules,

$$\langle\Delta r\rangle_{vib}{}^T = (3/2)a\langle(\Delta r)^2\rangle^T \tag{47}$$

If the harmonic approximation is used for $\langle(\Delta r)^2\rangle$ it is possible to express $\langle\Delta r\rangle_{vib}$ as[58]

$$\langle\Delta r\rangle_{vib} \approx \left(\frac{3h}{8\pi}\right)(-F_3F_2{}^{-\frac{3}{2}})\mu^{-1/2} \tag{57}$$

where

$$F_3 \equiv (1/3)(\partial^3 V/\partial r^3)_e \qquad F_2 \equiv (\partial^2 V/\partial r^2)_e$$

and the temperature dependence has been suppressed. Herschbach and Laurie found that F_3 and F_2 are approximately exponential functions of internuclear distance, each described by a family of curves which are

determined by the location of the bonded atoms in rows of the periodic table.[59]

$$(-1)^n F_n = 10^{-(r_e - a_n)/b_n} \tag{58}$$

Thus we write

$$\langle \Delta r \rangle_{\text{vib}} \cong (3h/8\pi)\mu^{-\frac{1}{2}} 10^{-D} \tag{59}$$

where

$$D \equiv (r_e - a_3)/b_3 - 3(r_e - a_2)/2b_2 \tag{60}$$

10^{-D} has units of $(\text{energy})^{-1/2}$. The constant in equation (59) is 19.35×10^{-3} if μ is in amu, and the a_2, b_2, a_3 and b_3 are reproduced in Table 7. A comparison of equation (59) with the $\langle \Delta r \rangle_{\text{vib}}$ calculated at 300 K using

TABLE 7

Herschbach–Laurie parameters.[59]

Row		a_2	a_3	b_2	b_3	Row		a_2	a_3	b_2	b_3
H	1	1.54	1.58	0.64	0.48	2	4	2.63	2.70	0.96	0.73
H	2	1.80	1.85	0.69	0.59	2	5	2.71	2.81	1.09	1.09
H	3	1.98	2.01	0.95	0.74	3	3	2.70	2.77	1.12	0.89
H	4	2.08	2.07	0.96	0.74	3	4	2.66	2.76	1.48	1.19
H	5	2.06	2.12	0.78	0.90	3	5	2.73	2.83	1.31	1.05
1	1	1.73	1.78	0.47	0.39	4	4	2.85	2.95	0.94	0.70
1	2	2.02	2.10	0.53	0.48	4	5	2.84	2.93	1.09	0.78
1	3	2.15	2.26	0.60	0.55	H	3T	1.82	1.92	1.04	0.86
1	4	2.36	2.41	0.76	0.57	H	4T	1.83		0.75	
1	5	2.47	2.48	0.87	0.68	H	5T	1.77		0.47	
2	2	2.40	2.48	0.70	0.61	1	3T	1.98		0.44	
2	3	2.54	2.57	0.98	0.72	1	4T	2.15		0.52	

equation (45) and the known spectroscopic constants of a large set of diatomic molecules[60] shows good overall agreement for $\langle \Delta r \rangle_{\text{vib}}$ values from 3 to 25×10^{-3} Å.[58] What this means is that it is possible to estimate $\langle \Delta r \rangle$ for a diatomic molecule by knowing only the bond length. Similarly

$$\langle (\Delta r)^2 \rangle = (h/4\pi)\mu^{-1/2} 10^{+d} \tag{61}$$

where $d \equiv (r_e - a_2)/2b_2$. 10^{+d} has units of $\text{length} \times \text{energy}^{-1/2}$.

Thus the reduced isotope shift can be expressed as

$$^1\Delta^R(\Delta, X) = \frac{h\mu^{-1/2}}{8\pi}[3 \times 10^{-D}(d\sigma/d\Delta r)_e + 10^d (d^2\sigma/d\Delta r^2)_e] \tag{62}$$

C. The electronic factor in isotope shifts: the change in shielding with bond extension

We have seen that the dynamic factor in isotope shifts is largely predictable and transferable for a given bond, e.g. C–F, from one molecule to the next. This means that the isotope shift carries primarily electronic information. This is shown by the correlation in Fig. 2. The change in shielding with bond extension is as much an index of the chemical bond as is the spin–spin coupling or the chemical shift. Therefore we shall consider in this section what is known about this index from theoretical and experimental sources.

1. The change in ^1H shielding with internuclear separation in H_2^+

The shielding in the H_2^+ molecule has been fully characterized over the entire range of internuclear separations by Hegstrom,[18] with relativistic calculations; it is represented in Fig. 3. We note several points about the behaviour of the ^1H shielding in this molecule. First, the shielding at the equilibrium configuration is greater than the diamagnetic shielding of the separated atoms, which is also found for ^{19}F in ClF but is unusual otherwise. In most diatomic molecules the nuclear shielding at the equilibrium separation, σ_e, is less than the diamagnetic shielding of the separated atoms. Second, the shielding decreases with bond extension away from equilibrium. This is typical for diatomic molecules. Only Li in LiH has shown exceptional behaviour.[43,51] This indicates that, if H_2^+ is at all typical, the minimum in the shielding function occurs at nuclear separations significantly greater than that at the equilibrium geometry. In Fig. 3 we have also sketched the potential energy curve $V(r)$ and the vibrational levels. With these we can readily see that vibrational averaging leads to deshielding and that the ^1H shielding in H_2^+ would decrease with increasing temperature as the higher vibrational levels become more populated. The mean bond displacement for HD^+ is less than that for H_2^+, leading to the correspondingly higher average shielding for ^1H in HD^+ compared to H_2^+, i.e. an isotope shift of the usual sign.

2. Derivatives of the perpendicular and parallel components of nuclear shielding in a diatomic molecule

We can illustrate $(d\sigma_\perp/d\Delta r)_e$ and $(d\sigma_\parallel/d\Delta r)_e$ for ^1H and ^{19}F in HF by means of a shielding density difference map.[61] The shielding density describes the contributions to shielding from various regions in the electronic distribution in the molecule in the same way that a charge density map shows the electronic distribution itself. The shielding density for the equilibrium HF geometry can be subtracted from the shielding density for the extended HF geometry, giving the density difference maps shown in Fig.
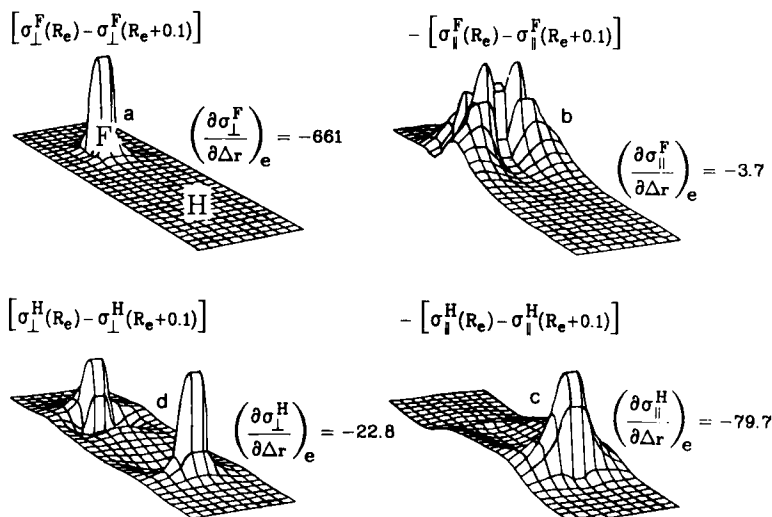
FIG. 6. Shielding density difference maps for ^{19}F and ^{1}H in the HF molecule upon bond extension, individually scaled. For comparison, extrema are: (a) ^{19}F($\perp$) 116.46, -10^{-3}; (b) ^{19}F($\parallel$) -0.076, 0.0128; (c) ^{1}H($\parallel$) -0.333, 0.0124; (d) ^{1}H($\perp$) 1.884, -2.003 (at H) and 1.123, -1.972 (at F), in arbitrary units. From reference 61, with permission.

6. These may be viewed as mappings of the distribution of $(d\sigma/d\Delta r)_e$, i.e. they show which regions of electronic distribution contribute to the change in shielding as the bond is extended. These are individually scaled so as to show the features of the $(d\sigma_\perp/d\Delta r)_e$ and $(d\sigma_\parallel/d\Delta r)_e$ density surfaces. The maximum values for each surface are shown in the figure caption. The derivatives obtained with this particular calculation (coupled Hartree–Fock calculation with gauge origin at F, using the Lie–Clementi basis set for HF) are also shown in the figure.

There are several points of interest in Fig. 6. First, the perpendicular component of the ^{19}F shielding in HF has a much larger derivative than the parallel component, whereas the derivatives of the parallel and perpendicular components have comparable magnitudes for ^{1}H shielding. The reason for this becomes apparent when it is recalled that $\sigma_\parallel$ is purely diamagnetic (for any gauge origin along the line of centres) whereas $\sigma_\perp$ has both diamagnetic and paramagnetic contributions. Since the diamagnetic contribution to shielding varies as $1/r$ (where r is the position of the electron relative to the nucleus) whereas the paramagnetic shielding varies as r^{-3}, it is reasonable that the paramagnetic shielding changes more drastically when the bond is extended. Proton shielding, on the other hand, is largely diamagnetic, so the changes with bond extension of the values of $\sigma_\perp$ and $\sigma_\parallel$ are comparable. Second, the ^{19}F shielding change with bond

extension comes from the immediate neighbourhood of the F nucleus with very minor contributions from the other regions in the molecule. On the other hand, the ^1H shielding change with bond extension originates not only from the vicinity of the ^1H nucleus but also from around the F nucleus, particularly for $(d\sigma_\perp^H/d\Delta r)_e$. The paramagnetic contribution to this component originates largely from the p orbitals on F. The changes in the parallel components $[(d\sigma_\parallel^H/d\Delta r)_e$ in Fig. 6 (b) and (d) are entirely diamagnetic] corresponding more closely to the charge density redistribution upon bond extension observed by Bader and Bandrauk[62] shown in Fig. 7. Charge is removed from along the internuclear axis and becomes concentrated in the perpendicular region. The quadrupolar character of the charge density difference observed in Fig. 7 is reflected in Fig. 6 (b) and (d) for the $(d\sigma_\parallel/d\Delta r)_e$.

FIG. 7. Charge redistribution upon bond extension in LiF and N_2 molecules. Positive contours correspond to an increase, negative to a decrease in electronic charge density. Displacement of nucleus marked by arrow is 0.132 a.u. for N_2, 0.232 a.u. for LiF. From reference 62, with permission.

The shieldings in diatomic molecules other than H_2^+ have only been calculated for separations very close to the equilibrium one. This allows derivatives of the shielding to be calculated. Some of Ditchfield's calculated derivatives for H_2, HF and LiH are shown in Table 8. He actually reported values up to 6th derivatives for HF and LiH.

The unusual positive $(d\sigma_\perp^{Li}/d\Delta r)$ shown in Table 8 leads to an unusual sign of the isotope shift for ^7Li. The explanation for this may be seen in Fig. 7; upon bond extension the charge polarization in the vicinity of the Li nucleus in LiF is primarily dipolar. The charge density is removed from the overlap region and builds up immediately in front of the Li nucleus.

TABLE 8

The shielding functions for H_2, HF and LiH, in ppm.[43]

Mol.	Component	σ_e	$(d\sigma/d\xi)_e$	$(d^2\sigma/d\xi^2)_e$
H_2	$\sigma_\perp^H$	26.0223	−14.9632	24.0505
	$\sigma_\parallel^H$	27.7056	−16.1798	23.0573
HF	$\sigma_\perp^H$	21.2063	−20.9333	88.3674
	$\sigma_\parallel^H$	44.2187	−73.1549	179.126
	$\sigma_\perp^F$	395.981	−605.969	−1998.51
	$\sigma_\parallel^F$	482.118	−3.4390	17.4407
LiH	$\sigma_\perp^H$	25.3210	−3.9974	−10.6593
	$\sigma_\parallel^H$	28.3655	−12.0785	19.5267
	$\sigma_\perp^{Li}$	88.9281	15.0629	−41.1407
	$\sigma_\parallel^{Li}$	101.605	−6.9587	12.7755

In Ditchfield's shielding calculations on LiH this unusual sign is shown to arise from a decrease in the local paramagnetic currents arising from $\sigma \rightarrow \pi^*$ magnetic field-induced mixing when the bond is extended, which results in an increase in $\sigma_\perp^{Li}$, an increase large enough to offset the decreases in the diamagnetic contributions.

3. Empirical estimates of $(d\sigma/d\Delta r)_e$

Derivatives of nuclear shielding can also be obtained from experiment. There are three sources: (i) molecular beam data on individual v and J states; (ii) $\sigma_0(T)$ data from dilute gas phase measurements extrapolated to zero pressure; (iii) isotope shifts.

Most molecular beam data provide nuclear spin-rotation constants C_{vJ} for a specific v,J state of the molecule. The relationship which has been established between the electronic part of the spin-rotation constant and the paramagnetic part of nuclear shielding[63,64] then allows the paramagnetic shielding tensor components for a given v,J state of the molecule to be calculated from the spin-rotation constants:

$$C_{vJ}^{elec} = k \left\langle \frac{\sigma^p}{R^2} \right\rangle_{vJ} \tag{63}$$

where k involves only fundamental constants. Theoretical calculations of the diamagnetic components are relatively easy since they depend only on the ground state electronic wavefunction. Putting these two parts together then allows the determination of $\langle\sigma\rangle_{vJ}$ from molecular beam data. When molecular beam spectra for more than one v,J state have been analysed, one can write the spin-rotation constants in terms of the same reduced

coordinate as in equation (26):[65]

$$C_{vJ}{}^{elec} = k \sum_n s_n \left\langle \frac{\xi^n}{R^2} \right\rangle_{vJ} \qquad (64)$$

In the analysis of the spin–rotation constant for a given v, the expansion coefficients s_n obtained by fitting several individual $C_J{}^{elec}$ are related to $(d^n\sigma^P/d\xi^n)_e$. Alternatively, one could write the relation between the paramagnetic shielding and the total spin–rotation constant (not just the electronic part) as:

$$\sigma^P = k(1+\xi)^2 C - b(1+\xi)^{-1} \qquad (65)$$

where k and b are known constants in terms of the equilibrium molecular geometry. By differentiating this equation with respect to ξ, $(d\sigma^P/d\xi)_e$ can be found in terms of $(dC/d\xi)_e$. This approach was used for F_2.[66] Using the measured spin–rotation constant,

$$\langle C \rangle/\text{kHz} = -(156.85 \pm 0.10) - (0.0024 \pm 0.0010)J(J+1)$$

one can identify

$$4(dC/d\xi)_e(B_e/\omega_e)^2 = -0.0024 \pm 0.0010 \qquad (66)$$

From this one may calculate $(d\sigma^P/d\xi)_e$ for ^{19}F in F_2 as -4080 ppm.

Another experimental source of shielding derivatives is the temperature dependence of shielding measured in the dilute gas phase in the limit of zero pressure. There are temperature dependent intermolecular effects which have to be removed in obtaining the zero-pressure limit. These are density dependent and are linear functions of density in the dilute gas.[16] Therefore, variable temperature measurements in samples of known density can give information on both $\sigma_0(T)$, the shielding in the zero-pressure limit, and $\sigma_1(T)$, the intermolecular shielding coefficient in the virial expansion (equation (2)). The fitting of the experimental data points described by $[\sigma_0(T) - \sigma_0(300)]$ to the $\langle\sigma\rangle^T - \langle\sigma\rangle^{300}$ of equation (38) leads to an empirical estimate of $(d\sigma/d\xi)_e$. Although equation (38) involves two parameters, $(d\sigma/d\xi)_e$ and $(d^2\sigma/d\xi)_e$, only the first derivative can be obtained from experiment. The rotational contribution, which has a linear dependence on temperature as seen in equation (38), dominates the temperature dependence, $\langle\sigma\rangle^{400K} - \langle\sigma\rangle^{300K}$, for example. This is shown very dramatically in Table 5. It is in fact not necessary for the rotational contribution to $\langle\sigma\rangle^{400} - \langle\sigma\rangle^{200}$ to be so overwhelming. A significant rotational contribution when combined with an anharmonic vibrational contribution makes the term in $(d\sigma/d\xi)_e$ dominant over the harmonic vibrational contribution which has the factor $(d^2\sigma/d\xi^2)_e$. Both vibrational contributions have the same dependence on temperature, that of $\langle v+\frac{1}{2}\rangle^T$, and on mass, as seen in equation (40). Thus the relative magnitudes of anharmonic and harmonic contribu-

tions to the isotope shift (shown in Table 6) also directly reflect the relative magnitudes of the anharmonic and harmonic contributions to the temperature dependence. We see in Table 6 that, except for LiH, the ratio of anharmonic/harmonic contributions which is the ratio $-3a_1(d\sigma/d\xi)_e/(d^2\sigma/d\xi^2)_e$ is better than 2.2–8. Any rotational contribution to the temperature dependence makes the $(d\sigma/d\xi)_e$ more important. Thus it is usually not possible to extract $(d^2\sigma/d\xi^2)_e$ from $\sigma_0(T) - \sigma_0(300)$ experimental data. At the same time this means that the one-parameter fit to the experimental data gives a good account of $(d\sigma/d\xi)_e$ essentially uncontaminated by $(d^2\sigma/d\xi^2)_e$ contributions.

There is a major problem associated with this source of $(d\sigma/d\xi)_e$, however. The $\sigma_0(T) - \sigma_0(300)$ data result after correcting for the temperature dependence of the reference (such as the substance used for the field-frequency lock). This is a small correction when compared to $\sigma_0(T) - \sigma_0(300)$ for ^{19}F. However, for other nuclei which have relatively small changes in σ_0 with temperature, the errors associated with the temperature dependence of the reference may be as large as the $\sigma_0(T) - \sigma_0(300)$ values themselves. This is found to be the case for ^{13}C in CH_4 and ^{11}B in BF_3. For ^{13}C in CO the reference temperature dependence is of the same order of magnitude as the $\sigma_0(T) - \sigma_0(300)$ for CO itself. This leads to systematic errors not reflected in the reported precision of the data. For ^{13}C in CO we reported a derivative that is too small to reproduce the experimental ^{18}O-induced isotope shift in the ^{13}C spectrum observed.[50] On the other hand, with the theoretical derivatives from Stevens and Karplus, we calculate an isotope shift which is -0.0472, in good agreement with the experimental value -0.0476 ± 0.0016 ppm. Some diatomic molecules for which derivatives have been estimated in this way are ^{13}C in CO $((d\sigma/d\Delta r) = -226)$,[67] ^{15}N in N_2 (-774),[67] ^{19}F in ClF (-2070)[57] and ^{19}F in F_2 (-4530),[57] all in ppm Å^{-1}. There are also some estimates for ^{1}H in HCl and HBr, but since the temperature dependence of ^{1}H shielding is very small these are probably not accurate.[68]

A third source of empirical estimates of $(d\sigma/d\xi)_e$ is the isotope shift itself. In those cases in which the ratio $[-3a_1(d\sigma/d\xi)]/(d^2\sigma/d\xi^2)_e$ is 8 or greater, the isotope shift will give a value within 12% (or better) of the true $(d\sigma/d\xi)_e$ if the observed isotope shift is fitted to only the linear part of equation (42). For an unfavourable case, ^{19}F in HF, this ratio is 2.2, which means that the isotope shift will give 145% of the true $(d\sigma/d\xi)_e$. Nevertheless, since the isotope shift is so much easier to measure than the temperature dependence of shielding in the gas phase in the zero-pressure limit, this is a valuable tool for this purpose. Furthermore, it is possible to measure isotope shifts in ions such as CN^-, PO_4^{3-} or NH_4^+, on which it would be very difficult to make gas-phase measurements. Thus, for these types of species the isotope shifts provide useful electronic information which is not

otherwise accessible. Diatomic molecules for which isotope shifts have been used to derive estimates of $(d\sigma/d\Delta r)$ are (-456 ± 15 for ^{13}C and -1150 ± 130 for ^{17}O),[50] CN$^-$ (-473 for ^{13}C and -873 for ^{15}N)[69] and H$_2$ (-11.5,[58] -12.1 [70]), all in ppm Å^{-1}.

Of course a combination of methods (ii) and (iii) would allow both first and second derivatives to be determined from experiment. An attempt to use a combination of (i) and (iii) for H$_2$ gives inconsistent results.[70]

IV. ONE-BOND ISOTOPE SHIFTS IN POLYATOMIC MOLECULES

A. *Ab initio* calculations: the water molecule

Ab initio methods of calculation have provided some highly accurate estimates of electric and magnetic properties of small molecules. However, almost all these calculations have been performed only at the equilibrium molecular geometries. An accurate calculation of NMR isotope shifts requires reliable quantum chemical calculations of the nuclear shielding surface near the equilibrium configuration. From such calculations it would be possible to obtain derivatives of the shielding with respect to geometry changes. These derivatives multiplied by the differences in the mean bond displacements, mean bond angle deformations, etc. which are obtained as thermal averages over a small part of the potential surface lead to calculated NMR isotope shifts according to equation (5). This has been done so far only for the water molecule. Coupled Hartree-Fock perturbation theory has been used[71] to calculate the ^{1}H and ^{17}O nuclear shielding surfaces. For equilibrium geometries ($r_{OH} = 0.9572$ Å; angle HOH $= 104.52°$), the origin of the vector potential of the external magnetic field is placed at the oxygen nucleus, and for non-equilibrium geometries the gauge origin is placed at the site on the Eckart axes that the oxygen nucleus would occupy in the equilibrium configuration of H$_2$^{16}O. The distance of the gauge origin from the oxygen nucleus is never more than 0.03 Å.

For the equilibrium configuration the following values of the diamagnetic and the paramagnetic parts of both the proton and oxygen shielding tensor components (all in ppm) are obtained.

For the oxygen shielding:

$$\sigma^d(O) = \begin{pmatrix} 415.311 & 0 & 0 \\ 0 & 417.169 & 0 \\ 0 & 0 & 416.02 \end{pmatrix}$$

$$\sigma^P(O) = \begin{pmatrix} -52.549 & 0 & 0 \\ 0 & -112.641 & 0 \\ 0 & 0 & -105.987 \end{pmatrix}$$

leading to

$$\sigma(O) = \begin{pmatrix} 362.762 & 0 & 0 \\ 0 & 304.529 & 0 \\ 0 & 0 & 309.839 \end{pmatrix} \qquad \sigma^O = 325.710 \text{ ppm}$$

For the proton shielding:

$$\sigma^d(H) = \begin{pmatrix} 31.480 & 0 & 21.497 \\ 0 & 7.701 & 0 \\ 18.026 & 0 & 22.712 \end{pmatrix}$$

$$\sigma^P(H) = \begin{pmatrix} 6.628 & 0 & -7.759 \\ 0 & 14.234 & 0 \\ -12.217 & 0 & 6.712 \end{pmatrix}$$

leading to

$$\sigma(H) = \begin{pmatrix} 38.108 & 0 & 17.738 \\ 0 & 21.935 & 0 \\ 5.809 & 0 & 29.424 \end{pmatrix} \qquad \sigma^H = 29.823 \text{ ppm}$$

The isotropic shielding can be directly compared with experimental values. For the proton shielding they estimated a σ_e value of 30.59 ± 0.02 ppm by combining the experimental value of 30.052 ± 0.0015 ppm[72] with a zero-point vibration correction of -0.54 ppm. For the oxygen shielding the agreement with an experimental value of $\sigma_e = 357 \pm 17$ ppm is less satisfactory. The experimental room temperature gas phase value is 344.0 ± 17.2 with a vibrational correction of -13.6.[73]

The calculation of the shielding surface was performed at forty-eight different nuclear geometries (sixteen of C_{2v} symmetry, thirty-two of C_s symmetry) over a range of $0.65 \text{ Å} < r < 1.25 \text{ Å}$ and $61° < \alpha < 155°$. The functional dependence of the oxygen and the proton shielding on $Я_1$, $Я_2$ and $\Delta\alpha$ has been calculated (Fig. 8). The protons are labelled 1 and 2 and the displacements from the equilibrium geometry are $Я_1$ (positive for an increase in the O-H_1 bond length), $Я_2$ (for the O-H_2 bond length), and $\Delta\alpha$ (positive for an increase in the HOH bond angle). Figure 8(a) shows how the oxygen shielding changes with $\Delta\alpha$ ($Я_1 = Я_2 = 0$). A minimum in the shielding surface near the equilibrium bond angle is close to $\Delta\alpha = +0.02$ rad. The fact that σ^O reaches a minimum at an angle coincident with the energy can be understood by the argument that angle change in either direction from the equilibrium weakens the bonding so that σ approaches its atomic value which is larger than for equilibrium. As is visible from Fig. 8(a), σ^O is sensitive to small bond angle deformations. Figure 8(b) gives a plot of σ^O against S_1, the actual displacement along the bond direction of each of

FIG. 8. Nuclear shielding function (in ppm) for H_2O: (a) σ^O vs. bond angle change; (b) σ^O vs. displacement along the bond direction of each of the two protons; (c) σ^H vs. bond angle change; (d) σ^{H_1} and σ^{H_2} vs. displacement along $O-H_1$. From reference 71, with permission.

the two protons. Figure 8(b) also shows that the oxygen shielding is very sensitive to changes in the O–H bond lengths.

The proton shielding as a function of $\Delta\alpha$ and $Я_1$ is given in Fig. 8(c) and (d). The dependence of σ^H on bond angle changes is small compared to bond length changes. An increase in the bond length leads to a decrease in the proton shielding. There are smaller (secondary) effects on σ^H, i.e. the change in $\sigma(H_2)$ due to a change in the other O–H bond ($Я_1$).

From a least-squares fit of their shielding data for different geometries to equation (4), Fowler et al. obtained altogether twenty-two independent derivatives of the proton and oxygen nuclear shielding with respect to geometry changes (up to fourth order). Some of these are given below.

For the oxygen shielding:

$$(\partial\sigma^O/\partial\Delta r)_e = -270.9 \text{ ppm Å}^{-1} \qquad (\partial\sigma^O/\partial\Delta\alpha)_e = -27.3 \text{ ppm rad}^{-1}$$

$$(\partial^2\sigma^O/\partial\Delta r^2)_e = -1045.6 \text{ ppm Å}^{-2} \qquad (\partial^2\sigma^O/\partial\Delta\alpha^2)_e = +138.8 \text{ ppm rad}^{-2}$$

For the proton shielding:

$$(\partial\sigma^{H_1}/\partial\Delta r_1)_e = -35.3 \text{ ppm Å}^{-1} \qquad (\partial\sigma^{H_1}/\partial\Delta r_2)_e = -4.6 \text{ ppm Å}^{-1}$$

$$(\partial\sigma^{H}/\partial\Delta\alpha)_e = -4.0 \text{ ppm rad}^{-1} \qquad (\partial^2\sigma^{H}/\partial\Delta\alpha^2)_e = -3.0 \text{ ppm rad}^{-2}$$

$$(\partial^2\sigma^{H_1}/\partial\Delta r_1^2)_e = +110.0 \text{ ppm Å}^{-2} \qquad (\partial^2\sigma^{H_1}/\partial\Delta r_2^2)_e = -24.5 \text{ ppm Å}^{-2}$$

The small magnitude of $(\partial\sigma^{O}/\partial\Delta\alpha)_e$ found in H_2O by Fowler et al. as well as by Schindler and Kutzelnigg[74] can be understood in terms of the changes in the bond pair and lone pair electron distributions with bond angle deformation. The lone pair has an important role to play in the ^{17}O shielding (as also in ^{33}S and ^{77}Se shielding in the other bent molecules H_2S, H_2Se, SO_2, SeO_2) because the highest occupied molecular orbital in molecules of this type consists primarily of a lone pair on the central atom, as indicated by theoretical calculations and supported by photoelectron spectral data. The lowest excitation energy corresponds to the magnetic dipole allowed b_1 (lone pair) $\rightarrow a_1$ excitation which therefore makes an important contribution to the paramagnetic term in the shielding according to Ramsey's theory.[64] Figure 9 shows the results of ab initio studies in H_2O, in which the bond lengths are held fixed at their equilibrium value and the bond angle is allowed to vary.[75] These diagrams show that, as the nuclei vibrate away from their equilibrium positions, the oxygen orbital lags behind whereas the orbitals centred on H completely follow the H nuclei. Also, the oxygen lone pair p character increases with increasing bond angle. Similar results are obtained for H_2S. The consequences of charge redistribution accompanying bond angle deformation are as follows. The lack of orbital following leads to a small magnitude of $(\partial\sigma^{O}/\partial\Delta\alpha)_e$. In the limit of complete orbital stasis $(\partial\sigma^{O}/\partial\Delta\alpha)_e \approx 0$. To a first approximation the increase in p character of the O lone pair with increasing bond angle gives a deshielding contribution, i.e. $(\partial\sigma^{O}/\partial\Delta\alpha)_e < 0$. This qualitative picture is consistent with the results of Fowler et al., and also with Schindler and Kutzelnigg's $(\partial\sigma^{O}/\partial\Delta\alpha)_e = -7 \text{ ppm rad}^{-1}$.

The next step in calculating the isotope shifts in the water molecule is the calculation of $\langle\Delta r\rangle$ and $\langle\Delta\alpha\rangle$. Fowler and Raynes[76] used the first method outlined in Section II.B.1. They obtained the oxygen and proton shielding for individual vibrational and rotational states, some of which are shown in Table 9. These shieldings for individual states cannot be measured experimentally because of the short lifetime of a molecule in a particular rovibrational state compared with the relatively long time scale of an NMR experiment. Thus all that can be obtained experimentally is an average value for a given temperature. The two methods described in Section II were employed to obtain the thermal average. Method 1 is a straightforward
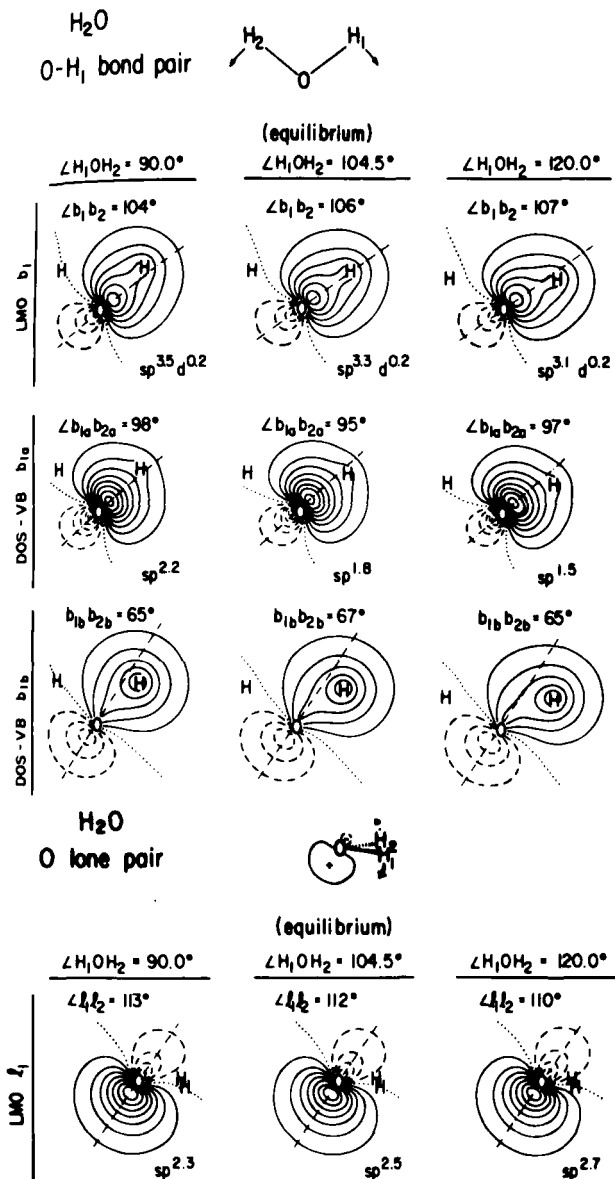
FIG. 9. Charge density maps illustrating bond pair and lone pair "orbital following" in H_2O with change in bond angle. From reference 75, with permission.

TABLE 9

Nuclear shielding σ^H and σ^O for the water isotopomers $H_2{}^{17}O$ and $D_2{}^{17}O$ in low rovibrational states, in ppm.[76]

State					$H_2{}^{17}O$		$D_2{}^{17}O$
v_1	v_2	v_3	J	τ	σ^H	σ^O	σ^O
		at r_e			29.820	325.56	325.56
0	0	0	0	0	29.276	312.44	316.12
0	0	0	1	−1	29.273	312.41	316.10
0	0	0	1	0	29.276	312.38	316.08
0	0	0	1	1	29.274	312.37	316.08
0	1	0	0	0	29.052	313.95	317.34
0	2	0	0	0	28.830	315.25	318.48
1	0	0	0	0	28.923	297.92	305.83
0	0	1	0	0	28.739	297.82	305.54
1	1	0	0	0	28.742	298.85	306.72
0	1	1	0	0	28.541	299.12	306.65

average, thus

$$\langle \sigma \rangle^T = \frac{\sum_{vJ\tau} (2J+1) g_{Ns} \langle \sigma \rangle_{vJ\tau} \exp(-E_{vJ\tau}/kT)}{\sum_{vJ\tau} (2J+1) g_{Ns} \exp(-E_{vJ\tau}/kT)} \tag{67}$$

where $E_{vJ\tau}$ stands for a particular rovibrational energy level and g_{Ns} is a factor which takes account of nuclear spin statistics. This method obviously requires the calculation of a very large number of energy levels (for example rotational levels are calculated as far as $J = 25$ and levels more than 5000 cm^{-1} above the zero point levels are excluded).[76]

In practice equation (67) is always a truncated summation over a finite number of rovibrational states. It is found that this sum does not converge very fast; the individual terms can even have alternating signs. In Table 10 the thermal average shieldings of the oxygen and proton in the water molecule obtained with this method and with the coth function (as used in equation (11)) are compared. The results are nearly identical for temperatures normally accessible in NMR spectrometers. For larger molecules it becomes impossible to calculate a sufficient number of rovibrational states in order to use the exact method for the thermal averaging, so the only practical way of calculating expectation values of molecular properties over different rotational and vibrational states for a given temperature is by using the harmonic approximation for the vibrational partition function.

The isotope effects on nuclear shielding in the water molecule are $^1H(^{18/16}O) = -0.002 \text{ ppm}$ $(-0.012 \pm 0.004 \text{ ppm})$[77] for the oxygen-induced shift on the protons, and $^{17}O(^{2/1}H, ^{2/1}H) = -3.68 \text{ ppm}$ $(-3.08 \pm 0.20 \text{ ppm})$[78]

for the deuterium-induced shifts on the oxygen nucleus in $D_2{}^{17}O$ compared to $H_2{}^{17}O$ (all at 300 K). The experimental values are given in parentheses. There are no gas phase data for comparison; both measurements were made on liquid phase samples in which hydrogen-bonding will almost certainly have somewhat different effects on different isotopomers.

TABLE 10

The thermal average shielding in water calculated using equation (67) and approximately using the coth function, equation (11).[76]

Temp. (K)	Proton shielding			Oxygen shielding		
	exact		approx.	exact		approx.
	o-$H_2{}^{16}O$	p-$H_2{}^{16}O$	$H_2{}^{16}O$	o-$H_2{}^{17}O$	p-$H_2{}^{17}O$	$H_2{}^{17}O$
0	29.272	29.275	29.275	312.413	312.443	312.443
30	29.272	29.275	29.273	312.394	312.409	312.397
60	29.270	29.271	29.270	312.354	312.356	312.351
100	29.267		29.267	312.296		312.290
150	29.263		29.263	312.216		312.214
200	29.258		29.258	312.139		312.137
250	29.254		29.254	312.061		312.061
300	29.250		29.250	311.983		311.985
350	29.245		29.245	311.906		311.910
400	29.240		29.241	311.830		311.836
450	29.235		29.236	311.755		311.763
500	29.230		29.231	311.681		311.692

The accurate calculation of isotope shifts in any property (bond length, nuclear shielding, etc.) is done by a difference approach, i.e. the property is calculated for both the reference molecule and the isotopically substituted molecule and the difference between them is obtained. This is the approach used in this review exclusively. Another approach is a direct one, in which isotopic substitution is considered as a perturbation of the reference molecule. The mass perturbation appears as a modification to the kinetic energy term in the vibration–rotation hamiltonian. The formulae for this double perturbation method have been derived by Fowler, and a more approximate version of the same approach is given by Mamayev and Sergeyev.[79] Fowler finds that (as expected) the mass perturbation approach works nearly as well as the difference approach when the fractional mass change is small (as for $^{16}O \rightarrow {}^{18}O$) but not so well (giving incorrect signs and magnitudes) when the fractional mass change is large (as for $H \rightarrow D$).

B. Calculation of mean bond displacements and mean bond angle deformations

In the following we describe applications of Bartell's approach to different molecular types, starting with some molecules where the force field up to at least cubic terms is known, and then some model potentials for other polyatomic molecules.

1. Triatomic molecules

The best description of the potential energy surface for polyatomic molecules is for linear triatomics, especially one in which many isotopic species provide an abundance of spectroscopic observables from which a least-squares refinement technique gives an anharmonic force field which is the best fit to the data. Of the polyatomic molecules, CO_2 and NNO probably have the most studied potential energy surface from the point of view of vibrational spectroscopy. The anharmonic force fields up to quintic and sextic terms have been obtained from the very large set of vibrational-rotational data belonging to ten isotopic species in the case of CO_2,[80-83] and eleven in the case of NNO.[84-86]

The general force field in terms of the true curvilinear coordinates for the linear triatomic molecule is:

$$V = K_{11}Я_1{}^2 + K_{22}Я_2{}^2 + K_{33}Я_3{}^2 + K_{13}Я_1Я_3$$
$$+ K_{111}Я_1{}^3 + K_{113}Я_1{}^2Я_3 + K_{133}Я_1Я_3{}^2 + K_{333}Я_3{}^2$$
$$+ K_{122}Я_1Я_2{}^2 + K_{223}Я_2{}^2Я_3 + \text{higher order terms} \qquad (68)$$

Here $Я_1$ denotes the displacement coordinate of the Y-X bond, $Я_3$ the displacement of the X-Z bond and $Я_2$ the bond angle deformation $\Delta\alpha$. Applying equation (13) by using the derivatives (14) we obtain

$$\langle \Delta r \rangle_{\text{vib}} = -[1/(2K_{11} + K_{13})]\{(3K_{111} + K_{113})\langle(\Delta r)^2\rangle$$
$$+ 2K_{113}\langle\Delta r_1\Delta r_3\rangle + [K_{122} - (1/r)K_{22}]\langle(\Delta\alpha)^2\rangle\} \qquad (69)$$

for the mean bond displacement due to vibration in CO_2 and two similar, but coupled equations for NNO.[34] Owing to the symmetry of the molecules the mean bond angle deformation must be zero, whereas the mean square amplitude of $\langle(\Delta\alpha)^2\rangle$ is non-zero. The rotational contribution which can be obtained in a closed form (Section II.B.2) has to be added. Table 11 shows some characteristic results obtained using a harmonic oscillator partition function (equation (11)). The results for $\langle \Delta r_{CO} \rangle^T$ in CO_2 are in excellent agreement with recent electron diffraction data,[87] and with an accurate calculation of $\langle \Delta r \rangle$ by Kohl and Hilderbrandt[88] using variational methods. For example, at 300 K we find the vibrational contribution to $\langle \Delta r_{CO} \rangle^T =$

TABLE 11

Mean bond displacement due to anharmonic vibration and rotation in linear triatomic molecules, all in 10^{-3} Å.[34]

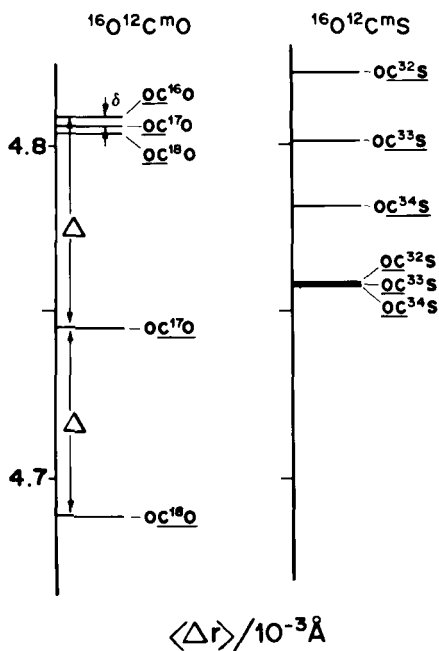|		$\langle \Delta r \rangle_{\text{vib}}^{T}$	$\langle \Delta r \rangle_{\text{rot}}^{T}$	$\langle \Delta r \rangle^{T}$
$^{13}C^{16}O_2$	250 K	4.4802	0.1718	4.6520
	300 K	4.5031	0.2062	4.7093
	350 K	4.5350	0.2405	4.7755
$^{15}N^{15}N^{16}O$				
$\langle \Delta r_{NN} \rangle^{T}$	250 K	4.9389	0.1425	5.0814
	300 K	4.9868	0.1710	5.1578
	350 K	5.0464	0.1995	5.2459
$\langle \Delta r_{NO} \rangle^{T}$	250 K	5.3217	0.2436	5.5652
	300 K	5.3556	0.2923	5.5479
	350 K	5.4044	0.3410	5.7453

FIG. 10. Mean bond displacements at 300 K in CO_2 and OCS, illustrating the primary effect (Δ), the secondary effect (δ) and the additivity of the effects. From reference 90, with permission.

0.0045 and $\langle \Delta r_{CO}^2 \rangle^T = 0.0012$, whereas Kohl and Hilderbrandt obtain 0.0040 and 0.0012, respectively.

In order to study the mass dependence of $\langle \Delta r \rangle^T$ we performed the calculation for different isotopomers of a symmetric (CO_2) and a non-symmetric (OCS)[89] linear triatomic molecule.[90] The results are shown in Fig. 10.

For bent triatomic molecules $\langle \Delta \alpha \rangle \neq 0$, so we also have to include the mean bond angle deformations, leading to three coupled equations to be solved. Such calculations were performed for several bent triatomic molecules.[14] The results shown in Table 12 can be summarized as follows. As is generally found for other molecules, vibrational and rotational contributions to the mean bond displacements $\langle \Delta r \rangle$ are positive. As usual an increase in temperature leads to an increase in the mean bond displacements, and for X–H bonds this is dominated by rotational contributions because the higher vibrational frequencies for these molecules lead to a smaller

TABLE 12

Mean bond displacement and mean bond angle deformation at 300 K, isotope effects ($\Delta_{iso} = \langle \Delta r \rangle_{light}^{300} - \langle \Delta r \rangle_{heavy}^{300}$, or $r\langle \Delta \alpha \rangle_{light}^{300} - r\langle \Delta \alpha \rangle_{heavy}^{300}$) and temperature dependence ($\Delta_T = \langle \Delta r \rangle^{400} - \langle \Delta r \rangle^{200}$, or $r\langle \Delta \alpha \rangle^{400} - r\langle \Delta \alpha \rangle^{200}$) for bent triatomic molecules.[14]

		$\langle \Delta r \rangle$			$r\langle \Delta \alpha \rangle$		
		vib.	rot.	total	vib.	rot.	total
H_2O	(10^{-2} Å)	1.915	0.088	2.003	0.218	−0.215	0.003
D_2O	(10^{-2} Å)	1.391	0.087	1.478	0.211	−0.201	0.010
Δ_{iso}	(10^{-3} Å)	5.237	0.006	5.243	0.075	−0.141	−0.066
Δ_T	(10^{-4} Å)	0.085	5.846	5.931	0.083	−14.340	−13.508
H_2S	(10^{-2} Å)	1.836	0.110	1.947	0.129	−0.067	0.062
D_2S	(10^{-2} Å)	1.318	0.110	1.428	0.126	−0.057	0.069
Δ_{iso}	(10^{-3} Å)	5.181	0.002	5.181	0.034	−0.104	−0.070
Δ_T	(10^{-4} Å)	0.309	7.364	7.673	0.249	−4.505	−4.256
H_2Se	(10^{-2} Å)	1.925	0.124	2.049	−0.183	−0.076	−0.260
D_2Se	(10^{-2} Å)	1.373	0.124	1.497	−0.101	−0.071	−0.172
Δ_{iso}	(10^{-3} Å)	5.514	0.001	5.515	−0.826	−0.054	−0.880
Δ_T	(10^{-4} Å)	0.553	8.272	8.825	2.286	−5.101	−2.815
O_2S	(10^{-2} Å)	0.471	0.046	0.516	0.283	−0.179	0.104
$^{18}O_2S$	(10^{-2} Å)	0.454	0.046	0.500	0.282	−0.176	0.106
Δ_{iso}	(10^{-3} Å)	0.171	0.001	0.172	0.015	−0.031	−0.016
Δ_T	(10^{-4} Å)	2.138	3.041	5.179	7.385	−11.965	−4.579

temperature dependence in the $(1/\omega) \coth(hc\omega/2kT)$ terms appearing in the vibrational averaging. The rotational contribution, on the other hand, is linear with temperature. The magnitude of the isotope effect on the bond length at 300 K is dominated by vibratior in all cases.

The vibrational contribution to the mean bond angle deformation, $\langle\Delta\alpha\rangle_{vib}$, is of either sign, i.e. in some of the molecules the average bond angle is greater than the equilibrium value and in others it is smaller. In all cases, however, $\langle\Delta\alpha\rangle_{vib}$ increases algebraically with increasing temperature, the changes with temperature being smaller for the hydrides owing to the greater vibrational frequencies. The rotational contribution to the mean bond angle deformation, $\langle\Delta\alpha\rangle_{rot}$, is negative for all bent triatomics. These findings can be understood in terms of the predominant centrifugal stretching effects arising from the rotation about the principal axis parallel to the line connecting the two end atoms. The isotope effects on $\langle\Delta\alpha\rangle$ upon substitution of the end atoms have different signs, a result of the different mass dependence of the rotational and vibrational contributions. The change with mass of $\langle\Delta\alpha\rangle_{vib}$ is of either sign but always such as to bring the mean bond angle closer to the equilibrium values as the masses of the end atoms increase.

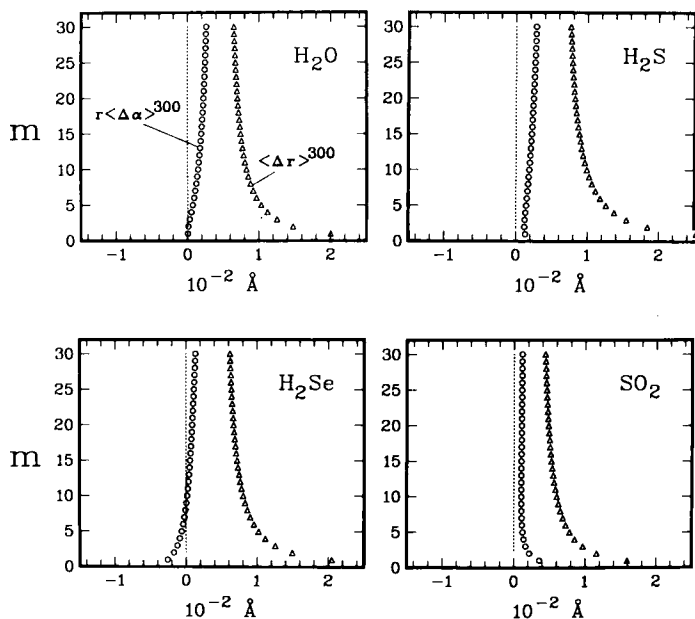FIG. 11. The mass dependence of $r\langle\Delta\alpha\rangle$ (shown as O) and $\langle\Delta r\rangle$ (shown as △) in bent triatomic molecules. The masses of the end atoms are varied arbitrarily while keeping the same force field. From reference 14, with permission.

On the other hand, the changes with masses of $\langle\Delta\alpha\rangle_{rot}$ is always of the same sign, the bond angle increasing with increasing mass. Altogether the mass dependence of $\langle\Delta r\rangle$ is stronger than that of $\langle\Delta\alpha\rangle$ in all cases. For example, $[\langle\Delta r_{XH}\rangle - \langle\Delta r_{XD}\rangle] \gg r[\langle\Delta\alpha_{HXH}\rangle - \langle\Delta\alpha_{DXD}\rangle]$ by a factor of 6 to 80. Figure 11 shows the mass dependence of $\langle\Delta r\rangle$ and $\langle\Delta\alpha\rangle$ for selected bent triatomic molecules. These calculations were carried out with arbitrarily assigned masses of 1–30 amu for the end atoms without changing the mass-independent constants in the force field. Figure 11 shows that even in bent triatomic molecules the $\langle\Delta\alpha\rangle$ term is not important for isotope shifts.

2. The Urey–Bradley model force field approach

A review by Duncan shows that uniquely determined general harmonic force fields (GHFF) are available for only selected molecules[91] and the general anharmonic force field is known for even fewer molecules. In most cases it is necessary to assume certain model potential functions. It has been shown[92] that a modified Urey–Bradley potential function[93] gives a reasonably good description of molecular vibrations. The Urey–Bradley force field (UBFF) has found its greatest application in the calculation of vibration frequencies of halogenated molecules. The number of independent UB force constants is usually less than that of the GHFF and they show a remarkable degree of transferability. This means that it is possible to use exactly the same set of UB force constants for all halomethanes to be compared, for example, a feature which makes the UB approach especially suitable for application to isotope effects.[11,94,33] The UB field is expressed as[95]

$$V = \sum_i [K_i' \, r_i \, \Delta r_i + \tfrac{1}{2} K_i (\Delta r_i)^2] + \sum_{i<j} [H_{ij}' \, r_{ij}^2 \, \Delta\alpha_{ij} + \tfrac{1}{2} H_{ij} (r_{ij} \, \Delta\alpha_{ij})^2]$$
$$+ \sum_{i<j} [F_{ij}' \, q_{ij} \, \Delta q_{ij} + \tfrac{1}{2} F_{ij} (\Delta q_{ij})^2] \tag{70}$$

where r is the bond length, α the bond angle, q the distance between atoms not bonded directly, and r_{ij} represents $(r_i r_j)^{1/2}$. K', K, H', H, F', F are the bond stretching, angle bending, and repulsive (between non-bonded atoms) force constants. The non-bonded distance coordinate Δq_{ij} can be expressed in terms of Δr_i, Δr_j and $\Delta\alpha_{ij}$ (equation 7 in reference 33).

To take into account the anharmonicity of vibration Bartell[96] suggested the following terms:

$$V_a = -\tfrac{1}{2} \sum_i a_i K_i (\Delta r_i)^3 + \tfrac{1}{2} \sum_i \sum_{j\neq i} (1/6q_{ij}) F_{ij}^3 (\Delta q_{ij})^3 \tag{71}$$

It seems reasonable to express the stretching part of V as a potential function similar to that of a diatomic molecule, so a Morse function (equation (34)) is used for the stretching anharmonicity.[96] F_{ij}^3, the cubic force constant

appropriate to non-bonded interactions, can be obtained as follows:

$$F^3 = q[\partial^3 V(q)/\partial q^3] \tag{72a}$$

$$V(q) = A \exp(-Bq) - Cq^{-6} \quad \text{for H–X interactions} \tag{72b}$$

$$V(q) = 4\varepsilon[(q_0/q)^{12} - (q_0/q)^6] \quad \text{for X–Y interactions} \tag{72c}$$

The parameters A, B, C, or ε and q_0 are available.[97,98] So far there is no sufficiently good model to describe the bending anharmonicity. Thus we neglect the H^3 terms in equation (71) even if they could become important in certain cases like pyramidal molecules of C_{3v} symmetry.[14]

In order to use Bartell's approach to calculate the mean bond displacements from a UB force field we need the additional derivatives of the non-bonded displacement coordinate Δq_{ij} with respect to the Cartesian displacement coordinates:

$$(\partial \Delta q_{ij}/\partial \Delta z_k) = s_{kj}\delta_{ik} = s_{ik}\delta_{jk} \tag{15c}$$

where δ_{ij} is the Kronecker delta and s_{ij} is a geometry factor:
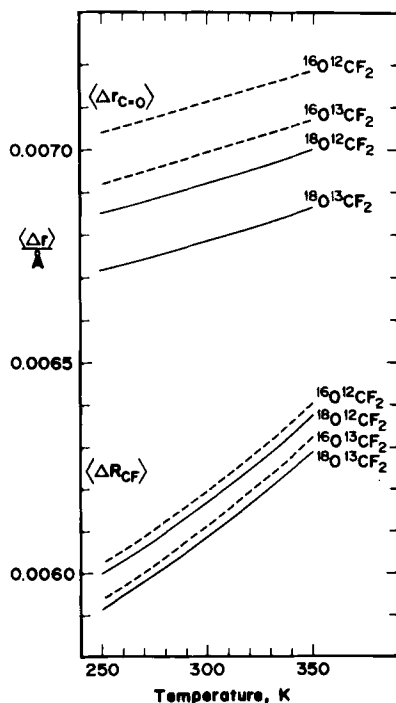
$$s_{kj} = (r_k - r_j \cos \alpha_{kj})/q_{kj}$$

FIG. 12. Mean bond displacement for various isotopomers of $O{=}CF_2$.[33]

Results for the mean bond displacement as a function of temperature for various isotopomers of carbonyl fluoride obtained from such calculations[33] are shown in Fig. 12.

3. Estimation methods for mean bond displacements

Although second derivative terms are not negligible in isotope shifts, for the purpose of obtaining estimates of isotope shifts we will consider only the term in the first derivative with respect to bond extension:

$$\sigma - \sigma^* \approx (\partial\sigma/\partial\Delta r)_e[\langle\Delta r\rangle - \langle\Delta r\rangle^*] \tag{73}$$

A method of estimating $\langle\Delta r\rangle$ which can be applied to an arbitrary bond to an end atom in a molecule would be very useful for predicting orders of magnitude of isotope shifts. This would allow one to determine *a priori* whether a particular isotopic substitution would be worthwhile to attempt for a given application. For the majority of molecules insufficient spectroscopic information is available to permit full dynamic calculations, so it is necessary to develop an approximation method in order to estimate the mean bond displacements for these molecules. It appears that stretching cubic constants for polyatomic molecules can be deduced from the bond length in the same way as for diatomic molecules. The Herschbach and Laurie parameters used for such estimation for diatomic molecules (Section III.B.3) are found to describe F_3 for polyatomic molecules as well.[58,59] Therefore we can use equation (59) to predict mean bond displacements in polyatomic molecules if the Morse anharmonic stretching accounts for most of the mean bond displacement.[58]

In Fig. 13 the plots of $\mu^{-1/2}10^{-D}$ *vs.* $\langle\Delta r\rangle_{vib}$ calculated for selected polyatomic molecules are compared with the results for some diatomic molecules.[58] A least-squares fit gives a slope of 22×10^{-3} rather than the 19.35×10^{-3} factor containing the fundamental constants in equation (59). The slope for the polyatomic molecules is somewhat larger because the other contributions due to bending and non-bonded interactions can be significant. Bartell has shown that, for molecules of the AX_n type, the Morse stretching contribution to $\langle\Delta r\rangle$ is only 64% in CH_4,[99] and only about 40% in SF_6.[100] However, equation (59) with a modified factor of 22×10^{-3} for polyatomics gives a satisfactory estimate of $\langle\Delta r\rangle$ from r_e. Therefore we shall use

$$\langle\Delta r\rangle_{vib}/\text{Å} \approx 22 \times 10^{-3}\mu^{-1/2}10^{-D} \tag{74}$$

where D is given by equation (60).

The rotational contribution to $\langle\Delta r\rangle$ is likewise easily estimated from r_e alone for an AX_n molecule:[99]

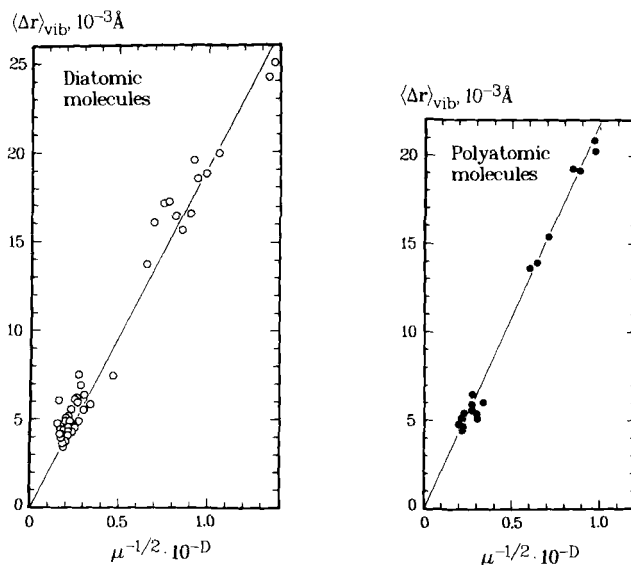$$\langle\Delta r\rangle_{rot} = 2\bar{E}_{rot}/(nF_2r_e) \tag{75}$$

FIG. 13. Test of approximation in equation (47) (straight line, slope $= 19.35 \times 10^{-3}$), against calculated mean bond displacements for diatomic molecules. The same method is applied to polyatomic molecules; the straight line is a least-squares fit to the data (slope $= 22 \times 10^{-3}$). From reference 58, with permission.

where $\bar{E}_{rot}$ is the classical average, kT for linear molecules, and $(3/2)kT$ for non-linear ones, and F_2 is expressed according to equation (58). However, we do not even need $\langle \Delta r \rangle_{rot}$ for estimating most isotope shifts. For bent triatomic molecules we already have seen that rotation does not play a significant role in the isotope shifts of the central atom upon end atom substitution. We have shown (Section III.A) that for diatomic molecules there is no rotational contribution to the isotope shift and for symmetrical substitution in molecular types CH_4, BF_3, SF_6, CO_2 there is also no rotational contribution to the isotope shift (Section II.B.2). We will see in Section IV.D that, even in unsymmetrical substitution in CH_4 isotopomers, the rotational contribution plays no role in the D-induced ^{13}C isotope shift. For the isotope shift of the end atom the rotational contribution is also not too important. For example, the dynamical factor relevant to $^2\Delta^1H(^{2/1}H)$ in CH_4-CH_3D is -2.687×10^{-4} Å from rotation and 5.53×10^{-3} Å from vibration, only 5% contribution from rotation. For $^1\Delta^1H(^{17/16}O)$ in $H_2^{16}O$-$H_2^{17}O$ the dynamical factor is -4.176×10^{-7} Å from rotation and 3.102×10^{-5} Å from vibration, only 1.4% rotational contribution.

C. The reduced isotope shift in polyatomic molecules

From dynamical calculations for different molecular types of different symmetries[33-35,14] we find in general (for any molecular type and any

substitution site) that the change in the mean bond displacement upon isotopic substitution can be expressed as follows:

$$\Delta = \langle \Delta r \rangle - \langle \Delta r \rangle^* = \langle \Delta r \rangle \frac{m' - m}{m'} f(m, m_A, \ldots) \tag{76}$$

The consequences of equation (76) for one-bond isotope shifts in NMR are clear if equation (73) holds (i.e. including only linear terms in the expansion of nuclear shielding in bond displacements). Comparing several isotopic species which differ in one mass m', from the parent species with mass m, we should get a constant value for the ratio $(\langle \Delta r \rangle - \langle \Delta r \rangle^*)/[\langle \Delta r \rangle \times (m' - m)/m']$. Furthermore, if the isotope shift can be approximated by equation (73), we should find $(\sigma - \sigma^*)/[(m' - m)/m'] = $ constant. An excellent test of this is provided by the $^{m'/m}$Se-induced ^{77}Se isotope shifts in diselenides. Gombler[101] measured the isotope shifts in $R_1{}^{77}$SeSeR$_2$ (R$_1$, R$_2$ = CF$_3$, CH$_3$) for $m = 74$, $m' = 76, 77, 78, 80, 82$ plotted in Fig. 14. Indeed we find a strictly linear behaviour of the isotope shifts $^1\Delta^{77}$Se($^{m'/74}$Se) $vs.$ $(m' - m)/m'$ (for $m = 74$) for all four molecules.[90] This seems to indicate that either the interpretation of isotope shifts using equation (73) is sufficient, or all of the dynamic variables $(\langle \Delta r \rangle^2)$, $(\langle \Delta \alpha \rangle^2)$, etc.) on which the shielding

FIG. 14. Effect of selenium isotopes on the ^{77}Se nuclear shielding in the diselenides R$_1{}^{77}$Se $^{m'}$Se R$_2$. (a) R$_1$ = R$_2$ = CH$_3$; (b) R$_1$ = R$_2$ = CF$_3$; (c) R$_1$ = CF$_3$, R$_2$ = CH$_3$; (d) R$_1$ = CH$_3$, R$_2$ = CF$_3$; from experimental results by Gombler.[101] This plot of $^1\Delta^{77}$Se($^{m'/74}$Se) = $\sigma(R_1{}^{77}$Se^{74}Se R$_2$) $- \sigma(R_1{}^{77}$Se $^{m'}$Se R$_2$) vs $(m' - 74)/m'$ illustrates the validity of equation (76). From reference 90, with permission.

depends are scaled by $(m'-m)/m'$ upon isotopic substitution. In fact we have found[102] in bent triatomic molecules that $\langle(\Delta\alpha)^2\rangle$, for example, does not scale by $(m'-m)/m'$.

By comparing the mean bond lengths of various isotopomers of several molecular types, we have found[90] a functional form

$$f(m, m_A, \ldots) \approx \frac{1}{2}\frac{m_A}{m_A+m}$$

that can reproduce the primary effect of isotopic substitution on the mean bond displacement for substitution at end atoms:

$$\Delta = \langle\Delta r\rangle - \langle\Delta r\rangle^* \approx \langle\Delta r\rangle\frac{m'-m}{m'}\cdot\frac{1}{2}\frac{m_A}{m_A+m} \tag{51}$$

that is, the same form as we had derived (equation (51)) for diatomic molecules. Thus, for a single substitution of m by m':

$$^1\Delta A(^{m'/m}X) \approx \left(\frac{\partial\sigma^A}{\partial\Delta r_{AX}}\right)_e [\langle\Delta r_{AX}\rangle - \langle\Delta r_{AX}\rangle^*]$$

$$\approx \left(\frac{\partial\sigma^A}{\partial\Delta r_{AX}}\right)_e \langle\Delta r\rangle \frac{m'-m}{m'}\cdot\frac{1}{2}\frac{m_A}{m_A+m} \tag{77}$$

On this basis we can use the same definition for the reduced isotope shift as for diatomic molecules, equation (54), which in this approximation can be identified with

$$^1\Delta^R(A, X) \approx \left(\frac{\partial\sigma^A}{\partial\Delta r_{AX}}\right)_e \langle\Delta r_{AX}\rangle + \frac{1}{2}\left(\frac{\partial^2\sigma^A}{\partial\Delta r_{AX}^2}\right)_e \langle(\Delta r_{AX})^2\rangle \tag{78}$$

and for 300 K, for a symmetrical AX_n molecule,

$$[\sigma_0^A(300\text{ K}) - \sigma_e] \approx n^1\Delta^R(A, X) \tag{79}$$

Thus we can obtain directly from experimental isotope shifts the same $[\sigma_0(300) - \sigma_e]$ that normally have been obtained from fitting the experimental $[\sigma_0(T) - \sigma_0(300)]$ function to dynamical calculations of $(\langle\Delta r\rangle^T - \langle\Delta r\rangle^{300})$.[103] Note that equation (79) is an approximation because, unlike equation (55) for diatomics, not all the quadratic terms which contribute to the rovibrational corrections to shielding in polyatomic molecules are included.

In Table 13 we present some experimental isotope shifts and the derived rovibrational corrections to the shielding in selected molecules. For CH_4, dynamical calculations including secondary vibrational effects on mean bond displacements,[35] yield for the rovibrational correction to the ^{13}C-shielding -2.985 ppm, to be compared to an estimate of -3.3 ppm. For ^{19}F

TABLE 13

The rovibrational correction to shielding, in ppm, and estimates of the derivatives $(\partial\sigma/\partial\Delta r)_e$, in ppm Å^{-1}, directly obtained from reduced isotope shifts (see references 14 and 58).

Nucl.	Mol.	m'/m	$-^1\Delta$	$-^1\Delta^R$	$[\sigma(300)-\sigma_e]$	$(\partial\sigma/\partial\Delta r)_{est}$
		(a) Highly symmetric molecules ($\langle\Delta\alpha\rangle = 0$)				
^{2}D	HD	$^{2/1}$H	0.0469	0.2814	-0.2814	-11.5
^{11}B	BH_4^-	$^{2/1}$H	0.138	0.6	-2.4	-26.7
^{13}C	CH_4	$^{2/1}$H	0.192	0.82	-3.3	-39
	CN^-	$^{15/14}$N	0.03 ± 0.005	1.87	-1.87	-380
	CO	$^{18/16}$O	0.0476 ± 0.0016	1.91	-1.91	-470
	CO_2	$^{18/16}$O	0.019	0.76	-1.53	-160
	CS_2	$^{34/32}$S	0.009	1.06	-2.12	-220
^{15}N	NH_4^+	$^{2/1}$H	0.307	1.32	-5.26	-65
	NO_3^-	$^{18/16}$O	0.056	2.16	-6.5	-410
	CN^-	$^{13/12}$C	0.075 ± 0.005	3.51	-3.5	-700
	N_2	$^{15/14}$N	0.0601 ± 0.002	3.49	-3.49	-900
^{17}O	CO	$^{13/12}$C	0.110 ± 0.011	4.88	-4.88	-1190
^{19}F	HF	$^{2/1}$H	2.5 ± 0.5	10.5	-10.5	-675
^{31}P	PO_4^{3-}	$^{18/16}$O	0.019 ± 0.002	0.52	-2.1	-120
^{55}Mn	MnO_4^-	$^{18/16}$O	0.59 ± 0.02	13.7	-55	-2490
^{95}Mo	MoO_4^{2-}	$^{18/16}$O	0.25 ± 0.01	5.26	-21	-1400
^{99}Tc	TcO_4^-	$^{18/16}$O	0.44 ± 0.06	9.2	-37	-2030
^{195}Pt	$PtCl_6^{2-}$	$^{37/35}$Cl	0.167	7.3	-43.8	-2530
	$PtBr_6^{2-}$	$^{81/79}$Br	0.028 ± 0.006	3.18	-19	-1470
		(b) Bent molecules ($\langle\Delta\alpha\rangle \neq 0$)				
^{17}O	H_2O	$^{2/1}$H	1.54	6.52	-13.0	-340
^{15}N	NH_3	$^{2/1}$H	0.65	2.77	-8.3	-140
	NO_2^-	$^{18/16}$O	0.138	5.13	-10.3	-990
^{31}P	PH_3	$^{2/1}$H	0.843	3.48	-10.4	-200
	PCl_3	$^{37/35}$Cl	0.019	1.5	-4.5	-310
	PBr_3	$^{81/79}$Br	0.006	1.72	-5.2	-370
^{77}Se	H_2Se	$^{2/1}$H	7.02	28.4	-56.9	-1540

in HF, calculations lead to -9.58 ppm (this work) shown in Table 4, -9.75 ppm,[104] and -11.23 ppm,[43] to be compared with -10.5 ppm from equation (79).

Another useful application of the reduced isotope shift is in the estimation of a derivative of nuclear shielding from a measured one-bond isotope shift with no other information other than a bond length. We use our empirical method of estimating $\langle\Delta r\rangle_{vib}$ for cases where it is not possible to perform a full dynamical calculation. We can apply this method to the estimation of the shielding derivatives from reported one-bond isotope shifts using

$$(\partial\sigma^A/\partial\Delta r)_e \approx {}^1\Delta^R(A, X)/\langle\Delta r_{AX}\rangle_{vib} \qquad (80)$$

Estimates of shielding derivatives using this equation are shown in Table 13. No other information except the bond length was used to obtain these derivatives. It is encouraging that they compare reasonably well with results from *ab initio* and other methods which require much more elaborate experiments or computations. Comparisons with other values are discussed in Section IV.F.

So far we have limited the discussion to molecules with vanishing mean bond angle deformations. We have shown in Section IV.B.1 that, for several bent triatomic molecules, the substitution of another isotope on an end position does not change $\langle \Delta \alpha \rangle$ significantly compared to the change in $\langle \Delta r \rangle$. The same holds for other bent molecules.[14] Fowler[71] has shown that the $\langle \Delta \alpha \rangle$ terms do not contribute significantly to the isotope shift in H_2O. The isotope shift is dominated in all cases by changes in the mean bond displacements rather than the changes in the mean bond angle deformations. This means that we can apply the same definition for a reduced isotope shift as a first order approximation for these molecules too. Table 13 includes some rovibrational corrections for bent molecules calculated in this way. For ^{17}O in H_2O Fowler *et al.* calculate -13.576,[76] to be compared with our estimate of -13.0. The agreement of our estimate with *ab initio* shielding calculations is encouraging.

If the substitution takes place at a non-end atom, we can no longer treat the isotope effect on the bond length like that in a diatomic molecule, because of the complex character of molecular vibrations. For non-end substitutions all contributions to $\Delta \langle \Delta r \rangle$ coming from bending vibrations, for example, are no longer negligible. The change of the mass of one non-end atom has an influence on all bonds connected to this atom, and we find the effect on $\langle \Delta r \rangle$ of an individual bond is always smaller than predicted by equation (51).[102] Nevertheless, for halogen-substituted methanes we can reproduce the effect of $^{13/12}C$ substitution on all bonds by a simple formula, modifying equation (51) only by an additional factor $m/(m + \frac{1}{2}m_A)$.

Equation (76) has another consequence: it allows us to correlate the dynamic factor $[\langle \Delta r \rangle - \langle \Delta r \rangle^*]$ with mean bond displacement in polyatomic molecules. By applying equation (74) or by doing the dynamical calculations for the same bond type, e.g. C–F,[94] we find that $\langle \Delta r \rangle$ increases with increasing bond length. Thus, the dynamic factor alone would lead to an opposite correlation between isotope shifts and bond length from that which is observed (e.g. see Fig. 2). The observations can only be expected if the magnitude of the electronic factor increases with decreasing bond length.

D. The additivity of NMR isotope shifts

One of the theoretically interesting and practically useful aspects of the isotope effect on NMR chemical shifts is the proportionality of the shift to the number of substituted atoms in equivalent positions. The practical

consequence of this is a spectrum with equally spaced peaks, the intensities giving an indication of the relative amounts of each isotopomer in the sample (Fig. 1). For example, the one-bond $^{2/1}$H-induced isotope shift in the ^{13}C spectrum of CH_nD_{4-n} isotopomers results in incremental isotope shifts as n goes from 0 to 4.[105] There are similar observations in other systems such as in PO_4^{3-},[106] $NH_{4-n}D_n^+$,[107] $BH_{4-n}D_n^-$,[108] $NH_{3-n}D_n$,[109] $PH_{3-n}D_n$.[110] Nor is this observation limited to one-bond isotope shifts. For example, the ^{59}Co spectrum of $Co(en)_3Cl_3$ in H_2O/D_2O solution shows 13 equally spaced peaks separated by 5.2 ppm, the peaks corresponding to all members of the isotopic homologous series in which the 12 exchangeable hydrogen atoms per molecule of the cobalt complex are replaced by deuterium atoms.[111] This additivity of the isotope effect on the chemical shift upon substitution in equivalent locations appears to be without exception, and the deviations from additivity usually appear to be small and have been noticed outside of experimental error only in isolated cases. There are some indications of additivity of mass effects in other forms of molecular spectroscopy. The sum of the squares of the vibrational frequencies of members of an isotopic homologous series is linearly related to the number of isotopes substituted, and this relation is valid for symmetry types which are common to all members of the series.[112] The sum of vibrational frequencies in $CH_{4-n}D_n$ is found empirically to depend on the number (n) of the substitutions by the heavy isotope, i.e. the zero-point energies of these molecules are linearly related to n.[113]

In Section IV.B.1 we have shown the mass effects on average nuclear positions in linear triatomic molecules. In the following we examine the origin of the observed additivity of the NMR isotope shift, determine if any systematic deviations from additivity can be expected, and how large they may be. An interesting molecule from the point of view of discussing the additivity of NMR isotope shifts is the methane molecule. The anharmonic force field of methane has recently been refined[114] to fit spectroscopic data from the isotopic species $^{12}CH_4$, $^{13}CH_4$, $^{12}CD_4$, $^{12}CH_3D$, $^{12}CHD_3$, and $^{12}CH_2D_2$. Six of the 13 cubic force constants are determined experimentally and the remaining cubic force constants are fixed at values derived from *ab initio* calculations.[115] We have calculated the mean bond displacements in the methane family $CX_{4-n}Y_n$ (X, Y = H, D, T), with the method described in detail elsewhere,[35] and find that the substitution effects on the vibrational contribution to mean bond displacements are strictly additive. Each substitution of a hydrogen by a deuterium shortens the appropriate bond by nearly the same amount Δ. The mean bond displacements in $^{12}CH_{4-n}T_n$ and $^{12}CD_{4-n}T_n$ exhibit the same strictly linear dependence on n.[35,90] We can express $\langle \Delta r_{CH} \rangle$ and $\langle \Delta r_{CD} \rangle$ in $^{12}CH_{4-n}D_n$ as follows. Let

$$d = \langle \Delta r_{CH} \rangle \text{ in } CH_4 \text{ at 300 K}$$

$$d - \Delta = \langle \Delta r_{CD} \rangle \text{ in } CD_4 \text{ at 300 K}$$

where $d = 2.0881 \times 10^{-2}$ Å and $\Delta = 5.5345 \times 10^{-3}$ Å. We find

$$\langle \Delta r_{CD} \rangle = d - \Delta + \delta_D(n) \tag{81a}$$

$$\langle \Delta r_{CH} \rangle = d + \delta_H(n) \tag{81b}$$

Similar relations can be found for the other series of isotopomers.[90] That is, for a given bond, substitution of an isotope involved in this bond had an effect Δ on its own mean bond length (a primary effect on the mean bond displacement); each substitution of an isotope at some other bonds has a much smaller effect δ (a secondary effect).

The rotational contribution (centrifugal stretching) to the mean bond displacement was calculated and is illustrated in Fig. 15 where the sum of all four $\langle \Delta r_i \rangle_{rot}$ is shown to be invariant to n:[90]

$$(4 - n)\langle \Delta r_{CH} \rangle_{rot} + n\langle \Delta r_{CD} \rangle_{rot} = 4 d_{rot} \tag{82}$$

where $d_{rot} = 5.2 \times 10^{-4}$ Å. The invariance of the centrifugal distortion to isotopic substitution which preserves T_d symmetry is pointed out in Section II.B.2. Here we find that, although there is a rotational effect on each bond,
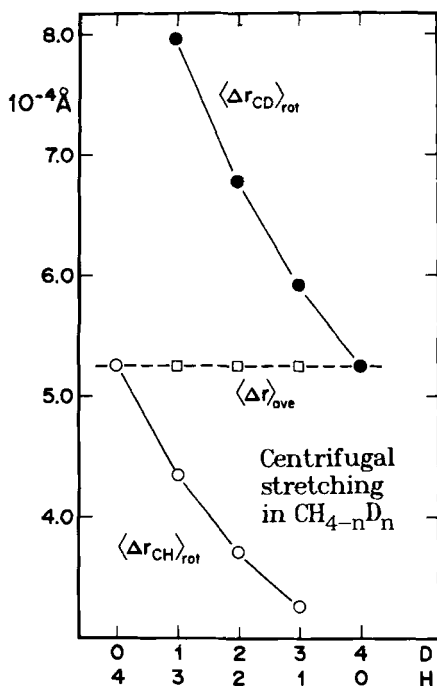

FIG. 15. The rotational contribution to mean bond displacement in the methanes. From reference 90, with permission.

the sum is also invariant, so the centrifugal distortion does not contribute to the isotope shift of the central nucleus.

The vibrational contribution to the isotope shift depends on

$$\sum_i \langle \Delta r_i \rangle_{\text{vib}} = (4 - n)\langle \Delta r_{\text{CH}} \rangle_{\text{vib}} + n \langle \Delta r_{\text{CD}} \rangle_{\text{vib}}$$

$$= 4d - n\Delta + \delta(n) \tag{83}$$

which is nearly linear with n, since $\delta(n) \ll \Delta$. The $^{2/1}$H-induced ^{13}C NMR isotope shift between any two isotopomers of $CH_{4-n}D_n$ can then be expressed, following equation (73), as

$$\sigma^C(CH_{4-n}D_n) - \sigma^C(CH_{4-n'}D_{n'}) = (\partial\sigma^C/\partial\Delta r)_e[(n' - n)\Delta + \delta(n) - \delta(n')]$$

$$\approx (\partial\sigma^C/\partial\Delta r)_e(n' - n)\Delta \tag{84}$$

Equation (84) is the basis for the near additivity of isotope shifts due to substitution at equivalent sites. If we leave out the term $[\delta(n') - \delta(n)]$ which is two orders of magnitude smaller than Δ, we have strict additivity: the magnitude of the shift is proportional to the number $(n' - n)$ of atoms which have been substituted by isotopes.

To test the general validity of the findings in the methanes we briefly return to the linear triatomic molecules. Figure 10 shows the results for single substitution in different isotopomers of CO_2 and OCS,[34] but the conclusions which follow are based on calculations for all possible isotopomers using $^{18/17/16}$O, $^{13/12}$C and $^{34/33/32}$S. As shown in Fig. 10 we find that substitution of a heavier isotope provides a drastic shortening of the average length of the bond directly attached to this isotope by a constant Δ, and as a secondary effect it shortens the other bond by a constant δ, where $\Delta \gg \delta$. We also find an empirical general additivity rule which is valid for all triatomics:

$$\langle \Delta r(^{m'}Y A ^{n'}X) \rangle_{\text{av}} - \langle \Delta r(^{m}Y A ^{n}X) \rangle_{\text{av}}$$

$$= [\langle \Delta r(^{m'}Y A ^{n}X) \rangle_{\text{av}} - \langle \Delta r(^{m}Y A ^{n}X) \rangle_{\text{av}}] \tag{85}$$

$$+ [\langle \Delta r(^{m}Y A ^{n'}X) \rangle_{\text{av}} - \langle \Delta r(^{m}Y A ^{n}X) \rangle_{\text{av}}]$$

where

$$\langle \Delta r \rangle_{\text{av}} \equiv \tfrac{1}{2}[\langle \Delta r_{AY} \rangle + \langle \Delta r_{AX} \rangle]$$

Thus, if we include only linear terms, for the shielding of the central atom in the linear triatomics,

$$\langle \sigma \rangle \approx \sigma_e + \left(\frac{\partial\sigma}{\partial\Delta r}\right)_e 2\langle \Delta r \rangle_{\text{av}} \tag{86}$$

The additivity of the isotope shift for the central atom which follows from

equations (85) and (86) may be written in the usual notation, for ^{13}C in OCS, for example:

$$^1\Delta^{13}C(^{18/16}O, {}^{34/32}S) = {}^1\Delta^{13}C(^{18/16}O) + {}^1\Delta^{13}C(^{34/32}S) \qquad (87)$$

Once again, additivity of isotope shifts is predicted on the basis of additivity of mass effects on $\langle \Delta r \rangle$.

Although the secondary isotope effects on the mean bond displacements are small, the term $[\delta(n') - \delta(n)]$ in equation (84) provides a theoretical basis for deviations from strict additivity of isotope shifts. If we include these small terms in calculating the isotope shifts for the methane family we find a deviation from additivity in the ratio $0:3:4:3:0$ for $n = 0$ to 4.[90] The isotope effects on the ^{13}C shifts in $CH_{4-n}D_n$ have been measured,[105] but the associated errors are not small enough to enable one to see these systematic deviations from additivity. On the other hand, excellent measurements have been carried out[107] for the ^{14}N shifts in the ammonium ion, $^{14}NH_{4-n}D_n{}^+$, with a precision of ± 0.001 ppm.[107] Deviations are found from the strict additivity of -0.014 ppm, -0.020 ppm, -0.014 ppm respectively for $n = 1, 2, 3$ which are in a ratio of $0:2.8:4:2.8:0$. Another example is the isotope shift of the ^{119}Sn nucleus in the $Sn(CH_3)_{4-n}(CD_3)_n$ system.[116] This system shows deviations from additivity in the same direction as those found for $NH_{4-n}D_n{}^+$, although the ratios are not $0:3:4:3:0$ exactly. Only if we can consider the CD_3 and CH_3 groups as point masses can the centrifugal stretching contribution be neglected, as in $CH_{4-n}D_n$. It should be noted that the ratio $0:3:4:3:0$ is strictly parallel to the results obtained[117] for deviations from additivity in zero-point energies in methanes using a model which treats the four bonds in $CH_{4-n}D_n$ as four coupled oscillators. The deviation from linear behaviour of the zero-point energy $vs.$ n plot comes from the term in the energy which corresponds to the mutual motion of two atoms in different oscillators from their equilibrium position. In our case the deviations from additivity come from the small secondary effects δ on the mean bond displacements, which are again a result of the coupled atomic motions in molecular vibrations.

E. Contributions from bond angle changes and higher order derivatives of the shielding surface

So far we have truncated equation (5) after the linear term in order to calculate or estimate isotope effects on nuclear shielding in polyatomic molecules. It is shown in Table 6 that this assumption is not unreasonable for many diatomics. The terms connected with higher order derivatives of the shielding surface contribute significantly less to the isotope shift than the linear ones. In some cases, however, the neglect of the second derivative term leads to significant error.

TABLE 14

Individual contributions to the isotope shift in the water molecule, in ppm.[38]

Term in equation (5)	$^1\Delta^{17}O(^{2/1}H, ^{2/1}H)$	$^1\Delta^1H(^{18/16}O)$
$(\partial\sigma/\partial\Delta r)_e$	-2.57	$-0.0021, -0.0003$ [b]
$(\partial\sigma/\partial\Delta\alpha)_e$	-0.01	$+0.0003$
$(\partial^2\sigma/\partial\Delta r^2)_e$	-1.31	$+0.0010, -0.0002$ [b]
$(\partial^2\sigma/\partial\Delta\alpha^2)_e$	$+0.45$	-0.0001
Total[a]	-3.68	-0.00017

[a] Including also third and fourth derivatives of shielding.
[b] The same bond and other bond contributions, respectively.

In Table 14 we show Fowler's[38] results for the H_2O molecule, indicating the relative contributions of terms involving the first and second derivatives of nuclear shielding. Although the observed ^{17}O isotope shift is only -3.08 ppm, the relative values of the calculated contributions to the total *ab initio* value of -3.68 ppm should indicate the relative importance of the various terms. We see that the largest contribution does indeed come from the term $(\partial\sigma/\partial\Delta r)_e\Delta\langle\Delta r\rangle$. There is, however, an important quadratic contribution $(\partial^2\sigma/\partial\Delta r^2)_e\Delta\langle(\Delta r)^2\rangle$. There is a smaller but non-negligible term in $(\partial^2\sigma/\partial\Delta\alpha^2)_e\Delta\langle(\Delta\alpha)^2\rangle$ and the remainder is due to 3rd and 4th derivatives of ^{17}O shielding.

For ^1H isotope shifts, the terms involving the bond angle are even less important. For ^1H isotope shifts, the term involving the primary derivative $(\partial\sigma^{H_a}/\partial\Delta r_{OH_a})_e$ gives the largest contribution, as might be expected.

There are several important conclusions from these results. (a) Neglecting the higher order contribution leads to an underestimation of the total isotope effect. (b) On the other hand, it becomes more clear from these findings that the isotope effects involving the bond angles are extremely small. They do not contribute significantly to the isotope shift (less than 1% for H_2O). This justifies using the same definition of a reduced isotope shift even for molecules with non-vanishing $\langle\Delta\alpha\rangle$. (c) Notice also that the contribution due to the harmonic bond angle changes which are associated with the derivative $(\partial^2\sigma/\partial\Delta\alpha^2)_e$ can have an opposite sign to the term in $\langle\Delta r\rangle$ and in $\langle\Delta r^2\rangle$.

If a change in the bond angle away from the equilibrium configuration weakens the bond (as in a linear triatomic molecule like OCO or a bent triatomic molecule like HOH) then a trace on the shielding surface along the $\Delta\alpha$ coordinate, such as that shown in Fig. 8(a), will have a minimum close to the equilibrium bond angle. This trace will be a function which is concave upward, i.e. increased shielding of the nucleus at the vertex of the

angle accompanies the opening of the bond angle as well as the closing of the bond angle. Such a shielding surface will therefore have $(\partial^2\sigma/\partial\Delta\alpha^2)_e > 0$, giving a positive contribution to the isotope shift since $\langle\Delta\alpha^2\rangle$, like $\langle\Delta r\rangle$ or $\langle(\Delta r)^2\rangle$, is greater for the isotopomer with lighter end atoms. The term $(\partial^2\sigma/\partial\Delta\alpha^2)_e\Delta\langle\Delta\alpha^2\rangle$ is especially important in linear molecules with low frequency bending vibrational modes. For acetylene, for example, a $^{2/1}$H-induced effect on the ^{13}C shift over one bond is -0.223 ppm whereas the effect over two bonds is larger (-0.438 ppm).[118] The observed small $^1\Delta^{13}$C($^{2/1}$H) is probably due to the partial cancellation of the negative linear and quadratic terms in Δr by the positive $(\partial^2\sigma/\partial\Delta\alpha^2)_e\Delta\langle\Delta\alpha^2\rangle$ term. Of course we cannot rule out a π contribution to the secondary derivative $(\partial\sigma^{C_1}/\partial\Delta r_{C_2H})_e$.

There is very little else known about $(\partial\sigma/\partial\Delta\alpha)_e$ or $(\partial^2\sigma/\partial\Delta\alpha^2)_e$. The observed negative sign, additivity, and dependence on $(m'-m)/m'$, even for isotope shifts in apex nuclei in bent systems, support the assumption of neglect of bond angle deformation contribution to the isotope shifts. The same assumption cannot always be made in the interpretation of the temperature dependence in the zero-pressure limit. It has been suggested that the unusual temperature dependence of ^{15}N in NH_3 and ^{31}P in PH_3 is due to contributions of bond angle deformations to the temperature dependence of nuclear shielding.[14] Unfortunately it has not been possible to obtain a quantitative simultaneous fit to the isotope shift and the temperature dependent chemical shift in the case of PH_3.

In Fig. 16 we compare several calculated $^{13/12}$C-induced isotope shifts on ^{19}F shielding with experimental values for a series of halomethanes.[11] The isotope effects are calculated only from the linear term in equation (5), but this time the derivatives $(\partial\sigma/\partial\Delta r_{CF})_e$ are obtained from fitting the experimentally measured temperature dependence of the nuclear shielding at the zero-pressure limit to a function[13,11,94]

$$\sigma_0(T) - \sigma_0(300 \text{ K}) \approx (\partial\sigma^F/\partial\Delta r_{CF})_{e,\text{emp}}[\langle\Delta r\rangle^T - \langle\Delta r\rangle^{300}]. \qquad (88)$$

We can see that there is a systematic trend in the deviation of the calculated values from the experimental isotope shifts. When one or two heavier nuclei like Cl are attached to the carbon the calculated isotope shifts are in good agreement with experiment whereas hydrogens lead to underestimation (as expected). The higher the percentage of rotational contributions to the temperature dependence of $\langle\Delta r\rangle$, the more accurate the empirical $(\partial\sigma/\partial\Delta r)_e$ which results from fitting $\sigma_0(T) - \sigma_0(300 \text{ K})$ data since the rotational term linearly dependent on temperature dominates the observed $\sigma_0(T)$. For CH_3F 65% of the temperature dependence of $\langle\Delta r\rangle$ is due to rotation,[11] so we expect to get a reasonably good empirical estimate of $(\partial\sigma/\partial\Delta r)_e$. For the others the rotational contribution to the temperature coefficient of $\langle\Delta r\rangle$
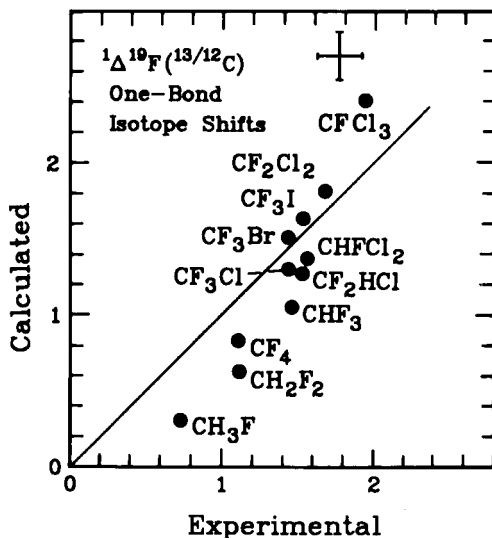
FIG. 16. Comparison of calculated (using equation (73)) and experimental ^{13}C-induced ^{19}F isotope shifts. From reference 11, with permission.

decreases with increasing masses of the other atoms attached to the carbon, down to only 10% rotation for $CFCl_3$.

Including the quadratic term in equation (88), we have

$$\sigma_0(T) - \sigma_0(300) \approx (\partial\sigma/\partial\Delta r)_e[\langle\Delta r\rangle^T - \langle\Delta r\rangle^{300}]$$

$$+ \tfrac{1}{2}(\partial^2\sigma/\partial\Delta r^2)_e[\langle(\Delta r)^2\rangle^T - \langle(\Delta r)^2\rangle^{300}] \qquad (89)$$

In polyatomic molecules there are of course many more quadratic terms than this. For the purpose of estimating the discrepancies between experimental and calculated isotope shifts in Fig. 16 let us consider only the term in $\langle(\Delta r)^2\rangle$. Furthermore, we will use the diatomic molecule approximation for the relationship between $\langle\Delta r\rangle$ and $\langle(\Delta r)^2\rangle$ (equation (47)). Then

$$\sigma_0(T) - \sigma_0(300) = \{(\partial\sigma/\partial\Delta r)_e + (1/3a)(1-f_T)(\partial^2\sigma/\partial\Delta r^2)_e\}$$

$$\times \{\langle\Delta r\rangle^T - \langle\Delta r\rangle^{300}\} \qquad (90)$$

where f_T is that fraction of the total temperature dependence $[\langle\Delta r\rangle^T - \langle\Delta r\rangle^{300}]$ which is due to rotation. Thus the empirical derivatives $(\partial\sigma/\partial\Delta r)_{e,emp}$ obtained from fitting $[\sigma_0(T) - \sigma_0(300)]$ will be

$$(\partial\sigma/\partial\Delta r)_{e,emp} = \{(\partial\sigma/\partial\Delta r)_e + (1/3a)(1-f_T)(\partial^2\sigma/\partial\Delta r^2)_e\} \qquad (91)$$

When the rotational contribution to $[\langle\Delta r\rangle^T - \langle\Delta r\rangle^{300}]$ is sizeable (i.e. $f_T \geqslant 0.3$), then $(\partial\sigma/\partial\Delta r)_{e,emp}$ should be very close to $(\partial\sigma/\partial\Delta r)_e$, because a is typically

around 2 Å^{-1} and the second derivative is of the same order of magnitude as the first derivative, so the neglected terms are about a factor of $(1 - f_T)/6$ smaller than $(\partial\sigma/\partial\Delta r)_e$. For much smaller rotational contributions the magnitude of the empirical first derivative is overestimated. In accounting for the ^{13}C-induced ^{19}F isotope shift using only the linear term in equation (5), we should expect to get values that are too small, since the $(\partial^2\sigma/\partial\Delta r^2)[\langle(\Delta r)^2\rangle - \langle(\Delta r)^2\rangle^*]$ terms have not been included. When using the empirical derivatives from the temperature-dependent shielding to calculate the isotope shift, we underestimate the magnitude of the isotope shift by an amount

$$(f_T - f_{iso})(1/3a)(\partial^2\sigma/\partial\Delta r^2)_e[\langle\Delta r\rangle - \langle\Delta r\rangle^*] \tag{92}$$

where f_{iso} is the fraction of $[\langle\Delta r\rangle - \langle\Delta r\rangle^*]$ that is due to rotation. In diatomic molecules f_{iso} is identically zero, and in polyatomic molecules it is typically less than 0.01. The different magnitudes of f_T lead to the systematic deviations observed in Fig. 16. For the CH_nF_{4-n} series the discrepancies between the calculated and experimental isotope shifts correlate with f_T values 0.31 to 0.65,[11] indicating a more or less constant value for $(\partial^2\sigma/\partial\Delta r^2)_e$. On the other hand, in the $CF_{4-n}Cl_n$ series, in which f_T ranges from 0.10 to 0.18,[94] the agreements between calculated and observed values are within experimental errors. This indicates that, for molecules with smaller rotational contribution to the temperature dependence ($f_T \ll 0.2$), the overestimation of $(\partial\sigma/\partial\Delta r)_{e,emp}$ partially compensates the error associated with the neglect of quadratic and higher order derivatives in the shielding expansion. Where the empirical first derivatives are closest to the true values the calculated isotope shifts are underestimated.

F. Estimation of one-bond isotope shifts for end atom substitution

In this section we discuss the general magnitudes of observed one-bond isotope shifts and provide estimates of others. We have shown that it is possible to estimate the isotope effect on the mean bond displacement in the case of end atom substitution so that we can obtain a value within 10% of the value one would obtain from a full dynamical calculation using an anharmonic force field. We have also shown that, except for ^1H or ^7Li, the term $(\partial\sigma/\partial\Delta r)_e\Delta\langle r\rangle$ gives 70–88% of the total calculated isotope shift in diatomic molecules and 70% of the calculated ^{17}O isotope shift in H_2O. With empirical shielding derivatives we can obtain around 75% of the observed ^{13}C-induced ^{19}F isotope shift in fluoromethanes with this term only.[11,94] Therefore it should be possible to estimate a one-bond isotope shift not previously measured, by using only the $(\partial\sigma/\partial\Delta r)_e\Delta\langle r\rangle$ term in the shielding. When isotope shifts are used in applications where a special synthesis is necessary in order to "tag" the molecule of interest, it would

be very useful to know *a priori* if the expected isotope shift is observable under experimental conditions. An order of magnitude estimate is easily within reach when the particular observed nucleus-substituted atom pair has previously been observed in any compound. In such a case the correlations which are shown in Fig. 2, and further discussed below, can narrow down the estimate easily to within 20% uncertainty. When the isotope shift for a particular observed nucleus-substituted atom pair has not been previously observed, it would be very useful to have an order of magnitude estimate in order to know whether the observation of the isotope shift is feasible, given that an NMR spectroscopist can generally predict linewidths to be expected under experimental conditions. Therefore we show here a method of estimation for one-bond isotope shifts proposed earlier.[119] Let us do this in parts. We wish to show how to estimate a one-bond isotope shift in the following situations:

(A) If an isotope shift has been previously observed for the same nucleus in an analogous compound, e.g. $^1\Delta^{31}P(^{34/32}S)$ from $^1\Delta^{31}P(^{18/16}O)$.

(B) If an isotope shift has been observed in an analogous compound for a different nucleus belonging in the same column of the periodic table as the desired one, e.g. $^1\Delta^{31}P(^{m'/m}X)$ from $^1\Delta^{15}N(^{m'/m}X)$.

(C) If no previously measured isotope shifts in analogues are known, and in the most general sense for an arbitrary previously unobserved nucleus-substituted atom pair.

We have shown that to a first approximation the one-bond isotope shift can be expressed by equation (77). In this expression the experimentally observed isotope shift consists of the product of two factors. The electronic factor reflects the sensitivity of nuclear shielding to bond extension and the dynamic factor reflects the average change in the molecular geometry on isotopic substitution. Let us first consider the dynamic factor. There are practical implications of equation (77) for measurements of isotope shifts. Quite apart from the advantage of a large chemical shift range for heavier nuclei, the mass dependence alone favours the observation of the chemical shift of a heavy nucleus upon substitution of a light neighbouring atom with an isotope. The most favourable case is the $^{3/1}H$-induced shift of a heavy nucleus. The largest experimentally observed one-bond isotope effect so far is the $^{2/1}H$-induced effect on the ^{77}Se shielding, -7.02 ppm per D in H_2Se.[4] In addition to the favourable fractional mass changes in the factor $(m' - m)/m'$, the factor $m_A(m_A + m)$ is close to 1.0. It would be wise to calculate the mass factors prior to attempting an isotope shift measurement. For example, in the Se–C bond the $^{13/12}C$-induced ^{77}Se shift is easily observable, whereas the $^{80/77}Se$-induced ^{13}C shift is not. A shift of $^1\Delta^{77}Se(^{13/12}C) = -0.683$ ppm is observed in $NCSe^-$, whereas no shift due to the Se isotopes in the ^{13}C spectrum has been found.[58] The mass factor $\frac{1}{2} \cdot (m' - m)/m' \cdot m_A/(m_A + m)$ is equal to 0.033 in the first case and 0.003

in the second. For a mass factor greater than 0.01 it should be feasible to observe any one-bond isotope effect on nuclear shielding with a medium-field high resolution spectrometer when linewidths are favourable. We also introduce the reduced one-bond shift equation (54)[58,119] as a means of removing most of the dependence of the measured isotope shifts on the masses. Thus $^1\Delta^R$ for ^{31}P in PH_3 can be directly compared to ^{31}P in PO_4^{3-} or to ^{15}N in NH_4^+. The range of values of $^1\Delta^R$ for a given observed nucleus therefore reflects the variation of $(\partial\sigma/\partial\Delta r)_e\langle\Delta r\rangle$ with nuclear environment. We have already shown that $\langle\Delta r\rangle$ is $15-20\times10^{-3}$ Å for hydrides and $4-7\times10^{-3}$ Å for most other bonds, and that it is possible to estimate $\langle\Delta r\rangle$ involving an end atom by knowing only the bond length, the masses and the rows of the periodic table of the pair of atoms.

Case (A) is therefore easily handled with the appropriate mass factors. The one-bond isotope shift $^1\Delta^{31}P(^{81/79}Br)$ in PBr_3 can be estimated as follows. From $^1\Delta^{31}P(^{37/35}Cl)$ in PCl_3, which is -0.019 ppm,[120] we calculate the reduced isotope shift (equation (54)) which is -1.50 ppm, approximately identified with $(\partial\sigma/\partial\Delta r_{PCl})_e\langle\Delta r_{PCl}\rangle$. At this point we can make a rough estimate and simply assume that

$$\langle\Delta r_{PCl}\rangle\approx\langle\Delta r_{PBr}\rangle \text{ and } (\partial\sigma/\partial\Delta r_{PCl})_e\approx(\partial\sigma/\partial\Delta r_{PBr})_e$$

In other words, we are estimating $^1\Delta^R(P, Br)\approx{}^1\Delta^R(P, Cl)$ from which we then calculate the desired isotope shift as -0.005 ppm. This shift has been reported as -0.006 ppm.[120] Another application would be the estimation of $^1\Delta^{31}P(^{34/32}S)$ in $P(v)$ compounds with a $P{=}S$ bond. The one-bond $^{18/16}O$-induced shift has been measured $(-0.0354$ ppm).[121] From this, following the same procedure as for the PX_3 example, we would obtain a reduced isotope shift of -0.96 ppm from which $^1\Delta^{31}P(^{34/32}S)=-0.0140$ ppm. A slightly better estimate can be obtained if we know the $P{=}O$ and $P{=}S$ bond lengths. Then we can find the ratio $\langle\Delta r_{PS}\rangle/\langle\Delta r_{PO}\rangle$:

$$\frac{\langle\Delta r_{PS}\rangle}{\langle\Delta r_{PO}\rangle}=\left(\frac{\mu_{PO}}{\mu_{PS}}\right)^{1/2}\frac{(10^{-D})_{PS}}{(10^{-D})_{PO}}=0.95$$

using $r_e=1.86$ and 1.52 Å respectively for $P{=}S$ and $P{=}O$ and the values of the parameters in Table 7. Thus we only need to assume that $(\partial\sigma^P/\partial\Delta r_{PS})_e\approx(\partial\sigma^P/\partial\Delta r_{PO})_e$.

$$^1\Delta^R(P, S)\approx{}^1\Delta^R(P, O)\langle\Delta r_{PS}\rangle/\langle\Delta r_{PO}\rangle=-0.91 \text{ ppm}$$

Then, as previously, we get an estimate for $^1\Delta^{31}P(^{34/32}S)=-0.0132$ ppm. We can also estimate $^1\Delta^{31}P(^{36/32}S)$ to be approximately twice as large because of the factor $(36-32)/36$ instead of $(34-32)/34$. These isotope shifts have recently been measured and reported as -0.0097 ppm and -0.0184 ppm.[122]

Also, the $^{34/32}S$-induced ^{95}Mo isotope shift in MoS_4^{2-}, which should have roughly the same value of $^1\Delta^R$ as MoO_4^{2-} $(-5.26$ ppm$)$, can be predicted

to be

$$-5.26 \text{ ppm} \times (34-32)/34 \times 1/2 \times 95/(95+32) = -0.11 \text{ ppm}$$

if electronic factors are about the same and $\langle \Delta r_{MoO} \rangle$ is comparable to $\langle \Delta r_{MoS} \rangle$. The measured value is -0.090 ppm.[123]

Let us now consider the electronic factor in more detail. The value of $(\partial\sigma/\partial\Delta r)_e$ for a given nucleus reflects the range of chemical shifts for that nucleus, since both are measures of the nuclear shielding sensitivity, the former to bond extension and the latter to changes in electronic structure. For example, the ratio of the *ab initio* theoretical ^{19}F shielding derivative $(\partial\sigma^F/\partial\Delta r_{HF})_e$ in HF to the empirical ^{1}H shielding derivative $(\partial\sigma^H/\partial\Delta r_{HH})_e$ in H$_2$ (-442 ppm Å^{-1}/-12.1 ppm Å^{-1})[43,70] is approximately the same as the ratio of the chemical shift ranges of ^{19}F and ^{1}H, about 800 ppm/20 ppm. Since the periodicity of the $\langle a_0^3/r^3 \rangle$ of the valence p or d orbitals of the observed nucleus has been found to be generally reflected in the ranges of chemical shifts,[124] it is possible to use $\langle a_0^3/r^3 \rangle$ in the same fashion (where $a_0 = 0.529$ Å). For example, the derivatives $(\partial\sigma^X/\partial\Delta r_{XH})_e$ for ^{11}B, ^{13}C and ^{15}N in BH$_4^-$, CH$_4$ and NH$_4^+$ have been estimated from observed $^{2/1}$H-induced isotope shifts; these are -27, -35 and -65 ppm Å^{-1} respectively,[58] or 0.76:1:1.85. These may be comapred with the values of $\langle a_0^3/r^3 \rangle$ for free atoms which are in the ratio 0.5:1:2.0,[125,126] roughly the same ratio as the observed ranges of chemical shifts for these nuclei. In CN$^-$ the ratio $(\partial\sigma^N/\partial\Delta r)_e$ to $(\partial\sigma^C/\partial\Delta r)_e$ is -872 ppm Å^{-1} to -473 ppm Å^{-1},[127,69] the same ratio as for the derivatives in NH$_4^+$ and CH$_4$ (1.85:1). In CO the ratio of $(\partial\sigma^O/\partial\Delta r)_e$ to $(\partial\sigma^C/\partial\Delta r)_e$ is -1150 to -456 ppm Å^{-1},[50] which is 2.5; this may be compared with the ratio of $\langle a_0^3/r^3 \rangle$ for the atoms, which is 3.5.

When the values of $\langle \Delta r \rangle$ are comparable, the reduced isotope shifts will appear to be related to one another in the same way as chemical shifts in general. In the above example, the $\langle \Delta r \rangle$ values for BH$_4^-$, CH$_4$ and NH$_4^+$ are similar (2–2.2×10^{-2} Å), so the reduced isotope shifts are related in very nearly the same way as the respective $(\partial\sigma/\partial\Delta r)_e$. Note, however, that $\langle \Delta r \rangle$ for bonds involving hydrogen are different from all others. Although the mean bond angle deformation $\langle \Delta\alpha \rangle$ is non-zero for NH$_3$ and PH$_3$,[14] it has been found that the $^{2/1}$H-induced isotope effect on X is dominated by the change in $\langle \Delta r \rangle$. It is found[109,110] that the ratio

$$\frac{^1\Delta^R(P, H) \text{ in PH}_3}{^1\Delta^R(N, H) \text{ in NH}_3} = 1.26$$

is comparable to the ratio of $\langle a_0^3/r^3 \rangle$ for the P and N atoms which is 1.4. Thus the trends relating magnitudes of isotope shifts to shielding sensitivity and the similarities of $\langle \Delta r \rangle$ for the bonds being compared lead to relationships between reduced shifts based on chemical shift ranges (or $\langle a_0^3/r^3 \rangle$) if the isotope shift of one chemical analogue is known. The method of

estimation for case (B) now becomes clear. Given that $^1\Delta^{95}Mo(^{18/16}O) = -0.25$ ppm,[128] by using the ratio of $\langle a_0^3/r^3\rangle$ for the $3d_{3/2}$ and $4d_{3/2}$ states of the atoms,[126] we can estimate $^1\Delta^{99}Tc(^{18/16}O)$ as follows. Take

$$(\partial\sigma^{Tc}/\partial\Delta r_{TcO}) \approx \frac{\langle a_0^3/r^3\rangle_{Tc}}{\langle a_0^3/r^3\rangle_{Mo}}(\partial\sigma^{Mo}/\partial\Delta r_{MoO})_e$$

and for a rough estimate let $\langle\Delta r_{TcO}\rangle \approx \langle\Delta r_{MoO}\rangle$. Then

$$^1\Delta^{99}Tc(^{18/16}O) \approx \frac{\langle a_0^3/r^3\rangle_{Tc}}{\langle a_0^3/r^3\rangle_{Mo}}{}^1\Delta^{95}Mo(^{18/16}O)\frac{99}{99+16}\frac{95+16}{95}$$

$$= -0.34 \text{ ppm}.$$

This compares well with the experimental value of -0.44 ± 0.06 ppm.[129]

There are fewer data on analogous compounds which involve replacement of non-end atoms. It is interesting, however, that the relationship holds even in the case of $^{13/12}$C-induced ^{199}Hg and ^{111}Cd shifts in Me_2Hg and Me_2Cd. Here the isotope shifts are of unusual sign, $+0.4$ ppm and $+0.14$ ppm respectively.[130,131] Nevertheless the reduced isotope shifts, 11.0 and 4.0 ppm, are in the same ratio as $\langle a_0^3/r^3\rangle$ of Hg and Cd.

TABLE 15

Observed and estimated (in parentheses) $^{2/1}$H-induced one-bond isotope shifts in hydrides, in ppm per D.[119]

H_2	BH_4^-	CH_4	NH_4^+	NH_3	H_2O	HF
-0.0402	-0.138	-0.192	-0.307	-0.65	-1.54	-2.5
		SiH_4		PH_3	H_2S	HCl
		(-0.4)		-0.843	(-2.2)	(-2.8)
		GeH_4		AsH_3	H_2Se	HBr
		(-1.1)		(-2.0)	-7.02	(-5.6)
		SnH_4		SbH_3	H_2Te	HI
		(-1.6)		(-3.0)	(-10.6)	(-7.9)
		PbH_4				
		(-2.9)				

The above examples indicate that predictions to within a factor of 2 are possible when chemically analogous compounds are compared. In Table 15 we show $^{2/1}$H-induced one-bond isotope shifts for various nuclei where they have been observed, and our predictions of the magnitudes of $^1\Delta$ for yet unknown shifts in parentheses. We present similar values and predictions for $^{18/16}$O-induced one-bond isotope shifts in Table 16. The predicted values

TABLE 16

Observed and estimated (in parentheses) $^{18/16}$O-induced one-bond isotope shifts, in ppm per ^{18}O.[119]

CO$_2$	NO$_2^-$	/	NO$_3^-$		O$_3$	
−0.019	−0.138		−0.056		(−0.26)	
			PO$_4^3$	SO$_2$ /	SO$_4^{2-}$	ClO$_4^-$
			−0.019	(−0.27)	(−0.026)	(−0.03)
			AsO$_4^{3-}$	SeO$_2$ /	SeO$_4^{2-}$	BrO$_4^-$
			(−0.06)	(−0.72)	(−0.06)	(−0.09)
				TeO$_2$ /	TeO$_4^{2-}$	IO$_4^-$
				(−1.6)	(−0.14)	(−0.16)

in Tables 15 and 16 are based on calculations of $\langle\Delta r\rangle$ using methods described in Section IV.B, and estimates of $(\partial\sigma/\partial\Delta r)_e$ based on correlations of the type described above.

Estimates can also be made by comparing non-analogous compounds for different nuclei in the same group of the periodic table. Here the estimate will not be as good as in the analogous compounds which we have used for case (A) and case (B). However, even if no other information regarding analogous compounds is available, this can lead to an estimate within a factor of 2–3. For example, to estimate $^1\Delta^{15}N(^{2/1}H)$ in NH$_4^+$ from $^1\Delta^{31}P(^{18/16}O)$ in PO$_4^{3-}$ (−0.019±0.002 ppm) we proceed as follows:

$$^1\Delta^{15}N(^{2/1}H) \approx {}^1\Delta^{31}P(^{18/16}O)\frac{\langle a_0^3/r^3\rangle_N}{\langle a_0^3/r^3\rangle_P}\frac{\langle\Delta r_{NH}\rangle}{\langle\Delta r_{PO}\rangle}\frac{\dfrac{2-1}{2}\dfrac{15}{15+1}}{\dfrac{18-16}{18}\dfrac{31}{31+16}}$$

Using equation (74) to estimate $\langle\Delta r\rangle$, this gives a value of −0.72 ppm, to be compared with the measured value, −0.307 ppm.[107]

Finally, it would be useful to have a way of making an order of magnitude estimate of the isotope shift that may be expected for a nucleus in any bond, at least a prediction of the feasibility of the observation. The derivatives $(\partial\sigma/\partial\Delta r)_e$ vary with structural factors by as much as 2-fold even for the same bond (^{19}F in C–F bonds in various halomethanes for example).[11,94] There are other variations in electronic factors for a given nucleus which imply that the derivatives $(\partial\sigma/\partial\Delta r)_e$ should have a spread of about a factor from 2 to 10. (These are discussed below.) In Table 17 we show the known ranges of $^1\Delta^R$ for various observed nuclei and in parentheses our predictions for other nuclei in any electronic environment. These predictions are based on two measured isotope shifts, $^1\Delta^{31}P(^{18/16}O)$ in PO$_4^{3-}$ and $^1\Delta^{15}N(^{18/16}O)$ in NO$_2^-$, and the $\langle a_0^3/r^3\rangle$ for the observed nucleus. From this table an

TABLE 17

Magnitudes of reduced isotope shifts observed for various nuclei, in ppm. Predicted[a,b] values for other nuclei are shown in parentheses.[119]

	H 0.375–0.81								
	Li (0.006–0.1)	Be (0.02–0.36)	B 0.6 (0.09–1.26)	C 0.2–1.87	N 1.3–5.1	O 6.5 (0.6–9)	F 0.6–10.5		
	Na (0.036–0.5)	Mg (0.1–1.6)	Al (0.2–2.6)	Si (0.3–4.8)	P 0.4–5.4	S (0.7–10.4)	Cl (1.1–14.8)		
	K (0.065–0.91)	Ca (0.2–2.3)	Ga (0.5–7.2)	Ge (0.9–11.9)	As (1.1–15.6)	Se 0.4–30	Br (2.0–28.1)		
	Rb (0.13–1.75)	Sr (0.3–4.1)	In (0.8–11.8)	Sn 6.5 (1.3–17.9)	Sb (1.8–24.4)	Te 1.6–9.7 (up to 31)	I (2.7–37.3)	Xe (3.3–46.3)	
	Cs (0.2–2.7)	Ba (0.4–5.9)	Tl (1.8–24.5)	Pb (2.4–33.2)	Bi (3.7–51)				
Sc (2.1–5.2)	Ti (2.8–7)	V 4.5 (3.6–9)	Cr 10.3 (4–9.9)	Mn 13.7 (5.5–13.7)	Fe (6.7–16.6)	Co 28.6 (8–19.8)	Ni (9.4–23.3)	Cu (0.2–2.5)	Zn (0.4–5)
Y (2.7–6.7)	Zr (3.8–9.3)	Nb (4.1–10.2)	Mo 4.1–5.3 (5.3–13.1)	Tc 9.2 (7.1–17.5)	Ru (7.5–18.7)	Rh (8.8–21.9)	Pd (9.7–23.9)	Ag (0.4–5.2)	Cd 4 (0.7–9.5)
La (3.9–9.6)	Hf (7.5–18.7)	Ta (9.3–23)	W (11.1–27.4)	Re (13.1–32.4)	Os (15.1–37.3)	Ir (17.4–43.1)	Pt 3.2–7.3 (18.6–46)	Au (0.9–12.4)	Hg 4–11 (1.5–20.7)

[a] The predictions are based on P in PO_4^{3-} for the lower limit and N in NO_2^- for the upper limit for the main groups.

[b] For the transition elements the predictions are based on MoO_4^{2-} and MnO_4^- respectively, i.e. for highly symmetric environments only. Furthermore, the factor ΔE^{-1} in the chemical shift depends on the ligands, so the given ranges should be multiplied by the factor by which ΔE^{-1} varies for a given transition element in its complexes compared to ions of the type MO_4^{m-}. For example, the observed values for Pt in $PtCl_6^{2-}$ and $PtBr_6^{2-}$ are smaller, whereas that for Co in $Co(CN)_6^{3-}$ is greater.

estimate of $^1\Delta$ can be made for nucleus A due to substitution of an end atom ^mX by $^{m'}X$ by multiplying the number in Table 17 by $(m' - m)/m'X\frac{1}{2}m_A/(m_A + m)$. Given no further information these estimates predict the feasibility of observation of any given one-bond isotope shift. This is based on the assumption that $\langle \Delta r \rangle$ is approximately the same for an arbitrary bond as for the P-O or N-O bond. Because of the fact that $\langle \Delta r \rangle$ is significantly different for X-H bonds in comparison to others, Table 17 is not suitable for predicting $^{2/1}$H-induced isotope shifts. For this the use of Table 15 and a case (B) approach would be more appropriate.

As an example we predict from Table 17 a $^{18/16}$O-induced shift on the ^{51}V shielding of $VO_4{}^{3-}$ in the range of -0.15 to -0.38 ppm, whereas the experiment yields -0.19 ppm.[132] For $^1\Delta^{19}F(^{34/32}S)$ we would predict -0.007 to -0.115 ppm. This may be compared with the experimental values which range from -0.0091 ppm to -0.0755 ppm for a variety of S-F bonds.[133-134] Equation (77) indicates that the least feasible observations are those of the shift in light nuclei A upon isotopic substitution of a heavy ligand X. The mass factors are unfavourable and the shielding derivative is expected to be small for the smaller chemical shift ranges typical of light nuclei.

G. Factors affecting $(\partial\sigma/\partial\Delta r)_e$

We have already seen that the dynamical factors in one-bond isotope shifts are fairly predictable and can even be estimated without a good force field because the mass-independent part of the dynamic factor is largely determined by the bond length and the rows of the periodic table of the pair of bonded atoms. In order to explain the correlations (a)-(d) which were noted in Section I, we look to the electronic factors $(\partial\sigma/\partial\Delta r)_e$. There are several systems for which these derivatives have been estimated. The results of dynamical calculations on a variety of molecules and the accompanying measurements of the temperature dependence of nuclear shielding in the zero-pressure limit provide empirical estimates of $(\partial\sigma/\partial\Delta r)_e$ according to equation (88). We use these as illustrative examples. Although most of the estimates of $(\partial\sigma/\partial\Delta r)_e$ which are now available are for ^{19}F shielding, the systematic trends which we have found for these derivatives are probably typical. In Table 18 we summarize the derivatives estimated from temperature-dependent shielding studies in the zero-pressure limit, from theoretical (ab initio) calculations, and from the reduced isotope shifts.

Examination of the derivatives in Table 18 reveals the following trends:

(a) $(\partial\sigma/\partial\Delta r)_e$ seems to be always negative, with rare exceptions, i.e. deshielding accompanies bond extension.

(b) $|(\partial\sigma/\partial\Delta r)_e|$ is smaller for nuclei in symmetric environments such as the octahedral, tetrahedral or trigonal planar nuclear sites.

(c) $|(\partial\sigma/\partial\Delta r)_e|$ generally increases with the chemical shift range of the observed nucleus, as we have already noted in the previous section.

TABLE 18

Derivatives of nuclear shielding with respect to bond extension, $(\partial\sigma^A/\partial\Delta r_{AX})_e$, and the absolute shielding σ_0^A (300 K).

Nucl.	Mol.	$(\partial\sigma^A/\partial\Delta r_{AX})_e$			Ref.	σ_0^A (300 K)	Ref.
		theory[a]	temp. depend.[b]	isot. shift			
[1]H	H$_2$	−20.7		−12.1	43, 70	26.363	70
				−11.5	58		
	LiH	−4.19			43	26.213	43
	CH$_4$	−25.6		−38	135, 35	30.611	72
	H$_2$O	−35.3			76	30.052	72
		−40.7			136		
	HF	−41.8, 42.6			43, 135	28.8	104
[11]B	BH$_4{}^-$			−26.7	58		
[13]C	CO	−413.7, −535			53, 137	3.2	138
		−640		−456	74, 50		
	CN$^-$			−473	69		
	CO$_2$		−221	−214	34, 50	60.9	139
	CH$_4$	−30, −40		−35	140, 35	197.35	72
	CH$_3$−CH$_3$	−31, −50(CH)			140	183.1	72
		−15(C−C), −6.3			140, 135		
	CH$_2$=CH$_2$	−26, −32(CH)			140	66.76	72
		−252, −188(C=C), −182.7			140, 135		
	CH≡CH	−4.5, −19(CH)			140	121.35	72
		−206, −110(C≡C), −103			140		
[15]N	CN$^-$			−873	69, 135		
	N$_2$		−774	−910	67, 141	−61.6	142
		−640, −1090			54, 74		

	NH$_4^+$			−65	58	223.8	142
	NO$_3^-$			−410	143	−131.8	142
	NO$_2^-$			−990	143	−365	5
^{17}O	CO	−479		−1150	53, 50	−42.3	73
		−1240			74		
		−1077, −1166			137, 135		
	H$_2$O	−270.9		−294	76, 14	344.0	73
		−285, −275			136, 135		
	CO$_2$			−1641	143	243.4	73
^{19}F	HF	−411, −444			52, 135	410.0	104
		−441.7			43		
	F$_2$		−4530		135, 57	−232.8	144
	ClF	−2782	−2070		57	637.1	144
	BF$_3$		−1115		103	327.2	144
	NF$_3$		−2500		143	50.3	144
	PF$_3$		−1200		143	228.3	144
	SiF$_4$		−1170		103	363.2	144
	SF$_6$		−2200		146	139.6	144
	COF$_2$		−1146		33	221.6	144
	CF$_4$		−1180		11	259.0	144
	CF$_3$Cl		−1630		94	224.4	144
	CF$_2$Cl$_2$		−2000		94	202.6	144
	CFCl$_3$		−2400		94	195.7	145
	CF$_3$Br		−1850		94	213.8	145
	CF$_3$I		−1950		94	199.6	145
	CH$_3$F	−131	−338		135, 11	471.0	144
	CH$_2$F$_2$		−725		11	339.1	145
	CHF$_3$		−1274		11	274.1	144
^{31}P	PO$_4^{3-}$			−120	58		
	PCl$_3$			−310	143		
	PBr$_3$			−370	143		

TABLE 18 (*cont.*)

Nucl.	Mol.	$(\partial\sigma^A/\partial\Delta r_{AX})_e$				$\sigma_0 A$ (300 K)	Ref.
		theory[a]	temp. depend.[b]	isot. shift	Ref.		
^{55}Mn	MnO_4^-			-2490	58		
^{77}Se	H_2Se			-1273	14		
^{95}Mo	MoO_4^{2-}			-1400	58		
^{99}Tc	TcO_4^-			-2030	58		
^{119}Sn	Bu_3SnH			-367	58		
^{195}Pt	$PtCl_6^{2-}$			-2530	58		
	$PtBr_6^{2-}$			-1470	58		

[a] Derivatives of the shielding of various nuclei (B, C, N, F, Si, P) have also been calculated at the CNDO/S level using a sum over states method.[147] The results agree qualitatively with those shown in this table (all $(\partial\sigma/\partial\Delta r)_e < 0$) although, as might be expected at this level of approximation, the magnitudes are considerably smaller in some cases and larger in others. As we have seen in Section III.C, the paramagnetic term, which is most difficult to calculate accurately, dominates the change in shielding with molecular geometry.

[b] The derivatives obtained from the temperature dependence in the zero-pressure limit are overestimated in those cases where the rotational contributions are small; see text Section IV.E for discussion of this.
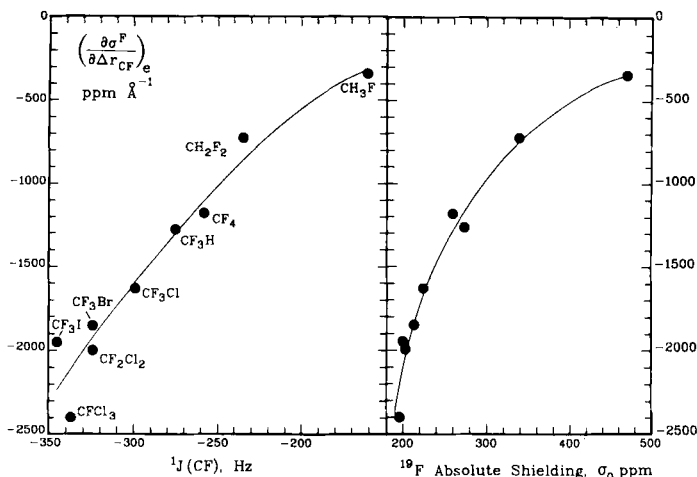
FIG. 17. Correlation of ^{19}F shielding derivatives with ^{13}C–F spin-spin couplings and the ^{19}F absolute shielding. From reference 11, with permission.

(d) $(\partial\sigma/\partial\Delta r)_e$ correlates with the absolute shielding σ_0. An example of this correlation is shown in Fig. 17 for ^{19}F in the C–F bond in fluoromethanes.[11] We have already seen in Section III that the theoretically calculated derivative of the paramagnetic term in the shielding has a larger magnitude than the derivative of the diamagnetic term. The more shielded nucleus has a smaller paramagnetic term. Thus the magnitude of $(\partial\sigma/\partial\Delta r)_e$ will be generally smaller for the more shielded nucleus. Another example is the ^{13}C shielding in CO, CN$^-$, CO$_2$, CH$_4$ in which the derivative is also smaller for the more shielded nucleus. The comparison is not as valid in this series because the bonds being extended do not involve the same atom. Nevertheless there is a clear trend. The consistently larger ^{13}C isotope shift upon D substitution in CH$_2$ groups compared to CH$_3$ groups is probably another example of the correlation of $(\partial\sigma/\partial\Delta r)_e$ with the absolute shielding; ^{13}C in CH$_2$ groups are generally less shielded than in CH$_3$ groups.

(e) $|(\partial\sigma/\partial\Delta r_{C\equiv O})_e|$ in CO (bond order ~3) is greater than $|(\partial\sigma/\partial\Delta r_{C=O})_e|$ in CO$_2$ (bond order ~2) for both O and C. Although there are not any other examples of $(\partial\sigma/\partial\Delta r)_e$ as a function of bond order, this particular example is illustrative. This also shows that $|(\partial\sigma/\partial\Delta r)_e|$ is greater for the shorter C$\equiv$O bond (1.128 Å) than the longer C=O bond (1.160 Å). Similarly, the magnitudes of $(\partial\sigma^F/\partial\Delta r_{CF})_e$ in CFH$_3$ and CF$_4$ correlate with bond lengths of 1.382 and 1.317 Å respectively. The shorter bond is associated with the larger derivative. We have already seen that the magnitude of the dynamic factor for a given bond type decreases with decreasing bond

length; therefore the electronic factor is responsible for the experimentally observed dependence of the isotope shift on bond/bond order.[3,134]

(f) $|(\partial\sigma^A/\partial\Delta r_{AX})_e|$ increases with increasing electronegativity of X, as for ^1H in the series HLi, H_2, H_4C, H_2O, HF, or ^{19}F in the series FH, F_4C, F_3N, FCl, F_2.

(g) $|(\partial\sigma/\partial\Delta r)_e|$ appears to be greater for nuclei with σ lone pairs, e.g. -990 for NO_2^- compared to -410 for NO_3^-, -310 and -370 for PCl_3 and PBr_3 respectively compared to -120 for PO_4^{3-}.

(h) $|(\partial\sigma/\partial\Delta r)_e|$ increases with increasing J. An example of this correlation is shown in Fig. 17 for ^{19}F shielding derivatives with respect to C–F bond extension and the corresponding $J(CF)$ for the fluoromethanes.[11]

These systematic trends in the derivatives account for the observed dependence of isotope shifts on electronegativity of substituents, bond order, etc.[8] Thus the electronic factor is mainly responsible for the observed correlations between the magnitude of the isotope shift and the bond order (or bond length), the spin–spin coupling, and the chemical shift which have been noted (as illustrated in Fig. 2).

V. ISOTOPE EFFECTS OVER MORE THAN ONE BOND

Isotope shifts due to substitution with a heavier atom at a site remote from the observed nucleus show the same general trends as one-bond isotope shifts. (i) The sign is still generally negative although some are positive, with some alternation of signs being observed in the same molecule. (ii) The magnitude reflects the chemical shift range of the observed nucleus. (iii) The magnitude is related to the fractional mass change. (iv) The effect is additive.

In the theoretical interpretation of n-bond isotope shifts ($n > 1$) we need to consider at least two contributions: (i) the secondary changes in shielding with extension of the remote bond due to a primary change in the mean bond length at the substitution site, and (ii) the primary change in shielding with extension of the bond directly involving the observed nucleus due to the secondary change in this mean bond length accompanying isotopic substitution at a remote site. We can write this as follows:

$$^n\Delta A(^{m'/m}X) = S\Delta + P\delta + \cdots \tag{93}$$

where $S \equiv (\partial\sigma^A/\partial\Delta r_{XY})_e$ is a secondary shielding derivative, $P \equiv (\partial\sigma^A/\partial\Delta r_{AZ})_e$ is a primary derivative, Δ is the primary change in the X–Y bond length, $\Delta = \langle\Delta r_{XY}\rangle - \langle\Delta r_{XY}\rangle^*$ when ^mX is replaced by $^{m'}X$ and $\delta = \langle\Delta r_{AZ}\rangle - \langle\Delta r_{AZ}\rangle^*$ is the secondary change in the A–Z bond length due to $^{m'/m}X$ substitution. There are also quadratic and higher order terms which have not been included in equation (93), as well as secondary–secondary

terms such as $(\partial\sigma^A/\partial\Delta r_{ZY})_e\delta'$ which should be generally smaller than the secondary-primary and primary-secondary terms shown in equation (93). The magnitudes of secondary second derivatives of the type $(\partial^2\sigma^A/\partial\Delta r_{XY}^2)_e$ are unknown for any molecule except water.[76] Therefore we will limit our discussion to terms shown in equation (93).

It is easy to see why n-bond isotope shifts are in general smaller than one-bond isotope shifts. While the latter involve a primary electronic factor and a primary dynamic factor, n-bond shifts $(n > 1)$ involve at least one secondary factor in each term. The further away the substitution site is from the observed nucleus, the smaller the secondary factor (either δ or S). In the water molecule in Fig. 8(d) it is clear that the change in the ^1H shielding upon extension of the other O–H bond is much less pronounced than the change upon extension of the immediate bond. The sign of the secondary shielding derivative or the secondary isotope effect on the bond length is not necessarily the same for most systems, because secondary effects are more dependent on the details of the electronic distribution and the potential surface. Thus positive signs for n-bond isotope shifts are quite possible.

The magnitude of the derivatives should still reflect the sensitivity of a given nucleus to its electronic environment, i.e. the secondary derivatives should be dependent on this sensitivity just as the primary derivatives have been shown to be. The dependence of Δ on fractional mass change has already been established in consideration of one-bond isotope shifts, whereas the dependence of δ on these factors has not. Finally, the additivity of 2-bond isotope shifts has also been established by the $CH_{4-n}D_n$ example.[90] This can be written as follows in terms of the primary (P) and secondary (S) derivatives of ^1H shielding:

$$\sigma^H(CH_{4-n}D_n) - \sigma^H(CH_{4-n'}D_{n'}) = (n'-n)\{S[\Delta-\theta(\delta)] + P\delta\}$$

neglecting rotational contributions. $\theta(\delta)$, the term of order δ, can be neglected relative to Δ, leading to $(n'-n)[S\Delta + P\delta]$, which is an isotope shift linearly dependent on the number of substitutions. Thus we see that the additivity extends to both terms in equation (93). The secondary change in the mean bond lengths is very small, e.g. for D substitution it is $\sim 1 \times 10^{-5}$ Å compared to the $\sim 5 \times 10^{-3}$ Å typical for a primary change as in $\Delta = \langle\Delta r_{CH}\rangle - \langle\Delta r_{CD}\rangle$. The numbers are of this relative order also for δ and Δ in H_2O.[76] Because of this, the term involving δ in equation (93) is usually much less important than the term involving Δ. It is possible to estimate the secondary shielding derivative S from a measured n-bond isotope shift if the primary shielding derivative P is known from other sources (such as the temperature dependence of shielding) and both Δ and δ are calculated with an adequate force field.

Some secondary derivatives obtained in this way are given in Table 19. We note that these are about one order of magnitude smaller than the values

TABLE 19

Derivatives of nuclear shielding with respect to extension of a remote bond $(\partial\sigma^A/\partial\Delta r_{XY})_e$.

Nucl.	Molecule	r_{XY}	$(\partial\sigma^A/\partial\Delta r_{XY})_e$	Ref.
^{1}H	H_2O	OH′	−4.6	76
	CH_4	CH′	−1.3	35
			−2.6	135
^{19}F	$CFCl_3$	CCl	−70	94
	CHF_3	CH	−84	11
	$S{=}CF_2$	CS	−284	102
	$F_2C{=}CFH$ (*trans*)	CH	−30	148
	(*cis*)	CH	−23	148
	(*gem*)	CH	−78	148
	$F_2C{=}CH_2$ (*trans*)	CH	−47	148
	(*cis*)	CH	−33	148
^{13}C	$H_3C{-}CH_3$	CH	−12.4	140
	$H_2C{=}CH_2$	CH	+5.3	140
	$HC{\equiv}CH$	CH	+12.5	140
^{17}O	UO_2^-	UO′	−300	102

of primary derivatives in Table 18. These secondary derivatives of nuclear shielding correlate with the spin–spin coupling constants over the same bond path. For example, the *cis*, *trans* and *gem* HF coupling constants in trifluoroethene are −2, +10 and +72 Hz respectively, the magnitudes being in the same order as the magnitudes of the secondary derivatives in Table 19. The chemical shifts upon substitution of atoms *cis*, *trans* and *gem* away from the observed nucleus also are in this relative order.[148]

The correlations found between isotope shifts and the spin–spin coupling constants or substituent effects on chemical shifts indicate that the dominating electronic factor in isotope shifts involves the same electronic transmission path. Furthermore, two-bond isotope shifts are found to correlate with the bond length at the substitution site.[134] These imply that the term $S\Delta$ is the one of major importance in determining the isotope shift. This is fortunate, since the secondary dynamic effects are sensitive to the fine details of the force field and require a reasonably good vibrational calculation to get even the sign of δ right. On the other hand, the magnitude of Δ is fairly easy to calculate or estimate as we have seen in Section IV.B. This is of practical importance because this allows the estimation of secondary derivatives $S = (\partial\sigma^A/\partial\Delta r_{XY})_e$ directly from $^n\Delta A(^{m'/m}X)$ knowing only the X–Y bond length and the masses m_Y, m' and m. Like substituent shifts and spin–spin coupling constants, the secondary derivatives of the shielding tell us the extent to which the electron distribution at one point in the molecule

is affected by the perturbations that occur at a remote site. This information is transmitted through bonds and therefore carries information about molecular structure. There are some interesting examples of this. The dihedral angle dependence of the three-bond isotope shift,[149] $^3\Delta^{13}C(^{2/1}H) =$ -0.080 ppm for $\theta \approx 0°$, -0.050 ppm for $\theta \approx 30°$ and $\geqslant -0.020$ ppm for $\theta \approx$ 90°, shows some dependence on proximity, not quite analogous to the Karplus relationship for vicinal coupling across the same electronic transmission path. The two- and three-bond isotope shifts in fluoroethanes show good correlations with couplings across the same transmission path:

$$|^3\Delta_{cis}{}^{19}F(^{2/1}H)| < |^3\Delta_{trans}{}^{19}F(^{2/1}H)| < |^2\Delta_{gem}{}^{19}F(^{2/1}H)|$$

in the same order as $^3J_{cis}(HF)$, $^3J_{trans}(HF)$ and $^2J_{gem}(HF)$ for several compounds,[148] which is also the same ordering as the magnitudes of the ^{19}F substituent shifts.

Long-range isotope shifts are observed in conjugated systems just as are coupling constants and substituent shifts. Some alternation of signs of isotope shifts is observed in such cases, as it is in the coupling over the same π system.[150] The same transmission of electronic information that gives rise to the shielding changes over many bonds in a π system upon chemical substitution also gives rise to the much smaller shielding changes upon isotopic substitution. The efficiency of the transmission of electronic information is indicated by the small secondary derivatives of shielding. These secondary derivatives are not easily calculated with *ab initio* methods since one needs to do calculations on fairly large molecules in order to study long-range effects. However, the semi-empirical methods which have been used for long-range couplings in conjugated systems may suggest a parallel approach for the calculation of secondary derivatives over the same pathways.

In the foregoing we have always implicitly assumed the Born-Oppenheimer approximation, i.e. that the rovibrational averaging occurs in the same potential energy surface and shielding surface for both isotopomers. The interpretation of the isotope shifts in terms of two factors, the dynamic and the electronic factor, is a consequence of the Born-Oppenheimer approximation and is not possible in cases where this separation is not valid, e.g. if Jahn-Teller effects occur. Other properties such as the electric dipole moment of HD or CH_3D are entirely due to a breakdown in the Born-Oppenheimer approximation. Although the observed effect, the chemical shift, is the same as that which would be observed if the hydrogen and the deuterium acted as if their electronegativities were different, it is not necessary to assume this. The NMR isotope shift data which have been reported so far can be interpreted with the foregoing theory without having to assume Born-Oppenheimer breakdown. Thus we would like to discourage the use of terms such as "isotope-induced inductive effect" of a deuterium

relative to a hydrogen,[151] or "hyperconjugation", which have been used in interpretation of some isotope shifts.[152] Both concepts imply that a Born-Oppenheimer breakdown is responsible for the observed isotope shift. In the cases when such models have been applied, the rovibrational averaging model within the context of the Born–Oppenheimer approximation is entirely sufficient.

VI. TEMPERATURE AND SOLVENT EFFECTS ON ISOTOPE SHIFTS

Figures 3 and 4 show that the rovibrationally averaged shielding changes with temperature in a parallel fashion for both isotopomers. Therefore, although the shielding temperature dependence may be large (e.g. it is calculated to be 1.56×10^{-3} ppm deg^{-1} for ^{19}F in HF in the range 100–500 K), the temperature dependence of the isotope shift will be very small, and probably very difficult to measure. In the case of the HD–D$_2$ system, Beckett and Carr[45] observed the temperature dependence of the isotope shift. Since the magnitude of the isotope shift at any one temperature can be used to obtain $(\partial\sigma/\partial\Delta r)_e$, and since this derivative can then be used to predict the temperature dependence of the shielding in both isotopomers, the magnitude and the temperature coefficient of the isotope shift are related to one another. Raynes and Panteli[70] have shown that the temperature dependence observed by Beckett and Carr is consistent in this way with the magnitude of the isotope shift at 300 K.

The temperature dependence of the isotope shift in diatomic molecules (other than H$_2$) is given by equation (40). The temperature dependent factor is $\{\coth(hc\omega/2kT) - (\mu/\mu^*)^{\frac{1}{2}} \coth[hc(\mu/\mu^*)^{\frac{1}{2}}\omega/2kT]\}$. For example, $^1\Delta^{19}$F($^{37/35}$Cl) in ClF has been calculated to be -0.0886 ppm at 300 K. In the temperature range 280–350 K the isotope shift in ClF changes from 1.027 to 0.93 times the value at 300 K.[39] The temperature factor shown above predicts that the magnitude of the isotope shift should decrease with increasing temperature for diatomic molecules. Similar factors for poly-atomic molecules lead to the same prediction for these as well. This temperature dependence has been verified experimentally for $^1\Delta^{19}$F($^{34/32}$S) in SF$_6$ and $^2\Delta^{19}$F($^{34/32}$S) in S=CF$_2$. The isotope shifts are -0.0552 ppm (at 225 K), -0.0530 ppm (at 293 K) for SF$_6$ and -0.0138 ppm (at 210 K) and -0.0119 ppm (at 293 K).[134] Somewhat larger changes have been observed in several other ^{34}S-induced ^{19}F isotope shifts in SOF$_2$, SO$_2$F$_2$, SO$_2$ClF and CF$_3$S(O)F,[134] which could be partly attributed to the larger amplitudes of motion in these fluxional molecules.

When unusual sign and/or unexpectedly large isotope shifts are observed, the possible involvement of chemical or conformational equilibria should

be investigated. These would exhibit temperature dependence and solvent effects which are larger than are normally observed for intrinsic isotope shifts. An example might be the unusual positive isotope shifts of ^{67}Zn in various zinc salts. It has been pointed out that these shifts may be due to solvent dependent equilibrium positions between inner- and outer-sphere complexes. The tendency for a halogen to enter the first coordination sphere is more pronounced in D_2O than in H_2O so the large positive shifts in $ZnBr_2/D_2O$ may be traced to an effective removal of D_2O ligands by bromide.[153] In those cases where conformational or chemical equilibria can be excluded with some certainty, the effects of intermolecular interactions on isotope shifts have been found to be small. For example, a linear density dependence of $^1\Delta^2D(^{2/1}H)$ has been measured in gas samples having densities up to 840 amagat; the magnitude of the isotope shift decreases with increasing density. This observation has been explained as follows:[17]

$$\sigma^{HD}(T, \rho) = \sigma_0^{HD} + \sigma_1^{HD}(T)\rho + \cdots$$
$$\sigma^{D_2}(T, \rho) = \sigma_0^{D_2} + \sigma_1^{D_2}(T)\rho + \cdots$$

$$(94)$$

$(\sigma_0^{D_2} - \sigma_0^{HD})$ is the isotope shift in the zero-pressure limit, and $(\sigma_1^{D_2} - \sigma_1^{HD})$ is the difference in the effects of binary collisions on the two species. Both σ_1 values are expected to be normal (i.e. negative). The greater magnitude of the σ_1 in D_2 molecules interacting with other (D_2 or HD) molecules is due to the more exposed deuterium nucleus in D_2 (where each D is $r_e/2$ from the centre of mass) compared to HD (where the D nucleus is $r_e/3$ from the centre of mass). A calculation using the nuclear site effect model gives -0.049×10^{-4} ppm amagat^{-1} for this difference, which compares favourably with the experimental result which is $-(0.059 \pm 0.026) \times 10^{-4}$ ppm amagat^{-1}. For polyatomic molecules dissolved in a liquid the solvent effect on the isotope shift may be considered in terms of the smaller average volume of a D atom undergoing vibrational averaging; compared to an H atom in the same bond, the solvent molecules can get closer to the D atom. Since differences in site factors are small, the solvent effects on isotope shifts are expected to be small except when specific interactions such as hydrogen bonding are involved. This is very fortunate because this allows the determination of accurate isotope shifts in solution where conditions can be arranged so as to obtain favourable linewidths, as opposed to the very difficult zero-pressure limit measurements.

VII. CONCLUSIONS

We have presented the theoretical basis for isotope shifts in NMR. We find that the theory gives a good account of generally observed trends as well as some of the more specific correlations with electronic structure and

with other molecular properties. In some specific cases in which *ab initio* calculations have been carried out the theory gives semi-quantitative agreement with experiment.

Isotope shifts are due to rovibrational effects and can be described by an electronic factor multiplied by a dynamic factor. The nearly uniform sign (negative) which is observed in one-bond isotope shifts comes from the nearly uniform sign (negative) of the electronic factor (the shielding increases as the bond gets shorter) combined with the widely observed shortening of the average bond length upon heavy isotope substitution.

The dynamic factor depends on the masses of the atoms involved in the bond. It has been possible to express the change in the mean bond length upon isotopic substitution in a simple form depending on the masses of the atoms involved in the bond, so that it becomes possible to estimate the dynamic factor from the bond length. The mass factor confirms the observed dependence of isotope shifts on the fractional change in mass. It favours the observation of isotope shift upon substitution of light atoms while observing heavy nuclei.

Because the dynamic factor is easily estimated, the electronic factor can be directly extracted from the measured isotope shift to a first approximation. Thus the one-bond isotope shift serves as an index of the chemical bond. The correlations of isotope shifts with other properties such as spin–spin coupling, bond order, bond length or electronegativity of substituents are then interpretable as manifestations of the sensitivity of the shielding derivative $(\partial\sigma/\partial\Delta r)_e$ to these chemical parameters.

Based on what we have shown here about the nature of the dynamic and electronic factors, it is possible to predict the order of magnitude of one-bond isotope shifts for any combination of atoms. Thus it is possible to make an *a priori* estimate of the feasibility of observation of one-bond isotope shifts involving any two atoms.

The additivity of isotope shifts has been shown to be due to the additive nature of mean bond length changes and provides an easily recognizable pattern in the spectrum, i.e. equally spaced peaks corresponding to each isotopomer with substitution at equivalent sites.

The isotope shift over more than one bond is interpreted in a similar way. Although there are secondary effects on bond lengths at nuclear sites remote from the substitution site, the important contribution seems to come from the primary change in bond length at the substitution site combined with a secondary electronic factor, the derivative of nuclear shielding with respect to the extension of a remote bond. Thus, with the given estimation methods for the dynamic factor, it is possible to obtain the change in nuclear shielding upon extension of a remote bond to a first approximation. This serves as an index of the electronic transmission path just as the spin–spin

coupling does, and is therefore a useful tool in characterizing molecular electronic structure.

Isotope shifts are thus understood in principle. However, the *ab initio* calculation of long-range isotope shifts has not yet been attempted. A suitable model for estimating the change in shielding upon remote bond extension would be very useful.

The unusual sign of a few one-bond isotope shifts is still to be explained, although some of these can be excluded from consideration because isotopic effects on chemical equilibrium may be involved.

The theoretical model discussed here has also been successfully applied to the primary and secondary effects of isotopic substitution on spin-spin couplings which are reported elsewhere.[154]

ACKNOWLEDGMENT

REFERENCES

1. H. Batiz-Hernandez and R. A. Bernheim, *Progr. NMR Spectrosc.*, 1967, **3**, 63.
2. (a) P. E. Hansen, in *Annual Reports on NMR Spectroscopy*, Vol. 15 (G. A. Webb, ed.), Academic Press, London, 1983, p. 105. (b) D. A. Forsyth, in *Isotopes in Organic Chemistry*, Vol. 6 (E. Buncel and C. C. Lee, eds), Elsevier, Amsterdam, 1984, p. 1.
3. W. Gombler, *J. Am. Chem. Soc.*, 1982, **104**, 6616.
4. H. J. Jakobsen, A. J. Zozulin, P. D. Ellis and J. D. Odom, *J. Magn. Reson.*, 1980, **38**, 219.
5. K. K. Andersson, S. B. Philson and A. B. Hooper, *Proc. Nat. Acad. Sci. USA*, 1982, **79**, 5871.
6. J. M. Risley, S. A. Defrees and R. L. Van Etten, *Org. Magn. Reson.*, 1983, **21**, 28.
7. M. Cohn and A. Hu, *J. Am. Chem. Soc.*, 1980, **102**, 913.
8. C. J. Jameson, in *Specialist Periodical Report on NMR*, Vol. 10 (G. A. Webb, ed.), Royal Society of Chemistry, London, 1981.
9. S. G. Frankiss, *J. Phys. Chem.*, 1963, **67**, 752.
10. R. D. Sammons, P. A. Frey, K. Bruzik and M. D. Tsai, *J. Am. Chem. Soc.*, 1983, **105**, 5455.
11. C. J. Jameson and H. J. Osten, *Mol. Phys.*, in press.
12. J. R. Everett, *Org. Magn. Reson.*, 1982, **19**, 86.
13. C. J. Jameson, *Mol. Phys.*, 1985, **54**, 73.
14. H. J. Osten and C. J. Jameson, *J. Chem. Phys.*, 1985, **82**, 4595.
15. N. F. Ramsey, *Phys. Rev.*, 1952, **87**, 1075.
16. C. J. Jameson, *Bull. Magn. Reson.*, 1980, **3**, 3.
17. C. J. Jameson, A. K. Jameson and D. Oppusunggu, *J. Chem. Phys.*, 1984, **81**, 2313.
18. R. A. Hegstrom, *Phys. Rev. (A)*, 1979, **19**, 17.
19. H. Wind, *J. Chem. Phys.*, 1965, **42**, 2371; **43**, 2956.
20. G. Riley, W. T. Raynes and P. W. Fowler, *Mol. Phys.*, 1979, **38**, 877.
21. P. W. Fowler, *Mol. Phys.*, 1981, **43**, 591.

22. P. W. Fowler, *Mol. Phys.*, 1982, **46**, 913; 1984, **51**, 1423.

23. E. B. Wilson, J. C. Decius and P. C. Cross, *Molecular Vibrations*, McGraw-Hill, New York, 1955.

24. A. R. Hoy, I. M. Mills and G. Strey, *Mol. Phys.*, 1972, **24**, 1265.

25. I. M. Mills, *J. Phys. Chem.*, 1976, **80**, 1187.

26. M. Toyama, T. Oka and Y. Morino, *J. Mol. Spectrosc.*, 1964, **13**, 193.

27. E. B. Wilson and J. B. Howard, *J. Chem. Phys.*, 1936, **4**, 260.

28. H. H. Nielsen, *Rev. Mod. Phys.*, 1951, **23**, 90.

29. G. Amat, H. H. Nielsen and G. Tarrago, *Rotation-Vibration of Polyatomic Molecules*, Dekker, New York, 1971.

30. R. W. James, *Physik. Z.*, 1932, **33**, 737.

31. L. S. Bartell, *J. Chem. Phys.*, 1963, **38**, 1827; 1979, **70**, 4581 (and references cited therein).

32. P. Ehrenfest, *Z. Physik* (Leipzig), 1927, **45**, 455.

33. C. J. Jameson and H. J. Osten, *J. Chem. Phys.*, 1984, **81**, 4915.

34. C. J. Jameson and H. J. Osten, *J. Chem. Phys.*, 1984, **81**, 2556.

35. H. J. Osten and C. J. Jameson, *J. Chem. Phys.*, 1984, **81**, 4288.

36. S. Cyvin, *Molecular Vibration and Mean Square Amplitudes*, Elsevier, Amsterdam, 1968.

37. K. Kuchitsu, in *Molecular Structures and Vibration* (C. J. Cyvin, ed.), Elsevier, Amsterdam, 1972, Ch. 12.

38. P. W. Fowler, private communications.

39. C. J. Jameson, *J. Chem. Phys.*, 1977, **66**, 4983.

40. J. L. Dunham, *Phys. Rev.*, 1932, **41**, 713, 721.

41. R. M. Herman and S. Short, *J. Chem. Phys.*, 1968, **48**, 1266; 1969, **50**, 572.

42. W. T. Raynes, A. M. Davies and D. B. Cook, *Mol. Phys.*, 1971, **21**, 123.

43. R. Ditchfield, *Chem. Phys.*, 1981, **63**, 185.

44. D. F. Evans, *Chem. and Ind.*, 1961, 1960.

45. J. R. Beckett and H. Y. Carr, *Phys. Rev.* (A), 1981, **24**, 144.

46. D. K. Hindermann and C. D. Cornwell, *J. Chem. Phys.*, 1968, **48**, 2017.

47. P. Morse, *Phys. Rev.*, 1929, **34**, 57.

48. A. D. Buckingham and W. Urland, Chem. Rev., 1975, **75**, 113.

49. L. S. Bartell, *J. Chem. Phys.*, 1955, **23**, 1219.

50. R. E. Wasylishen, J. O. Friedrich, S. Mooibroek and J. B. Macdonald, *J. Chem. Phys.*, 1985, **83**, 548.

51. R. M. Stevens and W. N. Lipscomb, *J. Chem. Phys.*, 1964, **40**, 2238.

52. R. M. Stevens and W. N. Lipscomb, *J. Chem. Phys.*, 1964, **41**, 184.

53. R. M. Stevens and M. Karplus, *J. Chem. Phys.*, 1968, **49**, 1094.

54. E. A. Laws, R. M. Stevens and W. N. Lipscomb, *J. Chem. Phys.*, 1971, **54**, 4269.

55. W. T. Raynes and G. Stanney, *J. Magn. Reson.*, 1974, **14**, 378.

56. A. Saika and H. Narumi, *Can. J. Phys.*, 1964, **42**, 1481.

57. C. J. Jameson, *J. Chem. Phys.*, 1977, **66**, 4977.

58. C. J. Jameson and H. J. Osten, *J. Chem. Phys.*, 1984, **81**, 4300. (Erratum: *J. Chem. Phys.*, 1985, **83**, 915.)

59. D. R. Herschbach and V. W. Laurie, *J. Chem. Phys.*, 1961, **35**, 458.

60. I. M. Mills, in *Theoretical Chemistry*, Vol. 1 (R. N. Dixon, ed.), Royal Society of Chemistry, London, 1974, p. 110.

61. C. J. Jameson and A. D. Buckingham, *J. Chem. Phys.*, 1980, **73**, 5684.

62. R. F. W. Bader and A. D. Bandrauk, *J. Chem. Phys.*, 1968, **49**, 1666.

63. W. H. Flygare, *J. Chem. Phys.*, 1964, **41**, 793.

64. N. F. Ramsey, *Phys. Rev.*, 1950, **77**, 567; **78**, 699.

65. J. Verberne, I. Ozier, L. Zandu and J. Reuss, *Mol. Phys.*, 1978, **35**, 1649.

66. D. K. Hindermann and L. L. Williams, *J. Chem. Phys.*, 1969, **50**, 2839.

67. C. J. Jameson, A. K. Jameson, S. Wille and P. M. Burrell, *J. Chem. Phys.*, 1981, **74**, 853.

68. W. T. Raynes and B. P. Chadburn, *J. Magn. Reson.*, 1973, **10**, 218; *Mol. Phys.*, 1972, **24**, 853.
69. R. E. Wasylishen, *Can. J. Chem.*, 1982, **60**, 2194.
70. W. T. Raynes and N. Panteli, *Mol. Phys.*, 1983, **48**, 439.
71. P. W. Fowler, G. Riley and W. T. Raynes, *Mol. Phys.*, 1981, **42**, 1463.
72. W. T. Raynes, in *Specialist Periodical Reports on NMR*, Vol. 7 (R. J. Abraham, ed.), Royal Society of Chemistry, London, 1978, p. 1.
73. R. E. Wasylishen, S. Mooibroek and J. B. Macdonald, *J. Chem. Phys.*, 1984, **81**, 1057.
74. M. Schindler and W. Kutzelnigg, *Mol. Phys.*, 1983, **48**, 781.
75. D. M. Chipman, W. E. Palke and B. Kirtman, *J. Am. Chem. Soc.*, 1980, **102**, 3377.
76. P. W. Fowler and W. T. Raynes, *Mol. Phys.*, 1981, **43**, 65.
77. B. Sredni and S. Pinchas, *J. Magn. Reson.*, 1972, **7**, 289.
78. O. Lutz and H. Oehler, *Z. Naturforsch.*, 1977, **32a**, 136.
79. P. W. Fowler, *Mol. Phys.*, 1983, **48**, 153; V. M. Mamayev and N. M. Sergeyev, *Chem. Phys. Lett.*, 1975, **34**, 317.
80. A. Chedin, *J. Mol. Spectrosc.*, 1979, **76**, 430.
81. Z. Cihla and A. Chedin, *J. Mol. Spectrosc.*, 1971, **40**, 337.
82. I. Suzuki, *J. Mol. Spectrosc.*, 1968, **25**, 479.
83. M. Lacy, *Mol. Phys.*, 1982, **45**, 253.
84. M. Lacy and D. H. Whiffen, *Mol. Phys.*, 1982, **45**, 241.
85. A. Chedin, C. Amiot and Z. Cihla, *J. Mol. Spectrosc.*, 1976, **63**, 348.
86. I. Suzuki, *J. Mol. Spectrosc.*, 1969, **32**, 54.
87. R. J. Mawhorter, M. Fink and B. T. Archer, *J. Chem. Phys.*, 1983, **79**, 170.
88. A. D. Kohl and R. L. Hilderbrandt, *J. Mol. Struct. Theochem.*, 1981, **85**, 325.
89. D. H. Whiffen, *Mol. Phys.*, 1980, **39**, 391.
90. C. J. Jameson and H. J. Osten, *J. Chem. Phys.*, 1984, **81**, 4293.
91. J. L. Duncan, in *Specialist Periodical Reports on Molecular Spectroscopy*, Vol. 3 (R. F. Barrow, D. A. Long and D. J. Millen, eds), Royal Society of Chemistry, London, 1975, p. 104.
92. T. Shimanouchi, *Pure Appl. Chem.*, 1963, **7**, 131.
93. H. C. Urey and C. A. Bradley, *Phys. Rev.*, 1931, **38**, 1969.
94. C. J. Jameson and H. J. Osten, *Mol. Phys.*, 1985, **55**, 383.
95. T. Shimanouchi, *J. Chem. Phys.*, 1949, **17**, 245.
96. K. Kuchitsu and L. S. Bartell, *J. Chem. Phys.*, 1962, **36**, 2460.
97. R. H. Boyd and L. Kesner, *J. Chem. Phys.*, 1980, **72**, 2179.
98. J. Kestin, S. T. Ro and W. Wakeham, *Physica*, 1972, **58**, 165.
99. L. S. Bartell, *J. Chem. Phys.*, 1963, **38**, 1827.
100. L. S. Bartell, S. K. Doun and S. R. Goates, *J. Chem. Phys.*, 1979, **70**, 4585.
101. W. Gombler, *J. Magn. Reson.*, 1982, **53**, 69.
102. H. J. Osten, unpublished calculations.
103. C. J. Jameson, *J. Chem. Phys.*, 1977, **67**, 2814.
104. D. K. Hindermann and C. D. Cornwell, *J. Chem. Phys.*, 1968, **48**, 4148.
105. M. Alei and W. E. Wageman, *J. Chem. Phys.*, 1978, **68**, 783.
106. O. Lutz, D. Nolle and D. Staschewski, *Z. Naturforsch.*, 1978, **38a**, 380.
107. R. E. Wasylishen and J. O. Friedrich, *J. Chem. Phys.*, 1984, **80**, 585.
108. B. E. Smith, B. D. James and R. M. Peachey, *Inorg. Chem.*, 1977, **16**, 2057.
109. W. M. Litchman, M. Alei and A. E. Florin, *J. Chem. Phys.*, 1969, **50**, 1897.
110. A. K. Jameson and C. J. Jameson, *J. Magn. Reson.*, 1978, **32**, 455.
111. M. R. Bendall and D. M. Doddrell, *Austral. J. Chem.*, 1978, **31**, 1141.
112. G. Herzberg, *Infrared and Raman Spectra of Polyatomic Molecules*, Van Nostrand Reinhold, New York, 1945.
113. H. J. Bernstein and A. D. E. Pullin, *J. Chem. Phys.*, 1953, **19**, 1409.

114. D. L. Gray and A. G. Robiette, *Mol. Phys.*, 1979, **37**, 1901.
115. P. Pulay, W. Meyer and J. E. Boggs, *J. Chem. Phys.*, 1978, **68**, 5077.
116. C. R. Lassigne and E. J. Wells, *J. Magn. Reson.*, 1978, **31**, 195.
117. J. Bigeleisen and P. Goldstein, *Z. Naturforsch.*, 1963, **21a**, 205.
118. Y. N. Luzikov and N. M. Sergeyev, *J. Magn. Reson.*, 1984, **60**, 177.
119. C. J. Jameson and H. J. Osten, *J. Am. Chem. Soc.*, 1985, **107**, 4158.
120. M. J. Buckingham, G. E. Hawkes, I. M. Ismail and P. J. Sadler, *J. Chem. Soc., Dalton Trans.*, 1982, 1167.
121. G. Lowe, B. V. L. Potter, B. S. Sproat and W. E. Hull, *J. Chem. Soc., Chem. Commun.*, 1979, 733.
122. C. Roeske, P. Paneth, M. H. O'Leary and W. Reimschussel, *J. Am. Chem. Soc.*, 1985, **107**, 1409.
123. O. Lutz, A. Nolle and P. Kroneck, *Z. Phys.* (A), 1977, **282**, 157.
124. C. J. Jameson and H. S. Gutowsky, *J. Chem. Phys.*, 1964, **40**, 1714.
125. R. G. Barnes and W. V. Smith, *Phys. Rev.*, 1954, **93**, 95.
126. T. A. Carlson, C. C. Lu, T. C. Tucker, C. W. Nestor and F. B. Malik, *Eigenvalues, Radial Expectation Values, and Potentials for Free Atoms from Z = 2 to 126 as calculated from Relativistic Hartree-Fock-Slater Atomic Wave Functions,* Oak Ridge National Laboratory, 1970, pp. 1-29.
127. R. E. Wasylishen, D. H. Muldrew and K. J. Friesen, *J. Magn. Reson.*, 1980, **41**, 341.
128. K. U. Buckler, A. R. Haase, O. Lutz, N. Muller, and A. Nolle, *Z. Naturforsch.*, 1977, **32a**, 126.
129. K. J. Franklin, C. J. L. Lock, G. B. Sayer and G. J. Schrobilgen, *J. Am. Chem. Soc.*, 1982, **104**, 5303.
130. J. Jokisaari and K. Raisanen, *Mol. Phys.*, 1978, **36**, 113.
131. J. Jokisaari, K. Raisanen, L. Lajunen, A. Passoja and P. Pyykko, *J. Magn. Reson.*, 1978, **31**, 121.
132. V. P. Tarasov, V. I. Privalov, Y. A. Buslaev and U. Eichhoff, *Z. Naturforsch.*, 1984, **39b**, 1230.
133. R. J. Gillespie and J. W. Quail, *J. Chem. Phys.*, 1963, **39**, 2555.
134. W. Gombler, *Z. Naturforsch.*, 1985, **40b**, 782.
135. D. B. Chesnut, private communications.
136. M. Schindler and W. Kutzelnigg, *J. Chem. Phys.*, 1982, **76**, 1919.
137. T. Weller, W. Meiler, H. J. Kohler, H. Lischka and R. Holler, *Chem. Phys. Lett.*, 1983, **98**, 541.
138. D. B. Newmann and J. W. Moskowitz, *J. Chem. Phys.*, 1969, **50**, 2216.
139. K. Jackowski and W. T. Raynes, *Mol. Phys.*, 1977, **34**, 465.
140. D. B. Chesnut and A. L. Helms, *Theoret. Chim. Acta* (Berlin), 1981, **58**, 163.
141. J. O. Friedrich and R. E. Wasylishen, *J. Chem. Phys.*, 1985, **83**, 3707.
142. C. J. Jameson, A. K. Jameson, D. Oppusunggu, S. Wille, P. M. Burrell and J. Mason, *J. Chem. Phys.*, 1981, **74**, 81.
143. C. J. Jameson and H. J. Osten, to be published.
144. C. J. Jameson, A. K. Jameson and P. M. Burrell, *J. Chem. Phys.*, 1980, **73**, 6013.
145. C. J. Jameson, A. K. Jameson and J. Honarbakhsh, *J. Chem. Phys.*, 1984, **81**, 5266.
146. C. J. Jameson, *Mol. Phys.*, 1980, **40**, 999.
147. B. T. Hamdi, D. J. Reynolds and G. A. Webb, *Org. Magn. Reson.*, 1984, **22**, 90.
148. H. J. Osten, C. J. Jameson and N. C. Craig, *J. Chem. Phys.*, 1985, **83**, 5434.
149. J. L. Jurlina and J. B. Stothers, *J. Am. Chem. Soc.*, 1982, **104**, 4677.
150. S. Berger and H. Kunzer, *Angew. Chem. Int. Ed. Engl.*, 1983, **22**, 321.
151. K. L. Servis and F. F. Shue, *J. Am. Chem. Soc.*, 1980, **102**, 7233.
152. J. R. Wesener and H. Gunther, *Tetrahedron Lett.*, 1982, **23**, 2845.
153. D. Rehder, *Magn. Reson. Rev.*, 1984, **91**, 125.
154. C. J. Jameson and H. J. Osten, *J. Am. Chem. Soc.*, in press.

NMR Spectroscopy of
Paramagnetic Haem Proteins

JAMES D. SATTERLEE

Department of Chemistry, University of New Mexico, Albuquerque, New Mexico, USA

I. INTRODUCTION

A. General remarks

In this report I have endeavoured to cover the years 1978–1984. This period has witnessed many important developments in the application of nuclear magnetic resonance spectroscopy to studies of paramagnetic haem proteins. Fundamental to this information explosion have been methodology developments that currently allow unequivocal resonance assignments. It has been well recognized that such assignments are required before detailed informa-

tion about three-dimensional solution structure and function can be routinely obtained. Consequently, much of this report concerns the methods that have been utilized to make unambiguous resonance assignments. In cases where these are made, NMR provides a unique window into the molecular basis of structure and dynamics.

For the most part this report concerns the proton NMR spectroscopy of haem proteins in solution. As a nucleus, protons have been the most widely used, although brief sections on carbon-13 and nitrogen-15 are included. For many well known reasons these latter nuclei are employed to a lesser extent than protons. Furthermore, the porphyrin ring of the various haem prosthetic groups, as well as the iron ion axial ligands, possess several protons which are easily identified and frequently occur in spectral windows away from the crowded region of 0–10 ppm that contains the many overlapping resonances of the polypeptide protons. These hyperfine shifts are unique to paramagnetic metalloproteins and I hope that this report will successfully describe how the structural elements of the haem crevice, combined with studies employing hyperfine shifts, can yield extremely detailed information.

It is not intended that this report should be exhaustive although I have endeavoured to include many pertinent references. I apologize in advance to any authors who may feel slighted by my treatment of their work. I assure them that this was unintentional on my part.

There have been several reviews written recently on topics that are related to this review,[1-4] and there is a recently published treatise that provides an excellent description of NMR methods applied to biological molecules.[5] Although the book by Jardetzky and Roberts does not explicitly treat paramagnetic haem proteins in detail, it provides interesting chapters on both intrinsic and extrinsic paramagnetic effects in biomolecules and gives excellent descriptions of techniques applied to many proteins.

B. Haem structures

Many of the properties of paramagnetic haem proteins depend upon the status of haem iron ion coordination. The most frequently encountered haem coordination structures in proteins are depicted in Fig. 1. This figure serves to define the porphyrin ring numbering system that is used, as well as the designation for the coordinated histidine and methionine ligands. It is useful to note that a biological naming system for these axial ligands is employed here. Thus, in histidine C_α is the proton-bearing carbon atom of the polypeptide chain and C_β is the next side chain carbon. The imidazole ring continues to be labelled in this manner with C_γ being the quaternary carbon which is bonded to C_δ and N_δ. It is this nitrogen that normally carries the proton. In the recent literature this position has been labelled

variously as N_ε or N_1. Finally, the imidazole ring is closed by N_ε and $C_{\varepsilon'}$. In this labelling scheme N_ε is the nitrogen that coordinates to the haem iron in the so-called proximal histidine. In haemoglobins and myoglobins this proximal histidine occurs in the primary sequence at position F-8. The imidazole C_ε has been named C_2 in the recent literature and C_δ has been called C_4.

The coordination structures and oxidation states that one normally encounters in haem proteins are indicated in Fig. 1 and Fig. 2. In haemoglobins the naturally occurring iron ion oxidation state is ferrous (Fe^{2+}). When the protein is in the deoxygenated form (deoxy) the iron ion is in a high spin state, with four unpaired electrons (Fig. 2B). This is characteristic of deoxy haemoglobins, deoxy myoglobin and certain other reduced proteins such as reduced horseradish peroxidase. The haem coordination structure can be presumed to include the four haem pyrrole nitrogens and the proximal histidine N_ε (Fig. 1A). This is nominally a 5-coordinate state, although a water molecule may occupy the sixth coordination position in some proteins. Water is a very weak field ligand, so regardless of its presence or absence (6-coordinate or 5-coordinate) the protein is in a high spin state. In deoxy haemoglobins and myoglobins the iron does not lie within a plane defined by the haem pyrrole nitrogens but projects out of the haem plane toward the proximal histidine. Although usually not as pronounced, the ferric (Fe^{3+}) oxidation state of most haem proteins also exhibits this out-of-plane displacement in the unligated (5-coordinate) state. For most of these "met" haem proteins there is evidence both for and against the claim that water occupies a position in the haem iron coordination sphere in the unligated state.

The high spin deoxy (ferrous forms), or unligated (ferric forms) states occur primarily for b-type haem proteins that have as their function ligand binding. These proteins are those that contain protohaem IX as their prosthetic group (Fig. 1A) in contrast to the c-type haem proteins (Fig. 1D) whose prosthetic group is covalently linked to the polypeptide chain via thioether bridges at haem positions 2 and 4. These same positions are occupied by vinyl groups in protohaem IX. Consequently, the removal of haems from b-type haem proteins to form the apo-protein is facile, as is the reconstitution of apo-globins with modified haems. The more common modified haems, which are derivatives of protohaem IX, that have been used in protein studies are shown in Fig. 3. In contrast, removal of haem c from its protein matrix is much harder and more complicated.

The ligated, 6-coordinate state appears in ferrous, ferric and ferryl forms of haem proteins. Crystallographic data reveal that in this type of structure the iron ion lies in the plane of the porphyrin ring. Neglecting the fact that the ligands are different, the local structure is best described by the structure that an octahedrally coordinated iron ion would have, albeit with different
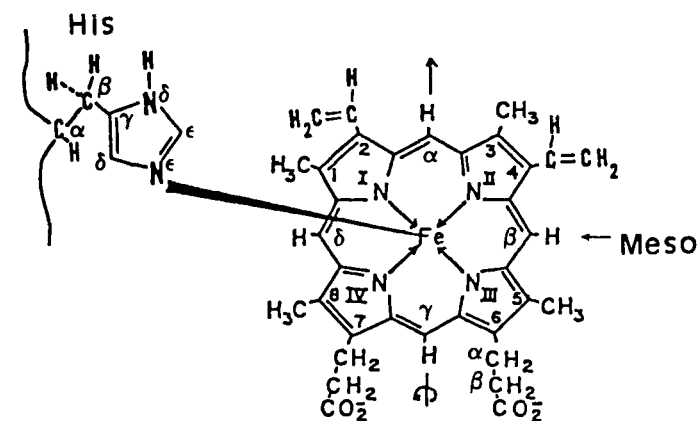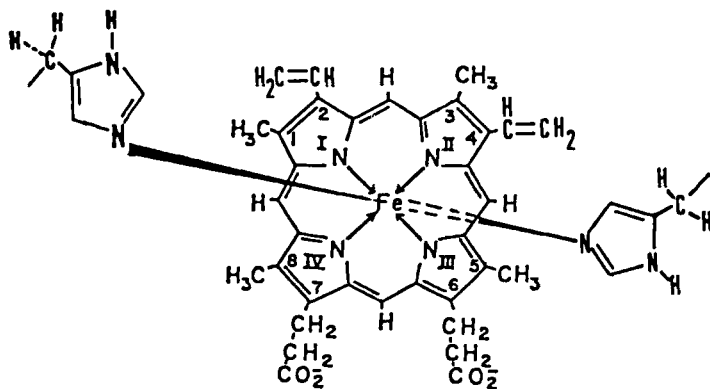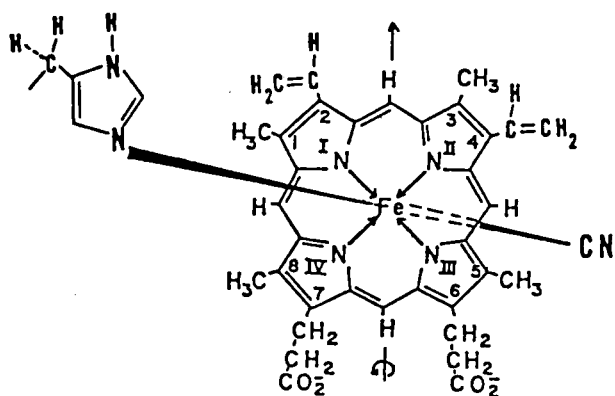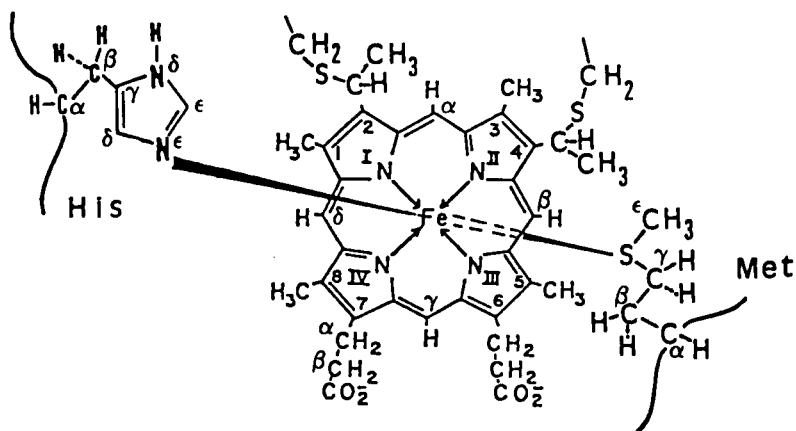
FIG. 1. Ligation states of the haem in various types of haem proteins. (A) high spin 5- or 6-coordinate native CcP, HRP, met-Mb, deoxy Hb, Mb; (B) b-type cytochromes; (C) CcP-CN, HRP-CN, met-Mb-CN, met-Hb-CN; (D) c-type cytochromes.
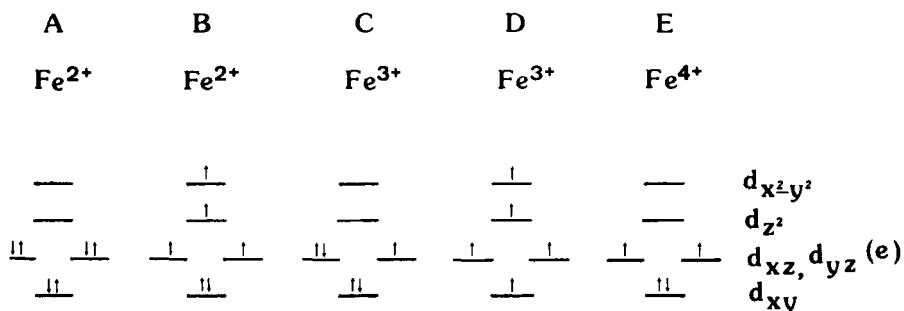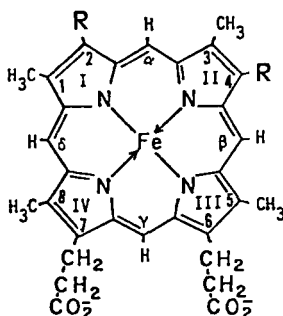
C

D

A	B	C	D	E	
Fe^{2+}	Fe^{2+}	Fe^{3+}	Fe^{3+}	Fe^{4+}	

$$d_{x^2-y^2}$$
$$d_{z^2}$$
$$d_{xz}, d_{yz} \; (e)$$
$$d_{xy}$$

FIG. 2.

FIG. 3.

2,4-R	Name
vinyl	protohaem IX
ethyl	mesohaem IX
proton	deuterohaem IX
2-proton	pemptohaem
4-vinyl	
2-vinyl	isopemptohaem
4-proton	

ligands. In the case of ferrous haemoglobins and myoglobins that have bound oxygen this structure is termed the oxy state. It is a diamagnetic haem form. Carbon monoxide also binds to ferrous haem proteins to yield 6-coordinate diamagnetic forms (Fig. 2A). This transition from unligated to ligated forms is accompanied by movement of the iron ion into the haem plane. In the case of oxygen binding to tetrameric haemoglobins this movement has been thought to be part of the allosteric "trigger" mechanism that results in the haemoglobin quaternary structure change from the T (tensed, deoxy) to the R (relaxed, oxy) state. In tetrameric ferric haemoglobins similar structural changes accompany ligation that involves iron

ion spin state changes. Ferric haem ligands such as azide and cyanide ions cause such changes.

In high spin, unligated ferric haem proteins (unligated form) a symmetric electronic ground state occurs for the haem iron(III) ion (Fig. 2D). This structure is typical for native haem peroxidase enzymes such as cytochrome *c* peroxidase (CcP) and horseradish peroxidase (HRP). Unligated, oxidized haemoglobins and myoglobins also have this type of structure. Upon binding a strong field ligand, such as cyanide ion, a ferric protein is converted to the low spin state. This electronic state has only a single unpaired electron as shown in Fig. 2C. The structure shown in Fig. 1B indicates that similar 6-coordination occurs naturally for b-type cytochromes. In this class of haem enzymes the imidazole rings of two histidines coordinate at the axial ligand positions. Similar 6-coordination occurs naturally for the c-type cytochromes. In this case nature has provided a histidine and a methionine (sulphur coordination) as the axial haem ligands. It should be pointed out that the axial ligands, in both of these cases, enforce the low spin state. Thus reduced, ferrocytochrome *c* is a diamagnetic molecule.

For ferric proteins capable of ligand binding, several types of ions are capable of being bound at the sixth coordination site, yet do not produce sufficiently strong ligand fields to convert the haem iron completely to the low spin state. These intermediate or mixed spin states are induced by such ions as OCN^-, SCN^-, N_3^- and OH^-. An excellent example of this is met-myoglobin hydroxide, which occurs in high pH solutions of the protein. The magnetic properties of this form reveal a reduction in magnetic moment which may be interpreted as one-third of the haem population existing in the low spin state. Current reviews exist that discuss the concept of intermediate spin porphyrin systems and their origin.[3,6,7]

One other structure is important in studies of haem proteins. For the haem peroxidases, which have come under scrutiny in recent years, the ferryl structure, consisting of haem iron formally oxidized to the +4 state and coordinated to any oxygen atom, is characteristic of the oxidized intermediates of these enzymes. For example, the hydrogen peroxide combination with horseradish peroxidase results in oxidation of the protein to Compound I, formally 2 equivalents above the ground state resting enzyme (ferric state). One-electron reduction of Compound I brings the protein into Compound II, oxidized 1 equivalent above the resting enzyme. Mössbauer data indicate similar iron electronic states for both Compound I and Compound II. Magnetic susceptibility studies indicate a triplet ground state ($S = 1$) for Compound II. Consequently, it may be concluded that the electronic structure for these two oxidized intermediates is as depicted in Fig. 2E. Similar, but not identical, oxidized intermediates are formed as a result of the hydrogen peroxide oxidation of cytochrome *c* peroxidase.

Besides the immediate coordination sphere of the haem there are other features of the haem crevice that have been considered to be important to protein function. Overall structural differences in the protein, that is, structural comparisons of cytochromes, peroxidases and haem-globins, particularly in the haem crevice, are undoubtedly relevant to a protein's function. Knowledge of the three-dimensional structure of proteins of interest is important to understanding articles such as this and those cited herein. Whereas structural comparisons are outside the scope of this book the reader is referred to two books containing extensive structure graphics,[8,9] in addition to the original literature.

These sources show that for b-type, ligand binding haem proteins several amino acids on the ligand binding side of the haem plane are situated in positions to affect ligand binding. The haem ligand binding site, on the distal side of the haem, is bordered by the E helix of the polypeptide chain in haemoglobins and myoglobins. Several amino acid side chains extend from the E helix toward the ligand binding site. For example, histidine E-7, the distal histidine (as opposed tö the proximal histidine that coordinates the iron ion), and valine E-11 occur in this structural region in normal mammalian myoglobins and haemoglobins. Other haem proteins have similar distal amino acids. In addition to the distal amino acids there are many possible haem contacts with amino acid side chains. Notable among these is the phenylalanine CD-1 that occurs in human haemoglobin subunits and in myoglobin. It is noted from the structures that this residue is positioned on the distal side of the haem so that the plane of its aromatic ring lies coplanar to the porphyrin ring.[8,9] This geometry has suggested the possibility of $\pi-\pi$ interactions. Similarly in myoglobin, histidine FG_2 appears on the proximal side of the haem and lies approximately parallel to it. These are two specific haem–protein contacts that are important to the information that follows; however, many such contacts occur.

C. Paramagnetic shifts

A paramagnetic haem iron ion has a dramatic influence on the NMR spectrum of a haem protein. The unpaired electron spins possess large individual magnetic moments which result in large magnetic fields at nearby nuclei. Consequently, the observed shifts for protons in the vicinity of a paramagnetic ion are quite large. In paramagnetic haem proteins observed proton shifts may range up to 150 ppm to high frequency and up to as much as 70 ppm to low frequency from a diamagnetic reference. Carbon shifts are much larger and an observed shift range of approximately 2500 ppm has been observed for ferric porphyrin complexes and met-haem proteins. Nitrogen shifts are somewhat smaller, with a range of about 1300 ppm having been observed. The theory that accounts for these large shifts has

been described in detail[10] and the essentials have been previously reviewed.[3,4,5,11] Recently, the current theory has been critically reviewed.[5] The conclusion that remains is that, although the present theory is complicated and rather unsuccessful in precisely calculating the observed shifts, it is very useful for understanding the source of interactions between nuclei and hyperfine fields in paramagnetic molecules. In fact, for highly symmetrical ferric porphyrins great insight into bonding effects has been the direct result of NMR experiments interpreted in terms of existing theory.[3,4,11] With the assumptions that the unsymmetrical natural porphyrins, even when included in the protein, behave in a fundamentally similar manner to the ferric porphyrin models, great insight can be gained concerning a haem protein's solution structure and function.

Given a firm realization of the limitations and approximations inherent in describing the paramagnetic shift phenomenon, it will be of value to describe the salient features for purposes of understanding later parts of this article. There are two contributions to the paramagnetic shift (hyperfine shift, isotropic shift), the contact and dipolar (pseudocontact) terms.

$$\delta_{para} = \delta_{con} + \delta_{dip} \tag{1}$$

Thus, the paramagnetic shift is seen to be the difference between the shift of a given nucleus in the paramagnetic molecule and its shift in a diamagnetic molecule of the same structure. Frequently, in ferric porphyrin and met-haem protein work the paramagnetic shifts have been reported for haem ring protons. In these cases the diamagnetic reference has been the zinc porphyrin.[11] In terms of the observed resonance shifts, which are now most frequently reported, there are both diamagnetic and paramagnetic contributions.

$$\delta_{obs} = \delta_{dia} + \delta_{para} \tag{2}$$

The contact shift (δ_{con}) has as its origin scalar coupling between electron spins and a given nucleus. In the most general case Kurland and McGarvey derived an expression for the contact shift in terms of the principal components of the electron g tensor (g_{ii}) and the molecular magnetic susceptibility tensor (χ_{ii}):[12]

$$\left(\frac{\Delta B}{B_0}\right)^{con} = -\frac{A}{3\gamma_N \hbar}\left[\frac{\chi_{xx}}{g_{xx}} + \frac{\chi_{yy}}{g_{yy}} + \frac{\chi_{zz}}{g_{zz}}\right] \tag{3}$$

In this equation $\Delta B/B_0$ represents the part of the observed shift, as a function of the applied magnetic field B_0, that is due to the contact interaction. In the case where a single spin level with an isotropic g tensor is populated, and in the limit of validity of the Curie law, this equation reduces to the simpler form generally applied to iron porphyrins:[4,5,11-13]

$$(\Delta B/B_0)^{con} = -Ag\beta S(S+1)/3\gamma_N \hbar kT \tag{4}$$

where A, the scalar, or hyperfine coupling, appears in these equations as a result of the scalar coupling, g is the electronic g factor, S is the total electron spin quantum number, and γ_N is the nuclear gyromagnetic ratio. The basis for interpreting the contact contribution, to the observed shift, in terms of metal ligand covalency originates in a relationship derived by McConnell[14] that relates A_H, the hyperfine coupling between a free radical and a proton on an aromatic fragment, to the unpaired spin density of the electron at the carbon to which the proton is attached, ρ_c:

$$A_H = Q\rho_c/2S \qquad (5)$$

Q is a constant (-63 MHz) for a given type of proton and strictly speaking must be evaluated independently for different aromatic systems. However, the greatest usefulness for equation (5) in ferric porphyrin systems has been due to the qualitative predictions that can be made rather than quantitative calculations. In this respect, the fact that Q has a negative value for protons directly attached to aromatic carbons indicates that positive π orbital spin density at the aromatic carbon results in low frequency proton shifts. Q for methyl groups attached to aromatic fragments is positive and not quite a constant, even for closely related structures, and high frequency shifts are predicted for protons of a methyl group attached to an aromatic carbon possessing positive unpaired electron spin density in a π type orbital. The value of equation (5) is its prediction that substitution of a methyl group by a proton (or vice versa) on the porphyrin ring will yield observed single proton and methyl group shifts of opposite direction and of approximately equal magnitude[11] *if* the unpaired spin density that is delocalized in the porphyrin molecular orbitals is predominantly of π nature.

In the case where unpaired electrons incompletely fill only π type iron d orbitals, populating these by both unpaired electrons and holes, π type delocalization of unpaired spin density can occur (low spin Fe^{3+}; Fig. 2). In principle for iron porphyrins both ligand-to-metal and metal-to-ligand charge transfer can occur. It is important to note that two e-type porphyrin-centred π molecular orbitals are of appropriate energy to interact with the iron ion e-type d orbitals (d_{xz}, d_{yz}). The $3e(\pi)$ is the highest filled porphyrin orbital. As a result, metal ligand covalency involving this orbital is of the ligand-to-metal charge transfer type. The $4e(\pi^*)$ is the lowest lying unfilled π molecular orbital on the porphyrin and would be involved in metal-to-ligand charge transfer. Because these two porphyrin centred molecular orbitals involve differing electron densities at different carbon positions on the porphyrin ring, the pattern of proton and carbon contact shifts, in principle, can be used to identify the symmetry properties of the π type orbital that contains the unpaired spin density.[11] In reality magnetic anisotropy occurs in low spin ferric haems, so the observed paramagnetic shifts are not entirely contact in origin. Consequently, any analysis must

involve separating the magnitudes of both dipolar and contact contributions to the observed shifts, so that the contact shift pattern alone may be analysed.

High spin ferric ions possess a totally symmetric electronic ground state (^6A) with an isotropic g tensor. Thus, to a first approximation the dipolar shift is zero, leaving only the contact shift to account for the observed spectra. Evidence for both σ and π delocalization mechanisms has been presented in studies of high spin ferric porphyrins.[11] Moreover, the neglect of dipolar shifts in high spin ferric systems is not strictly correct. Theory reveals that dipolar shifts can, in fact, result as a consequence of anisotropy in the zero field splitting,[10,12] although the magnitude of the dipolar shift contribution may be quite small in comparison with the contact shift contribution.

The dipolar, or pseudocontact, contribution to the paramagnetic shift results from through-space dipole coupling of the nuclear and electron magnetic moments. For carbon a term that is ligand centred must be added to the metal centred terms that are given in the following equations. The general equation is[10]

$$\left(\frac{\Delta B}{B_0}\right)^{\text{dip}} = -\tfrac{1}{2}\left\{[\chi_{zz} - \tfrac{1}{2}(\chi_{xx} + \chi_{yy})]\left(\frac{3\cos^2\theta - 1}{r^3}\right)\right.$$

$$\left. + \tfrac{1}{2}(\chi_{xx} - \chi_{yy})\left(a\frac{\sin^2\theta\cos 2\Omega}{r^3}\right)\right\} \tag{6}$$

where r is the metal-nucleus distance vector and the first and second terms in parentheses are the axial and rhombic geometric factors. The angles θ and Ω are, respectively, the angle between r and the z-axis of the molecule (frequently the principal symmetry axis) and the angle described by the projection of r on the x,y-plane and the x-axis. For metal porphyrins the z-axis is commonly the axis perpendicular to the haem plane (at least to a first approximation) and in proteins may include the iron–proximal histidine bond. With several simplifying assumptions that are generally not valid for either iron porphyrins, or haem proteins, equation (6) can be expressed as

$$\left(\frac{\Delta B}{B_0}\right)^{\text{dip}} = -\frac{\beta^2 S(S+1)}{9kT}(g_\parallel{}^2 - g_\perp{}^2)\langle[3\cos^2\theta - 1]/r^3\rangle \tag{7}$$

In particular, this equation is valid only for a single spin and in a molecule with axial symmetry. In fact, low spin ferric haem proteins exhibit highly anisotropic g tensors. For example, ferric cytochrome c from horse heart[7,5] yields $g_1 = 1.24$, $g_2 = 2.24$, $g_3 = 3.06$. As indicated later, knowledge of the magnitude of the dipolar shift and the three-dimensional structure of a protein can permit determination of the magnetic anisotropy.

In summary, it can be stated that, although the theoretical description of paramagnetic shifts is not good enough to permit quantitative calculations, the trends that these equations predict have been extremely useful in deriving information from both ferric porphyrins and haem proteins. Crucial to intepretations of haem protein data in these terms is the observation that a great amount of data indicate comparable shift contributions to corresponding protons in complexes of natural and synthetic porphyrins with identical axial ligands.[4,12] This provides a foundation for interpreting haem protein NMR spectra.

It is important to note that the explicit form of the observed shift includes the inverse temperature (equations (4) and (7)). For paramagnetic haem proteins the observed shifts are temperature dependent, a fact that can be used to advantage when resonances overlap. Obtaining spectra at different temperatures may improve resolution. One must also keep in mind the importance of reporting the temperature at which spectra are taken when studying paramagnetic haem proteins.

D. Paramagnetic effects on relaxation

The effect of paramagnetic centres on the relaxation times of neighbouring nuclei is to shorten the observed T_1 and T_2 severely. This enhancement of the relaxation rates (T_1^{-1}, T_2^{-1}) is described by two factors: (i) instantaneous dipole–dipole coupling between nuclei and unpaired electrons; (ii) hyperfine exchange coupling via the contact interaction. These two mechanisms are accounted for[17,18] by equations (8) and (9). The correlation times τ_c and τ_e for the

$$\frac{1}{T_{1,M}} = \frac{2}{15} \frac{\gamma_I^2 g^2 S(S+1)}{r^6} \left(\frac{3\tau_c}{1+\omega_I^2\tau_c^2} + \frac{7\tau_c}{1+\omega_S^2\tau_c^2} \right)$$

$$+ \frac{2}{3} S(S+1) \left(\frac{A}{\hbar} \right)^2 \left(\frac{\tau_e}{1+\omega_S^2\tau_e^2} \right) \tag{8}$$

$$\frac{1}{T_{2,M}} = \frac{1}{15} \frac{\gamma_I^2 g^2 S(S+1)\beta^2}{r^6} \left(4\tau_c + \frac{3\tau_c}{1+\omega_I^2\tau_c^2} + \frac{13\tau_c}{1+\omega_S^2\tau_c^2} \right)$$

$$+ \frac{1}{3} S(S+1) \left(\frac{A}{\hbar} \right)^2 \left(\frac{\tau_e}{1+\omega_S^2\tau_e^2} + \tau_e \right) \tag{9}$$

fluctuations of the coupled magnetic moment vectors due to the dipolar (first term) and scalar (second term)interaction are generally considered to consist of several components. These include the rotational correlation time (τ_r) for molecular tumbling and the electron spin–lattice relaxation time (T_{1e}) as well as exchange correlation times when chemical exchange is important. In these equations g is the electronic g factor of the ion, γ_I is

the nuclear gyromagnetic ratio, ω_S and ω_I are the electron and nuclear Larmor frequencies (respectively), S is the total electron spin quantum number and A is the scalar (hyperfine) coupling.

A simple equation is obtained when several restrictive approximations are made, including isotropic dipolar coupling and the fact that T_{1e} dominates τ_c and τ_e. The relative merits of making these assumptions have been discussed;[4,5,11,16] however, for the purposes of this discussion the form of the equations is of primary importance. The simpler equations (10) are given in the fast motion limit; the important feature relative to the subsequent discussion is the r^6 dependence of T_1.

$$T_{1N}^{-1}, T_{2N}^{-2} = \tfrac{4}{3}[S(S+1)g^2\beta^2\gamma_N^2/r^6]\tau_c + \tfrac{2}{3}S(S+1)(A/\hbar)^2\tau_e \quad (10)$$

An additional term contributes significantly to T_2^{-1} and therefore the observed linewidth. This term involves molecular tumbling modulation of the dipolar interaction between nuclear moments and the thermally averaged electron spin magnetic moment.[19,20] Under the same conditions as equation (10) the expression for this "Curie spin" contribution is defined by equation (11).

$$T_2^{-1} = \left[\frac{4\gamma_I^2\mu_S^4B_0^2}{45r^6(kT)^2}\right]\tau_r \quad (11)$$

For several cases the dipolar term in the relaxation equations dominates. This is true for both T_1^{-1} and T_2^{-1}. However, for large proteins that are rotating slowly ($\tau_r \approx 10^{-8}$ s) the Curie spin mechanism becomes important, especially at the higher fields now in common use for protein studies (4–11 Tesla). A description of the experimental detection of Curie spin line broadening is presented later.

The presence of a Curie spin effect may complicate the assignment of protons in low spin ferric complexes when the relaxation method is being employed. When the magnitude of the Curie spin effect can be eliminated by using low fields, or factored out by measuring linewidths at several applied fields, spin–lattice relaxation times can still profitably be used for assignments. Acknowledging the assumptions inherent in using equation (10) the ratio of T_1 values measured for any two nuclei in a molecule can be related to the ratio of the sixth power of their distances from the paramagnetic centre.[4,11] Given a value for one of the distances allows evaluation of the second distance. In this manner known structures for haems and haem proteins can frequently be used to assign unknown resonances. The haem methyl groups, with known (fixed) distances from the iron centre, are often used for the reference T_1 and r^{-6}. This method has been useful in making resonance assignments for the proximal and distal histidine protons in haem proteins. As mentioned above, the utility of these general equations for interpreting data has been most frequently used in proton

NMR spectroscopy. Slight modifications may be required when data from other nuclei are to be analysed. The requirement that ligand centred effects be considered for interpretation of ^{13}C data is an example.

E. Proton spectra

The magnitude of shifts encountered for ferric haem proteins is indicated in Fig. 4. This figure is a result of our work on the cytochrome c peroxidase: cytochrome c redox complex. Both proteins are in ferric states, but
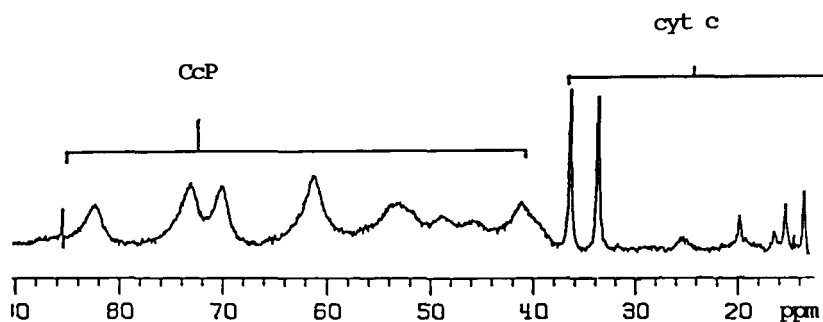

FIG. 4. High frequency region of the proton spectrum of a mixture of cytochrome c peroxidase and cytochrome c. The solution is 2.0 mM in each protein, 0.3 M KNO_3, pD = 6.8, 22 °C. Spectrum is taken at 360 MHz.

the peroxidase is high spin and cytochrome c is low spin. The shift equations indicate a proportionality to the quantity $S(S+1)$ and consequently to the paramagnetic moment of the iron centre through the relationship.

$$\chi_{ii} = \frac{g_{ii}^2 \beta^2 S(S+1)}{3kT} \tag{12}$$

Even with this rather simple picture it is obvious that larger shifts should appear for spin states with larger numbers of unpaired electrons. That is demonstrated for this spectrum by the known assignments of the peroxidase resonances which are broader and shifted further to high frequency. The assigned cytochrome c resonances exhibit smaller shifts.

From many porphyrin model studies and assignments made in haem proteins some generalizations emerge concerning the shift ranges exhibited by haem substituents in different spin and oxidation states. In high spin ferric states of haem proteins the haem methyls (pyrrole substituents) generally occur in the high frequency region, 50–90 ppm, whereas single protons of the haem pyrroles (vinyl H_α, propionic acid H_α) occur in the

area of 30–60 ppm to high frequency. The vinyl H_β protons occur to low frequency. The proximal histidine $N_\delta H$ occurs in the region 90–120 ppm. The ranges are approximate and show some variation if the haem group is not protohaem IX.

In low spin ferric haem proteins the haem methyls occur between 0 and 40 ppm to high frequency, with one or two usually occurring in the region 20–40 ppm. In cyanide complexes of smaller proteins one can generally resolve three of the four haem methyl groups. Single protons of the haem pyrrole substituents exhibit shifts further to low frequency from the methyls, but due to the dipolar (pseudocontact) shift resonances attributable to the protons of neighbouring amino acids may also occur in the range 10–30 ppm. Again, haem vinyl H_α resonances occur to high frequency whereas H_β resonances occur to low frequency. For c-type cytochromes the coordinated methionine methyl group lies in the range −15 to −30 ppm. Several other methionine single protons lie to low frequency but with smaller shifts. In deuteriohaemin reconstituted, cyanide ligated ferric b-type proteins ($S = 1/2$) the 2,4-H haem pyrrole resonances lie characteristically to low frequency as far as 30 ppm.

For the ferrous high spin case ($S = 2$) very small shifts are observed for the haem substituents[3,4,11] with haem methyl resonances in the low frequency region 5–20 ppm. In deuteriohaemin reconstituted proteins the pyrrole 2,4-H resonances occur in the region 40–70 ppm. In 90% H_2O solutions where exchangeable protons are seen the proximal histidine proton resonances occur in the range 50–75 ppm.

These shift ranges are only guidelines to serve as a first introduction to the correlation of observed shift positions with spin and oxidation state. For the purposes of this report many types of shifts appear in the tables that follow. For protons all of them are reported relative to 2,2-dimethyl-2-silapentane-5-sulphonate (DSS). For ^{13}C and ^{15}N the references employed are stated in the tables. High frequency shifts are taken as positive. In some instances authors have not reported the shifts for spectra that they present. Consequently, the shifts have been estimated from published spectra using various measuring devices. Errors are expected to be less than 0.5 ppm in such cases.

II. ASSIGNMENT METHODS

A. General

Achieving unambiguous resonance assignments is the prerequisite to realizing the full power of NMR in spectroscopic studies of haem proteins. Although there are some aspects of the solution behaviour of these proteins that can be studied in the absence of assignments, when specific resonance

assignments can be made for a given protein a barrier to detailed understanding of the molecular level events accompanying the protein's function is surmounted.

Specific deuterium labelling of protohaem IX and subsequent reconstitution into b-type haem proteins has become the most reliable and best used method for making unambiguous assignments of haem protons. The synthetic work of G. W. Kenner, Kevin Smith and their co-workers stands as a monument to great effort that has borne significant results in this regard. Without this pioneering synthetic work[21-30] the great expansion in our understanding of haem protein function that has taken place since 1978 would have been virtually impossible.

Prior to the use of isotopically enriched haems, model systems played a major role in interpreting haem protein NMR spectra. This aspect has recently been reviewed.[4] Illustrative of this method is the vinyl proton assignment made in met-myoglobin cyanide, which is based on the Curie behaviour of the spectrum of low spin ferric porphyrin models.[31,32] Two other methods, useful for resonance assignments, are discussed in the following sections. As for the use of model systems, employing nuclear Overhauser effects (NOE) and calculations based upon the current theory of the origin of paramagnetic shifts, each may be helpful when isotopically enriched porphyrins are unavailable, or for other reasons may not be employed.

B. Resonance assignments using deuterium labelled protohaem IX

Reconstituting b-type haem proteins with specifically deuteriated protohaem IX is relatively easy and the procedures are well known. Such a procedure leads to unambiguous resonance assignments; however, it is important to determine whether reconstitution procedures produce spectroscopically indistinguishable results compared to the native protein. This method has been used in making assignments in high spin ferric proteins such as met-myoglobin (Figs 5-7, Table 1) and peroxidases (Figs 8-13, Tables 2, 3). As described above, the ferric high spin proteins demonstrate large paramagnetic shifts of protons belonging to the haem group. Consequently, unambiguous assignments can be made for all haem methyl groups, most vinyl protons and, in fortuitous cases, the meso protons, as illustrated in Figs 5-13 and Tables 1-3.[33-37]

In the ligated forms of ferric haem proteins the degree of paramagnetism attributable to the haem centre varies with the strength of the axial ligand field (see above). Figure 14 shows the effectiveness of making haem methyl assignments in thiocyanate ligated met-myoglobin[36] whereas Figs 15 and 16 indicate assignments in cytochrome c peroxidase-azide.[37]
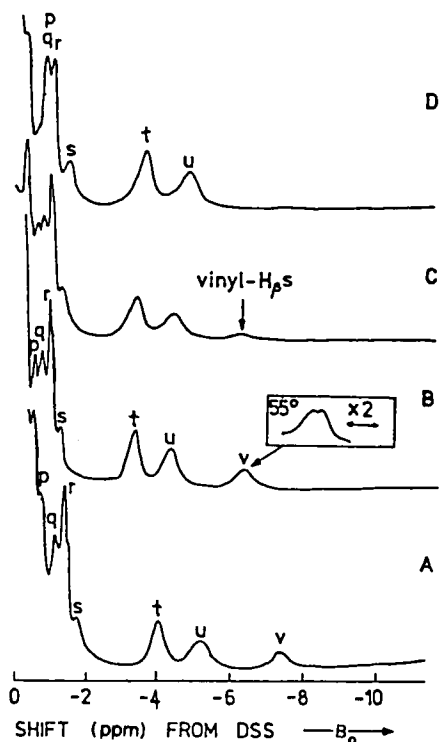
FIG. 5. 360 MHz ^{1}H NMR traces of the region 0-10 ppm to low frequency of DSS, of 2 mM protein solutions in 0.2 M NaCl in ^2H_2O, at p^{2}H 6.2 of: (A) met-Mb-^2H_2O at 25 °C; (B) met Mb-^2H_2O at 45 °C (the inset is peak v at 55 °C); (C) met-Mb-^2H_2O reconstituted with [2,4-($^2H_\beta$)$_4$]haemin at 45 °C; (D) deut-met-Mb-^2H_2O at 45 °C. The peaks with diminished intensity due to deuteriation are indicated by arrows. From reference 35, with permission.
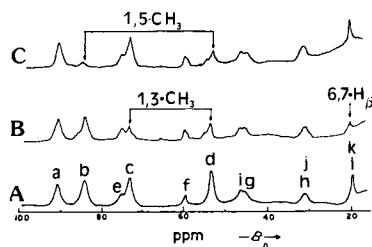

FIG. 6. 200 MHz ^{1}H NMR traces of the region 15-100 ppm to high frequency of DSS, at 27 °C and p^{2}H 6.2 of: (A) met-Mb-^2H_2O in 0.2 M NaCl in ^2H_2O; (B) met-Mb-^2H_2O reconstituted with [1,3-(C^2H_3)$_2$]haemin (also ~80% deuteriated at 6,7-H$_\beta$'s) in 0.2 M NaCl in ^2H_2O; (C) met-Mb-^2H_2O reconstituted with [1,5-(C^2H_3)$_2$]haemin, in 0.2 M NaCl in ^2H_2O. The peaks with reduced intensity due to deuteriation are indicated by arrows. From reference 35, with permission.
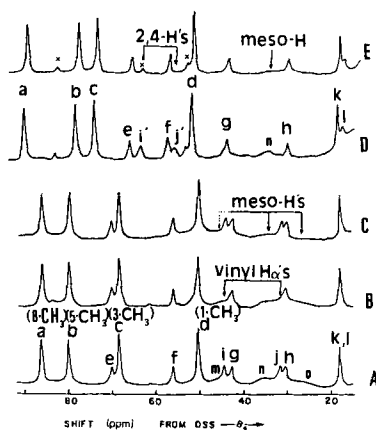
FIG. 7. 360 MHz ^{1}H NMR traces of the region .15–90 ppm to high frequency of DSS of 2 mM protein solutions in 0.2 M NaCl in ^2H_2O, 45 °C and p^2H 6.2 of: (A) met-Mb-^2H_2O: (B) met-Mb-^2H_2O reconstituted with [2,4-(2H$_\alpha$)$_2$]haemin; (C) met-Mb-^2H_2O reconstituted with [meso-(^2H)$_4$]haemin; (D) deut-met-Mb-^2H_2O; (E) deut-met-Mb-^2H_2O reconstituted with [2,4-(^2H)$_2$]deuteriohaemin (which also has some deuteriation of meso H's). The peaks with diminished intensities due to deuteriation are indicated by arrows. The peaks in D and E marked by x probably arise from a minor component of deut-met-Mb-^2H_2O which has the porphyrin rotated 180° about the α–γ meso positions. From reference 35, with permission.
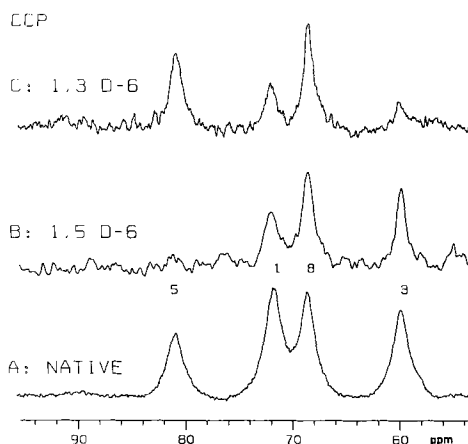

FIG. 8. Proton assignments of the haem methyl groups in cytochrome c peroxidase at 360 MHz, 25 °C and 0.1 M KNO$_3$; (A) cytochrome c peroxidase (native), pH 7.5; (B) [1,5-$^2H_6$]haemin reconstituted cytochrome c peroxidase, pH 7.2; (C) [1,3-$^2H_6$] haemin reconstituted cytochrome c peroxidase, pH 7.5. From reference 34, with permission.

TABLE 1

Chemical shifts for resolved resonances in met-aquo myoglobins.[a]

		met-Mb-^{2}H$_2$O	deut-met-Mb-^{2}H$_2$O
methyl	8 (a)	91.7 (~300)[b]	97.0 (~300)
	5 (b)	84.9	83.7
	3 (c)	73.2	79.2
	1 (d)	53.2	55.7
	e	75.5 (~250)	71.6 (250)
	f	59.2	61.2
	g	44.9	46.5
	h	30.9	30.6
vinyl H$_\alpha$	(i)	46.4	
	(j)	31.4	
pyrrole 2,4-H	i'		68.2 (350)
	j'		60.3
6,7-H$_\beta$	(k)	19.56 140)	20.17
	l	18.1(400)	17.8
meso H	(m)	~48	[c]
	(n)	37.4	~37
	(o)	~27	[c]
	y$_1$, y$_2$, y^3[d]	10.25, 9.67, 9.11	10.44, 9.76, 9.13
	p	−0.80	−0.74
	q	−1.17	−1.21
	r	−1.45	−1.47
	s	−1.81	−1.82
	t	−4.11 (110)	−4.13
	u	−5.24 (200)	−5.28
vinyl H$_\beta$	(v)[e]	−7.43	

[a] Shifts in parts per million at 360 MHz, 25 °C, and referenced to internal DSS.
[b] Linewidth in hertz at 360 MHz, given in parentheses.
[c] Other meso H not clearly resolved.
[d] Splits into two signals at 55 °C.
[e] Three single-proton resonances which exhibit weak Curie behaviour (linewidth ~50 Hz).
From reference 35, with permission.

The purely low spin paramagnetic state of b-type ferric haem proteins is conveniently achieved through cyanide ion binding. As described previously, the in-plane magnetic anisotropy in these ferric complexes may be such that not all haem protons may be resolved. In extreme cases as few as half of the predicted number of haem resonances may be observed. Nevertheless, the importance of making unambiguous assignments remains, particularly since non-haem protons may exhibit sizeable paramagnetic

TABLE 2

Proton resonance assignments in cytochrome c peroxidase and cytochrome c peroxidase-F.

Assignment	Cytochrome c peroxidase				Cytochrome c peroxidase-F			
	observed	hyper.[a]	av.[b]	spread	observed	hyper.	av.	spread
Methyls								
5	80.7	77.1			64.7	61.1		
1	71.5	67.9			53.8 (~1000)	50.2	54	13.4
8	68.4 (~550)	64.8	−66	21	60.8	57.2		
3	59.7	56.1			51.3	47.7		
Vinyls								
2-α	38.5	29.9	−34	9				
4-α	47.5 (~500)	38.9						
2-β	−10.8 (~200)	−17.1	−15.8	2.5				
4-β	−8.3	−14.6						

Shifts in ppm at 25 °C, referenced to residual H^2HO, reported relative to external DSS; linewidths given in parentheses in Hz at 360 MHz; negative sign indicates to low frequency of DSS.

[a] Hyperfine, or isotropic resonances obtained by referencing observed shifts to their corresponding diamagnetic positions.

[b] Average shift position for like protons.
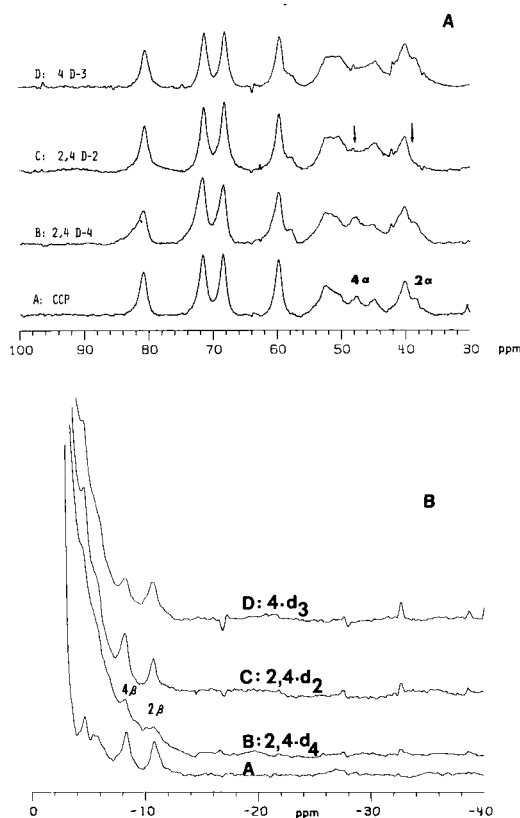
From reference 34, with permission.

FIG. 9. (A) Single haemin proton assignments for cytochrome c peroxidase at 360 MHz, pH 7.1–7.5, 25 °C; high frequency proton hyperfine shift region between 32 and 56 ppm, of cytochrome c peroxidase reconstituted with various deuteriated haemins: (A) cytochrome c peroxidase; (B) [2,4-β-^{2}H$_4$]haemin cytochrome c peroxidase; (C) [2,4-α^{2}H$_2$]haemin cytochrome c peroxidase; (D) [4-^{2}H$_3$]haemin cytochrome c peroxidase. Fig. 9B. (B) Low frequency single-proton assignments for cytochrome c peroxidase at 360 MHz, 25 °C. From reference 34, with permission.

dipolar (pseudocontact) shifts and complicate the observed spectrum. For example, the assignments shown for cytochrome c peroxidase-CN[37] in Figs 17 and 18 and horseradish peroxidase-CN[38,39] in Figs 19 and 20 indicate that a significant number of non-haem resonances occur in the hyperfine shift region outside the 0–10 ppm diamagnetic proton region. A large number of resonance assignments are summarized in Table 4 for ligated b-type[40] ferric haem proteins containing protohaem IX. Shifts and assignments of cyanide ligated ferric proteins that were reconstituted with unnatural derivatives of protohaem IX are presented elsewhere in this article.

TABLE 3

Chemical shifts for horseradish peroxidase and deuterio-HRP.

Peak[a]	Assignment	Horseradish peroxidase			Deuterio-HRP shift[b] at "pH" 7.0
		shift[b] at "pH" 7.0	change[c] in shift with "pH"	Change[d] in shift with IPA	
a_1	N_1H	95.8	1.0	~0	95.7
b_3	5-CH_3	78.6	0.6	−0.7	69.8
c_3	1-CH_3	71.9	−0.7	2.3	59.6
d_3	8-CH_3	68.3	0.8	−0.3	85.7
e_3	3-CH_3	52.6	0.3	0.3	69.6
f_1	vinyl H_α (2?)	69.5	0.3	0.8	
g_1	vinyl h_α (4?)	45.9	0.3	0.3	
h_1		51.3	−0.3	−0.3	~58
i_1	propionic acid	48.8	2.1	—[e]	49.7
j_1	H_α's (?) and	44.4	1.6	0.9	42.2
k_1	proximal	40.4	0	1.0	40.9
l_1	histidyl H_β's (?)	36.7	−0.3	1.3	36.0

m_1		33.2	0.9	1.4	34.8
n_1 to p_1		11.7, 11.3, 10.6	0.05, 0.06, 0	0	11.3, 10.9[e]
a'		−0.24	0	0	−0.12
b'		−0.57	0	0	− [e]
c_1		−0.67	0	0	−0.60
d'		−1.19	0	0	−1.22
e_1'		−1.71	−0.11	−0.1	− [e]
f_3'		−2.35	−0.04	−0.2	−2.33
g_3'		−2.65	−0.05	0	−2.65
h_1'		−3.96	−0.05	0	− [e]
i_1'	vinyl-H$_\beta$ (*trans*?)	−5.57	−0.11	−0.2	
j_1'	vinyl-H$_\beta$ (*trans*?)	−6.10	−0.30	− [e]	
k_1'		−8.9	0.2	0.3	−6.3

[a] The peak designations are as indicated in Fig. 1; the subscript refers to the number of protons giving rise to the peak, if determinable.

[b] Shift in ppm at 35 °C, in 0.2 M NaCl ^{2}H$_2$O, referenced to internal DSS.

[c] Change in shift (in ppm) upon lowering the "pH" from 7.0 to 5.2; high frequency shifts are positive.

[d] Change in shift (in ppm), upon addition of a 30-fold excess of IPA; high frequency shifts are positive.

[e] Not resolved.

From reference 33, with permission.
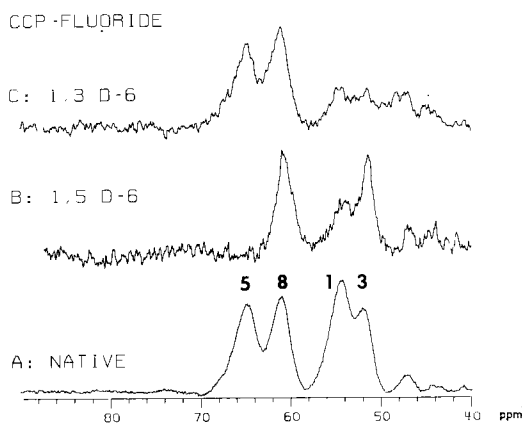
FIG. 10. Proton assignments of the haemin methyl groups in cytochrome c peroxidase-F at 360 MHZ, 0.1 M KNO_3, 25 °C: (A) cytochrome c peroxidase-F, pH 7.55; (B) $[1,5-{}^2H_6]$haemin reconstituted cytochrome c peroxidase-F, pH 7.65; (C) $[1,3-{}^2H_6]$haemin reconstituted cytochrome c peroxidase-F, pH 7.40. From reference 34, with permission.

The use of deuterium labelled porphyrin substitution for assigning haem resonances in ferrous forms of proteins has also been reported (reference 41 and ref. 26 therein) although the information content relative to that in the ferric forms has been questioned.[41] Linewidths in this haem electronic state are substantial even though the maximum deshielding is less than 18 ppm for haem substituents. The consequence of this state of affairs is that lower resolution is a complicating factor.

Aside from facilitating traditional lines of NMR and biochemical inquiry, the use of deuterium labelled haems has had a major impact on the controversy surrounding the origin of haem related multiple protein forms. For example, several proteins show multiple sets of paramagnetically shifted resonances as indicated in Table 4. One of the earliest quantitative NMR studies that revealed the simultaneous presence of two protein forms was the work of Keller and Wüthrich[42] on cytochrome b_5 (Fig. 21). Their original interpretation of the spectral heterogeneity was that it was due to isomerization of the amino acid proline. This is a completely reasonable interpretation given the fact that, whereas multiple positions for amino acid side chains are known,[43] the idea that the haem group might not enjoy the unique positioning within the protein inferred by crystallographers is a drastic concept. Nine years passed before LaMar and co-workers[40] demonstrated that two haem orientations, related by a 180° rotation of the haem about the $\alpha-\gamma$ meso axis (Fig. 22), exist in cytochrome b_5. These later data (Fig. 23, Table 5) rely upon reconstitutions using selectively deuteriated protohaem IX and derivatives of protohaem IX. Further work has demonstrated
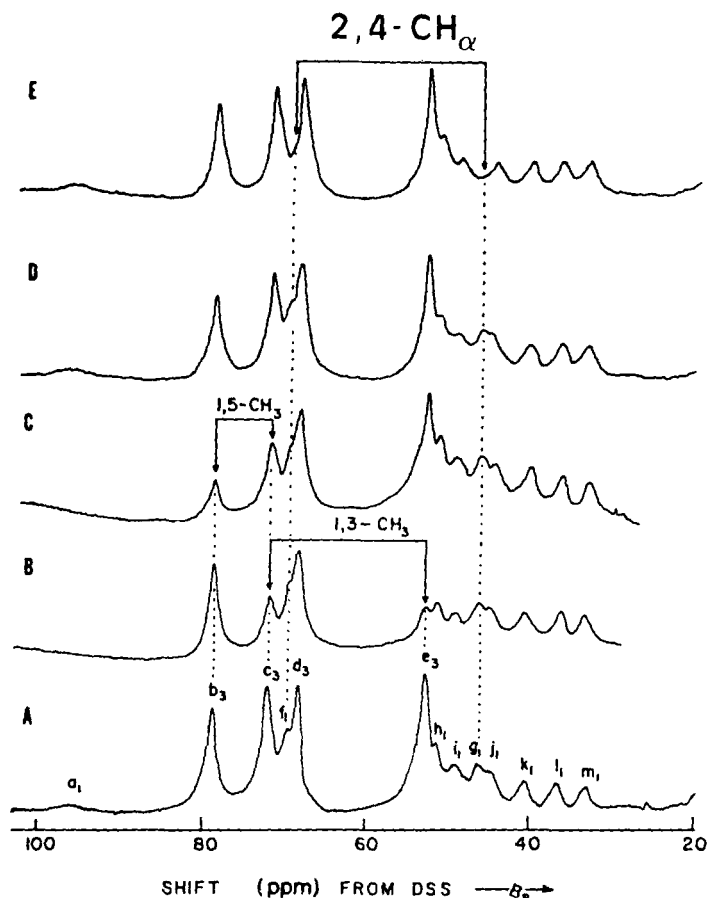
FIG. 11. High frequency portion of the 360 MHz proton NMR spectra of native horseradish peroxidase (A); [1,3-(C²H₃)₂]HRP (B); [1,5-(C²H₃)₂]HRP (C); [α,β,γ,δ-meso-²H₄]HRP (D); and [2,4-(α-C²H)₂]HRP (E) in ²H₂O at 35 °C, "pH" 7.0. The peaks with reduced intensities clearly indicating deuteriation are marked with arrows. The samples in traces B and C had been in ²H₂O for over 2 weeks so that the exchangeable peak a_1 is lost. From reference 33, with permission.

that this effect occurs in the native, ferric haemoglobins of *Chironomous thummi thummi*[44-48] larvae, the marine annelid *Glycera dibranchiata*[49] and sperm whale met-myoglobin.[50,51] This disordered haem phenomenon is also apparent in proteins reconstituted with protohaem IX derivatives that do not naturally occur, including myoglobin,[52] cytochrome *c* peroxidase,[53] horseradish peroxidase[54] and human haemoglobin.[55]

TABLE 4

Observed proton shifts on assigned haem substituents in several variously ligated ferric haem proteins.

Protein	Temp. (°C)	pH	Haem methyls 1	3	5	8
Sperm whale Mb-CN	25	6.8	18.7		27.4	13.0
Soybean Lb-CN	25	8.3	17.0		19.5	
C. thummi thummi (I) Hb-CN [a]	25	7.3		20.6		26.8
C. thummi thummi (III) Hb-CN [b]	25	6.0		21.7		28.9
C. thummi thummi (III) Hb-CN [c]	25	6.0	19.4	20.9	27.9	
C. thummi thummi (IV) Hb-CN [b]	26	6.0				28.4
C. thummi thummi (IV) Hb-CN [c]	25	6.0	18.5		27.9	
CcP-CN	24	7.2		31.2		27.3
HRP-CN	35	7.0		25.0		29.8
HRP-deutCN	35	7.0	22.3[e]	26.3	27.6[e]	31.6
Cytochrome b_5 [b]	25	8.0	11.9	14.1	22.0	2.7
Cytochrome b_5 [c]	25	8.0		30.8		27.3
Sperm whale Mb-OH	25	11.1	25.0	31.7	35.2	35.2
Sperm whale Mb-SCN	25	6.8	48.9	54.1	61.2	65.4
Sperm whale Mb-Im	25	8.3	25.9		39.0	15.9
Sperm whale Mb-N_3	25	7.2	26.2		31.6	24.4
CcP-N_3	24	7.4	25.8	36.8	31.9	38.9
Soybean Lb (nicotinate)[d]	25	7.2		19.5		27.9
Soybean Lb (pyridine)[d]	25	5.3		21.7		29.8
HbA-CN	25	6.5	15.7 (α) 15.0 (β)		21.8 (α) 21.5 (β)	
Carp Hb-CN	25	6.6	16.4 (α) 16.1 (β)		21.9 (α) 21.9 (β)	
Carp Hb-CN	25	9.0	21.4 (α) 20.9 (β)		17.8 (α) 16.9 (β)	
HRP compound I	25	7.0	51.8	90.2	74.6	10.3
HRP-deut-compound I	25	7.0	71.5	75.3	59.3	51.1

[a] Shifts inferred from assignments of CTT(III)-CN and CTT(IV)-CN.

[b] Major component.

[c] Minor component.

[d] These reported assignments are likely to be wrong in view of the incorrect assumption made in the NOE studies. Although unproven, the probable correct assignment is 1 = 19.5 and 21.7, respectively, and 5 = 27.9 and 29.8, respectively, for the nicotinate and pyridine ligated forms.

[e] Deuteriohaemin reconstituted HRP-CN exists in two different haem orientations; the 5,1 shifts are for a different orientation from the 8,3.

TABLE 4 (*cont.*)

	Haem vinyl groups						
2α	2β (*cis*)	2β (*trans*)	4α	4β	4β	$6,7\,\beta CH_2$	Ref.
17.9	−1.78	−2.44					25, 36
16.5	−6.9	−5.1				13.2, 11.6	84
			18.3	−3.14	−3.32		44, 46, 128
			16.5	−4.06	−3.29		44, 46, 128
			22.9	−2.51	−3.70		44, 46, 128
			17.3	−3.78	−3.27		44, 46, 128
			20.3	−4.15	−4.70		44, 46, 128
			15.9	−4.0	−2.2	−2.2	37
							38, 39, 41
							60
27.6	−6.9	−7.1					40
			18.0				40
							36
							36
							36
							36
17.6	−2.9	−5.6					37
			22.7	−8.5	−10.5	15.5, 13.2	82, 83
			21.4	−8.7	−10.6	22.9, 13.1	82, 83
							161
							161
							161
							161
							161
							161
							96
							96

FIG. 12. Low frequency portion of the 360 MHz proton NMR spectra of native horseradish peroxidase (A); $[2,4\text{-}(\beta\text{-}C^2H_2)_2]$HRP (B); and deuterio-HRP in ^2H_2O at, 35 °C, "pH" 7.0 (C). The peaks with reduced intensity due to deuteriation are marked by arrows. From reference 33, with permission.
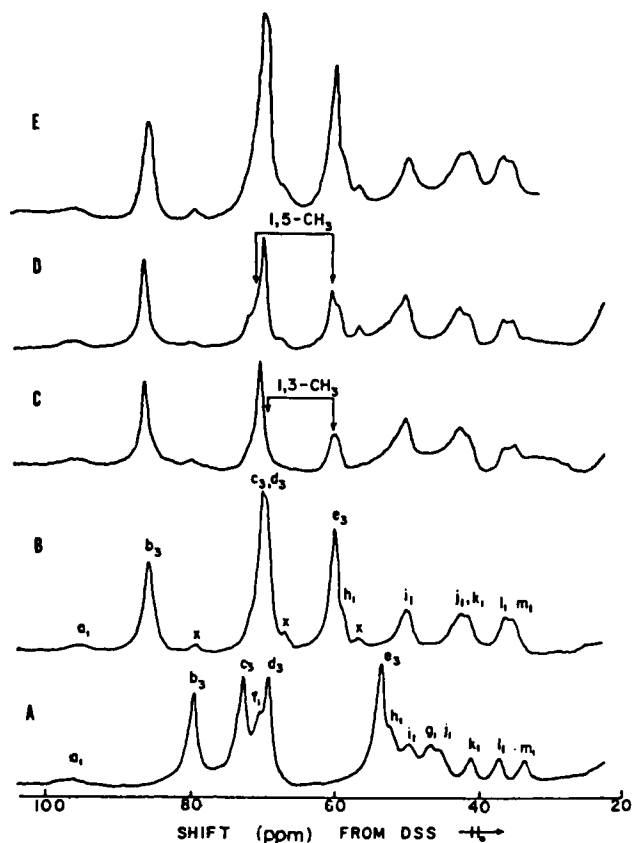
FIG. 13. High frequency portion of the 360 MHz proton NMR spectra of native horseradish peroxidase (A); deuterio-HRP (B); [1,3-$(C^2H_3)_2$]deuterio-HRP (C); [1,5-$(C^2H_3)_2$]deuterio-HRP (D); and [2,4-$(^2H)_2$]deuterio-HRP (E), all in ^2H_2O at 35 °C, "pH" 7.0 The peaks in B designated by x arise from the deuteriohaemin orientation, differing by 180° in rotation about the meso axis, from that exhibiting peaks *b* to *e*. Deuterio-HRP indicates HRP reconstituted with duteriohaemin. From reference 33, with permission.
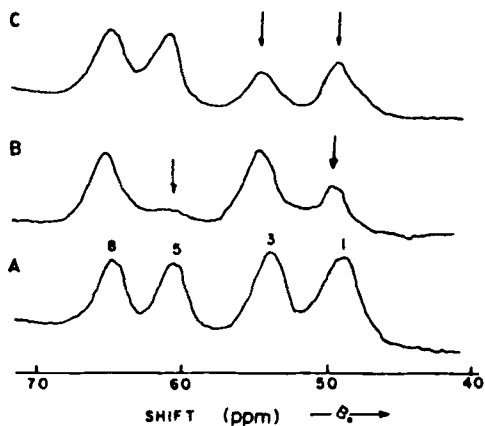
FIG. 14. Regions of the proton NMR spectra containing the haem methyl resonances at 25 °C, and referenced to internal 2,2-dimethyl-2-silapentane-5-sulphonate of: (A) native met-Mb-SCN; (B) met-Mb-SCN reconstituted with haemin deuteriated at methyl-1 (approx. 65%) and methyl-4 (90%); (C) met-Mb-SCN reconstituted with haemin deuteriated at methyl-1 (40%) and methyl-3 (60%). All proteins are in 0.1 M phosphate buffer, p^{2}H 6.8 (arrows indicate diminished intensities). Each of the peaks at 49 and 54 ppm contains a methyl and an additional single proton peak. From reference 36, with permission.
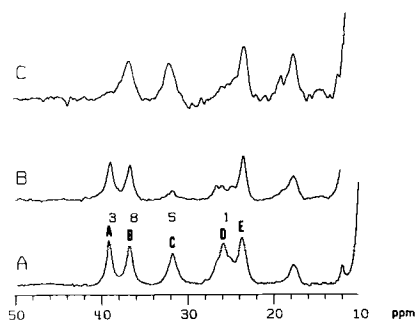
FIG. 15. Assignment of haemin methyl resonances in CcP-N$_3$ by deuteriation: (A) native CcP-N$_3$; (B) [1,5-^{2}H$_6$]haemin–CcP-N$_3$; (C) [1,3-^{2}H$_6$]haemin–CcP-N$_3$. The enzyme was in 0.1 M KNO$_3$, pHO$_3$, pH 7.4, 24 °C. From reference 37, with permission.
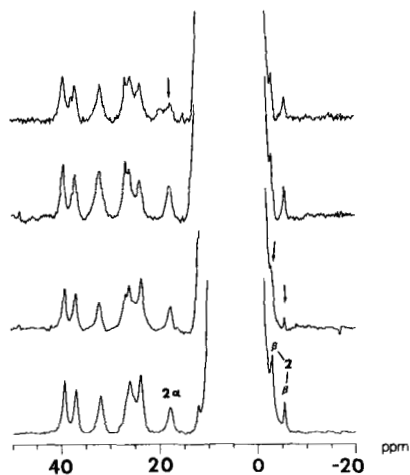
FIG. 16. Assignment of single proton resonances in CcP-N_3, by reconstitution with deuteriated haemins: (A) native CcP-N_3; (B) [2,4-$^2H_4$]haemin–CcP-N_3; (C) [4-$^2H_3$]haemin–CcP-N_3; (D) [2,4-$^2H_2$]haemin–CcP-N_3. Conditions are the same as described in Figure 15. Arrows indicate peaks displaying decreased intensity as a result of deuteriation. From reference 37, with permission.
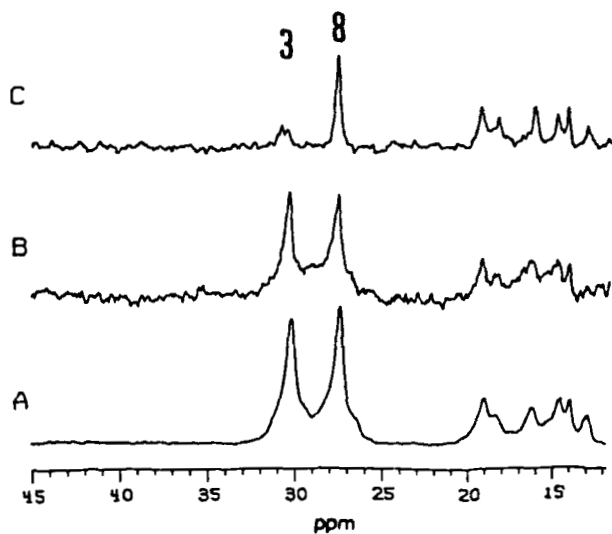

FIG. 17. Assignment of haemin methyl protons by deuteriation: (A) native CcP-CN; (B) CcP$_2$ reconstituted with [1,5-$^2H_6$]haemin; (C) CcP reconstituted with [1,3-$^2H_6$]haemin. The enzyme was in 0.1 M KNO$_3$, pH 7–7.4, at 24 °C. From reference 37, with permission.

TABLE 5

Hyperfine shifts at 25 °C (ppm, relative to DSS) for native and reconstituted ferricytochrome b_5.

Assignment	Protohaemin		Pemptohaemin		Isopemptohaemin		Deuteriohaemin
	major	minor	major	minor	major	minor	
1-CH$_3$	11.7 (X$_1$)	—^{a}	12.1 (X$_1$)	N.L.^{b}	11.8 (X$_1$)	N.L.	12.9 (X$_1$)
3-CH$_3$	14.4 (X$_3$)	30.8 (Y$_3$)	14.5 (X$_3$)	30.4 (Y$_3$)	16.2 (X$_3$)	31.0 (Y$_3$)	16.3 (X$_3$)
5-CH$_3$	21.8 (X$_5$)	—^{a}	21.0 (X$_5$)	N.L.	19.2 (X$_5$)	N.L.	18.7 (X$_5$)
8-CH$_3$	—^{a}	27.3 (Y$_8$)	N.L.	20.3 (Y$_8$)	N.L.	27.4 (Y$_8$)	N.L.
2-C$^\alpha$H	27.1 (X$_2$)	—^{a}			23.0 (X$_2$)	N.L.	
2-C$^\beta$H (cis)	−6.8 (X$_9$)	—^{a}			−7.4 (X$_9$)	N.L.	
2-C$^\beta$H (trans)	−7.0 (X$_{10}$)	—^{a}			−6.8 (X$_{10}$)	N.L.	
4-C$^\alpha$H	—^{a}	18.0 (Y$_4$)	N.L.	N.L.			
4-C$^\beta$H	—^{a}	—^{a}	N.L.	N.L.			
4-C$^\beta$H	—^{a}	—^{a}	N.L.	N.L.			
2-H			−29.1 (X$_2'$)	−21.6 (Y$_2'$)			−28.2 (X$_2'$)
4-H					−4.4 (X$_4'$)	−11.3 (Y$_4'$)	−4.8 (X$_4'$)
Im 2-H?^{c}	−13.6 (X$_{11}$)	−16.1 (Y$_{11}$)	−14.0 (X$_{11}$)	N.L.	−14.2 (X$_{11}$)	N.L.	−15.6 (X$_{11}$)
Im 4-H?	12.9 (X$_{12}$)	N.L.	N.L.	N.L.	N.L.	N.L.	N.L.

^{a} —, these resonances remain unresolved in the diamagnetic envelope 9–0 ppm.

^{b} N.L., not located. .

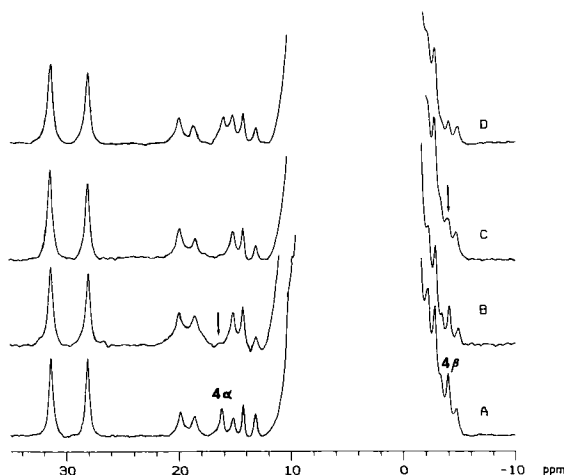^{c} ?, tentative.

From reference 40, with permission.

FIG. 18. Assignment of haemin vinyl protons by deuteriation in CcP-CN. Both high- and low-frequency regions are shown in this figure: (A) native CcP-CN; (B) α-vinyls deuteriated; (C) 4-vinyl group perdeuteriated (both α and β protons); (D) β-vinyl protons deuteriated. From reference 37, with permission.

C. Multiple irradiation techniques

The use of multiple irradiation methods, including various dynamic NOE experiments, for making protein assignments has been pioneered.[1,56-70] The general technique is to employ one or more of the following methods to make assignments in the diamagnetic (ferrous) form of the haem protein: steady state NOE, transient NOE, truncated driven NOE and, more recently, two-dimensional J-resolved spectroscopy.[1,56] Especially for smaller haem proteins one can anticipate future use of two-dimensional NOE correlations (NOESY)[56,71] and spin echo correlated spectroscopy (SECSY).[57]

After assignments are made in the ferrous, diamagnetic form (or ferric, paramagnetic form) saturation transfer experiments may be used in solutions which contain a mixture of oxidized and reduced forms of the same protein to arrive at assignments in the other oxidation state form of the protein. As an example of this technique, an assigned resonance in the ferrous (diamagnetic) form of the protein can be saturated by irradiation, and this irradiated spectrum is compared with a spectrum identically accumulated, with the exception that the irradiation frequency has been shifted to a position where no resonance appears. Comparison of the two spectra is usually done in the difference mode. When this is carried out on a protein solution containing both ferrous and ferric forms, a peak that appears in the difference spectrum is a peak in the ferric form that is linked by saturation transfer to the
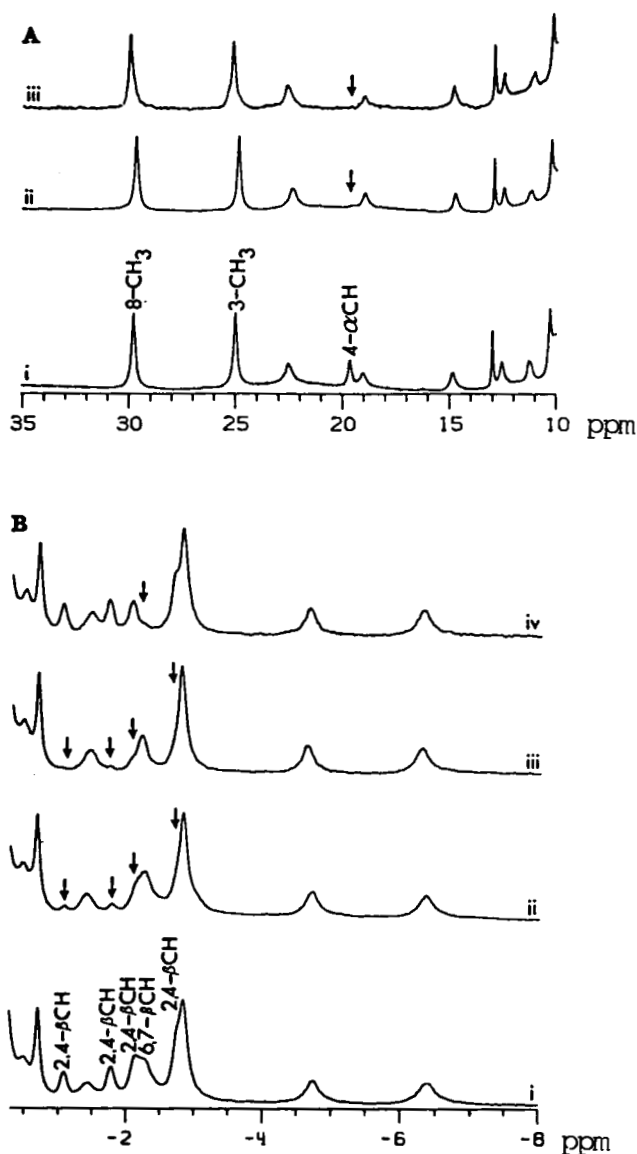
FIG. 19. Assignments by specific isotope labelling of the 360 MHz spectrum of HRP-CN at "pH" 7.0. Assignments are shown at 35 °C in A: (i) native HRP-CN, (ii) [2,4-(α-C^{2}H)]HRP-CN, and (iii) [4-α-C^{2}H]HRP-CN. Assignments are shown at 50 °C in B: (i) native HRP-CN, (ii) [2,4-(β-C^{2}H$_2$)]HRP-CN, (iii) [2,4-(β-C^{2}H$_2$),α,β,δ,γ-meso-^{2}H$_4$]HRP-CN, and (iv) [6,7-(β-C^{2}H$_2$)]HRP-CN. Peaks with clearly reduced intensities due to deuteriation are marked with arrows, and assignments are given on the bottom (native HRP-CN) trace. From reference 39, with permission.
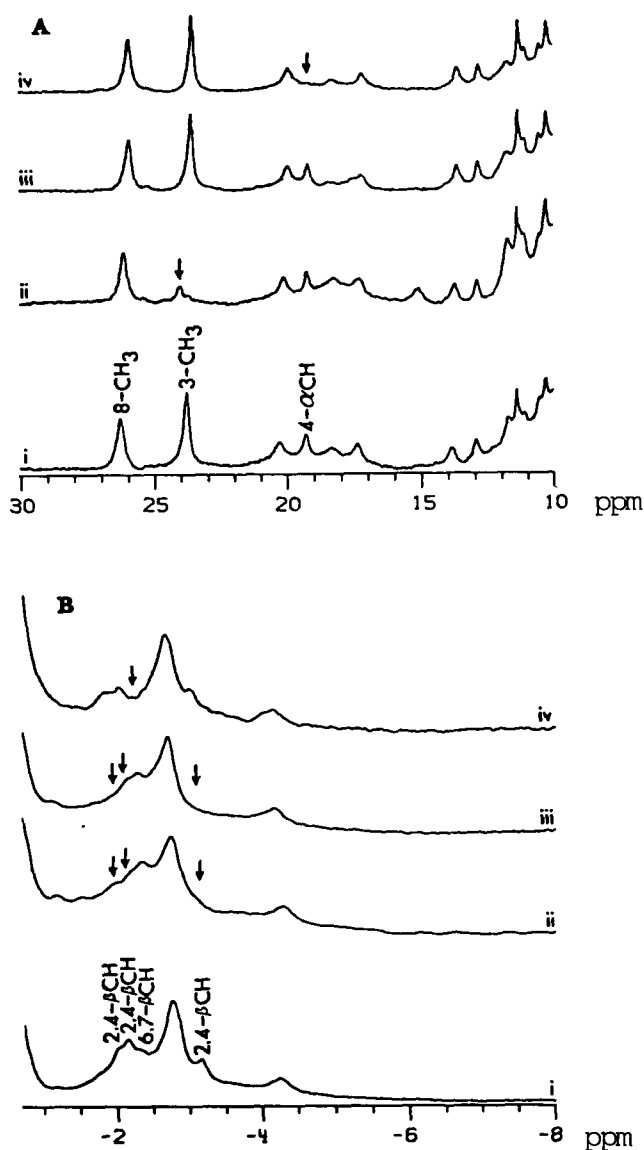
FIG. 20. Assignments by specific isotope labelling of the 360 MHz spectrum of HRP-CNa at "pH" 11.2 and 35 °C with A showing the high frequency assignments [(i) native HRP-CNa, (ii) [1,3-(C^{2}H$_3$)]HRP-CNa, (iii) [1,5-(C^{2}H$_3$)]HRP-CNa, (iv) [2,4-(α-C^{2}H)]HRP-CNa] and B the low frequency assignments [(i) native HRP-CNa, (ii) [2,4-(β-C^{2}H$_2$)]HRP-CNa, (iii) [2,4-(β-C^{2}H$_2$),α,β,γ,δ-meso-^{2}H$_4$]HRP-CNa, (iv) [6,7-(β-C^{2}H$_2$)]-HRP-CNa]. Peaks with clearly reduced intensities due to deuteriation are marked with arrows, and assignments are given on the bottom (native HRP-CNa) trace. From reference 39, with permission.
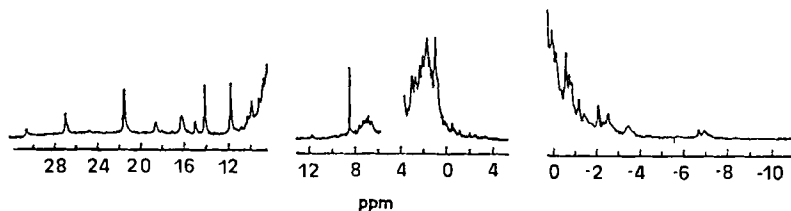
FIG. 21. 220 MHz proton NMR spectrum of 0.008 M ferricytochrome b_5 in 0.2 M deuteriated phosphate buffer (p^2H 6.3) at 29 °C. The three spectral regions are represented with different horizontal and vertical scales. The sharp line at −8.4 ppm comes from a low molecular weight component which could later be removed by exhaustive dialysis. From reference 42, with permission.
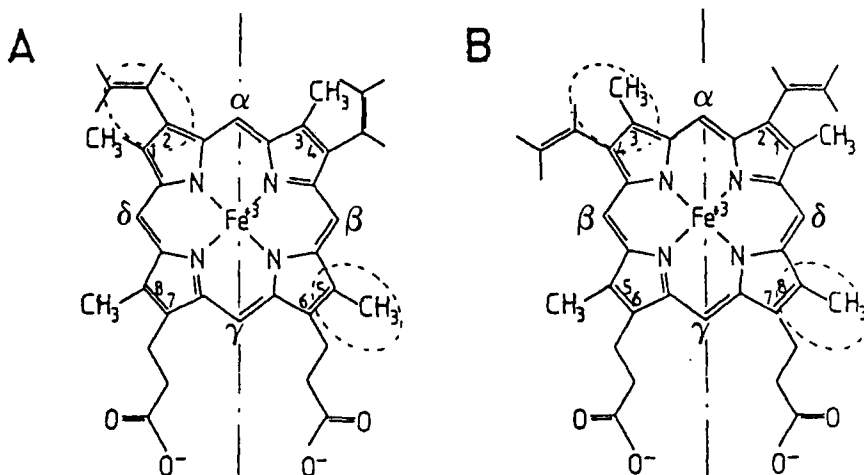
FIG. 22. The orientation of protohaemin in cytochrome b_5''' in the major component (A) and in the minor component (B). The regions of high electron spin density are marked by dashed circles. The drawing does not imply conclusions as to the rotational position of individual vinyl groups with respect to the haem in either orientation. From reference 40, with permission.

irradiated peak in the ferrous form. The choice of a peak in the ferric protein for irradiation is also possible. This technique is made possible by the rather fast electron exchange in the mixed oxidation state solution. Thus a given protein may exist in a rather fast dynamic equilibrium between oxidized (paramagnetic, ferric) and reduced (diamagnetic, ferrous) forms.

It is important to point out that the ferrous forms of haem proteins become diamagnetic only when a sufficiently strong field sixth ligand is
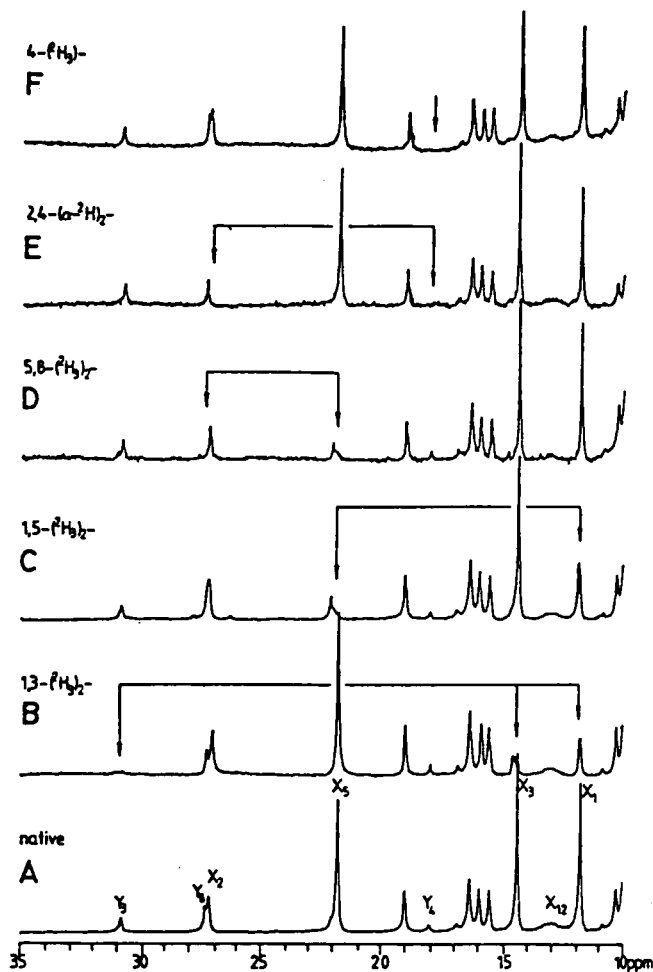
FIG. 23. The high frequency portion of the 360 MHz proton NMR spectra of ferricytochrome b_5 at 25 °C and pH 8 in ^2H_2O of: (A) native protein; (B) protein reconstituted with [1,3-$(C^2H_3)_2$]-protohaemin; (C) [1,5-$(C^2H_3)_2$]-protohaemin; (D) [5,8-$C^2H_3)_2$]-protohaemin; (E) [2,4-$(C^2H^\alpha)_2$]-protohaemin; and (F) [4-$C^2H=C^2H_2$]-protohaemin. The peaks with reduced intensities due to deuteriation are marked with arrows; residual intensity arises from incomplete deuteriation at the indicated positions. From reference 40, with permission.

available such as CO in the b-type haem proteins and methionine in c-type cytochromes. The types of studies described briefly in the foregoing have been widely applied in cytochromes c[58-79] and certain common myoglobins, haemoglobins[80,81] and leghaemoglobin.[82-84]

As an example of this method the assignments in cytochrome c-551 will be considered.[66] This protein is isolated from *Pseudomonas aeruginosa* and contains haem c (Figs 1, 24) at its active site. In addition, the porphyrin meso protons, $\alpha, \beta, \gamma, \delta$ in Fig. 1, and porphyrin methyl group protons, 1, 3, 5, 8 in Fig. 1, have previously been identified in the NMR spectrum of the ferrous protein.[77] Figure 24 reveals the projection of the axial methionine
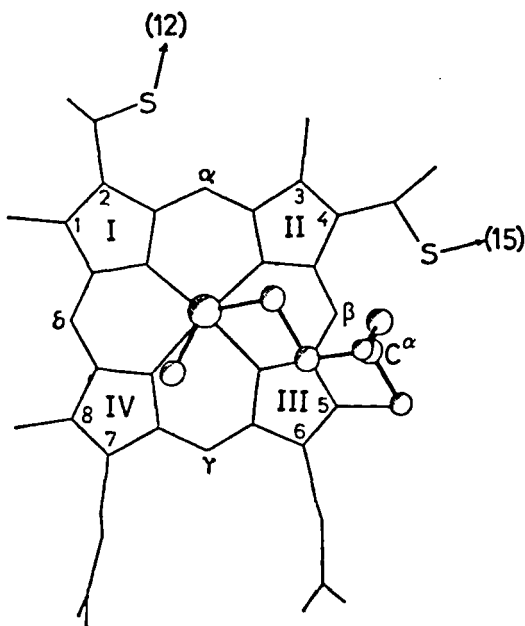
FIG. 24. Drawing of the haem group for c-type cytochromes based on the atomic coordinates of *Pseudomonas aeruginosa* ferrocytochrome c-551 obtained from the protein data bank. The view is perpendicular to the haem plane from the side of the axial methionine, whch is also indicated. The β-pyrrole positions are numbered from 1 to 8, the meso positions from α to δ and the pyrrole rings from I to IV. From reference 65, with permission.

on the haem plane as defined by crystallography.[65] Also the A_3X coupling pattern of the protons of the thioether covalent bridge to the polypeptide chain at haem positions 2 and 4 is assigned by proton homonuclear spin decoupling.
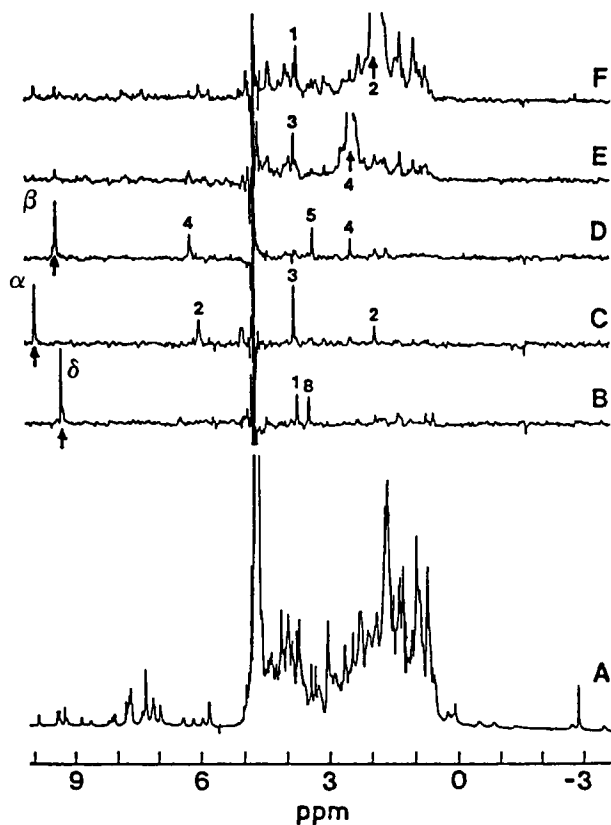
FIG. 25. (A) ^{1}H NMR spectrum at 360 MHz of a 0.002 M solution of ferrocytochrome c-551 in 0.05 M deuteriated phosphate buffer, pD 6.8, $T = 35°C$. (B to F) NOE difference spectra obtained upon irradiation at the positions indicated by the arrows. The individual assignments of the haem c resonances obtained from these experiments (see text) are also given, where the four haem ring methyls and the two thioether bridges are indicated by the number of the β-carbon atoms to which they are attached (Fig. 1). From reference 66, with permission.

The assignments made in this example are carried out using steady state NOE measurements. Figure 25 shows the proton spectrum of ferrocyto-chrome c-551 (A) and difference spectra obtained following proton irradi-ation at the resonance positions of the haem meso protons indicated by arrows in B–F. This figure contains the assignments which are made self-consistently from the NOE measurements and may be interpreted as follows. In Fig. 25B the meso-δ proton resonance is irradiated. According to the haem c structure in Fig. 24 the two closest protons are those of methyl resonances at haem positions 1 and 8. Consequently, these may be expected

to demonstrate significant Overhauser enhancements when the δ proton is irradiated. It is clear from Fig. 25B that two proton resonances between 3 and 4 ppm demonstrate intensity differences not cancelled in the difference spectrum, thereby indicating an Overhauser enhancement. Initially this pair of resonances can be ambiguously assigned to the 1,8 methyl pair. Further, NOE experiments provide the unique assignments shown in the figure. Continuing, irradiation of the α meso proton resonance (Fig. 2C) would be predicted from Fig. 24 to yield Overhauser enhancements to the thioether bridge protons at haem position 2 (two peaks) and the haem 3 position methyl protons (one peak). Such a pattern is observed. In this case no protons of the axial methionine lie close enough to the α meso proton to experience an NOE. Similarly, irradiation of the β meso proton would be expected to give a similar three-resonance difference spectrum from the haem 4 and 5 position substituents (Fig. 25D). From the coordinated S atom the methionine chain projects away from the haem, toward the viewer in Fig. 24, so that none of these protons is close to the haem β meso position. This accounts for the lack of NOE exhibited by the methionine side chain protons when the haem β meso proton is irradiated. Methyls 3 and 1 are unambiguously assigned by the NOE that each experience when position 4 (Fig. 25E) and 2 protons (Fig. 25F), respectively, are irradiated.

The assignments of the ferrous (diamagnetic) form haem methyl and meso proton resonances are thus complete. Saturation transfer experiments
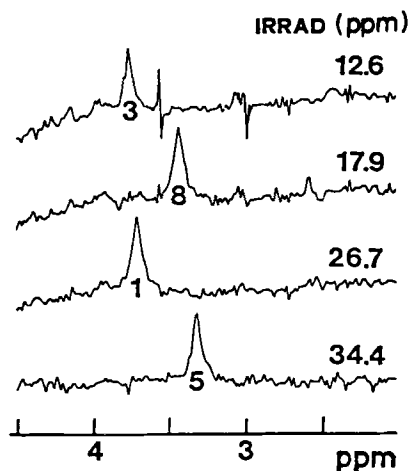

FIG. 26. Saturation transfer experiments in a mixed solution of 98% reduced and 2% oxidized cytochrome c-551, $T = 4\,°C$, total protein concentration 0.002 M. The traces correspond to the differences between spectra obtained with and without double resonance irradiation at the positions indicated, which correspond to the chemical shifts of the haem ring methyl groups (Fig. 1) in ferricytochrome c-551. From reference 66, with permission.

in solutions containing both oxidized and reduced forms of the protein are then carried out. In the ferric form cytochrome c-551 exhibits four proton resonances of relative integrated intensity corresponding to three protons each at 12.6, 17.9, 26.7 and 34.4 ppm. These paramagnetically shifted resonances are assigned to the haem methyls[77] and subsequent saturation transfer experiments are required for unambiguous assignment of these methyl groups through their correspondence to the assigned methyl groups of ferrocytochrome c-551.

The experimental results are shown in Fig. 26. Irradiation at each of the methyl resonance positions of the ferric forms produces a series of single resonance saturation transfer difference spectra. In Fig. 26 these are depicted as the result of spectra without double irradiation from which spectra where double irradiation is used (at 12.6, 17.9, 26.7 and 34.4 ppm, respectively)

TABLE 6

Assignments of the haem c ^{1}H NMR lines in cytochrome c-551 and hyperfine shifts of corresponding resonances in ferricytochrome c-551 and ferricytochrome c from horse heart.

	Cytochrome c-551		Horse heart cytochrome c
Assignment	chemical shift in reduced protein (ppm), $T = 27\,°C$	hyperfine shift[a] in oxidized protein (ppm), $T = 27\,°C$	hyperfine shift[a] in oxidized protein (ppm), $T = 35\,°C$
Meso proton α	9.87	−1.2	
Meso proton β	9.36	−10.1	
Meso proton γ	9.42	−2.7	
Meso proton δ	9.24	−11.0	
Ring methyl 1	3.69	21.1	3.9
Ring methyl 3	3.76	9.6	27.3
Ring methyl 5	3.32	28.8	6.9
Ring methyl 8	3.42	14.4	31.7
Thioether bridge 2:			
methine	5.97		
methyl	1.87	0.8	−3.6
Thioether bridge 4:			
methine	6.18		
methyl	2.44	−2.5	0.5

^{a} The hyperfine shift is the chemical shift difference between corresponding lines in the paramagnetic oxidized and the diamagnetic reduced protein. Positive numbers indicate shifts to high frequency.

From reference 66, with permission.

are subtracted. Table 6 summarizes the assignments and hyperfine shifts determined in this manner for cytochrome c-551.[66]

Many other cytochromes have been studied by this technique[58-79] or its variations. Steady state NOE measurements are, in fact, complicated by the presence of spin diffusion or cross-relaxation[85-91] which makes observed Overhauser enhancements less specific than would otherwise be desired. Transient NOE experiments,[1,92] which measure the establishment of Overhauser enhancements as a function of time, are useful for determining nearest neighbours and the pathway of spin diffusion. With this technique experiments can be suitably tailored to avoid, or take advantage of, spin diffusion.

Truncated driven NOE (TOE) measurements are another useful method for measuring initial NOE establishment rates.[1,58,71,72,80,81] These experiments may also be used to advantage when spin diffusion poses a problem for selectivity in steady state NOE measurements. Until 1983 one of the primary uses of TOE spectra was in assignments of axial ligand resonances in the diamagnetic, ferrous forms of cytochromes. This has resulted in important structural information concerning the chirality of the axially
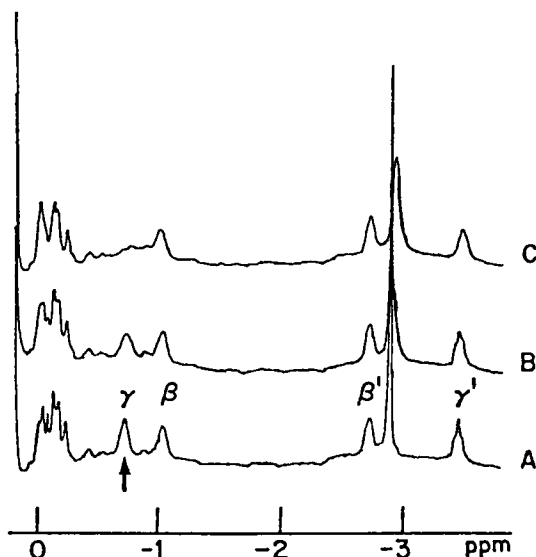

FIG. 27. Region from −4 to 0 ppm of the 360 MHz ^{1}H NMR spectra of *Pseudomonas aeruginosa* cytochrome c-551, protein concentration 2 mM, p^{2}H = 6.9, T = 52 °C. (A) Fully reduced cytochrome c-551; the sharp resonance at −2.90 ppm corresponds to ε-CH$_3$ and the four one-proton lines at −3.52, −2.72, −0.87 and −0.52 ppm to the β- and γ-methylene protons of the axial methionine (13). (B) Partially autoxidized solution containing ∼0.04% ferricytochrome c-551. (C) Partially autoxidized solution containing ∼0.4% ferricytochrome c-551. From reference 78, with permission.

coordinated methionine in c-type cytochromes.[63-65,69,71,78] During 1979 there appeared an article which indicated the feasibility of performing NOE measurements on the paramagnetic forms of haem proteins.[82] Subsequently this application has been expanded.[78,80,81,93,165] Examples of both of these methods, taken from the literature, will be briefly described.

   An interesting comparison of the haem coordination geometries in homologous cytochromes has arisen from TOE data obtained on cytochrome c-551 from *Pseudomonas aeruginosa* compared with horse cytochrome c.[64,78] Figure 27 shows the low frequency proton region of cytochrome c-551. The axial methionine methyl resonance is shown at −2.90 ppm for c-551 in Fig. 27 and occurs at a similar position in horse cytochrome c. The meso protons for the ferrous forms of both of these proteins occur between 9 and 10 ppm and are assigned as shown in Fig. 28. This figure also shows the time evolution of the Overhauser enhancement on the meso haem protons when the ε-CH_3 group of the axial methionine (Fig. 1) is irradiated. Comparing the cytochrome c (Fig. 28A) and cytochrome c-551 (Fig. 28B) TOE
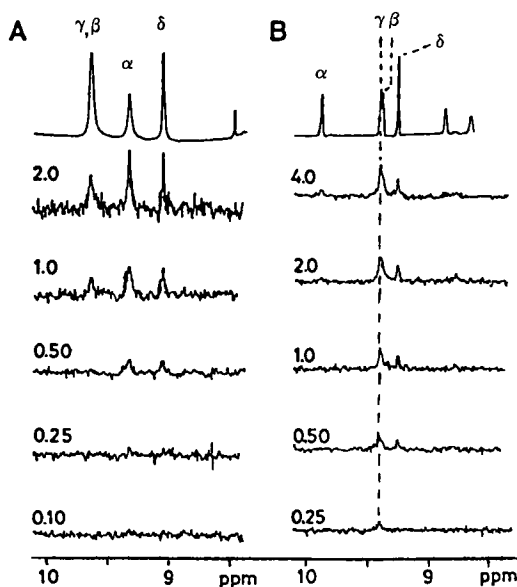

FIG. 28. Region from 8.5 to 10.0 ppm of the ^1H NMR spectra at 360 MHz of reduced horse cytochrome c (A) and cytochrome c-551 (B). The top traces show the normal Fourier transform spectra. The previously established assignments of the meso proton resonances (5,6) are also indicated. For each species a series of TOE difference spectra obtained with preirradiation of the ε-CH_3 resonance of the axial methionine (Fig. 2) are shown. The length of the preirradiation time, in seconds, is indicated with each trace. The protein concentration was 8 mM in both samples, which also contained 100 mM NaCl, p^2H 6.4, $T = 30\,°C$. From reference 78, with permission.

difference spectra from bottom to top shows the effect of successively longer irradiation of the ε-CH_3 group in each protein. The longer the irradiation time, the greater is the extent to which the Overhauser enhancement is driven. For cytochrome c (Fig. 28A) the α,δ meso protons exhibit larger NOE enhancements than the other meso protons. These are significant at irradiation times of 0.50 and 1.0 s. The analysis depends upon the fact that in the TOE pulse sequence,[58] $[-t_1(\omega_H)$—observe pulse—$t_2 - t_1(\omega_{off}$ resonance)—observe pulse—$t_2-]_n$, at reasonably short t_1 (the time of irradiation of ε-CH_3) the TOE enhancements are considered to reflect the nearest neighbour distance reliably. Interpreting the data of Fig. 28 follows this logic. Because the α,δ meso protons exhibit the largest Overhauser enhancements the ε-CH_3 must be spatially nearer to these meso positions than to the other meso positions. Consequently a physical position shown in Fig. 29A best fits the TOE data.

In contrast, for cytochrome c-551 (Fig. 28B) the γ,δ meso positions show greater enhancements at $t_1 = 0.5$ s. Using similar reasoning a spatial orientation depicted in Fig. 29B is most consistent with the data. The authors have correlated this different axial methionine chirality with circular dichroism data to show that the difference between the two cytochromes is maintained in the ferric protein.[78] They have used this information to rationalize the observed[59,66] differences in the paramagnetic NMR spectra of these two proteins. Similar TOE experiments could not be carried out on the ferric
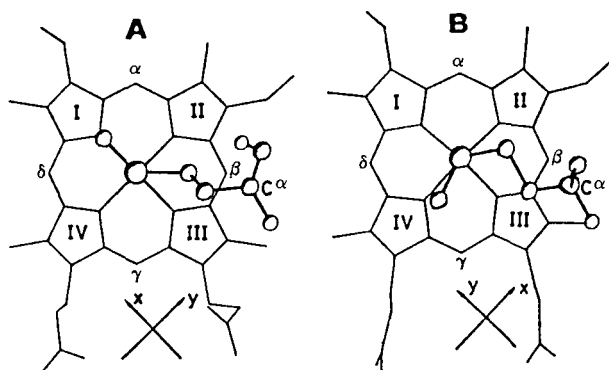

FIG. 29. Perspective computer drawing of the haem group and the axial methionine in (A) tuna ferricytochrome c (refined coordinates at 2.0 Å resolution from the protein data bank) and (B) *Pseudomonas aeruginosa* ferricytochrome c-551 (refined coordinates at 2.0 Å resolution obtained from Dr R. E. Dickerson). Tuna cytochrome c was selected as a representative example of the group of mammalian type cytochromes c which includes also horse cytochrome c. The view is in the direction perpendicular to the haem plane. The numbers and letters identify the four pyrrole rings (I–IV) and the meso protons (α–δ) of haem c, and the α carbon of the axial methionine (C^α). The directions of the principal axes c and y of the electronic g-tensor are also indicated. From reference 78, with permission.

forms of these enzymes. Aside from the perceived greater difficulty of performing TOE experiments on paramagnetic proteins, the haem meso protons in ferric proteins are extremely broad, frequently not observed, or assigned, and probably not amenable to accurate NOE-difference spectra manipulation.

In fact, the perceived complication of observing Overhauser enhancements in paramagnetic haem proteins apparently originates in the concept that the paramagnetism would provide an extremely efficient and fast relaxation pathway, thereby rendering NOEs too small to observe. However, it has been shown conclusively that negative steady state Overhauser effects can be observed in ferric haem proteins.[82,165] Work published in 1983–1984[80,81,165] indicates that TOE experiments on low spin ferric haem proteins can be useful in assigning the resonances of amino acid residues that lie in close proximity to the haem. This is particularly important given the potential role of haem–protein contacts in determining the active site chemistry in haem proteins.[80,81] Interpretation of TOE data in terms of group mobilities within the haem pocket has also been demonstrated[80,93] and that work has been chosen as an example of TOE applications in paramagnetic haem proteins.
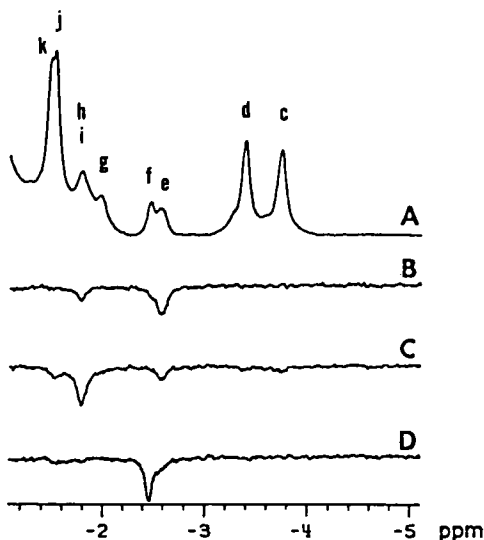

FIG. 30. Low frequency portion of the 360 MHz ^{1}H NMR spectra of met-Mb-CN in ^{2}H$_2$O, "pH" 10.4, 25 °C, and 0.2 M NaCl. (A) Reference spectrum, resolving peak e (2-H$_\beta$(trans)), but with peak i (2-H$_\beta$(cis)) merged with peak h. (B) Saturation of peak e, showing a NOE to composite peak h,i. (C) Saturation of composite peak h,i showing a NOE to peak e. (D) Saturation of peak f, showing an bsence of NOE to other peaks. Vertical scale ×2 for B, C, and D relative to A. From reference 93, with permission.

In the case of met-myoglobin cyanide, a low spin ferric protein (Fig. 1), extensive assignments of hyperfine resonances to specific haem peripheral substituents have been carried out according to the deuterium labelling methods described in the preceding section. The low frequency region of the spectrum contains two resonances of the 2 position vinyl group: 2-$H_\beta(trans)$ and 2-$H_\beta(cis)$ (see Fig. 1, Table 4). Both of these resonances overlap with other resonances in this spectral window; however, as demonstrated in Figs 30 and 31, each may individually be resolved at different pH values. These figures show the steady state NOE data obtained from irradiating the 2-$H_\beta(trans)$ (Fig. 30) and 2-$H_\beta(cis)$ (Fig. 31). When $H_\beta(cis)$ is irradiated the largest negative NOE is observed for the $H_B(trans)$, and oppositely, thereby establishing the connectivities.

For this vinyl fragment, $=CH_2$, a reasonable theoretical framework for interpreting the NOE data is a formal two spin approximation. As pointed out, in the TOE experiment the time dependence of the nuclear Overhauser enhancement η_I of the observed proton's peak, I, as a function of the time (T) that a second, interacting proton's resonance, S, is irradiated is given by

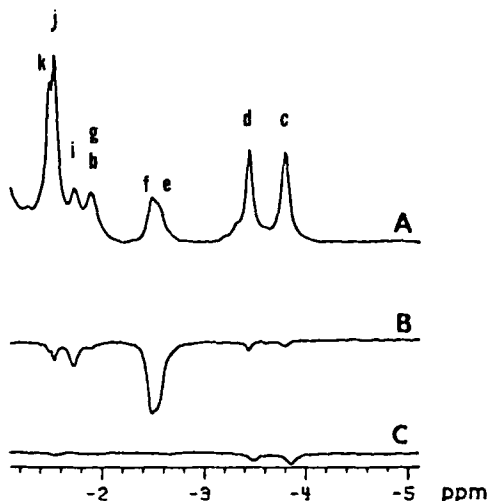$$\eta_I(T) = \frac{\sigma_{IS}}{\rho_I}(1 - e^{-\rho_i T}) \qquad (13)$$

FIG. 31. Low frequency portion of the 360 MHz ^{1}H NMR spectra of sperm whale met-Mb-CN in ^2H_2O, "pH" 8.5, 25 °C, and 0.2 M NaCL. (A) Reference spectrum. Peak i has been assigned to the 2-$H_\beta(cis)$ and peak e of composite peak e,f to 2-$H_\beta(trans)$. (B) Steady-state saturation of composite peak e,f showing a NOE to peak i and decoupler spillages to peaks k,j and c,d; vertical scale ×2 relative to A. (C) The decoupler is positioned at e, −4.8 ppm, showing spillage to peaks c and d; vertical scale ×2 relative to A. From reference 93, with permission.

In this case σ_{IS} is the cross-relaxation term that gives rise to the observed Overhauser enhancement and ρ_I is the intrinsic spin–lattice relaxation rate of nucleus I. The time dependent build-up of the 2-H$_\beta$(cis) enhancement as a function of irradiation time (t_1 in the TOE pulse sequence) of the 2-H$_\beta$(trans) is shown in Fig. 32. The authors have fitted these data to the
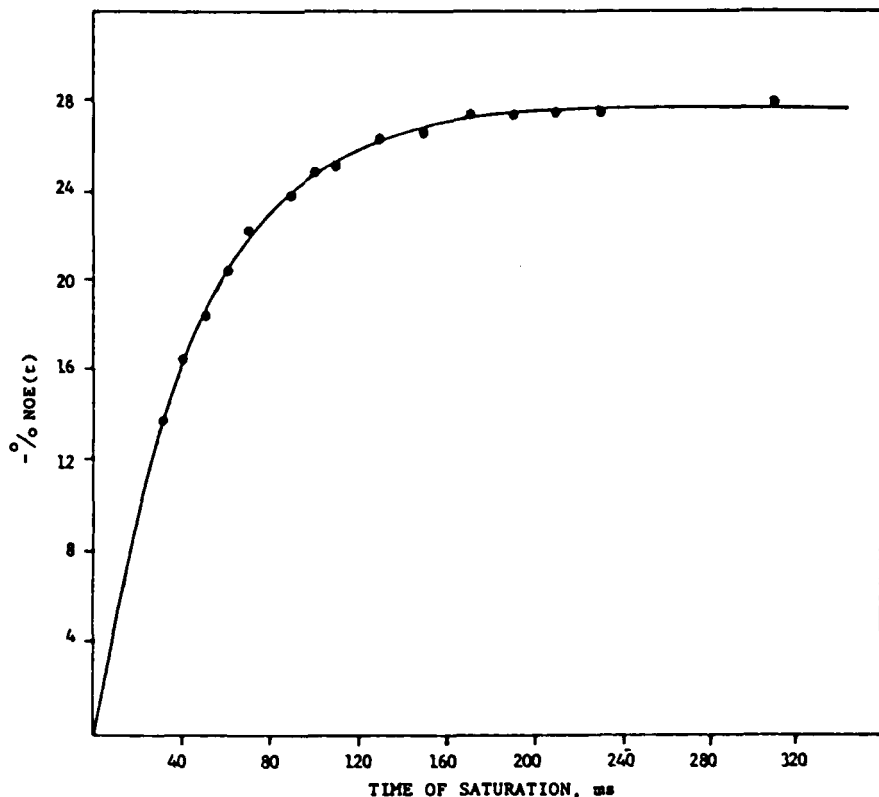

FIG. 32. Plot of time-dependent NOE of 2-H$_\beta$(cis) versus time saturation of 2-H$_\beta$(trans). Analysis of these data via in the text yields $\sigma(cis-trans) = -6.1$ Hz and $\rho_{cis} = 21.6$ s. From reference 93, with permission.

above equation to yield values of $\sigma = 6.1$ s^{-1}, $\rho_{cis} = 21.6$ s, and from this a calculated T_1 of 46 ms. Subsequent selective T_1 measurements yield an experimental T_1 (2-H$_\beta$(cis)) value of 55 ms, reinforcing the concept that a two spin approximation is valid. The observed cross relaxation rate in this instance, $\sigma_{cis-trans} = 6.1$ s^{-1}, is smaller than predicted by analysis of the spectral density function, given values used for the protein's correlation

time and the vinyl group interproton distance. The authors conclude that this difference is due to the presence of significant vinyl mobility at the haem 2 position.

It is important to emphasize that, for NOE measurements to be useful for making accurate assignments, one unambiguous proton resonance assignment must be obtained. This can be done by porphyrin deuterium isotope labelling in ferric haem proteins as just discussed, or in the ferrous haem protein. In the latter case, NOE assignments are then completely made in the ferrous protein and saturation transfer experiments allow assignments in the ferric form to be made. This method is discussed above in regard to cytochromes c; however, it should be pointed out that the relative ease in obtaining haemins deuteriated at the meso proton positions[94,95] makes this an easily instituted approach. The risk in proceeding without the firm assignment of at least one proton resonance is exemplified by an early incorrect set of assignments made for leghaemoglobin using the NOE method.[83] These were subsequently corrected using deuterium labelled protohaem IX.[84]

D. Assignments by comparison with model systems

The use of iron porphyrin model systems in making resonance assignments in haem proteins has been reviewed.[3,4,11,96] In view of the historical and continuing importance that model systems have had in interpretations of haem protein spectra it seems appropriate to describe briefly some of the important developments in iron porphyrin model systems since 1980. This survey is not intended to be exhaustive, nor will it refer to metalloporphyrin models other than those that contain iron, despite the fact that ruthenium and cobalt porphyrins have recently been advanced as models for the oxidized intermediates of haem peroxidase enzymes.[97]

The particular uses of iron porphyrin model systems that have evolved since 1980 have been for modelling specific iron spin and oxidation states. Models can be used in the least refined approximation to illustrate how spectra of particular types of well characterized iron porphyrins should appear in comparison with actual haem protein spectra.

One particularly interesting phenomenon has been the dramatic changes in the proton NMR spectrum when horseradish peroxidase Compound I is reduced to Compound II. The haem peroxidases, as a class, are ferrihaem enzymes. Upon reaction with hydrogen peroxide horseradish peroxidase (HRP) and cytochrome c peroxidase (CcP) both are initially oxidized 2 equivalents above the native state to the intermediate form named as Compound I.[98,99] HRP-I yields a nicely resolved set of hyperfine shifts.[100] Reduction by 1 equivalent to Compound II causes the change shown in Fig. 33, a loss of the well defined high frequency shift pattern.[100,101] For
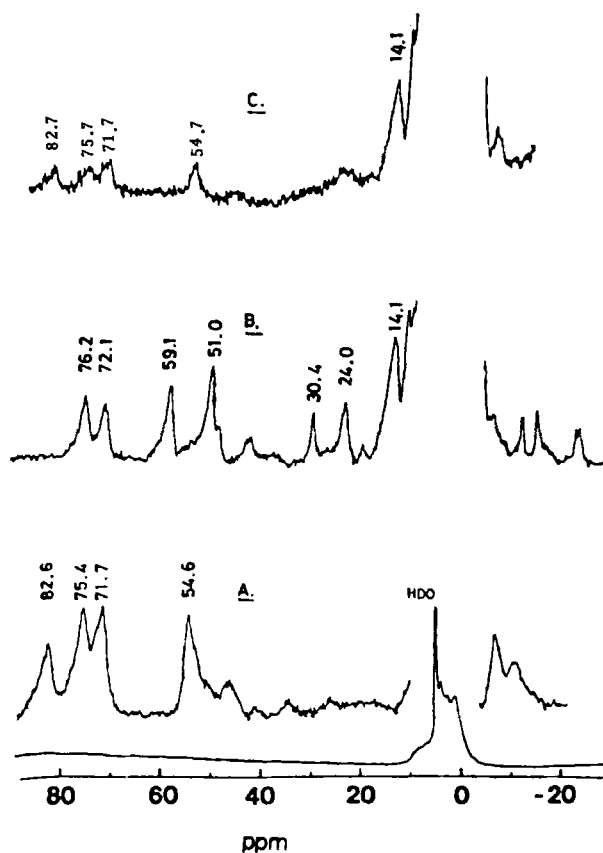
FIG. 33. 220 MHz proton NMR spectra of horseradish peroxidase and its reaction intermediates at 20 °C. All the samples are in 20 mM borate buffer at pH 9.2. (A) Ferric native horseradish peroxidase. (B) Compound I. Immediately after the addition of H_2O_2 to the HRP solution, 4 K transients of the spectrum were collected. The spectrum is contaminated with that of compound II. (C) Compound II. The spectrum was recorded just after adding p-cresol (oxidizable substrate) to the compound I solution. The peaks located at 50–85 ppm are due to the native recovered enzyme. From reference 100, with permission.

both CcP-I and CcP-II spectra similar to HRP-II are obtained (Fig. 34).[102] These dramatic spectral changes occur even though each of the two intermediate forms of both of these enzymes is thought to contain the ferryl moiety (iron(IV)-oxo; $Fe^{4+}=O$).[103,104]

HRP-I is further unique in that it contains a porphyrin π-cation free radical.[105,106] Furthermore, ferryl groups have been advanced as the molecular forms in the reactive intermediate of chloroperoxidase[99,107,108]
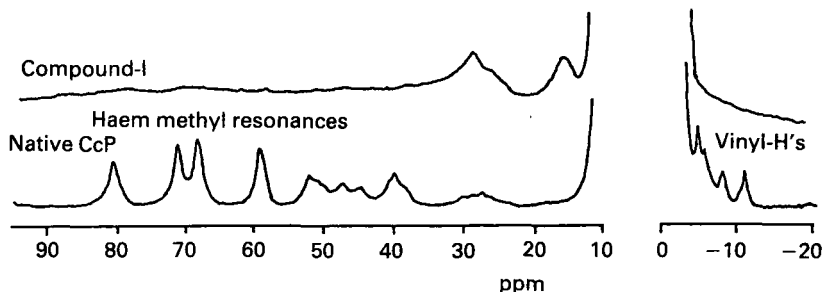
FIG. 34. Proton NMR spectra at 360 MHz of the hyperfine shifted resonances of native CcP in the ferric, high spin state, and the oxidized intermediate (CcP-I). Spectra were recorded at 21 °C, pH' = 7.4. The spectrum of CcP-I was accumulated within 12 min after addition of hydrogen peroxide to CcP. From reference 102, with permission.

and the product of the hydrogen peroxide reaction with myoglobin.[109] Moreover, given the similarity in spectra of the leghaemoglobin reaction product with hydrogen peroxide to HRP-II, CcP-I, CcP-II and oxidized myoglobin spectra, it is possible that a ferryl compound is also present there.[110]

Clearly, if successful modelling of the peroxidase intermediates is to occur, models are required of porphyrin cation free radicals and ferryl porphyrins. Models of iron porphyrin π cation free radicals have been studied,[111-113] as have a group of molecules that apparently possess the $Fe^{4+}=O$ group.[114,115] Specifically, using deuterium labelled octaethyl porphyrin (OEP), the porphyrin meso proton resonance has been assigned in the model ferryl compound N-methylimidazole-(OEP)-FeO, shown in Fig. 35. A comparison with HRP-II (Fig. 36A) reveals a set of resonances at ~15 ppm, in a position similar to the meso proton resonances. These are ultimately assigned by reconstituting HRP with protohaem deuteriated at the meso haem positions and subsequent formation of HRP Compound II. As demonstrated in Fig. 36B the resonances near 15 ppm exhibit reduced intensity in reconstituted HRP-II thereby confirming their assignment.

A second area where iron porphyrin model systems have helped delineate the correct resonance assignments is for the proximal ligand resonances in both ferrous and ferric haem proteins.[116-140,162] As indicated in the Introduction, histidine is the most frequently encountered haem proximal ligand. Substitution by other amino acids usually destabilizes the ferrous iron state resulting in autoxidation and loss of oxygen binding capacity for native haemoglobins and myoglobins. Several model systems were studied prior to 1978 with the purpose of determining the characteristic hyperfine shifts for ligand resonances coordinated to the haem iron. This particular area has been reviewed up to 1979,[4,11] and the results of model studies as well
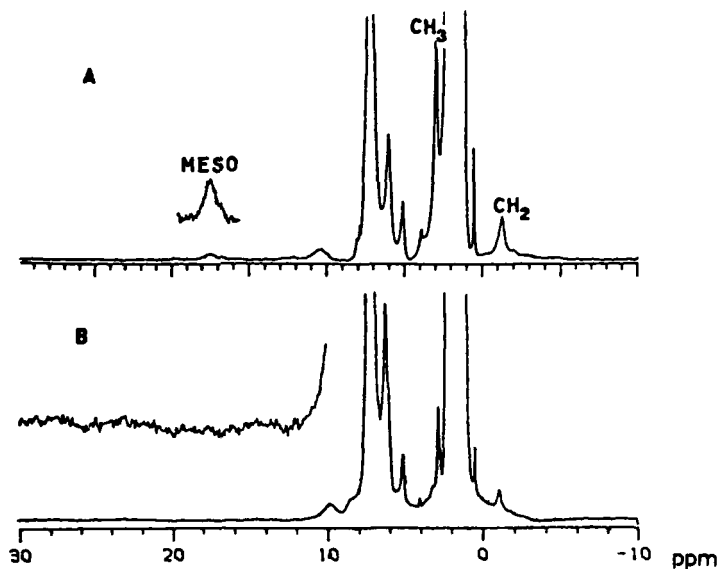
FIG. 35. ^{1}H NMR spectra at 360 MHz of: (A) (N-MeIm)(OEP)FeO at −80 °C; labelled peaks give the resonance assignment of peaks due to the thermally unstable intermediate; (B) (N-MeIm)(OEP-meso-d_4)FeO at −70 °C. Peaks due to the solvent (toluene-d_7) have been cut off. The peak at 6.5 ppm is due to excess N-MeIm; other peaks arise from iron(III) porphyrins. From reference 115, with permission.
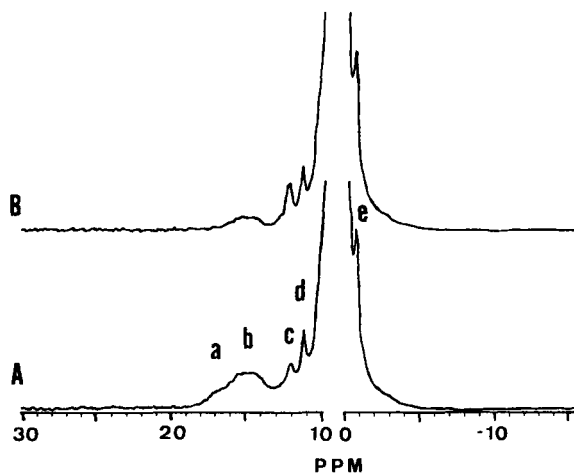

FIG. 36. Hyperfine shifted regions of the 360 MHz ^{1}H spectra of: (A) HRP-II and (B) [meso-^{2}H$_4$]HRP-II in 0.2 M NaCl 99.8% ^{2}H$_2$O at pH 9.2, 25 °C. The low frequency portions of the spectra (shifts greater than 0 ppm) are plotted at 1/4 the vertical scale of the high frequency portions. From reference 115, with permission.

TABLE 7

Description of modified and human mutant deoxy haemoglobins employed in studies of the proximal histidine $N_\delta - H$.

Protein	Description	Quaternary state [a]		Ref.
		pH 6.5	pH 9.0	
HbA	adult human haemoglobin	T	T	137, 139, 140
desArg(α141)HbA	HbA modified by removal of Arg141 in α chain of Arg141 in α chain	T	R	137, 138
desArg(α141)HbA + IHP	in presence of inositol hexaphosphate	T		137, 138
desHis(β146)Arg(α141)HbA	HbA modified by removal of His146 in β chain and Arg141 in α chain	R	R	137
desHis(β146)Arg(α141)HbA +IHP	in presence of inositol hexaphosphate	T		137
NESHbA	HbA modified by reaction of Cysβ93 sulphydryl groups with N-ethylmaleimide	T		124
NESdesArg(α141)HbA	NES HbA lacking Argα141	R	R	137, 138
NESdesArg(α141)HbA + IHP	in presence of inositol hexaphosphate	T		137, 138
desHis(β146)HbA	HbA with His146 in β chain removed	T	T	137
desHis(β146)HbA + IHP	in presence of inositol hexaphosphate	T		137
Hb Kempsey	human mutant β99(G1)Asp $\rightarrow$ Asn		R	139–141
Hb Kempsey	in presence of inositol hexaphosphate	T		139–141
Hb Osler	human mutant β145(HC2)Tyr $\rightarrow$ Asp			124
Hb McKees Rocks	human mutant β145(HC2)Tyr $\rightarrow$ terminal	T		124
Hb McKees Rocks + IHP		R		124
Hb–XL	cross-linked haemoglobin			124

Hb Boston[b] human mutant α58(E7)His $\rightarrow$ Tyr results in ferric α chain haem iron
Hb Iwate[b] human mutant α(F8)His-Tyr results in ferric α chain haem iron
Hb Milwaukee[b] human mutant β57(E11)Val $\rightarrow$ Glu results in ferric β chain haem iron

[a] Resemblance to quaternary structures of human HbA in deoxy and oxy forms defined in references 143, 142.

[b] met-haemoglobins useful in assigning resonances to a particular subunit.

as spectral comparisons made with modified, or naturally occurring, mutant haemoglobins (Table 7) have resulted in a great deal of recent data (Tables 8–10). The potential importance of having a direct spectroscopic probe of the proximal histidine is that fundamental processes of haem protein function are intimately related to the iron–histidine bond. From the proposed trigger mechanism for cooperative ligand binding in tetrameric haemoglobins,[141–143] to the stabilization of highly oxidized catalytic intermediates in haem peroxidases,[116,122] there has been much interest in the proximal histidine.

The first observation of the proximal $N_\delta H$ (Fig. 1) histidine protons in ferrous high spin haem proteins depended upon comparison with model systems and the fact that the imidazole $N_\delta H$ is expected to be deuterium-for-hydrogen exchangeable.[117] Similarly, observations of the $N_\delta H$ in low spin ferric haem proteins have depended on model studies[144,145] (Table 10). Moreover, the question of extensive hydrogen bonding[146,149] or, in the extreme, complete ionization of the proximal histidine[147,148] has resulted in several model studies concerning the properties of imidazolate complexes.[150–152] These have shown that deprotonation of coordinated imidazole does alter ligand binding properties and the proton NMR spectra of the resultant complexes.

However, to date, no native haem proteins have been demonstrated to possess an ionized proximal histidine.[116–125] Most of the strength of this statement comes from direct observation of the proximal histidine $N_\delta H$ using proton NMR spectroscopy. For the ferrous oxidation state this is illustrated in Fig. 37. Similar assignments have been rendered in the ferric oxidation state of several haem proteins as shown in Table 10, including the relevant references.

The question of how such assignments are arrived at can, in fact, be complicated and justifies some further explanation; for high spin, or deoxy, ferrous haem proteins comparison of protein spectra taken in D_2O buffer vs. H_2O buffer identifies the isotope exchangeable resonances. Those resonances appearing between 50 and 100 ppm are shown from model studies to be the proximal histidine $N_\delta H$. For tetrameric haemoglobins, such as human HbA, which consists of α and β subunits, a further question which results is: to which of the subunits (α, β) may the two $N_\delta H$ resonances be assigned? The approach taken is to use human mutant haemoglobins (Boston, Milwaukee, Iwate) in which the mutated subunits possess haem iron oxidized to the ferric state.[118,126] In this oxidized state the coordinated proximal histidine $N_\delta H$ resonance would not be seen in the 55–75 ppm region. Also mixed valency hybrids have been employed[118] with either one set or the other set of subunits in the oxidized state. These result in unambiguous assignments of the $N_\delta H$ resonances as shown in Table 8.[118,126]

TABLE 8

Observed shifts, in ppm, of proximal histidine $N_\delta H$ in ferrous deoxy forms of haemoglobins and myoglobin.

Protein	Temp.	pH	[g]β	[g]α		Ref.
HbA	25	6.8	75.9	63.1		117, 118
	26	6.4	76.1	63.9		124
HbA-$\alpha_2(\beta CN)_2$ [a]	25	6.5		62.4		120
HbA-$(\alpha CN)_2\beta_2$ [a]	25	6.5	74.7			120
HbA-α chain [b]	25	6.5		77.1		120
HbA-β chain β	25	6.5	86.5			120
Hb Boston	25	6.5	73.6			120
	27	6.7	76.0			126
Hb Milwaukee	25	6.5		62.8		120, 126
Hb Iwate	25	6.5	73.9			120
HbA-βPMB chain	25	6.5	76.5			120
HbA-αPMB chain	25	6.5		77.1		120
Hb Kempsey [d]	25	6.5	77.7	67.3		120
	27	6.4	76.8	67.1		119
Hb Kempsey [c] + IHP	25	6.5	77.1	64.6		120
	27	6.4	75.9	64.6		119
HbA + IHP	27	6.4	75.3	63.1		119
HbA + DPG	27	6.4	75.7	63.2		119
desHis(β146)HbA[c]	25	6.5	76.4	63.9		120
NESdesArg(α141)HbA[d]	25	6.5	78.2	75.9		120
	36	6.0	76.2	73.1		124
NESdesArg(α141)HbA[c] + IHP	36	6.0	73.2	64.5		124
NES HbA	36	6.0	73.5	62.6		124
Hb Osler	27	6.8	80.4	64.1		119
Hb Osler + IHP	27	6.8	78.5	63.8		119
Hb McKees Rocks[c] + IHP	36	6.4	77.2	62.7		124
Hb McKees Rocks[d]	27	6.8	78.3	63.9		119
desHis(β146)Tyr(β145)HbA[e] + IHP	36	6.4	77.5	62.4		124
Hb-XL[e]	26	6.4	75.7	64.1		124
Hb rabbit[f]	25	6.8	75.9	62.2		TW[i]
Hb carp[d]	31	6.3	80.7	72.9		123
	25	8.6	81.4	73.3		
Hb carp[c]	31	5.1	74.5	69.3		123
	25	6.0	74.9	70.0		
Sprm whale Mb	25	6.8			77.8	117
					78.2	127
					81.1[h]	127
C. thummi thummi Hb-I	25	7.0			~93.0	128
C. thummi thummi Hb-III	25	7.0			92.2	128
C. thummi thummi Hb-IV	25	7.0			91.0	128

[a] Mixed oxidation state tetramers.
[b] Isolated chains.
[e] Cross-linked using bis(3,5-dibromosalicyl) fumarate.
[g] Estimated accuracy in observed shifts is better than ±0.3 ppm reported relative to DSS.
[h] Myoglobin modified with cyanogen bromide so that histidine E-7 (distal) is chemically modified.

[c] T-like quaternary structure.
[d] R-like quaternary structure.
[f] New Zealand White.
[i] TW = this work.

TABLE 9

Observed shifts (ppm, relative to DSS) of proximal histidine $N_\delta H$ in Co(II) and Fe(II) haem proteins.

Protein	Temp.	pH	$\alpha(Co)_2$	$\beta(Co)_2$	$\alpha(Fe)_2$	$\beta(Fe)_2$	Ref.
Horseradish peroxidase	25	7.0				79.2	129
	25	9.0				86.1	129
R. rubrum cyt. c'	25	5.4				93.0	130
C. thummi thummi III-deut[a]	25	6.0				92.4	128
						94.0	128
C. thummi thummi IV-deut[a]						90.4	128
						92.8	128
$CoHb(\alpha Co)_2(\beta Co)_2$[b]	23	7.0	53.8	58.4			125
$CoHb(\alpha Co)_2(\beta Fe)_2$[b]	23	7.0	53.3			75.9	125
$CoHb(\alpha Fe)_2(\beta Co)_2$[b]	23	7.0		57.9	63.2		125
$CoHb(\alpha Co)_2(\beta Fe\text{-}CO)_2$[b]	23	7.0	61.4				125
$CoHB(\alpha Fe\text{-}CO)_2(\beta Co)_2$[b]	23	7.0		58.7			125
HbA	25	6.8			63.1	75.9	117, 118

[a] Deuteriohaemin reconstituted.

[b] Co(I)-protohaem reconstituted hybrids.

TABLE 10

Observed shift (ppm, relative to DSS) of proximal histidine $N_\delta H$ in variously ligated ferric forms of haem proteins.

Protein	Temp.	pH	Shift	Ref.
Horseradish peroxidase-CN	25	7.0	31.6	116, 38
Cytochrome c peroxidase-CN	22	7.0	28.3	122
Sperm whale Mb-CN	25	8.5	21.0	31, 133, 116
Elephant Mb-CN	40	8.6	19.7	43
D. dentriticum Hb-CN	27	7.6	17.2	162
Sperm whale Mb-H_2O	35	6.2	103	116, 134
Horseradish peroxidase	35	7.0	96	116
R. palustris cyt. c'	25	5.4	102	135
D. dentriticum Hb	25	7.3	96	162
Sperm whale Mb-N_3	25	6.0	33.0	136
C. thummi thummi Hb(III)-N_3	25	6.0	42.0	136

These assignments have been instrumental in opening up studies of ligation associated structure changes in the tetrameric haemoglobins.[119,120,123,124] Particularly important is the fact that inositol hexaphosphate (IHP) is effective in altering the apparent quaternary structure for several modified and mutant haemoglobins, within the ferrous, deoxy state (Tables 7, 8). For example, Hb Kempsey in the deoxy ferrous state
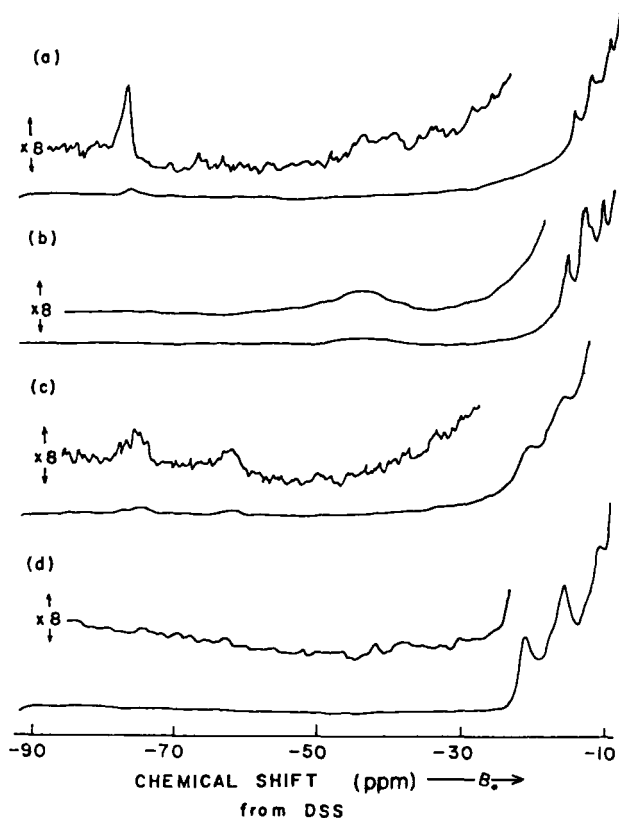
FIG. 37. Proton NMR spectra of deoxy myoglobin and haemoglobin. The high frequency NMR traces of: (a) 14 mM sperm whale deoxymyoglobin in 0.2 M NaCl.H$_2$O, pH = 6.8, 40 K transients; (b) 9 mM sperm whale deoxymyoglobin in 0.2 M NaCl, 99.8% D$_2$O, 'pH' = 7.0, 10 K transients; (c) 4 mM deoxyhaemoglobin A in 0.2 M NaCl.H$_2$O, pH = 6.0, 50 K transients; (d) 4 mM deoxyhaemoglobin A in 0.2 M NaCl, 99.8% D$_2$O, "pH" = 6.3, 50 K transients. Chemical shifts are referenced against internal DSS; probe temperature is 25 °C. From reference 117, with permission.

has a quaternary structure characteristic of the oxygenated form of normal human haemoglobin.[119] In the presence of IHP, deoxy Hb Kempsey can be switched to a quaternary structure resembling deoxy human HbA.[119] In another terminology, the molecule can be converted from the R to the T quaternary state.[119,137,143] The proximal histidine N$_\delta$H resonances in ferrous deoxy haem proteins exhibit characteristic shifts that have been used to study the effect of quaternary structure changes on the iron–histidine bonding.[119,120,124,160]

A similar effort has been undertaken using human hBA and carp haemo-globin.[161] The latter has been advocated as a protein capable of being switched between the T and R quaternary states in both ligated and unligated forms. These two proteins are studied in the ferrous, deoxy form and the ferric, cyanide ligated form. Figure 38 shows that carp haemoglobin in the ferrous, deoxy form exhibits two proximal histidine protons near 70 ppm where the N_δ should appear (Fig. 38B). These have been assigned to β (76 ppm) and α (70 ppm) subunits by analogy with HbA. Raising the pH converts this protein from a state resembling the T state in HbA to a state that resembles the R state. However, in the carp haemoglobin both the $N_\delta H$ resonances, and those with shifts of 15–25 ppm, are less well resolved and much broader than the corresponding peaks in HbA. This fact and data from the cyanide ligated carp met-haemoglobins has been taken as evidence for extensive haem centred heterogeneity in carp haemoglobin.[161] If sub-stantiated, this is significant in being the first reported observation of such heterogeneity in a native tetrameric haemoglobin. Additional results from this study indicate that carp met-azide haemoglobin can be switched from the R to the T state in a manner similar to human met-Hb-N_3.[162,163]
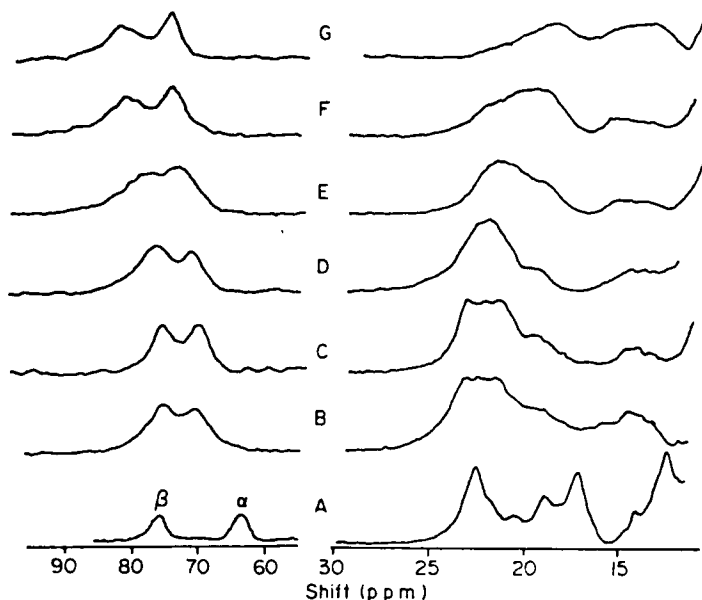

FIG. 38. Hyperfine shifted portions of the 200 MHz ^{1}H NMR spectra of: (A) deoxy HbA, pH 6.0; (B) carp deoxy Hb at pH 6.0 with 3 equivalents of IHP; (C to I) carp deoxy Hb in the absence of IHP at pH: C, 6.53; D, 7.57; E, 7.88; F, 8.33; G, 8.58. All proteins were in 90% H$_2$O/10% ^{2}H$_2$O at 25 °C. The ratio of the vertical scales for the region 60–90 ppm ($\times$6) and 12–30 ppm ($\times$1) is constant in A, B and C. From reference 161, with permission.

A related approach has been taken in an effort to obtain information on the partially ligated haemoglobin intermediates.[124] Hybrid haemoglobins of various ligation states have been used, but where either α or β subunits are created from globin chains reconstituted with protoporphyrin(ix)-cobalt(ii). The paramagnetism of cobalt +2 also leads to proximal histidine $N_\delta H$ shifts to high frequency.

Mixed valence hybrids have been employed as part of a continuing effort to elucidate the molecular details of haemoglobin ligation and its associated structural changes.[153–160] A large amount of work employing ferrous native haemoglobins has also been reported.[2] Among many significant conclusions, it has been shown for human haemoglobin mixed valence tetramers that α chain hyperfine resonances are sensitive to the ligation state of the β chains whereas the opposite is not indicated.[159,160]

Hyperfine resonances appearing between 6 and 20 ppm from the water resonance have been employed to study ferrous haemoglobin oxygenation and its quaternary and tertiary structural changes. Using mutant haemoglobins, attribution of the hyperfine resonances in this region to either α or β chains has been accomplished.[158] In combination with two other resonances, one that has been indicated as a tertiary structural marker[155] (6.4 ppm relative to HDO) and another assigned as a quaternary conformation indicator (9.4 ppm relative to HDO),[160] these resonances have been used to reach several conclusions. Among these are: (i) there is no preferential oxygen binding to the different types of haemoglobin chains in the absence of organic phosphates; (ii) in the presence of organic phosphates the α chains exhibit preferential oxygen ligation compared with the β chains; (iii) the structural changes induced by ligation are not concerted.

In high spin ferric haem proteins the assignment of the proximal histidine $N_\delta H$ is made primarily by analogy to the high spin ferrous proteins and the disappearance of a highly shifted ($\sim$90–100 ppm), single proton line when the solvent is changed from H_2O to D_2O.[116] For low spin ferric haem proteins the hyperfine shift region may consist of several isotope exchangeable resonances,[116,122,132,133] thereby complicating assignments. Consequently, the evidence for assigning the proximal histidine $N_\delta H$ resonance must be obtained from relaxation and pH behaviour of the isotope exchangeable resonances.[132,133] The use of relaxation measurements in this manner is illustrated in a later section.

E. Assignments by decoupling

In smaller proteins, those of approximate molecular weight 14 kD or less, it is frequently possible to assign resonances of a coupled spin system using common homonuclear decoupling methods. This has been done in assigning haem vinyl group protons directly in paramagnetic monomeric haemo-

globins.[44,83] It has also been employed to make assignments to haem c thioether bridge proton resonances and to elucidate the axial methionine's more complicated spin–spin coupling pattern in c-type ferrous cytochromes.[61,62,70,176] These assignments have subsequently been extended to c type ferricytochromes by saturation transfer experiments.

This technique has recently been employed to identify the α and β proton resonances of the haem coordinated histidine (His-18) in tuna ferricytochrome c^{165} (Fig. 39). Using a combination of nuclear Overhauser experiments and resolution enhanced spectra it is concluded that peaks labelled
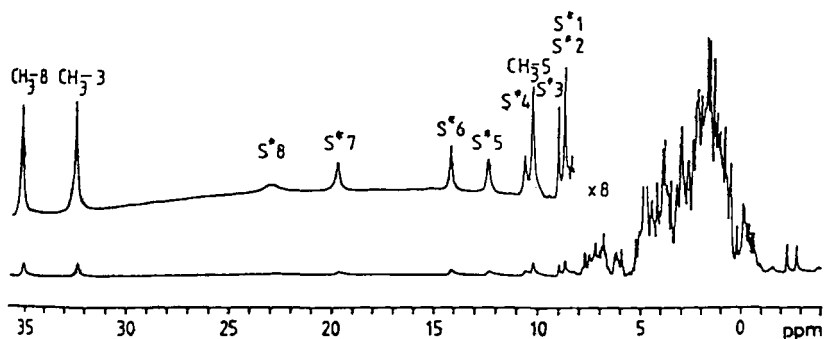
FIG. 39. 300 MHz ^{1}H NMR spectra of 4 mM tuna ferricytochrome c in ^{2}H$_2$O at 27 °C. S*1–S*8 are single proton resonances. S*1 and S*2 overlap at this temperature. From reference 165, with permission.

S*1, S*3, S*6 in Figs 39 and 40 belong to a coupled spin system. S*1 and S*6 are quite broad relative to S*3 which appears as a relatively narrow doublet. Irradiation at S*1 collapses the S*3 splitting (Fig. 40b) and irradiation at the frequency corresponding to peak S*6 exerts very little effect on S*3. The authors interpret these results to indicate that these three proton resonances reflect the $-C^\alpha HC^\beta H_2-$ spin system in histidine-18 (Fig. 1). They account for the different decoupling effects described above by employing a Karplus equation to calculate the expected couplings for this type of molecular fragment: $C^\alpha H(S*3)-C^\beta H_1$ (1.7 Hz) and $C^\alpha H-C^\beta H_2$ (11.6 Hz).

F. Assignments of amino acids not directly bonded to haem iron

Nuclear Overhauser effects, which are observed for protons of amino acids not directly bonded to the haem group, can be used to locate these residues spatially and, in conjunction with crystal structures and/or sequence homology comparisons, to make assignments. These assignments
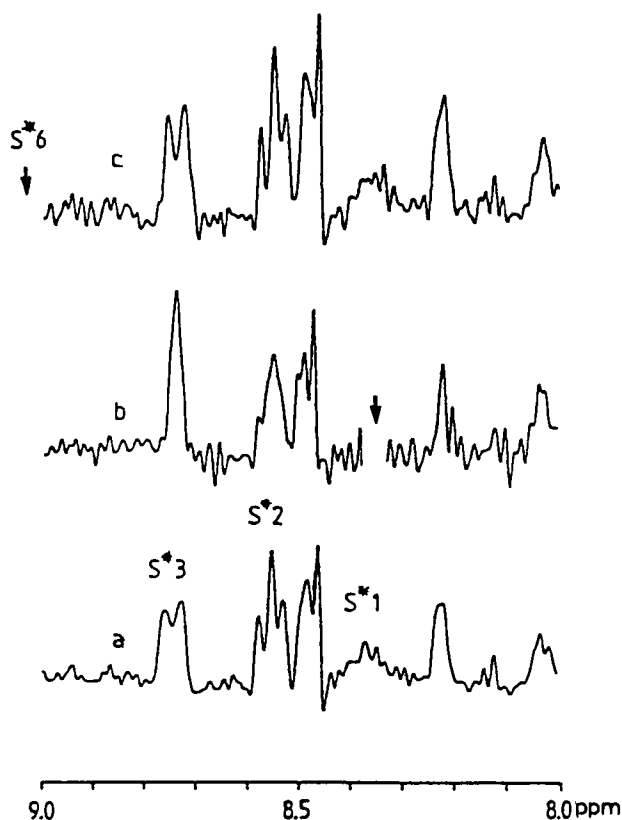
FIG. 40. Spin decoupling of S*1, S*3 and S*6 of 4 mM tuna ferricytochrome c at 37 °C: (a) resolution enhanced normal spectrum; (b) spin decoupling pulse applied to S*1, S*3 is decoupled and S*2 (Phe-10 para) is partially decoupled by the simultaneous irradiation of Phe-10 meta; (c) spin decoupling pulse applied to S*6. From reference 165, with permission.

can be refined if spin–spin coupling patterns are present through homonuclear decoupling experiments such as those described previously. For the most part this technique has been effectively demonstrated primarily for diamagnetic haem proteins, as in the case of S. platensis cytochrome c-553.[166]

A further extension of these techniques includes making a general inventory of the types of amino acids present in a given protein. Subsequently their characteristic proton coupling patterns and the general area of the spectrum in which a given type of amino acid is expected to yield proton resonances is considered. Further specific assignments can be made using Overhauser effects, decoupling, homology, comparison of calculated ring current shifts and crystal structures. Again, such methods depend upon

protein diamagnetism, knowledge of the primary sequence and three-dimensional structure.[167]

In studies of eukaryotic ferricytochromes c, resonances have been assigned within the spectral region between about 0 and 10 ppm. This region is populated by resonances both near to and far from the paramagnetic haem centre, and this fact serves as a reminder that highly temperature dependent resonances, indicating that these protons experience a significant paramagnetic field, can occur in this region. In fact, the shifts of these protons are very difficult to reconcile precisely with predictions made from ring current calculations or calculations using the paramagnetic shift equations due to the combination of effects that establishes any particular shift. The strategy adopted involves all the techniques mentioned in the preceding paragraph as well as the use of the extrinsic relaxation probes $[Cr(CN)_6]^{3-}$ and $[Cr(oxalate)_3]^{3-}$ which bind to specific sites on the surface of the cytochromes.[174] Some of the results for horse and tuna ferricytochromes c are presented in Table 11.[74] It should be pointed out that extrinsic relaxation probes can be employed for assigning haem resonances. Other than the complexes mentioned above, Gd^{3+} binds to haem propionates and broadens neighbouring proton signals, leading to assignments of the haem 5,8 methyl pair.[175]

One of the major problems encountered in the 0-10 ppm region of the proton spectrum is the rather poor resolution caused by the presence of overlapping resonances. For example, it has been calculated that the region of the proton spectrum where aliphatic protons resonate (5-6.5 ppm and 2.5 to -1 ppm) contains 600 resonances for a protein even as small as horse cytochrome c (~12 kD molecular weight).[73] Compared with this the aromatic region is predicted to contain resonances of only 47 protons.[73] Consequently, virtually all the studies mentioned in this section rely on one of several techniques for enhancing resolution. These include digital filtering with a sinebell function[169] and convolution difference methods.[170] In addition, a Carr-Purcell pulse sequence ($90°-\tau-180°-\tau$) has been employed to enhance resolution and discriminate multiplets in studies of the many histidine resonances of various ferric myoglobin forms.[171] The assignments are aided by homology comparisons of sperm whale, horse and pig metmyoglobins.

Another instance of homology considerations leading to an assignment of a functionally relevant amino acid is the identification of the titrating residue in myoglobins.[172] Many spectroscopic results indicate a pH dependent structural effect in the myoglobin haem crevice. Included in these are pH dependent hyperfine shifts.[172,173] Using haem methyl assignments, reconstituted protein and comparisons with elephant myoglobin the histidine at position FG3 has been proposed as the titrating residue.[172] These results clearly indicate a coupling between the electronic structures of histidine

TABLE 11

Comparison of tuna and horse ferricytochromes *c* NMR spectra.

	Horse		Tuna	
Assignment	resonance[a]	chemical shift (ppm)[b]	resonance[a]	chemical (ppm)[b]
His-26 C-2	A*4	7.62	TA*2	7.74
His-26 C-4	A*9	7.01	TA*11	7.02
Trp-59 C-2	A*11	6.86	TA*12	6.90
Trp-59 C-4 or C-7	A*6	7.57	TA*4	7.53
Trp-59 C-5 or C-6	A*16	6.31	TA*18	6.33
Trp-59 C-6 or C-5	A*15	6.54	TA*17	6.58
Trp-59 C-7 or C-4	A*7	7.37	TA*6	7.39
Tyr-74 *ortho*	A*5	7.62	TA*3	7.61
Tyr-74 *meta*	A*12	6.82	TA*13	6.82
Tyr-97/48(?)	A*10	7.01	TA*10	7.04
Tyr-97/48(?)	A*17	6.2	TA*19	6.3
Phe-82 *para*	A*2	8.26	TA*1	8.2
Phe-36 *ortho*	A*8	7.23	TA*8	7.17
Phe-36 *meta*	A*14	6.64	TA*16	6.73
Phe-36 *para*	A*13	6.76	TA*14	6.83
Phe-10 *ortho*	A*18	6.2	TA*20	6.32
Phe-10 *meta*	A*18	6.2	TA*20	6.32
Met-80 CH_3	M*1	−21.0	TM*1	−21.0
Ile-81/75(?)	M*2	−2.07	TM*2	−2.12
Ile 57 δCH_3	M*6	−0.18	TM*6	−0.07
Met-65 CH_3	M*19	1.94 ⎤	TM*16	1.96
N-Acetyl CH_3	M*20	1.97 ⎦	TM*17	1.96
Thr(?)	M*21	2.03	TM*18	2.05
Thr(?)	C*3	5.37	TC*3	5.33
Ala-15 CH_3	M*22	2.07	TM*19	2.08
Ala-15 αCH	C*4	5.63	TC*4	5.60
His-33 C-2	A*1	8.62	—	—
His-33 C-4	A*3	7.69	—	—
Trp-33 C-2	—	—	TA*7	7.37
Trp-33 C-4 or C-7	—	—	TA*5	7.39
Trp-33 C-4 or C-6	—	—	TA*9	7.12
Trp-33 C-6 or C-5	—	—	TA*15	6.72
Trp-33 C-7 or C-4	—	—	n.d.	n.d.

[a] A = aromatic; M = non-haem methyl; C = non-haem aliphatic.
[b] At pH 5.25 and 57 °C. N.D. = not determined.
From reference 74, with permission.

FG3 and the haem. The proposed interaction is via $\pi-\pi$ overlap, and the demonstration of such an effect adds another means by which active site (haem) properties may be influenced by the polypeptide chain. This result establishes the possibility that $\pi-\pi$ interactions within a haem pocket may be an effective and subtle way to regulate haem protein reactivity.

Examples of more direct methods for assigning those residues in close proximity to the paramagnetic haem site, which as a consequence may experience sizeable pseudocontact shifts and dipolar line broadening, are not plentiful in the literature. One such study which has previously been mentioned is that employing Overhauser effects and reconstituted protein to assign two methyl groups and two single proton resonances of isoleucine-99 in sperm whale myoglobin.[75] This amino acid lies close to haem position 4. Thus, the observation of large Overhauser enhancements to two methyl and two single proton resonances when the 4-H line of deuteriohaemin reconstituted met-myoglobin cyanide is saturated yields this assignment, and the relative orientation of the side chain is shown to be identical with that of the crystal structure.[75,76]

G. Assignments from calculations based on the hyperfine shift equations

Very early in the study of haem proteins by proton NMR two facts were appreciated. The first is that meaningful studies require resonance assignments. The working assumption of this report is that the goal of NMR studies of haem proteins is to elucidate the molecular level events associated with the particular function of the protein being studied. NMR is uniquely capable of providing such information along with solution structural information. Second, it was recognized that the pattern of resonances in paramagnetic haem proteins reflects either contact or pseudocontact shifts, or a combination of both.

Assuming that the observed resonance shifts in cytochrome b_5 are predominantly due to pseudocontact shifts and/or ring current shifts, it is possible[42] to calculate the predicted shift for every proton in this molecule. This approach relies upon known crystal structure data and ESR data and employs an equation for the specific case of a molecule that possesses a rhombic g tensor.[176] Since single crystal ESR measurements have not been carried out the g tensor axes are not uniquely located, so the procedure involves the search for a unique fit to the observed resonance pattern. Uniqueness is reported[42] despite the simplifying assumptions, such as use of the g tensor rather than the magnetic susceptibility tensor and neglect of contact contributions to the resonance positions.

This technique has been refined to include variations in linewidths between different resonances caused by differential dipolar relaxation and applied to resonance assignments in cytochrome c[59] and cytochrome b_5.[176]

The cytochrome b_5 study, along with work on met-myoglobin cyanide,[177] devotes attention to contact effects that contribute to the observed resonance positions. More recent work on tuna cytochrome c reveals that there is a linear trend, but not a precise correlation, between observed and calculated pseudocontact shifts for the methyl resonances of amino acids.[178]

Despite this work, widespread rationalization of observed resonance shifts with structure, employing the theoretical framework currently available, has not proceeded. The reasons for this must include the limited quantitative value of the hyperfine shift equations. This drawback originates in the necessity for understanding a very complicated electronic structure, including metal ion, porphyrin ring and axial ligands. In addition, precise structural information for the protein of interest must be known, and in the best circumstances the magnetic axes must be located.

Nevertheless, attempts are still being made to understand the origin of shifts in haem proteins,[179] and any such insights are to be welcomed. Recently, the observed methyl shift pattern in both high and low spin ferric porphyrin model systems and ferric haem proteins relative to the electronic structure of the ferric ion have been rationalized.[179] The results show that, as expected, the haem methyl resonances are probes of the electron distribution about the central metal ion. This idea was first advanced by Wüthrich who called attention to the pronounced C_2 symmetry (separation into pairs) of the methyl resonance pattern in cytochrome c.[59] Similar observations are made for met-myoglobin cyanide,[177] and the data of Table 12 show that C_2 symmetry is the rule for many c-type ferric cytochromes. This is also true for many low spin ferric b-type haem proteins (Table 4) including HRP-CN[37,38] and CcP-CN[36] where the 8,3 methyls occur as a pair, resonating near 20 ppm, and the 1,5 methyls are not observed, presumably because they are shifted to low frequency and are not resolved under the many overlapping resonances that occur between 0 and 10 ppm. This pattern of shifts reflects the asymmetry of the wavefunction containing the unpaired spin density. In the case of contact shifts this is likely to be a linear combination of metal centred and porphyrin centred atomic orbitals.[11,177] The origin of this C_2 symmetry has been the subject of much inquiry and is discussed in a later section.

It has also been shown that the pattern of haem methyl shifts can be fitted to an empirical equation that includes only rhombic perturbations on an unperturbed C_{4v} ground state.[179] It is thus clear that conclusions arrived at by comparing spectra of model systems and proteins are now placed on a firmer theoretical basis. These conclusions include the fact that the complexation of apo-protein with protohaemin results in greater triclinic perturbations of the electronic ground state of the haem than exist for the free haem in solution. In fact, only one substituted haem model has been identified that approaches the extent of rhombic perturbation that myoglobin

TABLE 12

Assigned proton NMR resonances in ferricytochrome c from various species.

	Temp.	pH[a]	Haem methyls				Axial methionine			Axial histidine	Ref.
			1	3	5	8	ε^1	γ^1	γ	c_δ-H	
c Horse heart	35	7.0	7.4	31.2	10.5	33.9					59
c Tuna	27		6.2	32.4	10.3	35.2					165
c S. cerevisiae Iso-1	35	6.7	7.9	30.6	11.2	33.9[c]	−23.6	−26.8	−31.0	25.5	62
c S. cerevisiae Iso-2	35	6.7		29.8	11.9	33.1[c]	−22.4	−24.7	−31.7	25.4	62
c C. krusei	35	7.2		29.8	10.9	32.4	−23.9	−25.1	−32.7	25.5	62
c_2 R. rubrum	20	6.0	10.8	30.1	15.1	33.9	−15.9	−13.3			63, 79
c-557 C. oncopelti	26	7.3	8.8	31.3	12.9	32.7					61
c-552 E. gracilis	33	7.5	13.2	33.2	17.4	38.5					69
c-5 P. mendocina	35	7.5	19.0	27.0	24.5	39.3	−10.2	−13.4			64
c-553 S. platensis	35	7.1	14.9	32.5	17.1	37.2	−9.1				166
c-553 D. vulgaris	35	7.0	20.7	23.4	22.1	30.7[c]	−8.7	−8.3			70
c-553 C. desulphuricans	35	7.0	14.4	29.7	20.4	36.8[c]	−9.5	−12.4			
c-551 P. stutzeri	35	6.8	22.1	12.3	31.9	17.6	−15.3	−12.7	−39.2		63
c-551 P. mendocina	35	7.0	22.0	13.8	31.2	17.9	−16.4	−9.3	−40.7		63
c-551 R. gelatinosa Iso-1	35	7.4	25.4	12.2	32.2	21.5	−9.9		−29.6		65
c-551 R. Gelatinosa Iso-2	35	7.4	29.6[c]	10.8	35.6	17.2[c]	−9.9		−25.1		65
c-551 P. aeruginosa	27	7.0	24.8	13.4	32.1	17.8					66
c-555 C. thiosulphatophilum	35	7.0	27.9	34.1	39.1	53.7					67

[a] pH's are not reported in tabular data from these references. Reported pH here is within ±0.6 pH unit for the range reported for all spectra in any given reference.

[b] All axial shifts reported at 20 °C.

[c] 1,8 resonances not unambiguously identified and the actual assignment may be reversed from that reported here.

exhibits (see below). Finally, it is to be noted that this analysis suggests a stronger influence of the triclinic perturbation in low spin ferric haem cases ($S = 1/2$) than in the high spin ferric haem cases ($S = 5/2$), which are shown to exhibit a ground electronic state symmetry of approximately C_{4v}.

H. Assignments of isotope exchangeable resonances using relaxation methods

It was previously mentioned that many of the data concerning assignments of proximal histidine $N_\delta H$ in low spin ferric haem proteins come from relaxation studies. Assignments of the distal histidine exchangeable ring NH and the FG2 histidine ring NH in sperm whale myoglobin come from dipolar relaxation measurements as well.

The principles of nuclear relaxation induced by paramagnetic ions are described in the Introduction. For the purposes of this section it is necessary to recall that, when dipolar relaxation dominates the nuclear relaxation mechanism, the ratio of relaxation rates for any two non-equivalent protons (a, b) describes a ratio of their respective distances from the paramagnetic centre. In this case the two protons at distances r_a and r_b from the haem iron ion exhibit relative T_1 values given by

$$\frac{T_{1a}}{T_{1b}} = \frac{r_a^6}{r_b^6} \tag{14}$$

Therefore, determination of T_{1a} and T_{1b}, *in circumstances for which metal centred dipolar relaxation is the sole contribution to the proton's spin–lattice relaxation time*, can yield the relative distances of the two protons (a, b). If one of these distances is well defined as, for example, a haem methyl group, the iron–nucleus distance for the remaining proton can be directly calculated. Note that the haem methyl is chosen as a standard because of its fixed geometry relative to the haem iron ion.

This method is illustrated for met-myoglobin cyanide[132] (Fig. 48). The proton NMR spectra of met-myoglobin cyanide in H_2O and D_2O are shown in Fig. 41. In H_2O solution the isotope exchangeable peaks labelled a–d appear between 12 and 24 ppm. The relative relaxation times (T_1) are calculated from the slopes of intensity plots shown in Fig. 42. These data for Mb-CN,[132,133] as well as data reported for met-leghaemoglobin cyanide[131] and Mb-CN reconstituted with protohaem derivatives that have various substituents at the 2,4 haem positions (which are occupied by vinyl groups in protohaem), are collected in Table 13.

There are several things to note from this table. Most interesting is that no distal histidine ring NH (Fig. 48) is identifiable in the spectrum of met-Lb-CN. Peak "a" in the met-Lb-CN spectrum is assigned to the proximal histidine $N_\delta H$. The latter "a" in this case refers to the initial labelling of the deuterium exchangeable peaks in which this is the highest
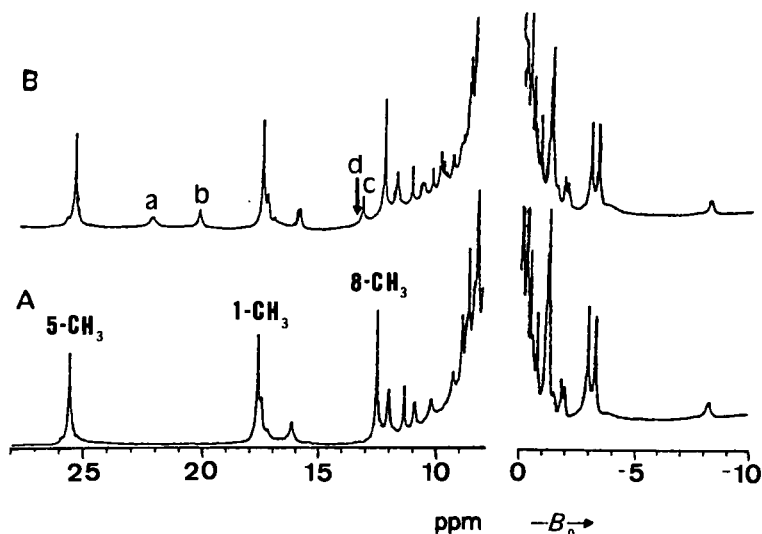
FIG. 41. 360 MHz ^{1}H NMR spectrum of the resolved resonances of sperm whale met-Mb-CN at 40 °C, pH 8.56 in 0.2 M NaCl. (A) ^2H_2O and (B) 90% H_2O/10% ^2H_2O with the H_2O signal saturated. The previous methyl assignments are included in A. Three of the four exchangeable proton signals of interest are labelled a–c in B; the position of d is indicated by an arrow. The intense, largely unresolved diamagnetic region is omitted. From reference 132, with permission.

frequency resonance of this type. Secondly, peak "a" in met-Mb-CN is assigned to the distal imidazole ring NH based on the fact that X-ray structures reveal it to be closer to the paramagnetic iron than the proximal histidine $N_\delta H$ (peak b). In such a position the distal histidine NH should experience more efficient dipole induced relaxation, as well as a greater shift. The lower part of Table 13 indicates that neither the shifts of these two protons (peaks a, b) nor their T_1 values are dramatically affected by reconstituting apo-myoglobin with modified haems. Finally, it should be mentioned that the assignments of peaks a and b, that are placed on a quantitative foundation by relaxation studies,[131–133,180] are in exact agreement with those of Sheard et al.[181] who use a semiquantitative assessment of expected contact and pseudocontact contributions to observed shifts in order to derive their assignments.

It is important to emphasize that measurements such as those just described are valid for conditions that yield good estimates of T_1. Consequently care must be taken to ensure that dynamic exchange processes are slow or halted altogether for the protons of interest. In fact, the dynamic exchange information that can be derived for isotope exchangeable protons of the haem pocket is of great importance to the overall dynamic picture

TABLE 13

Summary of shifts, relaxation times and distances for several cyanide ligated ferric sperm whale myoglobins and soybean ferric leghaemoglobin.[131–133,180]

Protein	pH	Temp.	Peak.	Assignment	X-ray structure (r-peak/r 1-CH$_3$)	T_1 (ms)	NMR data (T_1 peak/T_1 1-CH$_3$)$^{\mid}_{\S}$	Shift (ppm)
Mb-CN	8.6	25	a	distal histidine ring NH	0.67	9.3	0.66–0.70	22.1
	8.6	25	b	proximal histidine N$_\delta$H	0.81	25.5	0.77–0.82	20.3
	8.0	25	c	proximal histidine peptide NH	1.10	114	0.98–1.04	13.2
	8.6	25		1-CH$_3$	1.0	115		
Lb-CN	7.0	25	a	proximal histidine N$_\delta$H	0.81	35.2	0.77–0.80	18.3

<div align="center">Reconstituted Mb-CN</div>

Protein	pH	Temp.	Peak.	Assignment	X-ray structure (r-peak/r 1-CH$_3$)	T_1 (ms)	NMR data (T_1 peak/T_1 1-CH$_3$)$^{\mid}_{\S}$	Shift (ppm)
2,4 vinyl	8.6	25	a	distal histidine ring NH		8.7		23.5
	8.6	25	b	primal histidine N$_\delta$H		22.4		21.3
2,4 acetyl	8.6	25	a	distal histidine ring NH		8.0		22.9
	8.6	25	b	proximal histidine N$_\delta$H		22.4		21.9
2,4 bromo	8.6	25	a	distal histidine ring NH		8.3		24.0
	8.6	25	b	proximal histidine N$_\delta$H		23.1		21.1
2,4 ethyl	8.6	25	a	distal histidine NH		—		24.5
	8.6	25	b	proximal histidine N$_\delta$H		23.0		21.2
2,4 H	8.6	25	a	distal histidine ring NH		8.6		23.4
	8.6	25	b	proximal histidine N$_\delta$H		23.1		21.0

From reference 132, with permission.
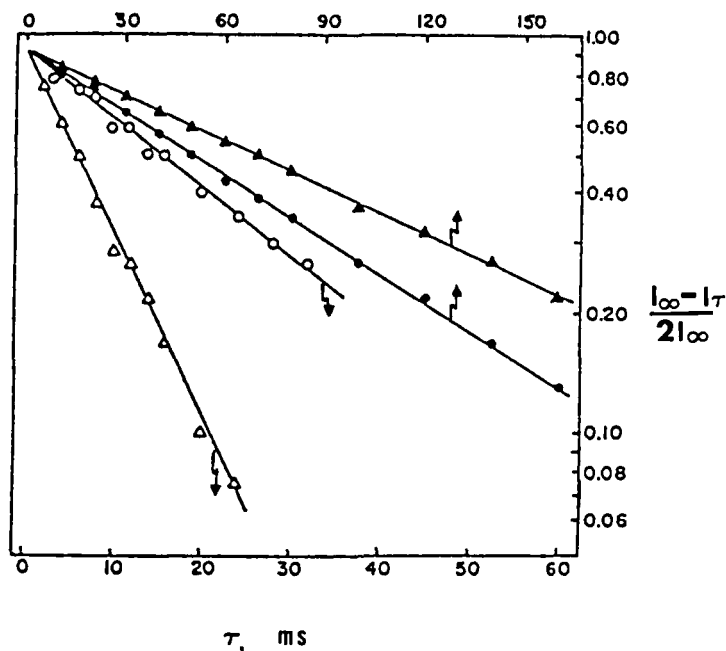
FIG. 42. Plots of $\ln(I_\infty - I_r)/2I_\infty$ versus τ for a 180°-τ-90° sequence T_1 determination for 1-CH$_3$ (▲), 5-CH (●), peak a (△), and peak b (○) of met-Mb-CN in 90% H$_2$O at 25 °C, pH 8.56. The saturation factor for peaks a and b is essentially unity under these conditions. The data for 1-CH$_3$, 5-CH$_3$, and peaks a and b refer to the upper and lower scales in τ, respectively. From reference 132, with permission.

of the haem site. A further complicating feature is the appearance of cross relaxation or spin-diffusion that might complicate the evaluation of T_1 by yielding curved semi-log intensity plots rather than straight lines as in Fig. 42.[85-91] This can result in inaccurate T_1 values and care must be exercised in analysing T_1 data for paramagnetic haem proteins. As examples we may consider the T_1 data for cytochrome c peroxidase-CN (Figs 17, 18) shown in Figs 43 and 44. In Fig. 43 the inversion recovery results are displayed by using a three-parameter fit and a plotting routine that is now a standard feature of most NMR software. The results appear to be described by a single exponential, with no hint of multiple exponential decay symbolic of extensive cross relaxation. However, a more critical treatment of the data (Fig. 44) reveals that the magnetization recovery is characterized by a fast component at short τ values (in the 180°-τ-90° sequence) and a slower component at longer τ values. Such deviations are not likely to be attributable to inaccuracy of the fully relaxed peak amplitude for the reason that τ values up to approximately 20 T_1 are employed. Moreover, these measure-
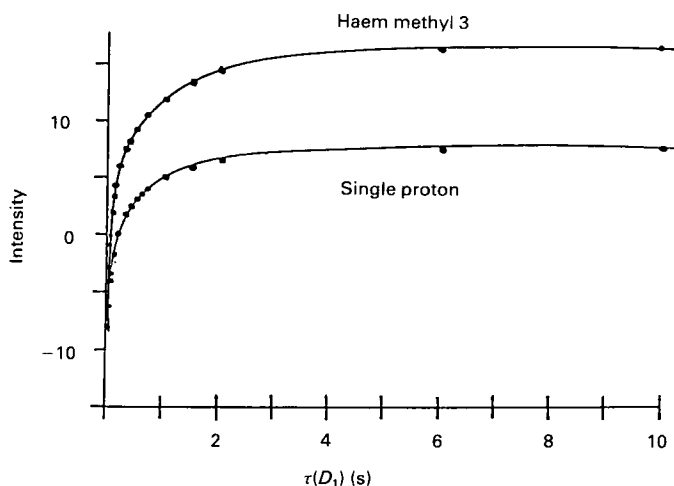
FIG. 43. Resonance intensity data as a function of the delay time in the 180°-D_1-90° pulse sequence for the CcP-CN haem methyl 3 and a single proton resonance at 14.3 ppm.
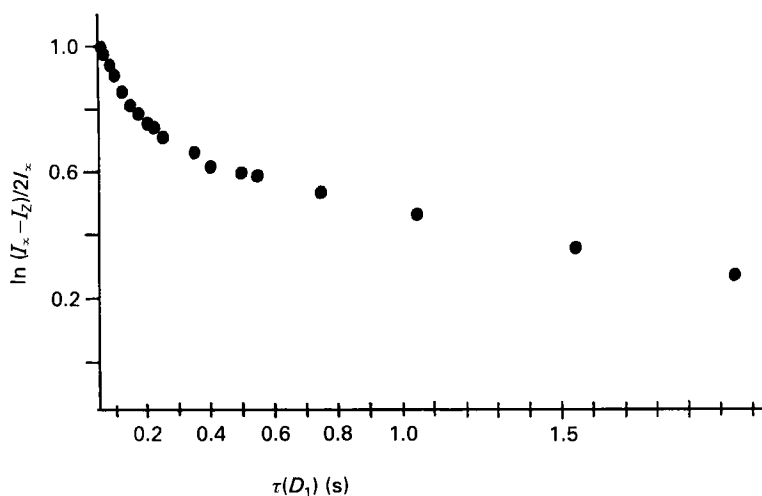
FIG. 44. Data taken from 180°-D_1-90° pulse sequence plotted logarithmically, experiments for CcP-CN haem methyl 3.

ments have been repeated five times and each result is identical to this. Furthermore, the inversion recovery pulse sequence used is one that contains composite 90° and 180° pulses.[182] Clearly, results such as these can lead to erroneous T_1 values which can themselves lead to erroneous calculated distances and ultimately to wrong assignments.

Another potentially complicating feature in relaxation studies is the "Curie spin" term in the paramagnetic relaxation equations. This mechanism results from motional modulation of the dipole–dipole interaction that occurs between a given nuclear magnetic moment and the thermally averaged magnetization of the unpaired electrons.[19,20] For large proteins that exhibit high magnetic susceptibilities and short electron spin–lattice relaxation times, measurements at several field strengths[130,183,184] reveal field dependent linewidths. This "Curie spin" contribution to the overall relaxation rate can be the dominant effect at high fields. The predicted behaviour is that resonance linewidths, a measure of T_2, should increase as B_0^2, the square of the applied magnetic field.[19,20,183,184]

The data presented thus far show that ferrous haem proteins do indeed exhibit such field dependent linewidths.[130,183,184] For example, the resonance line at -12.3 ppm in *Aplysia* deoxy myoglobin exhibits broadening from

TABLE 14

Summary of field dependent linewidths of selected resonance lines in both oxidation states of human haemoglobin A and sperm whale myoglobin.

Protein	Resonance at (ppm)	Temp.	B_0 (tesla)	ν_0 (MHz)	Observed linewidth (Hz)	Ref.
Ferrous						
Deoxy HbA	~23	23	2.1	90	114	184
		30	5.9	250	270	184
		30	8.5	360	460	184
Deoxy Mb	~11	39	2.1	90	43	184
		33	5.2	220	66	184
		37	8.5	360	89	184
		41	8.5	360	90	184
		29	8.5	360	117	184
Deoxy Mb	~15.5	39	2.1	90	38	184
		33	5.2	220	64	184
		37	8.5	360	89	184
		41	8.5	360	82	184
		29	8.5	360	120	184
Ferric						
Cytochrome *c'*	Haem methyl	25	2.3	100	140	130
		25	8.5	360	305	130
Mb-H$_2$O	Haem methyl	25	field independent		300	25
Mb-CN	Haem 5-CH$_3$	35	1.4	60	28	184
		32	2.3	100	28	184
		45	2.3	100	27	184
		37	5.2	220	28	184

an observed width at half maximum height of 14 Hz (at 60 MHz) to 37 Hz (at 220 MHz). Additional data are given in Table 14 for several ferrous and ferric haemoglobins and myoglobins. There are several consequences of this. The principal conclusion is that, in cases where Curie spin line broadening is expected, working at lower fields will offer spectra with narrower lines. Accordingly, resolution may actually decrease as the field strength is increased. Furthermore, working at higher temperatures, where the molecular tumbling is faster, will result in narrower lines at any given field strength. The data also suggest that the ferric oxidation state for *some* moderately sized proteins may not suffer complications from field dependent line broadening. Consider deoxy myoglobin, which shows extreme line broadening effects, with aquo met-myoglobin which has been reported to show no field dependent line broadening (Table 14). Note, however, that met-myoglobin azide has been reported to exhibit significant field dependent linewidths. In addition, the low spin forms of moderate to small proteins, typified by met-myoglobin cyanide, show linewidths independent of field. However, for cytochrome c peroxidase cyanide, a protein whose molecular weight is approximately 34 kD (*vs.* 16 kD for Mb), we have observed field dependent haem methyl linewidths even though this is a low spin ferric form.

Finally, it is necessary to point out that, in addition to causing broadening via dipole–dipole coupling, the Curie spin can relax by a scalar interaction. Therefore, manifestation of a Curie spin effect at protons via chemical exchange modulation or internal rotation modulation of the scalar coupling between particular protons and the Curie spin is also possible. This effect has been observed in complexes of Cr^{2+}.[185] As always, a carefully defined system with respect to chemical exchange or intramolecular rotation can ensure unambiguous definition of these effects.

I. Assignments by comparison with other proteins: less specific assignments

For many haem proteins the hyperfine resonances have not been assigned beyond noting relative intensities. Integration of a given set of hyperfine resonances can yield relative areas and, because single proton resonances can be assumed to exhibit the lowest integrated intensity (relative intensity of 1), methyl resonances can also be identified. These integrations rely on choosing clearly defined resonances in areas where baseline compensation due to infringement of the residual H_2O resonance or multiply overlapping resonances in the 0–10 ppm region is not required. We have used both internal and external standards. Cytochrome c is a convenient internal standard owing to its two, well resolved, haem methyls (Fig. 39).

Besides integrations, resolved hyperfine shifted methyl groups attributable to haem methyls may be classified from their characteristic shifts. For ferric haem proteins the unambiguous assignments which have been made show

that the haem methyl protons are highly deshielded (50–100 ppm). For low spin ferric haem proteins the haem methyl resonances are generally to low frequency of 30 ppm at 25 °C. By comparison, another feature of high spin, compared with low spin, ferric haem proteins is the larger linewidths of the haem methyl resonances in the former. The data in Table 15 bear out these generalizations for a large number of different ferric haem proteins in several different ligation states.
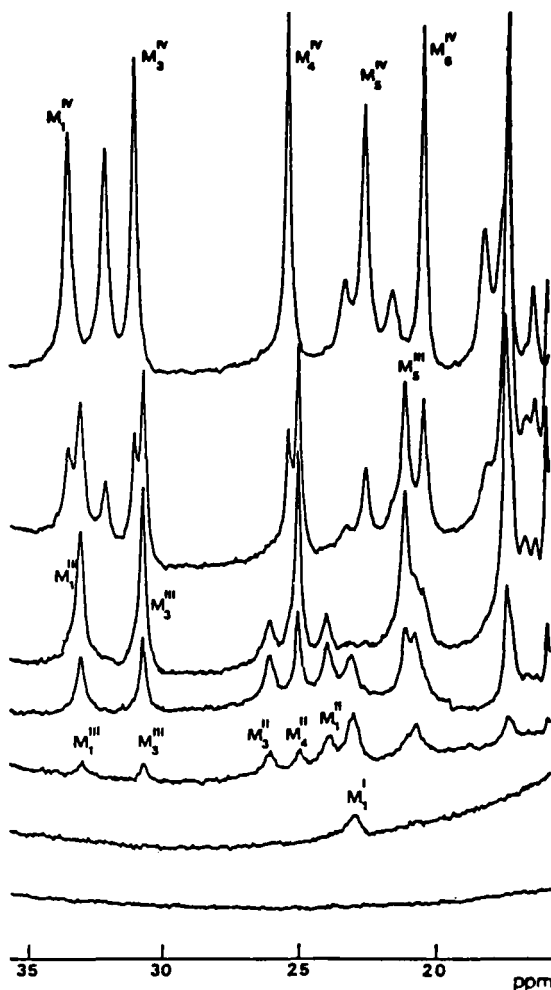

FIG. 45. 300 MHz NMR spectra of *D. gigas* cytochrome c_3 in different oxidation stages: detail of the high frequency region. The redox titration was carried out at 273 K and pH* = 7.2. From reference 187, with permission.

TABLE 15

Proton shifts of unassigned haem methyl groups in variously ligated ferric haem proteins.

Protein	Temp.	pH	Methyls									Ref.
D. gigas cytochrome c3[a]	0	7.2	34.0	32.7	31.6	25.9	23.1	20.9				187
P. palustris cytochrome c5556	27	7.0	32.0	31.5	24.1	23.8						188
A. tumefaceiens cytochrome c556	40	5.2	45	40.5	35.5	28						188
T. thermophilus cytochrome c552	27	6.9	34.6	33.5	17.1	12.6						186
D. vulgaris cytochrome c3[a]	25	6.8	26.7	26.1	19.4	17.3						189
G. dibranchiata Hb-CN[b,d]	24	6.8	21.0	20.1	20.0	19.7	18.7	18.3	18.1	13.7	13.3	TW[e]
Soybean Lb-N$_3$	25	7.0	23.1	21.7								83
D. dendriticum Hb-CN	25	7.7	21.8	15.7								164
P. perfectomarinus cytochrome c552[c]	22	7.2	38.7	21.3	21.8	21.2	19.8	16.2	11.6			190
HbA(αSH) chain CN	22	6.7	22.7	16.6								193
HbA(αSH) chain N$_3$	22	7.1	28.2	22.2	14.8							193
HbA(αSH) chain I$_M$	22	7.7	32.3	25.6								193
P. stutzeri CcP[c]	47	8.0	69.3	64.1	57.3	55.9	32.0	22.7				191
P. aeruginosa CcP[c]	20	6.0			50–60 ppm (broad)							192
R. molischianum cytochrome c'	26	5.6	80.0	71.0	67.5	64.0						188
R. rubrum cytochrome c'	26	6.4	84.5	79.8	69.1	64.7						194
G. dibranchiata Hb(II)	18	7.5	95.7	92.6	69.5	64.5						195
G. dibranchiata Hb(III)	18	6.5	96.2	92.3	69.2	64.2						195
G. dibranchiata Hb(IV)	18	6.6	94.0	89.7	66.9	62.9						195
D. dendriticum Hb	25	7.3	87.1	83.4	70.9	65.6						164
HbA(βSH) chain CN	22	7.2	21.5	15.6								193
HbA(βSH) chain N$_3$	22	7.0	25.8	20.6	12.2							193
HbA(βSH) chain I$_M$	22	7.6	30.7	24.3								193

HbACN (tetramer)	22	6.7	22.8	16.7	15.7				193
HbAN$_3$ (tetramer)	22	7.3	27.9	26.7	22.0	21.1	14.3	13.9	193
HbATM (tetramer)	22	7.4	32.2	26.4					193
HbA (tetramer)	22	5.2	86.3	84.4	73.0	58.9			193
HbA (tetramer) OCN	22	8.2	57.1	55.0	50.0	45.3			193
HbA (tetramer) HCOO	22	7.5	57.9	56.4	48.4	42.6			193
HbA (tetramer) F	22	6.8	56.4	53.2	49.3	44.0			193
HbA (tetramer) SCN	22	7.4	55.0	46.8					193
HbA (tetramer) NO$_2$	22	7.1	40.6	39.3					193
HbA(αSH) chain	22	6.1	86.6	84.3	74.7	58.6			193
HbA(αSH) chain OCN	22	7.7	57.4	55.5	49.9	45.2			193
HbA(αSH) chain HCOO	22	7.2	58.8	56.9	49.8	43.2			193
HbA(αSH) chain F	22	7.3	57.2	53.1	49.9	44.8			193
HbA(αSH) chain SCN	22	7.2	54.9	47.7					193
HbA(αSH) chain NO$_2$	22	7.4	42.0	36.2					193
HbA(βSH) chain	22	6.0	77.4	75.8	64.6	51.4			193
HbA(βSH) chain OCN	22	7.1	46.8	39.7	37.8				193
HbA(βSH) chain HCOO	22	6.9	51.8	42.2	38.9				193
HbA(βSH) chain F	22	6.9	56.5	51.7	43.7				193
HbA(βSH) chain SCN	22	6.8	45.1	40.4	37.9				193
HbA(βSH) chain NO$_2$	22	6.8	33.9	28.4	21.0	13.0			193
HbA(βpMB) chain	21	6.0	85.8		72.7	56.2			193

[a] A four-haem protein; not all of the 16 possible methyl groups have been reported; shifts for maximally oxidized protein reported here.

[b] Mixture of four proteins; not all of the 16 possible methyl groups have been identified.

[c] A two-haem protein; not all of the 8 possible methyl groups have been reported; shifts for maximally oxidized protein reported here.

[d] Upper case letters indicate the anion presumed bound to the haem ferric ion.

[e] This work.

Even at this rather superficial level of assignment useful studies of protein properties can be undertaken. The information obtained from the multiple haem proteins is one example.[187-192] Cytochrome c_3 is a molecule of molecular weight 13 kD that contains four haems.[187] These haems are of the c-type with thioether bridges to the protein polypeptide chain (Fig. 1) and they are axially bis-ligated by histidines. The spectra in Fig. 45 reveal the stepwise development of a spectrum containing hyperfine resonances characteristic of low spin ferric haems. An electron distribution scheme for the consecutive one-electron oxidation of each of four haems in a protein such as this is given in Fig. 46.[187] The correlation between these two figures is interesting. In Fig. 45 the fully reduced protein (bottom trace) shows no hyperfine resonances as a low spin ferrous protein should. This corresponds to state 15 on the far right of Fig. 46. Oxidation by one electron produces states 11-14 in Fig. 46 and a single hyperfine resonance in the second
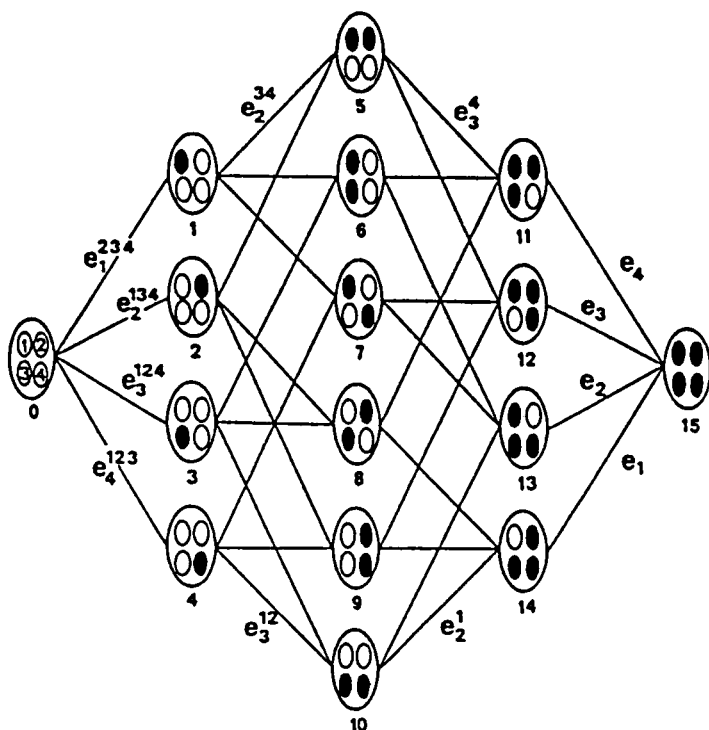
FIG. 46. Electron distribution scheme for a tetrahaem cytochrome. Oxidation states 0 and 15 refer respectively to the fully oxidized and fully reduced protein. e_i^{jkl} is the microscopic midpoint redox potential of haem i when haems j, k and l remain oxidized (● = haem reduced; ○ = haem oxidized). From reference 187, with permission.

spectrum up from the bottom in Fig. 45. In subsequent steps of reoxidation (bottom to top, Fig. 45) resonances characteristic of intermediate oxidation states (states 1–10, Fig. 46) appear. The top spectrum in Fig. 45 corresponds to the fully oxidized protein in which all haems are in the ferric state.

The analysis of such titration data is complicated,[187–190] but some conclusions can be mentioned. According to these authors intermolecular electron transfer between oxidation states characteristic of the distinct oxidation steps depicted in Fig. 46 is slow. The results further imply that intramolecular electron transfer, i.e. electron exchange between haems inside the same molecule, is rapid and that these four haems are interacting centres, contrary to conclusions drawn from ESR measurements.[196]

Two dihaem proteins have also been studied by Xavier and co-workers.[190,191] These are the dihaem cytochrome c-552 from *Pseudomonas perfectomarinus*[190] and the dihaem cytochrome c peroxidase from *Pseudomonas stutzeri.* The former protein is interesting because the difference in midpoint redox potentials of the two haems (H_1, H_2) is so large ($\Delta E = 354$ mV) that only one of the two potential intermediates occurs as a result of one-electron oxidation of the fully reduced state ($H_1 = H_2 = Fe^{2+}$). These two possibilities are (H_1^+, H_2) and (H_1, H_2^+), where + signifies an oxidized (ferric) haem. The one-electron oxidized intermediate state is unique (H_1^+, H_2), which allows for assignments of resonances to each of the haems.

Work on these multihaem proteins of low molecular weight (13 kD or less) is relevant to what one might expect for catalase, a tetrameric haem protein in which each of the subunits contains one haem.[197] These haems are coordinated to tyrosines which serve as proximal ligands rather than the histidines encountered in normal b-type haem proteins. In the one-proton NMR spectrum of bovine liver catalase published to-date[198] there are three major resonance bands at 61.4, 55.7 and 41.1 ppm which are probably attributable to overlapping haem methyl proton resonances from the four haem groups.

III. SELECTED PROBLEMS OF BIOLOGICAL RELEVANCE

Once assignments have been made it is possible to initiate NMR studies that are highly specific and answer questions pertinent to the function of a given protein, or class of proteins. Some of these are mentioned in Section II, in conjunction with assignment methods. In the sections that follow, several problems of biological importance are described. Owing to limited space not every worthy, or interesting, topic can be considered. Indeed, considering the rate at which new studies are being published, choosing the topics to describe was a formidable task. The literature is replete with

varied and interesting accounts and it is to be hoped that the interested reader will use the references as a springboard to the literature.

A. Analytical

Hyperfine shift patterns of both ferric high spin and ferric low spin haem proteins may be of general use as high resolution indicators of purity and homogeneity of sample preparations. In this respect, NMR can be complementary to more normal biochemical assays. In this section four examples are considered.

In some preparations of leghaemoglobin, isolated from soybean root nodules, a proton NMR spectrum of the ferric form consists of two haem methyl resonances between 20 and 25 ppm.[110] The appearance of these resonances indicates a predominantly low spin ferric state, despite the fact that, because this protein was used directly from isolation, one might have expected a spectrum characteristic of a high spin ferric protein. The suggestion is that leghaemoglobin has an usually high affinity for preservative materials used as bacterial growth inhibitors (N_3^-, CN^-) and has obtained one or more of these ions as haem ligands during the purification procedure. This illustrates the care that must be exercised in the biochemical manipulations required for protein isolation and purification.

The *Glycera dibranchiata* haemoglobins are another interesting case where NMR analysis suggests that further biochemical steps are required in order to obtain pure proteins. The history of this haemoglobin is as follows. In 1974 a crystal structure determination was carried out, on crystals of a protein grown from a haemoglobin solution that was isolated as a monomer protein fraction by gel filtration chromatography. This crystal structure as well as amino acid sequencing, along with purification and characterization methods based only on molecular weight, reinforces a concept that the monomer fraction is homogeneous. The uniqueness and importance of this crystallized protein lies in the fact that the distal histidine, which normally occurs at position E-7 in haemoglobins and myoglobins, is replaced by leucine in the *Glycera dibranchiata* haem crevice. Such a drastic replacement can potentially alter the properties of the ligand binding site by changing its polarity, by steric alterations and by more subtle effects, so this protein fraction becomes important to kineticists.

The first reported proton NMR spectra of the paramagnetic shift region 10–100 ppm indicated that there was significant heterogeneity present in fractions of this monomer haemoglobin isolated as for the structural and sequencing studies.[199] Subsequent extensive purification revealed the presence of three major haemoglobins and one or two minor haemoglobins, all of very similar molecular weight.[195] The haem methyl shift pattern of the ferric high spin forms (Table 15) indicates pronounced C_2 symmetry in the

unpaired electron distribution about the haem, an observation that is somewhat unusual for high spin ferric haem proteins. The nature of rhombic distortions for the electronic ground state in ferric high spin haem proteins most frequently conforms to C_4 symmetry.[179] What is also interesting about the *Glycera dibranchiata* monomer haemoglobins is that each component displays significant shift differences from each of the others. In the high spin ferric forms, methyl shift differences as great as 3 ppm are found for the differing component haemoglobins, indicating that subtle structural differences in these components may be affecting the electronic structures of their respective prosthetic groups.

A related case of biochemically undetected heterogeneity, that has been attributed to two similar proteins being present in a monomer haemoglobin preparation, has been reported.[164] A bile duct parasite common to herbivores, commonly called the liver fluke (*Dicrocoelium dendriticum*, Dd), possesses a monomeric haemoglobin. Despite a low sequence homology with other haemoglobins this protein possesses an exceptional amino acid replacement similar to that found in the *Glycera dibranchiata* haemoglobins. In this instance the distal histidine (E-7) is replaced by glycine, structurally a much smaller amino acid than the leucine found in *Glycera dibranchiata* haemoglobins, but similar in that it possesses a completely hydrocarbon side chain. In the ferric, cyanide ligated form of Dd haemoglobin close inspection of the hyperfine resonances reveals that they are composite in nature. Variable temperature and pH studies have identified two major constituent haemoglobins. It is concluded that the observed microheterogeneity is inconsistent with an origin due to rotational haem-protein isomers, but rather is due to the presence of closely related isozymes.[164]

Whereas these two immediately preceding examples involve cases of heterogeneity that is either confirmed or potentially biochemically resolvable, there are also instances where NMR has uniquely been able to detect silent mutations. One of these cases has been demonstrated for the *Chironomous thummi thummi* (CTT) haemoglobin-III.[200] Both Hb-III and Hb-IV from this species exhibit haem orientational disorder. The magnitude of this disorder is such that, in CTT Hb-III-CN, methyl resonances from the two orientations differ by at least 300 Hz at pH 5.0 and 25 °C. However, each methyl resonance is further split by an additional ~10 Hz. It is this secondary splitting that, the authors conclude, indicates the point mutation. Although reconstituting CTT Hb-III-CN with different haems changes the relative populations of the haem orientational isomers, the secondary peak splitting remains and, regardless of the haem, the estimated relative ratio of the two components of the secondary splitting remains constant at approximately 1.7:1. The point mutation in question was ultimately identified by amino acid sequencing to be the substitution of isoleucine by threonine at position 57 (E-6).

B. High pressure studies

Pressure induced changes that affect the structure and/or function of haem proteins have been studied by several techniques. Recently Morishima and Hara have published a series of papers in which they consider the effects of pressure on the hyperfine shifts in paramagnetic ferrous and ferric haemoglobins and myoglobins.[201-204] Their interest in pressure effects originates in several properties of haemoglobins; these include the quaternary structure switch $(T \leftrightarrows R)$ that accompanies oxygenation in tetrameric haemoglobins,[142,143] and consequently the idea that pressure might induce a quaternary structural change. Similarly it was thought that high pressure would alter the weak interactions (such as non-bonding interactions) that stabilize the haem crevice. Finally, the effect of pressure upon the haem iron ion spin state has been studied.[205,206]

Reasonably dramatic effects have been observed upon the proximal histidine $N_\delta H$ (His F-8) resonance in ferrous deoxy HbA as a result of increasing pressure. As shown in Table 16, the β subunit resonance shifts by 1.00 ppm whereas the α subunit resonance is not affected when the protein is exposed to 1300 atm pressure.[201] In the ferrous ligated forms (oxy, carbon monoxy) the resonance corresponding to the γ methyl group of

TABLE 16

Pressure dependence of proton resonances in selected human haemoglobin and sperm whale myoglobin complexes.[201-206]

Protein	Temp.	pH	Press. (atm)	Val. E-11		His F8		His E-7	Heam 1-CH$_3$
				α	β	β	α		
deoxy HbA	30	6.5	1			70.3	58.3		
	30	6.5	1300			71.3	58.6		
HbA-O$_2$	30	7.0	1	−7.1	−7.1				
	30	7.0	1300	−7.1	−7.3				
HbA-CO	30	7.0	1	−6.5	−6.5				
	30	7.0	1500	−6.6	−7.0				
HbA-CO	30	7.0	1	−6.4	−6.5				
+IHP	30	7.0	1100	−6.5	−7.0				
αCO	30	7.0	1	−6.5					
chains	30	7.0	800	−7.6					
βCO	30	7.0	1		−6.7				
chains	30	7.0	1100		−7.0				
Mb-CO	30	7.0	1	−7.1					
	30	7.0	1100	−7.1					
Mb-CN	30	7.8	1			16.4	18.6	22.2	
	30	7.8	800			16.4	17.2	21.9	
	30	7.8	1100			16.4	16.4	22.5	

value E-11 in the β subunit changes by 0.2–0.5 ppm when the protein solution is pressurized up to 1900 atm. However, again, the E-11 methyl resonance assignable to the α subunit exhibits no such shift. The conclusions that are drawn from these types of studies are as follows. The pressure effect is most pronounced for the β subunits of human HbA whether the intact tetramer is being studied or whether it is in the form of isolated β chains. The pressure induced changes are considered to be unrelated to change in quaternary structure, in keeping with suggestions from other methods.

In cyanide ligated met-myoglobin effects upon the proton NMR spectrum as pressure increases are demonstrated in Fig. 47. In this case the spectra
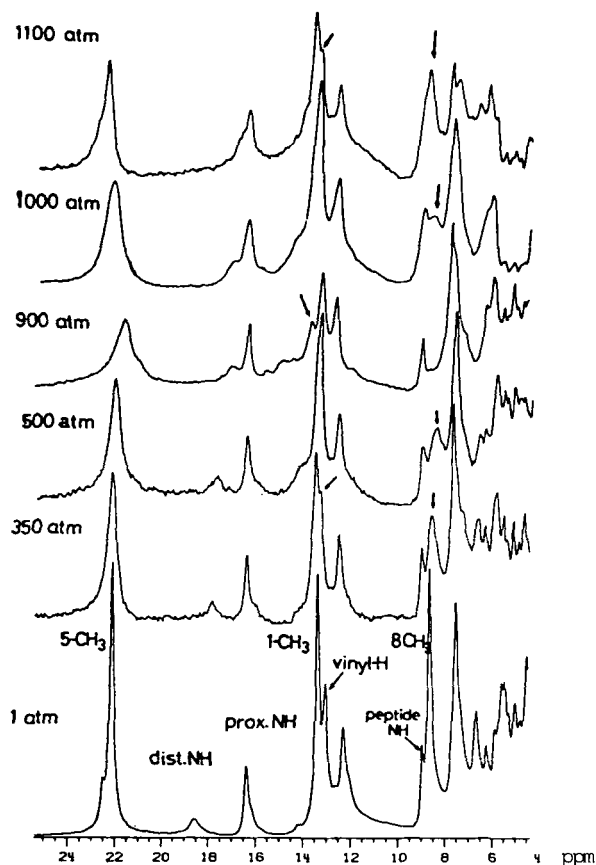
FIG. 47. Pressure dependence of proton NMR spectra for horse Mb-CN at 30 °C, pH 7.8, in 0.1 M Tris-HCl. The numbering of the haem methyl groups is shown in Fig. 48. From reference 202, with permission.

were obtained in 90% H_2O so that isotope exchangeable resonances are observed. Although all the lines broaden, the distal histidine (E-7) NH (Fig. 48) exhibits the most dramatic behaviour. As in the data discussed above for valine E-11, these results suggest a preferential effect of high pressure in the E helix, the distal side of the haem, near to the haem ligand binding site.

In another study[204] it has been demonstrated that pH induced spectral changes in ferrous deoxy des Arg (α141) haemoglobin are different from those induced by increased pressure. This is significant because this modified haemoglobin exists in a quaternary T-like state at pH 7.0 whereas at pH 8.5 it adopts a quaternary structure that is R-like (Table 7). In the T state no effect of pressure up to 1100 atm is observed. In the R state a resonance line at 6.4 ppm is shifted to 6.7 ppm, yet no evidence of conversion to the
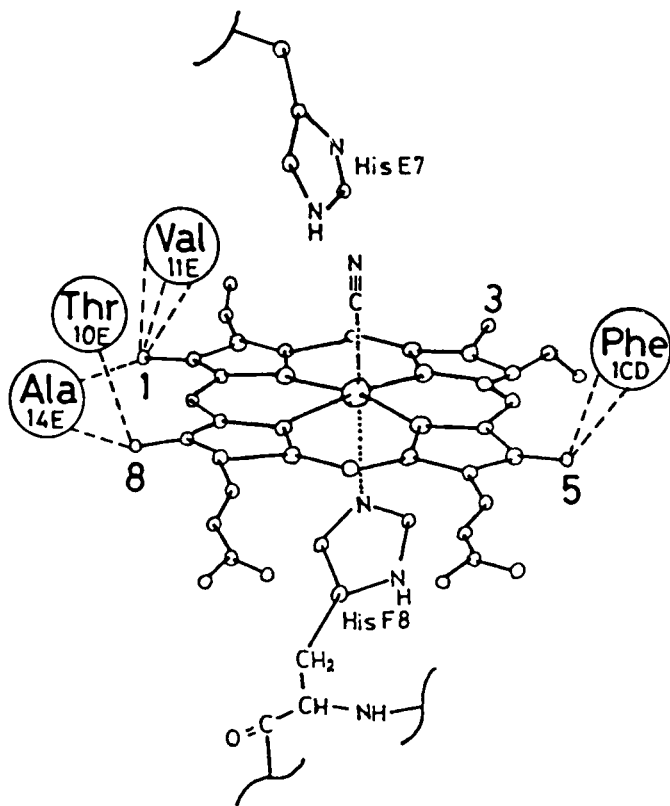
FIG. 48. Haem environmental structure of Mb-CN based on X-ray structural analysis. Open circles refer to residues which are in van der Waals contact with 1-, 5-, and 8 groups. The dotted lines stand for the interatomic contacts of 3.9 Å. From reference 202, with permission.

T state is obtained. The authors have concluded that this is further evidence that high pressure is incapable of inducing a quaternary structural change. Nevertheless, they do conclude that the observed shifts reflect pressure induced changes in the protein tertiary structure.[204]

C. Haem electronic structure

Several observations have suggested that the combination of haem with the three-dimensional polypeptide chain perturbs the electronic structure of the haem group compared with that of the free haem in solution. These haem-protein effects have been invoked to account for observed changes in the reactivity of haems compared with native proteins, as well as to describe how reactivities are different for different classes of proteins containing structurally identical haem groups. Peroxidases and myoglobins offer precisely such a comparison. The peroxidases are stable ferrihaem proteins whereas myoglobins are stable ferrohaem proteins. In fact, as indicated later, there are NMR discernible differences in the haem crevice structures of these two types of proteins.

Early NMR work on met-myoglobin cyanide[177] and c-type ferric cytochromes[66] called attention to the fact that the hyperfine shifts for the haem methyl groups of these proteins exhibit pronounced C_2 symmetry. The methyl group resonances appear to be grouped pairwise in the proton spectrum, with greater differences between the mean shift of each pair than between each of the two resonances comprising each pair. This phenomenon is clearly illustrated in Table 12.

Information on the source of this in-plane electronic asymmetry derives from studies of ferric porphyrin model systems as well as haem proteins. For low spin ferric porphyrin complexes it has been shown that the haem ring methyl resonance pattern is primarily governed by contact shifts, i.e. the pattern of the unpaired spin density distribution about the haem.[175] Because the contact contribution to the observed shifts of haem peripheral substituents, for unpaired spin density in π type porphyrin molecular orbitals, leads to deshielding,[175,177] the magnitude of the observed hyperfine shifts of haem methyl groups is a qualitative index of the extent of spin density delocalized onto the respective haem pyrrole rings by metal-porphyrin covalency.

A seminal observation is that the resonance positions for haem peripheral substituents overlap or occur within a very narrow range of frequencies for highly symmetric low spin ferric porphyrins.[4,11] Furthermore, the spread in resonance positions increases as porphyrin substituents are changed in such a way as to lower the haem's local site symmetry or to alter the electronegativity of the substituents.[4,11,175,207-210] Moreover, only in the case where the haem pyrrole 2,4 position substituents are groups such as sulphonate, acetyl,

formyl and cyanide does the spread of methyl shifts approach that observed
in low spin ferric haem proteins (Table 17). As a consequence it has been
considered that in-plane effects can modify the observed pattern of methyl
resonances. This is taken to indicate that peripheral contacts between the
haem and amino acids of the polypeptide chain could play a prominent
role in defining the pattern of electron delocalization.

TABLE 17

Spread of haem methyl resonances in 2,4-substituted derivatives of ferric protohaem dicyanide,
myoglobin cyanide, ferric cytochrome c and ferric cytochrome c cyanide.[175–209]

2,4-R	Ethyl	H	Vinyl	Acetyl	Formyl	Mb-CN	Cyt^+c	Cyt^+c-CN
Spread	0.35	5.27	4.99	17.42	19.4	21.9	27.8	11.5

In low spin ferric proteins a second possibility exists, as first advanced
in the case of met-Mb-CN,[177] that the plane of the proximal histidine defines
the pattern of electron spin delocalization over different halves of the
porphyrin ring. This view has been described in detail elsewhere.[11,207–210]
The fundamental property that allows this mechanism to operate is the
concept that the proximal histidine may interact with the iron centred
e-symmetry d orbitals, which in turn individually interact with porphyrin
$3e(\pi)$ type orbitals to reduce the degeneracy of the porphyrin $3e(\pi)$ type
orbitals. This could be accomplished by interaction of the proximal his-
tidine's imidazole ring π orbitals with the iron–porphyrin molecular orbitals.
A graphical picture of this type of interaction has been presented.[1,11,208–210]
In this model the result would be destabilization of one member of the
porphyrin $3e(\pi)$ pair and stabilization of the other, leading to the possibility
of an uneven distribution of electron density among the four porphyrin
pyrroles. This may result in a pairwise spread of methyl shifts. Models have
been developed that demonstrate the capability of coordinated imidazole
to induce a spread in haem methyl resonances[209] and pyrrole proton reson-
ances[208,210] when the rotational mobility of the coordinated imidazole is
restricted. Consequently these models have been of the chelated porphyrin
type where the coordinated imidazole is covalently attached to the periphery
of the porphyrin itself. Traylor and Berzinis have reported haem methyl
resonance spreads of 4.6 to 17.1 ppm,[209] whereas Walker[208,210] has reported
pyrrole proton resonance spreads as large as ~11 ppm. An additional effect,
that caused by "tension" in the iron–proximal imidazole bond, has been
studied using imidazole appended ferric porphyrins.[211] In these porphyrins
the imidazole containing arm is covalently attached to the porphyrin

periphery as in the models just described. By regulating the length of the arm, steric strain in the form of lengthening the iron–imidazole bond, or tilting of the imidazole plane, is induced. The consequence is the observation of up to an ~11 ppm splitting of the pyrrole proton resonance.[211]

The model that calls for proximal histidine steering of the unpaired electron distribution on the haem ring, thereby allowing proximal effects to determine the order and pattern of methyl proton resonances, provides a basis for interpreting the shift patterns in peroxidases and myoglobin. Figure 49 reveals the orientation of the proximal histidine imidazole plane, projected onto the haem ring for cytochrome c peroxidase (CcP) and myoglobin.[37] This figure is a summary of crystal structure data.
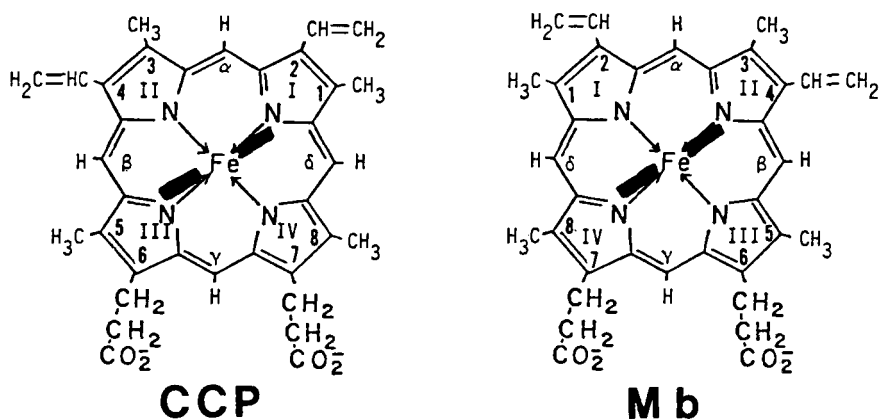
FIG. 49. Comparison of the proximal histidine (imidazole) plane projection onto the haemin for CcP and Mb. This view is along the proximal histidine–Fe bond and was formulated from the published crystal structures for each. Note the interchange of pyrroles I,II and III,IV in the two structures. This is equivalent to a 180° rotation about the α–γ (meso) axis. From reference 37, with permission.

The histidine π orbitals project perpendicularly to the imidazole plane and in the case of CcP are oriented so as to interact with the iron d_{yz} type orbital of e symmetry and one of the porphyrin $e(\pi)$ type orbitals that encompasses pyrroles II and IV. Removal of the π orbital degeneracy is predicted in such a manner that the methyl resonances on pyrroles II,IV (3-CH$_3$,8-CH$_3$) are expected to appear as a pair, widely separated from the 5-CH$_3$,1-CH$_3$ pair (pyrroles I,III). Only two methyl resonances are resolved in CcP–CN and these are the 3,8 pair that occur at 31.2, 27.3 ppm (Figs 17, 18). The 5,1 pair of resonances are unresolved under the broad envelope of resonances between 0 and 10 ppm. As predicted, the shift difference

between pairs of methyl group resonances (>18 ppm) is larger than the shift difference within a pair ($\Delta 3,8 = 3.9$ ppm). A similar case exists for horseradish peroxidase (HRP) (Fig. 19). HRP-CN displays a pair of 3,8 methyl resonances at 29.8 (8) and 24.9 (3) ppm at 35 °C. As for CcP-CN the 5,1 resonance pair are unresolved.

For sperm whale myoglobin the projection of the imidazole plane onto the haem ring is also shown in Fig. 49. Using the same model one would predict that pyrroles I and III should receive greater unpaired spin density than pyrroles II,IV. Consequently the appearance of 5-CH_3 (27.4 ppm) and 1-CH_3 (18.7 ppm) shifted to high frequency of either the 8 or 3 methyl resonances is understood (Table 4, Fig. 47). However, in this case the resonances are not as obviously classified in a pairwise manner. There are at least two reasons for this. In myoglobin there could be greater thermal motion of the imidazole ring, making the projection indicated in Fig. 49 symbolic only of the mean position. This would tend to equalize the unpaired spin density distribution about the porphyrin by less specifically removing the 3e(π) degeneracy. Another possibility is that, as in the first model studies discussed, haem–peptide peripheral contacts could modify the unpaired spin density distribution. This effect is believed to account for the inversion of order in the 3-CH_3,8-CH_3 pair in the two peroxidases studied so far.[37] In CcP-CN the 3-CH_3 is the most deshielded resonance of the pair whereas in HRP-CN it is the 8-CH_3 signal that lies to highest frequency. The interpretation of this phenomenon is that the ordering change between the two peroxidases is caused by an amino acid substitution in the primary sequence, thereby changing the nature of the haem contact. In the crystal structure of CcP, tryptophan-51 lies above pyrrole II (3-CH_3) whereas the position 51 residue in HRP is phenylalanine. Although no crystal structure has yet been published for HRP, in view of the obvious primary sequence homology in the B helix between these two proteins, it is reasonable to assume that phenylalanine-51 lies above pyrrole II in HRP.

It is interesting to note that the difference in the myoglobin and peroxidase shift pattern can be viewed, in the context of a fixed histidine–iron bond, as a rotation by 180° about the haem α-γ meso axis. It has been well documented that, within cyanide haemoglobins and myoglobins that demonstrate haem orientational heterogeneity, the 5,1 vs. 3,8 pairwise interchange also occurs (see above). Nevertheless, considering the functional distinction between peroxidases and myoglobin, the different haem orientations may form part of the molecular basis for the different properties of the two protein classes.

The c-type cytochromes with methionine and histidine axial ligands reveal that the orientation and conformation of the methionine ligand can also affect the unpaired spin density distribution on haem c. As in other low spin ferric haem proteins, the proton spectrum generally reveals only two

or three of the haem methyl resonances. An example of this effect is shown by a comparison of ferric horse heart cytochrome c, in which the haem 8-CH$_3$ (31.7 ppm) and 3-CH$_3$ (27.3 ppm, 35 °C) are the largest hyperfine shifts (Fig. 39, Table 12). Assuming, as in the models for b-type ferric haem proteins, that the contact contribution dominates the observed shifts, this pattern indicates the presence of greater spin density on haem pyrrole rings II and IV.[59] This observation has been rationalized on the basis that, because pyrrole II is the most solvent exposed pyrrole, such an electronic distribution could facilitate direct electron transfer.[59] This is not unreasonable in view of the fact that the computer modelled cytochrome c : cytochrome c peroxidase redox complex, based on crystal structures, indicates that the haem planes in the two proteins are approximately coplanar. This fact implies a type of π-π interaction involving haem groups on each protein as well as intervening amino acids.

An important observation is that ferric cytochrome c-551, from *P. aeruginosa*, displays a different methyl shift pattern (Table 12) in which the 1-CH$_3$ (21.1 ppm) and 5-CH$_3$ (28.8 ppm, 27 °C) pair appear to be the most deshielded.[66,78] This indicates that pyrroles I and III receive the most unpaired spin density. This result has been interpreted as being due to a 90° rotation in the orientation of the principal axes of the g tensor.[66] The functional implications remain the same as in cytochrome c because in this c-551 the available crystal structure shows a deletion in peptide fragment from residues 39 to 56 that exposes pyrrole III to the solvent.

Using NOE results in the diamagnetic ferrocytochromes it has been possible, in combination with circular dichroism experiments, to establish the chirality of the axial methione ligand. The correlation of methionine chirality with the identity of the high frequency haem methyl resonance pair shown in Table 18 is impressive evidence that the haem c electronic structure is governed, at least in part, by the orientation of the axial methionine. For the two methionine configurations R chirality is associated with the 8,3 methyl groups as the most deshielded pair, whereas for S chirality the 5,1 methyl groups exhibit the largest hyperfine shift. It should be noted that the available results suggest that the proximal histidine imidazole plane orientation is identical in all of these proteins, eliminating it as the determining factor.

Not all c-type cytochromes exhibit the same methionine chirality in both oxidation states. A recent observation indicates that for *Desulphovibrio desulphuricans* and *Desulphovibrio vulgaris* cytochromes c-553 the iron bound sulphur atom exhibits S chirality when the protein is reduced to the ferrous level, but R chirality in the ferric form. Moreover, the authors note that, although the axial histidine imidazole ring appears to be in an orientation identical to other c-type cytochromes, the axial methionine geometry is unique.[70]

TABLE 18

Correlation of coordinated axial methionine chirality with the haem methyl group resonances exhibiting the largest hyperfine shift in selected c-type ferric cytochromes.

Protein	Chirality	Assignment of high frequency resonances	Ref.
R. rubrum c	R	8,3	63
Horse c	R	8,3	66, 78
C. krusei c	R	8,3	62
E. gracilis c552	R	8,3	69
S. platensis c553	R		166
A. flos-aquae c553	R		212
R. rubrum c2	R	8,3	63
D. vulgaris c553	R	8,3	70
D. sulphuricans c553	R	8,3	70
P. stutzeri c551	S	5,1	63
P. mendocina c551	S	5,1	63
P. aeruginosa c551	S	5,1	46, 78
D. vulgaris c553 (reduced)	S		70
D. sulphuricans c553 (reduced)	S		70

IV. OTHER NUCLEI

Although proton NMR appears at this juncture to be the most readily useful technique for studying paramagnetic haem proteins, other nuclei are also potentially useful. In the sections that follow, reviews of the applications and potential application of ^{13}C and ^{15}N NMR are given. These are necessarily brief because so little has been published that specifically pertains to paramagnetic haem proteins. A principal reason for this is the significantly larger amounts of material required for these kinds of studies owing to the inherent lack of sensitivity of these other nuclei. Whereas proton NMR studies may be easily conducted on as little as 0.35 ml of a 0.001 M protein solution (~6 mg of protein for myoglobin), significantly higher concentrations (0.003–0.020 M) and larger sample volumes may be required in order to execute ^{13}C or ^{15}N NMR studies on isotopically *enriched* proteins in reasonable time periods. Many proteins are simply not available in such quantities.

A. Carbon-13

NMR studies using ^{13}C have focussed primarily on binding ^{13}C enriched ligands to the diamagnetic forms of haem proteins.[213,214] Other studies
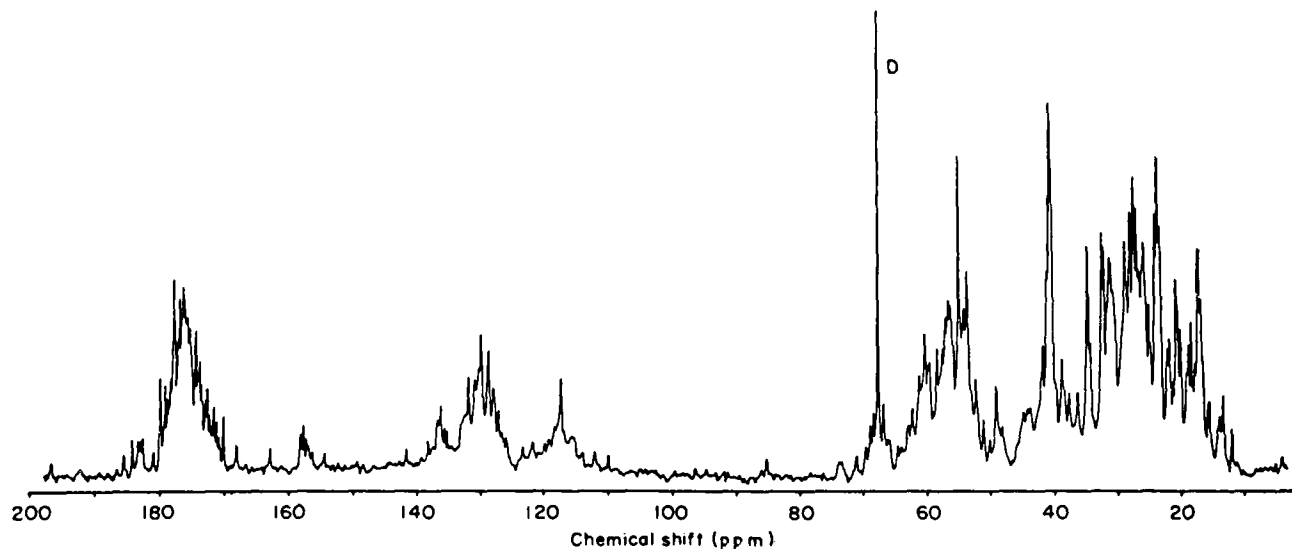
FIG. 50. The 75.5 MHz ^{13}C NMR spectrum of *Candida krusei* ferricytochrome *c*; 5 mM in ^2H_2O at pH 7 and 25 °C. The peak designated by D is from dioxan. Total acquisition time was 20 h. In the same way that the ^1H spectrum can be divided into regions, so can the ^{13}C spectrum. The group of resonances between 160 and 190 ppm come from carbonyls, the group between 150 and 160 ppm from arginine and tyrosine, the group between 110 and 150 ppm from other aromatics, and the group between 10 and 70 ppm from aliphatics. From reference 178, with permission.

involve the diamagnetic forms of haem proteins themselves.[215,216] In early studies natural abundance carbon spectra were obtained for met-myoglobin cyanide, horse heart ferricytochrome c, ferricytochrome c cyanide and *Candida krusei* ferricytochrome c.[178,215-217] In none of these cases were haem carbons identified. Figure 50 shows the natural abundance carbon spectrum of *C. krusei* ferricytochrome c and demonstrates the characteristic carbon resonance positions.[178] The principal result of these studies reveals the assignments of the aromatic carbon resonances although the proximal histidine C_γ resonance (imidazole quaternary carbon) is tentatively assigned in ferricytochrome c cyanide (123.6 ppm at 36 °C).[215-217]

Extensive work on ferric porphyrin models has resulted in elucidation of carbon resonance assignments for protohaem derivatives as well as synthetic ferric porphyrins.[218-221] The ^{13}C NMR spectrum of the bis-1-methylimidazole complex of ferriprotoporphyrin IX dimethyl ester is shown in Fig. 51. In comparison with the spectrum of Mb-CN,[215] [13]C enrichment at the haem 2,4 positions or the haem methyl groups provides the best promise for resolving haem resonances. Carbon shifts in low spin ferric
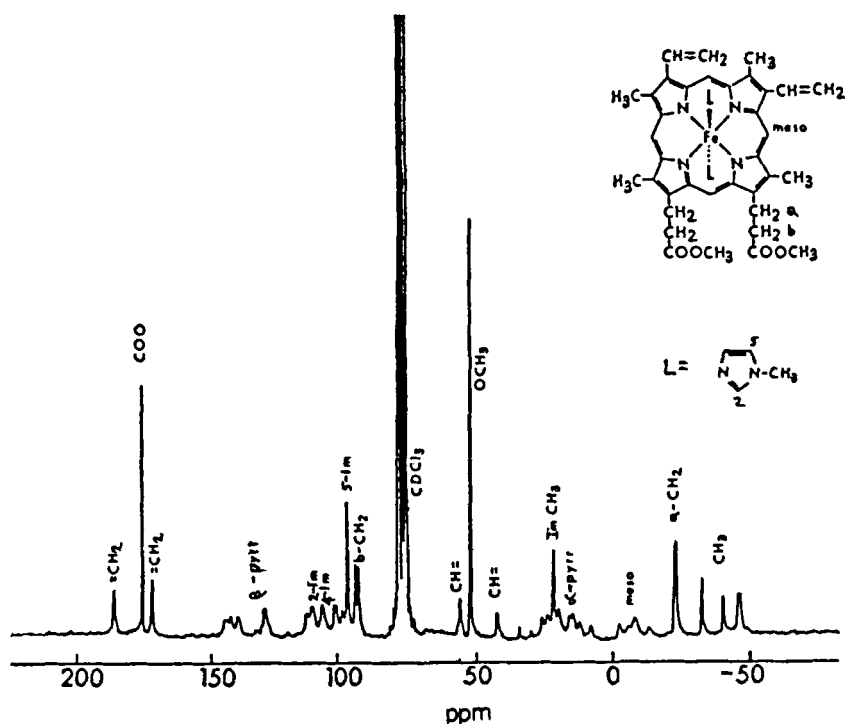
FIG. 51. Carbon-13 NMR spectrum of [FeProtDME(1-MeIm)$_2$]Cl, −22 °C, CDCl$_3$ solvent. From reference 218, with permission.

natural haem complexes are collected in Table 19.[218] Attention is called to the fact that synthetic methods for specific ^{13}C enrichment of haems have recently been published and it is likely that they will be a harbinger of increased ^{13}C NMR work involving particular attention to haem resonances.[30] One of the benefits of the effort that this will require is the additional information on the haem electronic structure that is derivable from ^{13}C NMR measurements.[218]

TABLE 19

Selected carbon-13 NMR resonances for iron(II) natural porphyrin–1-methylimidazole complexes.[a]

Carbon atom	Fe-Meso-DME	Fe-Prot-DME	Fe-Deut-DME	Fe-Ac-DME
ring CH_3	−38.4, −45.1,	−34.1, −42.5,	−32.3, −39.8,	−17.7, −23.9,
	−45.1, −51.7	−48.8, −49.1	−47.4, −51.1	−50.7, −59.6
mean value	−45.1	−43.6	−42.7	−38.0
av. dev. from mean	3.3	5.3	6.6	17.2
prop CH_2				
(a)	−24.2, −24.8	−24.0, −24.5	−21.2, −26.6	−17.0, −25.2
(b)	96.0, 94.5	94.9, 93.7	98.5, 88.4	96.0
COO	174.8	174.7	174.8, 174.3	174.5, 174.3
OCH_3	51.8	51.9	51.9	51.9
2,4-R	−26.6, −38.4[b]	55.7, 37.8[d]		159.1, 155.0[f]
	[c]	184.5, 171.3[e]		27.4[g]
Im-CH_3	21.7	21.0	20.8	19.0
Im-5-C	97.6	97.9	96.6	99.3

[a] Iron(III) porphyrin, 0.05 M; 1-MeIm, 0.2 M; −22 °C: TMS ref., $CDCl_3$ solvent.
[b] Ring CH_2.
[c] CH_3 signal is under solvent.
[d] CH=.
[e] CH_2=.
[f] C=O.
[g] CH_3.
From reference 218, with permission.

One other use of ^{13}C NMR in studies of paramagnetic ferric porphyrins should be mentioned. That is the observation of the coordinated cyanide ^{13}C resonance in dicyano ferric porphyrin complexes.[222] The data obtained are shown in Table 20. Because cyanide is a common ligand used to ensure a low spin iron ion in ferric haem proteins the model complexes are of some interest. The data indicate that changing the haem 2,4 position substituents only induces large shifts when charged groups are employed $(R_2 = R_4 = SO_3^-; Br)$, and even though temperature dependences of these resonances have not been reported it is expected that they will be large.

TABLE 20

Carbon-13 resonances for the coordinated cyano group of low spin iron(III) porphyrins.

Iron(III) complex	Porphyrin 2,4-R group	Cyano resonance
Protoporphyrin IX	$-CH=CH_2$	-2393
Mesoporphyrin IX	$-CH_2CH_2$	-2381
Deuterioporphyrin IX	$-H$	-2375
Dibromodeuterioporphyrin IX	$-Br$	-2359
Disulphonatedeuterioporphyrin	$-SO_3^-$	-2167
Haemin c	$-CH(CH_3)SCH_2-$	
	$CH(NH_2)COO^-$	-2300
meso-Tetrakis-(4-carboxyphenyl)por-phine		-1968
$K_3Fe(CN)_6$		-3583
$K_3Fe(CN)_6$		-3200

From reference 3, with permission.

B. Nitrogen-15

The use of ^{15}N enriched amino acids to study small proteins has been reported in the literature, but none of these studies involves haem proteins. As with ^{13}C, there is a lack of ^{15}N applications to haem proteins for many of the same reasons. ^{15}N NMR utilization has been recently reviewed.[223,230] The earliest account indicated that mobile side chains of haemoglobin could be observed.[224] The primary utility of ^{15}N NMR, as far as this report is concerned, has been to study the coordination of ^{15}N enriched cyanide ion to ferric porphyrins as well as haem proteins.[225-228] Some of these results are collected in Table 21. There are several trends. From the porphyrin data in the upper part of this table it is obvious that there is a dramatic solvent effect. Thus, in protohaemin IX dicyanide the observed shift changes by nearly 300 ppm as the solvent is changed from dimethyl sulphoxide (DMSO) to water. Similarly, there is about a 200 ppm shift linked to a *trans* effect as indicated by comparing protohaemin IX dicyanide with the complex in which one cyanide is replaced by 1-methylimidazole (1-CH$_3$Im). The *cis* effect, typified by comparing the first four porphyrins in either DMSO or methyl alcohol as solvent, is very small (of the order of 14 ppm).

These results suggest that the ^{15}N shift of $C^{15}N^-$ coordinated to ferric haem proteins can give information on proximal (*trans* effect) as well as distal (solvent effect) haem environments. The haem protein data in Table 21 include both solution and intraerythrocyte cases for haemoglobin. The quality of these spectra, particularly for the tetrameric haemoglobins, is especially poor. Broad lines and high noise levels are typical. Some variation with protein origin and pH are to be noted. In contrast, little variation with

TABLE 21

Observed ^{15}N shifts of $C^{15}N$ coordinated to ferric porphyrins and ferric haem proteins.

Complex	Solvent[a]	pH	Temp.	Observed shift[b]	Ref.
Porphyrins					
Protohaemin(IX)(CN)$_2$	DMSO		25	732	220
	pyr		25	696	220
	CH$_3$OD		25	506	220
	H$_2$O	9.2	25	448	220
Deuteriohaemin(CN)$_2$	DMSO		25	738	220
	CH$_3$OD		25	509	220
Mesohaemin(CN)$_2$	DMSO		25	720	220
	CH$_3$OD		25	496	220
OEP(CN)$_2$	DMSO		25	718	220
	CH$_3$OD		25	474	220
Protohaemin(CN)(1-CH$_3$Im)	DMSO		25	926	220
Proteins					
Human Hb-CN	H$_2$O	7.3	29	975, 1047	221
	H$_2$O	7.7	29	985, 1055	221
	H$_2$O	8.1	29	1081, 1083	221
Human Hb-CN	Intact erythrocyte H$_2$O	8.4	29	981, 1050	221
Dog Hb-CN	Intact erythrocyte H$_2$O	8.4	29	990, 1031	221
Rabbit Hb-CN	Intact erythrocyte H$_2$O	8.4	29	937, 1041, 1077	221
Rat Hb-CN	Intact erythrocyte H$_2$O	8.4	29	970	221
Horse Mb-CN	H$_2$O	5.7	25	931	219
	H$_2$O	6.9	—[c]	948	219
	H$_2$O	8.0	—[c]	939	219
	H$_2$O	9.0	—[c]	936	219
	H$_2$O	11.7	25	940	219
Sperm whale Mb-CN	H$_2$O	8.8	—[c]	945	219
	H$_2$O	6.6	—[c]	842	219
	H$_2$O	7.8	—[c]	847	219
	H$_2$O	9.0	—[c]	848	219
Lactoperoxidase CN	H$_2$O	7–8	25	423	222
Horseradish peroxidase CN	H$_2$O	7–8	25	578	222

[a] Abbreviations: DMSO = dimethyl sulphoxide, pyr = pyridine.
[b] Shifts relative to $^{15}NO_3{}^-$.
[c] Temperature not reported.

pH is observed for the myoglobins. Extremely significant is the fact that the peroxidase data[229] reveal much smaller shifts (by ~400 ppm) than for the oxygen binding haem-globins. From the protohaemin IX data in the upper part of the table it is obvious that low frequency shifts accompany the change to a more hydrogen bonding solvent (H_2O *vs.* DMSO), and the *trans* effect can exert an influence of about 200 ppm as well. It is interesting to note in this respect that proton NMR data indicate that the proximal histidine $N_\delta H$ is strongly hydrogen bonded in cyanide complexes of horse-radish and cytochrome *c* peroxidase.[121,122] Therefore, in comparison with myoglobin-CN, the proximal histidine in the peroxidases appears more imidazolate like. This could be the origin of the *trans* effect contribution to these observed shift differences.

ACKNOWLEDGMENTS

REFERENCES

1. R. M. Keller and K. Wüthrich, in *Biological Magnetic Resonance* (L. J. Berliner and J. Reuben, eds), Plenum Press, New York, Vol. 3, 1981, p. 1.
2. C. Ho and I. M. Russu, *Meth. Enzymol.*, 1981, **76**, 275.
3. H. Goff, in *Iron Porphyrins* (A. B. P. Lever and H. B. Gray, eds), Addison-Wesley, Reading, Mass., 1983, Part 1, p. 239.
4. G. N. LaMar, in *Biological Applications of Magnetic Resonance* (R. G. Shulman, ed.), Academic Press, New York, 1979, p. 305.
5. O. Jardetzky and G. C. K. Roberts, *NMR in Molecular Biology*, Academic Press, New York, 1981.
6. S. Mirtra, in *Iron Porphyrins* (A. B. P. Lever and H. B. Gray, eds), Addison-Wesley, Reading, Mass., 1983, Part 2, p. 1.
7. G. Palmer, in *Iron Porphyrins* (A. B. P. Lever and H. B. Gray, eds), Addison-Wesley, Reading, Mass., 1983, part 2, p. 43.
8. G. Fermi and M. F. Perutz, *Atlas of Molecular Structures in Biology: 2. Haemoglobin and Myoglobin* (D. C. Phillips and F. M. Richards, eds), Oxford University Press, Oxford, 1981.
9. R. E. Dickerson and I. Geis, *Hemoglobin*, Benjamin-Cummings, Menlo Park, Calif., 1983.
10. J. P. Jesson, in *NMR of Paramagnetic Molecules* (G. N. LaMar, W. D. Horrocks and R. H. Holm, eds), Academic Press, New York, 1973, p. 1.
11. G. N. LaMar and F. A. Walker, in *The Porphyrins* (D. Dolphin, ed.), Academic Press, New York, Vol. IVB, p. 61.
12. K. J. Kurland and B. R. McGarvey, *J. Magn. Reson.*, 1970, **2**, 286.
13. H. M. McConnell and R. E. Robertson, *J. Chem. Phys.*, 1958, **29**, 1361.

14. H. M. McConnell, *J. Chem. Phys.*, 1956, **24**, 764.
15. I. Salmeen and G. Palmer, *J. Chem. Phys.*, 1968, **48**, 2049.
16. T. J. Swift, in *NMR in Paramagnetic Molecules* (G. N. LaMar, W. D. Horrocks and R. H. Holm, eds), Academic Press, New York, 1973, p. 53.
17. I. Solomon, *Phys. Rev.*, 1955, **99**, 559.
18. I. Solomon and N. Bloembergen, *J. Chem. Phys.*, 1956, **25**, 261.
19. M. Gueron, *J. Magn. Reson.*, 1975, **19**, 58.
20. A. J. Vega and D. Fiat, *Mol. Phys.*, 1976, **31**, 347.
21. K. M. Smith, in *Porphyrins and Metalloporphyrins* (K. M. Smith, ed.), Elsevier/North Holland Biomedical Press, Amsterdam, 1975, p. 29.
22. J. H. Fuhrop and K. M. Smith, in *Porphyrins and Metalloporphyrins* (K. M. Smith, ed.), Elsevier/North Holland Biomedical Press, Amsterdam, 1975, p. 757.
23. J. A. S. Cavaleiro, A. M. d'A. Rocha Gonsalves, G. W. Kenner, K. M. Smith, R. G. Shulman, A. Mayer and T. Yamane, *J. Chem. Soc., Chem. Comm.*, 1974, 392.
24. A. M. d'A. Rocha Gonsalves, G. W. Kenner and K. M. Smith, *J. Chem. Soc., Chem. Comm.*, 1971, 1304.
25. A. Mayer, S. Ogawa, R. G. Shulman, T. Yamane, J. A. S. Cavaleiro, A. M. d'A. Rocha Gonsalves, G. W. Kenner and K. M. Smith, *J. Mol. Biol.*, 1974, **86**, 749.
26. K. M. Smith, F. Eivazi, K. C. Langry, J. A. P. Baptista de Almeida and G. W. Kenner, *Bioorg. Chem.*, 1979, **8**, 485.
27. G. W. Kenner and K. M. Smith, *Ann. New York Acad. Sci.*, 1973, **206**, 138.
28. K. M. Smith, *Accounts Chem. Res.*, 1979, **12**, 374.
29. B. Evans, K. M. Smith, G. N. LaMar and D. B. Viscio, *J. Am. Chem. Soc.*, 1977, **99**, 7070.
30. K. M. Smith, E. M. Fujinari, K. C. Langry, D. W. Parish and H. D. Tabba, *J. Am. Chem. Soc.*, 1983, **105**, 6638.
31. K. Wüthrich, R. G. Shulman and J. Peisach, *Proc. Nat. Acad. Sci. USA*, 1968, **60**, 373.
32. K. Wüthrich, R. G. Shulman, B. Wyluda and W. S. Caughey, *Proc. Nat. Acad. Sci. USA*, 1968, **62**, 636.
33. G. N. LaMar, J. S. deRopp, K. M. Smith and K. C. Langry, *J. Biol. Chem.*, 1980, **255**, 6646.
34. J. D. Satterlee, J. E. Erman, G. N. LaMar, K. M. Smith and K. C. Langry, *Biochim. Biophys. Acta*, 1983, **743**, 246.
35. G. N. LaMar, D. L. Budd, K. M. Smith and K. C. Langry, *J. Am. Chem. Soc.*, 1980, **102**, 1822.
36. G. N. LaMar, D. L. Budd and K. M. Smith, *Biochim. Biophys. Acta*, 1980, **622**, 210.
37. J. D. Satterlee, J. E. Erman, G. N. LaMar, K. M. Smith and K. C. Langry, *J. Am. Chem. Soc.*, 1983, **105**, 2099.
38. G. N. LaMar, J. S. deRopp, K. M. Smith and K. C. Langry, *J. Am. Chem. Soc.*, 1980, **102**, 4833.
39. J. S. deRopp, G. N. LaMar, K. M. Smith and K. C. Langry, *J. Am. Chem. Soc.*, 1984, **106**, 4438.
40. G. N. LaMar, P. D. Burns, J. T. Jackson, K. M. Smith, K. C. Langry and P. Strittmatter, *J. Biol. Chem.*, 1981, **256**, 6075.
41. G. N. LaMar, J. S. deRopp, K. M. Smith and K. C. Langry, *J. Am. Chem. Soc.*, 1983, **105**, 4576.
42. R. M. Keller and K. Wüthrich, *Biochim. Biophys. Acta*, 1972, **285**, 326.
43. R. Krishnamoorthi, G. N. LaMar, H. Mizukami and A. Romero, *J. Biol. Chem.*, 1984, **259**, 265.
44. G. N, LaMar, K. M. Smith, K. Gersonde, H. Sick and M. Overkamp, *J. Biol. Chem.*, 1980, **255**, 66.
45. G. N. LaMar, D. B. Viscio, K. Gersonde and H. Sick, *Biochemistry*, 1978, **17**, 361.
46. G. N. LaMar, M. Overkamp, H. Sick and K. Gersonde, *Biochemistry*, 1978, **17**, 352.
47. W. Ribbing, D. Krümpelmann and H. Rüterjans, *FEBS Lett.*, 1978, **92**, 105.

48. D. Krümpelmann, W. Ribbing and H. Rüterjans, *Eur. J. Biochem.*, 1980, **108**, 103.
49. I. Constantinidis, J. Mintorovitch and J. D. Satterlee, unpublished results.
50. T. Jue, R. Krishnamoorthi and G. N. LaMar, *J. Am. Chem. Soc.*, 1983, **105**, 5701.
51. G. N. LaMar, N. L. Davis, D. W. Parish and K. M. Smith, *J. Mol. Biol.*, 1983, **168**, 887.
52. G. N. LaMar, D. L. Budd, D. B. Viscio, K. M. Smith and K. C. Langry, *Proc. Nat. Acad. Sci.*, 1978, **75**, 5755.
53. J. D. Satterlee and J. E. Erman, *J. Am. Chem. Soc.*, 1981, **103**, 199.
54. G. N. LaMar, J. S. deRopp, K. M. Smith and K. C. Langry, *J. Am. Chem. Soc.*, 1980, **102**, 4833.
55. T. Jue and G. N. LaMar, *Biochem. Biophys. Res. Commun.*, 1984, **119**, 640.
56. A. Kumar, R. R. Ernst and K. Wüthrich, *Biochem. Biophys. Res. Commun.*, 1980, **95**, 1.
57. K. Nagayania, K. Wüthrich and R. R. Ernst, *Biochem. Biophys. Res. Commun.*, 1979, **90**, 305.
58. G. Wagner and K. Wüthrich, *J. Magn. Reson.*, 1979, **33**, 675.
59. R. M. Keller and K. Wüthrich, *Biochim. Biophys. Acta*, 1978, **533**, 195.
60. R. M. Keller and K. Wüthrich, *Biochim. Biophys. Acta*, 1980, **621**, 204.
61. R. M. Keller, D. Picot and K. Wüthrich, *Biochim. Biophys. Acta*, 1979, **580**, 259.
62. H. Senn, A. Eugster and K. Wüthrich, *Biochim. Biophys. Acta*, 1983, **743**, 58.
63. H. Senn and K. Wüthrich, *Biochim. Biophys. Acta*, 1983, **746**, 48.
64. H. Senn and K. Wüthrich, *Biochim. Biophys. Acta*, 1983, **747**, 16.
65. H. Senn and K. Wüthrich, *Biochim. Bioiphys. Acta*, 1983, **743**, 69.
66. R. M. Keller and K. Wüthrich, *Biochem. Biophys. Res. Commun.*, 1978, **83**, 1132.
67. H. Senn, M. Cusanovich and K. Wüthrich, *Biochim. Biophys. Acta*, 1984, **785**, 46.
68. H. Senn, M. Billeter and K. Wüthrich, *Eur. J. Biophys.*, 1984, **11**, 3.
69. R. M. Keller, A. Schejter and K. Wüthrich, *Biochim. Biophys. Acta*, 1980, **626**, 15.
70. H. Senn, F. Guerlesquin, F. Bruschi and K. Wüthrich, *Biochim. Biophys Acta*, 1983, **748**, 194.
71. R. M. Keller and K. Wüthrich, *Biochim. Biophys. Acta*, 1981, **668**, 307.
72. R. M. Keller and K. Wüthrich, *Biochim. Biophys. Acta*, 1980, **621**, 204.
73. G. R. Moore and R. J. P. Williams, *Eur. J. Biochem.*, 1980, **103**, 503.
74. G. R. Moore and R. J. P. Williams, *Eur. J. Biochem.*, 1980, **103**, 533.
75. R. Timkovich, M. S. Cork and P. V. Taylor, *Biochemistry*, 1984, **23**, 3526.
76. R. Timkovich and M. S. Cork, *Biochemistry*, 1984, **23**, 851.
77. R. M. Keller, K. Wüthrich and I. Pecht, *FEBS Lett.*, 1976, **70**, 180.
78. H. Senn, R. M. Keller and K. Wüthrich, *Biochem., Biophys. Res. Commun.*, 1980, **92**, 1362.
79. G. M. Smith, *Biochemistry*, 1979, **18**, 1628.
80. R. D. Johnson, S. Ramaprasad and G. N. LaMar, *J. Am. Chem. Soc.*, 1983, **105**, 7205.
81. S. Ramaprasad, R. D. Johnson and G. N. LaMar, *J. Am. Chem. Soc.*, 1984, **106**, 5330.
82. J. Trewhella, P. E. Wright and C. A. Appleby, *Nature*, 1979, **280**, 87.
83. J. Trewhella and P. E. Wright, *Biochim. Biophys. Acta*, 1980, **625**, 202.
84. G. N. LaMar, S. B. Kong, K. M. Smith and K. C. Langry, *Biochem. Biophys. Res. Commun.*, 1981, **102**, 142.
85. A. Kalk and H. J. C. Berendsen, *J. Magn. Reson.*, 1976, **24**, 343.
86. I. D. Campbell and R. Freeman, *J. Magn. Reson.*, 1973, **11**, 143.
87. J. D. Stoesz, A. G. Redfield and D. Malinowski, *FEBS Lett.*, 1978, **91**, 320.
88. P. J. Andree, *J. Magn. Reson.*, 1978, **29**, 419.
89. K. Akasaka, *J. Magn. Reson.*, 1981, **45**, 337.
90. K. Akasaka, *J. Magn. Reson.*, 1983, **51**, 14.
91. E. Sletten, J. T. Jackson, P. D. Burns and G. N. LaMar, *J. Magn. Reson.*, 1983, **52**, 492.
92. S. L. Gordon and K. Wüthrich, *J. Am. Chem. Soc.*, 1978, **100**, 7094.
93. S. Ramaprasad, R. D. Johnson and G. N. LaMar, *J. Am. Chem. Soc.*, 1984, **106**, 3632.
94. K. M. Smith, K. C. Langry and J. S. deRopp, *J. Chem. Soc., Chem. Comm.*, 1980, 1001.

95. J. H. Bradbury, J. A. Carver and M. W. Parker, *FEBS Lett.*, 1982, **146**, 297.
96. L. Latos-Grazynski, A. L. Balch and G. N. LaMar, *Adv. Chem. Ser.*, 1982, **201**, 661.
97. I. Morishima, Y. Takamuki and Y. Shiro, *J. Am. Chem. Soc.*, 1984, **106**, 7666.
98. H. B. Dunford and J. S. Stillman, *Coord. Chem. Rev.*, 1976, **19**, 187.
99. W. D. Hewson and L. P. Hager, in *The Porphyrins* (D. Dolphin, ed.), Academic Press, New York, 1979, Vol. VII, p. 295.
100. I. Morishima and S. Ogawa, *Biochemistry*, 1978, **17**, 4384.
101. I. Morishima and S. Ogawa, *Biochem. Biophys. Res. Commun.*, 1978, **83**, 946.
102. J. D. Satterlee and J. E. Erman, *J. Biol. Chem.*, 1981, **256**, 1091.
103. T. Mass, A. Ehrenberg and A. J. Bearen, *Biochemistry*, 1969, **8**, 4151.
104. T. Harami, Y. Maeda, U. Morita, A. Trautwein and U. Gonser, *J. Chem. Phys.*, 1977, **67**, 1164.
105. G. N. LaMar and J. S. deRopp, *J. Am. Chem. Soc.*, 1980, **102**, 395.
106. D. Dolphen and R. H. Felton, *Accounts Chem. Res.*, 1973, **7**, 26.
107. L. P. Hager, D. L. Daubek, R. M. Silverstein, T. T. Lee, J. A. Thomas, J. H. Hargis and J. C. Martin, *Oxidases Relat. Redox Syst. Proc. Int. Symp. 2nd 1971*, 1973, p. 311.
108. L. P. Hager, D. L. Daubek, R. M. Silverstein, J. H. Hargis and J. C. Martin, *J. Am. Chem. Soc.*, 1972, **94**, 4364.
109. M. Uyeda and J. Peisach, *Biochemistry*, 1981, **20**, 2028.
110. J. E. Erman and J. D. Satterlee, in *Electron Transport and Oxygen Utilization* (C. Ho, ed.), Elsevier/North Holland, Amsterdam, 1982, p. 223.
111. M. A. Phillippi, E. T. Shimomura and H. M. Goff, *Inorg. Chem.*, 1981, **20**, 1322.
112. P. Gaus, J. C. Marchen, C. A. Reed and J. R. Regnard, *Nouv. J. Chim.*, 1981, **5**, 203.
113. J. T. Groves, R. C. Haushalter, M. Nakamura, T. E. Nemo and B. J. Evans, *J. Am. Chem. Soc.*, 1981, **103**, 2884.
114. E. T. Shimomura, M. A. Phillippi, H. M. Goff, W. F. Scholz and C. A. Reed, *J. Am. Chem. Soc.*, 1981, **103**, 6778.
115. G. N. LaMar, J. S. deRopp, L. Latos-Grazynski, A. L. Balch, R. B. Johnson, K. M. Smith, D. W. Parish and R. J. Cheng, *J. Am. Chem. Soc.*, 1983, **105**, 782.
116. G. N. LaMar, V. P. Chacko and J. S. deRopp, in *The Biological Chemistry of Iron* (H. B. Dunford *et al.*, eds), Reidel, New York, 1982, p. 357.
117. G. N. LaMar, D. L. Budd and H. Goff, *Biochem. Biophys. Res. Commun.*, 1977, **77**, 104.
118. G. N. LaMar, K. Ragai, T. Jue, D. L. Budd, K. Gersonde, H. Sick, T. Kagimoto, A. Hayashi and F. Taketa, *Biochem. Biophys. Res. Commun.*, 1980, **96**, 1172.
119. S. Takahashi, A. K. L. C. Lin and C. Ho, *Biophys. J.*, 1982, **39**, 33.
120. K. Nagai, G. N. LaMar, T. Jue and H. F. Bunn, *Biochemistry*, 1982, **21**, 842.
121. G. N. LaMar, J. S. deRopp, V. P. Chacko, J. D. Satterlee and J. E. Erman, *Biochim. Biophys. Acta*, 1982, **708**, 317.
122. J. D. Satterlee and J. E. Erman, *Biochim. Biophys. Acta*, 1983, **743**, 149.
123. C. Dalvit, S. Miura, A. DeYoung, R. W. Noble, M. Cerdonio and C. Ho, *Eur. J. Biochem.*, 1984, **141**, 255.
124. S. Miura and C. Ho, *Biochemistry*, 1984, **23**, 2492.
125. T. Inubushi, M. Ikeda-Saito and T. Yonetani, *Biochemistry*, 1983, **22**, 2904.
126. S. Takashashi, A. K. L. C. Lin and C. Ho, *Biochemistry*, 1980, **19**, 5196.
127. Y. Shiro and I. Morishima, *Biochemistry*, 1984, **23**, 4879.
128. G. N. LaMar, R. R. Anderson, D. L. Budd, K. M. Smith, K. C. Langry, K. Gersonde and H. Sick, *Biochemistry*, 1980, **20**, 4429.
129. G. N. LaMar and J. S. deRopp, *J. Am. Chem. Soc.*, 1982, **104**, 5203.
130. G. N. LaMar, J. T. Jackson and R. G. Bartsch, *J. Am. Chem. Soc.*, 1981, **103**, 4405.
131. S. B. Kong, J. D. Cutnell and G. N. LaMar, *J. Biol. Chem.*, 1983, **256**, 3843.
132. J. D. Cutnell, G. N. LaMar and S. B. Kong, *J. Am. Chem. Soc.*, 1981, **103**, 3567.
133. G. N. LaMar, J. D. Cutnell and S. B. Kong, *Biophys. J.*, 1981, **34**, 217.

134. G. N. LaMar and J. S. deRopp, *Biochem. Biophys. Res. Commun.*, 1979, **90**, 36.
135. J. T. Jackson, G. N. LaMar and R. G. Bartsch, *J. Biol. Chem.*, 1983, **258**, 1799.
136. G. N. LaMar, R. Krishnamoorthi, K. M. Smith, K. Gersonde and H. Sick, *Biochemistry*, 1983, **23**, 6239.
137. J. V. Kilmartin, J. A. Hewitt and J. F. Wooten, *J. Mol. Biol.*, 1975, **93**, 203.
138. S. Ogawa, D. J. Patel and S. R. Simon, *Biochemistry*, 1974, **13**, 2001.
139. M. F. Perutz, J. E. Ladner, S. R. Simon and C. Ho, *Biochemistry*, 1974, **13**, 2163.
140. M. F. Perutz, A. R. Fersht, S. R. Simon and G. C. K. Roberts, *Biochemistry*, 1974, **13**, 2174.
141. H. F. Bunn, R. C. Wohl, T. B. Brandley, M. Cooley and Q. H. Gibson, *J. Biol. Chem.*, 1974, **249**, 7402.
142. J. Monod, J. Wyman and J. P. Changeaux, *J. Mol. Biol.*, 1965, **12**, 88.
143. M. F. Perutz, *Nature* (London), 1970, **228**, 726.
144. J. D. Satterlee and G. N. LaMar, *J. Am. Chem. Soc.*, 1976, **98**, 2804.
145. G. N. LaMar, J. S. Frye and J. D. Satterlee, *Biochim. Biophys. Acta*, 1976, **428**, 78.
146. J. S. Valentine, R. P. Sheridan, L. C. Allen and P. Kahn, *Proc. Nat. Acad. Sci. USA*, 1979, **76**, 1009.
147. T. Mincey and T. G. Traylor, *J. Am. Chem. Soc.*, 1979, **101**, 765.
148. J. Teroaka and T. Kitagawa, *Biochem. Biophys. Res. Commun.*, 1980, **93**, 674.
149. P. Stein, M. Mitchell and T. G. Spiro, *J. Am. Chem. Soc.*, 1980, **102**, 7795.
150. V. P. Chacko and G. N. LaMar, *J. Chem. Soc.*, 1982, **104**, 7002.
151. J. C. Schwartz, M. A. Stanford, J. N. Noy, B. M. Hoffman and J. S. Valentine, *J. Am. Chem. Soc.*, 1979, **101**, 3396.
152. M. A. Stanford, J. C. Schwartz, T. E. Phillips and B. M. Hoffman, *J. Am. Chem. Soc.*, 1980, **102**, 4492.
153. M. F. Perutz, J. K. M. Sanders, D. H. Chenery, R. W. Noble, R. R. Pennelly, L. W. M. Fung, C. Ho, I. Giannini, D. Pörschke and H. Winkler, *Biochemistry*, 1978, **17**, 3640.
154. K. J. Wiechelman, J. Fox, P. R. McCurdy and C. Ho, *Biochemistry*, 1978, **17**, 791.
155. G. Viggiano, K. J. Wiechelman, P. A. Chervenick and C. Ho, *Biochemistry*, 1978, **17**, 795.
156. G. Viggiano and C. Ho, *Proc. Nat. Acad. Sci. USA*, 1979, **76**, 3673.
157. G. Viggiano, N. T. Ho and C. Ho, *Biochemistry*, 1979, **18**, 5238.
158. C. Ho, C. H. J. Lam, S. Takahashi and G. Viggiano, in *Hemoglobin and Oxygen Binding* (C. Ho, ed.), Elsevier/North Holland, Amsterdam, 1982, p. 141.
159. S. Miura and C. Ho, *Biochemistry*, 1982, **24**, 6280.
160. C. Ho, L. W. M. Fung, K. J. Weichelman, G. Pifat and M. E. Johnson, in *Erythrocyte Structure and Function* (G. J. Brewer, ed.), Alan R. Liss, New York, 1975, p. 43.
161. G. N. LaMar, T. Jue, B. M. Hoffman and K. Nagai, *J. Mol. Biol.* 1984, **178**, 929.
162. S. Neya and I. Morishima, *J. Biol. Chem.*, 1981, **256**, 793.
163. S. Neya, S. Hada and N. Funasaki, *Biochemistry*, 1983, **22**, 3686.
164. J. Lecomete, G. N. LaMar, K. H. Winterhalter and J. D. G. Smith, *J. Mol. Biol.*, 1984, **180**, 357.
165. G. R. Moore and G. Williams, *Biochim. Biophs. Acta*, 1984, **788**, 147.
166. H. Senn, H. Böhme and K. Wüthrich, *Biochim. Biophys. Acta*, 1984, **789**, 311.
167. G. R. Moore, R. J. P. Williams, J. C. W. Chien and L. C. Dickson, *J. Inorg. Biochem.*, 1980, **12**, 1.
168. G. R. Moore and R. J. P. Williams, *Eur. J. Biochem.*, 1980, **103**, 493.
169. A. DeMarco and K. Wüthrich, *J. Magn. Reson.*, 1976, **2**, 201.
170. I. D. Campbell, C. M. Dobson, R. J. P. Williams and A. V. Xavier, *J. Magn. Reson.*, 1973, **11**, 172.
171. J. A. Carver and J. H. Bradbury, *Biochemistry*, 1984, **23**, 4890.
172. R. Krishnamoorthi and G. N. LaMar, *Eur. J. Biochem.*, 1984, **138**, 139.
173. T. Iuzaka and I. Morishima, *Biochim. Biophys. Acta*, 1975, **400**, 143.
174. A. P. Boswell, G. R. Moore and R. J. P. Williams, *Biochem. J.*, 1982, **201**, 523.

175. G. N. LaMar, D. B. Viscio, K. M. Smith, W. S. Caughey and M. L. Smith, *J. Am. Chem. Soc.*, 1978, **100**, 8085.
176. R. M. Keller, O. Groudinsky and K. Wüthrich, *Biochim. Biophys. Acta*, 1976, **427**, 497.
177. R. G. Shulman, S. H. Glarum and M. Karplus, *J. Mol. Biol.*, 1971, **57**, 93.
178. G. R. Moore, R. G. Ratcliffe and R. J. P. Williams, *Essays in Biochemistry*, 1983, **19**, 142.
179. A. Mayer and H. Eicher, *J. Mol. Catal.*, 1984, **23**, 151.
180. G. N. LaMar and R. Krishnamoorthi, *Biophys. J.*, 1983, **44**, 177.
181. B. Sheard, T. Yamane and R. G. Shulman, *J. Mol. Biol.*, 1970, **53**, 35.
182. R. Freeman, S. P. Kempsell and M. H. Levitt, *J. Magn. Reson.*, 1980, **38**, 453.
183. K. Wüthrich, J. Hochman, R. M. Keller, G. Wagner, M. Brunori and M. Giacometti, *J. Magn. Reson.*, 1975, **19**, 111.
184. M. E. Johnson, L. W. M. Fung and C. Ho, *J. Am. Chem. Soc.*, 1977, **99**, 1245.
185. G. N. LaMar and G. R. VanHecke, *J. Chem. Phys.*, 1970, **52**, 5676.
186. K. Hon-Nami, H. Kihara, T. Kitagawa, T. Miyazawa and T. Oshina, *Eur. J. Biochem.*, 1980, **110**, 217.
187. H. Santos, J. J. G. Moura, I. Moura, J. LeGall and A V. Xavier, *Eur. J. Biochem.*, 1984, **141**, 283.
188. G. R. Moore, G. J. McLune, N. J. Clayden, R. J. P. Williams, B. M. Alsaadi, J. Ångstrom, R. P. Ambler, P. VanBeeumen, P. Tempst, R. G. Bartsch, T. E. Meyer and M. D. Kamen, *Eur. J. Biochem.*, 1982, **123**, 73.
189. J. J. G. Moura, H. Santos, I. Moura, J. LeGall, G. R. Moore, R. J. P. Williams and A. V. Xavier, *Eur. J. Biochem.*, 1982, **127**, 151.
190. I. Moura, M. C. Liu, J. LeGall, H. D. Peck, W. J. Payne, X. V. Xavier and J. J. G. Moura, *Eur. J. Biochem.*, 1984, **141**, 297.
191. J. Villalain, I. Moura, M. C. Lie, W. J. Payne, J. LeGall, A. V. Xavier and J. J. G. Moura, *Eur. J. Biochem.*, 1984, **141**, 305.
192. N. Ellfolk, M. Rönnberg, R. Aasa, T. Vänngard and J. Ångstrom, *Biochem. Biophys. Acta*, 1984, **791**, 9.
193. S. Neya and I. Morishima, *J. Biol. Chem.*, 1979, **254**, 9107.
194. M. H. Emptage, A. V. Xavier, J. M. Wood, B. M. Alsaadi, G. R. Moore, R. C. Pitt, R. J. P. Williams, R. P. Ambler and R. G. Bartsch, *Biochemistry*, 1981, **20**, 58.
195. R. L. Kandler, I. Constantinidis and J. D. Satterlee, *Biochem. J.*, 1984, **226**, 131.
196. D. V. DerVartanian, A. V. Xavier and J. LeGall, *Biochem.*, 1978, **60**, 315.
197. M. R. N. Murthy, T. J. Reid, A. Sicignanco, N. Tanaka and M. G. Rossman, *J. Mol. Biol.*, 1981, **152**, 465.
198. I. Morishima and S. Ogawa, in *Oxidases and Related Redox Systems* (T. E. King, H. S. Mason and M. Morrison, eds), Pergamon Press, New York, 1982, p. 597.
199. R. L. Kandler and J. D. Satterlee, *Comp. Biochem. Physiol.*, 1983, **75B**, 499.
200. G. N. LaMar, R. R. Anderson, V. P. Chacko and K. Gersonde, *Eur. J. Biochem.*, 1983, **136**, 161.
201. I. Morishima and M. Hara, *J. Biol. Chem.*, 1983, **258**, 14428.
202. I. Morishima and M. Hara, *Biochemistry*, 1983, **22**, 4102.
203. I. Morishima and M. Hara, *J. Am. Chem. Soc.*, 1982, **104**, 6833.
204. I. Morishima and M. Hara, *Biochem. Biophys. Res. Commun.*, 1984, **121**, 229.
205. I. Morishima, S. Ogawa and H. Yamada, *J. Am. Chem. Soc.*, 1979, **101**, 7074.
206. I. Morishima, S. Ogawa and H. Yamada, *Biochemistry*, 1980, **19**, 1569.
207. G. N. LaMar, T. L. Bold and J. D. Satterlee, *Biochim. Biophys. Acta*, 1978, **498**, 189.
208. F. A. Walker, *J. Am. Chem. Soc.*, 1980, **102**, 3254.
209. T. G. Traylor and A. P. Berzinis, *J. Am. Chem. Soc.*, 1980, **102**, 2844.
210. F. A. Walker, J. Buehler, J. T. West and J. L. Hinds, *J. Am. Chem. Soc.*, 1983, **105**, 6923.
211. H. Goff, *J. Am. Chem. Soc.*, 1980, **102**, 3252.
212. E. Ulrich, D. W. Krogman and J. L. Markley, *J. Biol. Chem.*, 1982, **257**, 9356.

213. T. G. Perkins, J. D. Satterlee and J. H. Richards, *J. Am. Chem. Soc.*, 1983, **105**, 1350.
214. J. D. Satterlee, *Biochim. Biophys. Acta*, 1984, **791**, 384.
215. E. Oldfield, R. S. Norton and A. Allerhand, *J. Biol. Chem.*, 1975, **250**, 6381.
216. E. Oldfield, R. S. Norton and A. Allerhand, *J. Biol. Chem.*, 1975, **250**, 6368.
217. E. Oldfield and A. Allerhand, *J. Biol. Chem.*, 1975, **250**, 6403.
218. H. M. Goff, *J. Am. Chem. Soc.*, 1981, **103**, 3714.
219. M. A. Phillippi and H. M. Goff, *J. Chem. Soc., Chem. Comm.*, 1980, 455.
220. H. M. Goff, *Biochim. Biophys. Acta*, 1978, **542**, 348.
221. H. Goff, *J. Chem. Soc., Chem. Comm.*, 1978, 777.
222. H. Goff, *J. Am. Chem. Soc.*, 1977, **99**, 7723.
223. F. Blomberg and H. Rüterjans, in *Biological Magnetic Resonance* (L. J. Berliner and J. Reuben, eds), Plenum Press, New York, 1983, Vol. 5, p. 21.
224. D. Gust, R. B. Moon and J. D. Roberts, *Proc. Nat. Acad. Sci. USA*, 1975, **72**, 4696.
225. I. Morishma and T. Inubushi, *J. Chem. Soc., Chem. Comm.*, 1977, 616.
226. I. Morishima, T. Inubushi, S. Neya, S. Ogawa and T. Yonezawa, *Biochem. Biophys. Res. Commun.*, 1977, **78**, 739.
227. I. Morishima and T. Inubushi, *J. Am. Chem. Soc.*, 1978, **100**, 3568.
228. I. Morishima and T. Inubushi, *Biochem. Biophys. Res. Commun.*, 1978, **80**, 199.
229. H. Goff, private communication, 1985.
230. M. Witanowshi, L. Stefaniak and G. A. Webb, in *Annual Reports on NMR Spectroscopy* (G. A. Webb, ed.), Academic Press, London, Vol. 18, in press.

Nuclear Magnetic Relaxation and Models for Backbone Motions of Macromolecules in Solution

F. HEATLEY

Department of Chemistry, University of Manchester, Manchester, UK

I. INTRODUCTION

In recent years there have been significant developments, both practical and theoretical, in the study of macromolecular dynamics using nuclear magnetic relaxation. In the practical sphere the availability of high-field multinuclear Fourier-transform spectrometers, with sophisticated computer systems, has allowed the measurement of a wide range of independent relaxation parameters. In turn these data have stimulated increasingly realistic theoretical analyses of macromolecular motions, which cover a wide range of amplitudes and timescales. In solution the motions range from small-scale oscillations with amplitudes of the order of $10°$ and frequencies of the order of 10^{11} Hz, through segmental motions consisting typically of internal rotations through $120°$ at a frequency of 10^9 Hz, to overall molecular rotation at a frequency of perhaps as low as 10^5 Hz. The purpose of relaxation studies is to determine the nature and rates of those processes controlling relaxation.

This article is restricted to studies of macromolecules in dilute (or reasonably so) diamagnetic isotropic solutions where dipole-dipole coupling is averaged to zero. In principle, spectra are observed in which chemically shifted nuclei and spin-spin couplings are resolved. Thus, by studying relaxation of different nuclei, there is the possibility of drawing a detailed picture of the motions of different parts of the molecule. Furthermore, the article concentrates on the principles underlying the experimental and theoretical approaches to relaxation in synthetic and natural macromolecules, rather than providing a comprehensive survey of applications. Attention is directed mainly to backbone motions.

For a survey of earlier work on synthetic polymers, the reader is referred to the literature.[1] Wüthrich and Wagner,[2] and more recently Jardetzsky,[3] have reviewed some aspects of nuclear magnetic relaxation in natural macromolecules. Though containing little on NMR, a review on theoretical simulations of protein dynamics is illuminating for the picture of macromolecular motions that it provides.[4] Finally, it is worth mentioning the surveys of NMR studies of synthetic and natural molecules which appear annually in the Nuclear Magnetic Resonance volume of the Royal Society of Chemistry's Specialist Periodical Reports. These reviews include papers on the subject of this article. The basic concepts of pulsed FT NMR are described in several monographs.[5]

II. EXPERIMENTAL METHODS

This section briefly outlines techniques available to study nuclear relaxation. As described in more detail in the following section, relaxation parameters are related to molecular motion through a spectral density function, $J(\omega)$, which is expressed as a Fourier transform of a correlation function, $G(t)$, by

$$J(\omega) = \int_{-\infty}^{+\infty} G(t)\, e^{i\omega t}\, dt \tag{1}$$

The correlation function embodies the mechanisms and rates of the motions, and obtaining this function is the ultimate objective of relaxation studies. Unfortunately, magnetic relaxation measurements in a given magnetic field respond to values of $J(\omega)$ at a very limited number of frequencies, and it is not practicable to obtain $J(\omega)$ over a sufficiently wide frequency range and in sufficient detail to derive $G(t)$ from a reverse transformation of equation (1). However, by measuring several relaxation parameters at different resonance frequencies, $J(\omega)$ can be sampled discretely at a number of frequencies, giving some insight into the form of $G(t)$.

The most commonly performed relaxation measurement is that of the spin–lattice (or longitudinal) relaxation time, T_1. This parameter depends on $J(\omega_0)$ and $J(2\omega_0)$, where ω_0 is the resonance frequency. Using presently available commercial spectrometers, ω_0 spans the range 5–500 MHz depending on magnetic field and nucleus. T_1 is relatively easily measured using a variety of techniques such as inversion recovery or progressive saturation.[5] The phenomenon of cross-relaxation in spin–lattice relaxation gives rise to a number of interesting effects providing further dynamic information. Perhaps the most familiar of these is the nuclear Overhauser effect (NOE), which involves spectral densities at sum and difference frequencies $\omega_A + \omega_X$ and $|\omega_A - \omega_X|$ as well as individual resonance frequencies ω_A and ω_X. If A and X are different nuclear species, both $\omega_A + \omega_X$ and $|\omega_A - \omega_X|$ are in the same radiofrequency region as the resonance frequencies themselves. Although the NOE represents a different combination of $J(\omega)$'s from T_1, and is therefore an independent parameter, the information provided concerns the same part of the motional spectrum. However, if A and X are of the same species, the difference frequency $|\omega_A - \omega_X|$ is of the order of chemical shift, i.e. in the kHz region, and the NOE senses the spectral density at low as well as high frequencies. This attribute of the NOE has been exploited for both synthetic[1,7,8] and natural macromolecules.[6]

A relaxation experiment long in use for solid polymers but only recently[9] applied to solutions is spin–lattice relaxation in the rotating frame ($T_{1\rho}$). This parameter senses the spectral density at the resonance frequency in the rotating B_1 field, typically 10–100 kHz, and therefore extends the frequency range into the valuable audio region.

Measurements of spin–spin (transverse) relaxation times (T_2) are much less common than T_1, principally because of the difficulty of measurement. In principle, T_2 can be obtained from the linewidth at half-height, using the relation $T_2 = (\pi\delta\nu_{1/2})^{-1}$, but the T_2 contribution is frequently obscured by inhomogeneity broadening and line overlap. The spin–echo pulse sequence can be used,[5] but care is needed because of its high sensitivity to pulse imperfection.[10] Bain et al.[11] have recently described an alternative method, which involves measuring the signal intensity as a function of the offset of a saturating radiofrequency field. T_2 is of great significance in dynamic studies since it depends on $J(0)$, i.e. the area under the correlation function.

Several nuclei have been used to study macromolecular motions. The most important are ^{1}H and ^{13}C, since these occur naturally in practically all systems. Other nuclei that have been used are ^{2}H,[12–14] ^{15}N,[15] ^{19}F,[16] and ^{31}P.[17] The last of these is especially applicable to natural molecules. For ^{1}H nuclei the predominant relaxation mechanism is dipole–dipole (DD) interactions with other protons, though there may be a substantial contribution from paramagnetic centres, including dissolved oxygen, if present.

Although ^{1}H spectra have the advantage of high sensitivity, a serious disadvantage is the complexity of handling the large number of individual interactions in a typical polymer. For natural abundance saturated ^{13}C nuclei bonded to protons, the predominant mechanism is DD interaction with the attached protons. Theoretical analysis of the relaxation parameters is therefore relatively simple. For quaternary and unsaturated ^{13}C nuclei the situation is more complex. The chemical shielding anisotropy mechanism (CSA) is significant for unsaturated quaternary ^{13}C nuclei at all resonance frequencies, and for unsaturated protonated ^{13}C nuclei becomes increasingly so above 25 MHz. The same general behaviour probably applies to ^{15}N relaxation, though few studies have been made. Poor sensitivity is a disadvantage of both nuclei, in the absence of enrichment. For ^{19}F and ^{31}P nuclei the DD and CSA mechanisms are both operative, the balance depending on the proximity of other magnetic nuclei to the nucleus in question. Separating the contributions is relatively straightforward[18] in small molecules where the extreme narrowing condition applies ($\omega_0^2\tau_c^2 \ll 1$). In macromolecules, where this condition generally does not apply, the task is difficult. For ^{2}H nuclei the overwhelming mechanism is quadrupolar relaxation, which admits a particularly simple theoretical interpretation. Enrichment is usually required, however.

The measurement of relaxation parameters for different nuclear species in the same sample is one method of probing the frequency dispersion of the spectral density. However, if the molecular motions are anisotropic, as is usually the case in polymers, the relaxation mechanisms for each nucleus will in general have different correlation functions, and it is advisable to study each nucleus at different frequencies as well. From this summary it appears that the most precise characterization of macromolecular dynamics is likely to be obtained from T_1, T_2 and NOE measurements for ^{13}CH$_n$ groups over a range of resonance frequencies.

III. THEORY

A. Basic NMR theory

Consider first the cases of two nuclei relaxing entirely by their mutual dipolar interaction, and of a single nucleus relaxing by the quadrupolar mechanism. In each case relaxation arises from a fluctuating Hamiltonian which can be written as a scalar product of two second-rank spherical tensors:[19]

$$H = \sum_q (-1)^q F_q A_{-q}$$

where A_q contains spin operators and constants defining the magnitude of

the interaction and F_q is a function of the Euler angles[20] giving the orientation of the dipolar or electric field gradient tensors with respect to a reference frame. F_q is time-dependent because of random molecular motion, its average behaviour being expressed by a correlation function

$$G(t) = \langle F_q(\Omega, 0) F_q^*(\Omega, t) \rangle \tag{2}$$

where the symbol Ω represents the angles specifying the orientation of the dipolar vector or the principal axes of the electric field gradient tensors with respect to the external magnetic field. If these tensors are axially symmetric, the function $F_q(\Omega, t)$ is the same for both mechanisms and is equal to the element $D_{q0}^{(2)}(\Omega, t)$ of the Wigner rotation matrices.[20] For an isotropic solution, the correlation function is independent of q. Relaxation parameters are related to $G(t)$ through the function $J(\omega)$ defined in equation (1). Although polymer motion is often neither isotropic nor diffusional, it is helpful in understanding some important general properties of NMR relaxation to bear in mind the forms of $G(t)$ and $J(\omega)$ for the simple case of isotropic rotational diffusion:

$$G(t) = (1/5) \exp(-|t|/\tau_c) \tag{3}$$

$$J(\omega) = (2/5)\tau_c/(1 + \omega^2 \tau_c^2) \tag{4}$$

where τ_c is the correlation time. The expressions relating relaxation parameters to $J(\omega)$ are as follows:

(a) Dipolar relaxation of two identical nuclei, A_2, spin $I = 1/2$. Both longitudinal and transverse relaxation are exponential.

$$T_1^{-1} = 3C[J(\omega_A) + 4J(2\omega_A)] \tag{5a}$$

$$T_2^{-1} = (3/2)C[3J(0) + 5J(\omega_A) + 2J(2\omega_A)] \tag{5b}$$

where

$$C = \frac{1}{4}\left(\frac{\mu_0}{4\pi}\right)^2 \gamma^4 \hbar^2 r^{-6}$$

γ is the magnetogyric ratio, r is the internuclear distance (assumed constant) and μ_0 and $\hbar$ have their usual meanings. As τ_c (i.e. temperature) varies, T_1 passes through a minimum when $\omega_A \tau_c = 0.616$, whereas T_2 decreases monotonically as τ_c increases. In the extreme narrowing limit $(\omega_A^2 \tau_c^2 \ll 1)$ T_1 and T_2 are equal and independent of ω_A, whereas in the opposite extreme $(\omega_A^2 \tau_c^2 \gg 1)$ $T_1 \propto \omega_A^2$ and $T_2 \ll T_1$.

(b) Dipolar relaxation of two non-identical nuclei, AX, both spin $1/2$. The time-dependence of the longitudinal magnetization components M_{zA}

and M_{zX} is governed by the coupled equations

$$dM_{zA}/dt = -\rho_A(M_{zA} - M_{zA}{}^0) - \sigma(M_{zX} - M_{zX}{}^0) \qquad (6a)$$

$$dM_{zX}/dt = -\rho_X(M_{zX} - M_{zX}{}^0) - \sigma(M_{zA} - M_{zA}{}^0) \qquad (6b)$$

$$\rho_A = C[J(\omega_A - \omega_X) + 3J(\omega_A) + 6J(\omega_A + \omega_X)]$$

$$\rho_X = C[J(\omega_A - \omega_X) + 3J(\omega_X) + 6J(\omega_A + \omega_X)]$$

$$\sigma = C[6J(\omega_A + \omega_X) - J(\omega_A - \omega_X)]$$

$$C = \frac{1}{4}\left(\frac{\mu_0}{4\pi}\right)^2 \gamma_A{}^2 \gamma_X{}^2 \hbar^2 r^{-6}$$

The steady-state NOE of A on saturation of X is given by

$$\text{NOE} = 1 + \frac{\gamma_X}{\gamma_A}\left[\frac{6J(\omega_A + \omega_X) - J(\omega_A - \omega_X)}{J(\omega_A - \omega_X) + 3J(\omega_A) + 6J(\omega_A + \omega_X)}\right] \qquad (7)$$

The relaxation behaviour depends on whether A and X are of the same species or not. Consider first the homonuclear case. Here $|\omega_A - \omega_X| \ll \omega_A$ or ω_X and hence $J(\omega_A - \omega_X) \approx J(0)$, to all intents and purposes. The relaxation depends on the selectivity of the perturbation and the correlation time regime. For equal perturbation of A and X (non-selective pulses), both nuclei relax exponentially with the same T_1 which is identical to equation (5a). If only one nucleus (e.g. A) is perturbed (selective pulse), the recovery curve is in general bi-exponential, the time constants and relative magnitudes of the two contributions depending on whether $\omega_A{}^2\tau_c{}^2 \ll 1$ or $\omega_A{}^2\tau_c{}^2 \gg 1$. In the former case (fast motion) the recovery is effectively exponential with time constant.

$$T_{1A}{}^{-1} = \rho_A = C[J(\omega_A - \omega_X) + 3J(\omega_A) + 6J(\omega_A + \omega_X)] \qquad (8)$$

In the slow motion case the time constants are very different and equally weighted. The time constants are approximately equal to ρ and $\rho + \sigma$. Since in this regime $J(\omega_A - \omega_X) \gg J(\omega_A)$, $J(\omega_A + \omega_X)$, then $\rho \gg \rho + \sigma$, and the recovery consists of an initial rapid phase followed by a much slower second phase. Physically, the first stage represents transfer of spin energy from the perturbed to the unperturbed spin via the transition $\alpha\beta \leftrightarrow \beta\alpha$ (spin diffusion) at a rate given by $CJ(\omega_A - \omega_X)$. This process leads to internal equilibrium within the spin system, and is followed by much slower equilibration with the lattice via $\alpha \leftrightarrow \beta$ and $\alpha\alpha \leftrightarrow \beta\beta$ transitions represented by the $J(\omega_A)$ and $J(\omega_A + \omega_X)$ terms. During the recovery the initially unperturbed nucleus shows a transient NOE,[8] positive for $\omega_A{}^2\tau_c{}^2 \ll 1$ and negative for $\omega_A{}^2\tau_c{}^2 \gg 1$. As a function of τ_c the steady-state NOE is a sigmoid form with limits of 1.5 for $\omega_A{}^2\tau_c{}^2 \ll 1$ and 0 for $\omega_A{}^2\tau_c{}^2 \gg 1$. The latter represents saturation transfer from irradiated to observed nucleus. The NOE varies

with τ_c only over the approximate range $0.1 \lesssim \omega_A \tau_c \lesssim 10$. The relaxation time of A while X is kept saturated is given by equation (8). Because of the $J(\omega_A - \omega_X)$ term, this relaxation time behaves like T_2, i.e. it decreases monotonically as τ_c increases, and it provides a useful method of probing the low-frequency region.[21,22]

When A and X are of different species, one of them, X say, is usually a proton and broadband decoupling is normally used to simplify the A spectrum. Under these conditions, A relaxation is exponential with a relaxation time as given in equation (8). For the heteronuclear case, $|\omega_A - \omega_X|$ is of the same order of magnitude as ω_A, ω_X and $\omega_A + \omega_X$, and hence, as a function of τ_c, equation (8) behaves in a similar manner to equation (5a) already described. The NOE is given by equation (7), as in the homonuclear AX case, and varies with τ_c in the same way though with different limits. For the most common situation of a ^{13}C-^1H pair, the limits are 2.988 for $\omega_A^2 \tau_c^2 \ll 1$ and 1.15 for $\omega_A^2 \tau_c^2 \gg 1$.

Transverse relaxation measurements in the homonuclear case are usually made using the Carr–Purcell–Meiboom–Gill spin-echo sequence[23] with non-selective pulses. Provided the pulse interval is sufficiently short to suppress echo modulation from scalar coupling,[24] T_2 of both A and X is given by equation (5b) as for the A_2 case. For the heteronuclear case with X-decoupling, T_{2A} is given by

$$T_{2A}^{-1} = \frac{C}{2}[4J(0) + J(\omega_A - \omega_X) + 3J(\omega_A) + 6J(\omega_X) + 6J(\omega_A + \omega_X)] \quad (9)$$

Note that the X-decoupling must be in the continuous wave mode in order to avoid artificial shortening of T_2.[25]

(c) Quadrupolar relaxation. For a single nucleus of spin I and an axially symmetric electric field gradient, T_1 and T_2 are given by equations (5a) and (5b) except that the interaction constant C is

$$C = [e^2 qQ/4I\hbar(2I - 1)]^2$$

where $(e^2 qQ/h)$ is the quadrupole coupling constant in Hz.

B. Relaxation in multi-spin systems

In practice the simple systems described above are rarely encountered. In general there will be more than two interacting spins and possibly more than one mechanism. There are two exceptions which do effectively correspond to the simple situations. These are ^{13}C relaxation in a saturated $^{13}CH_n$ group with proton decoupling (heteronuclear dipolar relaxation, case (b)) and ^2H relaxation (quadrupolar relaxation, case (c)). In ^1H relaxation, in the absence of paramagnetic centres, the dominant mechanism is ^1H-^1H dipolar relaxation between nearest neighbours, so that coupling of relaxa-

tion encompasses all protons in the macromolecule. For ^{13}C, ^{19}F and ^{31}P nuclei, which usually occur in an isolated situation, relaxation arises from dipolar interaction with neighbouring protons, perhaps with a CSA contribution as well. The theory appropriate to a particular application therefore depends on the molecular structure. For the purpose of this article, the most important examples of multi-spin relaxation are ^{13}C relaxation in saturated ^{13}CH$_2$ and ^{13}CH$_3$ groups and multi-proton systems. Attention will be confined to these two cases.

A formal density matrix treatment of relaxation has been developed,[26] but the theory becomes prohibitively unwieldy for all except the simplest systems (see below). The theory requires the evaluation of cross-correlation functions between different interactions, as well as auto-correlation functions. If cross-correlation is neglected, as it usually is, the contributions of each relaxation source are additive. In the case of ^{13}C relaxation in ^{13}CH$_2$ and ^{13}CH$_3$ groups, dominated by dipolar interaction with attached protons, T_1^{-1} and T_2^{-1} are given by multiplying equations (8) and (9) by 2 or 3 as appropriate. Equation (7) still applies for the NOE. For longitudinal relaxation in ^{1}H systems, equations (6a) and (6b) can be generalized, giving for each spin an equation of the form

$$\frac{dM_{zi}}{dt} = -\rho_i(M_{zi} - M_{zi}^0) - \sum_{j \neq i} \sigma_{ij}(M_{zj} - M_{zj}^0) \qquad (10)$$

with

$$\rho_i = \sum_{j \neq i} C_{ij}[J(\omega_i - \omega_j) + 3J(\omega_i) + 6J(\omega_i + \omega_j)]$$

$$\sigma_{ij} = C_{ij}[6J(\omega_i + \omega_j) - J(\omega_i - \omega_j)]$$

$$C_{ij} = \frac{1}{4}\left(\frac{\mu_0}{4\pi}\right)^2 \gamma_H^4 \hbar^2 r_{ij}^{-6}$$

The applications of these equations to the specific examples of ^{1}H relaxation in vinyl polymers[21] and ^{1}H relaxation in proteins[6,27,28] has been described. In general, the relaxation of M_{zi} is multi-exponential, but under certain conditions the behaviour is simpler. For non-selective pulses and extreme narrowing, each spin relaxes at a characteristic rate with a relaxation time given approximately by

$$T_{1i}^{-1} = \rho_i + \sum_{j \neq i} \sigma_{ij} \qquad (11)$$

T_{1i} reflects the mobility and magnitude of local interactions experienced by that nucleus. In the opposite extreme of slow motion ($\omega_i^2 \tau_c^2 \gg 1$), all spins relax exponentially at the same rate because rapid spin-diffusion maintains a uniform spin temperature. The relaxation time is a population-weighted average of the individual T_1's given by equation (11). Thus

segmental detail is lost. However, it may be recovered by using a selective perturbation. Either the transient NOE following selective inversion[7,8] or the rate of development of the steady-state NOE following saturation of an individual peak[6] can be measured. In each case the other protons show differential responses dependent on the relaxation efficiency of their interactions with the perturbed nucleus.

Transverse relaxation in multi-proton systems is complex.[24] However, if a non-selective Carr–Purcell–Meiboom–Gill spin–echo sequence is applied, with a π pulse repetition rate much greater than the spread of resonance frequencies, theory suggests[24] that spin–spin coupled nuclei decay with the same relaxation rate which is an average of the individual relaxation rates given by generalizing equation (5b)

$$T_{2i}^{-1} = \tfrac{3}{2} \sum_{j \neq i} C_{ij}[3J(0) + 5J(\omega_i) + 2J(2\omega_i)] \tag{12}$$

In the absence of spin–spin coupling, each peak should relax with its characteristic relaxation time. This behaviour has been observed in solutions of poly(methyl methacrylate)[8,29] and poly(methyl acrylate),[30] where it is found that the spin-coupled backbone proton T_2's are almost identical, whereas the non-coupled side-group T_2's are quite different.

C. Cross-correlation effects

Relaxation in A_3 systems[31] and in AX_2 and AX_3 systems[32] has been rigorously analysed using density matrix theory, including cross-correlation effects. Cross-correlation manifests itself in non-exponential relaxation and in differing relaxation rates for the components of spin–spin multiplets. However, deviations from the simple additive scheme described above appear to be small if initial relaxation rates are considered and if there is no large motional anisotropy. There are few reports of cross-correlation effects in macromolecules. One example which has been described is that of markedly non-exponential methyl ^1H relaxation in poly(2,6-dimethyl-1,4-phenylene oxide),[33] where highly anisotropic motion arises from rapid methyl internal rotation superimposed on much slower backbone segmental motions. Cross-correlation effects in $^{13}CH_2$ and $^{13}CH_3$ systems remain a possibly fruitful area of investigation.

IV. CORRELATION FUNCTIONS FOR POLYMER MOTIONS

Dynamically, macromolecules fall into two broad classes, conveniently termed "stiff" and "flexible". The first class comprises those polymers with long-range structural order and which exist predominantly in one conformation. The most important examples of this type are polypeptides, either

natural (proteins, enzymes) or synthetic, which under appropriate conditions adopt a well defined conformation held together by intramolecular hydrogen bonds and other inter-residue links. There is a large relaxation contribution from relatively slow overall isotropic or anisotropic tumbling. The second class, "flexible" molecules, comprises those polymers with a large degree of conformational disorder, relaxation being controlled by small-scale segmental motions which are faster than overall tumbling. Members of this class include synthetic polymers such as polyolefins, polyethers, polyamides and polyesters and natural molecules such as polysaccharides, and polypeptides in conditions where the "rigid" conformation is disrupted. Backbone motion in the two classes has attracted different theoretical approaches, and it is convenient to divide this section accordingly, though the categories are not mutually exclusive. The total correlation function can be written as a product of overall and internal correlation functions

$$G(t) = G_0(t) G_i(t) \qquad (13)$$

This factorization is exact for isotropic rotation and independent motions, and it has been shown to be a good approximation in the anisotropic case.[34] In flexible chains $G(t)$ decays entirely by $G_i(t)$ (for sufficiently long chains), the effective motions being segmental. For stiff chains both terms may be important.

A. Models for flexible chains

In an earlier review[1] experimental data on the dependence of T_1 and T_2 in synthetic polymers on molecular weight, concentration and solvent were surveyed. It is found that T_1 and T_2 are independent of molecular weight above a fairly low critical value of 1000–10 000, depending on chemical structure, and independent of concentration below about 10 weight % polymer. It is concluded that, for sufficiently large molecules in dilute solution, relaxation is controlled by segmental motions unaffected by chain length or bulk solution viscosity. The size of the mobile segment depends on the polymer structure. In poly(alkenes), for example, the segment appears to be only one or two monomer units,[35] whereas in polyesters some effective segmental motions involve three or more repeat units.[36] Quantitatively the relaxation parameters at ca. 300 K correspond to correlation times in the extreme narrowing region or in the region of the T_1 minimum, depending on chain structure. The shorter correlation times are shown by polyethers and poly(1,4-dienes), and the longer times by vinyl polymers with either a large side-group (e.g. polystyrene) or multiple side-groups (e.g. poly(methyl methacrylate)). It was also observed that T_1 and T_2 depended quite markedly on the solvent, the correlation time increasing regularly with increasing viscosity (for good solvents). Thus the rate of segmental motion depends

not just on an intramolecular internal rotation barrier but also on a local solvent-dependent friction factor.

In view of the wide variety of possible segmental motions, with a wide variety of rates and mechanisms, it is not surprising that detailed quantitative examination of relaxation data shows that the isotropic rotational diffusion model for $G_1(t)$, equation (3), does not hold for flexible polymers. The inadequacy is shown particularly clearly by ^{13}C relaxation measurements where it is found[37] that T_1, T_2 and NOE measurements cannot simultaneously be simulated by the same value of τ_c. The observed NOE's are lower than predicted from the correlation time extracted from the T_1 data. In addition, it was observed[37b] that the value of T_1 at its minimum is up to a factor of 2 greater than predicted by equation (8). In ^{1}H relaxation, it is found[5,29,30] that T_2 is significantly less than T_1 even at temperatures well above that corresponding to the T_1 minimum, i.e. when extreme narrowing should apply.

Initial attempts[38] to rationalize the ^{13}C relaxation parameters by a common correlation function invoked the idea of an empirical distribution of correlation times, writing $G(t)$ as

$$G(t) = \int_0^\infty f(\tau_c) \exp(-|t|/\tau_c) \, d\tau_c \qquad (14)$$

where $f(\tau_c)$ is the normalized distribution function. The effect of such a distribution on the temperature dependence of relaxation parameters is to raise and broaden the T_1 minimum, displace the T_2 curve to shorter values and broaden the NOE inflection. The NOE may be substantially less than maximal and T_2 may be less than T_1 even though $\omega_0^2 \tau_0^2 \ll 1$, where τ_0 is the mean correlation time. Conversely, when $\omega_0^2 \tau_0^2 \gg 1$, a measurable NOE may be observable. However, a maximal NOE and equal T_1 and T_2 values are predicted if all correlation times meet the extreme narrowing condition. It can appear therefore that chain motion proceeds by a single isotropic process.

By using various distributions, it proved possible to rationalize experimental data sets in terms of the same correlation function.[39] More recently distributions have been used to analyse ^{13}C relaxation in polypropylene,[40] poly(but-1-ene),[40] terephthalic acid polyesters[41] and poly(4-vinyl-N-n-alkylpyridinium bromides),[42] and ^{1}H and ^{13}C relaxation in poly(L-lysine).[43] Wittebort et al. have used a rectangular distribution for ^{13}C relaxation in poly(L-lysine).[44]

However, these functions have not been universally successful. Distributions previously used[37] for ^{13}C relaxation are found to be unsatisfactory in a study of ^{1}H relaxation in poly(vinyl acetate),[21] which includes the measurement of [1]H–[1]H cross-relaxation rates. The discrepancy lies in the fact that the [13]C T_1 and NOE data probe the spectral density only over a limited

frequency range in the MHz region, whereas the ^{1}H data give information in the kHz region, as well as the MHz region. Thus the distribution used is capable of adjustment to match the observed dispersion of $J(\omega)$ in the MHz region, but not of adjustment to match $J(\omega)$ in the kHz region as well. Schaefer's distribution[38] also failed to give a satisfactory interpretation of ^{1}H relaxation in poly(2,6-dimethyl-1,4-phenylene oxide).[45] It would be possible to set up a distribution function capable of generating the observed frequency dispersion, but this would have suffered from the general objection to the use of any empirical distribution function, namely that there is no direct connection between such a distribution and the mechanism of segmental motions. Indeed, there is experimental evidence pointing to the necessity of incorporating the specific conformational transitions available to a particular polymer in an interpretation of relaxation data. For example, it has been found[46] that in *cis* polybutadiene the ratio of ^{13}C T_1 values for the CH and CH$_2$ groups is 1.4, not 2 as expected if the two groups experience identical general backbone motions. The observed ratio has been rationalized[46] in terms of a specific crankshaft-like conformational transition in which the CH and CH$_2$ groups reorient by different angles, resulting in different correlation functions. A further example is relaxation in polysulphones. ^{13}C relaxation parameters are found to be independent of molecular weight and comparable to those in vinyl polymers.[47-49] Relaxation is therefore controlled by segmental motions. However, in dielectric relaxation the maximum loss frequency varies strongly with molecular weight,[50] consistent with relaxation by overall tumbling. The conflict has been rationalized[47,48] in terms of specific segmental motions which reorient the C–H bond vectors but not the sulphone dipoles. Thus, in order to achieve a proper understanding of relaxation in polymers, it is necessary to relate relaxation data to the conformational transitions accessible to a particular molecule. In practice, because of the limited frequency range of NMR data, the most promising method is to deduce the correlation function for a suggested mechanism, and test it against as wide a variety of data as possible. Various approaches along these lines have been made, some seeking analytical solutions for the correlation function, and others using numerical computer simulation techniques. The majority of applications have dealt with saturated polymers of the polyvinyl or polyether type, which can be fairly realistically represented as a chain on a diamond lattice. It should be borne in mind that an acceptable theoretical correlation function must be non-exponential since, as described above, certain experimental data cannot be understood by an exponential form. However, the fact that a consistent interpretation was obtained by representing the correlation function as a distribution of exponential functions does not necessarily imply the existence of a number of different relaxation processes, though that may be the case. Since a non-exponential correlation function can

formally be represented as a distribution, discrete or continuous, of exponential functions, a single dynamic process could in principle be sufficient provided it results in a non-exponential correlation function.

Before discussing those papers with particular relevance to NMR, it is worth mentioning some more general considerations concerning segmental motions, with a view to obtaining guidance on the most likely processes. Two principal factors determine the rate of a conformational transition. Firstly there are intramolecular bond rotational energy barriers and secondly there are hydrodynamic forces hindering the motion of segments through the medium. The former favour those transitions requiring rotation about the least number of bonds, and the latter favour those requiring the least displaced volume. On these principles, Iwata[51] has developed a model of polymer dynamics in terms of "crankshaft" transitions, i.e. those consisting of motion of a segment by rotation about two collinear bonds. Only the segment between the bonds moves, the remainder being unaffected. More than 2300 possible transitions of this type were located in segments up to 18 bonds. Helfand[52] has investigated polymer conformational transitions more generally, classifying them according to the relative position in the initial and transition states of the "tails" attached to the segment undergoing the transition. Type 1* transitions are those which leave the tails undisturbed, e.g. crankshaft motions or the three- and four-bond transitions shown in Fig. 1; type 2* transitions are those in which the tails experience translation
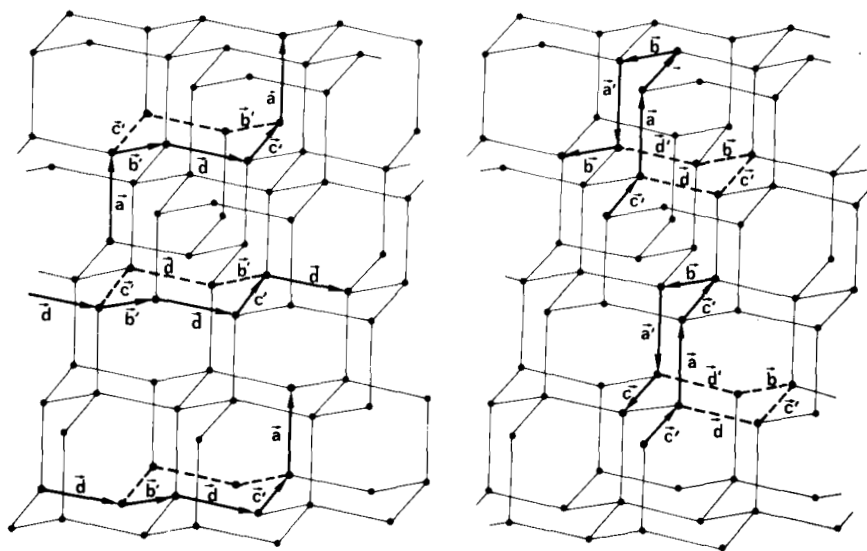
FIG. 1. Three-bond (left) and four-bond (right) transitions on a diamond lattice. From reference 80, with permission.

only, e.g. –ttt– ↔ –g$^+$tg$^-$–; and type 3* transitions are those in which the tails experience reorientation and translation, e.g. the rotation about a single bond. For the type 1* transition, Helfand has modified Kramer's theory of the rate of passage over a potential barrier, obtaining in the high-friction limit (diffusion control) a rate constant expressed as

$$k = \left[\frac{(\alpha_A \alpha_B)^{\frac{1}{2}}}{2\pi\Sigma\xi_i r_i^2}\right] \exp(-E^*/k_B T) \qquad (15)$$

ξ_i is the friction constant for atom i in the mobile unit, situated a distance r_i from the rotation axis. α_A and α_B are force constants such that the rotational potential energy near the initial state is approximated by

$$U(\phi) = \tfrac{1}{2}\alpha_A \Delta\phi^2$$

and near the transition state by

$$U(\phi) = E^* - \tfrac{1}{2}\alpha_B \Delta\phi^2$$

where $\Delta\phi$ is the angular deviation. The solvent influences the transition rate through the friction coefficient ξ_i. If ξ_i is proportional to the solvent viscosity η, the apparent activation energy of the transition rate (and hence correlation times) is $E^* + E_\eta$. Equation (15) clearly favours rotation of the smallest possible segment (to minimize $\Sigma\,\xi_i r_i^2$) about the fewest possible bonds (to minimize E^*).

The rates of type 2* and 3* transitions are less amenable to analysis. Intuitively one might expect these to be slower than type 1* because of the strong viscous drag on the bulky tails. However, initial approximate calculations,[53] subsequently verified by computer Brownian dynamics simulations and theoretical analysis,[54,55] show that this is not necessarily the case. It is found that the tails do not behave as rigid bodies but that, as the segment rotates, there is an accompanying distortion of the tails which diminishes with distance from the motional centre. After the barrier is crossed, the distortions themselves relax by translation and/or rotation of the tail. In many instances it is found that the extent of distortion of neighbouring bonds is so great as to lead to two simultaneous transitions. This is particularly likely when the first neighbour bond of the rotating bonds is *trans*, so that both single bond transitions and pair transitions such as ttg$^+$ ↔ g$^+$tt are observed. There is some experimental evidence that single bond rotations are an important relaxation process, notwithstanding the need for motion of the tails. For example, experimental activation energies for correlation times in vinyl polymers,[1] obtained using either a distribution of correlation times or a non-exponential correlation function from a lattice model, lie in the region of 25 ± 5 kJ mol^{-1}. Taking an approximate activation energy for solvent viscosity of 10 kJ mol^{-1}, we obtain a value of the order of $15 \pm$

5 kJ mol^{-1} for the intramolecular interactions. This is quite a low value, bearing in mind that the barrier in ethane[56] is 12 kJ mol^{-1}. It is certainly more consistent with a single bond rotation than with the two or more bond rotations necessary in type 1* transitions. Indeed, Boyd and Breitling[57] have calculated a value of c. 40 kJ mol^{-1} for the barrier in polyethylene for the three-bond motion in Fig. 1. For the five-bond crankshaft transition

$$-ttg^+tg^+tt- \leftrightarrow -g^+tg^+tg^+tg^- -$$
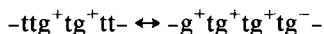
the barrier is calculated to be about 24 kJ mol^{-1}. Furthermore, from excimer fluorescence intensity measurements, Liao and Morawetz[58] have concluded that the process [1] $\rightleftharpoons$ [2] has the same activation energy whether this fragment is incorporated in a macromolecule or is in monomeric form.
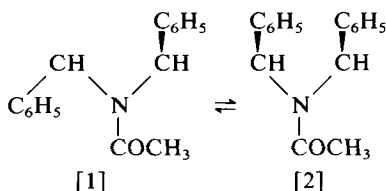
The first attempt to derive the correlation function appropriate to NMR relaxation for a specific molecular model of polymer transitions was developed using both Monte Carlo[59-64] and analytical methods.[65-69] The following summary of the analytical theory is based on references 67-69 and is referred to as the VJGM theory. It is assumed that the chain is distributed randomly on a tetrahedral lattice and that motion occurs by the type 1* three-bond and four-bond motions illustrated in Fig. 1. All other type 1* transitions can be reduced to series of these basic modes.[62] The general correlation function of the orientations of bonds p and q as defined in equation (2) can be written

$$G_{pq}(t) = \frac{1}{10}\left[3 \sum_i \sum_j P_i^q(0) P_j^p(t)(\mathbf{i} \cdot \mathbf{j})^2 - 1 \right] \tag{16}$$

where **i** and **j** are unit vectors along the four directions a, b, c and d in the lattice (Fig. 1) and $P_j^p(t)$ is the probability that p is along **j** at time t. For isotropic chains it can be assumed without loss of generality that bond q is directed along a at $t = 0$. For tetrahedral lattice angles, equation (16) becomes

$$G_{pq}(t) = \tfrac{4}{15}[P_a^p(t) - \tfrac{1}{4}] \tag{17}$$

For three-bond motions only with jump rate w_3, the time dependence of P_a^p is given by

$$\frac{\partial P_a^p}{\partial t} = w_3\left[\sum_{i,j \neq a} (P_{jia}^p - P_{aij}^p) + \sum i, j \neq a (P_{aij}^{p-2} - P_{jia}^{p-2}) \right] \tag{18}$$

where $P_{ijk}^{\ p}$ is the probability that bonds p, p+1, p+2 lie along **i**, **j**, **k**, respectively. Using the relation

$$\sum_{i,j \neq a} P_{aij}^{\ p} = P_a^{\ p} - \sum_i P_{aia}^{\ p}$$

equation (18) becomes

$$\frac{\partial P_a^{\ p}}{\partial t} = w_3 (P_a^{\ p-2} - 2P_a^{\ p} + P_a^{\ p+2}) \qquad (19)$$

If $P_a^{\ p}$ is treated as a continuous function of p, equations (17) and (19) can be rearranged to give the diffusion equation

$$\frac{\partial G_{pq}(t)}{\partial t} = 4w_3 \frac{\partial^2 G_{pq}(t)}{\partial p^2} \qquad (20)$$

solution of which for infinite chains gives an autocorrelation function

$$G_1(t) = \exp(|t|/\rho)\, \mathrm{erfc}(|t|/\rho)^{\frac{1}{2}} \qquad (21)$$

where the correlation time ρ is related to w_3 by

$$\rho = (\lambda^2 w_3)^{-1}$$

λ is a constant which depends on the conformational probabilities. If *trans* and *gauche* conformations are equally likely, $\lambda = \ln 9$. This correlation function decays rapidly initially, but at long times decays as $t^{-\frac{1}{2}}$. The diffusion form appears because the three-bond motion does not create new orientations, only an interchange.

If four-bond motions are also active, with transition rate w_4, equation (20) becomes

$$\frac{\partial G_{pq}(t)}{\partial t} = (3.16w_3 - 9.61w_4) \frac{\partial^2 G_{pq}(t)}{\partial p^2} - 4.74w_4 G_{pq}(t) \qquad (22)$$

Note that this equation contains a diffusion term and a loss term, the latter arising because the four-bond motions create and destroy bond orientations. Jones and Stockmayer[71] have given the solution of an equation of the same form as equation (22) (see below). The solution for the autocorrelation function is

$$G_1(t) = \exp(-|t|/\theta) \exp(|t|/\rho)\, \mathrm{erfc}(|t|/\rho)^{\frac{1}{2}} \qquad (23)$$

with $\theta = (4.74w_4)^{-1}$ and $\rho = [\lambda^2(3.16w_3 - 9.61w_4)]^{-1}$. This function decays more rapidly than equation (21) at long times because of the θ term. The

spectral density corresponding to equation (23) has been evaluated:[72]

$$J(\omega) = \frac{2\theta\rho(\theta - \rho)}{(\theta - \rho)^2 + \omega^2\theta^2\rho^2}\left\{\left(\frac{\theta}{2\rho}\right)^{\frac{1}{2}}\left[\frac{(1+\omega^2\theta^2)^{\frac{1}{2}}+1}{1+\omega^2\theta^2}\right]^{\frac{1}{2}}\right.$$
$$\left. + \left(\frac{\theta}{2\rho}\right)^{\frac{1}{2}}\left(\frac{\omega\theta\rho}{\theta - \rho}\right)\left[\frac{(1+\omega^2\theta^2)^{\frac{1}{2}}-1}{1+\omega^2\theta^2}\right]^{\frac{1}{2}} - 1\right\} \qquad (24)$$

It has also been suggested[69] that the $\exp(-|t|/\theta)$ term in equation (23) can account for deviation from the strict conditions of a tetrahedral lattice and rigid tails.

Although equation (23) resulted from the specific model of three- and four-bond motions, it was later recognized[70] that this correlation function is not special to this particular description. In general terms, the factors containing ρ represent processes of a cooperative nature leading to a diffusion of orientation along the chain, e.g. crankshaft or three-bond motions. The term $\exp(-|t|/\theta)$ represents processes leading to loss of orientation not necessarily with transitions of neighbouring bonds.

Jones and Stockmayer[71] have suggested two modifications to the three-bond VJGM model with the object of producing a faster decay of the correlation function at long times than is given by equation (21). The first is to relax the coupling between neighbouring bond orientations so that a bond may rotate even though its neighbours are not in the correct orientations for type 1* processes. Equation (20) is modified to

$$\frac{\partial G_{pq}(t)}{\partial t} = 4fw_3\frac{\partial^2 G_{pq}(t)}{\partial p^2} - 2w_3(1-f)G_{pq}(t) \qquad (25)$$

where $f \leqslant 1$ expresses the deviation from strict lattice conditions. Its solution is identical to equation (23) with $\theta = [2(1-f)w_3]^{-1}$ and $\rho = (\lambda^2fw_3)^{-1}$.

The second modification is to limit the conformational coupling to a finite chain segment, by imposing a sharp cut-off on the effects of directional coupling. This formulation is the one used by Jones et al. to analyse experimental data, and is referred to as the JS model. For the segment of $2m - 1$ bonds embracing the three-bond kinetic unit, equation (19) can be written in matrix form

$$\frac{\partial \mathbf{P}}{\partial t} = -w_3\mathbf{kP} \qquad (26)$$

where $\mathbf{k}$ is an $m \times m$ matrix with elements

$$k_{ij} = 2\delta_{ij} - \delta_{i,j-2} - \delta_{i,j+2}$$

Solution of equation (26) gives

$$P_a{}^P(t) = A + B\sum_j C_{jn}\exp(-\lambda_j w_3|t|)$$

where

$$C_{jn} = \left(\frac{2}{m+1}\right)^{\frac{1}{2}} \sin\left(\frac{jn\pi}{m+1}\right)$$

$$\lambda_j = 4\sin^2[j\pi/2(m+1)]$$

A and B are determined by the initial and final conditions. The correlation function is expressed as a discrete distribution of correlation times

$$G_1(t) = \frac{1}{5}\sum_{k=1}^{s} B_k \exp(-|t|/\tau_k) \tag{27}$$

with $s = (m+1)/2$ and $\tau_k = (w_3\lambda_k)^{-1}$. The spectral density is

$$J(\omega) = \frac{2}{5}\sum_{k=1}^{s} \frac{B_k\tau_k}{1+\omega^2\tau_k^2} \tag{28}$$

As m increases, the long time behaviour of equation (27) approaches the $t^{-\frac{1}{2}}$ dependence of equation (21) for an infinite segment. The distribution of correlation times in equation (28) is conveniently characterized by the harmonic mean τ_h and arithmetic mean τ_a:

$$\tau_h = \langle\tau_k^{-1}\rangle^{-1}; \ \tau_a = \langle\tau_k\rangle$$

τ_h is equal to $(2w_3)^{-1}$ for all m. Jones and Stockmayer[71] have given λ_k and B_k for m values of 3, 5 and 7.

   Yaris and co-workers[73-76] have pointed out that the Jones–Stockmayer finite matrix solution becomes unwieldy if the number of cooperating units is large, and have presented solutions of the continuum VJGM model for degrees of motional correlation intermediate between the infinite chain model [equation (20)] and the short segment sharp cut-off model [equation (26)]. Furthermore, recognizing that the diffusive equation (20) is a consequence of Markovian character rather than a specific property of the three-bond VJGM model, the form of equation (20) is retained with the microscopic rate parameter $4w_3$ replaced by an empirical diffusion constant D. It is noted that the solution of the diffusion equation is an integral over the wave vector of a plane wave. However, on physical grounds not all wave vectors should be allowed. A lower wavelength limit is set by the size of the smallest displaceable segment and an upper wavelength limit is set by the finite chain length. In practice the upper limit may be shorter than the chain length because a conformational displacement diffusing along the chain will be damped out by various dissipative processes. In the first modification[73] (the BY model) the upper limit is represented by a sharp cut-off. If k_A and k_B are the wave vectors for the long and short wavelength cut-offs, the correlation function is

$$G_1(t) = \frac{1}{10}\left(\frac{\pi}{t}\right)^{\frac{1}{2}} (\omega_B^{\frac{1}{2}} - \omega_A^{\frac{1}{2}})^{-1}\{\mathrm{erfc}[(\omega_A|t|)^{\frac{1}{2}}] - \mathrm{erfc}[(\omega_B|t|)^{\frac{1}{2}}]\}$$

where $\omega_{A(B)} = 2k_{A(B)}{}^2 D/5$. The corresponding spectral density is

$$J(\omega) = 2(\omega_B{}^{\frac{1}{2}} - \omega_A{}^{\frac{1}{2}})^{-1}\left\{ [4(2\omega)^{\frac{1}{2}}]^{-1}\left[\ln\left(\frac{\omega_B - (2\omega\omega_B)^{\frac{1}{2}} + \omega}{\omega_B + (2\omega\omega_B)^{\frac{1}{2}} + \omega}\right)\right.\right.$$

$$\left.- \ln\left(\frac{\omega_A - (2\omega\omega_B)^{\frac{1}{2}} + \omega}{\omega_A + (2\omega\omega_A)^{\frac{1}{2}} + \omega}\right)\right] + [2(2\omega)^{\frac{1}{2}}]^{-1}$$

$$\left.\times\left[\tan^{-1}\left(\frac{(2\omega\omega_A)^{\frac{1}{2}}}{\omega - \omega_B}\right) - \tan^{-1}\left(\frac{(2\omega\omega_A)^{\frac{1}{2}}}{\omega - \omega_A}\right)\right]\right\} \tag{29}$$

In the later approach[74] (the SY model) the sharp long-wavelength cut-off was replaced by the more physically reasonable device of an explicit damping added to the diffusion equation. Thus the master equation for the bond orientation probability is written as

$$\frac{\partial P}{\partial t} = \frac{\partial^2 P}{\partial x^2} - \beta P \tag{30}$$

where β is the damping constant. This equation results in a damped diffusion correlation function

$$G_1{}^{DD}(t) = \frac{1}{10}\left(\frac{\pi}{\delta t}\right)^{\frac{1}{2}} \exp(-\beta|t|) \, \mathrm{erf}[(\delta|t|)^{\frac{1}{2}}]$$

where

$$\delta = D\omega_c{}^2, \qquad \omega_c = (k_B{}^2 - \beta/D)^{\frac{1}{2}}$$

k_B is the short wavelength cut-off as before. There are only two adjustable parameters. The corresponding damped diffusion spectral density is

$$J_{DD}(\omega) = \delta^{-1}\left\{\frac{c(\omega)}{4k(\omega)}\ln\left[\frac{A(\omega)}{B(\omega)}\right] + \frac{s(\omega)}{2k(\omega)}\tan^{-1}\left[\frac{2k(\omega)s(\omega)}{k^2(\omega) - 1}\right]\right\} \tag{31}$$

with

$$A(\omega) = 1 - 2k(\omega)c(\omega) + k^2(\omega)$$

$$B(\omega) = 1 + 2k(\omega)c(\omega) + k^2(\omega)$$

$$k(\omega) = \left(\frac{\omega^2 + \beta^2}{\delta^2}\right)^{1/4}$$

$$c(\omega) = \{\tfrac{1}{2}[1 - \beta/(\omega^2 + \beta^2)^{\frac{1}{2}}]\}^{\frac{1}{2}}$$

$$s(\omega) = \{\tfrac{1}{2}[1 + \beta/(\omega^2 + \beta^2)^{\frac{1}{2}}]\}^{\frac{1}{2}}$$

The theories outlined above apply strictly to isolated chains with a uniform interaction with the medium along the chain contour. This condition should apply reasonably well for dilute solutions of loose random coils (i.e. a good

solvent). For more concentrated solutions, or for compact coil conforma-
tions, the dynamics are affected by chain–chain interactions. Skolnick and
Yaris[76] have extended their theory to include this effect, stimulated par-
ticularly by certain peculiarities of the poly(vinyl acetate)/toluene system
described below. The chain–chain interaction is modelled rather generally
in terms of scattering of waves at the chain contact point, leading to a
complex damped diffusion equation:

$$\frac{\partial P}{\partial t} = D\frac{\partial^2 P}{\partial x^2} - (\beta + i\gamma)P$$

Solution of this equation leads to a complex diffusion spectral density
identical to the damped diffusion model equation (31), except the frequency
is shifted by γ:

$$J_{CD}(\omega) = J_{DD}(\omega - \gamma) \tag{32}$$

In addition to these analytical approaches, two groups[53-55,59-64,77] have
studied polymer dynamics relevant to NMR using numerical simulations.
Monnerie and co-workers[59-64] have simulated motions in polyethylene and
polyethers using chains randomly generated on a tetrahedral lattice taking
account of both excluded volume and the energy difference between *gauche*
and *trans* rotational isomers. Three-bond and four-bond motions shown in
Fig. 1 are allowed. Chain motions are simulated with a Monte Carlo
technique in which, on each cycle, bonds are selected at random and
examined to see if a motion is geometrically allowed. If so, the motion is
performed or not, depending on the conformational energy of that particular
sequence. Finally, correlation functions for bond orientations are evaluated
from the evolution of the chain conformation. For poly(1,3-dioxolan) [PDO,
$(-OCH_2CH_2OCH_2-)_n$], polyoxetan [POP, $(-OCH_2CH_2CH_2-)_n$], poly-
tetrahydrofuran [PTHF, $(-OCH_2CH_2CH_2CH_2-)_n$] and polyethylene (PE)
the correlation functions are fitted reasonably well (and especially at long
times) by the function in equation (21). For poly(oxyethylene) [POE,
$(-OCH_2CH_2-)_n$] it is necessary to use equation (23) with $\theta/\rho = 150$, while
poly(oxymethylene) [POM, $(-OCH_2-)_n$] cannot be fitted with either
equation satisfactorily. The order of mobility is found to be:

$$POM < PDO < (POP \approx PTHF \approx PE) < POE$$

in qualitative agreement with ^{13}C T_1 values.[1,78] This order is understandable
in terms of the ground-state conformations accessible to each polymer. Thus
POM possesses a single predominant conformation, which does permit
three-bond motions. However, following such a transition, the most likely
event is the reverse, leading to no disorientation. On the other hand, in
POE there are a number of significantly populated conformations inter-
changeable by both three- and four-bond motions thus giving greater flexibil-

ity. PDO, POP, PTHF and PE are intermediate cases, moving predominantly by three-bond motions.

Helfand and co-workers[53-55,77] have pursued a different approach to simulating polymer dynamics, making use of the vastly increased power of modern computers. Their method is to solve numerically the Langevin equation of motion of a chain of carbon atoms moving in a viscous medium subject to forces from bond rotations, bond stretching and bond angle bending, as well as a random Brownian force. As mentioned earlier, it is found that for polyethylene chains single bond rotations are quite feasible, though cooperative transitions may also occur. Any associated movement of the tails initially takes place by distortion of neighbouring bond rotation angles. Weber and Helfand[77] have evaluated vector correlation functions for unit vectors oriented at different angles relative to the backbone. Those considered are the bond vector along a bond, the chord vector joining the mid-points of adjacent bonds, the out-of-plane vector perpendicular to the plane of the fragment and the bisector vector bisecting the C–C–C bond. It is found that the functions decay at considerably different rates, the order being

$$\text{out-of-plane} \approx \text{bisector} > \text{bond} > \text{chord}$$

Although these results apply to vector functions and not to second-order spherical harmonic functions arising in NMR relaxation, it may reasonably be inferred that dipole–dipole interactions oriented at different angles relative to the backbone will perhaps have different correlation functions. Hitherto it has generally been assumed that all interactions are dynamically equivalent, though it must be said that a lack of experimental data has prevented any other approach. The correlation functions are well represented by a semi-empirical function of the form

$$G(t) = (1 - \alpha) \exp(-\kappa_0 |t|) \exp(-\kappa_1 |t|) I_0(\kappa_1 |t|) + \alpha \exp(-\mu |t|) \quad (33)$$

where I_0 is a modified Bessel function and α, μ, κ_0 and κ_1 are constants. For the bisector and out-of-plane vectors, α is very small.

The theories outlined here only consider segmental motions. If the polymer molecular weight is sufficiently small, overall tumbling becomes sufficiently rapid to make a significant contribution to the spectral density at nuclear resonance frequencies. Assuming that the overall tumbling is isotropic and independent of internal motions, this contribution can be accommodated[71] by multiplying the segmental correlation function by the term $\exp(-|t|/\tau_R)$, where τ_R is the overall correlation time which for dilute solutions is given by

$$\tau_R = 2M\eta_0[\eta]/3RT \quad (34)$$

where M is the molecular weight, η_0 the solvent viscosity and $[\eta]$ the intrinsic viscosity.

F. HEATLEY

B. Applications of models for flexible macromolecules

The correlation functions described above have been applied to numerous macromolecules, the most common being the VJGM and the JS models, equations (24) and (28). Details of polymers studied and methods employed are summarized in Tables 1 and 2 respectively. In most cases several independent items of experimental data at two or more resonance frequencies have been measured, thus giving a stringent test of the validity of the function. In general it is found that all data can be satisfactorily simulated within the limits imposed by experimental errors, approximations in relaxation theory and uncertainties in geometrical parameters. A good example of the use of a variety of techniques, and of the agreement achievable between theory and experiment, is provided by the data[8] for isotactic poly(methyl methacrylate) shown in Figs. 2–5. In this polymer the backbone methylene protons are not equivalent due to the chain stereochemistry. Ignoring the remote ester methyl signals, there are three peaks whose relaxation can be studied, the two methylene protons designated A (low

TABLE 1

Relaxation studies using the VJGM model, equations (23) and (24).

Polymer[a]	Nucleus	Freq. (MHz)	Technique	Reference
PMPO, PPPO	^{1}H	60, 100, 250	T_1	79
	^{13}C	15, 25.2, 62.8	T_1, NOE	79
PS	^{13}C	25.2	T_1, NOE	37b
	^{13}C	15, 25.2	T_1, NOE	80
	^{1}H	60, 100	T_1, T_2	80
	^{1}H	80, 300	T_1, cross-relaxation rate	7, 22
PVAc	^{1}H	100, 300	T_1, cross-relaxation rate	21
PB	^{13}C	22.6, 90.5	T_1, NOE	81
s-PMMA	^{13}C	25.2	T_1, NOE	37b
	^{1}H	80, 300	T_1, T_2	29
i-PMMA	^{1}H	80, 300	T_1, T_2 transient NOE	8
PMA	^{1}H	80, 300	T_1, T_2,	30
AAP	^{13}C	25.2, 62.9	T_1, NOE	70
	^{1}H	20, 80	T_1	70

[a] Abbreviations: PMPO, PPPO, poly(2,6-dimethyl- and -diphenyl-phenylene oxide); PS, polystyrene; PVAc, poly(vinyl acetate); PB, poly(but-1-ene); s-PMMA, syndiotactic poly(methyl methacrylate); i-PMMA, isotactic poly(methyl methacrylate); PMA, poly(methyl acrylate); AAP, aryl-aliphatic polyesters.

TABLE 2

Relaxation studies using the JS model, equations (27) and (28).

Polymer[a]	Nucleus	Freq. (MHz)	Technique	Reference
PMFS, PPFS	^{19}F	28.2, 56.5	T_1, NOE	16
PMPO	^1H	30	T_1	33, 45
	^1H	20, 40, 62, 90	T_1	84
	^1H	0.043, 30, 90	T_1, $T_{1\rho}$	9
	^{13}C	22.6	T_1	84
PIB	^1H	100	T_1, cross-relaxation	85
	^{13}C	25, 67	T_1	85
PC	^1H	20, 30, 90	T_1	86–88
	^{13}C	22.6, 69.2	T_1	84, 86–88
	^1H	20, 40, 62, 90	T_1	84
PE	^1H	20, 40, 62, 90	T_1	84
	^{13}C	22.6	T_1	84
PVDC	^1H	59.8	T_1	89
	^{13}C	15	T_1, NOE	89
PSO	^{13}C	15	T_1, NOE	90
PMVK	^{13}C	15	T_1, NOE	91

[a] Abbreviations: PMFS, PPFS, poly(*meta*- and *para*-fluorostyrene); PMPO, see Table 1; PIB, poly(isobutene); PC, poly(bis-(4-hydroxyphenyl)-2,2-propane carbonate); PE, polyethylene; PVDC, poly(vinylidene chloride); PSO, poly(styrene oxide); PMVK, poly(methyl vinyl ketone).

field) and M (high field) and the α-methyl protons designated X. T_1 and T_2 measurements were made for all peaks at 300 MHz and T_1 measurements at 80 MHz from −20 to +140 °C. Also, at selected temperatures, the transient NOE of peak A following selective inversion of peak M is monitored to probe the rate of A–M cross-relaxation. Figure 2 shows the experimental data for 300 MHz. The T_1 curves pass through minima at 40 °C (A, M) and 10 °C (X). The lower temperature for X is due to internal rotation of the methyl group. Although the major contribution to the A and M relaxation is their mutual dipolar interaction within a methylene group, their T_1 values are not identical because of slightly different interactions with the X protons. At lower temperatures, T_{1A} and T_{1M} approach one another in value because of averaging by rapid cross-relaxation. At all temperatures T_{2A} and T_{2M} are essentially identical because the rapid repetition rate of the Carr–Purcell spin–echo train renders them effectively equivalent. It is noteworthy that, as the temperature increases, the value of T_2 approaches that of T_1 but remains somewhat lower.

To obtain the correlation times, the experimental data are compared with relaxation times calculated for a range of values of the correlation time ρ
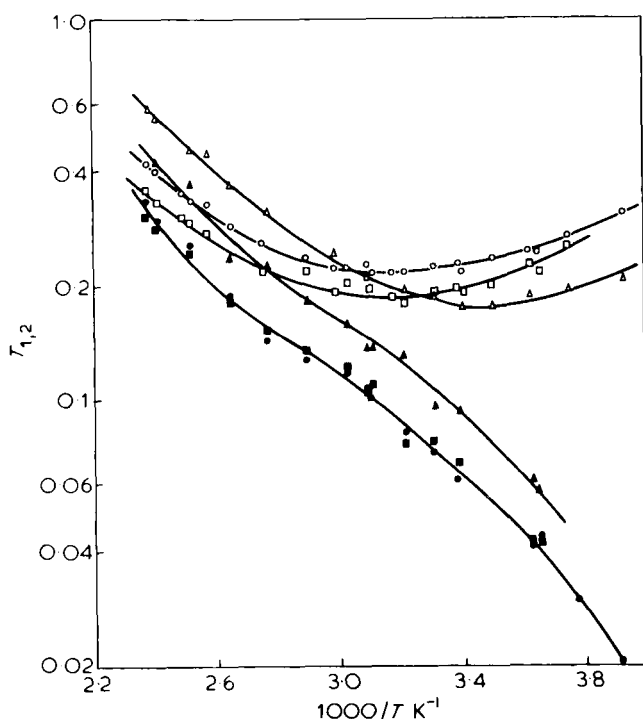
FIG. 2. ^{1}H relaxation times at 300 MHz for a 1% (w/w) solution of isotactic poly(methyl methacrylate), molecular weight 6.0×10^5, in toluene-d_8. $\bigcirc$ T_{1A}; $\square$ T_{1M}; $\triangle$ T_{1X}; $\bullet$ T_{2A}; $\blacksquare$ T_{2M}; $\blacktriangle$ T_{2X}. See text for designation of protons. From reference 8, with permission.

and the ratio ρ / θ. The calculations are performed using a set of coupled relaxation equations as in equation (10), assuming a purely intramolecular dipolar mechanism and including methyl internal rotation by jumps of 120°, with correlation time τ_G. The procedure is to select a value of ρ / θ, determine the value of ρ reproducing the observed T_{1A} at 300 MHz at each temperature, and then predict the remaining relaxation parameters expected for those values of ρ and ρ / θ. This is repeated for different ratios, and the predictions for each ratio are compared with experiment. The A and M relaxation times depend very little on τ_G, so the ratio τ_G / ρ is held fixed at unity while determining ρ and θ. Figures 3–5 show the resulting simulations of T_{2A} at 300 MHz, T_{1A} at 80 MHz and the transient NOE of A following selective inversion of M at two extreme temperatures. A comparison of experimental and predicted values permits a fairly precise determination of the best-fit ratio. Moreover, the three independent simulations, each of a very different
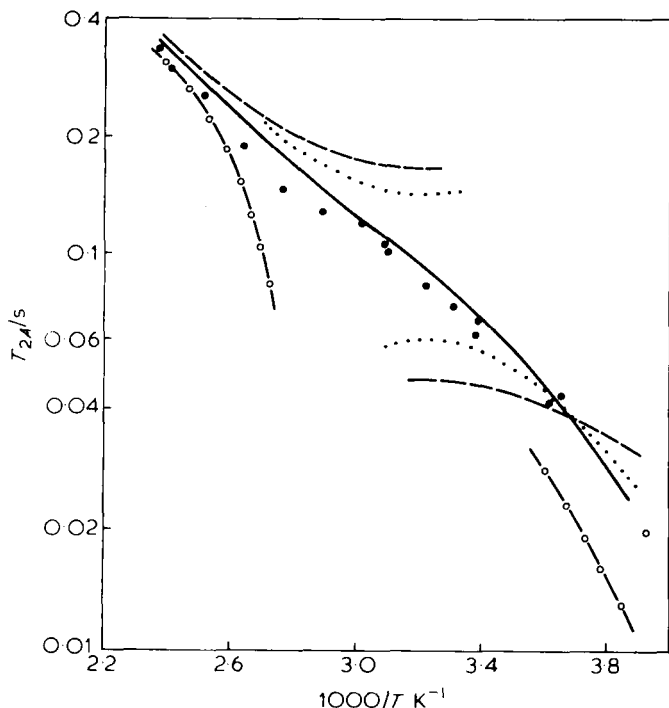
FIG. 3. Simulation of T_{2A} from Fig. 2 using the VJGM model as described in the text. The lines are predicted values for the following values of ρ/θ: 10 (dashed line); 1.0 (dotted line); 0.5 (continuous line); 0.1 (line with circles). τ_G/ρ is 1.0 for all curves except $\rho/\theta = 0.5$ for which $\tau_G/\rho = 0.6$. The symbols are experimental points. From reference 8, with permission.

nature, agree very well in giving a value of 0.5 for that ratio at all temperatures. The calculated relaxation times depend strongly on internuclear distances used, which are evaluated for the preferred chain conformations using standard bond lengths and angles. Although questionable perhaps, this method does appear to give reasonable relative distances since the calculated proportional relaxation contributions agree well with those measured by Hatada *et al.*[82] using selectively deuteriated polymers. Thus the proportions of methylene relaxation arising from methylene, methylene-methyl, methylene-methoxyl and intermethylene interactions are 58, 20, 0 and 22% respectively using the distances in reference 8, compared with experimental values[82] of 53, 17, 1 and 29%. Allowing reasonable uncertainties in the magnitudes of the distances produced an acceptable range for ρ/θ of 0.25–1.0.
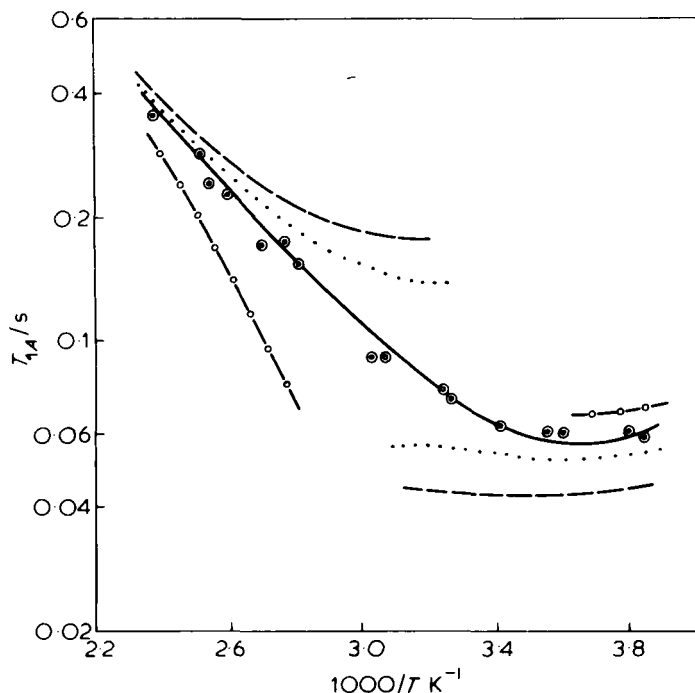
FIG. 4. Simulation of T_{1A} at 80 MHz for the sample in Fig. 2 using the VJGM model as described in the text. See Fig. 3 for designation of curves. From reference 8, with permission.

TABLE 3

[13]C relaxation parameters (times in ms) for polystyrene in hexachlorobutadiene (10% w/w) at 60 °C.

	T_{1C} (alpha) 15 MHz	T_{1C} (alpha) 25 MHz	T_{1C} (para) 15 MHz	T_{1C} (para) 25 MHz	NOE (para) 25 MHz	T_{2C} (para) 25 MHz
Experimental	79	42	82	50	2.0	26–41
Calculated[a]	76	49	82	53	1.9	33

[a] Obtained using the VJGM model with $\rho = 0.9$ ns and $\theta = 26$ ns.
From reference 80, with permission.

A further example of the use of the VJGM model is given in Table 3 which shows ^{13}C relaxation data at two resonance frequencies for a solution of polystyrene.[80] The agreement of the six experimental quantities with the predicted values is good.
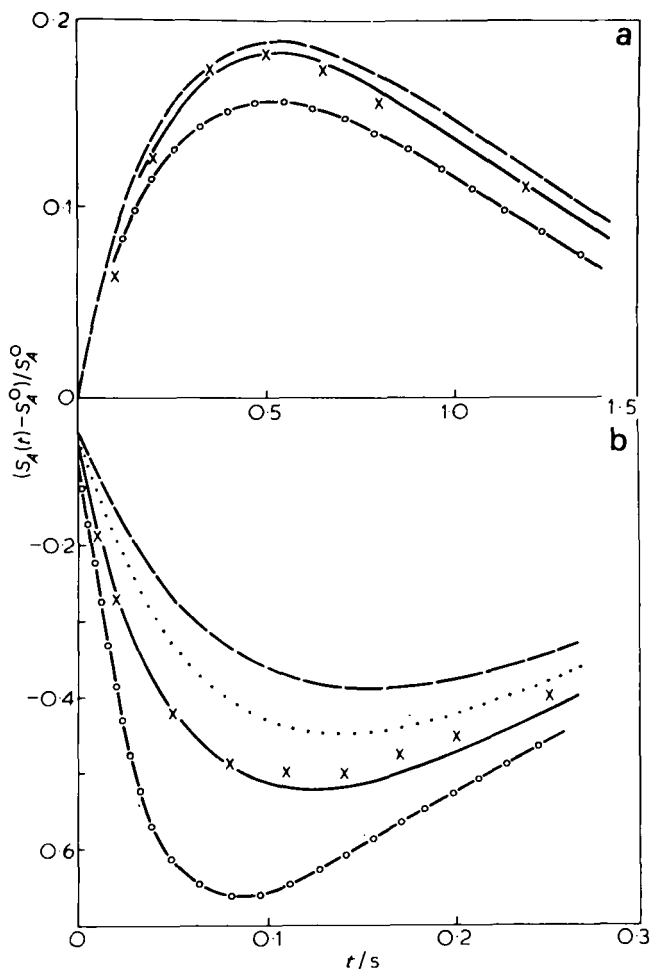
FIG. 5. Simulation of transient NOE's of the A resonance following selective inversion of the M resonance for the sample in Fig. 2 using the VJGM model as described in the text. (a) 140 °C; (b) −19 °C. See Fig. 3 for designation of curves. From reference 8, with permission.

Correlation times and activation energies for these two examples, and the other vinyl polymers in Table 1, are summarized in Table 4. It must be borne in mind that these results are those obtained for a particular set of internuclear distances considered appropriate by the authors. Allowing a reasonable uncertainty in the distances, the results quoted should be considered reliable only to a factor of 2 or so, either way. In spite of this qualification, some interesting features are evident which shed light on the physical properties of polymers in solution. In general it is found that ρ/θ

F. HEATLEY

TABLE 4

Correction times and activation energies for the VJGM models.

Polymer[a]	Ref.	Nucleus	Solvent[b]	Temp. (K)	ρ (ns)	ρ/θ	E_a (kJ mol^{-1})[c]
PMPO	79	^{1}H, ^{13}C	CDCl$_3$	323	0.55	0.05	
PVAc	21	^{1}H	toluene-d_8	228	400	100	
				298	1.5	0.2	11(θ)
				383	0.03	0.07	
PS	37b	^{13}C	PCE	303	4.0	0.4	21
	80	^{13}C	HCB	317	2.0	0.07	32
	80	^{1}H	HCB	317	2	1	
	22	^{1}H	CDCl$_3$	303	0.6	0.08	19
	22	^{1}H	CCl$_4$	303	1.6	0.08	25
	22	^{1}H	HCB	303	4.7	0.08	29
	22	^{1}H	CH/T	303	2.6	0.08	32
PB	81	^{13}C	PCE	258	4.7	0.9	
				313	0.54	0.33	22(ρ) 12(θ)
				403	0.056	0.1	
s-PMMA	37	^{13}C	ODCB	303	0.9	0.04	
	29	^{1}H	acetone-d_6	303	1.5	1.0	22
	29	^{1}H	toluene-d_8	313	1.5	0.7	24
	29	^{1}H	PhNO$_2$-d_5	303	5.3	0.8	25
	29	^{1}H	CD$_3$CN	313	1.9	0.9	29
i-PMMA	8	^{1}H	toluene-d_8	313	0.42	0.5	20
PMA	30	^{1}H	toluene-d_8	298	0.63	0.4	23

[a] For abbreviations see Table 1.

[b] PCE, pentachloroethane; HCB, hexachlorobutadiene; CH/T, 90% cyclohexane-d_{12}/10% toluene-d_8; ODCB, *ortho*-dichlorobenzene.

[c] Activation energy for correlation time in parentheses. If no correlation time specified, ρ/θ is essentially constant. Uncertainty 10–20%.

is less than unity, indicating the dominance of the diffusional characteristics of the motions. For PS there is a fairly wide variation in the best-fit parameters from different studies. To some extent this may arise from differences in geometry or experimental technique. For example, in the ^{13}C studies, Heatley and Begum[37b] use $r_{CH} = 110$ pm whereas Lauprêtre *et al.*[80] use 107 pm. The experimental data of the former authors with the latter bond length reduce ρ/θ from 0.4 to c. 0.2. The discrepancy between the best-fit ρ/θ values, from the two ^{1}H studies in hexachlorobutadiene, possibly lies in the fact that in reference 80 the lower frequency spectrometer is a non-Fourier transform pulse machine so that accurate measurements of individual proton T_1 values cannot be made. For s-PMMA there appears to be a significant difference between the ^{1}H and ^{13}C results, presumably due to different reorientation processes of the H–H and C–H vectors.

Two polymers, PS and s-PMMA, have each been studied in three good solvents and one poor one (CH/T and CD_3CN respectively). In each case ρ/θ depends very little on solvent, though the correlation times themselves vary systematically with viscosity for the good solvents. In the poor solvent the correlation times are longer than expected on the basis of solvent viscosity, due possibly to a less expanded conformation. The temperature dependence of ρ/θ for PVAc is exceptionally large, showing a sharp rise below $-10\,°C$. This is attributed to a phase transition also observed in dielectric relaxation.[83] Above the transition PVAc is a loose random coil, but below the transition it exists in a very compact conformation.

The aryl-aliphatic polyesters studied by Tekely et al.[70] are of the general structure [3]. The carbons labelled 4, 5 and 6 are individually resolved,

$$\left[-CO-\bigodot-\bigodot-\bigodot-\underset{4}{COO}CH_2\underset{5}{CH_2}\underset{6}{(\underbrace{OCH_2CH_2})_m}OCH_2CH_2O-\right]$$

[3]
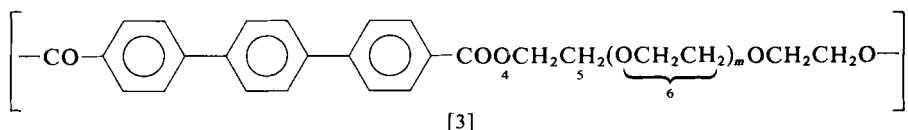
each giving slightly different ρ and θ values as summarized in Table 5. The longer the alkyl chain, the shorter the correlation times and the larger the θ/ρ ratio. The ρ processes are identified with fast type 1* or 2* motions and the θ processes with slower type 3* long-range motions.

TABLE 5

VJGM model parameters for aryl-aliphatic polyesters (deuteriochloroform solution at 300 K).

Line	$m = 2$		$m = 8$	
	ρ (ps)	θ (ns)	ρ (ps)	θ (ns)
4	24	1.3	17	1.3
5	20	1.2	15	1.2
6	28	1.1	21	0.9

From reference 70, with permission.

Turning to the JS model, the most thoroughly investigated system is poly(2,6-dimethyl-1,4-phenylene oxide) (PMPO), for which ^1H and ^{13}C T_1 values have been measured for a wide range of frequencies and molecular weights (Table 2). Backbone segmental motions can reasonably be represented by a diamond lattice model regarding the vertices as the oxygen atoms and the links as the $-C_6H_2(CH_3)_2-O-$ repeat unit. In addition, it is necessary

to include internal rotation of the aromatic ring about the *para* C–O bonds and of the methyl group about its C_3 axis. The latter is much faster than any other process. Assuming aromatic rotation by jumps of 180°, independently of backbone motions, equation (28) becomes

$$J(\omega) = \frac{2f}{5} \sum_{k=1} B_k \left\{ \frac{A'\tau_k}{1+\omega^2\tau_k^2} + \frac{B'\tau_{kr}}{1+\omega^2\tau_{kr}^2} \right\} \tag{35}$$

where

$$A' = (3\cos^2\Delta - 1)^2/4 + (3\sin^4\Delta)/4$$

$$B' = (3\sin^2 2\Delta)/4$$

$$\tau_{kr}^{-1} = \tau_k^{-1} + \tau_{i\rho}^{-1}$$

$\tau_{i\rho}$ is the correlation time for ring rotation. For interactions within the aromatic ring, Δ is the angle between the internuclear vector and the ring rotation axis and f is equal to 1. For interactions within the methyl group, Δ is the angle between the C_3 axis and the ring axis and $f = 3(\cos^2\alpha - 1)^2/4$ where α is the angle between the C_3 axis and the internuclear vector. Figures 6–8 compare experimental and simulated relaxation times. Figure 6 shows the methyl T_1 at 30 MHz as a function of molecular weight with the best-fit
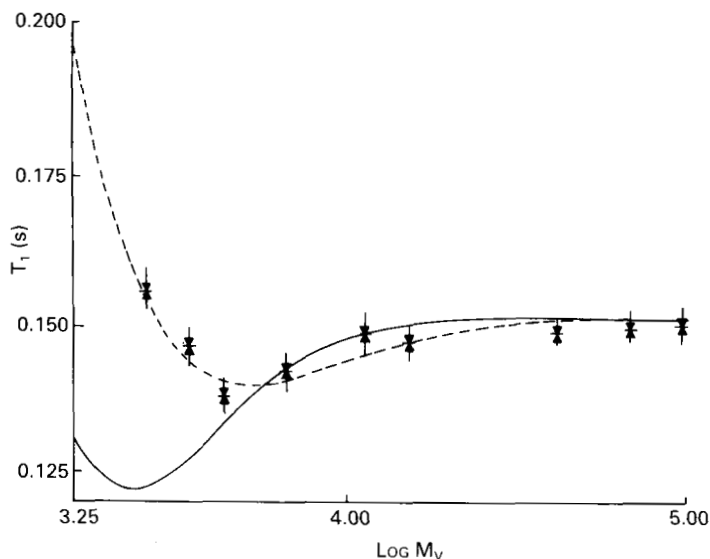
FIG. 6. Methyl proton T_1 *vs.* molecular weight for 10% (w/w) poly(2,6-dimethyl-1,4-phenylene oxide) in $CDCl_3$ at 20 °C and 30 MHz. The symbols are experimental values. The dashed line is a simulation using the JS model with $\tau_h = 5.3$ ns and $2m - 1 = 5$, assuming a polydispersity $M_w/M_n = 1.5$. The solid line is a prediction for monodisperse fractions. From reference 45, with permission.
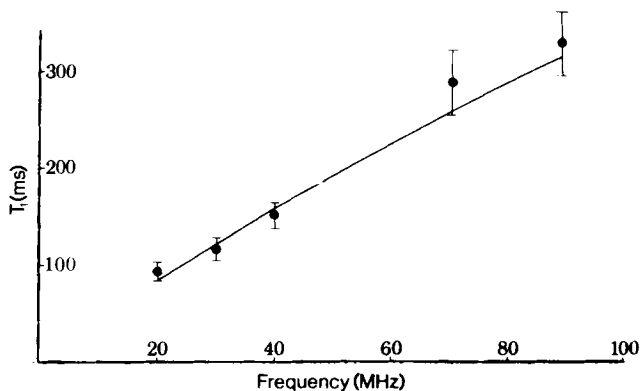
FIG. 7. Methyl proton T_1 vs. resonance frequency for 10% (w/w) poly(2,6-dimethyl-1,4-phenylene oxide) in $CDCl_3$ at 40 °C. The line is a prediction using the JS model with parameters from reference 45. From reference 84, with permission.
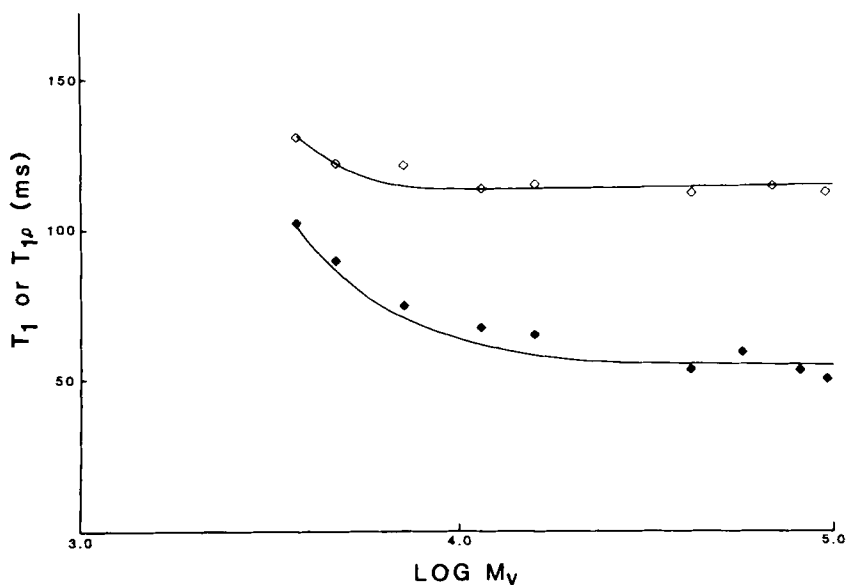
FIG. 8. Methyl proton T_1 and $T_{1\rho}$ vs. molecular weight for 10% (w/w) poly(2,6-dimethyl-1,4-phenylene oxide) in $CDCl_3$ at 40 °C. ◇ T_1 at 30 MHz; ◆ $T_{1\rho}$ at 42.6 KHz. The solid lines are predictions using the JS model with parameters from reference 45. From reference 9, with permission.

simulation for $\tau_h = 5.3$ ns and $2m - 1 = 5$. Below a molecular weight of ca. 10^4, overall molecular rotation contributes to relaxation. This is taken into account using equation (34) and a Schulz–Zimm molecular weight distribution function with $M_w/M_n = 1.5$. An unusual feature of the molecular weight

dependence is the minimum in T_1. This is a consequence of the predominance of the aromatic ring internal rotation which is approximately an order of magnitude faster than backbone rearrangements. Subsequent studies[9,84] at different frequencies have compared experimental data with those predicted using the correlation times derived from the earlier study.[45] As shown in Figs 7 and 8, the agreement is excellent, confirming the validity of the dynamic model.

TABLE 6

Correlation times, segment lengths and activation energies for the JS model.

Polymer[a]	Solvent[b]	Temp. (K)	τ_h (ns)	$2m-1$	E_a (kJ mol^{-1})[c]
PMFS	CDCl$_3$	298	0.24	9–13	
	C$_6$D$_6$	298	0.30	9–13	
PPFS	CDCl$_3$	298	0.33	9–13	
	CCl$_4$	298	0.10	9–13	
	C$_6$D$_6$	298	0.34	9–13	
PMPO	CDCl$_3$	293	3.0	5	$25(\tau_h)$
PIB	CCl$_4$	318	0.058	5	
PC	CDCl$_3$	263	0.37	5 ⎫	$11(\tau_a)$
	CDCl$_3$	333	0.059	13 ⎭	$19(\tau_h)$
	C$_2$D$_2$Cl$_4$	253	1.17	5 ⎫	
	C$_2$D$_2$Cl$_4$	313	0.20	9 ⎬	$21(\tau_h)$
	C$_2$D$_2$Cl$_4$	393	0.034	17 ⎭	
PE	decalin-d_{18}	363	0.0077	5	
PVDC	HMPA-d_{18}	313	0.22	5	$24(\tau_h)$
PMVK	dioxan-d_8	299	0.54	5	$20(\tau_h)$

[a] For abbreviations see Table 2.
[b] HMPA, hexamethylphosphoramide.
[c] Uncertainty 10–20%.

Table 6 summarizes the dynamic parameters obtained from applications of the JS model. Among the vinyl polymers, the fluorinated polystyrenes appear to have significantly greater dynamic correlation as judged by the $2m-1$ values. This is in agreement with the VJGM data in Table 4, where polystyrene has on the whole the lowest ρ/θ ratio. PMPO appears in both tables, but the motional parameters are not strictly comparable since, unlike the JS analysis,[9,45,84] the VJGM analysis[79] does not include aromatic ring rotation. O'Gara et al.[87] have compared the dynamics of four polycarbonates based on the PC structure, with a view to correlating solution motions and bulk properties. The diamond lattice motions are comparable in the polymers, but the aromatic ring rotations are strongly affected by the structural

variations. The freedom of the ring rotation correlates with impact resistance in the bulk polymer, indicating the important role of this process in energy dissipation.

The BY and SY models have been used by the authors to analyse experimental data obtained by other workers, principally the ^{1}H relaxation data[21] for poly(vinyl acetate) at 300 MHz. In this study three types of measurement are made on the backbone methine and methylene protons (labelled A and X respectively): (i) the T_1 value using the standard inversion recovery sequence; (ii) spin–lattice relaxation of A (or X) when the other group is saturated by a second frequency; (iii) the NOE of A (or X) due to saturation of the other. The time constants for relaxation with saturation of the other peaks are denoted by T_{AA} and T_{XX}. The Overhauser enhancements are expressed by the parameter η_A or η_X, defined by

$$\eta = (S_d - S_o)/S_o$$

where S_d and S_o are the intensities, in the presence and absence respectively, of the saturating field. T_{AA}, T_{XX}, η_A and η_X are related to cross-relaxation time constants T_{AX} and T_{XA} by the equations

$$\eta_A = 2T_{AA}/T_{AX}$$

$$\eta_X = 2T_{XX}/T_{XA}$$

$$T_{AX} = 2T_{XA}$$

These parameters involve spectral densities at the resonance frequency (300 MHz) and at the difference frequency $\omega_A - \omega_X$ (930 Hz), so the spectral density is probed over a wide range.

In the attempts to fit the data using the BY and SY models, equations (29) and (31), the motional parameters are first obtained from simulating T_{AA} and T_{XX} and then used to predict η_A and η_X. The results obtained are reported in Table 7. Both models fit the data equally well. The motional parameters are physically reasonable except at $-45\,°C$. For example, in the SY model at that temperature the fitting apparently gives $\beta > \delta$ which is equivalent to the damping length being less than the length of the smallest motional unit. Originally Heatley and Cox[21] analysed the data using the VJGM model, and they also found a large change in properties near $-10\,°C$ (Table 4 and earlier discussion). The various models thus agree in diagnosing gross qualitative changes in dynamic characteristics. It is this transition which prompted the modification[76] of the SY theory to incorporate chain-chain interactions leading to equation (32), and a renewed attempt to fit the low temperature NMR data. This time the best-fit motional parameters are obtained from simulating T_{AA}, T_{XX} and T_{AX} together. Multiple best-fit solutions for β and δ are obtained, one being non-physical with $\beta > \delta$, but the other being more reasonable in the sense that $\beta < \delta$. At low temperatures

TABLE 7

Analysis of ^{1}H relaxation data for poly(vinyl acetate) in toluene-d_8 at 300 MHz using the BY and SY models.

Experimental

T (°C)	T_{AA} (ms)	T_{XX} (ms)	η_A	η_X
−45	180	330	−0.9	−0.6
10	470	270	0.25	0.08
30	550	250	0	0
110	970	400	0.23	0.07

BY model, equation (29)

T (°C)	T_{AA} (ms)	T_{XX} (ms)	η_A	η_X	ω_A (10^8 s^{-1})	ω_B (10^8 s^{-1})
−45	202	279	−0.88	−0.61	2.6	2.6
10	470	270	−0.315	−0.091	0.213	518
30	550	250	−0.062	−0.014	0.101	356
110	970	400	0.063	0.013	1.77	1130

SY model, equation (31)

T (°C)	T_{AA} (ms)	T_{XX} (ms)	η_A	η_X	β (10^8 s^{-1})	δ (10^8 s^{-1})
−45	202	279	−0.88	−0.61	2.6	0.24
10	470	270	−0.315	−0.091	0.519	505
30	550	250	−0.062	−0.014	2.31	353
110	970	400	0.063	0.013	3.88	1210

From reference 75, with permission.

δ is substantially higher than at high temperatures and has a negative activation energy. It is pointed out[76] that δ is a product of a diffusion constant and a short wavelength cut-off, and that the negative activation energy could arise from normal temperature dependence of the diffusion constant (i.e. positive E_a) together with an increase in size of the smallest motional unit with temperature.

C. Comparison of models

The model correlation functions described above take an apparently wide variety of functional forms. However, when applied to the same set of experimental data, several groups have found little or nothing to choose between them. The case of the analysis of ^{1}H relaxation in poly(vinyl acetate)

using the VJGM, BY and SY models has been discussed above. Further examples are provided by the various models used to analyse [92] ^{13}C relaxation in polystyrene and ^{1}H and ^{13}C relaxation in polycarbonates.[88] For the polystyrene system the VJGM, JS and BY functions are used. From the comparison of experimental and simulated data in Table 8, all three models

TABLE 8

Comparison of experimental and calculated relaxation data for the methine carbon of isotactic polystyrene in *o*-dichlorobenzene at 35 °C and 22.6 MHz.

	T_1 (ms)	T_2 (ms)	NOE	Model parameters
Experiment[38]	65	26	1.8	
VJGM [equation (24)]	66	25	1.8	$\rho = 1.9$ ns $\theta = 35$ ns
JS [equation (28)]	65	28	2.07	$\tau_h = 1.0$ ns $2m - 1 = 17$
BY [equation (29)]	65	26	2.1	$\omega_A = 6.3 \times 10^6$ Hz $\omega_B = 4 \times 10^9$ Hz

From reference 92, with permission.

are acceptable within experimental error. As expected from this result, the spectral density functions shown in Fig. 9 are broadly similar in shape, and can be made to correspond very closely if measurements are confined to one or two decades of frequency. For the polycarbonate,[88] the JS model is compared with the correlation function of equation (33) with $\alpha = 0$. In spite of the differences in origin, the two models give satisfactory interpretations of the experimental data. For equation (33) the most important parameter is τ_1, the correlation time for cooperative transitions, which is comparable in size to the JS three-bond parameter τ_h. Thus it appears that the two models agree in characterizing the cooperativity of the chain motions. In the polyethylene simulations,[77] cooperative transitions are in the minority, the most important process being one-bond rotations. The concurrence with the JS model for polycarbonates perhaps reflects the more complicated repeat unit. Alternatively, the cooperative transitions may be composed of two close sequential single transitions. It is significant that both models of the segmental motion give similar values for the correlation times for internal rotation of the backbone aromatic rings.

Weber and Helfand[77] have compared their semi-empirical function equation (33) and the VJGM model equation (21), using the latter to replace the terms $\exp(-\kappa_1|t|)\, I_0(\kappa_1|t|)$ in equation (33). There is a general resemblance, with very good agreement at long times but not at short times.
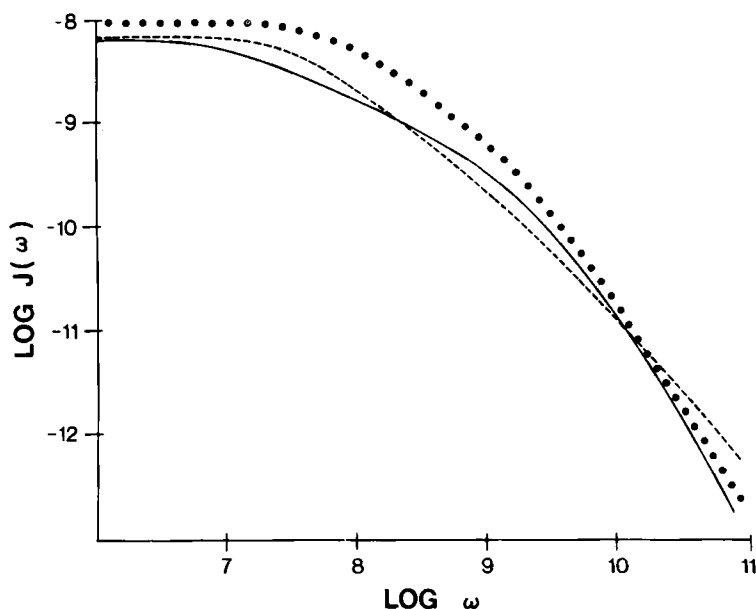
FIG. 9. Spectral density *vs.* frequency for models fitted to experimental data for a solution of isotactic polystyrene (Table 8). —— BY model; - - - VJGM model; ..... JS model. From reference 92, with permission.

It is clear that available experimental data can be fitted acceptably by several functions. Those described have been based to varying extents on a physically realistic model of conformational transitions, so their agreement is perhaps not surprising. Their physical significance has however been questioned,[93] and it has been shown that a highly idealized model of anisotropic rotations of a series of coaxial cylinders can generate a correlation function practically identical to the JS model. It is not sensible therefore to attach much physical significance to the derived motional parameters, though variations with temperature or polymer structure may suggest qualitative changes in motion. At present the limitations in accuracy and frequency range of NMR data appear to preclude a differentiation of the models described. The Weber–Helfand approach[77] appears to have a sounder basis, and it seems that it would be worthwhile to carry out a detailed study of both ^{1}H and ^{13}C relaxation in a suitable system to see if the correlation functions for internuclear vectors at different angles to the backbone do indeed differ in the way suggested by the dynamics simulations.

D. Models for stiff macromolecules

Most of the molecules falling under this heading are of biological origin, though synthetic polypeptides may also be members under suitable condi-

tions. An extensively studied example of the latter class is poly(γ-benzyl-L-glutamate) (PBLG) which forms a molecular solution of regular α-helices in dimethylformamide.[94] Table 9 gives experimental data[95] for the α-carbon relaxation in this system as a function of molecular weight, concentration,

TABLE 9

[13]C relaxation data for the α-carbon of PBLG in dimethylformamide-d_7 at 60 °C.

Mol. wt.[a]	Concn. (mg cm^{-3})	Temp. (°C)	Freq. (MHz)	T_1 (ms)	T_2 (ms)	NOE
35 000	50	60	75.5	320	11.0	1.2
81 000	50	60	75.5	489	6.1	1.5
35 000	50	60	25.1	75	10.3	—
81 000	50	60	25.1	147	6.0	1.1
35 000	50	30	25.1	90	9.1	—
81 000	50	30	25.1	160	2.9	—
81 000	100	60	75.5	532	3.8	—
81 000	50	60	75.5	489	6.1	—
81 000	25	60	75.5	500	7.2	—
81 000	12.5	60	75.5	—	7.6	—

[a] Fractions with $M_w/M_n = 1.08$.
From reference 95, with permission.

temperature and resonance frequency. In contrast to the class of flexible macromolecules, T_1 and T_2 are strongly dependent on molecular weight up to the highest value studied of 81 000, corresponding to a degree of polymerization of 500 or so. This value is much higher than the usual critical value at which the relaxation times reach a plateau in flexible polymers, and suggests a substantial, if not dominant, contribution to relaxation from overall molecular tumbling. In support of this conclusion we note that T_1 decreases with increasing temperature, that T_1 depends strongly on the resonance frequency and that T_2 is very much less than T_1. All these observations are consistent with relaxation via a slow process meeting the condition $\omega_0^2 \tau_c^2 \gg 1$.

However, there is abundant evidence that overall tumbling, although it may be the major process, is not the only contributor. For example, the NOE for molecular weight 81 000 increases from 1.1 at 25.1 MHz to 1.5 at 75.5 MHz, whereas for a single slow process the NOE should remain at its minimal value. Also, although T_1 increases with increasing resonance frequency, it does not do so in proportion to the square of the frequency. Similar anomalies in ^{13}C relaxation in haemoglobin, serum albumin and alumichrome have been summarized.[96] Furthermore, rotational correlation

times calculated from T_1 values assuming a rigid molecule differ significantly by up to a factor of 2 from correlation times obtained from light scattering.[96] Initial attempts to resolve these discrepancies in terms of rotational anisotropy[97,98] and free internal bond rotation[99] have been unsuccessful. For ^{13}C relaxation the possibility was also raised[98,100] that the mean C–H bond length could be rather greater than the commonly accepted value of 109 pm. However, the last explanation cannot explain the anomalous frequency dependence of the NOE, since the NOE is independent of the C–H distance for purely dipole–dipole relaxation.

A more satisfactory explanation of the observed relaxation behaviour can be found in terms of slow overall motion combined with limited amplitude rapid internal motions. The computer simulations of protein dynamics reviewed recently[4] show that the basic framework undergoes a wide spread of oscillatory motions (librations) such as vibrational bending modes and torsional oscillations, collectively resulting in excursions of the order of 10° of bonds from their average orientation. These motions have the effect of partially averaging dipole–dipole interactions, thus reducing the extent of correlation to be lost by the overall motion. The distinction between internal and overall motions has formed the basis for several practical approaches to relaxation in stiff chains, using various models for the internal motions.

Lipari and Szabo[34] have discussed in detail the general theory of relaxation by internal and overall motions, and they have evaluated correlation functions for various specific models for both processes. The overall motions may be represented in general by a rotational diffusion process with a degree of anisotropy depending on the molecule. For proteins and other molecules with an irregular folded backbone conformation approximating a spherical segment distribution, the assumption of isotropic rotation is appropriate. For molecules such as synthetic polypeptides and DNA fragments, which have extended helical conformations, overall rotation will be highly anisotropic, resembling that of a prolate ellipsoid. For isotropic rotation $G_0(t)$ is $\exp(-|t|/\tau_M)$ with $\tau_M = (6D)^{-1}$ where D is the rotational diffusion coefficient. For anisotropic rotation of a prolate ellipsoid, $G_0(t)$ is[101]

$$G_0(t) = \tfrac{1}{5}[\tfrac{1}{4}(3\cos^2\beta - 1)^2 \exp(-t/\tau_A) + \tfrac{3}{4}\sin^2 2\beta \exp(-t/\tau_B)$$
$$+ \tfrac{3}{4}\sin^4\beta \exp(-t/\tau_C)] \tag{36}$$

where

$$\tau_A^{-1} = 6D_\perp; \qquad \tau_B^{-1} = 5D_\perp + D_\parallel; \qquad \tau_C^{-1} = 2D_\perp + 4D_\parallel$$

$D_\parallel$ and $D_\perp$ are the rotational diffusion constants about the long and short axes respectively, and β is the angle between the interaction vector and the long axis.

The correlation function for internal motions can be written generally as

$$G_I(t) = \langle P_2(\boldsymbol{\mu}(0) \cdot \boldsymbol{\mu}(t)) \rangle$$

where $\boldsymbol{\mu}$ is a unit vector describing the orientation of the interaction vector in a reference frame rigidly attached to the macromolecule, and $P_2(x)$ is the second Legendre polynomial

$$P_2(x) = \tfrac{1}{2}(3x^2 - 1)$$

From the definition, $G_I(0) = 1$. Lipari and Szabo[34] also show that the limiting value of $G_I(t)$ as $t \to \infty$ can be written

$$G_I(\infty) = \int\!\!\int d\Omega_1 \, d\Omega_2 \, P(\Omega_1) P_2(\cos\theta_{12}) P(\Omega_2)$$

where Ω_1 and Ω_2 are the polar coordinates describing two states of $\boldsymbol{\mu}$, $P(\Omega)$ is the normalized orientational probability distribution of $\boldsymbol{\mu}$, and θ_{12} is the angle between $\boldsymbol{\mu}_1$ and $\boldsymbol{\mu}_2$. In general, for motions limited in amplitude, $G_I(\infty)$ is less than unity but not zero. Thus $G_I(t)$ decays from unity at $t = 0$ to an asymptotic value $G_I(\infty)$ as t increases. The value of $G_I(\infty)$ depends on the spatial restriction of the orientations of the interaction, while the form of the decay depends on the rate and mechanism of the motions. Lipari and Szabo have expressed $G_I(\infty)$ in terms of a generalized order parameter S by the relation

$$G_I(\infty) = S^2$$

The term "generalized order parameter" arises by analogy with the more familiar order parameter used in the analysis of NMR data in membranes[102] and liquid crystals.[103] $G_I(t)$ then becomes, in general,

$$G_I(t) = S^2 + (1 - S^2)f(t)$$

where $f(t)$ describes the time dependent part of $G_I(t)$ with the properties $f(0) = 1$ and $f(\infty) = 0$. In the general case, $G_I(t)$ has the form

$$G_I(t) = S^2 + \sum_{i=1} a_i \exp(-t/\tau_i) \tag{37}$$

where the length of the sum, the amplitudes a_i and the correlation times τ_i depend on the mechanism of the motion. The total correlation function (for isotropic overall tumbling) is then

$$G(t) = \frac{1}{5}\left[S^2 \exp(-t/\tau_M) + \sum_{i=1} a_i \exp(-t/\tau_i{}^*) \right]$$

where

$$(\tau_i{}^*)^{-1} = \tau_M{}^{-1} + \tau_i{}^{-1}$$

The spectral density is

$$J(\omega) = \frac{2}{5}\left[\frac{S^2\tau_M}{1+\omega^2\tau_M{}^2} + \sum_{i=1}\frac{a_i\tau_i{}^*}{1+(\omega\tau_i{}^*)^2}\right] \tag{38}$$

If all the internal motions are much faster than overall tumbling ($\tau_i \ll \tau_M$), and sufficiently rapid to meet the extreme narrowing condition for the largest frequency involved in a particular measurement, $J(\omega)$ becomes

$$J(\omega) = \frac{2}{5}\left[\frac{S^2\tau_M}{1+\omega^2\tau_M{}^2} + \sum_{i=1} a_i\tau_i\right] \tag{39}$$

which is equivalent to

$$J(\omega) = \frac{2}{5}\left[\frac{S^2\tau_M}{1+\omega^2\tau_M{}^2} + (1-S^2)\tau_e\right] \tag{40}$$

where τ_e is an effective correlation time defined by

$$(1-S^2)\tau_e = \sum_{i=1} a_i\tau_i$$

An identical alternative definition of τ_e which may be useful in some circumstances is

$$\tau_e = (1-S^2)^{-1}\int_0^\infty [G_I(t) - G_I(\infty)]\,dt \tag{41}$$

If any of the τ_i's are much slower than overall tumbling ($\tau_i \gg \tau_M$), the simple form of equation (40) is retained. For example, if $\tau_1 \gg \tau_M$ but $\tau_i \ll \tau_M$ for $i \geq 2$, one finds

$$J(\omega) = \frac{2}{5}\left[\frac{S'^2\tau_M}{1+\omega^2\tau_M} + (1-S'^2)\tau_e\right] \tag{42}$$

with $S'^2 = S^2 + a_1$ and $(1-S'^2)\tau_e = \sum_{i=2} a_i\tau_i$. If any of the τ_i's are comparable to τ_M, the more complex expression equation (38) applies.

When the overall motion is anisotropic rotational diffusion with axial symmetry, the total correlation function can be obtained by combining equations (36) and (37). With the same assumptions concerning relative rates of motion, as used to derive equation (40), the spectral density is given by

$$J(\omega) = \frac{2}{5}\{S^2[\tfrac{1}{4}(3\cos^2\beta - 1)^2\tau_A/(1+\omega^2\tau_A{}^2) + \tfrac{3}{4}(\sin^2 2\beta)\tau_B/(1+\omega^2\tau_B{}^2)$$
$$+ \tfrac{3}{4}(\sin^4\beta)\tau_C/(1+\omega^2\tau_C{}^2)] + (1-S^2)\tau_e\} \tag{43}$$

Equation (40) is described as "model-free", in the sense that in its derivation no particular mechanism is assumed for the internal motions. Provided the conditions of extreme narrowing and isotropic rotation condi-

tions are met, it provides a simple but generally useful representation of the spectral density with only three unknown parameters, and is capable of relatively straightforward experimental testing, for example by measurements of ^{13}C T_1, T_2 and NOE data at two resonance frequencies. The order parameter S depends only on the spatial restriction of the motion. However, the effective correlation time τ_e depends on the spatial restriction and the rate of motion. It is interesting to note that an expression identical to equation (40) has been used to interpret relaxation in micelles.[104] Here τ_M represents a slow process associated with overall micelle motions, and τ_e is associated with fast segmental motions within the micelle.

It is worth pointing out that equations (39) and (42) show that only limited information on internal motions is available from NMR data. For all motions in the extreme narrowing limit, only a single effective correlation time can be found. No information on motions much slower than overall tumbling can be obtained. The motions can be completely characterized only if they are comparable to overall motion and not in extreme narrowing. Note also that if the molecule is sufficiently small, so that $\omega^2 \tau_M^2 \ll 1$, the internal and overall motions cannot be separated, since $J(\omega)$ is independent of frequency.

Qualitatively a spectral density of the form of equation (40) allows a rationale of the inconsistencies mentioned earlier between experimental data and expectations for a rigid molecule. If the overall motion is very slow such that $\omega^2 \tau_M^2 \gg 1$, and the internal motions are significant such that $S^2 < 1$, then $J(\omega) \approx 2(1 - S^2)\tau_e/5$ and is independent of frequency. If, however, $S^2 = 1$, then $J(\omega) \approx 2S^2/(5\omega^2 \tau_M)$ and is strongly dependent on frequency. In the former case, the NOE's will take their maximal values and T_1 will be independent of frequency. In the latter case the values of the NOE's will be minimal and T_1 will vary as ω_0^2. Between these two extremes intermediate behaviour will be observed, depending on the relative contributions of the overall and internal motions. Thus T_1 may depend on ω_0, but may vary as some power between 0 and 2. As ω_0 increases, the relative contribution of the overall tumbling term decreases, so the NOE may increase. The incorporation of rapid internal motions increases T_1 and T_2 compared with their value in a rigid molecule, so the correlation times obtained using the rigid model are overestimated.

Lipari and Szabo[34] have evaluated the internal correlation function for a number of specific models. One particularly interesting group can be generally classed under the term "diffusion in a cone", which seems a reasonable model for oscillatory modes (vibrations and torsions). The librations are pictured as causing random motions of a bond within a cone with axis oriented along the equilibrium bond direction. Motions of this type have also been studied by several other groups.[96,105-108] The simplest model[96] is to treat the motion as diffusion around the surface of the cone,

i.e. as an internal rotation. If θ is the semi-angle of the cone and D_I the internal diffusion constant, in equation (40)

$$S = \tfrac{1}{2}(3 \cos^2 \theta - 1) \tag{44a}$$

$$(1 - S^2)\tau_e = \tfrac{1}{4}(3 \sin^2 2\theta + \tfrac{3}{4} \sin^4 \theta)/D_I \tag{44b}$$

A more realistic assumption is that the bond undergoes free diffusion anywhere within the cone.[105,106,109,110] The order parameter is

$$S = \cos \theta(1 + \cos \theta)/2 \tag{45}$$

and $G_I(t)$ is rigorously given by an infinite sum:

$$G_I(t) = S^2 + \sum_{i=1}^{\infty} a_i \exp(-b_i D_I t)$$

Kinoshita *et al.*[109] have calculated the coefficients a_i and b_i numerically. More conveniently, Lipari and Szabo[106] have shown that the time-dependent part can be represented accurately by a single exponential with effective correlation time τ_e obtained using equation (41), giving

$$D_I(1 - S^2)\tau_e = x_2(1 + x)^2 \{\ln[(1 + x)/2] + (1 - x)/2\}/[2(x - 1)]$$
$$+ (1 - x)(6 + 8x - x^2 - 12x^3 - 7x^4)/24$$

where $x = \cos \theta$. Thus equation (40) is a very good approximation. Using the same idea of free motion within a cone, but assuming reorientation by random jumps between a large number of discrete orientations, Howarth[105] has obtained a correlation function identical to equation (40) with S given by equation (45) and τ_e equal to the reciprocal of the mean jump rate.

Another physically reasonable model for internal motions is that of jumps between a number of discrete states as might apply for example to internal rotations of a C–C bond between distinct conformations. There may of course in addition be librational motions in each state. Wittebort and Szabo[19] have shown that for N states the correlation function can be expressed in terms of the eigenvalues and eigenvectors of an $N \times N$ matrix involving the jump rates and the geometry of the states. The correlation function takes the form of equation (37) with N terms in the sum. Note that the a_i and τ_i are composite functions, and do not necessarily represent individual rate processes. Explicit expressions for a two-state model have been given by Hogan and Jardetzky[17] and Lipari and Szabo,[110] the former restricting discussion to equal populations of each state. (Note that Lipari and Szabo have corrected an error in a formula of Hogan and Jardetzky.) The combined effects of internal rotation and librations have been discussed, for the case of the methyl group,[107,108] with particular reference to the situation of the methyl group attached directly to the backbone, as for example in an alanine residue in a protein. A simple but reasonable model assumes free rotation

of the methyl group superimposed on "diffusion in a cone" librations of the internal rotation axis. The following expression for the term $(1 - S^2)\tau_e$ in equation (40) is due to Brainard and Szabo:

$$(1 - S^2)\tau_e = \tfrac{5}{2}S_c^2/D_R + (1 - S_c^2)\{(6D_I)^{-1}$$
$$+ (D_I)^{-1}[\tfrac{3}{4}\sin^2 2\beta/(6 + \sigma) + \tfrac{3}{4}\sin^4 \beta/(6 + 4\sigma)]\}$$

where

$$\sigma = D_R/D_I - 1$$

D_R is the methyl rotation diffusion constant, D_I is the rotation axis diffusion constant, and β is the angle between the interaction vector and the rotation axis. S_c is the orientation parameter for the libration and is expressed in terms of cone semi-angle by equation (45). Lipari and Szabo[111] have pointed out that, if equation (40) is valid, it is not possible to determine D_R and D_I individually, since an infinite number of pairs can give the same τ_e value.

In order to investigate the range of validity of the approximate spectral densities, equations (40) and (43), Lipari and Szabo[34] have used these functions to fit synthetic data generated using exact formulae for various models such as equation (38). The best-fit values of the generalized parameters S^2 and τ_e are compared with their exact values. In summary, it is found that, if $S^2 \geq 0.3$, a set of measurements (T_1, T_2, NOE) at two fields gives fairly accurate values of S^2 and τ_e (within $\sim 15\%$), with little restriction on the magnitudes of τ_e, τ_M or ω_0. For lower values of S^2, down to 0.01, reasonably accurate determination of S^2 and τ_e within 25% requires the conditions $\tau_e/\tau_M < 0.1$ and $\omega_m \tau_e < 0.5$, where ω_m is the highest frequency involved in the experimental data. The greater the inequality between τ_e and τ_M, and the greater the conformity with extreme narrowing for τ_e, the smaller the error, reaching a few % for $\tau_e/\tau_M < 0.01$ and $\omega \tau_e < 0.1$. For anisotropic rotation, τ_M in these inequalities should be replaced with the shortest correlation time for the overall motion.

King, Jardetzky and co-workers[3,112-114] have described a formal theory of relaxation in systems with multiple motions, based on the theory of Markov processes. This requires that the dynamics can be represented by a set of transition probabilities from one state to another and that these probabilities are independent of the previous history. For a single motion, the spectral density for the correlation function of a dynamic variable F is[112]

$$J(\omega) = -2 \sum_n \frac{|\langle F, \phi_n \rangle|^2 \lambda_n}{\omega^2 + \lambda_n^2}$$

where ϕ_n and λ_n are the eigenfunctions and eigenvalues of a transition operator Ω constructed from the transition probabilities, i.e.

$$\Omega \phi_n = \lambda_n \phi_n$$

For multiple independent motions, M in number, the spectral density is

$$J(\omega) = -2 \sum_{n_1, n_2, \ldots, n_M} \frac{\left|\left\langle F, \prod_{k=1}^{M} \phi_{kn_k} \right\rangle\right|^2 \left(\sum_{k=1}^{M} \lambda_{kn_k}\right)}{\omega^2 + \left(\sum_{k=1}^{M} \lambda_{kn_k}\right)^2}$$

In practice the λ's are likely to fall into well spaced groups of near identical values, and this expression operationally becomes[114]

$$J(\omega) = -\frac{2}{5} \sum_{i=1}^{M} \frac{\bar{\alpha}_i \bar{\lambda}_i}{\omega^2 + \bar{\lambda}_i^2}$$

where the $\bar{\alpha}_i$ and $\bar{\lambda}_i$ are effective amplitudes and rates. The α_i are subject to the conditions $\bar{\alpha}_i \geqslant 0$ and $\sum \bar{\alpha}_i = 1$. Defining correlation times by $\tau_i = -(\bar{\lambda}_i)^{-1}$, this expression becomes

$$J(\omega) = \sum_{i=1}^{M} \frac{\bar{\alpha}_i \tau_i}{1 + \omega^2 \tau_i^2} \tag{46}$$

The formal similarity to equation (38) of Lipari and Szabo (and to equation (28) of Jones and Stockmayer) is obvious, though neither the division into overall and internal modes nor the distinction of different modes of internal motion is here made explicit. The approach results effectively in a discrete distribution of correlation times. If all the τ_i, and $M-1$ of the $\bar{\alpha}_i$ values are independent, then at least $M-1$ independent experimental measurements are required to characterize $J(\omega)$. In practice, because of experimental errors and the limited frequency range of NMR data, the number of independent terms capable of being solved with reasonable certainty is limited to three or less. Even so, such a solution requires that the $\bar{\alpha}_i$ are of reasonable magnitude, that the τ_i are fairly well separated and that $\omega^2 \tau_i^2 \geqslant 1$ for each τ_i for at least some of the measurement frequencies.

E. Applications to stiff molecules

Lipari and Szabo[111] have applied their model to ^{13}C experimental data for several biological macromolecules, including basic pancreatic trypsin inhibitor (BPTI), sperm whale myoglobin and bacterial dihydrofolate reductase. In each case isotropic rotation was assumed, the values of τ_M meeting the condition $\omega^2 \tau_M^2 \geqslant 1$. A spectral density of the form of equation (40) is assumed.

For BPTI, ^{13}C T_1's and NOE's are available[107] at 25.1 MHz and T_1's at 90.5 MHz for backbone and side-chain nuclei in several residues. For each nucleus, equation (40) gives a good representation of all relaxation parameters. For the α-carbon envelope, whose relaxation is determined by

backbone motions alone, the best-fit parameters are $\tau_M = 4.53$ ns, $\tau_e = 20.1$ ps and $S^2 = 0.874$. Since $\tau_e \ll \tau_M$ and $S^2 > 0.3$, the error in these values is quite small. The magnitude of S indicates substantial librational motions of the backbone. Assuming the diffusion in a cone picture for the sake of illustration, this value of S corresponds from equation (45) to a cone semi-angle of 17°. For several individually resolved methyl signals from alanine residues the values of τ_e are rather longer (40-70 ps) and the values of S^2 much smaller (0.013-0.058) than for the α-carbons. For these groups the internal motions consist of methyl rotation combined with the backbone librations detected in the α-carbon relaxation. The larger value of τ_e for the methyl would arise if the methyl rotation were slower than the librations, though still much faster than overall tumbling. The lower values of S^2 are a consequence of the greater degree of internal freedom. For methyl rotation without libration, the spectral density would effectively be that for anisotropic rotational diffusion, equation (36), where $D_\perp$ corresponds to overall rotation and $D_\parallel$ to the methyl rotation. For fast internal rotation $(D_\parallel \gg D_\perp$ and $D_\parallel{}^2 \ll \omega_0{}^2)$, equation (34) reduces to equation (40) with $S^2 = \frac{1}{4}(3\cos^2\beta - 1)^2$ where β is the angle between the C-H bond and the methyl symmetry axis. For tetrahedral geometry, $\beta = 70.5°$ and $S^2 = 0.111$. That the observed values of S^2, for the alanine methyls, are less than 0.111 is indicative of librational motions. Using the diffusion in a cone model, the libration cone semi-angle is calculated as 30-60°, depending on position. Interestingly, those residues Ala-27 and Ala-58 with semi-angles 50° and 60° respectively are located in regions predicted to have relatively high mobility by molecular dynamics simulations.[115]

For the myoglobin and dihydrofolate reductase the experimental data are less extensive than for BPTI and are limited to methyl carbons in the isoleucine and methionine moieties.[111] In each case the methyls have several internal rotation degrees of freedom, as well as librational modes. Although equation (40) gives a satisfactory representation, it is impossible to deduce any information on the backbone motions because of the many contributions to S^2 and τ_e.

Ribeiro et al.[114] have analysed ^{13}C relaxation in BPTI using equation (46). T_1, T_2 and NOE data are measured at 45 and 90 MHz. As a constraint on the fitting procedure, one of the correlation times, τ_1, is fixed at the value of 1.7 ns determined by depolarized light scattering for the overall rotational diffusion process. In the α-carbon region four peaks were studied, and the best-fit motional parameters obtained separately for the three measurements at each frequency. At least three terms in equation (46) are required, giving four unknown parameters. (It is unclear how four parameters are determined from only three experimental items.) The experimental and calculated relaxation data are given in Table 10, and the reported motional parameters in Table 11. One of the variable terms turns out to be

TABLE 10

Comparison of calculated and experimental ^{13}C relaxation data for α-carbon peaks of BPTI at 17 °C and pD 5; the motional parameters used in equation (46) to obtain the calculated values are given in Table 11.

Peak[a]	δ_c	Freq. (MHz)	T_1 (ms)[b] exp.	T_1 (ms)[b] calc.	T_2 (ms)[b] exp.	T_2 (ms)[b] calc.	NOE[b] exp.	NOE[b] calc.
1	51.14	45[c]	100	100	40	40	1.25	1.25
		45[c]	100	115	40	35	1.25	1.35
		90	200	220	70	60	1.15	1.25
2	51.74	45	120	120	60	60	1.45	1.45
		90	220	245	80	75	1.20	1.20
3	52.13	45	100	120	35	25	1.20	1.30
		90	250	275	55	50	1.15	1.20
4	53.55	45	105	105	45	45	1.30	1.30
		90	205	205	55	55	1.20	1.20

[a] The only assigned peak is peak 2 to Ala-58.
[b] Because of experimental errors all values are rounded to the nearest 5 or 10 in the third place, leading to the frequent identity of calculated and experimental values.
[c] Two solutions were found for this data set.
From reference 114, with permission.

TABLE 11

Best-fit motional parameters for the α-carbon peaks of BPTI at 17 °C and pD 5; the calculated relaxation times for these parameters and equation (46) are compared with experiment in Table 10.

Peak	Freq. (MHz)	τ_1 (ns)	α_1 (%)	τ_2 (ns)	α_2 (%)	τ_3 (ns)	α_3 (%)
1	45[a]	1.7	11	5	50	10	39
	45[a]	1.7	28	1.1	68	0.1	2
	90	1.7	35	5	52	0.002	13
2	45	1.7	23	5	41	0.05	36
	90	1.7	23	5	62	0.0011	15
3	45	1.7	13	10	80	0.17	6
	90	1.7	4	5	83	0.0011	13
4	45	1.7	2	5	74	0.033	24
	90	1.7	7	3.3	78	20	15

[a] Two solutions for this data set.
From reference 114, with permission.

slower than the fixed value of τ_1, suggesting some anisotropy in the overall motion. The average overall correlation time is comparable to Lipari and Szabo's value (see above). The remaining variable term produces a much shorter correlation time (except for peak 4 at 90 MHz), consistent with a fast librational motion. The average contribution is comparable to that of the composite internal motions in Lipari and Szabo's[111] analysis above. Ribeiro et al.[114] have also analysed methyl relaxation data in the same way, with similar conclusions to those of Lipari and Szabo.

Howarth[96] has analysed the frequency dependence of $\alpha - {}^{13}C$ relaxation in proteins and peptides, using the model of diffusion round the surface of a cone to represent the internal motions. The molecules include bovine serum albumin, lysozyme, alumichrome, gramicidin-S, luliberin and several myoglobins and haemoglobins. In general the experimental observations for all systems can be reconciled by the combination of overall tumbling and librations with a cone semi-angle of 20° and a correlation time of 10 ps. These values represent an internal motion contribution comparable to those obtained elsewhere.[111,114] The overall rotation correlation time is in much better agreement with values obtained from light scattering than the correlation times calculated assuming a rigid molecule.

For some macromolecules the assumption of isotropic overall rotation is inadequate. Systems such as nucleic acids and regular polypeptides can adopt highly extended helical conformations, whose overall motions are clearly anisotropic. A synthetic polypeptide which has been extensively studied[94] is helical poly(γ-benzyl-L-glutamate), for which the experimental data for $\alpha - {}^{13}C$ relaxation are discussed above (Table 9). Relaxation is simulated by a model of anisotropic rotational diffusion combined with Howarth's model[96] of diffusion on the surface of a cone [equations (43) and (44)]. To limit the degrees of freedom, the overall diffusion constants $D_\parallel$ and $D_\perp$ are assumed to be given by Perrin's equations[116] for rotation of an ellipsoid, as modified by Edsall[117] for a long helix:

$$D_\perp = \frac{3kT}{2\pi\eta d^3 N^3}\left[2\ln\left(\frac{dN}{R}\sqrt{\frac{2}{3}}\right) - 1\right]$$

$$D_\parallel = \frac{kT}{4\pi\eta R^2 dN}\left[1 - \frac{6R^2}{d^2 N^2}\ln\left(\frac{dN}{R}\sqrt{\frac{2}{3}}\right)\right] - D_\perp$$

where d is the length of the repeat unit, N is the degree of polymerization, R is the helix radius and η is the medium viscosity. An α-helix conformation was assumed, giving $d = 0.15$ nm and $R = 1.5$ nm. The angle β in equation (43) is 62°. To eliminate polymer–polymer interactions, experimental parameters were extrapolated to zero concentration. Figure 10 compares the experimental molecular weight dependence of T_1 and T_2 at 25.1 MHz with the calculated curves for various librational contributions. A perfectly
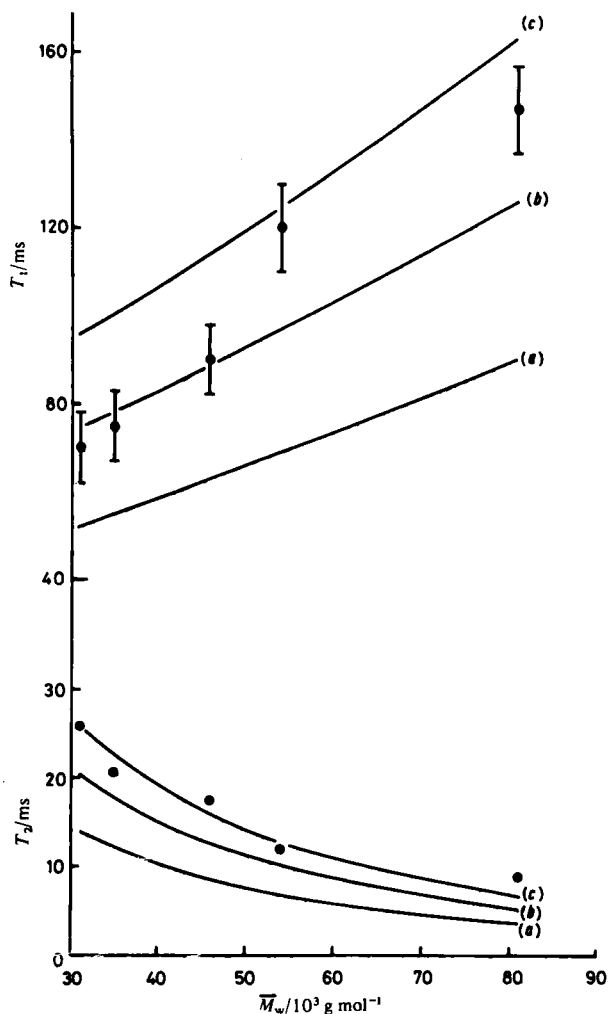
FIG. 10. α-Carbon T_1 and T_2 vs. molecular weight for poly(γ-benzyl-L-glutamate) in dimethylformamide-d_7 at 60 °C. ⬤ T_1; ● T_2 (extrapolated to $c = 0$). The curves are calculated as described in the text for (a) no libration, (b) libration with $D_1 = 1.7 \times 10^{10}$ s^{-1} and $\theta = 20°$, and (c) libration with $D_1 = 5.0 \times 10^{10}$ s^{-1} and $\theta = 25°$. From reference 95, with permission.

rigid molecule is clearly inadequate. The curves suggest best-fit values for D_1 of $(2-5) \times 10^{10}$ s^{-1} and θ of 20–25°, commensurate with the parameters suggested by Howarth[96] for proteins and peptides. These values of D_1 and θ also account for the frequency dependence of T_1 and the NOE.

   Several groups[17,110,118–122] have studied relaxation in fragments of deoxyribonucleic acid (DNA) which have been shown by electric dichroism

to behave effectively as rods.[123] In earlier studies inappropriate models such as isotropic rotation[118,119,121] or rigid anisotropic rotation[120] are used. Hogan and Jardetzky[17] have used a model of cylindrical anisotropic rotation with internal motions by two-state jumps. Lipari and Szabo considered the same model, as well as other versions of the internal process such as diffusion in a cone. The latter conclude that there is substantial internal mobility with correlation times of the order of 0.1-1 ns, but no unique picture of the motion could be differentiated.

Finally, it is worth pointing out that, although this section has been directed specifically towards stiff chains, the theoretical approaches are applicable with slight modification to flexible chains. Equation (38), for example, is formally identical to equation (28). Both Howarth[105] and Lipari and Szabo[111] have used the librational model to analyse relaxation in flexible chains, with satisfactory results. Lipari and Szabo[111] account for the effective anisotropy of backbone motion in such systems by assuming a simple two-exponential form for the overall correlation function:

$$G_0(t) = A \exp(-t/\tau_1) + (1 - A) \exp(-t/\tau_2)$$

where A, τ_1 and τ_2 are empirical parameters. This expression is shown to give a very close representation of the continuous correlation time distribution used for backbone motion in random coil poly(L-lysine).[45]

V. CONCLUSIONS

Because of limitations in accuracy, frequency range and relaxation theory, the potential of NMR relaxation in unambiguously characterizing a polymer correlation function is not at present being fulfilled. Nevertheless, the technique will continue to be useful, if interpreted with caution, since no other is able to give the same insight at the segmental level. Certainly NMR is valuable in a semi-quantitative manner when comparing different polymers, or different parts of the same polymer if the same model is used. At a basic level it is expected that NMR will have a vital role to play in testing the results of computer dynamics simulations should an NMR correlation function be computed for a realistic system.

REFERENCES

1. F. Heatley, *Progr. Nucl. Magn. Reson. Spectrosc.*, 1979, **13**, 47.
2. K. Wüthrich and G. Wagner, *Trends Biochem. Sci.*, 1978, **3**, 227.
3. O. Jardetzky, *Acc. Chem. Res.*, 1981, **14**, 291.
4. J. A. McCammon and M. Karplus, *Acc. Chem. Res.*, 1983, **16**, 187.

5. (a) D. Shaw, *Fourier Transform NMR Spectroscopy*, Elsevier, Amsterdam, 1976. (b) M. L. Martin, G. J. Martin and J. J. Delpuech, *Practical NMR Spectroscopy*, Heyden, London, 1979. (c) R. K. Harris, *Nuclear Magnetic Resonance Spectroscopy*, Pitman, London, 1983.
6. S. L. Gordon and K. Wüthrich, *J. Am. Chem. Soc.*, 1978, **100**, 7094.
7. F. Heatley and B. Wood, *Polymer*, 1979, **20**, 1512.
8. F. Heatley and M. K. Cox, *Polymer*, 1981, **22**, 190.
9. A. A. Jones and F. P. Shea, *J. Polymer Sci., Polymer Phys.*, 1982, **20**, 681.
10. R. L. Vold, R. R. Vold and H. E. Simon, *J. Magn. Reson.*, 1973, **11**, 283.
11. A. D. Bain, W. P. Y. Ho and J. S. Martin, *J. Magn. Reson.*, 1981, **43**, 331.
12. G. Hermann and G. Weill, *Macromolecules*, 1975, **8**, 171.
13. J. Schriever, J. C. Bunk and J. C. Leyte, *J. Magn. Reson.*, 1977, **27**, 45.
14. J. Schriever, L. H. Zuiderweg and J. C. Leyte, *Mol. Phys.*, 1977, **34**, 635.
15. P. L. Rinaldi, Chin Yu and G. C. Levy, *Macromolecules*, 1981, **14**, 551.
16. K. Matsuo, K. F. Kuhlmann, H. W. H. Yang, F. Geny, W. H. Stockmayer and A. A. Jones, *J. Polymer Sci., Polymer Phys.*, 1977, **15**, 1347.
17. M. E. Hogan and O. Jardetzky, *Proc. Nat. Acad. Sci. USA*, 1979, **76**, 6341; *Biochemistry*, 1980, **19**, 3640.
18. J. R. Lyerla and G. C. Levy, *Topics Carbon-13 NMR Spectrosc.* 1974, **1**, 79.
19. R. J. Wittebort and A. Szabo, *J. Chem. Phys.*, 1978, **69**, 1722.
20. D. M. Brink and G. R. Satchler, *Angular Momentum*, Oxford University Press, Oxford, 1961.
21. F. Heatley and M. K. Cox, *Polymer*, 1977, **18**, 225; F. Heatley, A. Begum and M. K. Cox, *Polymer*, 1977, **18**, 637.
22. F. Heatley and B. Wood, *Polymer*, 1978, **19**, 1405.
23. S. Meiboom and D. Gill, *Rev. Sci. Instrum.*, 1958, **69**, 688.
24. R. L. Vold and R. R. Vold, *J. Chem. Phys.*, 1974, **61**, 2525.
25. R. Freeman and H. D. W. Hill, *J. Chem. Phys.*, 1971, **55**, 1985.
26. A. G. Redfield, *Adv. Magn. Reson.*, 1965, 1, 1.
27. A. Kalk and H. J. C. Berendsen, *J. Magn. Reson.*, 1976, **24**, 343.
28. B. D. Sykes, W. E. Hull and G. H. Snyder, *Biophys. J.*, 1978, **21**, 137.
29. F. Heatley and M. K. Cox, *Polymer*, 1980, **21**, 381.
30. F. Heatley and M. K. Cox, *Polymer*, 1981, **22**, 288.
31. L. G. Werbelow and A. G. Marshall, *J. Magn. Reson.*, 1973, **11**, 299.
32. L. G. Werbelow and D. M. Grant, *Adv. Magn. Reson.*, 1977, **9**, 190.
33. R. P. Lubianez and A. A. Jones, *J. Magn. Reson.*, 1980, **38**, 331.
34. G. Lipari and A. Szabo, *J. Am. Chem. Soc.*, 1982, **104**, 4546.
35. M. Mauzac, J. P. Vairon and F. Lauprêtre, *Polymer*, 1979, **20**, 443.
36. P. M. Henrichs, J. M. Hewitt, G. A. Russell, M. A. Sandhu and H. R. Grashof, *Macromolecules*, 1981, **14**, 1770.
37. (a) J. Schaefer and D. F. S. Natusch, *Macromolecules*, 1972, **5**, 416; (b) F. Heatley and A. Begum, *Polymer*, 1976, **17**, 399.
38. J. Schaefer, *Macromolecules*, 1973, **6**, 882.
39. For a survey of earlier applications, see reference 1.
40. T. Asakura and Y. Doi, *Marcomolecules*, 1983, **16**, 786.
41. R. A. Komoroski, *J. Polymer Sci., Polymer Phys.*, 1979, **17**, 45.
42. D. Ghesquiere, C. Chachaty and A. Tsutsumi, *Macromolecules*, 1979, **12**, 775.
43. B. Perly, Y. Chevalier and C. Chachaty, *Macromolecules*, 1981, **14**, 969.
44. R. J. Wittebort, A. Szabo and F. R. N. Gurd, *J. Am. Chem. Soc.*, 1980, **102**, 5723.
45. A. A. Jones and R. P. Lubianez, *Macromolecules*, 1978, **11**, 126.
46. W. Gronski and N. Murayama, *Makromol. Chem.*, 1974, **177**, 3017; W. Gronski, *Makromol. Chem.*, 1977, **178**, 2949.
47. R. E. Cais and F. A. Bovey, *Macromolecules*, 1977, **10**, 757.

48. W. H. Stockmayer, A. A. Jones and T. L. Treadwell, *Macromolecules*, 1977, **10**, 762.
49. A. H. Fawcett, F. Heatley, K. J. Ivin, C. D. Stewart and P. Watt, *Macromolecules*, 1977, **10**, 765.
50. T. W. Bates, K. J. Ivin and G. Williams, *Trans. Faraday Soc.*, 1967, **63**, 1964, 1976.
51. K. Iwata, *J. Chem. Phys.*, 1973, **58**, 4184.
52. E. Helfand, *J. Chem. Phys.*, 1971, **54**, 4651.
53. E. Helfand, Z. R. Wasserman and T. A. Weber, *Macromolecules*, 1980, **13**, 526.
54. J. Skolnick and E. Helfand, *J. Chem. Phys.*, 1980, **72**, 5489.
55. E. Helfand and J. Skolnick, *J. Chem. Phys.*, 1982, **77**, 5714.
56. D. G. Lister, J. N. Macdonald and N. L. Owen, *Internal Rotation and Inversion*, Academic Press, London, 1978.
57. R. H. Boyd and S. M. Breitling, *Macromolecules*, 1974, **7**, 855.
58. T. P. Liao and H. Morawetz, *Macromolecules*, 1980, **13**, 1228. (Correction: *ibid.*, 1981, **14**, 231.)
59. L. Monnerie and F. Geny, *J. Chim. Phys.*, 1969, **66**, 1691, 1698.
60. F. Geny and L. Monnerie, *J. Chim. Phys.*, 1969, **66**, 1708, 1872.
61. F. Geny and L. Monnerie, *Macromolecules*, 1977, **10**, 1003.
62. F. Geny and L. Monnerie, *J. Polymer Sci., Polymer Phys.*, 1979, **17**, 131.
63. F. Geny and L. Monnerie, *J. Polymer Sci., Polymer Phys.*, 1979, **17**, 147.
64. F. Geny and L. Monnerie, *J. Polymer Sci., Polymer Phys.*, 1979, **17**, 173.
65. E. Dubois-Violette, F. Geny, L. Monnerie and O. Parodi, *J. Chim. Phys.*, 1969, **66**, 1865.
66. B. Valeur, L. Monnerie and J. P. Jarry, *Compt. Rend. Acad. Sci.*, 1974, **C278**, 589.
67. B. Valeur, J. P. Jarry, F. Geny and L. Monnerie, *J. Polymer Sci., Polymer Phys.*, 1975, **13**, 667.
68. B. Valeur, L. Monnerie and J. P. Jarry, *J. Polymer Sci., Polymer Phys.*, 1975, **13**, 675.
69. B. Valeur, J. P. Jarry, F. Geny and L. Monnerie, *J. Polymer Sci., Polymer Phys.*, 1975, **13**, 2251.
70. P. Tekely, F. Lauprêtre and L. Monnerie, *Macromolecules*, 1983, **16**, 415.
71. A. A. Jones and W. H. Stockmayer, *J. Polymer Sci., Polymer Phys.*, 1977, **15**, 847.
72. B. I. Hunt and J. G. Powles, *Proc. Phys. Soc.*, 1966, **88**, 513.
73. J. T. Bendler and R. Yaris, *Macromolecules*, 1978, **11**, 650. (Correction: F. Heatley and J. T. Bendler, *Polymer*, 1979, **20**, 1578.)
74. J. Skolnick and R. Yaris, *Macromolecules*, 1982, **15**, 1041. (Correction: *ibid.*, 1983, **16**, 491.)
75. J. Skolnick and R. Yaris, *Macromolecules*, 1982, **15**, 1046. (Correction: *ibid.*, 1983, **16**, 492.)
76. J. Skolnick and R. Yaris, *Macromolecules*, 1983, **16**, 266.
77. T. A. Weber and E. Helfand, *J. Phys. Chem.*, 1983, **86**, 2881.
78. G. Hermann and G. Weill, *Macromolecules*, 1975, **8**, 171.
79. F. Lauprêtre and F. Geny, *Eur. Polymer J.*, 1978, **14**, 401.
80. F. Lauprêtre, C. Noel and L. Monnerie, *J. Polymer Sci., Polymer Phys.*, 1977, **15**, 2127.
81. F. C. Schilling, R. E. Cais and F. A. Bovey, *Macromolecules*, 1978, **11**, 325.
82. K. Hatada, H. Ishikawa, T. Kitayama and H. Yuki, *Makromol. Chem.*, 1977, **178**, 2753.
83. S. Mashimo and K. Shinohara, *J. Phys. Soc. Japan*, 1973, **34**, 1141.
84. A. A. Jones, G. L. Robinson, F. E. Gerr, M. Bisceglia, S. L. Shostak and R. P. Lubianez, *Macromolecules*, 1980, **13**, 95.
85. A. A. Jones, R. P. Lubianez, M. A. Hanson and S. L. Shostak, *J. Polymer Sci., Polymer Phys.*, 1978, **16**, 1685.
86. A. A. Jones and M. Bisceglia, *Macromolecules*, 1979, **12**, 1136.
87. J. F. O'Gara, S. G. Desjardins and A. A. Jones, *Macromolecules*, 1981, **14**, 64.
88. J. J. Connolly, E. Gordon and A. A. Jones, *Macromolecules*, 1984, **17**, 722.
89. K. Matsuo and W. H. Stockmayer, *Macromolecules*, 1981, **14**, 544.
90. K. Matsuo, W. H. Stockmayer and S. Mashimo, *Macromolecules*, 1982, **15**, 606.

91. S. Mashimo, P. Winsor, P. H. Cole, K. Matsuo and W. H. Stockmayer, *Macromolecules*, 1983, **16**, 965.
92. A. A. Jones, G. L. Robinson and F. E. Gerr, *Carbon-13 NMR in Polymer Science* (W. M. Pasika, ed.), Am. Chem. Soc. Symposium Series 103, 1977, p. 271.
93. P. M. Henrichs, *Macromolecules*, 1981, **14**, 1770.
94. P. Doty, J. H. Bradbury and A. M. Holtzer, *J. Am. Chem. Soc.*, 1956, **78**, 947.
95. P. M. Budd, F. Heatley, T. J. Holton and C. Price, *J. Chem. Soc., Faraday Trans. 1*, 1981, **77**, 759.
96. O. W. Howarth, *J. Chem. Soc., Faraday Trans. 2*, 1978, **74**, 1031.
97. D. J. Wilbur, R. S. Norton, A. O. Clouse, R. Addleman and A. Allerhand, *J. Am. Chem. Soc.*, 1976, **98**, 8250.
98. M. Llinas, W. Meier and K. Wüthrich, *Biochim. Biophys. Acta*, 1977, **492**, 1.
99. R. B. Visscher and F. R. N. Gurd, *J. Biol. Chem.*, 1975, **250**, 2238.
100. K. Dill and A. Allerhand, *J. Am. Chem. Soc.*, 1979, **101**, 4376.
101. D. E. Woessner, *J. Chem. Phys.*, 1962, **37**, 647.
102. R. E. Jacobs and E. Oldfield, *Progr. NMR Spectrosc.*, 1982, **14**, 113.
103. P. Diehl and C. L. Khetrapal, *NMR Basic Principles and Progress*, 1969, **1**, 1.
104. U. Henriksson, L. Ödberg, J. C. Eriksonn and L. Westman, *J. Phys. Chem.*, 1977, **81**, 16.
105. O. W. Howarth, *J. Chem. Soc., Faraday Trans. 2*, 1979, **75**, 863.
106. G. Lipari and A. Szabo, *Biophys. J.*, 1980, **30**, 489.
107. R. Richarz, K. Nagayama and K. Wüthrich, *Biochemistry*, 980, **19**, 5189.
108. J. R. Brainard and A. Szabo, *Biochemistry*, 1981, **20**, 4618.
109. K. Kinoshita, S. Kawato and A. Ikegami, *Biophys. J.*, 1977, **20**, 289.
110. G. Lipari and A. Szabo, *Biochemistry*, 1981, **20**, 6250.
111. G. Lipari and A. Szabo, *J. Am. Chem. Soc.*, 1982, **104**, 4559.
112. R. King and O. Jardetzky, *Chem. Phys. Lett.*, 1978, **55**, 15.
113. R. King, R. Maas, M. Gassner, R. K. Nanda, W. W. Conover and O. Jardetzky, *Biophys. J.*, 1978, **24**, 103.
114. A. A. Ribeiro, R. King, C. Restivo and O. Jardetzky, *J. Am. Chem. Soc.*, 1980, **102**, 4040.
115. J. A. McCammon, B. R. Gelin and M. Karplus, *Nature* (London), 1977, **267**, 585; M. Karplus and J. A. McCammon, *ibid.*, 179, **277**, 578.
116. F. Perrin, *J. Phys. Radium*, 1934, **5**, 497.
117. J. T. Edsall, *The Proteins* (H. Neurath and K. Bailey, eds), Academic Press, New York, Vol. 1, Part B, Chap. 2, p. 668.
118. P. H. Bolton and T. L. James, *J. Phys. Chem.*, 1979, **83**, 3359.
119. P. H. Bolton and T. L. James, *J. Am. Chem. Soc.*, 1980, **102**, 25.
120. T. A. Early and D. R. Kearns, *Proc. Nat. Acad. Sci. USA*, 1979, **76**, 4165.
121. L. Klevan, I. M. Armitage and D. M. Crothers, *Nucleic Acids Res.*, 1979, **6**, 1607.
122. H. Shindo, *Biopolymers*, 1980, **19**, 509.
123. M. E. Hogan, N. Dattagupta and D. M. Crothers, *Proc. Nat. Acad. Sci. USA*, 1978, **75**, 195.

Nuclear Magnetic Resonance of Less Common Quadrupolar Nuclei

TORBJÖRN DRAKENBERG

Department of Physical Chemistry 2, University of Lund, Sweden

I. INTRODUCTION

Although most naturally occurring isotopes have a spin quantum number $I > \frac{1}{2}$, and therefore also have a quadrupole moment, the overwhelming majority of NMR studies deal with spin-$\frac{1}{2}$ nuclei, mostly ^{1}H, ^{13}C, ^{19}F and ^{31}P. It may appear surprising that even today, with the widespread use of modern NMR spectrometers capable of use at any frequency, the two nuclei ^{1}H and ^{13}C dominate the NMR field. One reason is the poor resolution that can be obtained for quadrupolar nuclei like ^{17}O and ^{33}S in organic molecules

due to the broad NMR resonances of these nuclei. When a quadrupolar nucleus is covalently bound the relaxation will be very efficient and only a few nuclei, with very low quadrupole moments (^{2}H, ^{6}Li, ^{7}Li, ^{9}Be, ^{11}B, ^{51}V), will give rise to lines that are not exceedingly broad. For the vast majority of quadrupolar nuclei NMR studies have to be restricted to situations where the electronic symmetry around the nucleus is cubic, or at least pseudocubic.

TABLE 1

Physical properties of quadrupolar nuclei.

Nucleus	Spin	Natural abundance (%)	Magnetic moment (μ_N)	Quadrupole moment (10^{-28} m^2)
^{39}K	3/2	93.1	0.391	0.094
^{85}Rb	5/2	72.2	1.348	0.26
^{87}Rb	3/2	27.8	2.741	0.13
^{133}Cs	7/2	100	2.564	−0.003
^{9}Be	3/2	100	−1.777	0.052
^{25}Mg	5/2	10.1	−0.855	0.22
^{43}Ca	7/2	0.13	−1.315	0.05
^{87}Sr	9/2	7.0	−1.089	0.36
^{137}Ba	3/2	11.3	0.931	0.28
^{45}Sc	7/2	100	4.7492	−0.22
^{138}La	5	0.089	3.684	0.51
^{139}La	7/2	99.9	2.7614	0.22
^{47}Ti	5/2	7.3	−0.7871	0.02
^{49}Ti	7/2	5.5	−1.1022	0.29
^{91}Zr	5/2	11.2	−1.3036	—
^{51}V	7/2	99.8	5.1392	−0.05
^{93}Nb	9/2	100	6.144	−0.22
^{181}Ta	7/2	99.98	2.371	+3.9
^{53}Cr	3/2	9.6	−0.4735 4	0.03
^{95}Mo	5/2	15.7	−0.9099	−0.015
^{97}Mo	5/2	9.5	−0.9289	0.17
^{55}Mn	5/2	100	3.4610	0.4
^{99}Tc	9/2	—	5.6847	0.34
^{61}Ni	3/2	1.2	−0.750	0.162
^{63}Cu	3/2	69.1	2.2206	−0.211
^{65}Cu	3/2	30.9	2.3789	−0.195
^{67}Zn	5/2	4.1	0.8733	0.16
^{69}Ga	3/2	39.8	2.011	0.232
^{71}Ga	3/2	60.2	2.555	0.146
^{115}In	9/2	95.7	5.507	1.161
^{73}Ge	9/2	7.6	−0.877	−0.29
^{75}As	3/2	100	1.439	0.3
^{121}Sb	5/2	57.3	3.363	−0.5
^{209}Bi	9/2	100	4.111	−0.4
^{33}S	3/2	0.8	0.6438	−0.064

Of course the efficient relaxation in low symmetry species can be used to advantage; for example, in exchanging systems with a dominating species of high symmetry the linewidth of the observed signal will be very sensitive to the amount of low symmetry species present.

In the previous review on less common quadrupolar nuclei in this series[1] the basic NMR properties were treated quite extensively especially for the alkali and alkaline earth metal ions. Since then a few review articles have appeared dealing with subjects very similar to this. These are collected in three recent volumes.[2-4]

Naturally there is not a clear and time independent definition of what should be considered a less common nucleus. In the present context it is of course a nucleus that is not studied very much by NMR, and this will directly exclude several quadrupolar nuclei from this review. In addition to the ones already excluded from the previous review in this series,[1] ^{2}H, ^{10}B, ^{11}B, ^{14}N, ^{17}O and the halogens, also ^{6}Li, ^{7}Li, ^{23}Na, ^{27}Al and ^{59}Co, will not be considered here because they cannot, in the reviewer's opinion, be thought of as less common. Both ^{27}Al and ^{59}Co have their own chapters in references 2 and 3, and lithium and sodium NMR has been extensively reviewed.[2-4] This review is intended to cover the literature for the five-year period from mid-1978 to mid-1983. NMR in the solid state and of ordered systems like liquid crystals has not been included. In Table 1 are collected the physical properties of the nuclei included in this review.

Throughout this chapter $W_{\frac{1}{2}}$ will be used for the width at half height of the signal in Hz, χ in MHz is the quadrupole coupling constant and δ in ppm is the chemical shift, positive for increasing frequency. θ, sometimes referred to, is the resonance frequency in a field where the proton resonance frequency for TMS is 100.00 MHz.

II. ALKALI METALS (EXCEPT Li AND Na)

During the period covered by this review two other reviews dealing with alkali metal NMR have been published and the reader interested in lithium or sodium NMR, or the basic aspects of alkali metal NMR, is referred to these reviews.[2-4]

A. Potassium-39

The ^{39}K isotope is the only one of the three potassium isotopes that has been used in NMR studies reviewed here.

Molten potassium salts at 200 °C have been studied[5] and the ^{39}K chemical shift is found to be quite sensitive to the nature of the counter-ion. Chemical shifts obtained are 13.1, 17.0 and 43 ppm for KSCN, $LiNO_3/KNO_3$ (43:57)

and NaOH/KOH (50:50), respectively. It is also interesting to note that the chemical shift for an aqueous solution of KSCN increases with concentration towards the value in the molten salt (Fig. 1).
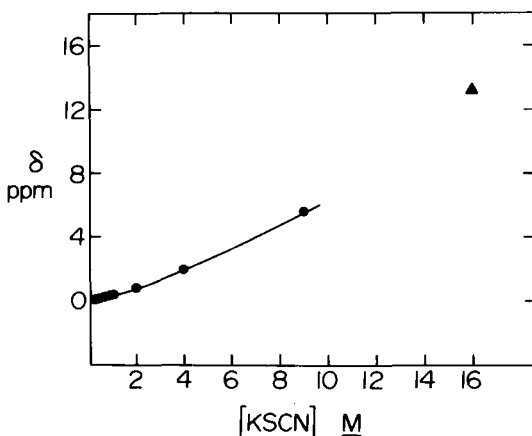
FIG. 1. ^{39}K resonance as a function of KSCN concentration in aqueous solution at 23 °C; ▲ indicates the ^{39}K resonance of molten KSCN at 200 °C. From reference 5, with permission.

Popov and co-workers[6-8] have used ^{39}K NMR to study the formation of complexes in non-aqueous media. ^{39}K chemical shifts, as well as the corresponding linewidths, show rather small changes with added 2,2'-bipyridine; in fact the variations are much smaller than those observed for ^{23}Na. The data show that the strength of interaction between 2,2'-bipyridine and alkali metal ions increases in the order $K^+ < Na^+ < Li^+$ and there is no detectable interaction with Cs^+.[6]

The complexation kinetics of K^+ ions to 18-crown-6 (18C6) in non-aqueous solvents have been studied using ^{39}K NMR.[7] A typical temperature dependence in ^{39}K T_2 is shown in Fig. 2 and this clearly shows the transfer from slow to fast exchange conditions. The lifetime of the solvated species is calculated from the equation

$$1/\tau_A = \frac{(1/T_{2B} - 1/T_2)(1/T_2 - 1/T_{2A})p_B}{1/T_{2av} - 1/T_2} \qquad (1)$$

where

$$1/T_{2av} = p_A/T_{2A} + p_B/T_{2B}$$

p_A, p_B, T_{2A} and T_{2B} are the populations and relaxation times in the solvated and complexed species, respectively, and $1/T_2 = \pi W_{\frac{1}{2}}$.
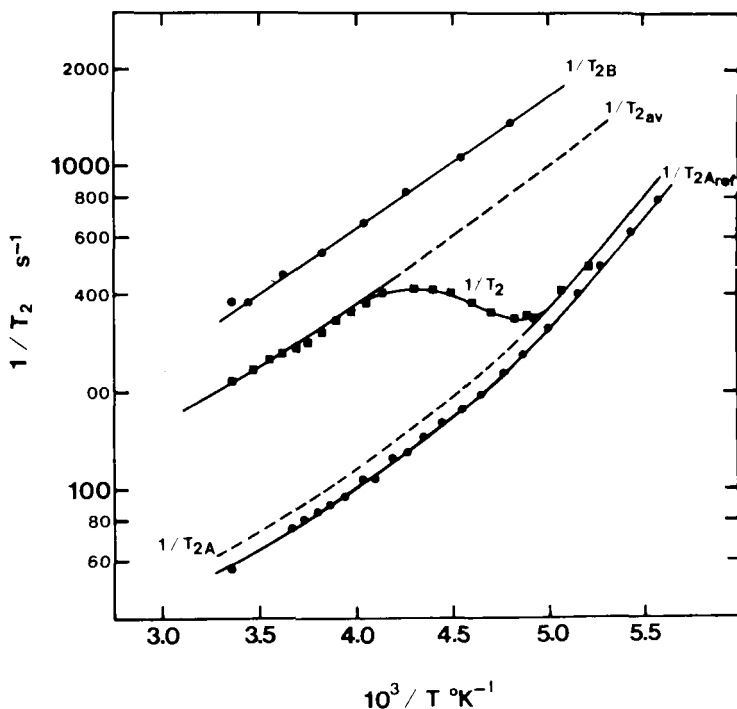
FIG. 2. Semilog plots of $1/T_2$ versus $1/T$ for ^{39}KI–18C6 solutions in methanol at ligand/K^+ ratios of 0 $(1/T_{2Aref})$, 0.5 $(1/T_2)$ and 1.0 $(1/T_{2B})$. From reference 7, with permission.

The semilog plots of $\log(1/\tau_A)$ versus $1/T$ are linear for all solvents and the activation energies for the exchange have been calculated (Table 2). The Arrhenius energy of activation varies dramatically from 9.2 kcal mol^{-1} for acetone and methanol solutions to 16.8 kcal mol^{-1} for 1,3-dioxolan solution; however, the free energy of activation varies only from 9.5 to 11.7 kcal mol^{-1}. The exchange may proceed via two mechanisms,[9] either a bimolecular process or a dissociative mechanism:

$$*K^+ + K^+ \cdot 18C6 \; \underset{k_{-1}}{\overset{k_1}{\rightleftharpoons}} \; *K^+ \cdot 18C6 + K^+ \qquad (2)$$

$$K^+ + 18C6 \; \underset{k_{-2}}{\overset{k_2}{\rightleftharpoons}} \; K^+ \cdot 18C6 \qquad (3)$$
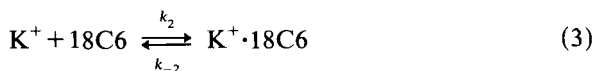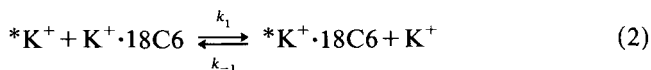
Both processes may contribute to the overall potassium ion exchange, and only if there is a contribution from the bimolecular process will the lifetime of the complex be concentration dependent. Schmidt and Popov,[7] however,

TABLE 2

Activation parameters for the $K^+\cdot18C6$ exchange in various solvents.[a]

Solvent	E_a (kcal mol^{-1})	$\Delta H^{\ddagger}$ (kcal mol^{-1})	$\Delta S^{\ddagger}$ (cal mol^{-1} K^{-1})	$\Delta G_{298}^{\ddagger}$ (kcal mol^{-1})
Acetone	9.2 ± 0.5	8.6 ± 0.5	-4 ± 2	9.8 ± 0.1
Acetone–1,4-dioxan	13.8 ± 0.5	13.2 ± 0.5	12 ± 2	9.6 ± 0.1
Methanol	9.2 ± 0.7	8.6 ± 0.7	-3 ± 3	9.5 ± 0.2
1,3-Dioxolan	16.8 ± 0.3	16.2 ± 0.3	15 ± 1	11.70 ± 0.01
1,3-Dioxolan[b]	15.5 ± 0.7	16.9 ± 0.7	11 ± 2	11.67 ± 0.03

[a] $18C6/K^+ = 0.5$.
[b] $18C6/K^+ = 0.25$.

discuss the exchange in terms of the lifetime of the solvated ion, and their conclusion that the exchange follows the bimolecular process is not convincing.

Contrary to $18C6\cdot K^+$ complexes, the cryptate $C222\cdot K^+$ provides well resolved ^{39}K resonances for both solvated and complex K^+ ions (Fig. 3).
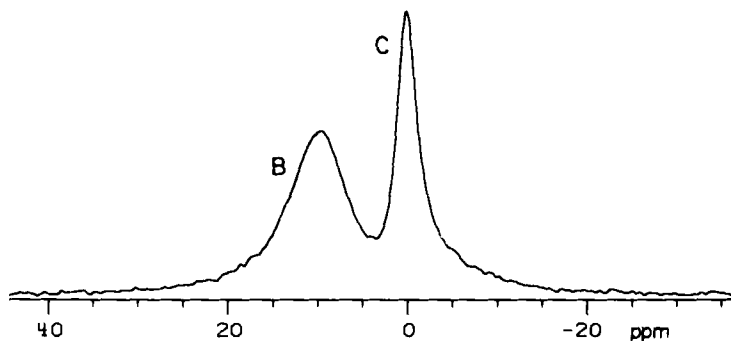
FIG. 3. ^{39}K NMR spectrum of a solution (methanol D$_2$O, 95:5) with 20 mM C222 and 30 mM KSCN; signal B is due to the $C222\cdot K^+$ complex and signal C to free, solvated, K^+ ions. From reference 10, with permission.

Shih and Popov[8] have studied the potassium complexes of C222, C221 and C211 in various solvents. The results are shown in Table 3. Neurohr et al.[10] have studied the complexes of several ligands in methanol–water (95:5); they have observed their relaxation behaviour in order to calculate the quadrupole coupling constants, χ, from the equation

$$1/T_1 = 1/T_2 = \frac{2\pi^2}{5}\chi\tau_c \tag{4}$$

TABLE 3

^{39}K chemical shifts^a in various solvents (δ_{free}) and in cryptates C222·K$^+$ and C221·K$^+$.

Solvent	δ_{free}	δ (C222·K$^+$)	δ (C221·K$^+$)
Nitromethane	−22.3	2.5	—
Methanol	−11.3	2.5	14.4
Acetone	−12.1	3.0	12.6
Dimethylformamide	−5.3	2.0	14.3
Acetonitrile	−1.8	2.4	13.5
Pyridine	0.2	—	15.0

^{a} The shifts are in ppm relative to potassium salt at infinite dilution in water.

The value of χ can be calculated only if there is an independent measure of the correlation time, τ_c, which could be determined from the ^{13}C relaxation times by assuming that the correlation time is the same for the ^{39}K$^+$ ion and ^{13}C nuclei in the ligand. The results are shown in Table 4. When the shift is dominated by the paramagnetic shielding term a linear relationship is expected between the shift and quadrupole coupling constant, as demonstrated for ^{23}Na.[11] The data in Table 4 indicate that for ^{39}K there is also a linear relationship between χ and the chemical shift.

TABLE 4

^{39}K linewidths ($W_{\frac{1}{2}}$), spin–lattice relaxation times (T_1), chemical shifts (δ) and quadrupole coupling constants (χ) for some potassium complexes.

Ionophore	$W_{\frac{1}{2}}$ (Hz)	T_1 (ms)	δ^a (ppm)	χ^b (MHz)
18-crown-6	117	2.6	−5.7	2.4
C222	129	2.3	−1.9	2.6
Valinomycin	248	1.3	−25.6	1.2
X-537A	250	1.3	−7.3	1.9^c

^{a} Recalculated to be the same scale as in Table 3 using a shift of −11.3 ppm for 30 mM KSCN in methanol-D$_2$O (95:5).
^{b} Calculated with the aid of τ_c from ^{13}C relaxation data.
^{c} Calculated assuming $\tau_c = 6 \times 10^{-11}$ s.

In a few cases ^{39}K has been used in biochemical studies,[12-15] and there is one report using ^{39}K NMR to study polysaccharide gels.[16] Detellier and Laszlo[12,13] have studied the role of alkali metal ions in the self assembly of 5'-guanosine monophosphate. These results are discussed in the next section.

B. Rubidium-87

Rubidium is the least studied alkali metal even though it has two quad-rupolar isotopes, [85]Rb and [87]Rb. [87]Rb has a reasonably high receptivity; however, its quadrupole moment, combined with the Sternheimer antishield-ing factor, results in lines that are seldom less than 200 Hz wide.

Khazaeli et al.[17] have studied the concentration dependence of the [87]Rb chemical shift and linewidth of the RbI signal in water, methanol and propylene carbonate. They find, in agreement with an earlier report,[18] that the variation of the chemical shift with concentration is non-linear for all solvents. Relationships much closer to linear are obtained when the chemical shifts are plotted versus the mean activity of the solute. Attempts to study the complex formation between Rb^{+} and 18C6 or C222 fail, probably because the [87]Rb resonance from the complexed ions is too broad to be observed.

In a study of the self assembly of 5'-guanosine monophosphate (5'-GMP) mainly ^{23}Na NMR, but also [39]K and [87]Rb NMR, has been used.[12] The authors perform a detailed analysis, mainly based on the ^{23}Na NMR data, resulting in the conclusion that 5'-GMP forms octameric aggregates with a correlation time of c. 10 ns. The aggregation from $(5'\text{-GMP})_4$ to $(5'\text{-GMP})_8$ is mediated by K^{+} ions, which can be seen from [39]K NMR as well as from ^{23}Na NMR. Figure 4 shows that the width of the [39]K resonance increases
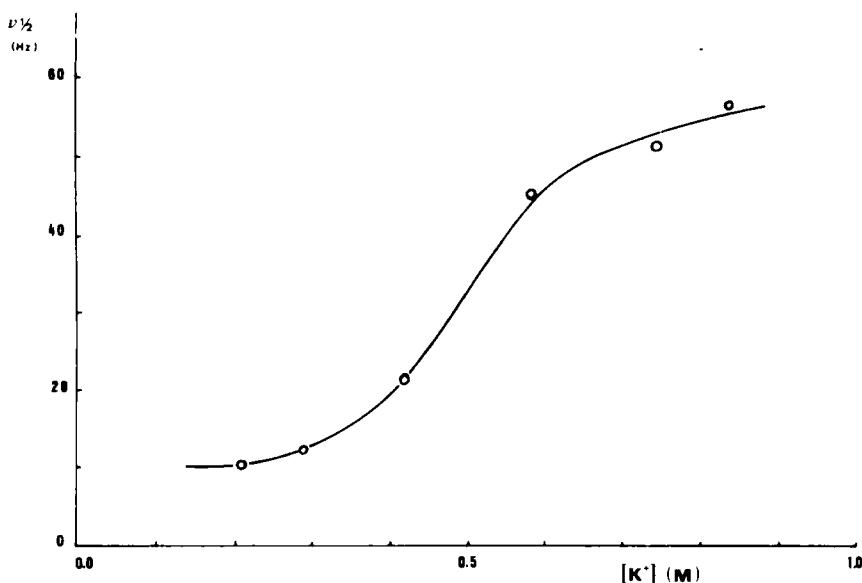
FIG. 4. Variation of the [39]K linewidth as a function of KCl concentration for a solution 0.1 M in (5'-GMP, Na$_2$). From reference 12, with permission.

with increasing KCl concentration in the presence of 0.1 M (5'-GMP, Na$_2$) and the width of the ^{23}Na resonance displays a similar dependence on the KCl concentration. This shows that increasing the K$^+$ concentration above c. 0.5 M creates new binding sites for both K$^+$ and Na$^+$, and furthermore that there are specific sodium sites which are not occupied by either potassium or rubidium.

Raushel and Villafranca[14] have used, among others, ^{39}K, ^{85}Rb, ^{87}Rb and ^{133}Cs NMR to study the binding of monovalent cations to pyruvate kinase. They demonstrate, using Mn^{2+} as a relaxation probe, that the Mn^{2+}-M$^+$ distance varies for the different monovalent cations, being smallest for K$^+$ (3.7 Å) and largest for Cs$^+$ (6.0 Å). They also show that, depending on the relaxation properties of the ions, they are sensitive to different Mn^{2+}-M$^+$ distances. ^{39}K$^+$, ^{85}Rb$^+$ and ^{87}Rb$^+$ can only be used for distances of up to 8 Å whereas ^{7}Li$^+$, ^{6}Li$^+$, ^{133}Cs$^+$ and ^{15}NH$_4{}^+$ can be used for distances between 12 and 20 Å and ^{14}NH$_4{}^+$ and ^{23}Na$^+$ are suitable for use at intermediate distances.

C. Caesium-133

The ^{133}Cs nucleus has a relatively high receptivity and a small quadrupole moment, making it attractive for NMR studies. In spite of these favourable properties there appear to be few people who have been working with this nucleus.[19-24] Khazaeli et al.[19] have studied the formation of ion pairs and triple ions of caesium salts in methylamine solutions using ^{133}Cs NMR and conductance measurements. Figure 5 shows the concentration dependence of the ^{133}Cs chemical shift for CsBPh$_4$, CsSCN and CsI. Since the limiting shift at infinite dilution has to be the same for all three salts, it is obvious that ion pair formation must be very strong for both CsBPh$_4$ and CsI, with half saturation values well below 1 mM. An attempt to treat these concentration variations as caused solely by ion pairing has not succeeded, and the authors therefore use the following model:

$$Cs^+ + X \xrightleftharpoons{K_{ip}} Cs^+ \cdot X^- \tag{5}$$

$$X^- + Cs^+ \cdot X^- \xrightleftharpoons{K_{ta}} X^- \cdot Cs^+ \cdot X^- \tag{6}$$

$$Cs^+ + Cs^+ \cdot X^- \xrightleftharpoons{K_{tc}} Cs^+ \cdot X^- \cdot Cs^+ \tag{7}$$
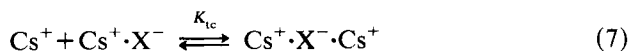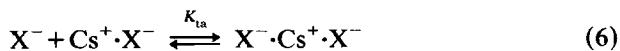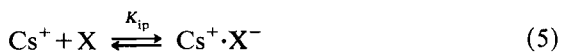
where K_{ip}, K_{ta} and K_{tc} are the formation constants of the ion pair and the anionic and cationic triple ions, respectively. The chemical shift can then be calculated from $\delta = \sum_i x_i \cdot \delta_i$, where x_i and δ_i are respectively the mole fraction and chemical shift of species i. This treatment, using some simplifying assumption like $K_{ta} = K_{tc}$ and $\delta(Cs^+ \cdot X^-) = \delta(Cs^+ \cdot X^- \cdot Cs^+)$, results in a
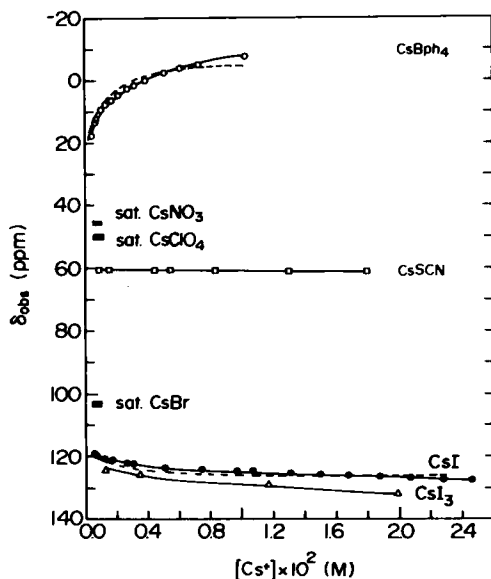
FIG. 5. Concentration dependence of the ^{133}Cs chemical shift of caesium salts in methyl-amine at 25 °C. The dashed curves are calculated using the simple ion pair model and the solid curves are calculated from the full model. From reference 19, with permission.

satisfactory agreement between observed and calculated chemical shifts. Also, thermodynamic parameters are calculated by using the concentration dependence of the ^{133}Cs chemical shift at various temperatures and assuming that the shift has a linear dependence on temperature. The values of K_{ip} obtained are 2.5×10^5 and 1.2×10^4 M^{-1} for CsI and CsBPh$_4$, respectively, and the chemical shifts for the ion pairs are found to be 124.5 ppm for CsI and -16.1 ppm for CsBPh$_4$. However, the association constant calculated from conductance data does not agree with the one derived from the NMR data, which the authors explain as being caused by the inadequacy of the conductance equation. Arkhipovich et al.[25] have used ^{133}Cs NMR and conductance measurements to study the association of Cs$^+$ ions with poly-ethylene oxide. They find, from competition experiments, that the binding strength decreases with increasing ionic radius.

In a series of papers Popov and co-workers have reported their studies on Cs$^+$ binding to crown ethers.[20-23] When larger rings, 21C7 to 30C10, are used the dependence of ^{133}Cs chemical shift on the ligand/Cs$^+$ ratio is in agreement with the formation of a 1:1 complex as seen in Fig. 6, and the
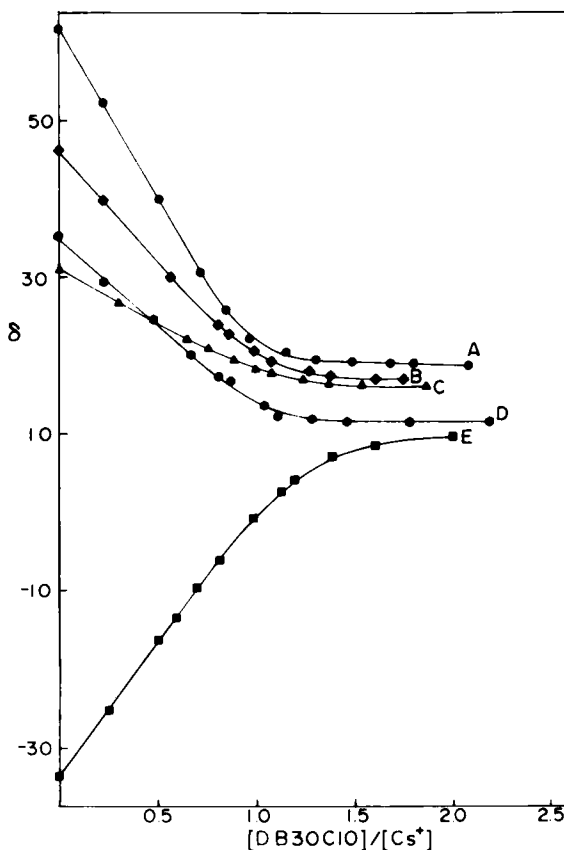
FIG. 6. ^{133}Cs chemical shifts at various [DB30C10]/[Cs^{+}] mole ratios in different solvents: A, nitromethane; B, methanol; C, acetone; D, pyridine; E, acetonitrile. From reference 21, with permission.

binding constants for Cs^{+} to the four ligands 21C7, 24C8, 27C9 and 30C10 in various solvents are found to be of the order of 10^{4} M^{-1}. Only for the solvents DMF and DMSO are significantly lower binding constants obtained. For the smaller ring 18-crown-6, however, the ^{133}Cs chemical shift variation is not explained without assuming the formation of more than the 1:1 complex as can be seen in Fig. 7. The variation in the ^{133}Cs chemical shift is linear in 18-crown-6/Cs^{+} ratios from 0 to 1 and the binding constant for the 1:1 complex can therefore only be given a lower limit of 10^{4} M^{-1}. Since it has been shown that the ion pair formation is very strong[19] this has to be taken into account when the binding constant for the 2:1 complex is calculated. In addition to ion pair and triple ion formation, equations
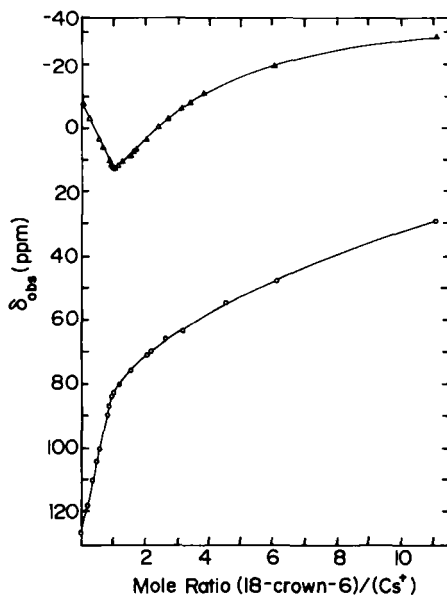
FIG. 7. ^{133}Cs chemical shifts versus $[18C6]/[Cs^+]$ mole ratios in methylamine at 25 °C: (upper curve) CsI at 0.02 M; (lower curve) $CsBPh_4$ at 0.01 M. From reference 22, with permission.

(5)–(7), the following equations are considered:

$$Cs^+ + C \overset{K_C}{\rightleftarrows} CsC^+ \tag{8}$$

$$Cs^+\cdot X^- + C \overset{K_X}{\rightleftarrows} CsC^+\cdot X^- \tag{9}$$

$$CsC^+ + X^- \overset{K_A}{\rightleftarrows} CsC^+\cdot X^- \tag{10}$$

$$CsC^+ + C \overset{K_{C2}}{\rightleftarrows} CsC_2^+ \tag{11}$$

$$CsC_2^+ + X^- \overset{K_{A2}}{\rightleftarrows} CsC_2^+\cdot X^- \tag{12}$$

$$CsC_2^+\cdot X^- \overset{K_{X2}}{\rightleftarrows} CsC^+\cdot X^- + C \tag{13}$$
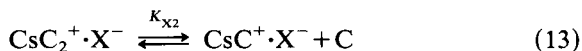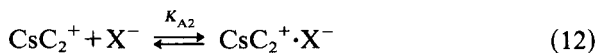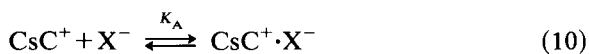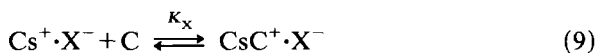
where C represents the crown ether. An analysis based on the above assumption, and assuming that $\delta(CsC_2^+) = \delta(CsC_2^+\cdot X^-)$, results in values for the chemical shifts of all species present in the solution, together with the thermodynamic parameters for the above equilibria. The chemical shifts are collected in Table 5.

In complexes with sufficiently slow metal exchange the NMR spectrum consists of separate signals for free (solvated) ions and complexes. Figure

TABLE 5

^{133}Cs chemical shifts (ppm) for some ion pairs, triple ions and 18-crown-6 (C) complexes in methylamine at 25 °C.

	Salt		
Species	CsI	CsBPh$_4$	CsSCN
Cs$^+$	60	60	60
Cs$^+\cdot$X$^-$	124.2	−13.1	60
X$^-\cdot$Cs$^+\cdot$X$^-$	469	−280	—
CsC$^+\cdot$X$^-$	82.7	9.0	32.5
CsC$_2^+$	−46.2	−49.4	—

8 shows a nice example of this, and furthermore the temperature dependence shows a variation from slow exchange at −40 °C to fast exchange at 60 °C.[24] The chemical shift of ^{133}Cs in a methanol solution containing an excess of C322 is temperature independent, contrary to the shielding effect found for free ions in the same solvent. This indicates that the Cs$^+$ ion is completely enclosed by the ligand, i.e. an inclusion complex. The result is not unexpected since the cavity in the C322 ligand is slightly larger than the caesium ion, which therefore fits inside the ligand. The ^{133}Cs chemical shift of a 1:1 mixture of caesium thiocyanate and cryptand C222 is temperature dependent, reaching a limiting value below −100 °C, $\delta = 244$ ppm. This is interpreted as being caused by an equilibrium between inclusion and exclusion Cs$^+\cdot$C222 complexes, with the inclusion complex dominating at low temperatures, since the low temperature ^{133}Cs chemical shift is independent of solvent. The very large ^{133}Cs deshielding for the Cs$^+\cdot$C222 inclusion complex (244 ppm) is explained as being caused by a strong overlap between the donor atoms (ring oxygens) and the outer p orbitals of the caesium ion. The ^{133}Cs shielding of the exclusion complex, where no such strong orbital overlap is forced on the caesium ion, is expected to be greater than that from the inclusion complex, in agreement with the analysis of the temperature dependence data.

III. ALKALINE EARTH NUCLEI

During the past few years there has been increasing interest in using ^{25}Mg and ^{43}Ca NMR in studies of biochemical interest, whereas little attention has been paid to more basic studies. A few review articles covering ^{25}Mg and ^{43}Ca have appeared.[3,4,26,27] Beryllium, strontium and barium have been almost neglected.
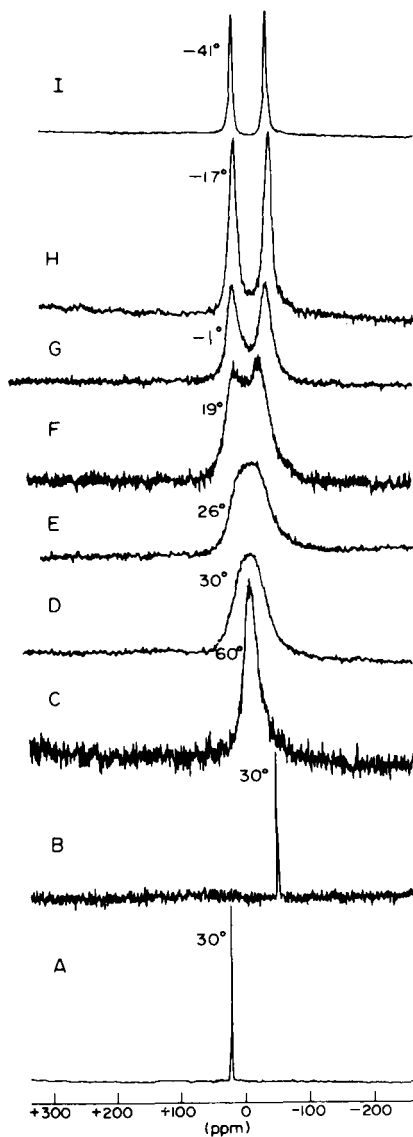
FIG. 8. ^{133}Cs spectra of: (A) a solution containing CsSCN and excess of C322; (B) uncomplexed Cs$^+$ in methanol; (C to I) a methanol solution 0.05 M in C322 and 0.10 M in CsSCN at various temperatures. From reference 24, with permission.

A. Solvation studies

Heubel and Popov[28] have studied the solvation of Mg^{2+} in various solvents by ^{25}Mg NMR. In agreement with earlier studies,[29] they find that in water solution there is no change in the ^{25}Mg chemical shift due to variation in concentration or counter-ion, and the observed broadening at higher concentrations can best be explained as being caused by viscosity effects. In non-aqueous solvents, however, quite dramatic effects are observed on ^{25}Mg chemical shifts as a function of Mg salt concentration.[28] By adding I_2 to magnesium halide solutions in acetonitrile or propylene carbonate, Heubel and Popov[28] show convincingly that the ^{25}Mg shift changes are caused by ion pairing. Addition of I_2 changes the shift almost linearly up to a $Mg:I_2$ ratio of 2. Further addition of I_2 does not affect the ^{25}Mg shift. The shift variation is caused by the formation of the bulky XI_2^- ion, which does not form ion pairs as readily as the X^- ion itself. This effect is much less pronounced in polar solvents like DMF, and even MeOH and DMSO, where ion pairing between Mg^{2+} and X^- is much reduced. Another manifestation of the ion–ion interaction in non-polar solvents is the broad ^{25}Mg NMR signals observed in these solvents.

Bouhoutsos-Brown and Bryant[30] have found that the width of the ^{25}Mg signal depends on the amount of water added to a methanol solution of $MgCl_2$ at $-40\,°C$. The linewidth is found to increase monotonously up to a $H_2O/MeOH$ ratio of 0.15, whereafter it stays essentially constant. In solutions containing small amounts of water the signal is strongly non-Lorentzian. This is explained as being caused by the coexistence of at least two species giving rise to ^{25}Mg NMR signals with different linewidths and in slow exchange with each other. The broad resonance should be assigned to one or more species containing a mixture of H_2O and MeOH ligands in the first coordination sphere and the narrow resonance is assigned to the symmetrical methanol complex. There has been a recent study of the solvation of calcium in various solvents using ^{43}Ca NMR.[31] In this work the concentration dependence of the ^{43}Ca chemical shift is studied for several solvents, including water. It is found that the ^{43}Ca shift is much more concentration dependent, in water, when using oxyanions like NO_3^- or ClO_4^- instead of halides as counter-ions. This is explained as being caused by the higher tendency of the oxyanions to form contact ion pairs, because these ions are less hydrated in water than the halide ions. On the one hand, for non-aqueous solutions, it is found that with methanol there is a 25 ppm shielding increase in the concentration range 0.15–1.5 M for $CaCl_2$, whereas there is a shielding decrease of c. 5 ppm for $Ca(ClO_4)_2$ in the same concentration range. On the other hand, in dimethylformamide solution there is no concentration dependence in the ^{43}Ca shift. These studies have not been performed at concentrations below 0.15 M, making

an extrapolation to infinite dilution uncertain, but there is a correlation between the Gutman donicity scale[32] and the estimated shifts at infinite dilution.[31]

B. Complex formation

Rode et al.[33] have studied the effect of N-substitution in amides on their interaction with ^{7}Li, ^{23}Na and ^{9}Be. For ^{9}Be the largest effect is observed for DMF, which causes a shielding increase of c. 2.5 ppm relative to formamide. They have tried to correlate the shifts with calculated atomic charges or orbital densities at the metal nucleus, but with little success. Similarly Kraft et al.[34] have tried to correlate the chemical shifts observed for ^{7}Li, ^{23}Na, ^{39}K, ^{25}Mg and ^{43}Ca caused by complexation with dicarbonyl ligands. Again the agreement between observed chemical shifts and ab initio calculated electron populations is not satisfactory.

Gaines et al.[35] have studied several beryllaboranes and a few other compounds by ^{9}Be NMR, and they also observed the first example of a ^{9}Be-^{11}B spin coupling (in ^{11}B NMR). Several (C_5H_5)BeX compounds, all having very highly shielded ^{9}Be resonances with very little dependence on X, have been studied. The high shielding is ascribed to paramagnetic ring current effects from the C_5H_5 ring.

The Wehrlis[36] have used ^{9}Be NMR to study $BeCl_2$ dissolved in dry acetonitrile. At room temperature they observe two narrow and one broad signal all within 1.7 ppm. At $-40\,°C$ four resonances are observed with chemical shifts ranging from 0 to -2.68 ppm. The signals are assigned as shown in Fig. 9. Addition of Cl^- ions to the solution results in an increase in the intensity of the 0 and -1.26 ppm signals and a decrease in the -2.68 ppm signal whereas water addition (moist air) results in the appearance of two new resonances at -1.15 and -2.32 ppm which are assigned to $BeCl_2(H_2O)_2$ and $BeCl(H_2O)_3{}^+$ or $BeCl_2(H_2O)CH_3CN$, respectively.

Bouhoutsos-Brown et al.[37] have studied the pH dependence of the ^{25}Mg NMR signal from a solution containing equimolar amounts of Mg^{2+} and EDTA. In the pH interval between 7 and 9 they observe two ^{25}Mg resonances with widely different linewidths and, apparently, the same chemical shift. This once more shows that the ^{25}Mg chemical shift does not vary much, and the interesting parameters in ^{25}Mg NMR studies are therefore the relaxation rates and the linewidth. The sharp line observed by Bouhoutsos-Brown et al.[37] also shows that the exchange

$$Mg^* + MG \cdot EDTA \rightleftarrows Mg + Mg^* EDTA$$
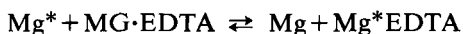
is slow on the NMR time scale even though the binding constant is not very large for the Mg·EDTA complex in this pH interval. This is in agreement with an "on" rate for Mg^{2+} limited by the "off" rate of the water molecules
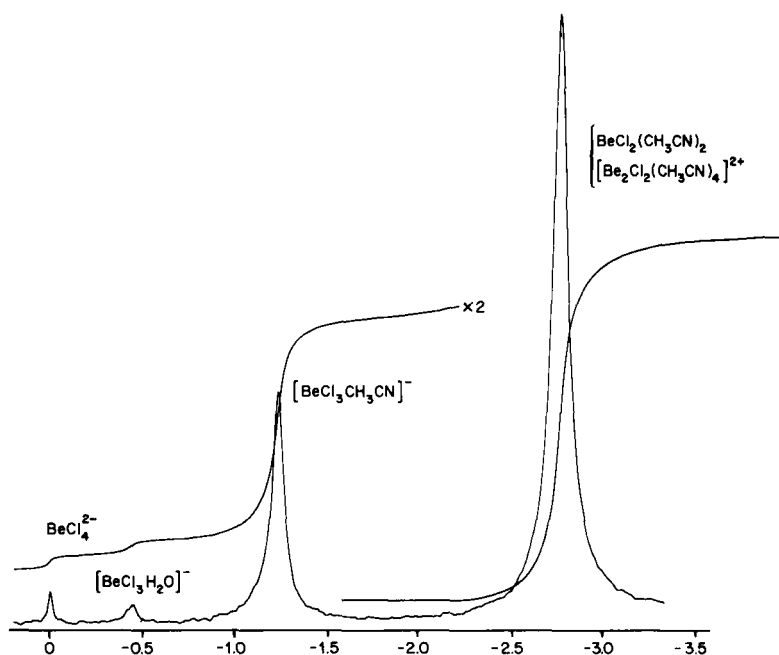
FIG. 9. 56.2 MHz ^{9}Be spectrum of 0.018 M anhydrous beryllium chloride in acetonitrile recorded at −40 °C; peak assignments are as indicated. From reference 36, with permission.

from the solvated Mg^{2+} ion.[38] For ^{43}Ca, however, the broadening caused by complexation to EDTA is small and two well resolved resonances, from free and complexed Ca^{2+} ions, have been observed.[31,37,39] In addition, the values of χ have been determined for ^{43}Ca in Ca·EDTA and Ca·EGTA to be 0.5 and 2.1 MHz, respectively.[39] ^{43}Ca chemical shifts from −40 to 30 ppm have been observed for complexes containing either only oxygen ligands or a mixture of oxygen and nitrogen ligands.[27] Complexes which may use only oxygens in the coordination show high ^{43}Ca shielding whereas the ^{43}Ca complexes of EDTA, EGTA and EDTMP are deshielded, all relative to the Ca^{2+}(aq.) ion. It should be noted that there is a four-fold increase in the value of χ in passing from ^{43}Ca(EDTA) to ^{43}Ca(EGTA),[39] showing that the value of χ can be very sensitive to variations in the geometry of the complex.

C. Biochemical applications

The main development in the area of alkaline earth NMR is undoubtedly in applications to biochemical problems. These studies have developed

along two different lines. Either an excess of metal ions ($^{25}Mg^{2+}$ or $^{43}Ca^{2+}$) over possible binding sites on a protein or any other macromolecule is used and the effect on the "free" signal transferred via exchange from ions bound is studied, or equimolar ratios metal:site are used and the NMR signals from ions bound to the macromolecule are studied directly. The uses of ^{25}Mg and ^{43}Ca NMR in the study of calcium binding proteins have been reviewed recently.[40] ^{25}Mg and ^{43}Ca NMR have been used to study the metal ion binding to prothrombin fragment 1.[41-43] pH titration studies have shown that the Mg^{2+} binding has pK_a values at 4.2 and above 7. The low pK value agrees well with that found for small γ-carboxyglutamic acid containing peptides. The high pK has no counterpart in small peptides, indicating that groups other than the carboxyls are involved in the calcium and magnesium binding. Competition between Mg^{2+} and Ca^{2+} for the binding sites in fragment 1 has also been studied.[43] These experiments show that the two ions only partly compete for the same sites. For example, a study of the ^{25}Mg linewidth as a function of pH at high Ca^{2+} concentration shows that the high pK value has disappeared. Accordingly it is shown that for calcium, observed by ^{43}Ca NMR, dependence of the low pK_a value is suppressed by the addition of magnesium, whereas the dependence of the high pK_a value remains largely unaffected. Sarasua et al.[44] have used ^{43}Ca and ^{25}Mg NMR to study the metal ion binding to human blood clotting factor XIII. They find for this protein that the binding of calcium is significantly stronger than that of magnesium, but these dissociation constants are much higher than those found for fragment 1.

^{25}Mg and ^{43}Ca NMR have been used extensively to study metal binding to calcium binding proteins.[45-56] In the first studies on metal binding to parvalbumin[45,46] a large excess of metal ions was used and only effects transferred to free ions via exchange could be studied. It was thus found that the exchange rate of the two strongly bound Ca^{2+} ions is slow, resulting in a sharp ^{43}Ca NMR signal from the free ions.[45] For magnesium under similar conditions, however, the ^{25}Mg signal broadens significantly and a temperature dependence typical for intermediate exchange is observed.[46] Furthermore, it is observed that magnesium and calcium compete, with about the same binding constant, for the site causing this broadening. This shows that the site observed cannot be either of the two strong calcium binding sites since they are known to have binding constants for Ca^{2+} that are several orders of magnitude higher than those for Mg^{2+}.

In more recent work, especially using ^{43}Ca NMR, calcium concentrations in the mM range have been used, which has enabled the direct study of NMR signals of protein bound ions.[50,52] By doing so it is possible to determine not only the product of the correlation time, τ_c, and χ but also the values themselves. This is possible because the correlation time is sufficiently long to result in the breakdown of the extreme narrowing

condition, and therefore, by measuring T_1 and T_2, τ_c is calculated from the equation

$$T_2/T_1 = \frac{0.2J(\omega) + 0.8J(2\omega)}{0.3J(0) + 0.5J(\omega) + 0.2J(2\omega)} \tag{14}$$

where $J(\omega) = \tau_c/(1 + \omega^2\tau_c^2)$ and χ is calculated from

$$1/T_1 = \frac{3\pi^2}{10} \cdot \chi^2 \cdot \frac{2I+3}{I^2(2I-1)}[0.2J(\omega) + 0.8J(2\omega)] \tag{15}$$

It is thus found that the correlation time for the ^{43}Ca nucleus is the same as that for the whole protein, showing that the mobility of the Ca^{2+} ion within the sites is very limited. In several cases ^{43}Ca NMR has been used to determine the Ca^{2+} ion exchange rate,[47,48,54] resulting in "off" rates of 10^3, 10^3 and $600\,s^{-1}$ for prophospholipase A_2, calmodulin and troponin C, respectively. These numbers are calculated from the temperature dependence of the ^{43}Ca NMR lineshape, and a scheme for performing the calculations has been published.[56]

Shimizu and co-workers[57-60] have also used ^{25}Mg and ^{43}Ca to study metal–protein interaction. They have used a large excess of metal ion; they consistently discuss the linewidth of the signal from bound ions which they appear never to observe. They have in this way studied the interaction between ^{25}Mg^{2+} and creatine kinase[57] and acetate kinase,[60] and the interaction between ^{43}Ca^{2+} and thermolysin[58] and tetrahymena calmodulin.[59]

Bishop et al.[61] have shown that ^{25}Mg^{2+} can be used to study the interaction between magnesium ions and proteins, serum albumin and an Fe protein of nitrogenase. Using previously determined numbers of binding sites[62,63] they have derived linewidths for the bound ^{25}Mg^{2+} ions of 2750 Hz for the nitrogenase and 1000 Hz for serum albumin. These values are surprisingly small and could be the result of slow exchange, which has not been properly checked for.

The interaction of Mg^{2+} and Ca^{2+} with DNA has been studied with ^{25}Mg and ^{43}Ca NMR. First Reimarsson et al.[64] showed that the ^{25}Mg NMR signal has a temperature dependence indicative of intermediate exchange, whereas for Ca^{2+} the temperature dependence of the ^{43}Ca resonance shows that this ion is in slow exchange up to the melting temperature of the DNA helix. Rose et al.[65,66] have made more thorough studies showing that the ^{25}Mg resonance is non-Lorentzian, which can be interpreted as either being due to a long correlation time in the bound site resulting in a breakdown of the extreme narrowing approximation, or it could be caused by overlapping signals, of different linewidths, which are in slow exchange.

Urry et al.[67] have used ^{43}Ca NMR to study the binding of Ca^{2+} ions to the polypentapeptide of elastin (Val-Pro-Gly-Val-Gly). They first measured T_1 as a function of temperature for a 50 mM $CaCl_2$ solution and found that

there is a strong and non-linear dependence; however, their value at room temperature agrees well with the one reported previously, $T_1 = 1.33$ s at 28 °C.[68] For a solution which is 190 mM in pentamers Urry *et al.*[67] are able to estimate a binding constant for Ca^{2+} of 9 M^{-1} from the dependence of the ^{43}Ca NMR linewidth as a function of total calcium concentration, whereas for a pentamer concentration of 1.9 M at 20 °C the data indicate that there is more than one binding site for Ca^{2+} ions on the pentamer. Finally, at higher temperatures (38 °C) the data indicate that there is a positive cooperativity in the calcium binding.

IV. MAIN GROUPS III AND IV

A. Gallium-69, gallium-71 and indium-115

Accurate determinations of the ratios of chemical shifts $(^{71}Ga)/(^2H) = 1.986\ 668\ 67$ and $(^{115}In)/(^2H) = 1.427\ 469\ 2$ have been performed[69] and extrapolated to infinite dilution. The authors have also determined the ratio $\nu(^{69}Ga)/\omega(^{71}Ga) = 0.787\ 014\ 68$.
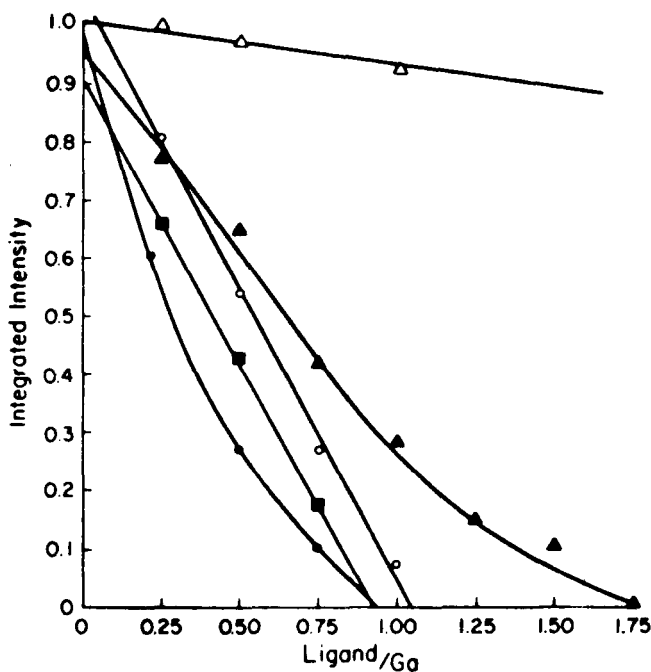
FIG. 10. The relative intensities of the $Ga(D_2O)_6^{3+}$ resonance in the presence of EDTA

In the light of the use of the radioactive isotope ^{67}Ga to localize tumours, it has been of interest to use [71]Ga NMR to study the interaction of Ga^{3+} with various buffers and chelating agents in solution.[70-72] It has thus been found that the addition of EDTA, NTA, lactate or phosphate progressively diminishes the intensity of the $^{67}Ga(D_2O)_6^{3+}$ resonance, without the appearance of any new signals.[70] The variation in the intensity of the $^{71}Ga(D_2O)_6^{3+}$ resonance as a function of added ligands is shown in Fig. 10. These plots indicate that the stoichiometry for both the EDTA and the NTA complexes is 1:1 whereas it is more than 1:1 for the lactate–Ga complex. The buffers TRIS, HEPES and MOPTS are found to have only a weak effect on the [71]Ga resonance. In a more thorough NMR study, of the interaction between Ga^{3+} and phosphate, a broad [71]Ga resonance at −273.2 ppm from $GaCl_4^-$ (compared to $Ga(H_2O)_6^{3+} = -247.7$ ppm) is observed upon addition of phosphate. This signal never amounts to more than about 30% of the total gallium population even when the $Ga(H_2O)_6^{3+}$ signal disappears, indicating that further, even broader, signals are present but not observable. This conclusion is also confirmed by means of ^{31}P NMR which shows several resonances and therefore clearly indicates the presence of several species in slow exchange with each other.[70]

For both [71]Ga and [115]In it has been found that the chemical shifts in the halide and mixed halide complexes cannot be explained by a simple additiv-

TABLE 6

[71]Ga and [115]In chemical shifts for various $M\,X_n\,Y_m\,Z_{4-m-n}$ complexes in dichloromethane.

Complex	$\delta(^{71}Ga)^a$ (ppm)	$\delta(^{115}In)^a$ (ppm)
MCl_4^-	0	0
MCl_3Br^-	−39	−52[b]
$MCl_2Br_2^-$	−83	−117[b]
$MCl_3Br_3^-$	−132	−187[b]
MBr_4^-	−186	−259
MCl_3I^-	−126	−187
$MCl_2I_2^-$	−290	−416
$MClI_3^-$	−485	−686
MI_4^-	−705	−999
MBr_3I^-	−300	−418
$MBr_2I_2^-$	−425	−606
$MBrI_3^-$	−561	−797
MCl_2BrI^-	−179	−258[b]
$MClBr_2I^-$	−237	−337[b]
$MClBrI_2^-$	−356	−513[b]

[a] Chemical shifts from reference 73.

[b] From reference 75.
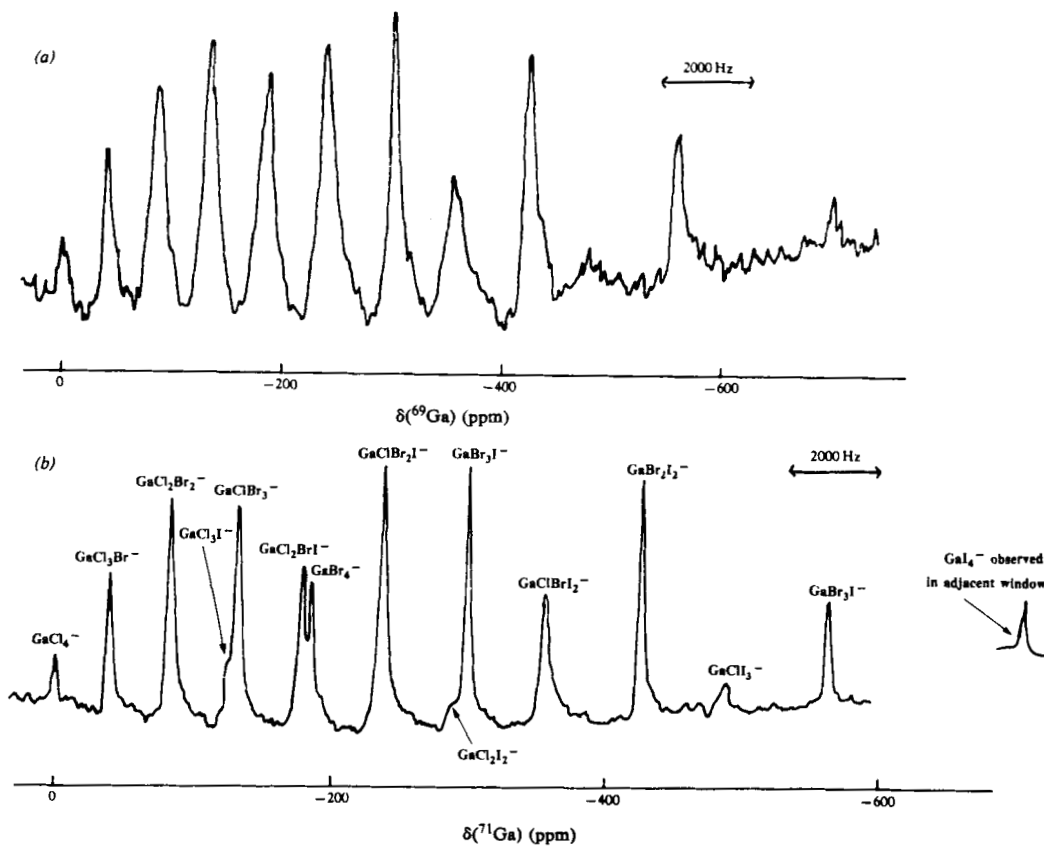
FIG. 11. (a) ^{69}Ga NMR and (b) ^{71}Ga NMR spectra of a mixture of $GaCl_4^-$, $GaBr_4^-$ and GaI_4^-. From reference 73, with permission.

ity model,[72] nor are they strictly correlated with the sum of the electronegativities of the halides.[73,74] However, using the pairwise additivity model, all chemical shifts can be reproduced to within a couple of ppm for ^{71}Ga. As can be seen from Table 6 and Fig. 11, all fifteen $^{71}GaCl_nBr_mI_{4-n-m}$ species are resolved, whereas for ^{69}Ga only twelve resonances are resolved. For ^{115}In Colton et al.[73] have not resolved the resonances from the $InCl_nBr_{4-n}$ complexes since for mixtures of $InCl_4^-$ and $InBr_4^-$ only a broad resonance is observed; however, McGarvey et al.[75] show a spectrum with five resolved resonances for such a mixture. They also show that the ^{115}In chemical shift of $InCl_4^-$ depends strongly on added Cl^-, indicating the formation of complexes with more than four Cl^-, e.g.

$$InCl_4^- + Cl^- \rightleftarrows InCl_5^{2-} \tag{16}$$

$$InCl_5^{2-} + Cl^- \rightleftarrows InCl_6^{3-} \tag{17}$$
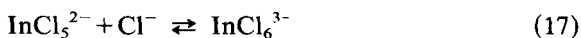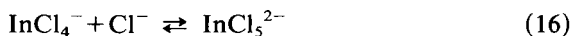
From the dependence of the ^{115}In shift on added $(C_6H_5)_4PCl$ in acetonitrile (Fig. 12), McGarvey et al.[75] have calculated the binding constants $K_5 = 350\ M^{-1}$ and $K_6 = 10\ M^{-1}$ and the chemical shifts of -115 and -235 ppm for $InCl_5^{2-}$ and $InCl_6^{3-}$. Surprisingly they do not mention if there is any line broadening during this titration. It is anticipated that signal broadening will occur when a considerable amount of the low symmetry compound $InCl_5^{2-}$ is formed.
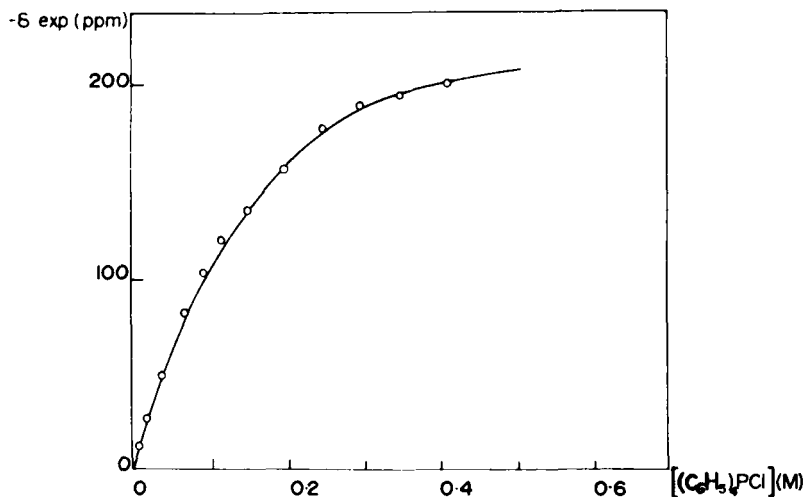
FIG. 12. ^{115}In chemical shift as a function of added $(C_6H_5)_4PCl$ in acetonitrile for a 0.1 M $[(C_6H_5)_4P][InCl_4]$ solution. From reference 75, with permission.

B. Germanium-73

The only quadrupolar nucleus in the main group IV is ^{73}Ge which has been almost neglected by NMR spectroscopists, probably mainly due to its low receptivity, magnetic moment $-0.877\ \mu N$ and natural abundance 7.6%. Pestunovich et al.[76] have used the INDOR technique to obtain the ^{73}Ge chemical shift from a series of complexes of the type [1]. The chemical
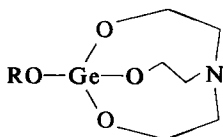
[1]

shifts, relative to Me$_4$Ge, are -53.4, -55.2, -55.2, -60.6, -63.4 and -73.8 ppm for $R = Me_3Sn$, H, Me_3Ge, Me, Pr and Me_3Si, respectively.

V. MAIN GROUPS V AND VI

A. Arsenic-75, antimony-121, antimony-123 and bismuth-209

Of the group V quadrupolar nuclei (except ^{14}N) only antimony-121 and bismuth-209 have been studied during the reviewing period. It is quite surprising that there apparently is no study of ^{121}Sb NMR using a high field FT spectrometer, especially in the light of the fact that Kidd and Spinney[77] were unable to detect all of the possible $SbCl_nBr_{6-n}$ signals at low fields. Goetz-Grandmont and Leroy[78] using a higher field have reported cis/trans isomers for $SbCl_4Br_2$, but not for $SbCl_3Br_3$ or $SbCl_2Br_4$. Kidd and Spinney[77] have analysed the shift data for the $SbCl_6$-$SbBr_6$ system using the pairwise additivity model, and the agreement between the calculated and observed shifts is shown in Table 7. They conclude that they observe only the cis isomers and also exclude the possibility of a fast cis-trans isomerization. Judging from the linewidth data reported,[77] it is very likely that the observed $SbCl_3Br_3$ isomer is the fac isomer since the corresponding line is quite sharp. According to calculations,[79] the effective field gradient in the fac isomer should be zero.

Bismuth-209 has a natural abundance of 100% and a sensitivity, relative to that of the proton, of 0.127; however, the quadrupole moment of $-0.38 \times 10^{-28}\ m^2$ and a large Sternheimer antishielding factor confine studies to symmetric species. The only study relevant for this review concerns the BiF_6^- ion.[80] Its ^{209}Bi NMR spectrum consists of seven well resolved lines ($W_{\frac{1}{2}} = 44$ Hz) with the intensity ratio $1:6:15:20:15:6:1$ expected for a nucleus coupled to six identical spin-$\frac{1}{2}$ nuclei. The coupling $^1J(^{209}Bi-^{19}F) =$

TABLE 7

^{121}Sb chemical shifts and linewidths for the [SbCl$_n$Br$_{6-n}$]$^-$ ions in acetonitrile.

Species	δ_{obs} [a] (ppm)	δ_{calc} [b] (ppm)	$W_{\frac{1}{2}}$ [c] (Hz)
SbCl$_6^-$	0	+1	290
SbCl$_5$Br$^-$	−380	−383	1100
cis-SbCl$_4$Br$_2^-$	−780	−778	800
fac-SbCl$_3$Br$_3^-$	−1180	−1183	250
cis-SbCl$_2$Br$_4^-$	−1590	−1589	1850
SbClBr$_5^-$	−2005	−2005	1250
SbBr$_6^-$	−2430	−2432	790

[a] From reference 77.
[b] Calculated using the pairwise additivity model, reference 77.
[c] From reference 78.

3828 ± 3 Hz is considerably larger than the one estimated previously in the solid state, 2700 Hz.[81] The exact resonance frequency of ^{209}Bi in BiF$_6^-$ is given to be $\theta = 16.017\,649 \pm 10$ Hz at 25 °C, and a saturated solution of Bi(NO$_3$)$_3$ in concentrated HNO$_3$ has a ^{209}Bi chemical shift of −24 ppm from BiF$_6^-$.

B. Sulphur-33

Vold et al.[82] and Ancian et al.[83] have used the linewidth of the ^{33}S NMR signal from CS$_2$ to determine the value of χ for ^{33}S,[82] and to study the molecular reorientation of CS$_2$, neat[82] and in alkanes.[83] The value of χ is calculated to be 14.9 ± 0.3 MHz by using previously determined correlation times[84] and a ^{33}S linewidth of 358 Hz at 15 °C. The value of χ for CS$_2$ is similar to those earlier reported for $C \equiv S$ (12.835 MHz)[85] and S=O (15.9 MHz);[86] however, it is significantly smaller than those for O=C=S (29.07 MHz)[87,88] and HN=S (27.5 MHz).[87] Dousmanis et al.[89] conclude that the Stokes–Einstein model does not hold for the reorientation of CS$_2$ in various alkanes and that the reorientation does not follow either the J or M diffusion models. However, neat CS$_2$ appears to reorient according to the J diffusion model.[84] Hinton and Shungu[90] and Haid et al.[91] have studied the ^{33}S relaxation of SO$_4^{2-}$. They report that the spin–lattice relaxation time increases with decreasing concentration, and Hinton and Shungu[90] have determined the activation energy of 2.5 kcal mol^{-1} for the process governing the relaxation, from the temperature dependence of T_1. It is interesting to note that, even though both groups report that T_1 for ^{33}S in SO$_4^{2-}$ increases with decreasing concentration, the absolute values given for the same concentration differ by about a factor of 2, indicating that the

TABLE 8

^{33}S chemical shifts and linewidths in organic compounds.
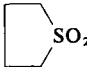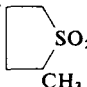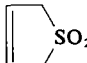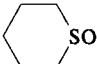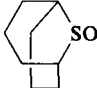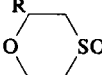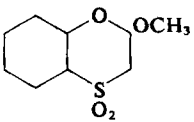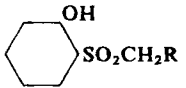
Compound		δ (ppm)	$W_{\frac{1}{2}}$ (Hz)	Ref.
CH_3SO_2		-7	50	92, 94
$CH_3CH_2SO_2$		6	70	94
$(CH_3)_2CHSO_2$		23	160	94
$(CH_3)_3CSO_2$		38	160	94
$CH_3(CH_2)_2SO_2$		7	130	92, 94
$CH_3(CH_2)_3SO_2$		8	180	94
$(C_6H_5)_2SO_2$		-23	130	92, 94
$(CH_3 \cdot C_6H_4)_2SO_2$		-17	140	94
$(HO \cdot C_6H_4)_2SO_2$		-15		94
$(CH_2{=}CH)_2SO_2$		-26	60	92
$(C_6H_5CH_2)_2SO_2$		2	120	94
(five-membered ring with R substituent, SO_2)	$R = H$	42	50	92, 94
	$R = CH_3$	37	60	92
	$R = NH_2$	33	80	92
	$R = OH$	36	100	92
(H_3C- and CH_3-substituted ring, SO_2)		37	90	92
(ring with double bond, SO_2)		32	50	92, 94
(six-membered ring, SO_2)		-6	50	94
(bicyclic ring, SO_2)		-3	190	94
(O-containing ring with R, SO_2)	$R = H$	-13	100	94
	$R = OCH_2CH_3$	-13	100	94

TABLE 8 (cont.)

Compound		δ (ppm)	$W_{\frac{1}{2}}$ (Hz)	Ref.
[structure: bicyclic ring with O, OCH₃, S, O₂] α		−5	200	94
	β	−15	200	94
[structure: ring with OH, SO₂CH₂R] R = CH₃		13	130–600*	94
	R = CH₂OH	10	150–1000*	94

* Solvent dependent.

ion–ion interaction is stronger for Rb^+-SO_4^{2-} as used by Haid et al.[91] than for NH_4^+-SO_4^{2+} as used by Hinton and Shungu.[90] The ^{33}S NMR signal from organic compounds is normally too broad to be observed, and only when the sulphur atom is in a symmetrical environment is observation of the ^{33}S resonance possible. Faure et al.[92] and Harris and Evans[93] have thus studied the ^{33}S NMR shielding and linewidth data for several sulphones and a few sulphonic acids (Table 8).

VI. TRANSITION ELEMENTS

A. Group IIIв

Both ^{45}Sc and ^{139}La are high sensitivity nuclei; however, they also have appreciable quadrupole moments, $\sim 0.22 \times 10^{-28}$ m^2, resulting in broad resonances except when in symmetric environments. Lutz and co-workers[94] have reinvestigated the dependence, upon the addition of HCl, of the ^{45}Sc linewidth and chemical shift of $ScCl_3$ in water. They are unable to reproduce earlier results[95] with abrupt changes in chemical shift and linewidth as a function of added HCl. Judging from the data,[94] there is no formation of any contact ion pairs between Sc^{3+} and Cl^- before quite high HCl concentrations are used (Fig. 13). It is also interesting to note that there is a strong broadening of the line at low acid concentrations, which seems to be independent of the $ScCl_3$ concentration. This broadening occurs only for $HCl:ScCl_3 < 0.5$, which is not easily explained as being caused by the formation of an unsymmetrical $ScCl_3$ complex. Lutz and co-workers[94] have also studied $Sc_2(SO_4)_3$ as a function of H_2SO_4 concentration, which results
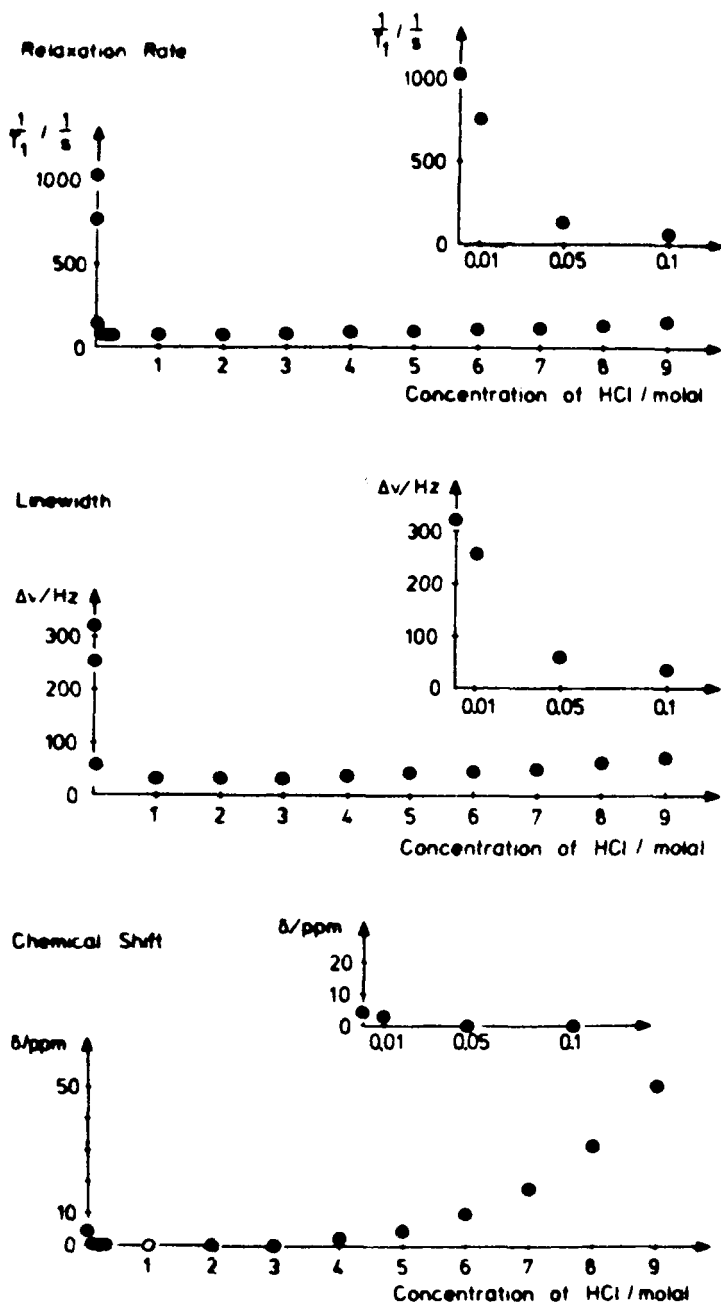
FIG. 13. Chemical shift, linewidth and longitudinal relaxation rate of [45]Sc in 0.11 M aqueous solution of ScCl$_3$ as a function of added HCl. From reference 94, with permission.

in a small variation of ^{45}Sc shifts and relaxation rates. They are able to obtain a ^{45}Sc signal from a strongly basic solution, which is assigned to Sc(OH)$_4^-$, $\delta = 115.7$ ppm. Tarasov et al.[96] have studied the concentration dependence of ^{45}Sc linewidth and shift for ScCl$_3$ and Sc(ClO$_4$)$_3$ solutions. They conclude that the low concentration effect, which is counter-ion independent, is caused by the formation of aquo-hydroxy complexes, whereas the high concentration effect, counter-ion dependent, is caused by the formation of inner sphere complexes which are more stable than the corresponding lanthanum complexes.

TABLE 9

^{43}Sc chemical shifts for some triethyl phosphate (TEP) and tributyl phosphate (TBP) complexes.

Complex	δ^{TEP} (ppm)	δ^{TBP} (ppm)
ScCl$_6^{3-}$	−249	−249
ScCl$_4$L$_2^{2-}$	−166	−166
cis-ScCl$_3$L$_3$	−134	−136
trans-ScCl$_3$L$_3$	−119	−121
cis-ScCl$_2$L$_4^+$	−82	−84
trans-ScCl$_2$L$_4^+$	−67	−70
ScClL$_5^{2+}$	−27	−31
ScL$_6^{3+}$	26.5	—

Buslaev et al.[97] have studied mixed Cl$^-$-triethyl phosphate (TEP) and Cl$^-$-tributyl phosphate (TBP) complexes with Sc^{3+}. The chemical shifts are collected in Table 9. It is interesting to note that, even for non-symmetrical complexes, ScCl$_3$(TEP)$_3$ and ScCl$_2$(TEP)$_4$, resolved ^{45}Sc-^{31}P coupling patterns are detected. By referring to calculations of electric field gradients in other non-symmetric complexes[79] it is concluded that the resolved multiplet structures can be assigned to the cis isomers of ScCl$_3$(TEP)$_3$ and ScCl$_2$(TEP)$_4$ (Fig. 14).

Lutz and Oehler[98] have continued their careful measurements on ^{138}La and thus determined $\nu(^{138}$La$)/\nu(^{139}$La$) = 0.934\,067\,94$, in agreement with an older value of 0.934 07.[99] These authors have measured the solvent isotope effect in H$_2$O/D$_2$O and find $\delta_{iso} = -1.6$ ppm, which can be compared to −4.3 ppm for ^{89}Y,[100] and −6.2 ppm for ^{45}Sc.[94] It therefore appears that δ_{iso} decreases with increasing atomic number in group IIIB, which is the inverse of that found in other groups. No explanation for this anomaly has been found so far.[99]

Tarasov et al.[96] have followed the ^{139}La shift and linewidth as a function of either salt concentration or added acid for LaCl$_3$, La(NO$_3$)$_3$ and
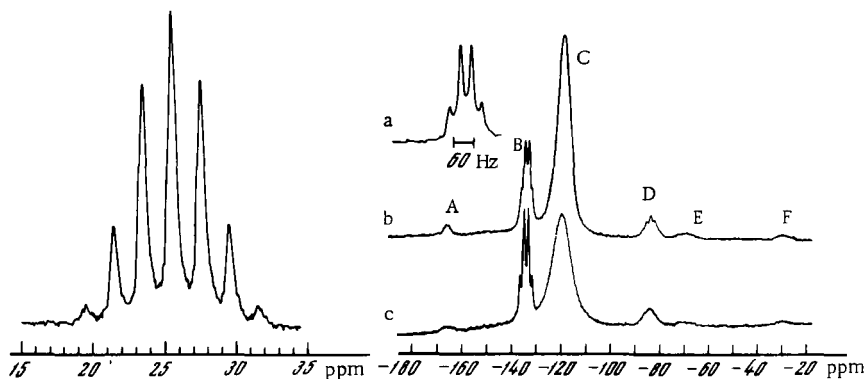
FIG. 14. ^{45}Sc NMR spectra at 19.474 MHz of a solution with a triethyl phosphate/ScCl$_3$ ratio ~3 at 30 °C for (a) and (b) and 0 °C for (c). From reference 97, with permission.

La(ClO$_4$)$_3$, and explained the shielding decrease found in the LaCl$_3$ solution at high salt concentration as being caused by changes in the hydration shell:

$$La(H_2O)_9^{3+} \rightleftarrows La(H_2O)_8^{3+} \qquad (18)$$
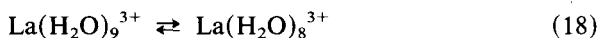
The position of equilibrium, indicated by equation (18), should be shifted to the right in more concentrated solutions.

A study of ^{139}La shifts and linewidths for LaCl$_3$ in mixed H$_2$O–methanol solvents shows that for up to 50% methanol there is no formation of contact ion pairs whereas at more than 50% both the shift and linewidth indicate the formation of new species in solution.[101] X-ray data show that in 100% methanol there are dimers with one bridging chorine,[102] and it is therefore reasonable to assume that this also exists in the mixed solvents with higher methanol contents.

Lanthanum–carboxylic acid complexes have also been studied,[103,104] and using reported stability constants[105] it is possible to calculate the chemical shift for LaX^{2-} to be 100, 50, 22 and 0 ppm for X = CH$_3$COO$^-$, ClCH$_2$COO$^-$, Cl$_2$CHCOO$^-$ and Cl$_3$COO$^-$, respectively.[102] Also, the shift for the La·EDTA complex is reported to be 570 ppm.

Table 10 shows some chemical shifts and linewidths for several lanthanum complexes in acetonitrile solution.[106]

B. Group IVв

Titanium is unusual in the sense that it has two isotopes, ^{47}Ti and ^{49}Ti, with almost the same gyromagnetic ratio. The resonance frequencies differ by only 266 ppm. Hao et al.[107] have determined the Ti chemical shifts for several TiX$_4$, TiX$_6^{2-}$ and (C$_5$H$_5$)$_2$TiX$_2$ complexes with X = F, Cl, Br or I (Table 11). The data show that ^{47,49}Ti display the inverse halogen dependence

TABLE 10

Lanthanum-139 chemical shifts and linewidths for various complexes in acetonitrile.

Complex	δ^a (ppm)	$W_{\frac{1}{2}}$ (Hz)
$[La(MeCN)_n]^{3+}$	−129	380
$[La(luto)_8]^{3+}$	−122	2700
$[La(NO_3)_6]^{3-}$	−60	260
$[La(DMF)_8]^{3+}$	−39	1700
$[La(pyo)_8]^{3+}$	4	2800
$[La\{CH(OCCF_3)_2\}_4]^-$	33	7000
$[La\{P(NMe_2)_3O\}_6]^{3+}$	66	930
$[La(DMSO)_8]^{3+}$	82	1800
$[La\{OS(CH_2)_3CH_2\}_8]^{3+}$	93	2600
$[La\{N(CH_2CO_2)_3\}_2]^{3-}$	202	7800
$[La(NO_2)_6]^{3-}$	342	600
$[La(Et_2NCS_2)_4]^{-1}$	710	2100
$[LaCl_6]^{3-}$	851	200
$[LaBr_6]^{3-}$	1090	500
$[La(en)]^{3+}$	40	3800
$[La(en)_4]^{3+}$	400	3800
$[La(dien)]^{3+}$	122	7700
$[La(dien)_3]^{3+}$	450	2400

^{a} Chemical shift from $La(H_2)_n^{3+}$.

TABLE 11

Chemical shifts and linewidths for some titanium and zirconium complexes.

Compound	$\delta(^{49}Ti)$ (ppm)	$W_{\frac{1}{2}}(^{49}Ti)$ (Hz)	$\delta(^{91}Zr)$ (ppm)	$W_{\frac{1}{2}}(^{91}Zr)$ (Hz)
MCl_4	0	3	—	—
MBr_4	482.9	3	—	—
MI_4	1278.3	10	—	—
MF_6^{2-}	−1162.7	7	−191.1	50
MCl_6^{2-}	—	—	601.2	245
MBr_6^{2-}	8.2	40	—	—
Cp_2MF_2	−1036.5	30	—	—
Cp_2MFCl	−928.3	90	—	—
Cp_2MCl_2	−771.6	30	−121.9	276
Cp_2MClBr	—	—	−65.9	237
Cp_2MBr_2	−668.3	30	0	19
Cp_2MICl	−661.2	120	—	—
Cp_2MIBr	−595.1	35	—	—
Cp_2MI_2	−517.2	30	126	134
$Cp_2M(N_3)_2$	−930.9	500	—	—
$Cp_2M(NCS)_2$	−962.3	25	—	—
$M(NEt_2)_4$	−204.8	150	—	—
$M(OPr^i)_4$	−858.3	80	—	—

as noted previously.[108] The same has been shown to be true for ^{91}Zr.[109] It is found that ^{47,49}Ti and ^{91}Zr have almost identical chemical shift sensitivities towards halogen substituents, which is somewhat surprising since normally this sensitivity increases upon passing down a group. Hao et al.[107] have found that the ^{19}F spin coupling in $MF_6{}^{n-}$ complexes decreases across a row and increases upon descending a group, when compared as reduced couplings, $^1K(M-F)$. The same group has measured the spin–lattice relaxation of ^{47,49}Ti in $TiF_6{}^{2-}$ as a function of concentration in water, and for $TiCl_4$ in toluene as a function of temperature. These measurements result in $T_1(^{49}Ti)/T_1(^{47}Ti)$ ratios close to the calculated value of 3.43. The variable temperature data are used to calculate the activation energies for molecular reorientation to be 1.34 and 1.39 kcal mol^{-1} for $^{47}TiCl_4$ and $^{49}TiCl_4$, respectively.

Sayer et al.[110] have used ^{91}Zr NMR to study the $Zr(BH_4)_4$ complex. Using ^{1}H, ^{11}B or ^{1}H and ^{11}B decoupling, spectra as shown in Fig. 15 are obtained. It is thus clear that both ^{1}H and ^{11}B are spin coupled to the central ^{91}Zr nucleus, with couplings of $^2J(Zr-H) = 28$ Hz and $^1J(Zr-B) = 80$ Hz. The ^{1}H coupling pattern is in agreement with all sixteen protons being coupled to the ^{91}Zr nucleus with the same coupling value. For this to apply, two conditions must be fulfilled: (1) slow intermolecular exchange of the BH_4
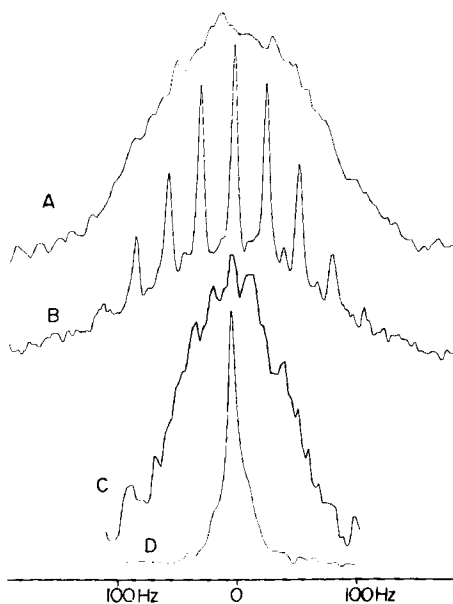
FIG. 15. ^{91}Zr NMR spectra of $Zr(BH_4)_4$ at 25 °C: (A) fully coupled; (B) ^{11}B decoupled; (C) ^{1}H and ^{11}B decoupled. From reference 110, with permission.

ligands; (2) fast intramolecular exchange making all four protons within each BH_4 group identical.

C. Group VB

^{51}V continued to be a popular nucleus for NMR studies, which is not surprising in the light of its high sensitivity, 40% of that for protons. Also the low quadrupole moment of $7.3 \times 10^{-31}\ m^2$ results in lines which are not extremely broad even for non-symmetrical compounds. Studies of vanadates have thus continued by using a high field spectrometer, and the chemical shifts for fifteen different vanadates, from VO_4^{3-} to $V_6O_{18}^{6-}$, have been assigned[111] with chemical shifts ranging from -538 to -590 ppm, using $VOCl_3$ as a shift reference. The decavanadate ion has been reinvestigated.[112] Studies of the kinetics of the breakdown of, for example, $V_4O_{12}^{4-}$ show surprisingly enough that this is not correlated with the OH^- concentration but with that of HVO_4^{2-}. Furthermore, the line broadening of the two species $V_4O_{12}^{4-}$ and HVO_4^{2-} shows that the reaction cannot be a simple exchange $A^* + A_4 \rightleftarrows A^*A_3 + A$ but that there must also exist a long-lived pentamer. Peroxo complexes of vanadium have been studied by ^{51}V NMR, resulting in chemical shifts ranging from -543 ppm for $VO(OO)^+$ to -845 ppm for $VO(OO)_3^{3-}$.[113]

Gillespie and Rao[114] have studied the aqueous solution of $Na(NH_4)_2VO_2F_4$-HF and re-evaluated a previous assumption of the presence of VOF_4^- ions,[115] and Buslaev et al.[116] have studied similar systems in acetonitrile.

A series of complexes, $CpV(NO)_2L$, where L is a Lewis base bound to the V nucleus via C, P, S, N or O, has been found to have a shift range of almost 800 ppm. It is found that the ^{51}V shielding decreases with increasing electronegativity of the coordinating atom, $P < S < N < O$.[117,119] It is thus possible to conclude that both dimethyl sulphoxide and dimethylformamide are coordinated to vanadium via their oxygens. Likewise it is concluded that 4-cyanopyridine is coordinated via its pyridine nitrogen and not its cyano group. For some other complexes it has been found that the shift increases for the ligands in the order $R_2NO^- < O_2^{2-} < O^{2-}$.[118-120]

From the ^{51}V shift in complexes of the types $V(CO)_5EZ_3^-$ and $CpV(CO)_2EZ_3$, where E is P, As, Sb or Bi, it is found that independent of Z there is a general trend in the chemical shift. The ^{51}V shielding decreases for the ligands in the order $SbZ_3 < PZ_3 < AsZ_3 < BiZ_3$.[121] Rehder[122] has also studied the effect of the bulkiness in complexes like $CpV(CO)_3PR_3$ and of ring size in various complexes with a bidentate ligand, $Ph_2P(CH_2)_nPPh_2 \cdot L$, on the ^{51}V shift. It is found that the chemical shift increases with increasing cone angle[123] for the PR_3 ligand, in agreement with an increasing P–V distance. As shown in Fig. 16, except for $CpV(CO)_2L$, there is a minimum
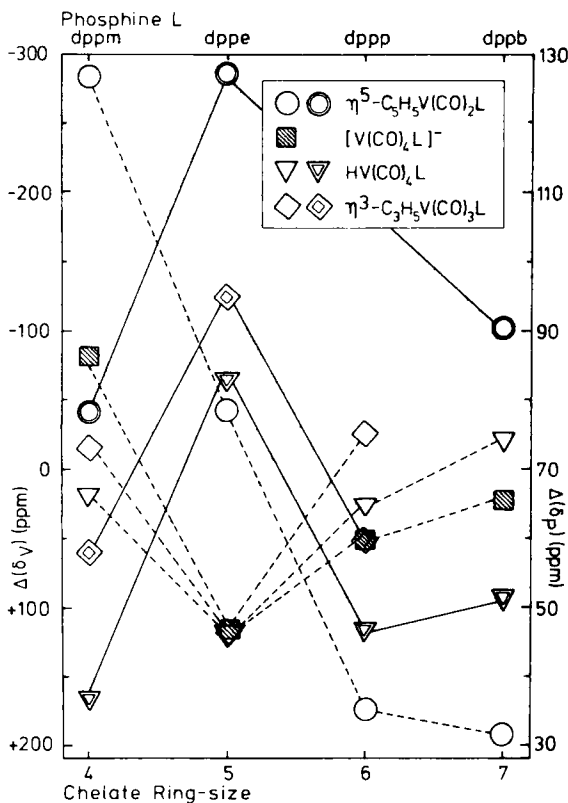
FIG. 16. ^{31}P coordination shift $\Delta(\delta_p)$ and chelate contribution to ^{51}V chemical shift (dashed lines) as a function of ring size. From reference 122, with permission.

in the ^{51}V chemical shift when L forms a 5-membered ring with vanadium and a maximum in the shift in the coordinating ^{31}P resonance for the same ring size. The temperature variation in the ^{51}V chemical shift and linewidth for VO(OPr^i)$_3$ shows some unexpected features.[124] As shown in Fig. 17, the linewidth of the ^{51}V resonance from VO(OPr^i)$_3$ in n-pentane goes through a maximum at about 230 K, which resembles what may be expected for a system in intermediate exchange. At about the same temperature there is an irregularity in the temperature dependence of the ^{51}V chemical shift, which could be caused by an exchange process. Similar, but less pronounced, effects are seen for other solvents, except for tetrahydrofuran where the temperature dependences are quite normal. In a comparative study of the chemical shifts of vanadium, niobium and manganese complexes it is found that the ^{93}Nb has a dependence on chelate ring size which is similar to that of ^{51}V.[125-127]
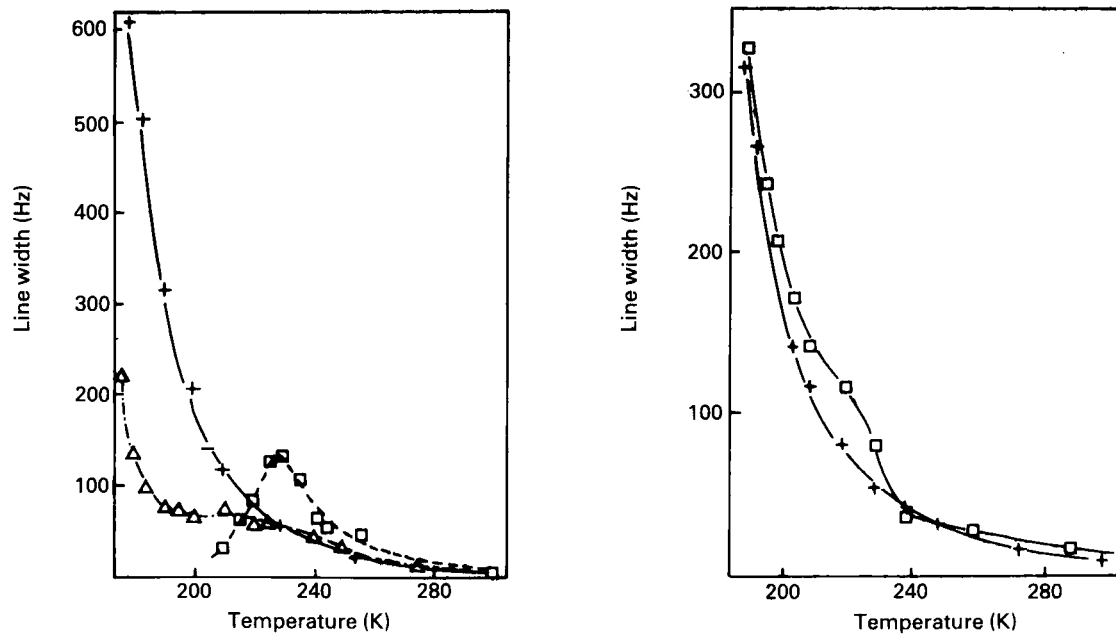
FIG. 17. Temperature dependence of the linewidth of ^{51}V signals of $VO(OPr^i)_3$ in various solvents.
Upper: $VO(OPr^i)_3$ in THF (0.86 M: +); n-pentane (1.72 M: □); Et_2O (1.72 M: △).
Lower: $VO(OPr^i)_3$ in THF (0.86 M: *); methylcyclohexane (0.86 M: □). From reference 124, with permission.
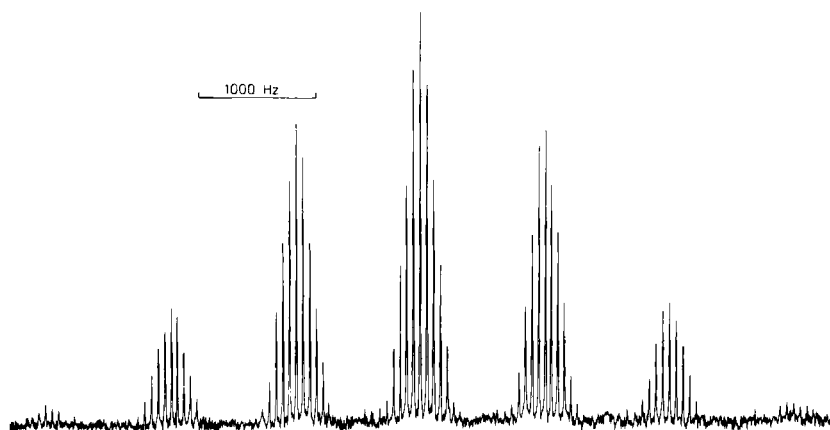
FIG. 18. The 22.00 MHz ^{93}Nb spectrum of $[Et_4N][Nb(PF_3)_6]$. From reference 178, with permission.

Figure 18 shows clearly that well resolved spectra from ^{93}Nb can be obtained from highly symmetrical complexes. It is also interesting to note that the quadrupolar nucleus ^{93}Nb gives much better resolved lines than the dipolar nuclei ^{31}P and ^{19}F for the $Nb(PF_3)_6^-$ complex.[128] The same phenomenon has been observed[114] for $VO_2F_4^{2-}$ and can be explained by

TABLE 12

^{93}Nb chemical shifts for the complexes
$[Nb(NCS)_n(SCN)_mCl_{6-n-m}]^-$.

Complex	δ (ppm)
$NbCl_6^-$	0
$NbCl_5NCS$	−232
cis-$NbCl_4(NCS)_2$	−457
cis-$NbCl_3(NCS)_3$	−681
cis-$NbCl_2(NCS)_4$	−902
$NbCl(NCS)_5$	−1118
$Nb(SCN)_6$	−780
cis-$Nb(SCN)_4(NCS)_2$	−947
trans-$Nb(SCN)_4(NCS)_2$	−940
trans-$Nb(SCN)_2(NCS)_4$	−1125
$Nb(SCN)(NCS)_5$	−1235
trans-$Nb(SCN)_2Cl_4$	−220
trans-$Nb(SCN)_4Cl_2$	−475
$Nb(SCN)_5Cl$	−633
$Nb(SCN)_2(NCS)_2Cl_2$	−670

using an extension of Pople's treatment[129] of the lineshape of a spin-$\frac{1}{2}$ signal which is spin coupled to a quadrupolar nucleus.

The system $[Nb(NCS)_n(SCN)_mCl_{6-n-m}]^-$ can theoretically give rise to fifty-six different configurations. Kidd and Spinney[130] have been able to detect sixteen different ^{93}Nb resonances with a shift range of 1342 ppm for this system. Using the pairwise additivity model[131] they are able to assign the observed sixteen resonances as shown in Table 12. The calculation also shows that all fifty-six configurations should have signals separated by no less than 7 ppm, making it possible to observe all species present in sufficient concentration without serious signal overlap.

D. Group VIB

During the review period the interest in ^{53}Cr NMR has been very scarce, most probably owing to the low receptivity of this nucleus. However, Haid et al.[91] have measured the relaxation time, T_1, for CrO_4^{2-} ions as a function of concentration from 0.5 to 3.0 M K_2CrO_4. They extrapolated the relaxation to zero concentration, $(T_1)_0 = 55$ ms. The scarcity of data available for ^{53}Cr is in contrast to the quite extensive amount available for the NMR nuclides of the second element in this group, ^{95}Mo and ^{97}Mo. Most of the work has been concentrated around molybdenum carbonyl complexes, but there are a few papers dealing with oxomolybdenum complexes. In fact there are so many papers published during the review period dealing with molybdenum NMR that it is questionable whether molybdenum should be considered to be a less common quadrupolar nucleus. I have, however, decided to include it in this review.

Kroneck et al.[132] have used ^{17}O, ^{33}S, ^{95}Mo and ^{97}Mo NMR to study the oxothiomolybdates MoO_nS_{4-n} in aqueous solution. Even though the authors have used both ^{95}Mo and ^{97}Mo, the ^{95}Mo isotope is the one of choice for NMR studies because it has both a higher receptivity and a smaller quadrupole moment than ^{97}Mo. The authors find a large, 500–600 ppm, shift for each oxygen replaced by a sulphur. For ^{95}Mo the resonances are quite narrow for all the oxothiomolybdates, $\leqslant 10$ Hz. In fact the ^{95}Mo NMR resonance for MoS_4^{2-} is sufficiently narrow to show the ^{32}S-^{34}S isotope effect.[132] Gheller et al.[134] have likewise determined ^{95}Mo chemical shifts for the $MoO_nSe_{4-n}^{2-}$ species. $MoSe_4^{2-}$ in acetonitrile has the most highly deshielded ^{95}MO NMR signal observed so far, $\delta = 3339$ ppm, relative to MoO_4^{2-}. For the binuclear complex [2] it is observed that the ^{95}Mo resonance

[2]
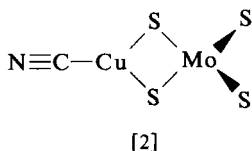
is shielded by between 350 and 400 ppm, compared to MoS_4^{2-}, and for another similar but less well characterized complex the ^{95}Mo resonance is further shielded and appears to be close to that of MoO_2S_2.

There has been a considerable amount of interest in oxymolybdenum complexes,[135-139] partly motivated by the existence of the MoO_2 or $MoOS$ moiety in enzymes.[140] It has thus been found that replacement of O by S in the series $[MoO_nS_{2-n}(R_2NO)_2]$ shifts the ^{95}Mo resonance by c. 700 ppm to higher frequency,[137] whereas replacement of an O or N ligand by a thiolate sulphur causes an increasing shift of 200–400 ppm.[137] All reported ^{95}Mo chemical shifts of MoO_3 complexes with EDTA and EDTA-like complexes fall in a narrow range between 63 and 70 ppm.[138] When an alkaline solution of MoO_4^{2-} is acidified the ^{95}Mo NMR signal broadens and at pH 6 one reasonably sharp and one broad signal are observed (Fig. 19). The broad signal has been assigned to the polynuclear species $Mo_7O_{24}^{6-}$.[138]
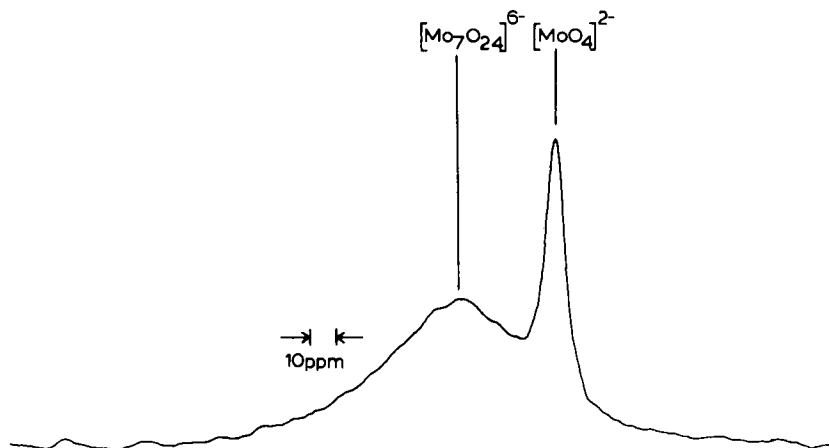
FIG. 19. ^{95}Mo NMR spectrum of 1 M $Na_2MoO_4 \cdot 2H_2O$ in H_2O at pH 6. From reference 138, with permission.

Gheller et al.[141] have studied a few Mo(IV) and Mo(V) complexes, mostly multinuclear complexes. $Mo_3^{IV}O_4$ and its complexes have resonances between 990 and 1162 ppm, and $Mo_2^VO_4$ and its EDTA and L-cysteine complexes resonate between 434 and 604 ppm. Mo(IV)aq is oxidized by air to Mo(V)aq, which can be seen in the ^{95}Mo spectra where a new resonance appears for a Mo(IV)aq solution after prolonged storage. The PDTA complexes of both Mo_3O_4 and Mo_2O_4 result in ^{95}Mo NMR spectra containing two resonances (Fig. 20) which for $[Mo_2O_4(PDTA)]^{2-}$ are assigned to the two non-equivalent Mo sites, a result of the asymmetric PDTA ligand.
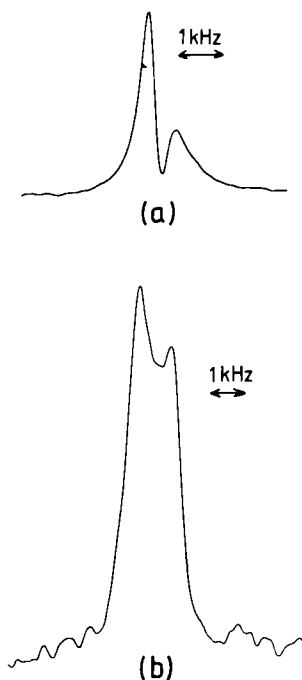
FIG. 20. ^{95}Mo NMR spectrum of: (a) $Na_2[Mo_2O_4(PDTA)]\cdot4H_2O$ in H_2O, pH 5.5; (b) $Na_4[(Mo_3O_4)_2(PDTA)_3]\cdot14H_2O$ in H_2O, pH 5.5. From reference 141, with permission.

Most of the Mo(II) complexes studied by ^{95}Mo NMR are of the type $CpMo(CO)_nL$;[142-146] however, there are two binuclear complexes, $Mo_2(O_2CPr^n)_4$ and $Mo_2(O_2CCF_3)_4$,[141] which have been observed with ^{95}Mo NMR. These have formally quadruple bonds between the two Mo nuclei, and their shifts are far removed from the normal range for Mo(II) species (-100 to -2072 ppm); $\delta[Mo_{II}{}^2(O_2CCF_3)_4] = 4026$ ppm and $\delta[Mo_2{}^{II}(O_2CPr^n)_4] = 3730$ ppm are in fact the most deshielded ^{95}Mo resonances observed to date.[141] The most highly shielded Mo(II) resonance is the one from $[Cp(CO)_3MoSnMe_3]$ with a shift of -2072 ppm.[143]

Several Mo(O) complexes have been studied by ^{95}Mo NMR,[142-144,147-158] with a chemical shift range of -450 to -2200 ppm. Most of the data are for complexes where one or more CO ligand has been replaced by phosphines or phosphites. In some cases, especially for PF_3,[151] the shift changes are surprisingly small considering the large shift range for ^{95}Mo; however, in most cases the shifts for the various complexes are well resolved. The $^1J(^{95}Mo-^{31}P)$ spin coupling has been observed and is found to be different for phosphines (130-150 Hz) and phosphites (210-240 Hz). A shielding increase in the order $PPh_3 < AsPh_3 < SbPh_3$ has been found for both
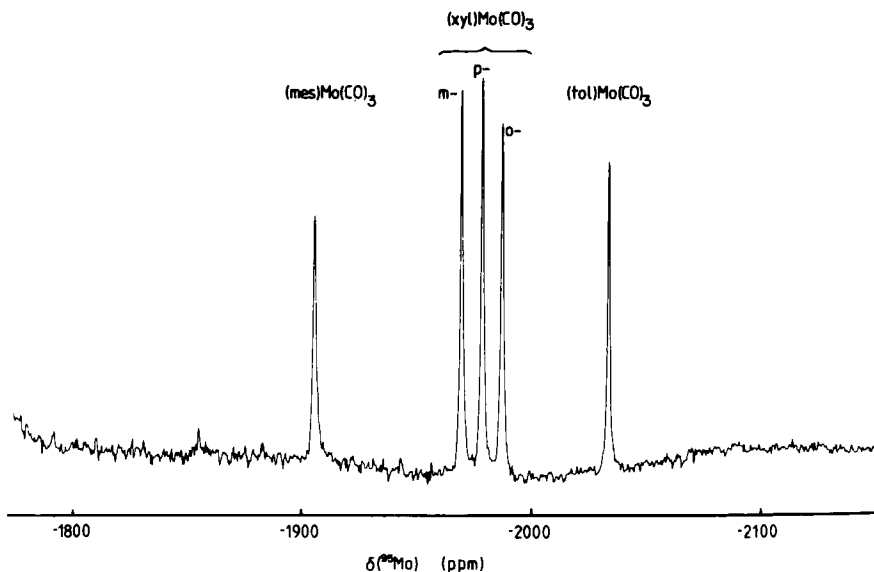
FIG. 21. Room temperature ^{95}Mo NMR spectrum of a mixture of [(arene)Mo(CO)$_3$] derivatives (arene = mes, *m*-, *m*- and *o*-xyl and tol) in CH$_2$Cl$_2$, each approximately 0.2 M. From reference 147, with permission.

Mo(CO)$_5$L[144,149,156] and Mo(CO)$_4$L$_2$ [149] complexes, analogous to that found for the isoelectronic vanadium species.[159]

Donovan-Mtunzi *et al.*[158] have studied the effect of nitrogen ligation to Mo, and find that nitrogen ligation causes deshielding relative to phosphorus or CO ligation, with increasing deshielding in the order MeCN < pyridine < piperidine < N$_2$ < NO.

In a study of arene-molybdenum(0) tricarbonyl derivatives Masters *et al.*[147] have shown that the ^{95}Mo resonances from *ortho-*, *meta-* and *para-*(xyl)Mo(CO)$_3$ complexes are well resolved (Fig. 21) with a spread of 17 ppm, and Minelli *et al.*[148] have shown that the ^{95}Mo(II) resonances for

[3]

[4]
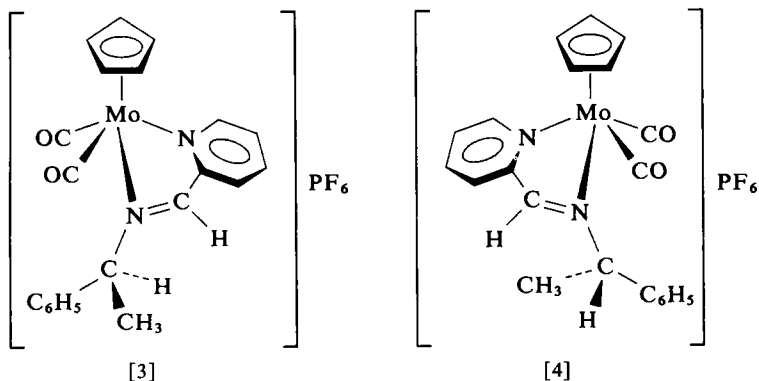
the isomers [3] and [4] are separated by 14 ppm. From the two examples it is evident that ^{95}Mo NMR can become a powerful tool in studies of stereochemistry in metal complexes.

E. Group VIIB

Of the naturally occurring quadrupolar nuclei in this group ^{55}Mn has the lowest quadrupole moment, 0.4×10^{-28} m^2, compared to 2.8×10^{-28} m^2 for ^{185}Re. Even for ^{55}Mn this means that only for highly symmetric environments will there be an observable signal; for ^{185}Re the sharpest line reported is 1.3 kHz for Re(CO)$_6$,[160] and for ReO$_4^-$ it is 14 kHz.[161] It is therefore not surprising that very few reports on ^{55}Mn, ^{185}Re and ^{187}Re have appeared.[160-162] In fact almost as much has been done on the radioactive ^{99}Tc nucleus.[161,163] Like other transition metals the group VIIB nuclei have large chemical shift ranges: -2373 to 490 ppm for ^{55}Mn, -3672 to 806 ppm for ^{99}Tc, and -3400 to 0 ppm for ^{195}Re, all relative to MO$_4^-$.

Franklin et al.[163] have studied TcO$_4^-$ enriched in ^{17}O (21.9%) and ^{18}O (42.7%) which result in the ^{99}Tc spectrum shown in Fig. 22. As previously
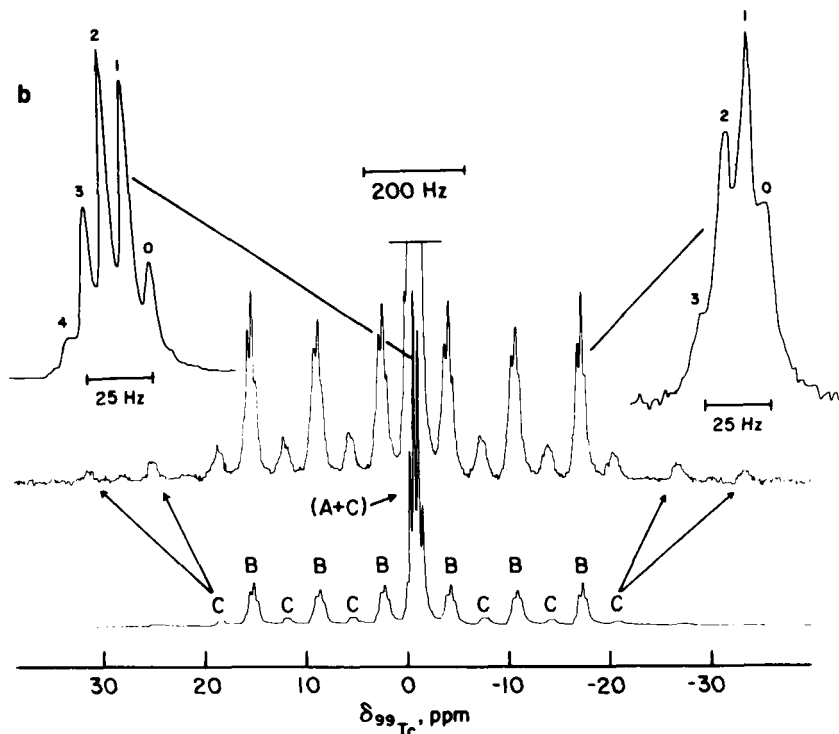
FIG. 22. ^{99}Tc NMR spectrum of ^{17}O (21.9%) and ^{18}O (42.7%) enriched KTcO$_4$ in H$_2$O at 25 °C. Isotopic isomers are denoted by (A) Tc ^{16}O$_x$ ^{18}O$_{4-x}$, (B) Tc ^{17}O ^{16}O$_x$ ^{18}O$_{3-x}$ and (C) Tc ^{17}O$_2$ ^{16}O$_x$ ^{18}O$_{2-x}$. From reference 163, with permission.

shown for ^{55}Mn ^{164} and ^{97}Mo,^{165} the ^{17}O relaxation is sufficiently slow to result in well resolved multiplets, a decet in the ^{17}O spectrum and six lines from Tc^{17}OO$_3^-$ and eleven from Tc^{17}O$_2$O$_2^-$ in the ^{99}Tc NMR spectrum. In addition to these multiplets there is extra fine structure due to the ^{16}O/^{18}O isotope effect on the ^{99}Tc resonances of 0.22 ppm, which should be compared to 0.56 ppm, for ^{55}Mn and 0.25 ppm for ^{97}Mo.

F. Group VIIIв

Another blank spot on the NMR periodic table was removed when Brevard and Granger[167,168] and Dykstra and Harrison[169] detected the ^{99}Ru and ^{101}Ru NMR signals. Brevard and Granger[167] first used RuO$_4$, 1.02 M in CCl$_4$, to show the possibilities of ^{99}Ru and ^{101}Ru NMR. They obtain sharp signals with $W_{\frac{1}{2}} = 0.8$ Hz for ^{99}Ru and 9 Hz for ^{101}Ru, which suggests that even non-symmetrical Ru compounds could result in reasonably narrow ^{99}Ru NMR signals. Measured T_1 values are used to calculate the ratio of the quadrupole moments, $Q(^{101}$Ru$)/Q(^{99}$Ru$) = 5.45$, which is in reasonable agreement with earlier data.[170,171] In the same way they calculate the ratio $Q(^{189}$Os$)/Q(^{101}$Ru$) = 4.63$, which is significantly larger than that (1.73) calculated from other data.[170,171] The discrepancy is explained in terms of a greater sensitivity of the ^{189}Os outer electronic sphere to molecular collisions since the f electrons may play an important role.

Ru(CN)$_6^{4-}$ in water has been suggested as an NMR reference since it is easy to handle and has a low frequency NMR signal, resulting in positive
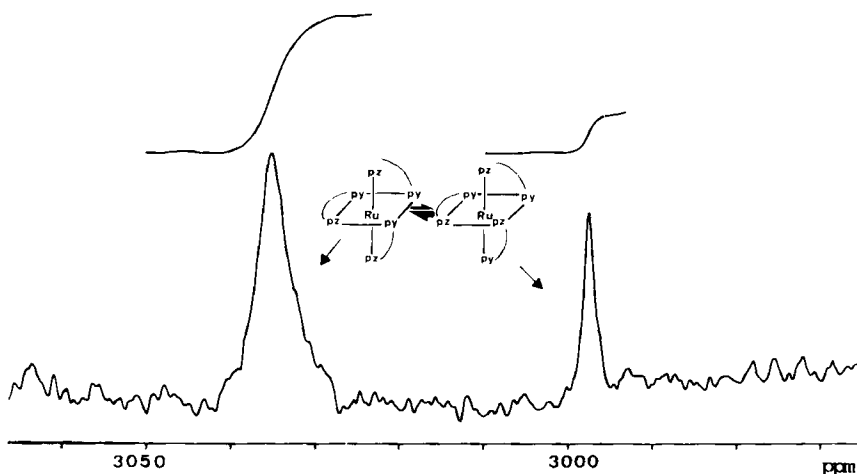
FIG. 23. ^{99}Ru NMR spectrum of tris[1(2-pyridyl)-3,5-dimethylpyrazole]ruthenium(II) hexafluorophosphate showing the *mer-fac* isomerism induced by the ligands (py = pyridine, pz = pyrazole). From reference 167, with permission.

TABLE 13

Chemical shifts and linewidths for some ^{99}Ru complexes.

Compound	Solvent	δ (ppm)	$W_{\frac{1}{2}}$ (Hz)	Ref.
RuCp$_2$	CH$_2$Cl$_2$	−1270	—	168
Ru$_3$(CO)$_{12}$	C$_6$H$_6$	−1208	—	168
Ru(CNCH$_3$)$_6$SO$_4$	D$_2$O	−112	15	169
KRu(CN)$_6$	D$_2$O	0	1.6	168, 169
fac-Ru(CO)$_3$I$_3$PPN^a	acetone	56	10	169
mer-Ru(CO)$_3$I$_3$PPN	acetone	356	75	169
fac-Ru(CO)$_3$Cl$_3$PPN	acetone	816	112	169
Ru(CO)$_3$Cl$_3$Cs	acetone	976	—	168
Ru$_2$(CO)$_6$Cl$_4$	acetone	1204	—	168
Ru(SnCl$_3$)$_5$Cl^{4-} (NH$_4^+$)$_4$	CH$_3$CN	1554	—	168
RuO$_4$	CCl$_4$	2021	—	168
Ru(CO)$_2$Cl$_4^{2-}$ (Cs$^+$)$_2$	D$_2$O	2523	—	168
Ru(bpy)$_3$Cl$_2$	D$_2$O	4518	—	168
mer-Ru(LL')$_3$(PF$_6$)$_2$^{b}	CH$_3$CN	5040	—	168
fac-Ru(LL')$_3$(PF$_6$)$_2$	CH$_3$CN	5003	—	168
Ru(NH$_3$)$_6$Cl$_2$	D$_2$O	7821	—	168
Ru(LL')$_3$$^{2+}$	CH$_3$CN	5018	—	170
		5059		
Ru(bpy)(LL')$_2$$^{2+}$	CH$_3$CN	4920	—	170
		5013		
		5050		
Ru(bpy)$_2$(LL')$^{2+}$	CH$_3$CN	4801	—	170
Ru(bpy)$_3$$^{2+}$	CH$_3$CN	4609	—	170

^{a} PPN represents the bis(triphenylphosphine)iminium cation.

^{b} LL' represents [1-(2-pyridyl)-3,5-dimethylpyrazole].

shift values for most compounds. One drawback with this reference is its large temperature coefficient, 0.7 ppm K^{-1}.[169] The Ru chemical shifts reported so far are collected in Table 13. It is interesting to note that the chemical shift is sufficiently sensitive to the symmetry of the Ru complex to result in separate resonances for the mer and fac isomers of, for example, the tris[1-(2-pyridyl)-3,5-dimethylpyrazole] ruthenium complex as shown in Fig. 23. It therefore seems likely that ^{99}Ru NMR, which gives sharper signals than with ^{101}Ru, can become a useful technique in the study of organoruthenium compounds. This has recently been further exemplified by Steel et al.[172] who have studied the complexes Ru(bpy)$_n$[(1-(2-pyridyl)-3,5-dimethylpyrazole]$_{3-n}$ with ^{99}Ru NMR. They are able to observe three ^{99}Ru resonances from the complex with one bpy ligand.

The only magnetically active nickel isotope, ^{61}Ni, has a spin $I = 3/2$, magnetic moment $= -0.75$ μN and a natural abundance of 1.19%, resulting

TABLE 14

^{61}Ni chemical shifts, ^{31}P–^{61}Ni couplings and linewidths for some nickel complexes.

Compound	δ (ppm)	J (^{31}P–^{61}Ni) (Hz)	$W_{\frac{1}{2}}$ (Hz)	Ref.
Ni(PF$_3$)$_4$	−929.1	482	20	174
Ni(P(OMe)$_3$)$_4$	−742.2	398	80	174
Ni(P(OEt)$_3$)$_4$	−703.0	405	90	174
Ni(CO)$_4$	0	—	3.9	174
Ni(PBu$_3$)(CO)$_3$	56.6	232	—	173
Ni(CO)$_3$P(Me$_3$Si)Bu$_2$	58.9	197	—	173
Ni(CO)$_3$P(Me$_3$Ge)Bu$_2$	59.2	203	—	173
Ni(CO)$_3$P(Me$_3$Si)$_2$Bu	81.8	161	—	173
Ni(CO)$_3$P(Me$_2$Ge)$_2$Bu	87.0	197	—	173
Ni(CO)$_3$P(Me$_3$Sn)Bu$_2$	92.8	206	—	173
Ni(PCl$_3$)$_4$	266.9	450	20	174

in low receptivity. Consequently, few NMR studies using ^{61}Ni have been published. Schumann et al.[173] and Hao et al.[174] have, however, used ^{61}Ni NMR to study some nickel–phosphine complexes (Table 14). As long as tetrahedral complexes are used, reasonably narrow ^{61}Ni NMR resonances are obtained, and for Ni(PF$_3$)$_4$ both $^1J(^{61}$Ni–^{31}P) = 482 Hz and $^2J(^{61}$Ni–^{19}F) = 28 Hz could be observed.[174] Most spectroscopic evidence seems to indicate that the degree of back-donation is greater to PF$_3$ than to CO.[175] However, as discussed above, NMR studies on ^{51}V and ^{93}Nb suggest that at least for these two nuclei CO should be a better π acceptor. For Ni, on the other hand, the ^{61}Ni NMR resonance for the Ni(PF$_3$)$_4$ complex is shifted by 929 ppm to lower frequency of that from Ni(CO)$_4$, also in agreement with ^{59}Co NMR results.

G. Groups I$_B$ and II$_B$

Of the quadrupolar nuclei in these two groups, only ^{63}Cu, ^{65}Cu and ^{67}Zn have been studied by NMR. All three nuclei have high quadrupole moments, −0.211, −0.195 and 0.16 × 10^{-28} m^2 respectively, so only species with high symmetry at the metal nucleus will result in observable NMR signals. Both copper isotopes have reasonably high magnetic moments and natural abundances giving rise to high sensitivity. It might therefore appear surprising that these nuclei have been so widely neglected by NMR spectroscopists; however, the results currently available[176,177] clearly point out the difficulties. The most narrow ^{63}Cu resonance observed so far seems to be 115 Hz for Cu^I[P(OCH$_3$)$_3$]$_4$$^+$, whereas more typical linewidths are above 500 Hz (Table 15). Despite the broad lines it has been possible to resolve the ^{63}Cu–^{31}P

TABLE 15

^{63}Cu chemical shifts, linewidths and $^{63}Cu-^{31}P$ couplings for some tetrahedral complexes.

Compound	δ (ppm)	$W_{\frac{1}{2}}$ (Hz)	$J(^{63}Cu-^{31}P)$ (Hz)	Ref.
$Cu[P(OCH_3)]_4$	−6	166	1223	177
$Cu[P(OC_2H_5)_3]_4$	0	137	1209	177
$Cu[P(OC_4H_9)_3]_4$	3	430	1312	177
$Cu[P(CH_3)_2(C_6H_5)]_4$	159	2750	—	177
$Cu[P(OCH_3)(C_6H_5)_2]_4$	90	4250	—	177
$Cu[P(OCH_3)_2(C_6H_5)]_4$	48	530	1109	177
$Cu[P(OC_4H_9)(C_6H_5)_2]_4$	85	4130	—	177
$Cu[P(OC_4H_9)_2(C_6H_5)]_4$	46	650	1200	177
$Cu[CH_3CN]_4$	−90	500	—	176

spin–spin coupling in several $Cu[P(OR)_3]_4{}^+$ and $Cu[PR'_n(OR')_{3-n}]_4{}^+$ complexes, and the values obtained show that $^1J(^{63}Cu-^{31}P)$ is larger for phosphite than for phosphine complexes, in agreement with results for other metals.[156,178]

Kroneck et al.,[178] Ochsenbein and Schläpfer[180] and Marker and Gunter[181] have studied the temperature dependence of the width and shift of the ^{63}Cu resonances from $Cu(CH_3CN)_4{}^+$, $Cu(C_5H_5N)_4{}^+$ and $Cu[P(OC_2H_5)_3]_4{}^+$. For $Cu(CH_3CN)_4{}^+$ the shift is found to be strongly temperature dependent, −0.75 ppm K^{-1}, and the linewidth goes through a minimum. These two observations have been explained as being caused by chemical exchange between $Cu(CH_3CN)_4{}^+$ and a less symmetric complex. Thus, as long as the relaxation rate of the less symmetric, not observable, complex is fast compared to the exchange rate between the complexes, the width of the observed resonance is given by the equation

$$\Delta \nu_{\frac{1}{2}} = \frac{2\pi}{5} \cdot \chi \cdot \tau_c + \frac{1}{\pi \tau_m} \qquad (19)$$

where τ_c is the correlation time and τ_m the lifetime of the observed ^{63}Cu nucleus, and both are temperature dependent in a similar fashion. The temperature dependence of the ^{63}Cu shift from $Cu[P(OC_2H_5)_3]_4{}^+$ in $CHCl_3$ is much smaller, −0.1 ppm K^{-1}, and therefore Kroneck et al.[178] have suggested that this resonance should be used as a shift standard for copper NMR. Also for $Cu[P(OC_2H_5)_3]_4{}^+$ the linewidth has a minimum as a function of temperature, but at a significantly higher temperature than for $Cu(CH_3CN)_4{}^+$. Marker and Gunter[181] have performed a thorough study of the relaxation behaviour of $Cu[P(OCH_3)]_4{}^+$ and $Cu[P(OC_2H_5)_3]_4{}^+$ as a function of temperature. They confirm the conclusion drawn by Kroneck et al.[178] regarding the presence of low symmetry species in addition to the

tetrahedral complex. They have used both ^{63}Cu and ^{31}P to study the relaxation of the ^{63}Cu nucleus since not only the ^{63}Cu resonance but also the ^{31}P resonance linewidth depends on the relaxation rate of the ^{63}Cu nucleus. A detailed analysis of these temperature dependences results in activation energies for both the reorientational and exchange processes: 12.6 and 17.7 kJ mol^{-1} respectively for Cu[P(OC$_2$H$_5$)$_3$]$_4$$^{+}$, and 13.1 and 15.3 kJ mol^{-1} respectively for Cu[P(OCH$_3$)$_3$]$_4$$^{+}$. The lower activation energy for the exchange of the P(OC$_2$H$_5$)$_3$ ligand, as compared to P(OCH$_3$)$_3$, is in agreement with the notion that the bulkier ligand should have the faster exchange.[182]

^{67}Zn is a low receptivity nucleus with a natural abundance of 4.1% and a magnetic moment of 0.784 μ_N. This together with its quadrupole moment is a reasonable explanation as to why this biochemically interesting metal has been almost neglected by NMR spectroscopists. However, Carson and Dean[183] have studied a series of symmetrical thiolatozincates (Table 16)

TABLE 16

^{67}Zn chemical shifts and linewidths for some thiolatozincates and Zn(SePh)$_4$$^{2-}$.

Complex	Temp. (K)	δ^a (ppm)	$W_{\frac{1}{2}}$ (Hz)
Zn(SMe)$_4$$^{2-}$	297	362	110
Zn(SPr^i)$_4$$^{2-}$	297	352	1200
Zn(SPh)$_4$$^{2-}$	303	267	1050
Zn$\left(\begin{smallmatrix} \diagup S \rceil \\ \diagdown S \rfloor \end{smallmatrix}\right)_2$$^{2-}$	363	418	1200
Zn(SePh)$_4$$^{2-}$	363	224	830

^{a} Shift relative to 2 M Zn(ClO$_4$)$_2$ at 297 K.

and discuss the possibility of using ^{67}Zn NMR to study the zinc binding protein metallothionein, which has been extensively studied by ^{113}Cd NMR.[184] The linewidths observed, from 110 Hz for Zn(SMe)$_4$$^{2-}$,[183] are not too promising for studies on even small proteins like metallothioneins. A quite considerable shift range is found for the Zn(SR)$_4$$^{2-}$ complexes, c. 150 ppm, and a further shielding increase of 40 ppm for Zn(SePh)$_4$$^{2-}$. These shifts parallel those determined for ^{113}Cd, but they are somewhat smaller than expected.[185,186]

Li and Popov[187] have studied the solvation of various zinc salts in aqueous, non-aqueous and mixed solvents. They find that the ^{67}Zn resonance from Zn(NO$_3$)$_2$ depends strongly on the nature of the solvent (water, DMSO or methanol); however, it remains independent of concentration, thus indicating that there is no formation of contact ion pairs. Figure 24 shows that
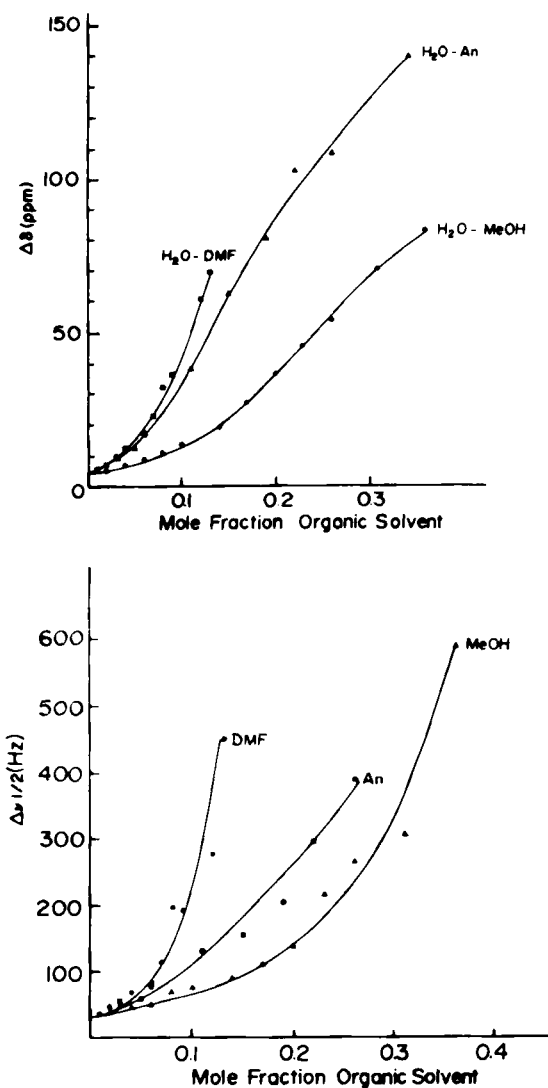
FIG. 24. (Upper) ^{67}Zn chemical shift. (Lower) linewidth of 0.163 M ZnCl$_2$ solution in binary solvent mixtures. From reference 187, with permission.

both chemical shift and linewidth for a ZnCl$_2$ solution depend strongly on the solvent mixture. The deshielding of the ^{67}Zn resonance is consistent with enhanced complex formation with increasing non-aqueous solvent in the solvent mixture. An attempt has been made[187] to study complex formation, but with little success. The crown ethers 12C4, 15C5 and 18C6

apparently do not form any complexes with Zn^{2+} and the resonance from $^{67}Zn(EDTA)$ is too broad to be observed.

Shimizu and Hatano have tried to use ^{67}Zn NMR to study the binding of Zn^{2+} ions to small ligands like imidazole and carboxylic acids,[188,189] and to proteins.[190,58] The lesson from their work is that one has to be very careful when interpreting data on ^{67}Zn NMR, and especially for zinc–protein interactions. The reviewer prefers not to discuss these papers further because he strongly disagrees with the authors' conclusions.

VII. CONCLUSIONS

Most naturally occurring quadrupolar nuclei have now been studied by NMR, and the widespread use of modern NMR equipment has in many cases facilitated these studies. However, in not a few cases it has been found that the dead time of modern spectrometers, especially at low frequencies, is quite long. My personal impression is that the manufacturers of multi-purpose NMR spectrometers have neglected the fact that probe ringing (acoustic ringing) can in many cases be the limiting factor when one wants to observe broad lines. The probe ringing may also become a problem when observing narrow signals over a wide spectral width; see, for example, the distorted lineshapes obtained in Fig. 20 due to the use of a long dead-time.

A majority of the NMR studies of quadrupolar nuclei are now to be found in the field of applications. They are performed with the aim of solving, or at least shedding more light on, a given chemical or biochemical problem. Of course there are, and will always be, some "pure" NMR studies and also some methodological studies.

It seems that more chemists, and a few biochemists, are becoming aware of the possibilities of using NMR of quadrupolar nuclei; however, the increase in these uses of NMR is not as great as one might have foreseen five years ago, and the spin-$\frac{1}{2}$ nuclei are still dominating the NMR world and will probably be doing so for a long time to come.

ACKNOWLEDGMENT

REFERENCES

1. F. Wehrli, in *Annual Reports on NMR Spectroscopy*, Vol. 9 (G. A. Webb, ed.), Academic Press, London, 1979, p. 125.
2. *NMR of Newly Accessible Nuclei*, Vol. 1 (P. Laszlo, ed.), Academic Press, New York, 1983.

3. *NMR of Newly Accessible Nuclei*, Vol. 2 (P. Laszlo ed.), Academic Press, New York, 1983.
4. *The Multinuclear Approach to NMR Spectroscopy* (J. B. Lambert and F. G. Riddell, eds.), Reidel, Boston, 1983.
5. E. Schmidt and A. I. Popov, *Spectroscopy Lett.*, 1981, **14**, 787.
6. E. Schmidt, A. Hourdakis and A. I. Popov, *Inorg. Chim. Acta*, 1981, **52**, 91.
7. E. Schmidt and A. I. Popov, *J. Am. Chem. Soc.*, 1983, **105**, 1873.
8. J. S. Shih and A. I. Popov, *Inorg. Chem.*, 1980, **19**, 1689.
9. E. Shchori, J. Jagur-Grodzinski and M. Shporer, *J. Am. Chem. Soc.*, 1973, **95**, 3842.
10. K. J. Neurohr, T. Drakenberg, S. Forsén and H. Lilja, *J. Magn. Reson.*, 1983, **51**, 460.
11. J. P. Kintzinger and J. M. Lehn, *J. Am. Chem. Soc.*, 1974, **96**, 3313.
12. C. Detellier and P. Laszlo, *J. Am. Chem. Soc.*, 1980, **102**, 1135.
13. C. Detellier, A. Paris and P. Laszlo, *Compt. Rend. Acad. Sci.* (D), 1978, **286**, 781.
14. F. M. Raushel and J. J. Villafranca, *Biochemistry*, 1980, **19**, 5481.
15. J. J. Villafranca and F. M. Raushel, *Fed. Proc.*, 1982, **41**, 2961.
16. V. J. Morris and P. S. Belton, *J. Chem. Soc., Chem. Commun.*, 1980, 983.
17. S. Khazaeli, J. L. Dye and A. I. Popov, *Spectrochim. Acta*, 1983, **39A**, 19.
18. C. Deverell and R. E. Richards, *Mol. Phys.*, 1966, **10**, 551.
19. S. Khazaeli, A. I. Popov and J. L. Dye, *J. Phys. Chem.*, 1982, **86**, 4238.
20. M. Shamsipur, G. Rounaghi and A. I. Popov, *J. Solution Chem.*, 1980, **9**, 701.
21. M. Shamsipur and A. I. Popov, *J. Am. Chem. Soc.*, 1979, **101**, 4051.
22. S. Khazaeli, A. I. Popov and J. L. Dye, *J. Phys. Chem.*, 1982, **86**, 5018.
23. S. Khazaeli, J. L. Dye and A. I. Popov, *J. Phys. Chem.*, 1983, **87**, 1830.
24. E. Kauffmann, J. L. Dye, J. M. Lehn and A. I. Popov, *J. Am. Chem. Soc.*, 1980, **102**, 2274.
25. G. N. Arkhipovich, S. A. Dubrovskii, K. S. Kazanskii, N. V. Ptitsina and A. N. Shupik, *Eur. Polym. J.*, 1982, **18**, 569.
26. D. M. Rose, M. L. Bleam, P. A. Tovo, M. T. Record and R. G. Bryant, in *Biochemical Structure Determination by NMR* (A. A. Bothner-By, A. Glickson and B. D. Sykes, eds.), Dekker, New York, 1981.
27. O. Lutz, in *The Multinuclear Approach to NMR Spectroscopy* (J. B. Lambert and F. G. Riddell, eds.), Reidel, Boston, 1983.
28. P. H. Heubel and A. I. Popov, *J. Solution Chem.*, 1979, **8**, 283.
29. L. Simeral and G. E. Maciel, *J. Phys. Chem.*, 1978, **80**, 552.
30. E. Bouhoutsos-Brown and R. G. Bryant, *J. Inorg. Nucl. Chem.*, 1981, **43**, 3213.
31. R. M. Farmer and A. I. Popov, *Inorg. Nucl. Chem. Lett.*, 1981, **17**, 51.
32. V. Gutman and E. Wychera, *Inorg. Nucl. Chem. Lett.*, 1966, **2**, 257.
33. B. M. Rode, T. Pontani and G. Heckmann, *J. Chem. Soc., Faraday Trans. 1*, 1978, **74**, 71.
34. H. G. Kraft, P. Peringer and B. M. Rode, *Inorg. Chim. Acta*, 1981, **48**, 135.
35. D. F. Gaines, K. M. Coleson and D. F. Hillenbrand, *J. Magn. Reson.*, 1981, **44**, 84.
36. F. W. Wehrli and S. L. Wehrli, *J. Magn. Reson.*, 1982, **47**, 151.
37. E. Bouhoutsos-Brown, D. M. Rose and R. G. Bryant, *J. Inorg. Nucl. Chem.*, 1981, **43**, 2247.
38. H. Dieber, M. Eigen, G. Ilgrenfritz, G. Maass and R. Winkler, *Pure Appl. Chem.*, 1969, **20**, 93.
39. T. Drakenberg, *Acts Chem. Scand.*, 1982, **A36**, 79.
40. H. J. Vogel, T. Drakenberg and S. Forsén, in *NMR of Newly Accessible Nuclei*, Vol. 1 (P. Laszlo, ed.), Academic Press, New York, 1983.
41. P. Robertson, R. G. Hiskey and K. A. Koehler, *J. Biol. Chem.*, 1978, **253**, 5880.
42. H. C. March, P. Robertson, M. E. Scott, K. A. Koehler and R. G. Hiskey, *J. Biol. Chem.*, 1979, **254**, 10268.
43. P. Robertson, K. A. Koehler and R. G. Hiskey, *Biochem. Biophys. Res. Commun.*, 1979, **86**, 265.
44. M. M. Sarasua, K. A. Koehler, C. Skrzynia and J. M. McDonagh, *J. Biol. Chem.*, 1982, **257**, 14102.

45. J. Parello, H. Lilja, A. Cavé and B. Lindman, *FEBS Lett.*, 1978, **89**, 191.
46. A. Cavé, J. Parello, T. Drakenberg and B. Lindman, *FEBS Lett.*, 1979, **100**, 148.
47. T. Andersson, T. Drakenberg, S. Forsén, T. Wieloch and M. Lindström, *FEBS Lett.*, 1981, **123**, 115.
48. T. Andersson, T. Drakenberg, S. Forsén and E. Thulin, *FEBS Lett.*, 1981, **125**, 39.
49. S. Forsén, T. Andersson, T. Drakenberg, E. Thulin and T. Wieloch, in *Advances in Solution Chemistry* (Bertini *et al.*, eds.), Plenum Press, 1981.
50. T. Andersson, T. Drakenberg, S. Forsén, E. Thulin and M. Swärd, *J. Am. Chem. Soc.*, 1982, **104**, 576.
51. T. Andersson, T. Drakenberg, S. Forsén and E. Thulin, *Eur. J. Biochem.*, 1982, **126**, 501.
52. S. Forsén, T. Andersson, T. Drakenberg, E. Thulin and M. Swärd, *Fed. Proc.*, 1982, **41**, 2981.
53. S. Forsén, T. Andersson, T. Drakenberg, H. Lilja and E. Thulin, *Period. Biol.* (Jugoslavia), 1983, **85**, 31.
54. S. Forsén, A. Andersson, T. Drakenberg, O. Teleman, E. Thulin and H. J. Vogel, in *Calcium Binding Proteins 1983* (B. de Bernard *et al.*, eds.), Elsevier North Holland, Amsterdam, 1983.
55. S. Forsén, *Inorg. Chim. Acta*, 1983, **79**, 39.
56. T. Drakenberg, S. Forsén and H. Lilja, *J. Magn. Reson.*, 1983, **53**, 412.
57. T. Shimizu and M. Hatano, *Biochem. Biophys. Res. Commun.*, 1982, **104**, 720.
58. T. Shimizu and M. Hatano, *Biochem. Biophys. Res. Commun.*, 1982, **104**, 1356.
59. T. Shimizu, M. Hatano, S. Nagao and Y. Nozawa, *Biochem. Biophys. Res. Commun.*, 1982, **106**, 1112.
60. T. Shimizu and M. Hatano, *Inorg. Chim. Acta*, 1983, **80**, L37.
61. E. O. Bishop, S. J. Kimber, B. E. Smith and P. J. Beynon, *FEBS Lett.*, 1979, **101**, 31.
62. R. M. Frye, H. Lee and G. A. Rechnitz, *Clin. Biochem.*, 1974, **7**, 258.
63. E. O. Bishop, M. D. Lambert, D. Orchard and B. E. Smith, *Biochim. Biophys. Acta*, 1977, **482**, 286.
64. P. Reimarsson, J. Parello, T. Drakenberg, H. Gustavsson and B. Lindman, *FEBS Lett.*, 1979, **108**, 439.
65. D. M. Rose, M. L. Bleam, M. T. Record, and R. G. Bryant, *Proc. Nat. Acad. Sci. USA*, 1980, **77**, 6289.
66. D. M. Rose, C. F. Polnaszek and R. G. Bryant, *Biopolymers*, 1982, **21**, 653.
67. D. W. Urry, T. L. Trapane and C. M. Venkatachalam, *Calcif. Tissue Int.*, 1982, **34**, S41.
68. B. Lindman, S. Forsén and H. Lilja, *Chem. Scr.*, 1977, **11**, 91.
69. J. Kodweiss, O. Lutz, W. Messner, K. R. Mohn, A. Nolle, B. Stütz and D. Zepf, *J. Magn. Reson.*, 1981, **43**, 495.
70. C. H. F. Chang, T. P. Pitner, R. E. Lenkinski and J. D. Glickson, *Bioinorg. Chem.*, 1978, **8**, 11.
71. R. E. Lenkinski, C. H. F. Chang and J. D. Glickson, *J. Am. Chem. Soc.*, 1978, **100**, 5383.
72. R. Haron, J. Gairin and G. Commenges, *Inorg. Chim. Acta*, 1980, **46**, 63.
73. R. Colton, D. Dakternieks and J. Hauenstein, *Aust. J. Chem.*, 1981, **34**, 949.
74. B. R. McGarvey, M. J. Taylor and D. G. Tuck, *Inorg. Chem.*, 1981, **20**, 2010.
75. B. R. McGarvey, C. Owens Trudell, D. G. Tuck and L. Victoriano, *Inorg. Chem.*, 1980, **19**, 3432.
76. V. A. Pestunovich, S. N. Tandura, B. Z. Shterenberg, N. Yu. Kromova, T. K. Gar, V. F. Mironov and M. G. Verenkov, *Izv. Akad. Nauk SSSR, Ser. Khim.*, 1980, 959.
77. R. G. Kidd and H. G. Spinney, *Can. J. Chem.*, 1981, **59**, 2940.
78. G. J. Goetz-Grandmont and M. J. F. Leroy, *Z. Anorg. Allg. Chem.*, 1983, **496**, 40.
79. V. P. Tarasov, V. I. Privalov and Yu. A. Buslaev, *Mol. Phys.*, 1978, **35**, 1047.
80. K. Morgan, B. G. Sayer and G. J. Shrobilgen, *J. Magn. Reson.*, 1983, **52**, 139.
81. E. Fukushima, *J. Chem. Phys.*, 1971, **55**, 2463.

82. R. R. Vold, S. W. Sparks and R. L. Vold, *J. Magn. Reson.*, 1978, **30**, 497.
83. B. Ancian, B. Tiffon and J. E. Dubois, *Chem. Phys. Lett.*, 1979, **65**, 281.
84. H. W. Spiess, D. Schweitzer, U. Haerberlen and K. H. Hausser, *J. Magn. Reson.*, 1971, **5**, 101.
85. R. C. Mockler and G. R. Bird, *Phys. Rev.*, 1955, **98**, 1837.
86. T. Amano, E. Hirota and Y. Monuo, *J. Phys. Soc. Japan*, 1967, **22**, 399.
87. J. R. Eshbach, R. E. Hillger and M. W. P. Strandberg, *Phys. Rev.*, 1952, **85**, 532.
88. C. H. Townes and S. Geschwind, *Phys. Rev.*, 1948, **44**, 1113.
89. G. C. Dousmanis, T. M. Sanders, C. H. Townes and H. J. Zeiger, *J. Chem. Phys.*, 1953, **21**, 1416.
90. J. F. Hinton and D. Shungu, *J. Magn. Reson.*, 1983, **54**, 309.
91. E. Haid, D. Köhnlein, G. Kössler, O. Lutz and W. Schich, *J. Magn. Reson.*, 1983, **55**, 145.
92. R. Faure, E. J. Vincent, J. M. Ruiz and L. Léna, *Org. Magn. Reson.*, 1981, **15**, 401.
93. D. L. Harris and S. A. Evans, *J. Org. Chem.*, 1982, **47**, 3355.
94. E. Haid, D. Köhnlein, G. Kössler, O. Lutz, W. Messner, K. R. Mohn, G. Nothaft, B. Van Reiklen, W. Schich and N. Steinhauser, *Z. Naturforsch.*, 1983, **38a**, 317.
95. G. A. Melson, D. J. Olszanski and A. K. Rahimi, *Spectrochim. Acta*, 1977, **33A**, 301.
96. V. P. Tarasov, G. A. Kirakosyan, S. V. Trots, Yu. A. Buslaev and V. T. Panyushkin, *Koord. Khim.*, 1983, **9**, 205.
97. Yu. A. Buslaev, G. A. Kirakosyan and V. P. Tarasov, *Dokl. Akad. Nauk SSSR*, 1982, **264**, 1405.
98. O. Lutz and H. Oehler, *J. Magn. Reson.*, 1980, **37**, 261.
99. P. B. Sogo and C. D. Jeffries, *Phys. Rev.*, 1955, **99**, 613.
100. C. Hassler, J. Kronenbitter and A. Schwenk, *Z. Physik*, 1977, **A280**, 117.
101. D. C. McCain, *J. Inorg. Nucl. Chem.*, 1980, **42**, 1185.
102. L. S. Smith, D. C. McCain and D. L. Wertz, *J. Am. Chem. Soc.*, 1975, **97**, 2365.
103. P. L. Rinaldi, S. A. Khan, G. R. Choppin and G. R. Levy, *J. Am. Chem. Soc.*, 1979, **101**, 1350.
104. C. A. M. Vijverberg, J. A. Peters, A. P. G. Kieboom and H. van Bekkum, *Rec. Trav. Chim. Pays-Bas*, 1980, **99**, 287.
105. D. D. Ensor and G. R. Chopin, *J. Inorg. Nucl. Chem.*, 1980, **42**, 1477.
106. D. F. Evans and P. H. Missen, *J. Chem. Soc., Dalton Trans.*, 1982, 1929.
107. N. Hao, B. G. Sayer, G. Dénè, D. G. Bickley, C. Detellier and M. J. McGlinchey, *J. Magn. Reson.*, 1982, **50**, 50.
108. R. G. Kidd, R. W. Matthews and H. G. Spinney, *J. Am. Chem. Soc.*, 1972, **94**, 6686.
109. B. G. Sayer, N. Hao, G. Dénès, D. G. Bickley and M. J. McGlinchey, *Inorg. Chim. Acta*, 1981, **48**, 53.
110. B. G. Sayer, J. I. A. Thompson, N. Hao, T. Birchall, D. R. Eaton and M. J. McGlinchey, *Inorg. Chem.*, 1981, **20**, 3748.
111. E. Heath and O. W. Howarth, *J. Chem. Soc., Dalton Trans.*, 1981, 1105.
112. O. W. Howarth and J. R. Hunt, *J. Chem. Soc., Dalton Trans.*, 1979, 1389.
113. M. A. Habayeb and O. E. Hileman, *Can. J. Chem.*, 1980, **58**, 2255.
114. R. J. Gillespie and U. R. K. Rao, *J. Chem. Soc., Chem. Commun.*, 1983, 422.
115. J. V. Hatton, Y. Saito and W. G. Schneider, *Can. J. Chem.*, 1964, **43**, 47.
116. Yu. A. Buslaev, V. D. Kopanev, A. A. Konovalova, S. V. Bainova and V. P. Tarasov, *Dokl. Akad. Nauk SSSR*, 1978, **243**, 1175.
117. M. Herberhold and H. Trampisch, *Z. Naturforsch.*, 1982, **37b**, 614.
118. M. Herberhold and H. Trampisch, *Inorg. Chim. Acta*, 1983, **70**, 143.
119. F. Näumann and D. Rehder, *J. Organometal. Chem.*, 1981, **204**, 411.
120. D. Rehder and K. Wieghardt, *Z. Naturforsch.*, 1981, **36b**, 1251.
121. R. Talay and D. Rehder, *Chem. Ber.*, 1978, **111**, 1978.
122. D. Rehder, *J. Magn. Reson.*, 1980, **38**, 419.

123. C. A. Tolman, *Chem. Rev.*, 1977, **77**, 313.
124. K. Paulsen, D. Rehder and D. Thoennes, *Z. Naturforsch.*, 1978, **33a**, 834.
125. D. Rehder, H. C. Bechthold, A. Kececi, H. Schmidt and M. Siewing, *Z. Naturforsch.*, 1982, **37b**, 631.
126. H. C. Bechthold and D. Rehder, *J. Organometal. Chem.*, 1982, **233**, 215.
127. H. C. Bechthold and D. Rehder, *J. Organometal. Chem.*, 1981, **206**, 305.
128. D. Rehder, H. C. Bechthold and K. Paulsen, *J. Magn. Reson.*, 1980, **40**, 305.
129. J. A. Pople, *Mol. Phys.*, 1958, **1**, 168.
130. R. G. Kidd and H. G. Spinney, *J. Am. Chem. Soc.*, 1981, **103**, 4759.
131. R. G. Kidd and H. G. Spinney, *J. Inorg. Nucl. Chem.*, 1973, **12**, 1967.
132. P. Kroneck, O. Lutz and A. Nolle, *Z. Naturforsch.*, 1980, **35A**, 226.
133. O. Lutz, A. Nolle and P. Kroneck, *Z. Physik*, 1977, **A282**, 157.
134. S. F. Gheller, P. A. Gazzana, A. F. Masters, R. T. C. Brownlee, M. J. O'Connor, A. G. Wedd, J. R. Rodgers and M. R. Snow, *Inorg. Chim. Acta*, 1981, **54**, L131.
135. K. A. Christiansen, P. E. Miller, M. Minelli, T. W. Rockway and J. H. Enemark, *Inorg. Chim. Acta*, 1981, **56**, L27.
136. E. C. Alyea and J. Topich, *Inorg. Chim. Acta*, 1982, **65**, L95.
137. S. F. Gheller, T. W. Hambley, P. R. Traill, R. T. C. Brownlee, M. J. O'Connor, M. R. Snow and A. G. Wedd, *Aust. J. Chem.*, 1982, **35**, 2183.
138. M. A. Freeman, F. A. Schultz and C. N. Reilley, *Inorg. Chem.*, 1982, **21**, 567.
139. M. Minelli, J. H. Enemark, K. Weighart and M. Hahn, *Inorg. Chem.*, 1983, **22**, 3952.
140. J. L. Johnson, in *Molybdenum and Molybdenum Containing Enzymes* (M. P. Coughlan, ed.), Pergamon Press, Oxford, 1980, p. 345.
141. S. F. Gheller, T. W. Hambley, R. T. C. Brownlee, M. J. O'Connor, M. R. Snow and A. G. Wedd, *J. Am. Chem. Soc.*, 1983, **105**, 1527.
142. A. F. Masters, R. T. C. Brownlee, M. J. O'Connor, A. G. Wedd and J. D. Cotton, *J. Organometal. Chem.*, 1980, **195**, C17.
143. J. Y. LeGall, M. M. Kubicki and F. Y. Petillon, *J. Organometal. Chem.*, 1981, **221**, 287.
144. S. Dysart, I. Georgic and B. E. Mann, *J. Organometal. Chem.*, 1981, **213**, C10.
145. R. T. C. Brownlee, A. F. Masters, M. J. O'Connor, A. D. Wedd, H. A. Kimlin and J. D. Cotton, *Org. Magn. Reson.*, 1982, **20**, 73.
146. M. Minelli, J. L. Hubbard, K. A. Christensen and J. H. Enemark, *Inorg. Chem.*, 1983, **22**, 2652.
147. A. F. Masters, R. T. C. Brownlee, M. J. O'Connor and A. G. Wedd, *Inorg. Chem.*, 1981, **20**, 4183.
148. M. Minelli, T. W. Rockway, J. H. Enemark, H. Brunner and M. Muschiol, *J. Organometal. Chem.*, 1981, **217**, C34.
149. E. C. Alyea, R. E. Lenkinski and A. Somogyvari, *Polyhedron*, 1982, **1**, 130.
150. P. Jaitner and W. Wohlgenannt, *Monatsh. Chem.*, 1982, **113**, 699.
151. J. T. Bailey, R. J. Clark and G. C. Levy, *Inorg. Chem.*, 1982, **21**, 2085.
152. G. T. Andrews, I. J. Colquhorun, W. McFarlane and S. O. Grim, *J. Chem. Soc., Dalton Trans.*, 1982, 2353.
153. M. M. Kubicki, R. Kergout, J. Y. LeGall, J. E. Guerchais, J. Douglade and R. Mercier, *Aust. J. Chem.*, 1982, **35**, 1543.
154. E. C. Alyea, G. Ferguson and A. Somogyvari, *Organometallics*, 1983, **2**, 668.
155. G. M. Gray and R. J. Gray, *Organometallics*, 1983, **2**, 1026.
156. A. F. Masters, G. E. Bossard, T. A. George, R. T. C. Brownlee, M. J. O'Connor and A. G. Wedd, *Inorg. Chem.*, 1983, **22**, 908.
157. G. M. Gray and C. S. Kraihanzel, *Inorg. Chem.*, 1983, **22**, 2959.
158. S. Donovan-Mtunzi, M. Hughes, G. J. Leigh, H. M. Ali, R. L. Richards and J. Mason, *J. Organometal. Chem.*, 1983, **246**, C1.
159. D. Rehder, *Chem. Ber.*, 1978, **111**, 1978.

160. A. Kececi and D. Rehder, *Z. Naturforsch.*, 1980, **36b**, 20.
161. R. G. Kidd, *J. Magn. Reson.*, 1981, **45**, 88.
162. D. Rehder, R. Kramolowsky, K. G. Steinhäuser, U. Kunze and A. Antoniadis, *Inorg. Chim. Acta*, 1983, **73**, 243.
163. K. J. Franklin, C. J. L. Lock, B. G. Sayer and G. J. Schrobilgen, *J. Am. Chem. Soc.*, 1982, **104**, 5303.
164. A. R. Haase, O. Lutz, M. Müller and A. Nolle, *Z. Naturforsch.*, 1976, **31a**, 1427.
165. K. U. Buckler, A. R. Haase, O. Lutz, M. Müller and A. Nolle, *Z. Naturforsch.*, 1977, **32a**, 126.
166. O. Lutz, A. Nolle and P. Kroneck, *Z. Physik*, 1977, **A282**, 157.
167. C. Brevard and P. Granger, *J. Chem. Phys.*, 1981, **75**, 4175.
168. C. Brevard and P. Granger, *Inorg. Chem.*, 1983, **22**, 532.
169. R. W. Dykstra and A. M. Harrison, *J. Magn. Reson.*, 1982, **46**, 338.
170. S. Buettgenbach, M. Herschel, G. Meisel, E. Schroedl, W. Witte and W. J. Childs, *Z. Physik*, 1974, **269**, 189.
171. S. Buettgenbach, R. Dicke, H. Gebauer and M. Herschel, *Z. Physik*, 1977, **A280**, 217.
172. P. J. Steel, F. Lahousse, D. Lerner and C. Marzin, *Inorg. Chem.*, 1983, **22**, 1488.
173. H. Schumann, M. Meissner and H. J. Kroth, *Z. Naturforsch.*, 1980, **35b**, 639.
174. N. Hao, M. J. McGlinchey, B. G. Sayer and G. J. Schrobilgen, *J. Magn. Reson.*, 1982, **46**, 158.
175. R. A. Head, J. F. Nixon, N. P. C. Westwood and R. J. Clark, *J. Organometal. Chem.*, 1978, **145**, 75.
176. O. Lutz, H. Oehler and P. Kroneck, *Z. Naturforsch.*, 1978, **33a**, 1021.
177. P. Kroneck, O. Lutz, A. Nolle and H. Oehler, *Z. Naturforsch.*, 1980, **35a**, 221.
178. P. Kroneck, J. Kodweiss, O. Lutz, A. Nolle and D. Zept, *Z. Naturforsch.*, 1982, **37a**, 186.
179. R. L. Kreiter and J. G. Verkade, *Inorg. Chem.*, 1969, **8**, 2115.
180. U. Ochsenbein and C. W. Schläpfer, *Helv. Chim. Acta*, 1980, **63**, 1926.
181. A. Marker and M. J. Gunter, *J. Magn. Reson.*, 1982, **47**, 118.
182. C. A. Tolman, *J. Am. Chem. Soc.*, 1970, **92**, 2956.
183. G. K. Carson and P. A. W. Dean, *Inorg. Chim. Acta*, 1982, **66**, 157.
184. I. M. Armitage and Y. Boulanger, in *NMR of Newly Accessible Nuclei*, Vol. 2 (P. Laszlo, ed.), Academic Press, New York, 1983, p. 337.
185. G. K. Carson, P. A. W. Dean and M. J. Stillman, *Inorg. Chim. Acta*, 1981, **56**, 59.
186. G. K. Carson and P. A. W. Dean, *Inorg. Chim. Acta*, 1982, **66**, 37.
187. Zhi-fen Li and A. I. Popov, *J. Solution Chem.*, 1982, **11**, 17.
188. T. Shimizu, M. Kodaka and M. Hatano, *Biochem. Biophys. Res. Commun.*, 1982, **106**, 988.
189. M. Kodaka, T. Shimizu and M. Hatano, *Inorg. Chim. Acta*, 1983, **78**, L55.
190. T. Shimizu and M. Hatano, *Inorg. Chim. Acta*, 1983, **76**, L177.

This Page Intentionally Left Blank

Platinum NMR Spectroscopy

P. S. PREGOSIN

Laboratorium für Anorganischen Chemie, ETH-Zentrum, Zürich, Switzerland

I. INTRODUCTION

The chemistry of platinum spans a gap which includes heterogeneous catalysts for automobiles,[1] homogeneous catalysts for organic synthesis[2] and cancer drugs.[3] Consequently it is not a mystery to find an increasing number of chemists expressing an interest in ^{195}Pt nuclear magnetic resonance. This isotope is moderately abundant (33.7%) and has a relatively large magnetic moment 1.0398 (μ/μ_B), both of which contribute to making ^{195}Pt NMR measurements relatively easy, e.g. this author's experience suggests that 10^{-2} M solutions give signals in a matter of minutes. Nevertheless the many hundreds of recorded spectra would not have been so readily obtained were it not for the favourable spin–lattice and spin–spin relaxation times of this nucleus. Since all these factors are indeed arranged so as to shine favourably on ^{195}Pt, it is worth describing the moderately more technical studies in which platinum NMR has been involved.

II. METHODOLOGY

The existing literature shows that ^{195}Pt in the oxidation states 0, +2 and +4 possesses spin–lattice relaxation times, T_1, in the range *ca.* 0.014 to 8.31 s,[4-10] with most values less than 2 s.

ABBREVIATIONS

Me methyl; Et ethyl; Pr^n n-propyl; Pr^i i-propyl; Bu^n n-butyl; Bu^t t-butyl; cy cyclohexyl; Bz benzyl; Tol p-tolyl; Mes = mesityl = 2,4,6-trimethylphenyl; py pyridine; en ethylenediamine.

The short T_1 values are normally attributed to efficient relaxation via the chemical shielding anisotropy (CSA) and spin rotation (SR) contributions which can be described as given in the equations

$$1/T_1(\text{CSA}) = (2/15)\nu^2 B_0^2(\sigma_\| - \sigma_\perp)^2 \tau_c \qquad (1)$$

$$1/T_1(\text{SR}) = (2\pi I kT)(2C_\perp^2 + C_\|^2)\tau_J/3 \qquad (2)$$

In equation (1) σ is a measure of the shielding and can be anisotropic, and τ_c is a molecular reorientation correlation time. In equation (2) C is a spin rotation tensor and τ_J the anglar momentum correlation time. The temperature dependence in equation (2) is significant since $T_1(\text{SR})$ decreases with increasing temperature, whereas the opposite is true for $T_1(\text{CSA})$. Recent work[4,5] has emphasized the importance of the CSA term, e.g. T_1 for the relatively symmetric tetrahedral molecule $[\text{Pt}(\text{P}(\text{OEt})_3)_4]$ is relatively long, 8.31 s (4.7 T, 310 K), but T_1 for the 2-coordinate bent complex $[\text{Pt}(\text{PPr}^i_3)_2]$ is only 0.097 s under the same conditions. These data, when combined with field dependence studies which reveal ca. four-fold decrease in T_1 when B_0 is doubled (the T_1 for $[\text{Pt}(\text{PPr}_3^i)_2]$ is only 0.025 s at 9.4 T), nicely illustrate the importance of CSA relaxation for ^{195}Pt. A similar field dependence has been found for $[\text{Pt}(\text{acac})_2]$.[7] However, the importance of spin rotation should not be forgotten. For $[\text{Pt}(\text{PMe}_3)_4)]$, at 9.4 T where CSA
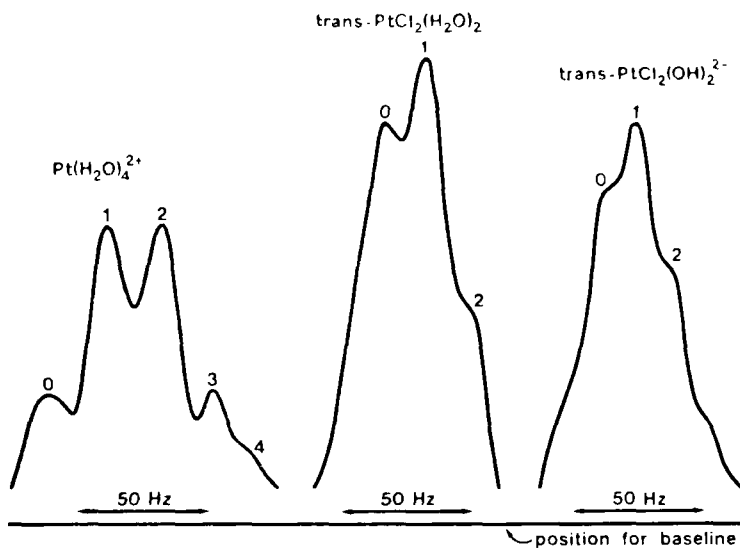
FIG. 1. Platinum-195 NMR spectra of $\text{Pt}(\text{H}_2\text{O})_4^{2+}$, trans-$\text{PtCl}_2(\text{H}_2\text{O})_2$, and trans-$\text{PtCl}_2(\text{OH})_2^{2-}$ equilibrated in isotopic water. The mole fraction of ^{16}O compared to ^{18}O is ca. 1.6:1. The numbers denote number of H_2^{18}O coordinated. The base-line noise is about 5% of the highest peak. From reference 14, with permission.
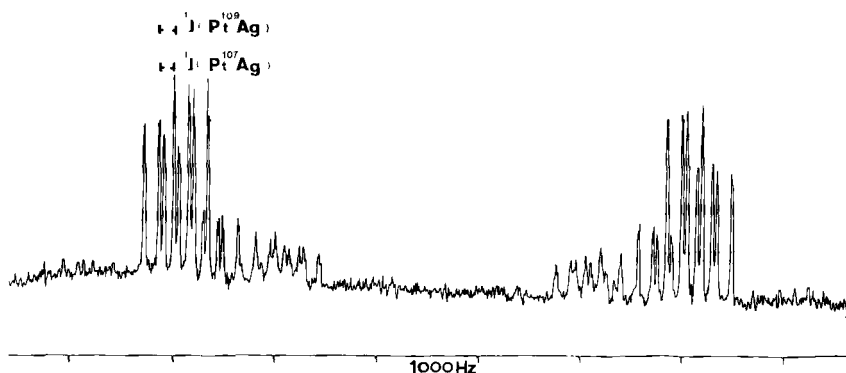
FIG. 2. ^{195}Pt-{^{1}H} spectrum of the cluster [Pt$_3$(μ-CO)$_3$(PPr$^i_3$)$_3${Ag(PPr$^i_3$)}]$^+$ in which an Ag(PPr$^i_3$)$_3^+$ caps the Pt triangle. ^1J(Pt–^{107,109}Ag) = 195 Hz. (K. H. Dahmen and L. M. Venanzi, unpublished results, ETH, 1985.)

relaxation should be important, the observed temperature dependence[5] is suggestive of spin rotation relaxation, i.e. $T_1 = 1.5$ s at 310 K and 5.1 s at 243 K. A listing of ^{195}Pt T_1 values may be found in Table 1. There have been several reports concerned with the approximate magnitude of the ^{195}Pt CSA[11,12] which for $\Delta\sigma$ seems to be of the order of thousands of ppm.

The spin-spin relaxation relation time, T_2, varies very markedly as a function of the coordinated ligands. Although spectra containing well resolved ^{195}Pt lines are common enough,[13] several examples are instructive. Gröning et al.[14] have measured ^{195}Pt NMR spectra for the ^{16}O,^{18}O isotopomers of [Pt(H$_2$O)$_4$]$^{2+}$, trans-[PtCl$_2$(H$_2$O)$_2$] and trans-[PtCl$_2$(OH)$_2$]$^{2-}$ (see Fig. 1) and have used these data in studying the kinetics of H$_2$O exchange, whereas Dahmen and Venanzi[15] have used the transition metal resonance to show that silver is incorporated in their cluster (see Fig. 2). Unfortunately there are many examples of broad ^{195}Pt resonances and most of these arise from complexes containing ligand atoms with moderate to large quadrupole moments, e.g. ^{14}N, ^{79,81}Br, ^{127}I. Figure 3 shows the line broadening due to the ^{14}N in trans-[PtCl$_2$(ethylene)(NH$_2$C$_6$H$_4$-p-CH$_3$)],[16] relative to its ^{15}N enriched isotopomer. For a number of complexes with nitrogen ligands the ^{14}N relaxation is sufficiently slow to allow the observation of ^1J(^{195}Pt-^{14}N) values (see below and in Tables section).

There are further negative consequences of the relatively short ^{195}Pt relaxation times as illustrated by Figs 4 and 5.[17] These spectra show ^{1}H resonances which are coupled to platinum, as a function of magnetic field strength (Fig. 4) and temperature (Fig. 5). As B_0 increases, the CSA contribution shortens the Pt T_1 such that the ^{1}H linewidths are adversely affected. Lowering the temperature also causes a decrease in the Pt T_1(CSA) with a
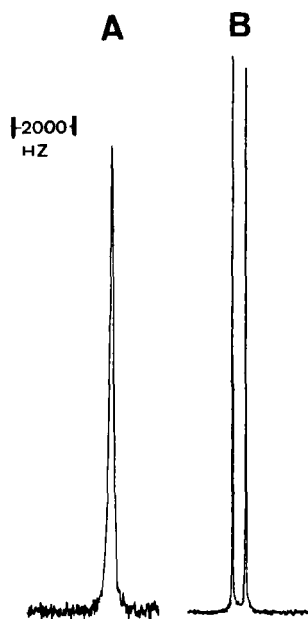
FIG. 3. ^{195}Pt NMR spectrum of (A) *trans*-[PtCl$_2$(C$_2$H$_4$)(NH$_2$C$_6$H$_4$-*p*-CH$_3$)] and (B) the same, enriched with 95 atom % ^{15}N. $\delta = -3013; J = 244$ Hz. (H. Moriyama and P. S. Pregosin, unpublished results.)
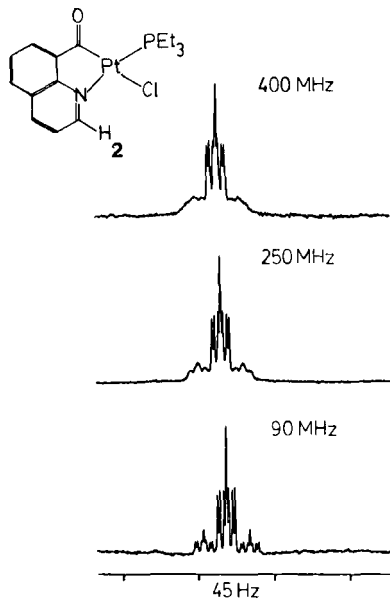
FIG. 4. ^{1}H NMR spectra for the proton *ortho* to nitrogen in the metallated complex [PtCl(COC$_9$H$_6$N)(PEt$_3$)] at magnetic field strengths corresponding to 400, 250 and 90 MHz for ^{1}H. ^3J(Pt–H) = 27.1 Hz. Note that the ^{195}Pt satellites are sharpest at 90 MHz. From reference 17, with permission.
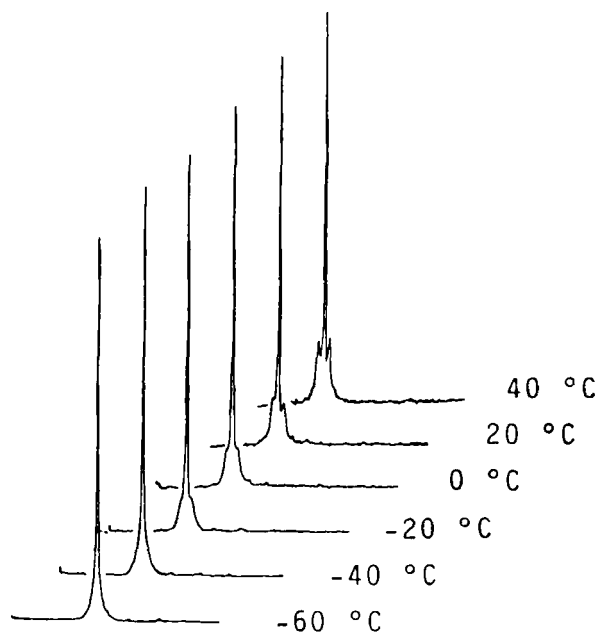
FIG. 5. Temperature dependence of the aldehyde proton of *trans*-[PtCl$_2$(PEt$_3$)(quinoline-8-aldehyde)] in the range −60 to 40 °C. From reference 17, with permission.

similar broadening of the satellite lines. One can easily imagine a problem where slowing a chemical process, via temperature, would be accompanied by this thermal decoupling thereby thwarting a structure proof based on ^nJ(Pt–L) data. Equally frustrating would be a case where signal overlap prompted a high field ^{1}H spectrum only to lose the information due to the CSA relaxation. (This author has experienced both cases.) In any case, broad ^{195}Pt satellites in ^{1}H, ^{13}C and ^{15}N, and occasionally ^{31}P, NMR spectroscopy are quite likely, especially in dimeric and higher molecular weight complexes where τ_c and σ will be important. Temperature is also an important parameter affecting the relation of quadrupolar nuclei and can be used to sharpen a ^{195}Pt–^{14}N interaction.[18,19]

III. REFERENCING

The most commonly used chemical reference is the platinum(IV) dianion PtCl$_6{}^{2-}$ in aqueous solution. There is a solvent dependence[13] of this anion, nevertheless several authors[10,20] have found this convenient, despite the broad line due to the unresolved ^{35,37}Cl isotopomers (resolvable* at 9.4 T[21]).

This reference material is commercially available, and relatively stable; however, in addition to the unfavourable linewidth, $PtCl_6^{2-}$ is a high frequency reference with the consequence that most reported δ values will be negative, i.e. they will appear to low frequency of the reference. An acceptable solution to the problem is to reference platinum resonances using a frequency scale defining the proton signal of tetramethylsilane as exactly 100 000 000 MHz. This provides a reference in which platinum signals appear routinely to high and low frequencies so that the user must adjust to negative numbers in any case. Both scales are in common usage. In an earlier report we have related the two scales using the relationship $\delta(PtCl_6^{2-}) = \delta(\text{frequency scale}) - 4533$ ppm.

IV. CHEMICAL SHIFTS

Metal chemical shifts are dominated by changes in the paramagnetic screening contribution, σ_p, to the total shielding.[22] This term has been discussed in some detail for other nuclides and may be abbreviated as shown in the equation

$$\sigma_p \propto -\langle r^{-3} \rangle \sum_j^{occ} \sum_k^{unocc} (E_k - E_j)^{-1} C \qquad (3)$$

where r is an average distance of a d electron from the nucleus, E_k and E_j are energies of unoccupied and occupied molecular orbitals and C is a complicated sum containing the coefficients of the d (and other) orbitals used in the LCAO summation to develop the various molecular orbitals. There have been a number of attempts to calculate and/or estimate ^{195}Pt chemical shifts,[23] and several of these have met with qualitative success. There seems to be general agreement concerning the importance of the $E_k - E_j$ terms; however, since these will depend upon the nature of the complex, it is difficult to find a single empirical expression which satisfactorily accommodates all the ^{195}Pt data. Nevertheless, Juranic[25] and Goodfellow and co-workers[23] have achieved some impressive results with Pt(IV) and Pt(II) complexes, respectively, and Saito and his group,[24] using extended Hückel methods, have been successful with a small range of Pt(0) derivatives. Goodfellow has recently summarized the situation.[22b] Figure 6 shows a plot of $\delta(^{195}Pt)$ versus a parametrized σ_p for a series of Pt(IV) complexes. Despite this progress it is not likely that theory will be able to pinpoint a platinum resonance position in a complicated molecule in the near future.

---

* There are also H/D and $^{12}C/^{13}C$ isotope effects on $\delta(^{195}Pt)$.[170]
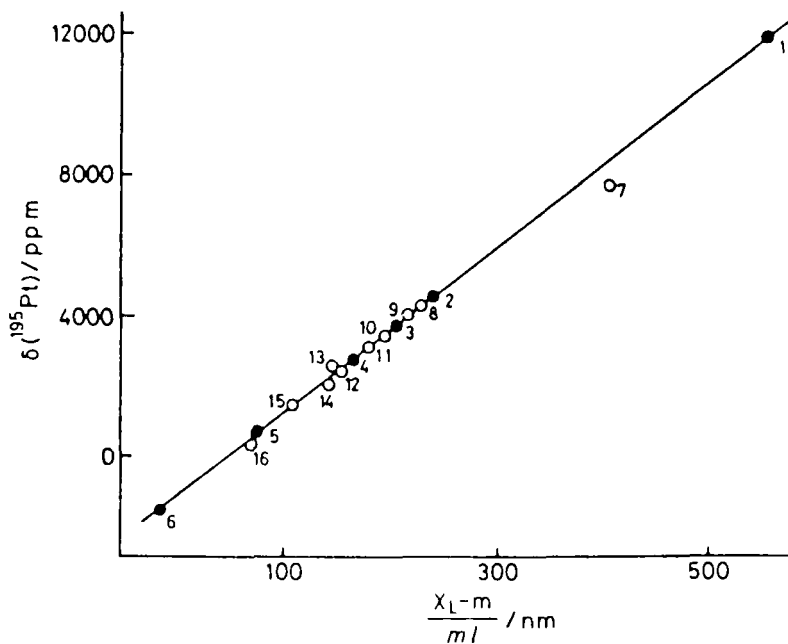
FIG. 6. Linear dependence of ^{195}Pt chemical shifts in platinum(IV) complexes on the parametrized paramagnetic shielding term. Complexes: 4, $[PtBr_6]^{2-}$; 5, $[Pt(CN)_6]^{2-}$; 6, $[PtI_6]^{2-}$; 7, fac-$[PtCl_3F_3]^{2-}$; 8, $[PtBrCl_5]^{2-}$; 9, $[PtBr_2Cl_4]^{2-}$; 10, $[PtCl_5(CNMe)]^-$; 11, $[PtBr_5Cl]^{2-}$; 12, cis-$[PtCl_4(CNMe)_2]$; 13, $trans$-$[PtCl_4(PMe_3)_2]$; 14, cis-$[PtCl_4(PMe_3)_2]$; 15, mer-$[PtCl_3(PMe_3)_3]^+$; 16, $[PtI(CN)_5]^{2-}$. From reference 25, with permission.

Nevertheless there are certain characteristic positions for complex types within the *ca.* 15 000 ppm range of ^{195}Pt chemical shifts, and this brings us to a few frequently (but not always) valid generalizations.

(A) Substitution of a relatively hard A-type ligand, e.g. H_2O or Cl^-, for one which is softer and consequently coordinates strongly to Pt(II), e.g. H^-, CH_3^-, Ph^-, AsR_3, PR_3, induces a relatively large change in $\delta(^{195}Pt)$ (500–1000 ppm or more), e.g.

trans-$[PtCl_3L]^-$ (ref. 23)

L	H_2O	Cl	SMe_2	$AsMe_3$	PMe_3
$\delta(^{195}Pt)$	−1180	−1715	−2757	−3173	−3500

trans-$[PtClR(PEt_3)_2]$[185]

R	Cl	COPh	$SnCl_3$	Ph	H	CH_3	SiH_3[26]
$\delta(^{195}Pt)$	−3916	−4532	−4790	−4857	−4875	−5003	−5067

(B) The Pt chemical shift is a function of the halogen, with low frequency shifts associated with increasing atomic number, e.g.

$PtX_3(AsMe_3)^-$ (ref. 23)

X	Cl	Br	I
$\delta(^{195}Pt)$	−3173	−3869	−5446

$X_2(CO)Pt-Pt(CO)X_2^2$ (ref. 27)

X	Cl	Br	I
$\delta(^{195}Pt)$	−4160	−4335	−4709

(C) There is a rough dependence of the chemical shift on oxidation state, e.g. $PtCl_6^{2-} = 0$, $PtCl_4^{2-} = ca. -1620$; however, here the chemist must exercise caution.

(a) The nature of the ligand is as important as the oxidation state, e.g. $Pt(PEt_3)_4$,[28] $\delta = -5262$ is at *higher* frequency than *trans*-$[PtI_2(PEt_3)_2]$,[23] $\delta = -5553$, although the coordination number is 4 in both cases.

(b) The chemical shift of the metal in $[PtL_n]$ depends *strongly* on n, despite the formal zero oxidation state (see accompanying table). Note once

^{195}Pt chemical shifts in complexes of $Pt(0)$[28]

L in PtL_n	$n = 4$	$n = 3$	$n = 2$
PMe_3	−4909		
PMe_2Ph	−4842		
$PMePh_2$	−4783		
PEt_3	−5262	−4526	
PBu^n_3	−5356	−4511	
$PTol_3$		−4589	
$P(CH_2Ph)_3$		−4439	
PPr^i_3			−6607
Pcy_3		−4567	−6555
PBu^t_2Ph			−6526

Tol = p-tolyl; cy = cyclohexyl.

again that the zerovalent $[Pt(PEt_3)_3]$ at $\delta = -4526$ appears at *higher* frequency than either *trans*-$[PtI_2(PEt_3)_2]$,[23] $\delta = -5553$, or *trans*-$[PtHCl(PEt_3)_2]$, $\delta = -4875$, but that the tetrahedral complexes $[Pt(PEt_3)_4]$, $\delta = -5262$, and $[Pt(PBu^n_3)_4]$, $\delta = -5356$, are shifted to much lower frequency. The 2-coordinate complexes $[PtL_2]$, L = PPr^i_3, Pcy_3, PBu^t_2Ph are found at even lower frequency, $\delta = -6526$ to −6607. These seemingly contradictory examples should serve to remind the reader that the sum of the differences $(E_k - E_j)$ is what (partly) affects $\delta(^{195}Pt)$ and not oxidation state

or coordination number. These latter are chemically and didactically useful tools which should be related to the chemical shift.

(D) $\delta(^{195}Pt)$ is a function of complex geometry. This effect can be quite marked as in the square planar PMe_3 complexes *cis-* and *trans-* $[PtCl_2(PMe_3)_2]$,[23] $\delta = -4408$ and -3950, $\Delta\delta = 458$, respectively, or far more modest as in the octahedral dianions *cis-* and *trans-*$[PtCl_2Br_4]^{2-}$, $\Delta\delta = 13$ ppm,[29] or *cis-* and *trans-*$[PtCl_2(OH)_4]^{2-}$, $\Delta\delta = 24$ ppm;[30] see Tables 13 and 16 for data on simple salts of Pt(IV). As might be expected, replacement of Cl, by Br, or OH^- in the complexes $[PtCl_nX_{6-n}]^2$, X = Br, OH, has a larger effect than the differences arising from the geometric isomers (*ca.* 300 for X = Br,[29] 500–600 for X = OH[30]). Interestingly, in the anions $[PtCl_nBr_{6-n}]^{2-}$, $\delta(^{195}Pt)$ correlates with the sum of the Rochow electronegativities for the halogens.[29]

The recent chemical shift literature shows no developing pattern, rather it would seem that $\delta(^{195}Pt)$ values are often collected just to have them. Indeed, this is reflected in the increasing number of metal shifts which appear in footnotes. The general trend in the chemistry is clear in that the number of reports containing ^{195}Pt data on organometallic complexes has steadily increased. As a sampling of these I note several on platinum–methyl complexes,[31-34] one of which reports a correlation of $\delta(^{195}Pt)$ with $\delta(^{77}Se)$,[31] and various others concerned with alkyl,[35,36] aryl,[37] olefin,[38,39] cyclometallated,[40-42] isonitrile,[43] phosphine[44,45] (phosphate[46]) and hydride[47] complexes.

Before moving to couplings I note two attractive chemical shift applications: the first involves the demethylation of methylcobalamin,[48] where the platinum resonance is used to follow the reaction of $PtCl_6^{2-}$ with the methyl cobalt complex, and the second concerns the low temperature ^{195}Pt study of [1], which reveals conformational isomers.[49]

[1]
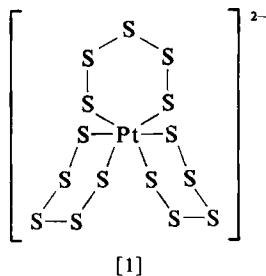
V. COUPLINGS

^{195}Pt is a very desirable "coupling partner". The large gyromagnetic ratio, 5.7505 $(\nu/10^7 \text{ rad T}^{-1} \text{ s}^{-1})$, combined with its position in the periodic table,
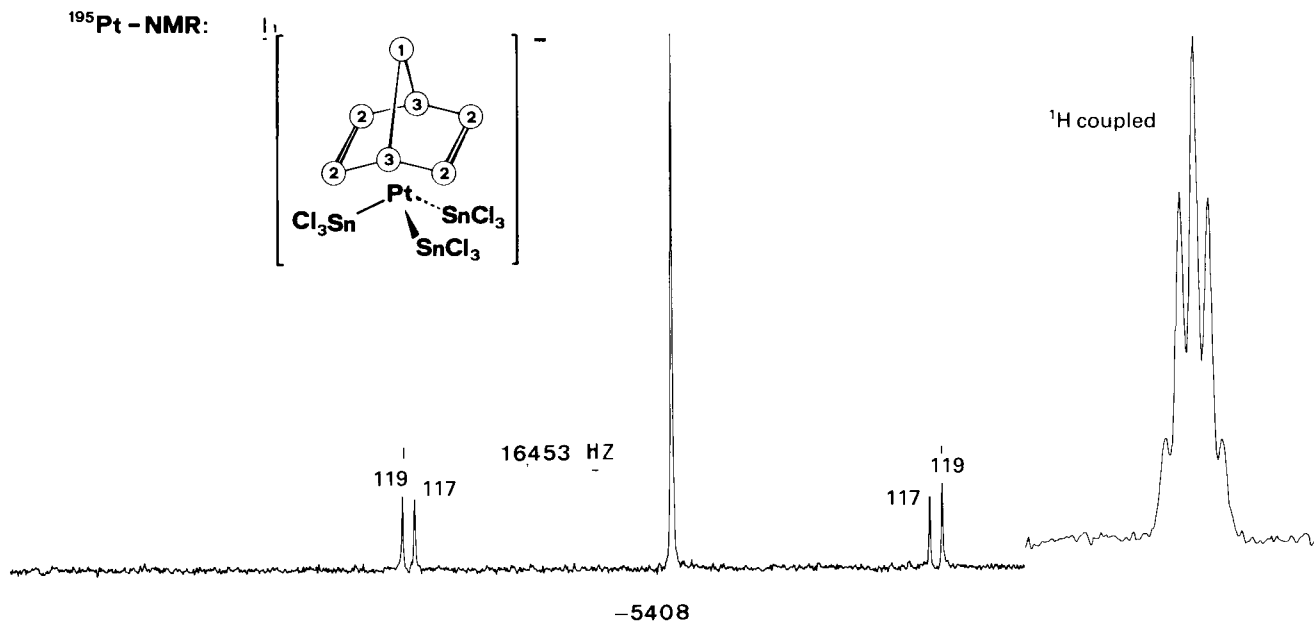
FIG. 7. ^{195}Pt-{^{1}H} spectrum of the anion [Pt(SnCl$_3$)$_3$(norbornadiene)]$^-$ showing ^{117}Sn and ^{119}Sn couplings. The inset, above, shows the ^{1}H-coupled spectrum (main band). (H. Rüegger, PhD thesis, ETH, Zürich, 1983.)

gives a product which, in terms of the contact expression[22a]

$$^1J(^{195}Pt-L) \propto \gamma_{Pt}\gamma_L|\Psi_{S.L}(0)|^2|\Psi_{S.Pt}(0)|^2$$

$$\times \sum_j \sum_k (E_k - E_j)C_{j,Pt}\, C_{j,L}\, C_{k,Pt}\, C_{k,L} \qquad (4)$$

(where L is a suitable ligand atom coupling partner) leads to relatively large one-bond spin–spin couplings. The E and C terms have the same meaning as in equation (3). Spectra demonstrating novel $^1J(Pt-L)$ splittings are shown in Figs 7–9, where platinum couples to ^{207}Pb, $^{117,119}Sn$ and ^7Li (Fig. 2 contains a platinum–silver coupling). The most routinely encountered one-bond interactions are $^1J(Pt-^{31}P)$, $^1J(Pt-^{13}C)$, $^1J(Pt-^1H)$ and $^1J(Pt-^{15}N)$.

There is some information on the signs of $^nJ(Pt-L)$.* McFarlane[50] has shown that $^1J(Pt-P)$ is positive in cis- and trans-[PtCl$_2$(PEt$_3$)$_2$], and this has been confirmed subsequently for a variety of methyl-phosphine organo-platinum complexes[51,52] as well as in simple coordination complexes of PMe$_3$,[53] PF$_3$,[54] and P(OMe)$_3$.[54] $^1J(Pt-H)$ in the complexes [PtHL(PEt$_3$)$_2$]$^+$

Frequency / Hz
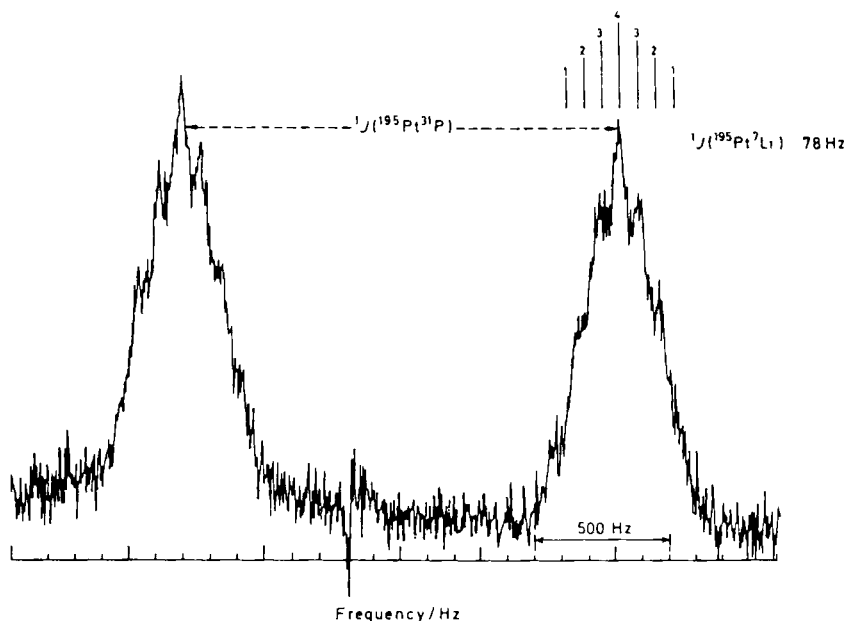
FIG. 8. 42.8 MHz ^{195}Pt NMR spectrum of trans-[Pt(μ-Li)(C$\equiv$CPh)$_2$(Bu^n)(PEt$_3$)]$_2$ (in C$_6$D$_6$, 27 °C, ^1H broad band decoupled). The splitting pattern due to spin–spin coupling between ^{195}Pt and two equivalent ^7Li nuclei ($I = 3/2$) is shown. The presence of ^6Li (natural abundance 7.42%, $I = 1$) will contribute to the intensities, in particular to those of the inner lines since $J(^{195}Pt-^6Li) = 0.38J(^{195}Pt-^7Li)$. From reference 15c, with permission.

* Henceforth the superscripts will be omitted.
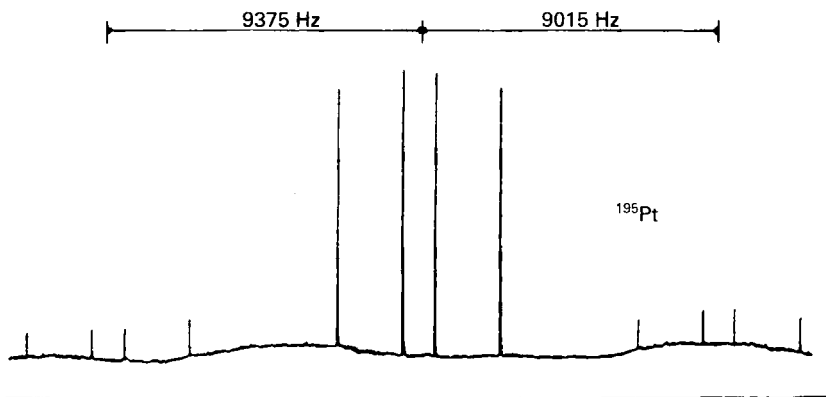
FIG. 9. ^{195}Pt-$\{^1H\}$ NMR spectrum of cis-[PtPh(PbPh$_3$)(PPh$_3$)$_2$] at 21.31 MHz, showing the asymmetry of the satellites relative to the central multiplets. From reference 15b, with permission.

is also positive,[55] L = PH$_3$, PH$_2$Me, PHMe$_2$, PMe$_3$, PEt$_3$, as is ^1J(Pt–C) in the carbonyl compounds cis- and trans-[PtCl$_2$(^{13}CO)(PEt$_3$)][56] and [PtCl(Ph)(^{13}CO)(PEt$_3$)].[56] In the few reported examples, ^1J(Pt–Se) is positive.[57,58] $^3J(Pt-P-C-H)$ has been shown in many examples[53,59] to be positive, as has $^2J(Pt-C-F)$,[51] but $^2J(Pt-C-H)$ is negative.[34,51] ^1J(Pt–Pt) has been determined to be positive[60] in the dimeric complexes [Pt$_2$(CNMe)$_6$]$^{2+}$ and [Pt$_2$\{(CF$_3$)$_2$CO\}(1,5-COD)$_2$].

Platinum is one of the few transition metals where 2-,3-,4- (square planar and tetrahydral), 5- and 6-coordination is to be found. Generally the coordination numbers 2 to 5 give larger ^1J(Pt–L) values than the related 6-coordinate complexes since the former are associated with the lower oxidation states, Pt(0) and Pt(ii), whereas the latter normally represents Pt(iv). This is readily understood in terms of the C coefficients which have a larger percentage s character in the lower oxidation states. Indeed, in some simple molecules ^1J(Pt–L) follows the % s character in the Pt–L bond in a semi-quantitative way. For PtL$_6$ versus PtL$_4$ one would predict the value $^1J\{$Pt(iv)-d^{2}sp$^3\}/^1J\{$Pt(ii)-dsp$^2\}$ to be ca. 0.67. The observed ratios are: 0.577–0.711 for ^1J(Pt–P) in PMe$_3$ complexes;[61] 0.442–0.625 for PX$_3$ complexes,[62] X = F, Cl, Br, OMe, Me; 0.712 for ^1J(Pt–C) in the pair [PtCl$_3$(CO)]$^-$ and [PtCl$_5$(CO)]$^-$;[62] 0.79 for ^1J(Pt–^{14}N) in the pair trans-[PtCl$_2$(NMe$_3$)$_2$] and trans-[PtCl$_4$(NMe$_3$)$_2$];[61] 0.71 and 0.67 for cis-[PtX$_2$(^{15}NH$_2$(CH$_2$)$_{11}$CH$_3$)$_2$][63] and cis-[PtX$_4$(^{15}NH$_2$(CH$_2$)$_{11}$CH$_3$)$_2$], X = Cl, Br, respectively. The trend is clear and qualitatively supports the validity of using equation (4) in discussing changes in ^1J(Pt–L). In addition to the well documented ^1J(Pt–H),[64,65] ^1J(Pt–C)[65-67] and ^1J(Pt–P) values,[67] there

are several relatively uncommon additions to the literature in the form of
^1J(Pt-B),[68] ^1J(Pt-Se),[57,58,69,70] ^1J(Pt-Te)[71,72] and ^1J(Pt-Ag).[73] Compilations
of couplings can be found in the tables section.

VI. APPLICATIONS

Most of the applications involving $\delta(^{195}$Pt) can be classified by utilizing:
(i)   Chemical equivalence (symmetry)
(ii) Ligand induced effects and molecular structure
(iii) ^nJ(Pt-L) as a probe for structure and bonding
(iv) Shift correlation.
Point (i) is nicely illustrated by [2] whose ^{195}Pt spectrum reveals two
types of Pt(ii), as shown in Fig. 10. Despite the four intervening bonds,
^4J(Pt-Pt) is 363 Hz.[74]

[2]
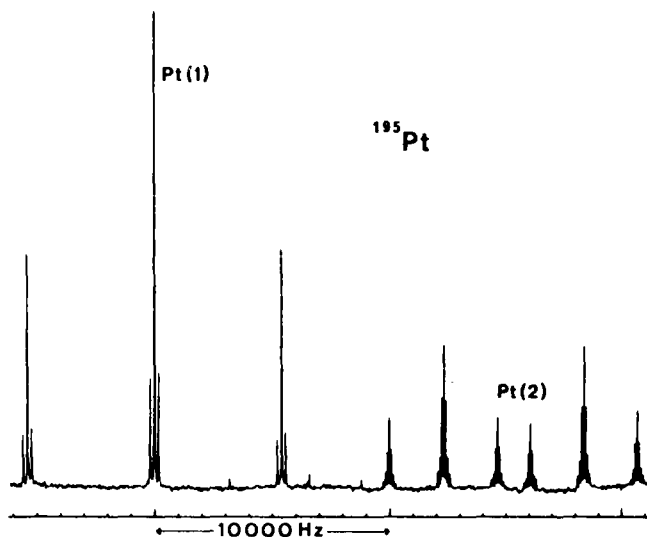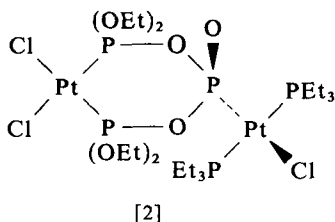
FIG. 10. ^{195}Pt-$\{^1$H} NMR spectrum of complex [2]. From reference 74, with permission.

The isomers [3a] and [3b][75] (Mes = mesityl) illustrate point (ii) in that changing from a phosphorus ligand to a pseudo-olefin induces a shielding
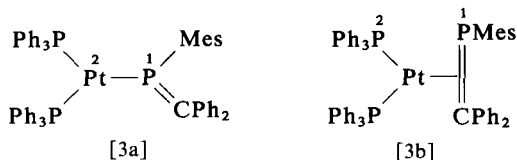
increase, in keeping with literature expectations (Table 2). Still on point (ii), inversion of one SCN from tetrakis-S-[Pt(SCN)$_4$]$^{2-}$, $\delta = -3961$, to [Pt(NCS)(SCN)$_3$]$^{2-}$, $\delta = -3431$, is accompanied by the high frequency shift expected when a "softer" sulphur ligand is replaced by the somewhat harder nitrogen end of the thiocyanate.[76] This type of linkage isomerism has been studied in detail.[77,78]

Despite the sensitivity of the chemical shift, ^nJ(Pt-L) data, point (iii), have proved to be the workhorse in solution structural problems. The two examples cited above do not actually require ^{195}Pt data. The ^1J(Pt-P^1) values readily differentiate [3a] from [3b] (the latter being a modest 500 Hz, the former 4940 Hz), and the ^nJ(Pt-N) values immediately identify the two SCN linkage isomers since ^1J(Pt-N) is of the order of several hundred Hz and ^3J(Pt-N) $\leqslant 20$ Hz.

Of the various ^1J(Pt-L) interactions noted above, ^1J(Pt-P) and ^1J(Pt-C) have received the most coverage. There are two review articles with compilations of the former[67,79] (see also Tables 2 and 3), and Mann and Taylor's text[80] on organometallic complexes is an important source for the latter. In view of the increasing importance of hydride complexes in transition metal chemistry a sampling of ^1J(Pt-H) values is given in Table 4.

A. ^1J(Pt-N) and the *trans* influence

Changes in ^1J(Pt-L) with *trans* ligand provide one method of determining the *trans* influence (the extent to which a ligand labilizes the bond *trans* to it in the ground state at equilibrium) and form the basis of a widely used structural tool. Since the *trans* influence is an important concept in the chemistry and spectroscopy of platinum(ii), and as the nitrogen chemistry of Pt(ii) and Pt(iv) has become the focus of many bioinorganic laboratories, it seems worthwhile to explore the connection between ^1J(Pt-N) and the *trans* influence.

One-bond platinum-nitrogen couplings currently range from 88 Hz[81] to *ca.* 755 Hz,[82,83] with [4] and [5] currently representing extremes. As I find no mention of a ^1J value for a platinum nitrile, i.e. L$_n$Pt-^{15}N≡CR, it is reasonable to assume that the full range has not yet been attained. For a single ligand, e.g. ^{15}NH$_2$R [84] or a Schiff's base,[85] the value of ^1J(Pt-N) is a

[4]

[5]

(X = Cl, 757 Hz,[83] n = 2; X = H_2O,
754 Hz,[82] n = 1; $^{15}NO_2$ *trans* to X)
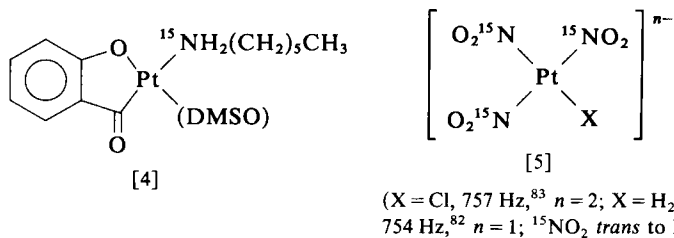
function of the *trans* ligand, L, as shown in the accompanying scheme in which X and Y are a variety of ligands that may be either neutral or anionic (see Tables 6 and 7 for details). In some cases the *cis* ligands have been held constant, so the data directly mirror the *trans* influence. In others (where X and Y are shown) the couplings are a composite of the *trans* influence of L and the varying *cis* influences of X and Y. Carbon ligands

138–336 Hz[84]   294–494 Hz[85] ^{15}N = $^{15}NH_3$ 232–410 Hz
                                                $^{15}NO_2$ 452–757 Hz[82,83]
                                                ^{15}NCS* 287–707 Hz[76–78]

* $^1J(Pt-15N)/^1J(Pt-^{14}N)$ taken as 1.4
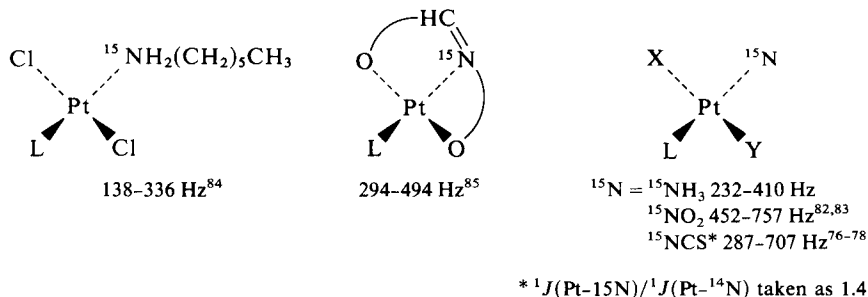
trans to ^{15}N reduce $^1J(Pt-N)$ as do PR_3 ligands, although to a lesser extent. Halogen and oxygen ligands result in relatively large one-bond couplings. A typical sequence for $^1J(Pt-N)$ and other one-bond $^1J(Pt-L)$ values is:

H_2O > halogen > amine > DMSO (a sulphur donor)

> AsR_3 > PR_3 > carbon ligand

with the *trans* influence of the ligand decreasing with increasing value of $^1J(Pt-L)$. The 232–410 Hz range indicated for the square planar NH_3 complexes[86–90] is probably typical for biologically pertinent L ligands, but need not represent the entire spread for an sp^3 nitrogen, e.g. see [4]. In any case, there are marked differences as a function of the ligand L, and this empiri-

[6]   [7]
$^1J(Pt-N)$ = 392, 358 Hz $^1J(Pt-N)$ = 280 Hz
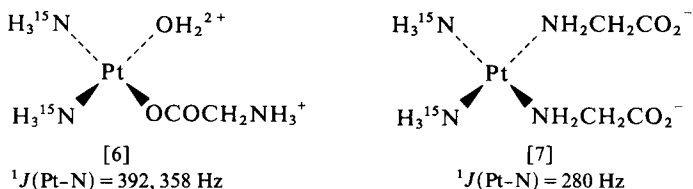
cism can be used to advantage, e.g. glycine reacts with the cancer drug precursor $[Pt(NH_3)_2(H_2O)_2]^{2+}$ to give complexes with the glycine oxygen coordinated (pH 1.5–4.5), [6]; however, at higher pH values the nitrogen becomes sufficiently active to yield [7] and these structural changes are reflected in the changes in $^1J(Pt–N)$. It is worth noting that, in general, different types of ligand are detectable from both $^1J(Pt–N)$ [90a] and ^{195}Pt [90b] data. A similar dependence of $^1J(Pt–N)$ has been observed[91] in the ethylenediamine complexes [8] and [9].

[8]
$^1J(Pt–N) = 421$

[9]
$^1J(Pt–N) = 319$ Hz
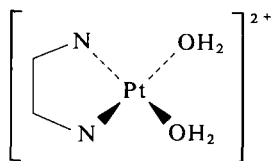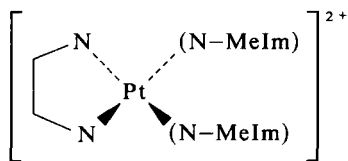
(N–MeIm = N-methylimidazole)

The NMR data for the anti-tumour drugs which involve complexes of Pt(IV) are sparse,[88,92] so related *trans* influence correlations must await further work.

Before departing from this chemistry I note several studies[93–96] concerned with ^{195}Pt shifts of dimeric and trimeric hydroxy bridged ammine platinum compounds. These are readily distinguishable from related monomers using the metal chemical shift data, and this can be important as these higher molecular weight materials are thought to be toxic.[93] For example, the trimer $[Pt(\mu\text{-OH})(NH_3)_2]_3^{3+}$ has $\delta = -1505$, whereas the dimer $[Pt(\mu\text{-OH})(NH_3)_2]_2^{2+}$ appears at $\delta = -1153$.

A dimer such as [10] is also distinguishable from a pyridonate bridged dimer[95] such as [11].
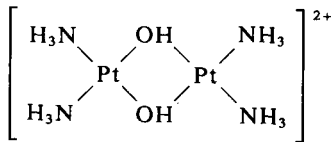
[10]
$\delta = -1153$
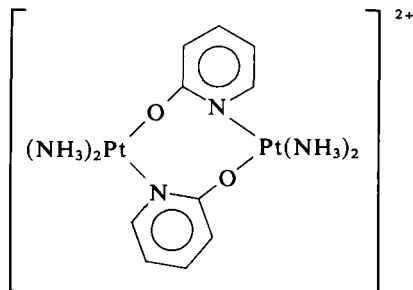
[11]
$\delta = -1810$

The dependence of $^1J(Pt-N)$ on the *trans* ligand for an sp^2 nitrogen is not nearly as well documented[76-78,82,85] but is qualitatively similar to that for an sp^3 nitrogen. Changing the *trans* ligand markedly affects the one-bond coupling as shown below:

	N *trans* to:	$^1J(Pt-N)$
trans-PtCl$_2$(pyridine)(PPh$_3$) [97]	PPh$_3$	248
trans-PtCl$_2$(2,4-Me$_2$-pyridine)(C$_2$H$_4$) [18]	CH$_2$=CH$_2$	408
cis-PtCl$_2$(pyridine)(PPh$_3$) [97]	Cl	441

For closely related ligands, e.g. pyridines and imines,[96,98,99] there are only modest differences in $^1J(Pt-N)$. Specifically, for some ethylene complexes (see scheme) the values fall in the range 379–426 Hz. However, should the chemistry change, as in [12] (see scheme) where we have increased the coordination number, both $^1J(Pt-N)$ and $\delta(^{195}Pt)$ respond significantly.[100]

sp^2 nitrogen ligand	$^1J(Pt-N)$
2,4-Me$_2$-pyridine [96]	408
2,4,6-Me$_3$-pyridine [96]	426
p-ClC$_6$H$_4$N=CMe$_2$ [98]	396
p-CH$_3$C$_6$H$_4$N=CMe$_2$ [98]	400
CH$_3$N=C(Me)R [99]	379
Bu^{t}N=C(Me)R [99]	403

[12]
$^1J(Pt-N) = 135, 178$ Hz [100]
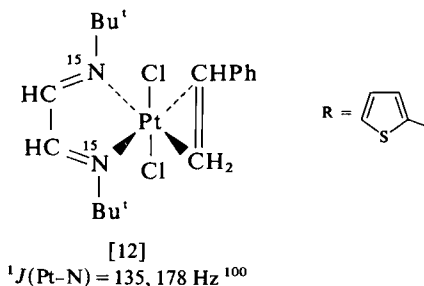
Tables 5–13 contain an extensive collection of $^1J(Pt-N)$ couplings. Those terms in equation (4) which are required to change in order to account for the observed *trans* influence have already been discussed at length.[62,84,85,101-103]

B. Pt–Pt couplings in higher molecular weight complexes

The chemistry of dimers and clusters is of increasing interest and chemical relevance. One consequence of this development is a growing NMR literature concerned with complexes with metal–metal interactions. In the case of platinum this has led to a burgeoning, if somewhat perplexing,

collection of $^nJ(\text{Pt-Pt})$ couplings. It is now well established[13] that $^nJ(\text{Pt-Pt})$ values do not correlate well with Pt–Pt bond lengths; nevertheless there are some few observations which, when taken together, provide useful structural probes. It seems reasonable to begin with $^nJ(\text{Pt-Pt})$ values where the metals are separated by two bonds, i.e. when the molecule contains the fragment [13], so that we can later better understand the significance of the results for molecules possessing a bridged metal–metal bond, i.e. [14]. It is known[52,60,104-114] that $^2J(\text{Pt-Pt})$ values are of the order of hundreds of Hz for a variety of molecules having bridging units of type [13]. For X = halogen,

$$
\begin{array}{cc}
\text{X} & \text{X} \\
\diagup\ \diagdown & \diagup\ \diagdown \\
\text{Pt}\quad\text{Pt} & \text{Pt}\text{---}\text{Pt} \\
[13] & [14]
\end{array}
$$
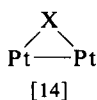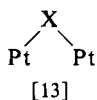
the values fall in the range 125–391 Hz;[23,60,104] for S^{2-} or RS^- the range is 202–969 Hz,[52,105,106] with the lowest value known to be negative[52] in sign. When the coupling goes via a bridging phosphorus atom, the observed values are +259 to +667,[108] and there is a single value through a bridging CH_2 of 370 Hz.[107] The chemistry of the bridging hydride ligand has delivered many suitable complexes[108-115] which reveal this spin-spin interaction at 92–886 Hz. The 92 Hz value arises from [15];[115] however, note that for [16] the metal–metal coupling is 2853 Hz,[116] and consequently structure [16] is

$$
\begin{array}{cc}
\text{R}_3\text{Si}\text{------}\text{H}\quad\text{PR}'_3 & \text{H}\text{------}\text{SiR}_2\quad\text{PR}'_3 \\
\diagdown\ \diagup\ \diagdown\ \diagup & \diagdown\ \diagup\ \diagdown\ \diagup \\
\text{Pt}\quad\text{Pt} & \text{Pt}\text{------}\text{Pt} \\
\diagup\ \diagdown\ \diagup\ \diagdown & \diagup\ \diagdown\ \diagup\ \diagdown \\
\text{R}'_3\text{P}\quad\text{H}\text{------}\text{SiR}_3 & \text{R}'_3\text{P}\quad\text{SiR}_2\text{------}\text{H} \\
[15] & [16] \\
J(\text{Pt-Pt}) = 92\ \text{Hz} & J(\text{Pt-Pt}) = 2853\ \text{Hz}
\end{array}
$$
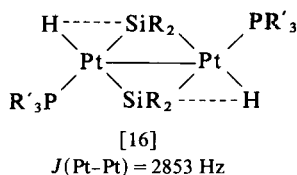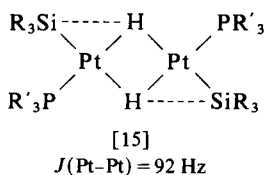
sketched with a metal–metal interaction. The $R_3Si \cdots H$ notation is meant to suggest some H–Si character. As an aside I note that, in addition to the $^nJ(\text{Pt-Pt})$ value, the solution structure proof for complexes [15] and [16] as well as [17][112] and [18][111] makes extensive use of the values of $^1J(\text{Pt-H}_T)$ and $^1J(\text{Pt-H}_B)$ which differ considerably, the latter being much smaller.

$$
\begin{array}{cc}
\left[\begin{array}{c}
\text{L}\qquad\text{L} \\
|\qquad\quad| \\
\text{R}\text{---}\text{Pt}\text{---}\text{H}_B\text{---}\text{Pt}\text{---}\text{H}_T \\
|\qquad\quad| \\
\text{L}\qquad\text{L}
\end{array}\right]^+
&
\left[\begin{array}{c}
\text{L}\quad\ \text{H}_B\quad\text{L} \\
\diagdown\ \diagup\ \diagdown\ \blacktriangledown \\
\text{Pt}\qquad\text{Pt}\text{---}\text{H}_T \\
\diagup\ \diagdown\ \diagup\ | \\
\text{L}\qquad\text{H}_B\quad\text{L}
\end{array}\right]^+ \\
[17] & [18] \\
^1J(\text{Pt-Pt}) = 366\ \text{Hz} & ^1J(\text{Pt-Pt}) = 325\ \text{Hz} \\
(\text{L} = \text{PEt}_3, \text{R} = \text{Ph}) & (\text{L} = \text{PPh}_3)
\end{array}
$$
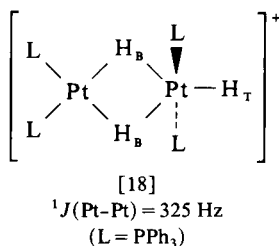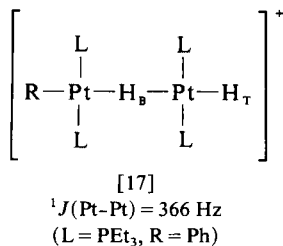
Further, all these complexes have $^1J(\text{Pt-P})$ *and* $^3J(\text{Pt-P})$ values, and the presence of the latter is diagnostic for a higher molecular weight complex. These proton and phosphorus couplings can also be quite valuable when dealing with mixed metal dimers, e.g. [19][117] and [20].[118]
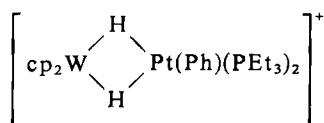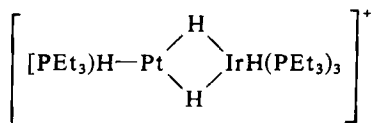
[19]　　　　　　　　　　　　　　[20]

Returning to $^nJ(\text{Pt-Pt})$, we see that, apart from [16], for molecules where the platinum–platinum interaction is considered to be weak or non-existent, the spin–spin coupling between the two metals is less than 1 kHz.

For dimeric complexes with definite platinum–platinum bonds[60,119–130] the $^1J(\text{Pt-Pt})$ values are usually larger, and for Pt(I) and Pt(II) complexes[119,120,127] often >3 kHz. Thus for complexes such as [21][120] and [22][128]
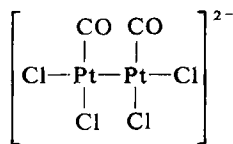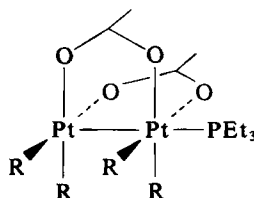
[21]　　　　　　　　　[22]
$^1J(\text{Pt-Pt}) = 5250$ Hz　　$^1J(\text{Pt-Pt}) = 6541$ Hz
　　　　　　　　　　　　(R = Ph)

the NMR data clearly reveal the presence of the Pt–Pt bond, with compound [23] providing an extreme example.[123]
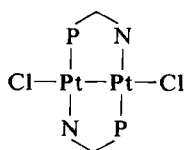
P⌒N = 2-diphenylphosphinopyridine

[23]　$^1J(\text{Pt-Pt}) = 10\,269$ Hz

Although [21] to [23] are clear examples, there is evidence pointing to a substantial dependence of $J(\text{Pt-Pt})$ on the remaining coordination sphere. Complexes [24] and [25] possess only modest Pt–Pt couplings. Interestingly, such molecules have phosphorus ligands *trans* to the metal–metal bond and, viewing each centre separately, such a ligand will exert a large *trans* influence thereby weakening the Pt–Pt interaction.[120] In summary, we are

$$\left[\begin{array}{c} \overset{L}{\underset{|}{}}\ \ \overset{L}{\underset{|}{}} \\ EtMe_2P-Pt-Pt-PMe_2Et \\ \underset{L}{\overset{|}{}}\ \ \underset{L}{\overset{|}{}} \end{array}\right]^{2+}$$

[24]
$J(Pt-Pt) = 525$ Hz [120]
(L = CH$_3$N≡C)

$$\begin{array}{c} Et_2P-S \\ |\ \ \ | \\ (PhO)_3P-Pt-Pt-P(OPh)_3 \\ |\ \ \ | \\ S-PEt_2 \end{array}$$
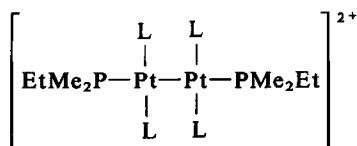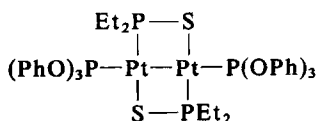
[25]
$J(Pt-Pt) = 465$ Hz [124]

safe in assigning significant Pt-Pt bonding to a dimer when the spin-spin coupling is considerably more than 1 kHz but the converse is not true (X-ray crystallography is still the most reliable general method). Consider the problem posed by complexes [26] and [27]. The former arises from the

[26]
$J(Pt-Pt) = 400$ Hz
(Pt-Pt distance = 3.010 Å)

[27]
$J(Pt-Pt) = 332$ Hz
(Pt-Pt distance = 2.769 Å)
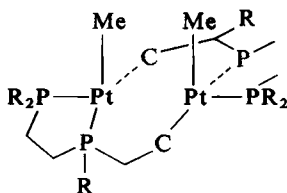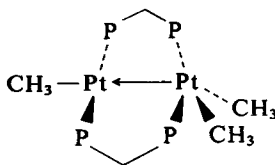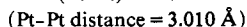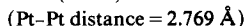
cyclometallation of diphos (Ph$_2$PCH$_2$CH$_2$PPh$_2$),[131] whereas the latter contains bridging Ph$_2$PCH$_2$PPh$_2$ ligands.[132] Compound [27] is thought to contain a Pt(II)-Pt(II) donor-acceptor bond, but [26] is not considered to have an appreciable Pt-Pt interaction. Whatever the extent of the bonding between the two metals, the value of $J(Pt-Pt)$ does not seem a reliable indicator. It is worth remembering that compound [2] shows a long-range coupling, $^4J(Pt-P-O-P-Pt)$, of 363 Hz,[74] so four-bond interactions for [26] and [27] are worth considering.

In an analogous fashion the interpretation of $J(Pt-Pt)$ data for small and large clusters is clouded by our lack of knowledge with regard to signs, and by the uncertainty relating to the size of $^2J(Pt-X-Pt)$ for a molecule with fragment [14]. Typically, clusters contain bridging carbonyl ligands, e.g. [28], and possess $J(Pt-Pt)$ values between 750 and 1840 Hz.[60,131-136] The trinuclear cluster [28] has several platinum-platinum coupling pathways, e.g. $^1J(Pt-Pt)$, $^2J(Pt-C-Pt)$, $^2J(Pt-Pt-Pt)$, and as we only observe (or calculate) a composite of all the contributions it is difficult to use this parameter with confidence. Once again values substantially in excess of 1 kHz have been shown, empirically, to be associated with short Pt-Pt separations and presumed Pt-Pt bonds. Just as with the dimers, the converse is not true, i.e. small $J(Pt-Pt)$ values are not necessarily associated with

long and/or weak Pt–Pt interactions, e.g. $[Pt_3(\mu\text{-}CNBu^t)_3(CNBu^t_3)]$,[60] an analogue of [28] with bridging and terminal $CNBu^t$ ligands, has $J(Pt\text{-}Pt) = 188$ Hz. Not all the chemistry surrounding $J(Pt\text{-}Pt)$ is ambiguous. The trimetallic compound [29] shows a very modest 57 Hz spin–spin interaction
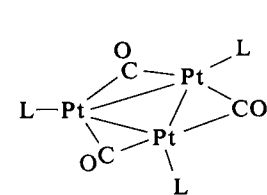
[28]

$J(Pt\text{-}Pt) = 1371–1770$ Hz [60,132]

(L = tertiary phosphine)
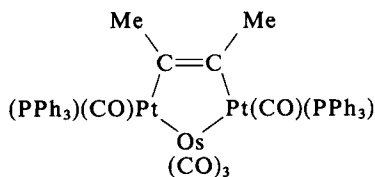
[29]

$J(Pt\text{-}Pt) = 57$ Hz

(Pt–Pt distance = 3.033 Å)

between the two metals[137] and does indeed[137] have the metals separated by more than 3 Å. Since this section has emphasized higher molecular weight complexes it is appropriate to mention the extensive studies[138–147] on clusters (many with bridging carbene and carbyne moieties[138–145]) in which ^{195}Pt data are given.
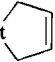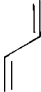
Summarizing the entire applications section, although the platinum chemical shift is both sensitive to subtle and gross changes in the metal coordination sphere, it is still somewhat underdeveloped in comparison with the potential offered by $^nJ(Pt\text{-}L)$. Although many $^1J(Pt\text{-}L)$ values are readily understood, there are still some unanswered questions.

VII. TABLES

The following material is intended to provide the user with a qualitative view of platinum chemical shift and spin coupling data. The shift data are given with respect to external $PtCl_6^{2-}$, and where this is not the case, i.e. a frequency reference is employed, the number has been converted using $\delta(PtCl_6^{2-}) = \delta(21.4 \text{ MHz}) - 4533$. The reader is urged to consult the original literature since the experimental conditions are not specified and these contribute significantly to $\delta(^{195}Pt)$. This listing is not intended to be comprehensive. Perhaps undue emphasis has been given to reports associated with the various aspects of organometallic chemistry; nevertheless it is hoped that the coordination chemist will find his way through the ensemble of group IV and V ligands to the metal.

TABLE 1

Some spin–lattice relaxation times for ^{195}Pt.[a]

Complex	T_1 (s)			Ref.
Na_2PtCl_6	1.35, 0.3			9, 10
H_2PtCl_6	1.28			9
H_2PtBr_6	0.32			
H_2PtI_6	1.11			9
Na_2PtCl_4	0.46, 0.7			9, 10
H_2PtCl_4	0.46			9
H_2PtBr_4	0.37			9
$[Pt(en)_2]Cl_2$	0.28			9
$K_2[Pt(SCN)_4]$	0.83			9
$K_2[Pt(CN)_4]$	1.09			9
sym-trans-$[Pt(\mu\text{-Cl})Cl(PBu_3)]_2$	ca. 100 ms, 21.1 T			8
	ca. 10.5 ms, 58.7 T			
$(Bu_4N)[PtCl_3(pyridine)]$	34.8 ms (CD_3CN)			6
	14.3 ms ($CDCl_3/CD_3CN$, 7:2)			

Pt(⌒⌒⟋)$_2$L

	T_1 (s)			Ref.
L = $(Ph_2P)_2CH_2$	0.5			4
$(cy_2PCH_2)_2$	0.21			4
$(Ph_2PCH_2)_2$	0.16			4
$(Pr^i{}_2PCH_2)_2Pt$	0.45			4
$(Me_3P)_2Pt$	0.83			4
$Pt(1,5\text{-COD})_2$	0.15			4
$(Ph_3P)_2Pt$	0.25			4
	0.17			4
$(Bu^t{}_2PCH_2)_2Pt$				

	9.4[b]	7.0[b]	4.7[b]	
$Pt(PPr^i{}_3)_2$	0.025	0.046	0.097	5
$Pt(PBu^t{}_3)_2$	0.031	0.053	0.123	5
$Pt(Pcy_3)_2$	0.0085	0.017		5
$Pt(P\{OC_6H_4\text{-}o\text{-}CH_3\}_3)_3$	0.56			5
$Pt(PEt_3)_3$	2.4	2.37	4.15	5
$Pt(P\{OEt\}_3)_4$	5.6	6.2	8.31	5
$Pt(PMe_3)_4$	1.5	1.5	1.44	5

[a] 2.11 T for references 9 and 10; 6.3 T for reference 6; 9.4 T for reference 4.
[b] B_0 in Tesla, 310 K.

TABLE 2

^{195}Pt chemical shifts for monomeric Pt(0) complexes.

Complex		$\delta(^{195}Pt)$	$J(Pt-P)$	Ref.
Pt(1,5-COD)$_2$		−4636		
Pt($\bigsqcup\times$)(PPh$_3$)$_2$		−5102	3393	4
Pt(η^2-C$_4$H$_6$)(R$_2$PCH$_2$-)$_2$		−5239	3248	4
			3227	
R = Bu^t			69	
cy		−5230		4
Pt(CF$_3$C≡CCF$_3$)(PPh$_3$)$_2$		−4645		34
Pt(CF$_2$=CF$_2$)(PPh$_3$)$_2$		−4791		34
Pt(CH$_2$=CH$_2$)(PPh$_3$)$_2$		−5065		34
Pt(RC≡CR')(PPh$_3$)$_2$				
R = Ph	R' = Ph	−4741	3452	24
Ph	Me	−4727	3377	24
			3454	
Ph	CO$_2$Me	−4710	3403	24
			3741	
Ph	H	−4690	3464	24
			3547	
Et	Et	−4689	3425	24
Me	CO$_2$Me	−4682	3366	24
			3803	
Me	Me	−4674	3420	24
H	H	−4658	3626	24
CO$_2$Et	CO$_2$Et	−4655	3722	24
CO$_2$Me	CO$_2$Me	−4653	3722	24
CF$_3$	CF$_3$	−4645	3595	24
Ph	CN	−4640	3336	24
			3772	
CO$_2$CH$_2$CF$_3$	CO$_2$CH$_3$CF$_3$	−4626	3726	24
Me	CN	−4598	3303	24
			3864	
H	CN	−4573	3434	24
			3887	
CN	CN	−4586	3696	24
Pt(CF$_2$=CF$_2$)(PEt$_3$)$_2$		−4784		23
Pt{(CF$_3$)$_2$CO}(PEt$_3$)$_2$		−4941		23
Pt(PMe$_2$Ph)$_4$		−4728		23
Pt(P(OMe)$_3$)$_4$		−5830		23
PtP$_2$				
P = Pr$^i_3$		−6585^a	4155	5
		−6607		28
PBu$^i_3$		−6479^a	4399	5
Pcy$_3$		−6501	4180	5
		−6555		28
PBu$^t_2$Ph		−6526		28

TABLE 2 (cont.)

Complex	$\delta(^{195}Pt)$	$J(Pt-P)$	Ref.
PtP$_3$			
P = P{O(o-CH$_3$C$_6$H$_4$)}$_3$	−4858	6968	5
PEt$_3$	−4510[b]	4202	5
	−4526		28
PPh$_3$	−4583[c]	4455	5
PTol$_3$	−4589		28
PBu$_3$	−4511		28
PBz$_3$	−4439		28
Pcy$_3$	−4567		28
PtP$_4$			
P = P(OEt)$_3$	−5750[a]	5374	5
PMe$_3$	−4856[a]	3835	5
	−4909		28
PMe$_2$Ph	−4842		28
PMePh$_2$	−4783		28
PEt$_3$	−5262		28
PBu$^n_3$	−5356		28
Pt{P^1(Mes)=CPh$_2$}(P^{2}Ph$_3$)$_2$			
η^1	−4410	4360 (P^2)	75
		4940 (P^1)	
η^2	−4847	3380 (P^2)	75
		500 (P^1)	

[a] 258 K.

[b] 243 K.

[c] 193 K.

TABLE 3

Some one-bond platinum–phosphorus couplings.

Complex	$\delta(^{31}P)$	$^1J(Pt–P)$	Ref.
$Pr_4N[PtX_3(PMe_3)]$			61
X = Cl	−30.6	3674	
Br	−31.5	3542	
I	−32.2	3377	
$Pt_2X_4(PMe_3)_2$			61
X = Cl	−23.2	3824	
Br	−24.5	3682	
I	−26.4	3480	
cis-$PtX_2(PMe_3)_2$			61
X = Cl	−24.0	3480	61
	−24.9	3489	148
Br	−23.8	3426	61
	−25.1	3439	148
I	−26.0	3306	61
	−27.3	3317	148
$trans$-$PtX_2(PMe_3)_2$			
X = Cl	−15.8	2379	61
	−15.8	2386	148
Br	−20.4	2336	61
	−21.5	2324	148
I	−32.2	2230	61
	−32.3	2236	148
CN	−19.6	2120	61
$[PtX(PMe_3)_3]PF_6$			148
X = Cl	−26.9	3370	
	−12.0	2231	
Br	−25.5	3406	
	−15.6	2233	
I	−26.1	3329	
	−20.3	2227	
$PtH_2(PEt_3)_2$			110a
cis	18.9	1984	
$trans$	27.7	2764	
$PtH_2(PMe_3)_2$			110a
cis	−21.7	1875	
$trans$	21.1	2594	
$trans$-$PtHX(PEt_3)_2$			150
X = Cl	23.2	2723	
Br	21.8	2685	
I	19.8	2632	
CN	20.3	2685	
NCO	22.5	2715	
NCS	23.1	2700	
SCN	20.8	2619	
NO_3	26.5	2824	

TABLE 3 (*cont.*)

Complex	$\delta(^{31}P)$	$^1J(Pt–P)$	Ref.
NO$_2$	22.0	2768	
N$_3$	23.2	2730	
trans-PtHX(Pcy$_3$)$_2$			116
X = C$_6$F$_5$	37.5	2760	
C$_6$F$_3$H$_2$	37.3	2795	
1,3-C$_6$F$_2$H$_3$	37.5	2810	
OC$_6$F$_5$	40.5	2897	
OC$_6$H$_5$	39.9	2866	
pyrrole-H	36.7	2813	
HNC$_6$F$_5$	36.1	2845	
C$_6$H$_5$	17.2	2793	
trans-PtH(C$_6$F$_5$)(PEt$_3$)$_2$	18.5	2684	116
trans-PtH$_2$(Pcy$_3$)$_2$	52.8	2872	116
[PtX(PMe$_3$)$_4$]X			148
X = Cl	−30.1	2465	
Br	−31.8	2497	
I	−35.4	2420	
[Pt(PMe$_3$)$_4$](BF$_4$)$_2$	−21.5	2230	
PtI$_2$(PMe$_3$)$_3$	−38.2 (1)	4082	
	−30.3 (2)	2164	
cis-PtCl$_2$(PEt$_3$)$_2$	9.0	3502	
trans-PtCl$_2$(PEt$_3$)$_2$	12.1	2394	
[PtCl(PEt$_3$)$_3$]ClO$_4$	9.9	3442	
	17.6	2263	
cis-PtCl$_2$(PBu$^n_3$)$_2$	0.9	3505	
trans-PtCl$_2$(PBu$^n_3$)$_2$	4.5	2379	
[PtCl(PBu$^n_3$)$_3$]ClO$_4$	1.4 (1)	3441	
	10.2 (2)	2267	
cis-PtCl$_2$(PTol$_3$)$_2$	12.2	3694	
trans-PtCl$_2$(PTol$_3$)$_2$	18.4	2595	
[PtCl(PTol$_3$)$_3$]ClO$_4$	18.7 (1)	3645	
	29.8 (2)	2475	
cis-PtCl$_2$(PPh$_3$)$_2$	13.8	3678	16
trans-PtCl$_2$(PPh$_3$)$_2$	20.1	2637	16
[PtX$_3$(Ph$_3$)]$^-$			149
X = Cl Y = F	50.2	7464	
Br F	52.1	7257	
I F	60.3	6959	
X = Cl Y = Cl	90.0	6182	
Br Cl	90.7	5869	
I Cl	92.7	5371	
X = Cl Y = OCH$_3$	58.3	6020	
Br OCH$_3$	60.1	5932	
I OCH$_3$	74.3	5753	

TABLE 3 (*cont.*)

Complex	$\delta(^{31}P)$	$^1J(Pt-P)$	Ref.
trans-PtClR(PPh$_3$)$_2$			151
R = Ph	24.5	3157	
C$_6$H$_4$OCH$_3$-*p*	24.2	3148	
Tol	24.0	3169	
C$_6$H$_4$Cl-*p*	23.9	3095	
trans-PtXPh(PPh$_3$)$_2$			152
X = Br	21.3	3091	
I	23.6	3130	
SCN	21.0	3075	
cis-PtR$_2$(PPh$_3$)$_2$			151
R = Ph	18.4	1763	
C$_6$H$_4$OMe-*o*	15.3	2012	
mesityl	2.7	1736	
C$_6$H$_4$Cl-*p*	17.9	1813	
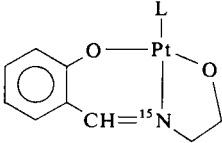
TABLE 4

^{1}H NMR data for some hydride complexes.

Compound	^{1}H(τ)	^1J(Pt–H)	Ref.
trans-PtHX(PEt$_3$)$_2$			
X = NO$_3$	33.6	1322	153
O—N=O	29.4	1003	153
NCO	27.7	1080	153
NCS	27.6	1086	153
Cl	26.8	1275	153
Br	25.55	1346	153
SCN	22.95	1233	153
I	22.65	1369	153
CN	17.6	778	153
Ph	16.67	648	154
H	12.96	790	110
trans-PtHL(PEt$_3$)$_2$$^+$			
L = C$_2$H$_4$	17.20	908	155
py	29.32	1106	156
CO	14.76	967	156
Bu^{t}NC	17.13	895	156
P(OPh)$_3$	15.21	872	156
P(OMe)$_3$	14.54	846	156
PPh$_3$	16.51	890	156
PEt$_3$	16.24	790	156
trans-PtHX(PMePh$_2$)$_2$			157
X = Cl	26.40	1260	
Br	24.90	1302	
I	22.09	1332	
NO$_3$	32.90	1316	
NCS	27.02	1072	
SCN	22.18	1204	
CN	17.37	768	
trans-PtHL(PMePh$_2$)$_2$$^+$			157
L = 2-methylpyridine	27.20	1080	
2,4,6-trimethylpyridine	26.53	1073	
p-CH$_3$C$_6$H$_4$NC	16.10	872	
PMePh$_2$	15.39	840	
acetone	33.60	1458	

TABLE 5

$\delta(^{195}Pt)$, $^1J(Pt–N)^a$ and the *trans* influence.

Compound	δ	J
$[PtCl_2L(^{15}NH_2(CH_2)_5CH_3)]$ [84]		
L = PBu^n_3	−3612	138.3
$PMePh_2$	−3597	155.9
$P(p\text{-}CH_3C_6H_4)_3$	−3489	158.8
$AsBu^n_3$	−3328	183.8
$AsMePh_2$	−3324	208.8
$As(p\text{-}CH_3C_6H_4)_3$	−3322	207.4
$^{14}NH_2(CH_2)_5CH_3$	−2130	286.8
C_2H_4	−3006	283.9
Cl	−2215	336^b
Cl	−2805	295.6^c
$PtCl_2L(^{15}NHMe_2)]$ [158]		
L = $^{15}\overset{+}{N}HMe_2\overset{'}{C}H_2CH_2^-$		107
PPh_3		171
DMSO		$226\text{-}244^d$
aliphatic amine		$278\text{-}290^e$
C_2H_4		299
Cl^-		$312\text{-}350^e$
Br^-		$334\text{-}340^e$

$$\text{[structure: L—Pt with O—Pt—O ring, benzene ring, } CH=^{15}N]$$

L = PBu^n_3	−2510	249.1
$P(OEt_3)$	−2647	303.0
$P(p\text{-}CH_3C_6H_4)_3$	−2511	323.6
$AsBu^n_3$	−2207	366.2
CN(cyclohexyl)	−2364	397.1
$As(p\text{-}CH_3C_6H_4)_3$	−2233	416.2
DMSO	−2463	431
piperidine	−1630	464.7
$^{15}NH_2(CH_2)_5CH_3$	−1532	478.0
pyridine.	−1598	494.2

Structures (1)–(8): platinum complexes

(1) H_3N, Cl, Pt, H_3N, Cl

(2) H_3N, Cl^+, Pt, H_3N, NH_3

(3) H_3N, Cl, Pt, Me_2SO, Cl

(4) H_3N, Cl, Pt, Cl, Me_2SO

(5) H_3N, Cl^+, Pt, Me_2SO, NH_3

(6) H_3N, Cl^+, Pt, H_3N, Me_2SO

(7) H_3N, NH_3^{2+}, Pt, H_3N, Me_2SO

(8) N, Cl^-, Pt, O, Cl

TABLE 5 (*cont.*)

$$
\text{HO} \quad \text{N} \diagdown \text{Pt} \diagup \text{Cl} \qquad \text{Cl} \diagup \text{Pt} \diagdown \text{Me}_2\text{SO}
$$

(9)   (10)   (11)

$$\text{N} \frown \text{O} = \text{H}_2\text{NCH}_2\text{CO}_2^-$$

| Complex[f] | δ (ppm) | $^1|J(^{195}\text{Pt}-^{15}\text{N})|$ (Hz), *trans* to | | |
		Cl^-	NH_3	Me_2SO
(1)	−2097	312.2	—	—
(2)	−2354	317	278	—
(3)	−3046	336	—	—
(4)	−3067	—	—	232
(5)	−3126	—	287	—
(6)	−3147	340.0	—	233.8
(7)	−3224	—	288	232
(8)	−1602	317	—	—
(9)	−3110	—	—	244
(10)	−2747	—	—	226
(11)	−2902	330	—	—

For *cis*-Pt(NH$_3$)$_2$ complexes,[g] the order of *trans* influences based on ^1J is:

Ligand:	H_2O	CO_2^-	OH^-	Cl^-	NH_3	S-met
^1J (Hz):	390	360	340	310	285	265

[a] Values are in Hz; $J = {}^1J(^{195}\text{Pt}-^{15}\text{N})$.

[b] *cis*-PtCl$_2$(^{15}NH$_2$(CH$_2$)$_5$CH$_3$)$_2$].

[c] *cis*-[PtCl$_2$(^{15}NH$_2$)(CH$_2$)$_5$(CH$_3$)(C$_2$H$_4$)].

[d] From reference 86.

[e] Data from reference 63.

[f] Data from reference 86

[g] Data from reference 88.

TABLE 6

NMR data for some thiocyanate complexes.[a]

Complex	Isomer	$\delta(^{195}\text{Pt})$	$^1J(\text{Pt}-^{14}\text{N})$	Ref.
trans-[Pt(CNS)$_2$(NMe$_3$)$_2$]	NN	-2224	504 ± 2	77
trans-[PtCl(NCS)(NMe$_3$)$_2$]		-2090	460 ± 10	
trans-[Pt(AsMe$_3$)$_2$(CNS)$_2$]	SS	-4495		
	NS	-4159	330 ± 5	
	NN	-3733	370 ± 10	
trans-[Pt(AsMe$_2$Et)$_2$(CNS)$_2$]	SS	-4497		
	NS	-4163	330 ± 5	
	NN	-3737		
trans-[Pt(AsMeEt$_2$)$_2$(CNS)$_2$]	SS	-4494		
	NS	-4162	310 ± 10	
	NN	-3739	390 ± 10	
trans-[Pt(AsEt$_3$)$_2$(CNS)$_2$]	NS	-4147		
	NN	-3714	395 ± 10	
cis-[Pt(CNS)$_2$(SbMe$_3$)$_2$]	SS	-4950		
trans isomer	SS	-4570		
trans-[Pt(CNS)$_2$(SMe$_2$)$_2$]	SS	-4146		
	NS	-3726	373 ± 2	
	NN	-3198	451 ± 2	
trans-[Pt(CNS)$_2$(SeMe$_2$)$_2$]	SS	-4363		
	NS	-3897	375 ± 2	
	NN	-3338	440 ± 2	
cis-[Pt(CNS)$_2$(PMe$_3$)$_2$]	NS	-4564		
	NN	-4372		
cis-[Pt(CNS)$_2$(PMe$_2$Et)$_2$]	NS	-4519	205 ± 5	
	NN	-4423	220 ± 10	
cis-[Pt(CNS)$_2$(PMeEt$_2$)$_2$]	NS	-4544	245 ± 5	
	NN	-4442	220 ± 5	
cis-[Pt(CNS)$_2$(PEt$_3$)$_2$]	NS			
	NN	-4434		
trans-[Pt(CNS)$_2$(PEt$_3$)$_2$]	NN	-3870	424 ± 2	
Pt(CNS)$_3$L$^-$				
L = NMe$_3$	NSN	-2605	460 ± 5	
	NNN	-2088		
PMe$_3$	SSS	-4354		
	NSS	-3985	355 ± 5	
	NSN	-3578	439 ± 5	
	SNS	-4094	205 ± 5	
	NNS	-3830		
	NNN	-3519		
PMe$_2$Et	SSS	-4369		
	NSS	-4015	340 ± 10	
	SNS	-4118	215 ± 5	
	NNS	-3858		

TABLE 6 (cont.)

Complex	Isomer	$\delta(^{195}Pt)$	$^1J(Pt-^{14}N)$	Ref.
AsMe$_3$	SSS	−4305		
	NSS	−3891	353 ± 5	
	SNS	−3957	290 ± 10	
	NNS	−3636		
L = AsMe$_2$Et	SSS	−4318		
	NSS	−3906	360 ± 5	
	SNS	−3982	270 ± 5	
	NNS			
SbMe$_3$	SSS	−4374		
	NSS	−3935		
SMe$_2$	SSS	−4067		
	NSS	−3602	370 ± 5	
	NSN	−3035	450 ± 30	
	SNS	−3589	360 ± 10	
	NNS	−3231		
SeMe$_2$	SSS	−4174		
	NSS	−3676	375 ± 5	
	NSN	−3087	438 ± 5	
	SNS	−3682	368 ± 10	
TeMe$_2$	SSS	−4441		
	NSS	−3928	367 ± 5	
	NSN	−3343		

	δ	$^1J(Pt-^{15}N)$	$^3J(Pt-^{15}N)$	
(Bu$^n_4$N)$_2$[Pt(SC^{15}N)$_4$]	−3961	—	12	76
(Bu$^n_4$N)$_2$[Pt(^{15}NCS)(SC^{15}N)$_3$]	−3431	525	12	
trans-[Pt(^{15}NCS)$_2$(PBu$^n_3$)$_2$]	−3881	589	—	
trans-[Pt(^{15}NCS)(SC^{15}N)(PBu$^n_3$)$_2$]	−4244	491	20	
trans-[Pt(SC^{15}N)(PBu$^n_3$)$_2$]	−4526	—	20	

[a] The coordinated atoms of the thiocyanate group are given in order around the metal starting from the group next to L; e.g. SNS indicates NCS *trans* to L. SS indicates two sulphur coordinated ligands, NS indicates one N and S bound thiocyanate, NN signifies two N-coordinated ligands.

TABLE 7

^{195}Pt NMR data for some nitrogen complexes.
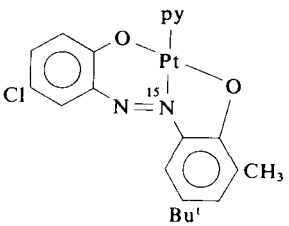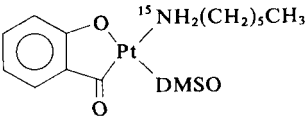
	$\delta(^{195}Pt)$	$^1J(Pt-^{15}N)$	Ref.
(structure: py, O, Pt, O, Cl, $^{15}N=N$, CH$_3$, Bu^t)		523	159
$PtCl_2(PhCH=CH_2)(t\text{-}Bu^{15}N=CH)_2$	−1996	135	100
		178	
		(^{15}N trans to styrene CH_2)	
${PtCl_2(PBu^n_3)}_2(t\text{-}Bu^{15}N=CH)_2$	−3412	211	100
$PtCl_2(PBu^n_3)(t\text{-}Bu^{15}N=CH)_2$	−3415	217	100
$PtCl_2(PBu^n_3)(N\text{-ligand})$			100
pyridine	−3505		
2,6-dimethylpyridine	−3451		
n-hexylamine-^{15}N	−3612	138	
aniline-^{15}N	−3601	103	
t-butylamine	−3534	159	
$Pt(Ph^{15}NSO)(PPh_3)_2$		136 ± 10	160
(structure: O, Pt, $^{15}NH_2(CH_2)_5CH_3$, DMSO, O)		88 Hz	13
trans-$PtCl_2(C_2H_4)(p\text{-}ClC_6H_4{}^{15}NH_2)$	−3011	242	99
trans-$PtCl_2(C_2H_4)(p\text{-}CH_3C_6H_4{}^{15}NH_2)$	−3013	244	99
Cyanate complexes	δ	$^1J(Pt-^{14}N)$	77
trans-$Pt(NCO)_2(NMe_3)_2]$	−2054	420	20
trans-$PtCl(NCO)(NMe_3)_2]$	−1975	470	10
cis-$[Pt(NCO)_2(PMeEt)_2]$	−4350	200	20
cis-$[Pt(NCO)_2(SMe_2)_2]$	−3328	330	5
cis-$[Pt(NCO)_2(SeMe_2)_2]$	−3458	300	5
cis-$[PtCl(NCO)(SeMe_2)_2]$	−3580	300	10
trans-$[PtCl(NCO)(SeMe_2)_2]$	−3580	305	10

TABLE 8

Chemical shifts and $^1J(^{195}Pt–^{15}N)$ couplings for some platinum(II) NO_2 complexes.

Complex[83]	$\delta(^{195}Pt)$	J (Hz) *trans* to		
		Cl^-	Br^-	NO_2^-
$[PtCl_4]^{2-}$	−1631			
$[PtCl_3Br]^{2-}$	−1858			
trans-$[PtCl_2Br_2]^{2-}$	−2101			
cis-$[PtCl_2Br_2]^{2-}$	−2111			
$[PtClBr_3]^{2-}$	−2380			
$[PtBr_4]^{2-}$	−2676			
$[Pt(NO_2)Cl_3]^{2-}$	−1671	589		
trans-$[Pt(NO_2)Cl_2Br]^{2-}$	−1828		570+[a]	
cis-$[Pt(NO_2)Cl_2Br]^{2-}$	−1878	580		
cis-$[Pt(NO_2)ClBr_2]^{2-}$	−2057		568	
trans-$[Pt(NO_2)ClBr_2]^{2-}$	−2104	570		
$[Pt(NO_2)Br_3]^{2-}$	−2303		562	
trans-$[Pt(NO_2)_2Cl_2]^{2-}$	−1797			470
trans-$[Pt(NO_2)_2ClBr]^{2-}$	−1994			459
trans-$[Pt(NO_2)_2Br_2]^{2-}$	−2209			452
cis-$[Pt(NO_2)_2Cl_2]^{2-}$	−1797	679		
cis-$[Pt(NO_2)_2ClBr]^{2-}$	−1949	665	665	
cis-$[Pt(NO_2)_2Br_2]^{2-}$	−2120		651	
$[Pt(NO_2)_3Cl]^{2-}$	−1949	757		535
$[Pt(NO_2)_3Br]^{2-}$	−2087	665	745	522
$[Pt(NO_2)_4]^{2-}$	−2187			592

Complex[82]	$\delta(^{195}Pt)$	*trans* to	
		NO_2^-	O
$Pt(NO_2)_4^{2-}$	−2166	594	
$(H_2O)Pt(NO_2)_3^-$	−1928	531	754
$Pt(NO_2)_3(OH)^{2-}$	−1780	583	626
$Pt(NO_2)_2(C_2O_4)^{2-}$	−1487		748
cis-$(H_2O)_2Pt(NO_2)_2$	−1777		679
trans-$(H_2O)_2Pt(NO_2)_2$	−1780	470	
$Pt(NO_2)_2(PBu^n_3)_2$ [161]			
cis		390[b]	
trans		453	

[a] One peak partially hidden.
[b] *trans* to PBu^n_3

TABLE 9

^{15}N and ^{195}Pt NMR shifts (ppm) and one-bond couplings (Hz) for some Pt(II) and Pt(IV) diammines.

Complex[a]	$\delta(^{195}Pt)$	$\delta(^{15}N)$	$^1J(^{195}Pt-^{15}N)$	Solvent
Platinum(IV)				
c,t-Pt(NH$_3$)$_2$(mal)(OH)$_2$	+1570	—	—	D$_2$O/H$_2$O$_2$
c-Pt(C$_3$H$_7$NH$_2$)$_2$(OH)$_4$	+1521	—	249	D$_2$O
c,c,t-Pt(C$_3$H$_7$NH$_2$)$_2$Cl$_2$(OH)$_2$	+881	—	266	D$_2$O
c,c,t-Pt(NH$_3$)$_2$Cl$_2$(OH)$_2$	+860	−37.9	275	H$_2$O/H$_2$O$_2$
c-Pt(NH$_3$)$_2$Cl$_4$	−145	−30.5	247	H$_2$O
Platinum(II)				
[Pt(NH$_3$)$_2$(OH)]$_2^{2+}$	—	−81.7	342	H$_2$O
[Pt(NH$_3$)$_2$(OH)]$_3^{3+}$	−1499	−79.1	339	H$_2$O
c-Pt(NH$_3$)$_2$(H$_2$O)$_2^{2+}$	−1590	−89.0	387	H$_2$O
Pt(NH$_3$)$_2$(Etmal)	−1694	−83.7	366	H$_2$O
Pt(NH$_3$)$_2$(CBDCA)	−1723	—	360	H$_2$O
Pt(en)(H$_2$O)$_2^{2+}$	−1914	−51.9	411	H$_2$O
c-Pt(NH$_3$)$_2$Cl$_2$	−2048	—	302	DMF
	−2097	—	312	DMSO
	−2168	—	312	H$_2$O

Complex[b]	$\delta(^{195}Pt)$
[Pt(NH$_3$)$_2$(OH)]$_2$(NO$_3$)$_2$	−1153
[Pt(NH$_3$)$_2$(OH)]$_3$(NO$_3$)$_3$	−1505
cis-[Pt(NH$_3$)$_2$(H$_2$O)$_2$](NO$_3$)$_2$	−1588[c]
[Pt$_2$(NH$_3$)$_4$(C$_5$H$_4$NO)$_2$]$_2$(NO$_3$)$_4$	−1308
	−2261
[Pt$_2$(NH$_3$)$_4$(C$_5$H$_4$NO)$_2$](NO$_3$)$_2$	−1810
cis-[Pt(NH$_3$)$_2$(C$_5$H$_4$NOH)(H$_2$O)](NO$_3$)$_2$	−2015[d]
cis-[Pt(NH$_3$)$_2$(C$_5$H$_4$NOH)$_2$](NO$_3$)$_2$	−2495[d]

[a] Data from reference 88.
[b] At pH = 4.2, except where noted. Data from reference 95.
[c] pH = 2.0.
[d] At pH = 4.2. This species is partially deprotonated.

TABLE 10

^{195}Pt and ^{15}N NMR parameters.

Compound[a]	$\delta(Pt)^b$	$\delta(^{15}N)^c (J(^{195}Pt-^{15}N)^d)$ trans H_2O	trans A^{m-}
$[Pt(NH_3)_2(H_2O)_2](ClO_4)_2$ (I)	−1583.7	−85.83 (390.6)	
$(Pt(NH_3)_2(H_2O))_2(\mu\text{-}OH)^{3+}$	−1546.8	−83.13 (396.5)	−81.83 (339.3)
$(Pt(NH_3)_2(OH))_2(\mu\text{-}OH)^+$	−1516.3		−73.98 (298)^e
			−82.15 (334)^f
$Pt(NH_3)_2(ONO_2)(H_2O)^+$	−1598.4	−85.47 (403.4)	−85.47 (377.8)
$Pt(NH_3)_2(OSO_3)(H_2O)$	−1550.0	−85.10 (395.5)	−86.80 (378.2)
$Pt(NH_3)_2(OPO_3H_2)(H_2O)^+$	−1502.1	−85.54 (392.6)	−86.46 (377.2)
$Pt(NH_3)_2(OPO_3H)(H_2O)$	−1522	−85.8^i	−85.8^j
$(Pt(NH_3)_2)_2(\mu\text{-}OH)(\mu\text{-}PO_4H)^+$	−1480.6	—	−79.30 (342)^f
			−83.38 (366)^g
$Pt(NH_3)_2(O_2CCH_3)(H_2O)^+$	−1585.0	−87.19 (393.6)	−81.67 (348.1)^h
$Pt(NH_3)_2(O_2CCH_3)_2$	−1581.5	—	−83.12 (349.1)^h
$(Pt(NH_3)_2)_2(\mu\text{-}OH)(\mu\text{-}O_2CCH_3)^{2+}$	−1548.2	—	−77.36 (351.1)^f
			−83.01 (376.9)^h

^{a} Data for ^{15}N-substituted compounds, in H_2O (~0.3 M). All compounds have cis ammine ligands.

^{b} All values to lower shielding from aqueous Na_2PtCl_6.

^{c} All values to lower shielding from external $^{15}NH_4^+$.

^{d} Coupling constants in Hz, measured from ^{15}N spectra.

^{e} trans to terminal hydroxide.

^{f} trans to bridging hydroxide.

^{g} trans to phosphate.

^{h} trans to acetate.

^{i} Peaks coincident with peak from (I). Pt–N coupling not clearly resolved.

TABLE 11

^{195}Pt and ^{15}N NMR data.[89]

Compound[a]	$\delta(\text{Pt})$[b]	^{15}N(ammine)[c]		ligand *trans* to NH$_3$	^{15}N(gly)[c]	
		$\delta(\text{N})$	$J(\text{Pt-N})$		$\delta(\text{N})$	$J(\text{Pt-N}$
Pt(H$_2$O)$_3$(O$_2$CCH$_3$)$^{+d}$	-20 (s)					
Pt(H$_2$O)$_3$(glyH-O)$^{2+}$	-8.1 (s)				$+8.95$	0
Pt(H$_2$O)$_2$(glyH-O)$_2$$^{2+}$	-35.5 (s)				$+8.95$	0
	-42.3 (s)				$+8.95$	0
Pt(H$_2$O)$_3$(midaH$_2$-O)$^{2+}$	-2 (s)					
Pt(NH$_3$)$_2$(O$_2$CCH$_3$)(H$_2$O)$^{+e}$	-1585.0 (dd)	-87.19	393.6	H$_2$O		
		-81.67	348.1	-O$_2$C-		
Pt(NH$_3$)$_2$(glyH-O)(H$_2$O)$^{2+}$	-1582.2 (dd)	-87.19	392.1	H$_2$O	$+9.00$	0
		-82.64	358.4	O(gly)		
Pt(NH$_3$)$_2$(midaH$_2$-O)(H$_2$O)$^{2+}$	-1579.4 (dd)	-87.28	392.5	H$_2$O		
		-82.78	362.3	O(mida)		
Pt(NH$_3$)$_2$(O$_2$CCH$_3$)$_2$^{e}	-1581.5 (t)	-83.12	349.6	-O$_2$C-		
Pt(NH$_3$)$_2$(glyH-O)$_2$$^{2+}$	-1573.8 (t)	-83.85	359	O(gly)	$+9.00$	0
Pt(NH$_3$)$_2$(gly-N,O)$^+$	-2128.6 (ddd)[f]	-84.91	331.1	O(gly)	-54.43	275.0
		-64.93	301.3	N(gly)		
Pt(NH$_3$)$_2$(midaH-N,O)$^+$	-2080.4 (br t)	-76.40	355.4	O(mida)		
		-68.90	306.6	N(mida)		
Pt(NH$_3$)$_2$(gly-N)(OH)	-2126 (dt)	^{g}	287^h	OH	-47.9	314^h
		^{g}	287^h	N(gly)		
Pt(NH$_3$)$_2$(gly-N)$_2$	-2661 (tt)	-65.2	280	N(gly)	-49.3	312

[a] All ammine complexes with ^{15}N-substituted ammine, and *cis*.

[b] Shifts to lower shielding from PtCl$_6$$^{2-}$; s = singlet, d = doublet, t = triplet, br = broad.

[c] Shifts to lower shielding from ^{15}NH$_4$$^+$; coupling constants (Hz) from ^{15}N spectrum, except wher otherwise noted.

[d] From reference 80.

[e] From reference 90.

[f] For fully ^{15}N-substituted compound.

[g] Overlaps with other peaks.

[h] From ^{195}Pt spectrum.

TABLE 12

Platinum NMR data on some cancer related complexes.

Complex	$\delta(^{195}\text{Pt})$	$^1J(\text{Pt}-^{14}\text{N})$	Ref.
$\text{Pt}(\text{NH}_2\text{CH}_2\text{CH}_2\text{O})_2\text{Cl}_2{}^a$	284	195	92
trans-$\text{Pt}(\text{NH}_2\text{CH}_2\text{CH}_2\text{OH})_2(\text{OH})_2\text{Cl}_2$	881	190	92
trans,trans,cis-$\text{Pt}(\text{OH})_2\text{Cl}_2(\text{NH}_3)_2$	860	196	92
$\text{Pt}(\text{H}_2\text{O})_2(1,2\text{-diaminocyclohexane})^{2+}$	−1898	285	94
$[\text{Pt}(\mu\text{-OH})(1,2\text{-diaminocyclohexane})]_2{}^{2+}$	−1462	142	94
$[\text{Pt}(\mu\text{-OH})(1,2\text{-diaminocyclohexane})]_3{}^{3+}$	−1757	140	94
$\text{Pt}(\text{OH})_2(1,2\text{-diaminocyclohexane})$	−1796		94
		$^1J\ (\text{Pt}-^{15}\text{N})$	
$\text{Pt}(\text{H}_2\text{O})_2(^{15}\text{NH}_3)_2{}^{2+}$		389	91
		287 (NH$_3$)	91
$\text{Pt}(^{15}\text{NH}_3)_2(1\text{-methylimidazole-}^{15}\text{N}_2)^{2+}$		437 (N3)	
		26 (N1)	
$\text{Pt}(\text{H}_2\text{O})_2(\text{en-}^{15}\text{N}_2)^{2+\ b}$		421	91
		319 (en)	91
$\text{Pt}(\text{en-}^{15}\text{N}_2)(1\text{-methylimidazole-}^{15}\text{N}_2)^{2+}$		429 (N3)	
		26 (N1)	
$\text{Pt}(\text{H}_2\text{O})_2(1\text{-methylimidazole-}^{15}\text{N})_2)^{2+}$		579 (N3)	91
		33 (N1)	
$\text{Pt}(\text{H}_2\text{O})(\text{en-}^{15}\text{N}_2)(1\text{-methylimidazole-}^{15}\text{N}_2)^{2+}$		411, 327 (en)	91
$\text{Pt}(^{15}\text{py})\text{Cl}(\text{PPh}_3)\{\text{C}(=\text{CMe}_2)\text{CH}_2\text{py}\}^+$	−404^c	266	97
	−3936^d	143	97
$\text{PtCl}_2(^{15}\text{py})\text{PPh}_3$			
trans	−3560	248	97
cis	−3400	441	97
trans-$\text{PtCl}_2(\text{NHMe}_2)(\text{PPh}_3)$	−3650	170	97
$[\text{Pt}(^{15}\text{NHMe}_2)\text{Cl}(\text{PPh}_3)\{\text{C}(=\text{CMe}_2)\text{CH}_2\text{NHMe}_2\}]^+$	−4093	$\left\{\begin{array}{l} 207 \\ 73^e \end{array}\right.$	97
$\begin{array}{c}\text{NMe}_2-\text{CH}_2 \\ \quad\mid\qquad\mid \\ \text{Cl}-\text{Pt}---\text{C} \\ \quad\mid\qquad\quad\diagdown \\ \text{PPh}_3\qquad\text{CMe}_2\end{array}$	−3809	159	97

^{a} *cis*-N,N *trans*-O,O *cis*-dichloro isomer.
^{b} en = ethylenediamine.
^{c} py *trans* to PPh$_3$.
^{d} py *trans* to C ligand.
^{e} $^3J(\text{Pt}-\text{N})$.

TABLE 13

Chemical shifts and couplings for some platinum(IV) complexes.[a]

Complex[b]	δ(ppm)	J(Hz) *trans* to		
		Cl⁻	Br⁻	NO₂⁻
(1) [PtCl₆]²⁻	0			
(2) [PtCl₅Br]²⁻	−287			
(3) *cis*-[PtCl₄Br₂]²⁻	−584			
(4) *trans*-[PtCl₄Br₂]²⁻	−585			
(5) *fac*-[PtCl₃Br₃]²⁻	−893			
(6) *mer*-[PtCl₃Br₃]²⁻	−894			
(7) *cis*-[PtCl₂Br₄]²⁻	−1214			
(8) *trans*-[PtCl₂Br₄]²⁻	−1216			
(9) [PtClBr₅]²⁻	−1548			
(10) [PtBr₆]²⁻	−1894			
(11) [Pt(NO₂)Cl₅]²⁻	384	394		
(12) *trans*-[Pt(NO₂)Cl₄Br]²⁻	86	393		
(13) *cis*-[Pt(NO₂)Cl₄Br]²⁻	146		366	
(14) *mer, trans*-[Pt(NO₂)Cl₃Br₂]²⁻	−227	400		
(15) *fac, cis*-[Pt(NO₂)Cl₃Br₂]²⁻	−217	400		
(16) *mer, cis*-[Pt(NO₂)Cl₃Br₂]²⁻	−160		367	
(17) *cis, mer*-[Pt(NO₂)Cl₂Br₃]²⁻	−536	403		
(18) *cis, fac*-[Pt(NO₂)Cl₂Br₃]²⁻	−471		366	
(19) *trans, mer*-[Pt(NO₂)Cl₂Br₃]²⁻	−481		360	
(20) *trans*-[Pt(NO₂)ClBr₄]²⁻	−860	403		
(21) *cis*-[Pt(NO₂)ClBr₄]²⁻	−801		372	
(22) [Pt(NO₂)Br₅]²⁻	−1135		372	
(23) *trans*-[Pt(NO₂)₂Cl₄]²⁻	500			336
(24) *trans*-[Pt(NO₂)₂Cl₃Br]²⁻	[210]			[339]
(25) *trans*-[Pt(NO₂)₂Cl₂Br₂]²⁻	[−86]			[339]
(26) *trans*-[Pt(NO₂)₂Cl₂Br₂]²⁻	[−95]			[339]
(27) *trans*-[Pt(NO₂)₂ClBr₃]²⁻	−397			342
(28) *trans*-[Pt(NO₂)₂Br₄]²⁻	−713			342
(29) *cis*-[Pt(NO₂)₂Cl₄]²⁻	862	424		
(30) *cis*-[Pt(NO₂)₂Cl₃Br]²⁻	563	427		
(31) *cis*-[Pt(NO₂)₂Cl₃Br]²⁻	614	430	399	
(32) *cis*-[Pt(NO₂)₂Cl₂Br₂]²⁻	248	430		
(33) *cis*-[Pt(NO₂)₂Cl₂Br₂]²⁻	310	427	391	
(34) *cis*-[Pt(NO₂)₂Cl₂Br₂]²⁻	360		394	
(35) *cis*-[Pt(NO₂)₂ClBr₃]²⁻	−11	433	397	
(36) *cis*-[Pt(NO₂)₂ClBr₃]²⁻	51		397	
(37) *cis*-[Pt(NO₂)₂Br₄]²⁻	−276		405	
(38) *mer*-[Pt(NO₂)₃Cl₃]²⁻	1043	446		360
(39) *mer*-[Pt(NO₂)₃Cl₂Br]²⁻	[756]	[446]		[360]
(40) *mer*-[Pt(NO₂)₃Cl₂Br]²⁻	[804]		[415]	[360]
(41) *mer*-[Pt(NO₂)₃ClBr₂]²⁻	[456]	[446]		[363]
(42) *mer*-[Pt(NO₂)₃ClBr₂]²⁻	512		415	363
(43) *mer*-[Pt(NO₂)₃Br₃]²⁻	207		421	369

TABLE 13 (*cont.*)

Complex[b]	δ(ppm)	J(Hz) *trans* to		
		Cl⁻	Br⁻	NO₂⁻

Complex^b	δ(ppm)	Cl^-	Br^-	NO_2^-
(44) *fac*-[Pt(NO₂)₃Cl₃]²⁻	1375	460		
(45) *fac*-[Pt(NO₂)₃Cl₂Br]²⁻	1133	466	427	
(46) *fac*-[Pt(NO₂)₃ClBr₂]²⁻	885	467	424	
(47) *fac*-[Pt(NO₂)₃Br₃]²⁻	631		430	
(48) *trans*-[Pt(NO₂)₄Cl₂]²⁻	1280	.		376
(49) *trans*-[Pt(NO₂)₄ClBr]²⁻	[995]			[376]
(50) *trans*-[Pt(NO₂)₄Br₂]²⁻	[695]			[376]
(51) *cis*-[Pt(NO₂)₄Cl₂]²⁻	1594	488		391
(52) *cis*-[Pt(NO₂)₄ClBr]²⁻	1368	486	459	394
(53) *cis*-[Pt(NO₂)₄Br₂]²⁻	1136		455	394
(54) [Pt(NO₂)₅Cl]²⁻	1833	518		415
(55) [Pt(NO₂)₅Br]²⁻	1629		482	415
(56) [Pt(NO₂)₆]²⁻	[2080]			[439]

^{a} Data from reference 83. D₂O solutions. $^1J(^{195}Pt-^{15}N)$.

^{b} For compounds (23)–(47) the terms *cis* and *trans*, etc., refer to the geometrical arrangement of the nitrito groups. For (12)–(21) these terms refer to the arrangement of the halides except in (12), (13), (20) and (21) where they refer to the arrangement of NO₂⁻ and the single halide. The listed couplings remove other ambiguities. In compound (25) the bromides are *cis*, in (26) they are *trans*. The values given in square brackets are those predicted for the nine unobserved species.

TABLE 14

^{195}Pt chemical shifts^a and $^nJ(^{195}$Pt$-^{195}$Pt$)$ couplings in some zerovalent and polymetallic complexes.

Complex	$\delta(^{195}$Pt$)$		$^1J(^{195}$Pt$-^{195}$Pt$)$		Ref.
$[Pt_3(CO)_6]^{2-}$	-4581				131
$[Pt_6(CO)_{12}]^{2-}$	-4500				131
$[Pt_9(CO)_{18}]^{2-}$	-4463 (2)				131
			822		
	-5045 (1)				
$[Pt_{12}(CO)_{24}]^{2-}$	-4426				131
			750		
	-5078				
$[Pt_{15}(CO)_{30}]^{2-}$	-4411 (2)				131
	-5020 (1)				
	-5091 (2)				
$[Pt_3(\mu_2$-CO$)_3(PR_3)_3]$					132
$PR_3 = $ P(cyclohexyl)$_3$	-4392		1571		132
PPr$^i_3$	-4530		1607		132
PPr$^i_2$Ph	-4450		1610		132
P(CH$_2$Ph)Ph$_2$	-4448		1619		132
PBu$^t_2$Me			1770		60
PEt$_2$Bu^t	-4445		1595		133
	Pt^1	Pt^{2,3}	Pt^1, Pt^2	Pt^2, Pt^3	
Pt$_3(\mu$-CO$)_3$L$_4$					133
L = PEt$_3$	-3908	-3883	586	1830	
PMe$_2$Ph	-3760	-3949	507	1840	
PMePh$_2$	-3828	-3970			
PEt$_2$Bu^t	-3836	-3758	385	1808	
P(CH$_2$Ph)Ph$_2$	-3855	-4066			
Pt$_4(\mu$-CO$)_5$L$_4$					134
L = PEt$_3$	-4180		1072		
PMe$_2$Ph	-4162		1110		
PMePh$_2$	-4191		1124		
PtOs$_3(\mu$-H$)_2(\mu$-CH$_2)($CO$)_{10}($Pcy$_3)$	$-3488, -4361$ two isomers				146
$[Os_2Pt_2(\mu$-H$)_2($CO$)_8($PR$_3)_2]$ (butterfly cluster)					
PPh$_3$			1744		135
P(cyclohexyl)$_3$			1542		135
$[OsPt_2($CO$)_5($PPh$_3)_2(\mu_3$-MeC$_2$Me$)]$			57		137
$[FeWPt(\mu_3$-CC$_6$H$_4$Me-4$)($CO$)_6) \times$ (PMe$_2$Ph$)(\eta$-C$_5$H$_5)_2]$	-4924				144
$[W_2Pt(\mu$-CC$_6$H$_4$Me-4$)_2($CO$)_4(\eta$-C$_5$H$_5)_2]$	-2882		$^1J(^{195}$Pt$-^{183}$W$) = 177$		143
$[Rh_2Pt(\mu$-CO$)_2($CO$)_2(\mu$-C$_5$Me$_5)_2]$	-4481		$^1J(^{195}$Pt$-^{103}$Rh$) = 15$		145
$[Rh_2Pt(\mu$-CO$)_2($COD$)(\mu$-C$_5$Me$_5)_2]$	-3599				145
$($Bu$_4$N$)_2[$PtRh$_4($CO$)_{12}]$	-4146		$^1J($Pt$-$Rh$) = 44$		162
PtFe$_3(\mu_3$-C(OCH$_3))(\mu$-H$)($CO$)_{10}($PPh$_3)$	-4417				163

TABLE 14 (*cont.*)

Complex	$\delta(^{195}Pt)$	$^1J(^{195}Pt-^{195}Pt)$	Ref.
	Pt_A −3743 Pt_B −4036	1730	136
$P\frown P = (Ph_2P)_2CH_2$			
$PtL_2(\mu\text{-}CO)(\mu\text{-}\sigma\text{: }\eta^3\text{-}C_6H_4CH_3\text{-}$ $p)W(CO)cp$			138a
L = PMe$_3$	−4659		
PMe$_2$Ph	−4644		
PMePh$_2$	−4683		
$PtL_2(\mu\text{-}X)(\mu\text{-}CHTol)W(CO)_nL_{2-n}$			138b
L = PMe$_3$ X = CO $n=2$	−4289		
PMe$_2$Ph CO ⌒ 2	−4326		
PMe$_3$ CO 1	−4548		
PMe$_2$Ph CO 1	−4551		
PMe$_3$ H 2	−5539, −5556		
PMe$_2$Ph H 2	−5552		
$PtL_2(\mu\text{-}CO)(\mu\text{-}CHTol)W(RC\equiv CR)cp$			138c
L = PMe$_3$ R = Me	−5239		
PMe$_2$Ph Me	−5204		
PMe$_2$Ph Ph	−5167		
PMePh$_2$ Ph	−5136		
$Pt(CO)(\mu\text{-}CR(Tol)(\mu\text{-}$ $Ph_2PCH_2PPh_2)W(CO)_4$			139
R = Me	−4158		
H	−4221		
C≡CBu^t	−3698		
SC$_6$H$_4$Me-p	−4342		
$Pt(Ph_2PCH_2PPh_2)(\mu\text{-}$ $CMe(OMe))W(CO)_5$	−4396		140
$[Pt(CO)(\mu\text{-}CMe)(\mu\text{-}$ $Ph_2PCH_2PPh_2)W(CO)_4]^+$			140
BF$_4^-$	−3462		
$[Pt_2(\mu\text{-}(SiMe_3C\equiv CSiBu^tMe_2))(COD)_2]$	−3914		142
A = O	−3709	+5355	60
NH	−3916	+6235	60
$[L_2Pt(\mu\text{-}PhC\equiv CPh)PtL'_2]$			
L = L' = PMe$_3$		470	60
L = PMe$_3$, L'L' = PhC≡CPh	−4693	1006	60
$[(P(OMe)_3)_2Pt\!\left(\begin{smallmatrix}CPh\\CPh\end{smallmatrix}\!\!>\!CO\right)\!Pt(P(OMe)_3)_2]$		1976	129b

TABLE 14 (*cont.*)
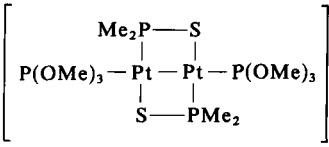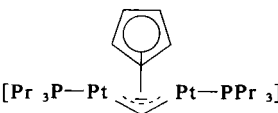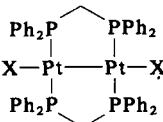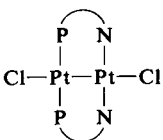
Complex	$\delta(^{195}Pt)$	$^1J(^{195}Pt-^{195}Pt)$	Ref.
$[Pt_3(\mu\text{-}C\equiv NBu^t)_3(C\equiv NBu^t)_3]$		188	60
$[\{PtCl(CO)(PPh_3)\}_2]$		760	60
$[\{Pt(C\equiv NMe)_3\}_2]^{3+}$	−4568	+507	60

$$\begin{bmatrix} & Me_2P\text{---}S & \\ & | \quad\quad | & \\ P(OMe)_3 - Pt - Pt - P(OMe)_3 \\ & | \quad\quad | & \\ & S\text{---}PMe_2 & \end{bmatrix}$$

Complex	$\delta(^{195}Pt)$	$^1J(^{195}Pt-^{195}Pt)$	Ref.
$[Pr_3P\text{---}Pt \overset{\text{cp}}{\cdots} Pt\text{---}PPr_3]$	−5139	410	60

$$\begin{matrix} Ph_2P & & PPh_2 \\ | & & | \\ X\text{---}Pt\text{----}Pt\text{---}X \\ | & & | \\ Ph_2P & & PPh_2 \end{matrix}$$

Complex	$\delta(^{195}Pt)$	$^1J(^{195}Pt-^{195}Pt)$	Ref.
		188	60
X = Cl		8197	60
Br		8828	60
I		9007	60
trans-Pt$_2$(cp)$_2$(CO)$_2$Pt$_2(\mu$-OAc)$_2$Ph$_4$(PR$'_3$)	−2140	9400	129a
			128
R = OMe		6044	
Et		6541	
Pt$_2$X$_4$(CO)$_2^{2-}$			119
X = Cl	−4160	5250	
Br	−4335	4770	
Pt$_2$BrI$_3$(CO)$_2^{2-}$	−4474, −4732	4087	119

$$\begin{matrix} & \overset{\frown}{P \quad N} & \\ & | \quad\quad | & \\ Cl\text{---}Pt\text{---}Pt\text{---}Cl \\ & | \quad\quad | & \\ & \underset{\smile}{P \quad N} & \end{matrix}$$

Complex	$\delta(^{195}Pt)$	$^1J(^{195}Pt-^{195}Pt)$	Ref.
		10 269	123

P⌢N = 2-diphenylphosphinopyridine

Complex	$\delta(^{195}Pt)$	$^1J(^{195}Pt-^{195}Pt)$	Ref.
Pt$_2(\mu$-SPR$_2$)$_2$L$_2$ (structure [25])			124
R = cy L = P(OPh)$_3$		495	
Et P(OPh)$_3$		465	
Et P(OPh)$_2$Ph		366	
OEt P(OEt)$_2$Ph		95	
Et C≡NCH$_3$		1022	
Ph C≡NBu^t		1163	
Pt$_2$(O$_2$P-O-PO$_2$)$_4$X$_2^{4-}$			126
X = Cl	−4236		

TABLE 14 (cont.)
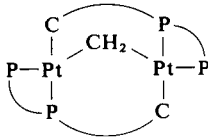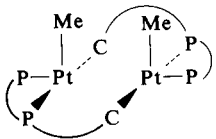
Complex	$\delta(^{195}\text{Pt})$	$^{1}J(^{195}\text{Pt}-^{195}\text{Pt})$	Ref.
X = Br	−4544		
I	−5103		
$Pt_2(SO_4)_4(H_2O)_2{}^{2-}$	1753		127
$Pt_2(PO_4H)_4(H_2O)_2{}^{2-}$	1796		127
$Pt_2(SO_4)_4Cl_2{}^{4-}$	1720		127
$Pt_2(PO_4H)_4Cl_2{}^{4-}$	1822		127
$Pt_2(SO_4)_4Br_2{}^{4-}$	1592		127
$Pt_2(PO_4H)_4Br_2{}^{4-}$	1744		127
$Pt_2(SO_4)_4Cl(H_2O)^{3-}$	1809	3464	127
	1638		
$Pt_2(PO_4H)_4Cl(H_2O)^{3-}$	1890	5342	127
	1713		
$Pt_2(SO_4)_4Br(H_2O)^{3-}$	1866	3472	127
	1440		
$Pt(PO_4H)_4Br(H_2O)^{3-}$	1973	5349	127
	1550		
$K_4[Pt_2(H_2P_2O_5)_4]\cdot2H_2O$	−5139		165
$Pt_2(\mu\text{-}Sn\{acac\}_2)_3$		4663	125
$Cl\text{-}Pt(\mu\text{-}Ph_2PCH_2PPh_2)_2PtH_2{}^{+}$		1320	121

$\overbrace{P\ \ P}\ \ C = Ph_2PCH_2CH_2PPh_2C_6H_4\text{-}2$		370	107

$\overbrace{P\ \ P}\ \ C$ as above		400	130a
$dl\text{-}[Clcy_2PPt(\mu\text{-}Pcy)]_2$		+259	108
$dl\text{-}[ClPh_2PPt(\mu\text{-}PPh)]_2$		+342	108
$dl\text{-}[CH_3Ph_2PPt(\mu\text{-}PPh)]_2$		+667	108
$meso\text{-}[Clcy_2PPt(\mu\text{-}Pcy)]_2$		+639	108
$(PEt_3)_2(Ph)Pt(\mu\text{-}H)Pt(Ph)(PEt_3)_2$	−4549	164	114
$(PEt_3)_2(Tol)Pt(\mu\text{-}H)Pt(Tol)(PEt_3)_2$		163	114
$(Ph_3P)PhPt(\mu\text{-}H)(\mu\text{-}PPh_2)Pt(PPh_3)_2{}^{+}$	−5349	500	113
$CH_3Pt(\mu\text{-}H)(\mu\text{-}dppm)PtCH_3{}^{+}$		464	109
$Pt_4H_2(PBu^t{}_3)_4$	−3933		166

TABLE 14 (*cont.*)
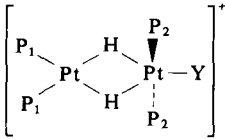
Complex	$\delta(^{195}\text{Pt})$	$^1J(^{195}\text{Pt}-^{195}\text{Pt})$	Ref.
$[(CH_3)_2Pt(\mu\text{-}Ph_2PCH_2PPh_2)_2PtCH_3]$		332	130b
$[\{Pt(\mu\text{-}H)(PBu^t{}_2Me)(Si(OEt)_3)\}_2]$	-4577	92	115
$[Pt(C_6H_5)(PEt_3)_2(\mu\text{-}H)PtH(PEt_3)_2]$		366	111

$$\left[\begin{array}{c} P_1 \diagdown \quad H \diagdown \quad \overset{P_2}{\underset{\underset{P_2}{\vdots}}{\overset{\blacktriangledown}{Pt}}}-Y \\ \diagup \quad Pt \quad \diagup \\ P_1 \qquad H \end{array}\right]^+$$

Complex	$\delta(^{195}\text{Pt})$	$^1J(^{195}\text{Pt}-^{195}\text{Pt})$	Ref.
$P_1 = P_2 = PEt_3,\ Y = Ph$			
5-coordinate[a]	-4369	796	112, 113
4-coordinate	-5265		
$P_1 = P_2 = PEt_3,\ Y = H$[b]	$\begin{cases} -4855 \\ -5204 \end{cases}$	886	112, 113
$P_1 = P_2 = P(\text{cyclohexyl})_3,\ Y = H$[c]	$\begin{cases} -4812 \\ -5328 \end{cases}$	268	112, 113
$P_1 = P_2 = PPh_3,\ Y = H$[d]	$\begin{cases} -4756 \\ -5104 \end{cases}$	325	112, 113
$P_1 = PPh_3,\ P_2 = P(\text{cyclohexyl})_3$[e]	$\begin{cases} -4908 \\ -5255 \end{cases}$	701	112, 113
$[Pt_2H_3(Bu^t{}_2P(CH_2)_nPBu^t{}_2)_2]^+$			
R = 2		815.4	164
R = 3		840.2	164
sym-trans-$[Pt_2X_4L_2]$			
X = Cl L = PEt_3		193	104
Cl PPr_2Bu^t		125	104
Cl $PBu^n{}_3$		199	104
Cl $PPr^n{}_3$		200	60
Cl PMe_2Et		177	60
Cl $PMeEt_2$		190	60
Br PMe_2Et		219	60
Br $PPr^n{}_3$		239	60
I $PBu^n{}_3$		380	104
I PMe_2Et		377	60
I $PMeEt_2$		383	60
I $PPr^n{}_3$		391	60
Cl PMe_3	-3410		23
Cl $AsMe_3$	-3034		23
Cl $AsEt_3$	-3023		a
Cl $AsPr_3$	-3008		a
Cl $AsPr^i{}_3$	-2983		a
Cl $AsBu^n{}_3$	-3014		a
Br PMe_3	-3985		23
Br $AsMe_3$	-3701		23
Br $SbMe_3$	-3772		23
I PMe_3	-5297		23

TABLE 14 (*cont.*)

Complex		$\delta(^{195}Pt)$	$^1J(^{195}Pt-^{195}Pt)$	Ref.
I	AsMe$_3$	-5212		23
I	SbMe$_3$	-5386		23
I	SMe$_2$	$\begin{cases} -4827 \\ -4795 \end{cases}$		23
	two isomers			
$[(PPr^n_3)_2Pt(\mu\text{-}Cl)_2Pt(PPr^n_3)_2]^{2+}$		-4255	137	23
$[Cl_3Pt^1(\mu\text{-}SeMe_2)Pt^2Cl_2(SeMe_2)]$				
Pt$_1$		-2807	516	60
Pt$_2$		-3749		
$[(P)ClPt(\mu\text{-}X, Y)PtCl(P)]$				
$X = Cl, X = S(CH_2Ph)_2$		-3884	390	8
$P = PBu^n_3$				
$X = Y = S(CH_2Ph)_2$		-3843	880	8
$P = PBu^n_3$				
$X = Y = SPh$		-4018		8
$P = PMe_2Ph$				
$X = Y = SEt$		-3807		8
$P = PMe_2Ph$				
$Pt_2(\mu\text{-}S)(\mu\text{-}SCH_3)(PPh_3)_4]I$			969	106
$Pt_2(\mu\text{-}SMe)_2(CH_3)_2(PMe_2Ph)_2$			-202	52
$[Pt(PMe_2Ph)_4]$		-4728		23
$[Pt(P(OMe)_3)_4]$		-5830		23
$[Pt(FPOC_6H_4O)_4]$		-5629		59
$[Pt(FP(OPh)_2)_4]$		-5590		59
$[Pt(PEt_3)_2(CO(CF_3)_2)]$		-4941		23
$[Pt(C_2F_4)(PEt_3)_2]$		-4784		23
$[Pt(C_2F_4)(PPh_3)_2]$		-4791		34
$[Pt(C_2H_4)(PPh_3)_2]$		-5065		34

[a] G. Balimann, Ph.D. thesis, ETH Zürich, 1977.

TABLE 15

^{195}Pt chemical shifts^a of nitrate, sulphate, phosphate, acetate, and chloride complexes of Pt(H$_2$O)$_4^{2+}$.

	Complexes			
Anion	mono	bis (*cis* and *trans*)	tris	tetrakis
NO$_3^-$	−24	−57 −59	−96	
SO$_4^{2-}$	+74	+133 +164		
H$_2$PO$_4^-$	+145	+267 +292	+424	+602
CH$_3$COO$^-$	−20			
Cl$^-$	−350	−811 (*cis*) −644 (*trans*)	−1185	−1625

^{a} Measured relative to an aqueous solution of Na$_2$PtCl$_6$. From reference 90b.

TABLE 16

^{195}Pt shift data for some simple salts of Pt(IV).

		[PtCl$_6$(OH)$_{6-n}$]$^{2-}$ ^{a}	[PtCl$_6$Br$_{6-n}$]$^{2-}$ ^{b}
$n = 0$		3290	−1879
$n = 1$		2797	−1529
$n = 2$	*cis*	2361	−1191
	trans	2337	−1206
$n = 3$	*fac*	1851	−865
	mer	1828	−879
$n = 4$	*cis*	1278	−566
	trans	1260	−578
$n = 5$		663	−277
$n = 6$		−3	0 ^{b}
H$_2$PtI$_6$		−6300 ^{c}	
H$_2$PtBr$_6$		−1860 ^{c}	

^{a} Alkaline aqueous solution, pH = 10–12; data from reference 30.
^{b} As Bu$_4$N$^+$ salts in acetone. (Bu$_4$N)$_2$PtCl$_6$ arbitrarily assigned zero; data from reference 29.
^{c} Data from reference 187.

TABLE 17

The effect of ligand and geometric isomerization on $\delta(^{195}Pt)$.[a]

	L =	PMe_3	$AsMe_3$	$SbMe_3$	SMe_2	$SMePh$
cis-$PtCl_2L_2$		−4408	−4291	−4612	−3551	−3488
cis-$PtBr_2L_2$		−4636	−4625	−5019	−3879	−3858
cis-PtI_2L_2		−4588		−5816		−4686
cis-$PtClBrL_2$		−4517	−4448	−4797	−3707	−3664
cis-$PtClIBr_2$				−5138	−4025	−4021
cis-$PtBrIL_2$				−5385	−4224	−4224
trans-$PtCl_2L_2$		−3950	−3780		−3424	−3385
trans-$PtBr_2L_2$		−4473	−4378		−3899	−3879
trans-PtI_2L_2		−5539	−5518		−5789	−4805
trans-$PtClBrL_2$			−4075		−3660	−3629
trans-$PtClIL_2$		−4741	−4655	−4749	−4141	−4118
trans-$PtBrIL_2$			−4963	−5131	−4375	−4365
$PtCl_3L^-$		−3500	−3173	−3143	−2757	
$PtBr_3L^-$		−4119	−3869	−3928	−3415	
PtI_3L^-		−5506	−5446	−5642	−4973	

	L =	$SeMe_2$	$TeMe_2$	$P(OCH_3)_3$	$SOMe_2$
cis-$PtCl_2L_2$		−3735	−4369	−4371	−3477
cis-$PtBr_2L_2$				−4599	−3778
cis-PtI_2L_2				−5102	
cis-$PtClBrL_2$				−4476	−3619
cis-$PtClIBr_2$				−4669	
cis-$PtBrIL_2$				−4820	
				NMe_3	
trans-$PtCl_2L_2$		−3504		−1886	
trans-$PtBr_2L_2$		−4041		−1988	
trans-PtI_2L_2		−4819	−5664		
trans-$PtClBrL_2$		−3769		−1935	
trans-$PtClIL_2$		−4304			
trans-$PtBrIL_2$		−4573			
$PtCl_3L^-$		−2769	−3059		−2998
$PtBr_3L^-$		−3476	−3826		−3641
PtI_3L^-		−5129	−5528		

[a] The anions have Pr_4N^+, Ph_4P^+ or Bu_4N^+ cations; data from reference 23.

TABLE 18

The effect of different phosphorus ligands on $\delta(^{195}Pt)$.[a]

L	$[PtCl_3L]^-$	cis-$[PtCl_2L_2]$	$trans$-$[PtCl_2L_2]$
PMe_3	−3500	−4408	−3950
PEt_3	−3540	−4490, −4475	−3938, −3916
PPr^n_3	−3520	−4442	
PBu^n_3	−3524	−4448	−3929
PMe_2Ph	−3511	−4403	
PEt_2Ph		−4426	−3964
$PMePh_2$	−3515	−4439	
PPh_3	−3513		
$P(p\text{-}ClC_6H_4)_3$		−4428	
$P(p\text{-}CH_3OC_6H_4)_3$		−4407	
$P(OMe)_3$	−3496		
$P(OEt)_3$		−4363	
$P(OPh)_3$		−4298	
PF_3	−3626		
$PF_2(OMe)$	−3584		
$PF(OMe)_2$	−3534		
$PCl(OMe)_2$	−3425		
$PCl_2(OMe)$	−3354		

[a] From reference 23.

TABLE 19

^{195}Pt chemical shifts of some arsine complexes.[a]

Compound	$\delta(^{195}Pt)$	$\Delta\nu_{1/2}$
cis-[PtCl$_2$(AsEt$_3$)$_2$]$^-$	−4363	~400
cis-[PtCl$_2$(AsPr$^n_3$)$_2$]	−4321	~170
cis-[PtCl$_2$(AsMe$_2$Ph)$_2$]	−4287	~180
cis-[PtCl$_2$(AsMePh$_2$)$_2$]	−4323	~190
cis-[PtCl$_2$(AsPh$_3$)$_2$]	−4351	~115
cis-[PtCl$_2$(AsTol$_3$)$_2$]	−4352	~80
cis-[PtCl$_2$(AsBzPh$_2$)$_2$]	−4325	~160
trans-[PtCl$_2$(AsEt$_3$)$_2$]	−3710	~105
trans-[PtCl$_2$(AsPr$^n_3$)$_2$]	−3703	~75
trans-[PtCl$_2$(AsBu$^n_3$)$_2$]	−3709	~55
trans-[PtCl$_2$(AsPr$^i_3$)$_2$]	−3596	~130
trans-[PtCl$_2$(AsMe$_2$Ph)$_2$]	−3771	~100
trans-[PtCl$_2$(AsMePh$_2$)$_2$]	−3792	~100
trans-[PtCl$_2$(AsPh$_3$)$_2$]	−3803	~65
trans-[PtCl$_2$(AsTol$_3$)$_2$]	−3801	~40
sym-trans-[Pt$_2$Cl$_4$(AsEt$_3$)$_2$]	−3023	~225
sym-trans-[Pt$_2$Cl$_4$(AsPr$^n_3$)$_2$]	−3008	~200
sym-trans-[Pt$_2$Cl$_4$(AsBu$^n_3$)$_2$]	−3014	~135
sym-trans-[Pt$_2$Cl$_4$(AsPr$^i_3$)$_2$]	−2983	
trans-[PtCl$_4$(AsPr$^n_3$)$_2$]	−1023	~115
cis-[PtCl$_2$(PBu$^n_3$)(PTol$_3$)]	−4412	<3

[a] Data from the Ph.D. thesis of G. Balimann, ETH Zürich, 1977.

TABLE 20

^{195}Pt chemical shifts of some olefin complexes of Pt(II).

Compound		$\delta(^{195}Pt)$	Ref.
$[PtCl_3(C_2H_4)]^-$		$-2743, -2785$	23, 167
$(Pr_4N)[PtCl_3(n\text{-octene})]$		-2718	23
trans-$[PtCl_2(amine)(C_2H_4)]$			168
$\quad$ MeNH$_2$		-3040	
$\quad$ EtNH$_2$		-3020	
$\quad$ Pr^{i}NH$_2$		-3008	
$\quad$ PhCH$_2$NH$_2$		-3030	
$\quad$ PhCH(CH$_3$)NH$_2$		-3016	
$\quad$ PhCH(Bu^t)NH$_2$		-2990	
$\quad$ Me$_2$NH		-3074	
$\quad$ EtMeNH		-3049	
$\quad$ Pr^{i}MeNH		-3030	
$\quad$ PhCH$_2$MeNH		-3047	
$\quad$ (S)-PhCH(CH$_3$)MeNH			
$\quad\quad$ S.S.		-3045	
$\quad\quad$ S.R.		-2996	
$\quad$ piperidine		-3087	
$\quad$ 2,6-Me$_2$-piperidine		-2953	
trans-$[PtCl_2(substituted\ pyridine)(C_2H_4)]$			18
$\quad$ 2,4,6-(CH$_3$)$_3$		$-2871^a\ (-2849)^b$	
$\quad$ 2,6-(CH$_3$)$_2$		-2877	
$\quad$ 2,4-(CH$_3$)$_2$		$-2930^a\ (-2909)^b$	
$\quad$ 2-CH$_3$		-2937	
$\quad$ 4-N(CH$_3$)$_2$		-2980	
$\quad$ 4-CH$_3$		-2979	
$\quad$ 4-H		-2979	
$\quad$ 4-Cl		-2986	
$\quad$ 4-COCH$_3$		-2984	
$\quad$ 4-CN		-2992	
trans-$[PtCl_2(piperidine)(cis\text{-}2\text{-butene})]$		-2943	167
trans-$[PtCl_2(piperidine)(trans\text{-}2\text{-butene})]$		-2941	167
trans-$PtClBr_2(C_2H_4)]^-$		-3360	23
cis-$[PtCl_2Br(C_2H_4)]^-$		-3062	23
cis-$[PtClBr_2(C_2H_4)]^-$		-3155	23
$(NPr^n_4)[PtBr_3(C_2H_4)]$		-3473	23
trans-(N, olefin)-$[PtCl(N\text{-}Me\text{-}S\text{-}proline)(olefin)]$			
$\quad$ propene	R	-2532	169
	S	-2532	
$\quad$ *trans*-2-butene	R	-2523	169
	S	-2523	
$\quad$ Bu^t-ethylene	R	-2495	169
	S	-2490	
$\quad$ *p*-chlorostyrene	R	-2391	169
	S	-2402	

TABLE 20 (*cont.*)

Compound		$\delta(^{195}\text{Pt})$	Ref.
styrene	R	−2391	169
	S	−2395	
p-methoxystyrene	R	−2365	169
	S	−2371	
[PtCl$_2$(1,5-COD)]		−3361	34
[PtMe$_2$(1,5-COD)]		−3594	34
[PtPh$_2$(1,5-COD)]		−3624	34
[Pt(*p*-ClC$_6$H$_4$)$_2$(1,5-COD)]		−3626	34
[Pt(*p*-PhC$_6$H$_4$)$_2$(1,5-COD)]		−3624	34
[Pt(*p*-CH$_3$C$_6$H$_4$)$_2$(1,5-COD)]		−3618	34
[Pt(*p*-FC$_6$H$_4$)$_2$(1,5-COD)]		−3614	34
[Pt(*o*-CH$_3$C$_6$H$_4$)$_2$(1,5-COD)]		−3536	34
[PtCl$_3$(H$_2$C=C=CH$_2$)]$^-$		−2496	39
cis-[PtCl$_2$(H$_2$C=C=CH$_2$)(PPr$^n_3$)]		−3633	39
cis-[PtCl$_2$(H$_2$C=C=CH$_2$)(PMe$_2$Et)]		−3639	39

[a] CDCl$_3$.

[b] Acetone.

TABLE 21

^{195}Pt chemical shifts of complexes with some carbon ligands.

Compound	$\delta(^{195}\text{Pt})$	Ref.
cis-[PtMe$_2$(PMe$_2$Ph)$_2$]	−4594	34
cis-[PtMe$_2$(PMePh$_2$)$_2$]	−4649	34
cis-[Pt(AsEt$_3$)$_2$Ph$_2$]	−4584	34
trans-[Pt(AsEt$_3$)$_2$Ph$_2$]	−4475	34
trans-[Pt(Me)I(PMe$_2$Ph)$_2$]	−4963	34
trans-[Pt(Br)Me(PMe$_2$Ph)$_2$]	−4671	34
trans-[Pt(Me)Cl(PMe$_2$Ph)$_2$]	−4484	34
trans-[Pt(Me)I(PMePh$_2$)$_2$]	−4965	34
trans-[PtMe(PMe$_2$Ph)$_2$(SePh)]	−4833	34
cis-[Pt(Me)Cl(PMe$_2$Ph)$_2$]	−4522	34
trans-[Pt(CF$_3$)I(PMe$_2$Ph)$_2$]	−4629	34
trans-[Pt(Me)I(PEt$_3$)$_2$]	−4857	34
trans-[Pt(Me)Cl(PEt$_3$)$_2$]	−4509	34
trans-[Pt(AsMe$_3$)$_2$IMe]	−4859	34
trans-[Pt(AsMe$_3$)$_2$(Br)Me]	−4616	34
trans-[Pt(AsMe$_3$)$_2$(Me)Cl]	−4474	34
trans-[Pt(AsMe$_3$)$_2$(Br)Ph]	−4405	34
trans-[Pt(AsMe$_2$Ph)$_2$(Me)I]	−4929	34
trans-[Pt(AsMe$_2$Ph)$_2$(Br)Me]	−4681	34
trans-[Pt(AsMe$_2$Ph)$_2$(Me)Cl]	−4532	34
[{PtMe$_3$(μ_3-I)}$_4$]	−2769	34
fac-[PtMe$_3$I(tmen)]	−2413	34
fac-[PtMe$_3$I(py)$_2$]	−2515	34
fac-[Pt(AsMe$_2$Ph)$_2$(Br)Me$_3$]	−3815	34
fac-[PtMe$_3$I(PMe$_2$Ph)$_2$]	−4289	34
fac-[PtBrMe$_3$(PMe$_2$Ph)$_2$]	−3989	34
fac-[PtMe$_3$Cl(PMe$_2$Ph)$_2$]	−3831	34
fac-[PtMe$_3$I(PMePh$_2$)$_2$]	−4239	34
fac-[PtMe$_3$I(PMe$_3$)$_2$]	−4353	34
fac-[PtMe$_3$I(dppe)]	−4517	34
[PtBr$_2$Me$_2$(py)$_2$]	−2251	34
[PtMe$_2$I$_2$(py)$_2$]	−3347	34
[PtMe$_2$I$_2$(PMe$_2$Ph)$_2$]	−4387	34
[PtMe$_2$I$_2$(PEt$_3$)$_2$]	−4288	34
[PtBr$_2$Me$_2$(PMe$_2$Ph)$_2$]	−3816	34
[PtMe$_2$Cl$_2$(PMe$_2$Ph)$_2$]	−3515	34
[PtMe$_2$Cl$_2$(PMe$_2$Ph)$_2$]	−3109	34
[PtBr$_3$Me(PMe$_2$Ph)$_2$]	−3732	34
[PtMe$_2$(CF$_3$)I(PMe$_2$Ph)$_2$]	−3997	34
[PtMe$_2$(CF$_3$)I(PMe$_2$Ph)$_2$]	−3919	34
[PtBrMe$_2$(C$_3$H$_5$)(PMe$_2$Ph)$_2$]	−3929	34
[PtMe$_2$(C$_3$H$_5$)Cl(PMe$_2$Ph)$_2$]	−3793	34
[PtBrMe$_2$(CH$_2$Ph)(PMe$_2$Ph)$_2$]	−3894	34
[PtMe$_2$(COMe)Cl(PMe$_2$Ph)$_2$]	−4554	34
[PtBrMe$_2$(COMe)(PMe$_2$Ph)$_2$]	−4676	34

TABLE 21 (*cont.*)

Compound	$\delta(^{195}\text{Pt})$	Ref.
$[\text{Pt}\{(\text{CH}_2)_3\}\text{Cl}_2(4\text{Me-py})_2]$	−1389	34
$[\text{PtBr}_2\{(\text{CH}_2)_3\}(4\text{Me-py})_2]$	−1865	34
$[\text{Pt}\{(\text{CH}_2)_3\}\text{Cl}_2(\text{py})_2]$	−1359	34
$[\text{PtBr}_2(\text{CH}_2)_3(\text{py})_2]$	−1874	34
cis-$[\text{Pt}\{(\text{CH}_2)_4\}(\text{PMe}_2\text{Ph})_2]$	−4677	34
cis-$[\text{Pt}(\text{OC}(\text{CH}_3)=\text{CHCOCH}_2)(\text{PPh}_3)_2]$	−4227	36
cis-$[\text{Pt}(\text{OC}(\text{CH}_3)=\text{CHCOCH}_2)(\text{P}(\textit{p}\text{-ClC}_6\text{H}_4)_3)_2]$	−4230	36
cis-$[\text{Pt}(\text{OC}(\text{CH}_3)=\text{CHCOCH}_2)(\text{AsPh}_3)_2]$	−4214	36
cis-$[\text{PtCl}_2(\text{C}(=\text{CH}_2)\text{CH}_2\text{NEt}_3)(\text{PPr}^n_3)]$	−3891	41
$[\text{PtCl}(\text{C}(=\text{CH}_2)\text{CH}_2\text{NHBu}^t)(\text{PPr}^n_3)]$	−3704	41
$[\text{Pt}_2\text{Cl}_2(\text{C}(=\text{CH}_2)\text{CH}_2\text{NHMe})_2(\text{PPr}^n_3)_2]$	−4113	41
cis,cis,trans-$[\text{PtBr}_2(\text{C}_6\text{F}_5)_2(\text{PEt}_3)_2]$	−3151	37
mer,trans-$[\text{PtCl}_3(\text{C}_6\text{F}_5)(\text{PEt}_3)_2]$	−2369	37
mer,trans-$[\text{PtBr}_3(\text{C}_6\text{F}_5)(\text{PET}_3)_2]$	−3298	37
trans-$[\text{PtCl}(\text{C}_6\text{F}_5)(\text{PEt}_3)_2]$	−4441	37
trans-$[\text{PtBr}(\text{C}_6\text{F}_5)(\text{PEt}_3)_2]$	−4548	37
trans-$[\text{PtI}(\text{C}_6\text{F}_5)(\text{PEt}_3)_2]$	−4843	37
$(\text{NBu}_4)_2[\text{Pt}(\text{CN})_4]$	−4707	170
$\text{K}_2[\text{Pt}(\text{CN})_4]$	−4746	170
$(\text{NBu}_4)_2[\text{PtCl}_2(\text{CN})_4]$	−2481	170
$\text{K}_2[\text{PtCl}_2(\text{CN})_4]$	−2624	170
$(\text{NBu}_4)_2[\text{PtBr}_2(\text{CN})_4]$	−3349	170
$\text{K}_2[\text{PtBr}_2(\text{CN})_4]$	−3598	170
$(\text{NBu}_4)_2[\text{PtBrCl}(\text{CN})_4]$	−2944	170
$(\text{NBu}_4)_2[\text{PtI}_2(\text{CN})_4]$	−4714	170
$\text{K}_2[\text{PtI}_2(\text{CN})_4]$	−4790	170
$\text{K}_2[\text{PtCl}(\text{CN})_5]$	−3294	170
$(\text{NBu}_4)_2[\text{PtI}(\text{CN})_5]$	−4033	170
$\text{Na}_2[\text{PtI}(\text{CN})_5]$	−4214	170
$(\text{NBu}_4)_2[\text{Pt}(\text{CN})_6]$	−3321	170
$\text{K}_2[\text{Pt}(\text{CN})_6]$	−3866	170
$[\text{PtCl}_2(\text{CO})(\text{PMe}_3)]$	−4164	59
$[\text{PtBr}_2(\text{CO})(\text{PMe}_3)]$	−4404	59
$[\text{PtI}_2(\text{CO})(\text{PMe}_3)]$	−4928	59
$[\text{PtClBr}(\text{CO})(\text{PMe}_3)]$ Cl *trans* to CO	−4295	59
Br *trans* to CO	−4255	59
$[\text{PtClI}(\text{CO})(\text{PMe}_3)]$	−4513	59
$[\text{PtBrI}(\text{CO})(\text{PMe}_3)]$	−4655	59
$[\text{PtCl}(\text{CO})(\text{PMe}_3)_2]\text{BF}_4$	−4471	59
$[\text{PtBr}(\text{CO})(\text{PMe}_3)_2]\text{BF}_4$	−4594	59
$(\text{NPr}^n_4)[\text{PtCl}_2\text{R}(\text{CO})]$		
R = Me	−3869	171
Et	−3876	171
Pr^n	−3881	171
Pr^i	−3806	171
Bu^n	−3880	171
Ph	−3655	171

TABLE 21 (*cont.*)

Compound		$\delta(^{195}Pt)$	Ref.
$[PtCl_2(CO)(PEt_3)]$	*cis*	−4207	56
	trans	−3840	
$[PtClPh(CO)(PEt_3)]$	P *cis* to CO	−4345	56
	P *trans* to CO	−4168	
$[PtClPh(CO)(PMePh_2)]$	P *trans* to Cl	−4288	56
	P *trans* to CO	−4201	
	P *trans* to Ph	−4067	
$[Pt(OC_6H_4CO)L_2]$			
L = PBu^n_3		−4304	172
$P(p\text{-}CH_3C_6H_4)_3$		−4316	172
$P(OEt)_3$		−4380	172
$P(OPr^i)_3$		−4390	172

TABLE 22

^{195}Pt chemical shifts of some complexes with Si, Ge and Sn ligands.

Compound	$\delta(^{195}Pt)$	Ref.
trans-[PtCl(SiH$_3$)(PEt$_3$)$_2$]	−5067	26
trans-[PtCl(SiH$_2$F)(PEt$_3$)$_2$]	−4935	26
trans-[PtCl(SiH$_2$Cl)(PEt$_3$)$_2$]	−4992	26
trans-[PtCl(SiHCl$_2$)(Pet$_3$)$_2$]	−4853	26
trans-[PtCl(SiH$_2$CCH)(PEt$_3$)$_2$]	−5049	26
trans-[PtCl(SiH$_2$CCCF$_3$)(PEt$_3$)$_2$]	−5035	26
trans-[PtBr(SiH$_2$Br)(PEt$_3$)$_2$]	−5061	26
trans-[PtBr(SiHBr$_2$)(PEt$_3$)$_2$]	−4902	26
trans-[PtI(SiH$_3$)(PEt$_3$)$_2$]	−5270	26
trans-[PtI(SiH$_2$Cl)(PEt$_3$)$_2$]	−5198	26
trans-[PtI(SiH$_2$I)(PEt$_3$)$_2$]	−5164	26
trans-[PtI(SiH$_2$)(PEt$_3$)$_2$]$_2$S	−5181	26
trans-[PtI(SiH$_2$)(PEt$_3$)$_2$]$_2$Se	−5168	26
trans-[PtI(SiH$_2$SeSiH$_3$)(PEt$_3$)$_2$]	−5178	26
trans-[PtI(SiHICCH)(PEt$_3$)$_2$]	−5110	26
trans-[PtCl(GeH$_2$Cl)(PEt$_3$)$_2$]	−4904	26
trans-[PtI(GeH$_3$)(PEt$_3$)$_2$]	−5317	26
trans-[PtI(SiH$_2$NHSiH$_3$)(PEt$_3$)$_2$]	−5262	173
trans-[PtI(SiH$_2$)]$_2$NH	−5250	173
trans-[PtI(SiH$_2$NSiH$_3$)$_2$(PEt$_3$)$_2$]	−5240	173
trans-[PtI(SiH$_2$P(SiH$_3$)$_2$)(PEt$_3$)$_2$]	−5177	173
trans-[PtCl(SnCl$_3$)(PEt$_3$)$_2$]	−4780	174
trans-[Pt(SnCl$_3$)$_3$(PEt$_3$)$_2$]$^-$	−5152	174
trans-[Pt(SnCl$_3$)$_3$(P(OEt)$_3$)$_2$]$^-$	−5234	174
trans-[Pt(C$_6$H$_5$)(SnCl$_3$)(PEt$_3$)$_2$]	−4799	174
trans-[PtH(SnCl$_3$)(PEt$_3$)$_2$]	−5302	175
trans-[PtH(SnCl$_3$)(PPh$_2$CH$_2$Ph)$_2$]	−5322	175
trans-[PtH(SnCl$_3$)(PPh$_3$)$_2$]	−5195	175
trans-[Pt(C(CO$_2$Et)=CHCO$_2$Et)(SnCl$_3$)(PPh$_3$)$_2$]	−4771	175
trans-[PtCl(SnCl$_3$)(P(*p*-ClC$_6$H$_4$)$_3$)$_2$]	−4812	176
cis-[PtCl(SnCl$_3$)(P(*p*-CH$_3$OC$_6$H$_4$)$_3$)$_2$]	−4742	176
cis-[PtCl(SnCl$_3$)(P(*p*-CH$_3$C$_6$H$_4$)$_3$)$_2$]	−4718	177
trans-[PtCl(SnCl$_3$)(AsEt$_3$)$_2$]	−4857	177
cis-[PtCl(SnCl$_3$(As(*p*-CH$_3$C$_6$H$_4$)$_3$)$_2$]	−4785	177
trans-[PtCl(SnCl$_3$)(As(*p*-CH$_3$C$_6$H$_4$)$_3$)$_2$]	−4835	177
trans-PtCl(SnCl$_3$)(PEt$_3$)$_2$	−4779	177
trans-PtCl(SnCl$_3$)(Ptr$^n_3$)$_2$	−4746	177
cis-PtCl(SnCl$_3$)(P(OPr^i)$_3$)$_2$	−4551	178
trans-Pt(SnCl$_3$)$_2$(PR$_3$)$_2$		
R = OEt	−5132	178
OPr^i	−5136	178
Et	−5082	177
Pr^n	−5061	177
Pt(SnCl$_3$)$_3$L$_2$$^-$		
L = PPr$^n_3$	−5120	177

TABLE 22 (*cont.*)

Compound	$\delta(^{195}\text{Pt})$	Ref.
L = AsEt$_3$	−5400	177
AsMe$_3$	−5363	177
P(OMe)$_3$	−5390	178
P(OPh)$_3$	−5629	178
Pt(SnCl$_3$)$_4$(PEt$_3$)$^{2-}$	−5633	178
cis-PtCl$_2$(SnCl$_3$)L$^-$		178
L = PEt$_3$	−4359	
PTol$_3$	−4329	
P(OEt)$_3$	−4310	
P(OPh)$_3$	−4311	
AsEt$_3$	−4275	
AsPh$_3$	−4284	
trans-PtCl(SnCl$_3$)$_2$L$^-$		178
L = PEt$_3$	−4728	
PTol$_3$	−4617	
AsEt$_3$	−4857	
cis-PtCl(SnCl$_3$)$_2$(AsEt$_3$)$^-$	−4738	178
PtCl$_3$(SnCl$_3$)$^{2-}$	−2748	179
cis-PtCl$_2$(SnCl$_3$)$_2$$^{2-}$	$\begin{cases}-4202 \\ -6415\end{cases}$	179 180
PtCl(SnCl$_3$)$_3$$^{2-}$	−4829	179
Pt(SnCl$_3$)$_4$$^{2-}$	−5615	179
Pt(SnCl$_3$)$_5$$^{3-}$	$\begin{cases}-5894 \\ -4701\end{cases}$	179 181
PtH(SnCl$_3$)$_4$$^{3-}$	−5824	179
PtH(SnCl$_3$)$_2$(PEt$_3$)$_2$$^-$	−5396	179
[Pt(μ-Cl)$_n$(SnCl$_3$)$_{2-n}$L]		179
$n = 2$ L = PEt$_3$	−3409	
1 PEt$_3$	−3419, −4270 ^2J(Pt–Pt) = 238 Hz	
0 PEt$_3$	−4320	
2 PTol$_3$	−3353	
1 PTol$_3$	−3293, −4157	
0 PTol$_3$	−4178	
2 AsEt$_3$	−3069	
1 AsEt$_3$	−3045, −4170	
0 AsEt$_3$	−4231	
trans-PtCl$_{2-n}$(SnCl$_3$)$_n$(1-R-3,4-dimethylphosphole)^a		182
R = CH$_3$ n = 1	−4940	
CH$_3$ 2	−5442	
Bu^n 2	−5463	
Bu^t 1	−5006	
Bu^t 1 *cis* isomer	−4885	
Bu^t 2	−5470	
Ph 1	−4775	
Ph 2	−5436	
Bz 1	−5312	

TABLE 22 (*cont.*)

Compound	$\delta(^{195}\text{Pt})$	Ref.
R = Bz 2	−5480	
$\text{Pt}_2(\text{SnCl}_3)_2(\mu\text{-Ph}_2\text{PCH}_2\text{PPh}_2)_2$	−4990	183
$\text{Pt}_2\text{Cl}(\text{SnCl}_3)(\mu\text{-Ph}_2\text{PCH}_2\text{PPh}_2)_2$	−5387	183
	−4343	
$\text{Pt}_2(\text{SnCl}_3)_2(\mu\text{-CH}_2)(\mu\text{-Ph}_2\text{PCH}_2\text{PPh}_2)_2$	−4901	183
$\text{Pt}_2(\text{SnCl}_3)_2(\mu\text{-S})(\mu\text{-Ph}_2\text{PCH}_2\text{PPh}_2)_2$	−4958	183
$\text{Pt}_2(\mu\text{-SnCl}_2)\text{Cl}_4(\text{CO})_2$	−4165	184
trans-$\text{PtR}(\text{SnCl}_3)(\text{PEt}_3)_2$		185
R = CH_3	−5003	
CH_2Ph	−4945	
COC_6H_5	−4532	
$\text{C}_6\text{H}_4\text{-}p\text{-NO}_2$	−4800	
$\text{C}_6\text{H}_4\text{-}p\text{-CF}_3$	−4832	
$\text{C}_6\text{H}_4\text{-}p\text{-Br}$	−4844	
$\text{C}_6\text{H}_4\text{-}p\text{-H}$	−4857	
$\text{C}_6\text{H}_4\text{-}p\text{-OCH}_3$	−4862	
$\text{C}_6\text{H}_4\text{-}p\text{-CH}_3$	−4864	
$\text{C}_6\text{H}_4\text{-}m\text{-NO}_2$	−4829	
$\text{C}_6\text{H}_4\text{-}m\text{-CF}_3$	−4844	
$\text{C}_6\text{H}_4\text{-}m\text{-Br}$	−4851	
$\text{C}_6\text{H}_4\text{-}m\text{-OCH}_3$	−4856	
$\text{C}_6\text{H}_4\text{-}m\text{-CH}_3$	−4868	
cis-$\text{Pt}(Z)\text{Ph}(\text{PPh}_3)_2$		186
Z = SnPh_3	−4808	
SnPh_2Cl	−4780	
SnPhCl_2	−4786	
SnPh_2Br	−4785	
SnPhBr_2	−4788	
SnPh_2I	−4797	
SnPh_2NCS	−4796	
$\text{SnPh}_2(\text{SPh})$	−4784	
$\text{SnPh}_2(\text{SCH}_2\text{Ph})$	−4799	
cis-$\text{PtCl}(Z)(\text{PPh}_3)_2$		186
Z = SnMe_2Cl	−4715	
SnBu_2Cl	−4750	
SnBu^t_2Cl	−4615	
SnMeCl_2	−4722	
SnBu^nCl_2	−4699	
SnPhCl_2	−4704	
cis-$\text{PtBr}(Z)(\text{PPh}_3)_2$		186
Z = SnMe_2Br	−4963	
SnBu^n_2Br	−4929	
SnMeBr_2	−4928	
SnBu^nBr_2	−4880	
SnPhBr_2	−4788	
trans-$\text{PtCl}(Z)(\text{PPh}_3)_2$		186
Z = SnMe_2Cl	−4837	

TABLE 22 (*cont.*)

Compound	$\delta(^{195}\text{Pt})$	Ref.
Z = SnBu$^n_2$Cl	−4907	
SnMeCl$_2$	−4790	
SnBu^{n}Cl$_2$	−4779	
SnPhCl$_2$	−4827	
trans-PtBr(Z)(PPh$_3$)$_2$		186
Z = SnMe$_2$Br	−5040	
SnBu$^n_2$Br	−5035	
SnMeBr$_2$	−4963	
SnBu^{n}Br$_2$	−4913	
SnPhBr$_2$	−4977	

^{a} Relative to H$_2$PtCl$_6$.

TABLE 23

^{195}Pt data for some miscellaneous complexes.

Complex		$\delta(^{195}\text{Pt})$		Ref.
trans-PtX$_2$(n-pentylpyridine)$_2$				188
X = Cl		−1961		
Br		−2109		
I		−3127		
cis-PtCl$_2$(SMe$_2$)$_2$^{a}		−3551		189
trans-PtX$_2$(SMe$_2$)$_2$				189
X = Cl		−3419		
Br		−3898		
I		−5152		
cis-PtCl$_2$(SeMe$_2$)$_2$		−3749		189
trans-PtCl$_2$(SeMe$_2$)$_2$		−3501		189
trans-PtBr$_2$(SeMe$_2$)$_2$		−4035		189
PtXMe$_3$(MeSeCH=CHSeMe)				31

	meso-1	DL	*meso*-2
X = Cl	−3221	−3405	−3256
Br	−3329	−3547	−3429
I	−3532	−3803	−3726

Complex		$\delta(^{195}\text{Pt})$	Ref.
Pt{η^2-(SR)(SnPh$_3$)C=S}(PPh$_3$)$_2$			190
R = CH$_3$		−4976	
C$_3$H$_5$		−4964	
CH$_2$Ph		−4961	
Pt{η^2-(SR^1)(P(S)R$^2_2$)C=S}(PPh$_3$)$_2$			191
R^1 = Me R^2 = Ph		−4999	
CH$_2$Ph Ph		−4993	
Me cy		−4944	
CH$_2$ cy		−4922	

^{a} Taken as −3551 (see Table 17).

REFERENCES

1. B. Harrison, B. J. Cooper and A. J. J. Wilkins, *Platinum Metals Reviews*, 1981, **25**, 14.
2. C. Consiglio, P. Pino, L. I. Flowers and C. H. Pittman, *J. Chem. Soc., Chem. Comm.*, 1983, 612; J. C. Bailar, in *Inorganic Compounds with Unusual Properties* (R. B. King, ed.), American Chemical Society, 1979, p. 1.
3. B. Rosenberg and L. Van Camp, *Cancer Res.*, 1970, **30**, 1799; S. J. Lippard, *Science*, 1982, **218**, 1075.
4. R. Benn, R. D. Reinhardt and A. Rufinski, *J. Organometal. Chem.*, 1985, **282**, 291.
5. R. Benn, H. M. Büch and R. D. Reinhardt, *Magn. Reson. Chem.*, 1985, **23**, 559.
6. K. Lystback and H. Bildsoe, *Magnetic Resonance in Chemistry*, 1985, **23**, 263.
7. J. J. Dechter and J. Kowalewski, *J. Magn. Reson.*, 1984, **59**, 146.
8. J. Y. Lallemand, J. Soulié and J. C. Chottard, *J. Chem. Soc., Chem. Comm.*, 1980, 436.
9. J. J. Pesek and W. R. Mason, *J. Magn. Reson.*, 1977, **25**, 519.
10. W. Freeman, P. S. Pregosin, S. N. Sze and L. M. Venanzi, *J. Magn. Reson.*, 1976, **22**, 473.
11. D. M. Doddrell, P. F. Barron, D. E. Clegg and C. Bowie, *J. Chem. Soc., Chem. Comm.*, 1982, 576.
12. H. J. Keller and H. H. Rupp, *Z. Naturforsch.*, 1971, **26a**, 785; H. H. Rupp, *ibid.*, p. 1937.
13. P. S. Pregosin, *Coord. Chem. Rev.*, 1982, **44**, 247.
14. O. Gröning, T. Drakenberg and L. I. Elding, *Inorg. Chem.*, 1982, **21**, 1820.
15. (a) K. H. Dahmen and L. M. Venanzi, unpublished results, ETH Zürich, 1985. (b) S. Carr, R. Colton and D. Dakternieks, *J. Magn. Reson.*, 1982, **47**, 156. (c) A. Sebald, B. Wrackmeyer, C. R. Theocharis and W. Jones, *J. Chem. Soc., Dalton Trans.*, 1984, 747.
16. H. Moriyama and P. S. Pregosin, unpublished results, ETH Zürich, 1984.
17. C. Anklin and P. S. Pregosin, *Magnetic Resonance in Chemistry*, 1985, **23**, 671.
18. H. Motschi, S. N. Sze and P. S. Pregosin, *Helv. Chim. Acta*, 1979, **62**, 2068.
19. I. M. Ismail, S. J. S. Kerrison and P. J. Sadler, *Polyhedron*, 1982, **1**, 57.
20. S. J. S. Kerrison and P. J. Sadler, *J. Magn. Reson.*, 1978, **31**, 321.
21. I. M. Ismail, S. J. S. Kerrison and P. J. Sadler, *J. Chem. Soc., Chem. Comm.*, 1980, 1175.
22. (a) R. G. Kidd and R. J. Goodfellow, in *NMR and the Periodic Table* (R. K. Harris and B. E. Mann, eds), Academic Press, London, 1978, and references therein. (b) R. J. Goodfellow, in *Multinuclear NMR* (J. Mason, ed.), Plenum Press.
23. P. L. Goggin, R. J. Goodfellow, S. R. Haddock, B. F. Taylor and I. R. H. Marshall, *J. Chem. Soc., Dalton Trans.*, 1976, 459.
24. Y. Koie, S. Shinoda and Y. Saito, *J. Chem. Soc., Dalton Trans.*, 1982, 1082.
25. W. Juranic, *J. Chem. Soc., Dalton Trans.*, 1984, 1537.
26. D. W. Anderson, E. A. V. Ebsworth and D. W. H. Rankin, *J. Chem. Soc., Dalton Trans.*, 1973, 2370.
27. N. M. Boag, P. L. Groggin, R. J. Goodfellow and I. R. Herbert, *J. Chem. Soc., Dalton Trans.*, 1983, 1101.
28. I. Georgii, B. E. Mann, B. F. Taylor and A. Musco, *Inorg. Chim. Acta*, 1984, **86**, L81.
29. P. S. Pregosin, M. Kretschmer, W. Preetz and G. Rimkus, *Z. Naturforsch.*, 1982, **37b**, 1422.
30. C. Carr, P. L. Goggin and R. J. Goodfellow, *Inorg. Chim. Acta*, 1984, **81**, L25.
31. E. W. Abel, S. Bhorgava, K. G. Orrell, A. W. G. Platt, V. Sik and S. Cameron, *J. Chem. Soc., Dalton Trans.*, 1985, 345.
32. A. R. Middleton, G. Wilkinson, M. B. Hursthouse and N. P. Walker, *J. Chem. Soc., Dalton Trans.*, 1982, 663.
33. H. Suitkamp, D. J. Stufkens and K. Vrieze, *J. Organometal. Chem.*, 1979, **169**, 107.
34. J. D. Kennedy, W. McFarlane, R. J. Puddephatt and P. J. Thompson, *J. Chem. Soc., Dalton Trans.*, 1976, 874.
35. O. J. Scherer and J. Jungmann, *J. Organometal. Chem.*, 1981, **208**, 153.

36. S. Okeya, Y. Nakamura, S. Kawaguchi and T. Hinomoto, *Inorg. Chem.*, 1981, **20**, 1576.
37. C. Crocker, R. J. Goodfellow, J. Cimino and R. Uson, *J. Chem. Soc., Dalton Trans.*, 1977, 1448.
38. M. D. Waddington and P. W. Jennings, *Organometallics*, 1982, **1**, 385.
39. J. R. Briggs, C. Crocker, W. S. McDonald and B. L. Shaw, *J. Chem. Soc., Dalton Trans.*, 1981, 121; *ibid.*, 1982, 457.
40. L. Chessot, E. Müller and A. von Zelewsky, *Inorg. Chem.*, 1984, **23**, 4249.
41. J. R. Briggs, C. Crocker, W. S. McDonald and B. L. Shaw, *J. Chem. Soc., Dalton Trans.*, 1981, 575.
42. P. G. Pringle and B. L. Shaw, *J. Chem. Soc., Dalton Trans.*, 1984, 849.
43. C. R. Langrick, P. G. Pringle and B. L. Shaw, *J. Chem. Soc., Dalton Trans.*, 1984, 1233.
44. S. Cenini, F. Porta, M. Pizzotti and C. Crotti, *J. Chem. Soc., Dalton Trans.*, 1985, 163.
45. D. W. Bruce, R. F. Jones and D. J. Cole-Hamilton, *J. Chem. Soc., Dalton Trans.*, 1984, 2249.
46. J. J. MacDougall, J. H. Nelson and F. Mathey, *Inorg. Chem.*, 1982, **21**, 2145.
47. W. R. Meyer and L. M. Venanzi, *Angew. Chem. Int. Ed. Engl.*, 1984, **23**, 529.
48. Y. T. Fanchiang, J. J. Pignatello and J. M. Wood, *Organometallics*, 1983, **2**, 1748.
49. F. G. Riddell, R. D. Gillard and F. L. Wimmer, *J. Chem. Soc., Chem. Comm.*, 1982, 332.
50. W. McFarlane, *J. Chem. Soc. (A)*, 1967, 1922.
51. J. D. Kennedy, W. McFarlane and R. J. Puddephatt, *J. Chem. Soc., Dalton Trans.*, 1976, 745.
52. J. D. Kennedy, I. J. Colquhoun, W. McFarlane and R. J. Puddephatt, *J. Organometal. Chem.*, 1979, **197**, 479.
53. P. L. Goggin, R. J. Goodfellow, J. R. Knight, M. G. Norton and B. F. Taylor, *J. Chem. Soc., Dalton Trans.*, 1973, 2220.
54. C. Crocker, P. L. Goggin and R. J. Goodfellow, *J. Chem. Soc., Dalton Trans.*, 1976, 2494.
55. E. A. V. Ebsworth, J. M. Edward, F. J. S. Reed and J. D. Whitelock, *J. Chem. Soc., Dalton Trans.*, 1978, 1161.
56. G. K. Anderson, R. J. Cross and D. S. Rycroft, *J. Chem. Res. (S)*, 1980, 240.
57. S. J. Anderson, P. L. Goggin and R. J. Goodfellow, *J. Chem. Soc., Dalton Trans.*, 1976, 1959.
58. I. M. Blacklaws, E. A. V. Ebsworth, D. W. H. Rankin and H. E. Robertson, *J. Chem. Soc., Dalton Trans.*, 1978, 753.
59. J. Browning, P. L. Goggin, R. J. Goodfellow, M. G. Norton, A. J. M. Rattray, B. F. Taylor and J. Mink, *J. Chem. Soc., Dalton Trans.*, 1977, 2061.
60. N. M. Boag, J. Browning, C. Crocker, P. L. Goggin, R. J. Goodfellow, M. Murray and J. L. Spencer, *J. Chem. Res. (S)*, 1978, 228.
61. P. L. Goggin, R. J. Goodfellow, S. R. Haddock, J. R. Knight, F. J. S. Reed and B. F. Taylor, *J. Chem. Soc.*, 1974, 523.
62. C. Crocker, P. L. Goggin and R. J. Goodfellow, *J. Chem. Soc., Chem. Comm.*, 1978, 1056.
63. P. S. Pregosin, H. Omura and L. M. Venanzi, *J. Am. Chem. Soc.*, 1973, **95**, 2047.
64. J. P. Jesson, in *Transition Metal Hydrides* (E. L. Muetterties, ed.), Marcel Dekker, New York, 1971, p. 100.
65. T. G. Appleton, H. C. Clark and L. E. Manzer, *Coord. Chem. Rev.*, 1973, **10**, 335.
66. H. C. Clark, J. E. H. Ward and K. Yasufuku, *Can. J. Chem.*, 1975, **53**, 186; M. Chisholm, H. C. Clark, J. E. H. Ward and K. Yasufuku, *Inorg. Chem.*, 1975, **14**, 894, and references therein.
67. P. S. Pregosin and R. W. Kunz, ^{31}P and ^{13}C NMR of transition metal phosphine complexes, in *NMR Basic Principles and Progress*, Springer Verlag, Heidelberg, Vol. 16, 1979.
68. J. D. Kennedy and B. Wrackmeyer, *J. Magn. Reson.*, 1980, **38**, 529, and references therein.
69. E. W. Abel, K. G. Orrell and A. W. G. Platt, *J. Chem. Soc., Dalton Trans.*, 1983, 2345.
70. W. H. Pan and J. P. Fackler, *J. Am. Chem. Soc.*, 1978, **100**, 5783.
71. H. J. Gysling, N. Zimbulyadis and J. A. Robertson, *J. Organometal. Chem.*, 1981, **209**, C41.

72. P. L. Goggin, R. J. Goodfellow and S. R. Haddoch, *J. Chem. Soc., Chem. Comm.*, 1975, 176.
73. A. F. M. J. van der Ploeg, G. van Koten and C. Brevard, *Inorg. Chem.*, 1982, **21**, 2878.
74. D. E. Berry, G. W. Bushnell, K. R. Dixon and A. Pidcock, *Inorg. Chem.*, 1983, **22**, 1961.
75. T. A. Ban der Knoup, F. Bickelhaupt, J. G. Kraaykamp, G. van Koten, J. P. C. Bernards, H. T. Edyes, W. S. Veeman, E. de Boer and E. J. Baerends, *Organometallics*, 1984, **3**, 1804.
76. P. S. Pregosin, H. Streit and L. M. Venanzi, *Inorg. Chim. Acta*, 1980, **38**, 237.
77. S. J. Anderson, P. L. Goggin and R. J. Goodfellow, *J. Chem. Soc., Dalton Trans.*, 1976, 1959.
78. S. J. Anderson and R. J. Goodfellow, *J. Chem. Soc., Dalton Trans.*, 1977, 1683.
79. P. S. Pregosin, in ^{31}P *NMR Spectroscopy* (J. Verkade and L. Quin, eds), Verlag Chemie Int., 1986.
80. B. E. Mann and B. F. Taylor, ^{13}C *NMR Data for Organometallic Compounds*, Academic Press, London, 1981.
81. Cited in ref. 13, p. 266.
82. F. E. Wood and A. L. Balch, *Inorg. Chim. Acta*, 1983, **76**, L63.
83. S. J. S. Kerrison and P. J. Sadler, *J. Chem. Soc., Dalton Trans.*, 1982, 2363.
84. H. Motschi, P. S. Pregosin and L. M. Venanzi, *Helv. Chim. Acta*, 1979, **62**, 667.
85. H. Motschi and P. S. Pregosin, *Inorg. Chim. Acta*, 1980, **40**, 141.
86. S. J. S. Kerrison and P. J. Sadler, *J. Chem. Soc., Chem. Comm.*, 1977, 861.
87. M. Chikuma and R. J. Pollock, *J. Magn. Reson.*, 1982, **47**, 324.
88. I. M. Ismail and P. J. Sadler, in *Metal Chemotherapeutic Agents* (S. J. Lippard, ed.), ACS Symposium Series No. 209, American Chemical Society, 1983, p. 171.
89. T. G. Appleton, J. R. Hall and S. F. Ralph, *Inorg. Chem.*, 1985, **24**, 673.
90. T. G. Appleton, R. D. Berry, C. A. Davis, J. R. Hall and H. A. Kimlin, *Inorg. Chem.*, 1984, **23**, (a) 3514, (b) 3521.
91. M. Alec, P. J. Vergamini and W. E. Wageman, *J. Am. Chem. Soc.*, 1979, **101**, 5415.
92. R. Kuroda, S. Neidle, I. M. Ismail and P. J. Sadler, *J. Chem. Soc., Dalton Trans.*, 1983, 823.
93. B. Rosenberg, *Biochemie*, 1978, **60**, 859.
94. D. S. Gill and B. Rosenberg, *J. Am. Chem. Soc.*, 1982, **104**, 4398.
95. L. S. Hollis and S. J. Lippard, *J. Am. Chem. Soc.*, 1983, **105**, 3494.
96. M. Chikuma, K. C. Ott, R. J. Pollack, O. A. Gansow and B. Rosenberg, unpublished results.
97. M. Green, J. K. K. Sarhan, I. D. Ross, I. M. Ismail and P. J. Sadler, unpublished results.
98. A. Albinati, H. Moriyama, H. Rüegger, P. S. Pregosin and A. Togni, *Inorg. Chem.*, 1985,
99. I. M. Al-Najjar, S. S. Al-Showiman and H. M. Al-Hazimi, *Inorg. Chim. Acta*, 1984, **89**, 57.
100. H. van der Poel, G. van Koten, D. M. Grove, P. S. Pregosin and K. H. A. Ostoja Starzewski, *Helv. Chim. Acta*, 1981, **64**, 1174.
101. L. M. Venanzi, *Chem. in Britain*, 1968, **4**, 162.
102. H. Motschi, C. Nussbaumer, P. S. Pregosin, F. Bachechi, P. Mura and L. Zambonelli, *Helv. Chim. Acta*, 1980, **63**, 2071.
103. P. B. Hitchcock, B. Jacobson and A. Pidcock, *J. Chem. Soc., Dalton Trans.*, 1977, 2043, 2038; G. W. Bushnell, A. Pidcock and M. A. R. Smith, *ibid.*, 1975, 572; F. F. Mather, A. Pidcock and G. J. N. Rapsey, *ibid.*, 1973, 2095.
104. A. A. Kiffen, C. Masters and J. P. Visser, *J. Chem. Soc., Dalton Trans.*, 1975, 1311; R. Huis and C. Masters, *ibid.*, 1976, 1796.
105. J. Soulié, J. Y. Lallemand and R. C. Rao, *Org. Magn. Reson.*, 1979, **12**, 67.
106. C. E. Briant, C. J. Gardner, T. S. A. Hor, N. D. Howells and D. M. P. Mingos, *J. Chem. Soc., Dalton Trans.*, 1984, 2645.

107. D. P. Arnold, M. A. Bennett, G. M. McLaughlin and G. B. Robertson, *J. Chem. Soc., Chem. Comm.*, 1983, 34.

108. R. Glaser, D. J. Kountz, R. D. Waid, J. C. Gallucci and D. W. Meek, *J. Am. Chem. Soc.*, 1984, **106**, 6324.

109. M. P. Brown, S. J. Cooper, A. A. Frew, L. M. Muir, K. W. Muir, R. J. Puddephatt and M. A. Thomson, *J. Chem. Soc., Dalton Trans.*, 1982, 299.

110. (a) R. S. Paonessa and W. C. Trogler, *Inorg. Chem.*, 1983, **22**, 1038. (b) T. H. Tulip, Y. Yamagota, T. Yoshida, R. D. Wilson, J. A. Ibers and S. Otsuka, *Inorg. Chem.*, 1979, **18**, 2239.

111. G. Bracher, D. M. Grove, L. M. Venanzi, F. Bachechi, P. Mura and L. Zambonelli, *Angew. Chem. Int. Ed. Engl.*, 1978, **17**, 778.

112. G. Bracher, D. M. Grove, P. S. Pregosin and L. M. Venanzi, *Angew. Chem. Int. Ed. Engl.*, 1979, **18**, 155.

113. F. Bachechi, G. Bracher, D. M. Grove, B. Kellenberger, P. S. Pregosin and L. M. Venanzi, *Inorg. Chem.*, 1983, **22**, 1031.

114. D. Carmona, R. Thouvenot, L. M. Venanzi, F. Bachechi and L. Zambonelli, *J. Organometal. Chem.*, 1983, **250**, 589.

115. M. Ciriano, M. Green, J. A. K. Howard, J. Proud, J. L. Spencer, F. G. A. Stone and C. A. Tsipsis, *J. Chem. Soc., Dalton Trans.*, 1978, 801.

116. M. Anburn, M. Ciriano, J. A. K. Howard, M. Murray, N. H. Pugh, J. L. Spencer, F. G. A. Stone and P. Woodward, *J. Chem. Soc., Dalton Trans.*, 1980, 659.

117. R. Naegeli, A. Togni and L. M. Venanzi, *Organometallics*, 1983, **2**, 926.

118. P. Boron, A. Musco and L. M. Venanzi, *Inorg. Chem.*, 1982, **21**, 4192.

119. N. M. Boag, P. L. Goggin, R. J. Goodfellow and I. R. Herbert, *J. Chem. Soc., Dalton Trans.*, 1983, 1101.

120. I. R. Herbert, Ph.D. dissertation, University of Bristol, 1984.

121. M. C. Grossel, R. P. Moulding and K. R. Seddon, *J. Organometal. Chem.*, 1983, **247**, C32.

122. M. P. Brown, J. R. Fisher, R. J. Puddephatt and K. R. Seddon, *Inorg. Chem.*, 1979, **18**, 2808.

123. J. P. Farr, F. E. Wood and A. L. Balch, *Inorg. Chem.*, 1983, **22**, 3387.

124. B. Messbauer, H. Meyer, B. Walther, M. J. Heeg, A. F. M. Maqsudur Rohman and J. P. Oliver, *Inorg. Chem.*, 1983, **22**, 272.

125. G. W. Bushnell, D. T. Eadic, A. Pidcock, A. R. Sam, R. D. Holmes-Smith and S. R. Stobart, *J. Am. Chem. Soc.*, 1982, **104**, 5837.

126. C. Che, W. P. Schaefer, H. B. Gray, M. L. Dickson, P. B. Stein and D. M. Roundhill, *J. Am. Chem. Soc.*, 1982, **104**, 4253.

127. T. G. Appleton, J. R. Hall, D. W. N. Neate and S. F. Ralph, *Inorg. Chim. Acta*, 1983, **77**, L149.

128. D. M. Grove and K. Vrieze, unpublished results.

129. (a) N. M. Boag, R. J. Goodfellow, M. Green, B. Hessner, J. A. K. Howard and F. G. A. Stone, *J. Chem. Soc., Dalton Trans.*, 1983, 2585. (b) W. E. Carroll, M. Green, J. A. K. Howard, M. Pfeffer and F. G. A. Stone, *J. Chem. Soc., Dalton Trans.*, 1978, 1472.

130. (a) D. P. Arnold, M. A. Bennett, G. M. McLaughlin, G. B. Robertson and M. J. Whittaker, *J. Chem. Soc., Chem. Comm.*, 1983, 32. (b) M. P. Brown, S. J. Cooper, A. Frew, L. M. Muir, K. W. Muir, R. J. Puddephatt, K. R. Seddon and M. A. Thomson, *Inorg. Chem.*, 1981, **20**, 1500.

131. C. Brown, B. T. Heaton, A. D. C. Towl, P. Chini, A. Fumagalli and G. Longoni, *J. Organometal. Chem.*, 1979, **181**, 233.

132. A. Moor, P. S. Pregosin and L. M. Venanzi, *Inorg. Chim. Acta*, 1981, **48**, 153.

133. A. Moor, P. S. Pregosin and L. M. Venanzi, *Inorg. Chim. Acta*, 1982, **61**, 135.

134. A. Moor, P. S. Pregosin, L. M. Venanzi and A. J. Welch, *Inorg. Chim. Acta*, 1984, **85**, 103.

135. L. J. Farrugia, J. A. K. Howard, P. Mitroprachachon, F. G. A. Stone and P. Woodward, *J. Chem. Soc., Dalton Trans.*, 1981, 1274.

136. M. C. Grossel, R. P. Moulding and K. R. Seddon, *J. Organometal. Chem.*, 1983, **253**, C50.

137. L. F. Farrugia, J. A. K. Howard, P. Mitrprachachon, F. G. A. Stone and P. Woodward, *J. Chem. Soc., Dalton Trans.*, 1981, 162.

138. J. C. Jeffery, J. C. V. Laurie, I. Moore, H. Rayay and F. G. A. Stone, *J. Chem. Soc., Dalton Trans.*, 1984, 1563; J. C. Jeffery, I. Moor and F. G. A. Stone, *ibid.*, p. 1571; J. C. Jeffery, I. Moore, H. Tayay and F. G. A. Stone, *Ibid.*, p. 1581.

139. K. A. Mead, I. Moore, F. G. A. Stone and P. Woodward, *J. Chem. Soc., Dalton Trans.*, 1983, 2083.

140. M. R. Awang, J. C. Jeffery and F. G. A. Stone, *J. Chem. Soc., Dalton Trans.*, 1983, 2091.

141. R. D. Barr, M. Green, J. A. K. Howard, T. B. Marder, I. Moore and F. G. A. Stone, *J. Chem. Soc., Chem. Comm.*, 1983, 746.

142. N. M. Boag, M. Green, J. A. K. Howard, F. G. A. Stone and H. Wadepohl, *J. Chem. Soc., Dalton Trans.*, 1981, 862.

143. T. V. Ashworth, M. J. Chetcuti, J. A. K. Howard, F. G. A. Stone and S. J. Wisbey, *J. Chem. Soc., Dalton Trans.*, 1981, 763.

144. M. Chetcuti, M. Green, J. A. K. Howard, J. C. Jeffery, R. M. Mills, G. N. Pain, S. J. Porter, F. G. A. Stone, A. A. Wilson and P. Woodward, *J. Chem. Soc., Chem. Comm.*, 1980, 1057.

145. N. M. Boag, M. Green, R. M. Mills, G. N. Pain, F. G. A. Stone and P. Woodward, *J. Chem. Soc., Chem. Comm.*, 1980, 1171.

146. I. J. Farrugia, M. Green, D. R. Hankey, M. Murray, A. G. Orpen and F. G. A. Stone, *J. Chem. Soc., Dalton Trans.*, 1985, 177; I. F. Farrugia, J. A. K. Howard, P. Mitrprachachon, F. G. A. Stone and P. Woodward, *ibid.*, 1981, 155.

147. M. Green, K. A. Mead, R. M. Mills, I. D. Salter, F. G. A. Stone and P. Woodward, *J. Chem. Soc., Chem. Comm.*, 1982, 51.

148. R. Favez, R. Roulet, A. A. Pinkerton and D. Schwarzenbach, *Inorg. Chem.*, 1981, **19**, 1356.

149. C. Croder, P. L. Goggin and R. J. Goodfellow, *J. Chem. Soc., Dalton Trans.*, 1976, 2497.

150. J. Socrates, *J. Inorg. Nucl. Chem.*, 1969, **34**, 1667.

151. C. Eaborn, K. J. Odell and A. Pidcock, *J. Chem. Soc., Dalton Trans.*, 1978, 1288.

152. F. H. Allen and A. Pidcock, *J. Chem. Soc. (A)*, 1968, 2700.

153. J. Powell and B. L. Shaw, *J. Chem. Soc.*, 1965, 3879.

154. D. P. Arnold and M. A. Bennett, *Inorg. Chem.*, 1984, **23**, 2110.

155. A. J. Deeming, B. F. G. Johnson and J. Lewis, *J. Chem. Soc., Dalton Trans.*, 1973, 1848.

156. M. J. Church and M. J. Mays, *J. Chem. Soc. (A)*, 1968, 3075.

157. H. C. Clark and H. Kurosawa, *J. Organometal. Chem.*, 1972, **36**, 399.

158. I. M. Al-Najjar, M. Green, S. J. S. Kerrison and P. J. Sadler, *J. Chem. Res. (S)*, 1979, 206.

159. P. S. Pregosin and E. Steiner, *Helv. Chim. Acta*, 1976, **59**, 376.

160. R. Meij, Ph.D. dissertation, Amsterdam, 1978.

161. P. S. Pregosin and L. M. Venanzi, *Chem. in Britain*, 1978, **14**, 276.

162. A. Fumagalli, S. Martinengo, P. Cini, D. Galli, B. F. Heaton and R. Della Pergola, *Inorg. Chem.*, 1984, **23**, 2947.

163. M. Green, K. A. Mead, R. M. Mills, I. D. Salter, F. G. A. Stone and P. Woodward, *J. Chem. Soc., Chem. Comm.*, 1982, 51.

164. T. H. Tulip, Y. Yamogata, T. Yoshida, R. D. Wilson, J. A. Ibers and S. Otsuka, *Inorg. Chem.*, 1979, **18**, 2239.

165. M. A. Filomena, D. Remedious, P. J. Sadler, S. Neidle, M. R. Sanderson, A. Subbiah and R. Kuroda, *J. Chem. Soc., Chem. Comm.*, 1980, 13.

166. P. W. Frost, J. A. K. Howard, J. L. Spencer and D. G. Turner, *J. Chem. Soc., Chem. Comm.*, 1981, 1104.

167. P. S. Pregosin and L. M. Venanzi, *Helv. Chim. Acta*, 1975, **58**, 1548.

168. P. S. Pregosin, S. N. Sze, P. Salvadori and R. Lazzaroni, *Helv. Chim. Acta*, 1977, **60**, 2514.
169. S. Shinoda, Y. Yamaguchi and Y. Saito, *Inorg. Chem.*, 1979, **18**, 673.
170. C. Brown, B. T. Heaton and J. Sabounchei, *J. Organometal. Chem.*, 1977, **142**, 413.
171. J. Browning, P. L. Goggin, R. J. Goodfellow, N. W. Hurst, L. G. Mallinson and M. Murray, *J. Chem. Soc., Dalton Trans.*, 1978, 872.
172. H. Motschi, P. S. Pregosin and H. Rüegger, *J. Organometal. Chem.*, 1980, **193**, 397.
173. E. A. V. Ebsworth, J. M. Edward and D. W. H. Rankin, *J. Chem. Soc., Dalton Trans.*, 1976, 1673.
174. K. H. A. Ostoja Starzewski and P. S. Pregosin, *Angew. Chem. Int. Ed. Engl.*, 1980, **19**, 316.
175. P. S. Pregosin, *Chimia*, 1981, **35**, 43.
176. P. S. Pregosin and S. N. Sze, *Helv. Chim. Acta*, 1978, **61**, 1848.
177. K. H. A. Ostoja Starzewski, P. S. Pregosin and H. Rüegger, *Helv. Chim. Acta*, 1982, **65**, 785.
178. A. Albinati, P. S. Pregosin and H. Rüegger, *Inorg. Chem.*, 1984, **23**, 3223.
179. P. S. Pregosin and H. Rüegger, *Inorg. Chim. Acta*, 1984, **86**, 55.
180. N. W. Alcock and J. H. Nelson, *J. Chem. Soc., Dalton Trans.*, 1982, 2415.
181. J. H. Nelson and N. W. Alcock, *Inorg. Chem.*, 1982, **21**, 1196.
182. M. S. Holt, J. J. MacDougall, F. Mathey and J. H. Nelson, *Inorg. Chem.*, 1984, **23**, 449.
183. K. Seddon, University of Oxford, unpublished results.
184. R. J. Goodfellow and I. R. Herbert, *Inorg. Chim. Acta*, 1982, **65**, L161.
185. A. Albinati, U. von Gunten, P. S. Pregosin and H. J. Rüegg, *J. Organometal. Chem.*, 1985, **295**, 239.
186. S. Carr, R. Colton and D. Dakternieks, *J. Organometal. Chem.*, 1983, **249**, 327.
187. A. von Zelewski, *Helv. Chim. Acta*, 1968, **51**, 802.
188. A. Pidcock, R. E. Richards and L. M. Venanzi, *J. Chem. Soc. (A)*, 1968, 1970.
189. W. McFarlane, *J. Chem. Soc., Dalton Trans.*, 1974, 324.
190. S. W. Carr, R. Calton, D. Dakternieks, B. F. Hoskins and R. J. Steen, *Inorg. Chem.*, 1983, **22**, 3700.
191. S. W. Carr, R. Calton and D. Dakternieks, *Inorg. Chem.*, 1984, **23**, 720.

This Page Intentionally Left Blank

Index